METHODS FOR DETECTING DEFECTS IN COMPOSITE REHABILITATED CONCRETE STRUCTURES

Final Report

SPR 336

RESEARCH

Oregon Department of Transportation

METHODS FOR DETECTING DEFECTS IN COMPOSITE REHABILITATED CONCRETE STRUCTURES

Final Report

SPR 336

by

Vistasp M. Karbhari, Henning Kaiser, Rajiv Navada, Kumar Ghosh, Luke Lee
Department of Structural Engineering
University of California - San Diego
La Jolla, CA 92093-0085

for

Oregon Department of Transportation
Research Group
200 Hawthorne SE, Suite B-240
Salem OR 97301-5192

and

Federal Highway Administration
400 Seventh Street SW
Washington, D.C. 20590

April 2005

Technical Report Documentation Page

1. Report No.	2. Government Accession No.	3. Recipient's Catalog No.
FHWA-OR-RD-05-09		

4. Title and Subtitle	5. Report Date
METHODS FOR DETECTING DEFECTS IN COMPOSITE REHABILITATED CONCRETE STRUCTURES	April 2005
	6. Performing Organization Code

7. Author(s)	8. Performing Organization Report No.
Vistasp M. Karbhari, Henning Kaiser, Rajiv Navada, Kumar Ghosh, Luke Lee Department of Structural Engineering University of California - San Diego La Jolla, CA 92093-0085	

9. Performing Organization Name and Address	10. Work Unit No. (TRAIS)
Oregon Department of Transportation Research Unit 200 Hawthorne SE, Suite B-240 Salem, Oregon 97301-5192	11. Contract or Grant No. SPR 336

12. Sponsoring Agency Name and Address			13. Type of Report and Period Covered
Oregon Department of Transportation Research Unit 200 Hawthorne SE, Suite B-240 Salem, Oregon 97301-5192	and	Federal Highway Administration 400 Seventh Street SW Washington, D.C. 20590	Final Report 14. Sponsoring Agency Code

15. Supplementary Notes

16. Abstract

Fiber reinforced polymer (FRP) composites are increasingly being used to rehabilitate under-strength or deteriorating concrete structural elements and to prolong useful service-life of bridge structures. The rehabilitation is conducted through the external bonding of FRP strips onto the concrete substrate using either the wet layup process or the adhesive bonding of prefabricated strips. While the method has been shown to be extremely effective, there is a need for the development of expertise relating to identification of defects during inspection.

This report addresses four specific aspects of defect identification: (1) identification of the types of defects in composite-strengthened concrete structural elements; (2) determination of the potential effect of selected defects on the performance and integrity of the structural system; (3) identification of state-of-the-art quality assurance and non-destructive evaluation (NDE) technologies that can be used for detecting defects; and (4) preliminary investigation of selected technologies that have a high likelihood of being successfully used for purposes of quality assurance.

Potential defects are identified, classified by type and stage at which they could occur, and their effects are listed. Criticality of selected defect types is assessed using an experimental fracture mechanics based approach. The range of NDE techniques identified is assessed based on pertinent characteristics required for inspection in the field, and the techniques are classified based on applicability. Two techniques – thermography (representative of a non-contact local technique) and vibration based modal analysis coupled with a damage detection approach (representative of a global technique) – are explained in more depth with examples of use.

17. Key Words	18. Distribution Statement
Fiber reinforced polymer (FRP) composites; rehabilitation; strengthening; repair; defects; delamination; disbond; non-destructive evaluation; thermography; damage detection; effects.	Copies available from NTIS, and online at http://www.oregon.gov/ODOT/TD/TP_RES/

19. Security Classification (of this report)	20. Security Classification (of this page)	21. No. of Pages	22. Price
Unclassified	Unclassified	424 + appendices	

SI* (MODERN METRIC) CONVERSION FACTORS

APPROXIMATE CONVERSIONS TO SI UNITS

Symbol	When You Know	Multiply By	To Find	Symbol
		LENGTH		
in	inches	25.4	millimeters	mm
ft	feet	0.305	meters	m
yd	yards	0.914	meters	m
mi	miles	1.61	kilometers	km
		AREA		
in^2	square inches	645.2	millimeters squared	mm^2
ft^2	square feet	0.093	meters squared	m^2
yd^2	square yards	0.836	meters squared	m^2
ac	acres	0.405	hectares	ha
mi^2	square miles	2.59	kilometers squared	km^2
		VOLUME		
fl oz	fluid ounces	29.57	milliliters	ml
gal	gallons	3.785	liters	L
ft^3	cubic feet	0.028	meters cubed	m^3
yd^3	cubic yards	0.765	meters cubed	m^3
NOTE: Volumes greater than 1000 L shall be shown in m^3.				
		MASS		
oz	ounces	28.35	grams	g
lb	pounds	0.454	kilograms	kg
T	short tons (2000 lb)	0.907	megagrams	Mg
		TEMPERATURE (exact)		
°F	Fahrenheit	(F-32)/1.8	Celsius	°C

APPROXIMATE CONVERSIONS FROM SI UNITS

Symbol	When You Know	Multiply By	To Find	Symbol
		LENGTH		
mm	millimeters	0.039	inches	in
m	meters	3.28	feet	ft
m	meters	1.09	yards	yd
km	kilometers	0.621	miles	mi
		AREA		
mm^2	millimeters squared	0.0016	square inches	in^2
m^2	meters squared	10.764	square feet	ft^2
m^2	meters squared	1.196	square yards	yd^2
ha	hectares	2.47	acres	ac
km^2	kilometers squared	0.386	square miles	mi^2
		VOLUME		
ml	milliliters	0.034	fluid ounces	fl oz
L	liters	0.264	gallons	gal
m^3	meters cubed	35.315	cubic feet	ft^3
m^3	meters cubed	1.308	cubic yards	yd^3
		MASS		
g	grams	0.035	ounces	oz
kg	kilograms	2.205	pounds	lb
Mg	megagrams	1.102	short tons (2000 lb)	T
		TEMPERATURE (exact)		
°C	Celsius	1.8C+32	Fahrenheit	°F

*SI is the symbol for the International System of Measurement

ACKNOWLEDGEMENTS

The authors gratefully acknowledge the assistance and support of Dr. Charles Sikorsky of the California Department of Transportation, and of Dr. Paul Schuman (now at Simpson, Gumpertz and Heger) while he was a student in the Department of Structural Engineering at the University of California San Diego. They also acknowledge the role of Dr. Sikorsky in developing the example provided in Chapter 7.

DISCLAIMER

METHODS FOR DETECTING DEFECTS IN COMPOSITE REHABILITATED CONCRETE STRUCTURES

TABLE OF CONTENTS

REPORT APPENDICES

LIST OF FIGURES

LIST OF TABLES

1.0 INTRODUCTION

1.1 INTRODUCTION

This document provides a summary of the research conducted under a contract of the Oregon Department of Transportation with the University of California – San Diego, with the primary objectives as follows:

- Identification of the types of defects in composite-strengthened concrete structural elements
- Determination of the potential effect of defects on the performance and integrity of the structural system
- Identification of state-of-the-art quality assurance and non-destructive evaluation (NDE) technologies that can be used for detecting defects, and
- Development of the technologies that have a high likelihood of being successfully used for purposes of quality assurance.

Results of the study are reported in the following chapters with the chapters being organized to read as self-contained documents, albeit with a link from one to the next. This is done to enable ease of reference and use. A brief summary of each chapter is provided below. Figure 1.1 provides a ready reference for the reader in pinpointing location of pertinent information.

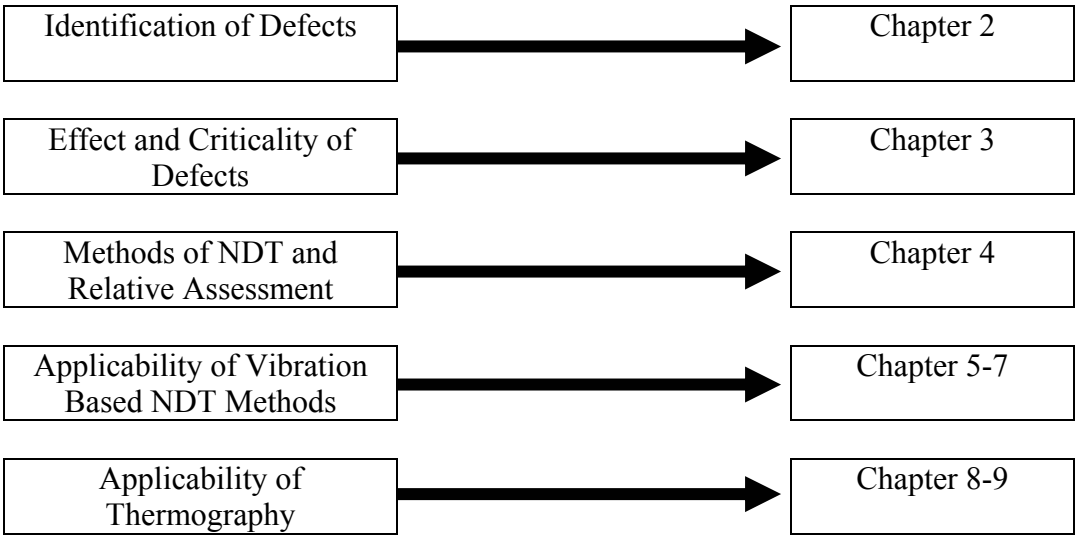

Figure 1.1: Report structure

1.2 OVERVIEW OF CHAPTER 2

This chapter provides the identification and classification of potential defects based on stage at which they could occur. Schematics and photographs of defect types are provided and potential effects of these defects are described. This chapter enables an engineer/inspector to rapidly gain knowledge about the following:

(a) types of defects,
(b) stages of rehabilitation at which they could occur, and
(c) causes and effects of these classes of defects.

1.3 OVERVIEW OF CHAPTER 3

This chapter provides a broad classification of defects identified in chapter 2 according to their effect on immediate degradation of structural integrity, durability, and aesthetics. A preliminary guideline of defect size, location, and density is provided, and limited guidance related to repair of these defects is provided.

1.4 OVERVIEW OF CHAPTER 4

This chapter provides a state-of-the art review of potential non-destructive testing (NDT) techniques for defect detection in carbon-fiber reinforced polymer (CFRP) materials, with emphasis on use in rehabilitation of concrete. This review covers past and current projects, including industrial applications, research projects, and methods under current industrial development. Both theoretical and practical aspects of each individual technique are addressed, including information on equipment, portability, data storage, and their capabilities and limitations. These findings serve to assess the suitability of each individual method towards in-situ inspection of CFRP-rehabilitated concrete components, and they provide the basis for the selection of two methods for further development.

1.5 OVERVIEW OF CHAPTERS 5-7

Methods for structural health monitoring of civil structures provide a means to evaluate the remaining useful life and capacity of the structure. Knowledge of a structure's useful life allows for the development of a systematic repair or replacement strategy for civil structures, maximizing the performance of the structures. Inherent in the structural health monitoring strategy is a nondestructive evaluation (NDE) technique to evaluate the condition and behavior of the structural system in its current state. However, most nondestructive testing (NDT) techniques available are localized methods such as ultrasonic testing, acoustic emission, magnetic field methods, radiography, eddy-current methods, and thermal field methods, which require the vicinity of damage be known a priori. While these local NDT methods can prove useful for the interrogation of structures and characterization of damage once the area of damage

has been identified, methods for global nondestructive evaluation are necessary for large civil structures.

The need for global NDE methods has led to an increased interest in the examination of the dynamic characteristics of a structure. The use of information related to the vibration properties (in particular, modal properties) can be effective in evaluating the safety of a structure, monitoring vibrations of the structure, improving analysis and design procedures, assessing design codes, and monitoring the in-service behavior of structures. Here, modal parameters refer to natural frequencies, mode shapes, which are often used as a measure of structural change over a period of time or after a repair or a major event such as an earthquake, blast, etc. By developing an effective procedure to acquire the modal properties of a structure, an analysis of the global capacity of the structure is possible based on the premise that modal parameters directly correspond to the mechanical properties, i.e., stiffness and mass of a structure.

An evaluation of the modal parameters of a structure at periodic time intervals allows for monitoring of changes in the mechanical properties, thus providing a means to measure the change in capacity of a structure as damage accumulates over time. In Chapter 5 an overall review of methods of dynamic testing is provided, followed by a review of damage detection methods in Chapter 6. A demonstration of the implementation of this form of NDT as a means of assessing the FRP rehabilitation is detailed in Chapter 7. This chapter also details procedures for conducting the evaluation with flow charts for steps.

1.6 OVERVIEW OF CHAPTERS 8-9

Based on a review of NDE techniques, the use of dynamic testing in conjunction with damage detection algorithms and IR thermography, were determined to have high potential for use in defect detection in FRP rehabilitated concrete structures. Chapter 8 provides a review of the use of IR thermography, including steps for its use and samples of defect identification. A case study is provided in Chapter 9 to demonstrate the implementation of the method and to provide a correlation between defect effects as measured through IR thermography and through structural response.

1.7 APPENDICES

Two appendices are provided. Appendix 1 explains the development of a methodology for the quantitative assessment of the effect of defects, based on a fracture mechanics approach, and provides limited sample results for some defect types. Appendix 2 provides results of a more in-depth study related to environmental and size effects of selected defects. These appendices thus provide quantitative assessment of selected defects already identified in Chapter 3. It is noted that defect criticality as related to FRP rehabilitation of concrete is as yet a new field; thus assessment at a quantitative level is largely undefined. Significant research is ongoing at a number of universities and institutions worldwide. The contents of Appendices 1 and 2 provide among the first quantitative assessments of these defects.

2.0 IDENTIFICATION AND DESCRIPTION OF POTENTIAL DEFECTS

2.1 INTRODUCTION

2.1.1 Materials

For centuries, composite materials have been used extensively for a broad range of applications. Beginning with simple man-made substances like reinforced clay or ceramics, concrete soon became of interest for construction purposes due to its ease of production and generally low cost. Today, it is the most widely used composite construction material.

From the 1970's onwards, polymer reinforced composite materials became increasingly popular, especially for use in the aerospace and defense industry. This interest was initiated by the demand for an extremely lightweight material, which would also be extremely resistant to most environmental factors and exhibit excellent strength and stiffness characteristics. Such materials typically consist of a load-bearing component (fibers) and a stress-transferring component (polymer matrix), which encapsulates the fibers.

The two polymer families available are thermoplastics and thermosets. While thermoplastics contain long molecular chains, which have the capability of sliding over each other, thermosets incorporate a stiffer molecular structure consisting of a highly cross-linked three-dimensional network. Because of the molecular structure thermoplastics may be melted and reshaped, whereas once formed thermosets cannot be reshaped or reformed and suffer degradation at temperatures higher than their glass transition temperatures. Due to considerations of cost, processing ease and durability in specific environments, thermosetting resin systems are more widely used in civil infrastructure applications. This report, for the most part, therefore emphasizes only thermosetting resin systems and composites derived thereof.

As indicated, the matrix serves as the fiber-encapsulating media, which transfers stresses between fibers and, in addition, protects them from aggressive environmental factors, like water, chemicals, abrasion, etc. Examples of matrices commonly used in civil infrastructure applications are polyesters, vinylesters and epoxies, the latter generically having the least shrinkage and highest strength/stiffness properties, as depicted in Table 2.1.

Table 2.1: Mechanical properties of selected resins [1]

Resin Type	Elastic modulus *E [GPa]*	Strength σ *[MPa]*	Cure shrinkage *[%]*	Strain to failure ε *[%]*
Polyester	3.1 – 4.6	50 – 75	5 – 12	1.0 – 6.5
Vinylester	3.1 – 3.3	70 – 81	2.1 – 3.5	3.0 – 8.0
Epoxy	2.6 – 3.8	60 - 85	1 - 5	1.5 – 8.0

If desired, users may add diluents, pigments or fillers to modify resin viscosity or appearance. To initiate and control cure of the resin, carefully metered amounts of hardeners, catalysts, initiators and inhibitors are mixed into the resin. The time span over which resins remain in liquid form prior to gel and vitrification can vary significantly, depending on factors like resin system makeup, ambient temperature and bulk resin volume.

An important property of thermoset polymers is their glass transition temperature T_g, which represents the range of temperatures (although usually specified as a single temperature level) over which the resin, or composite, changes response from a glassy, or elastic mode, to a rubbery, or viscoelastic mode. Consequently, a cured resin system must not be exposed to temperatures close to T_g, as this will result in substantial changes in elastic response and matrix damage.

The vast majority of fibers used in current applications belong to the glass, aramid and carbon varieties. For applications that do not demand extremely high strength and stiffness, glass fibers are preferred. However, their use on concrete is limited due to the susceptibility of the fibers to moisture and especially alkali-induced degradation. Aramid fibers have found high appreciation in impact related applications, such as bulletproof vests, and in structural applications wherein impact or abrasion resistance is essential. A typically low bond between fibers and matrix allows for high-energy absorption, but it limits their use in structural applications. Carbon fibers are essentially inert to environmental influences and have the highest levels of stiffness. However, they are limited to fairly low levels of strain. Table 2.2 presents a comparison of mechanical properties of some representative fibers and structural steel.

Table 2.2: Longitudinal properties of selected reinforcement [1]

Material	Density ρ [kg/m^3]	Elastic modulus E [GPa]	Tensile Strength σ_l [MPa]
E-Glass	2570 – 2600	69 – 72	3.5 – 3.7
Kevlar 49	1440	131	3.6 – 4.1
Carbon (HS)	1700 – 1900	160 – 250	1.4 – 4.9
Carbon (HM)	1750 – 2000	338 – 436	1.9 – 5.5
Carbon Steel	7790	205	0.6

Commonly, carbon fibers are supplied in yarns (also referred to as bundles, strands or tows) by 3000, 6000, 12000, etc., indicating the amount of individual fibers included in each fiber tow. This high number indicates their extremely small diameter, usually in the order of 10μm [1].

Depending on manufacturing technique, fibers can be designed for either high-strength, high-modulus or a combination of both. Herein, notations like ‘HS’ or ‘HM’ represent ‘high-strength’ and ‘high-modulus’, respectively. These properties largely depend on the precursor type and heat treatment employed during manufacture of the fibers. Apart from high strength and stiffness, carbon fibers can tolerate high temperatures and most corrosive environments.

To promote a good bond between fibers and the surrounding matrix, a suitable surface treatment (sizing) of the fibers is essential. The manufacturer typically provides information on resin/fiber compatibility.

To provide the user with a manageable fiber structure, yarns are arranged in specific reinforcement formations. Possible methods of integrating fiber tows include weaving, braiding, knitting or randomly oriented fiber mats. Depending on the intended use, fibers can be aligned in an almost infinite amount of variations to resist stresses in multiple directions. Some basic patterns include unidirectional (UD) or multidirectional weaves, schematically shown in Figure 2.1.

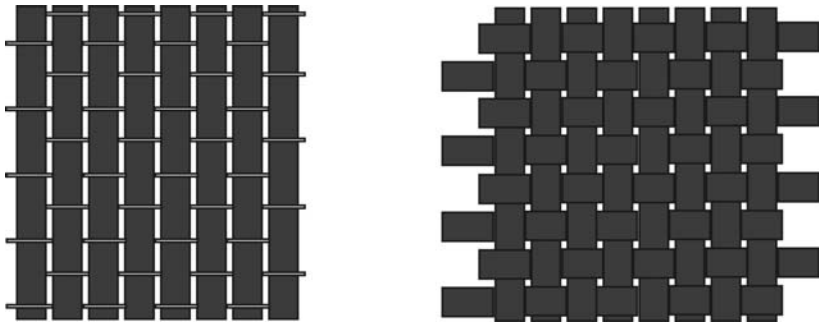

unidirectional multidirectional (plain weave)

Figure 2.1: Geometry of common weave patterns

2.1.2 Manufacturing methods

Successful incorporation of fibers within the resin can be obtained via a wide range of methods, including wet layup, spray-up, preimpregnated (prepreg) layup, liquid molding and others. Due to the simplicity and the flexibility of manual production, wet layup remains the most widely used process.

In wet layup, dry sheets of fabric are typically placed inside a mold, and resin is added between each layer to ensure full saturation. Using rollers or squeegees, resin is then forced to penetrate the fabric and completely wet-out the fibers. The part may be left to cure at ambient conditions; however, enhanced mechanical properties may be obtained via application of vacuum pressure and external heat. While vacuum pressure leads to higher degrees of fiber compaction and saturation of the fibrous architecture by the resin system, lower part thickness and smaller resin voids, high temperature cure promotes crosslinking.

Upon achieving sufficient “green strength”, which may actually be much lower than 100% cure, the composite is demolded. Degree of cure largely depends on the resin stoichiometry, as well as ambient conditions. Due to the chemical nature of polymer crosslinking, high moisture content

can result in incomplete cure. Low temperatures cause a similar effect, which makes outdoor manufacturing of composites particularly susceptible to these effects.

Preimpregnated material typically contains unidirectional fibers that have been impregnated and partially cured prior to use. Prepreg is used for manufacturing of parts in the aerospace industry that demand a relatively high fiber volume fractions V_f, high dimensional stability, and high quality (see Section 1.3). The material is much thinner compared to conventional fabric, thus a higher number of layers is required to form a composite with identical thickness.

Prepreg sheets are supplied on rolls with a layer of backing paper (peel ply) between adjacent layers. Upon installation, the backing paper is removed and the plies are stacked to form the desired composite structure. Due to the preimpregnation with a partially cured resin system, prepreg rolls must be stored in a freezer to retard the steady progression of cure. Prior to installation, thawing should take place in the original container to prevent condensation.

2.1.3 Mechanical and thermal properties

Both mechanical and thermal properties of composite materials are governed by the properties of the individual components. Unlike steel, composites are anisotropic materials, as they show significantly different properties in longitudinal and transverse directions, with respect to the fiber axis. Figure 2.2 indicates the rapid decrease of tensile stiffness with increasing off-axis angles for unidirectional and woven composite materials.

A quasi-isotropic material, i.e. with similar properties in all directions, can only be obtained by using chopped strand mats with randomly oriented fibers. Chopped fiber materials, however, are not nearly as stiff and strong as their continuous counterparts.

Although fibers are the main contributors to strength and stiffness, good adhesion between fibers and matrix as well as stress transfer between adjacent fibers is an absolute necessity for high material performance. In composite design, mechanical properties are mostly governed by the ratio of fiber volume to overall material volume, V_f. An increase in V_f results in a composite with higher strength and stiffness. Nevertheless, in practical applications, V_f is limited to roughly 55-65% for prepreg material and only 30 to 55% for wet layup, depending on weave geometry, resin viscosity, stacking order, degree of layer compaction as well as cure conditions.

Due to the anisotropic nature of composites, thermal properties are often different in multiple directions. Under normal ambient conditions, the coefficient of thermal expansion of carbon fibers is positive in the transverse direction and negative in the longitudinal direction, resulting in a longitudinal contraction of the composite material upon temperature increase. Most so-called 'room-temperature' epoxy resins have a T_g in the order of 60-80°C, indicating the maximum operating temperature of the composite. These resin systems are often available 'off-the-shelf' and the previously mentioned temperature limit must be considered prior to installation in hot environments.

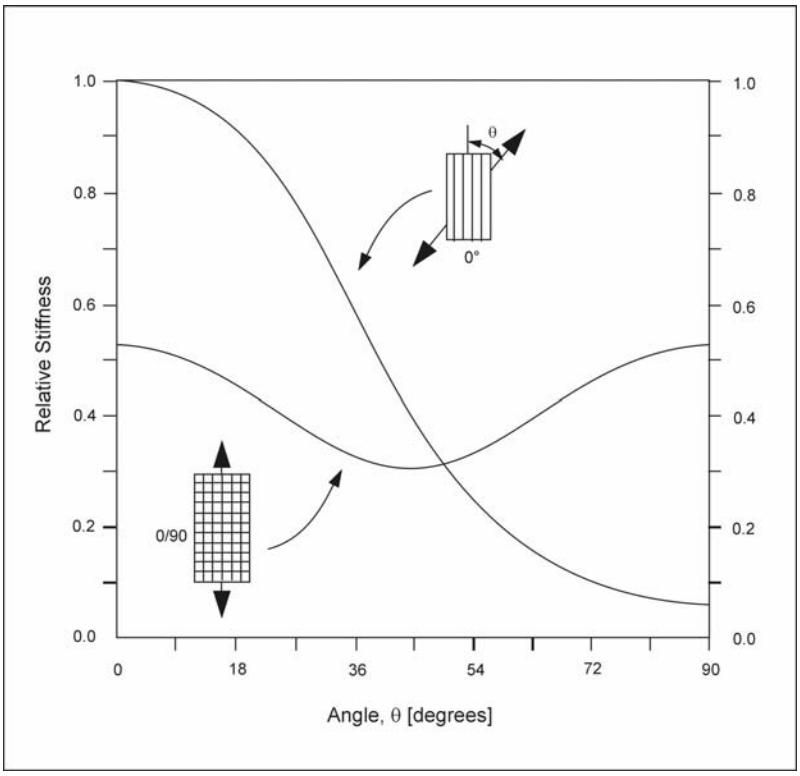

Figure 2.2: Effect of test angle upon in-plane stiffness of unidirectional and biaxial laminates [2]

2.1.4 Structural applications

A steady increase in the number of deteriorating infrastructure has forced civil engineers to seek viable rehabilitation methods, capable of significantly extending the service lifetime of a structure. While many concrete structures, such as bridges or dams, were designed and constructed during the mid-20th century, more than 50 years of continuously increasing traffic, along with the exposure to harsh environments, has led to an unexpected degree of physical and chemical damage, experienced in substantial amounts of cracking, spalling and deterioration of internal steel reinforcement.

To date, a large number of concrete rehabilitation measures have involved the application of external reinforcement schemes, typically in the form of epoxy bonded steel plates [3,4]. Researchers have recently focused on using fiber reinforced polymer (FRP) composites for external strengthening, to make use of their high strength and stiffness as well as excellent environmental resistance [5, 6, 7]. Figure 2.3 depicts a typical application scheme for composite materials on concrete surfaces.

Figure 2.3: Strengthening of concrete bridge deck

External strengthening is typically applied to account for structural degradation due to in-service conditions as well as additional flexural and shear loads, which were not included in the initial design of a structure. Furthermore, long-term exposure to the environment might have caused substantial damage in form of concrete cracking, spalling and exposure of corroded steel reinforcement. Through external bonding of composite materials, flexural and shear capacities of members such as columns, bridge girders or floor slabs may be significantly increased. Herein, the material is bonded to the concrete substrate using appropriate resin systems. To ensure adequate bonding, the concrete substrate is sandblasted, serving two main purposes: 1) the weak cement paste layer is removed; and 2) exposure of aggregate enhances mechanical interlock between adhesive and substrate.

While strength and stiffness of the composite material are important to the system's overall efficiency, the composite-substrate adhesive layer must primarily provide adequate stress transfer capabilities. Unless the adhesive material is specifically designed for adhesion, stress transfer and environmental resistance, the rehabilitation will lack performance and eventually undergo rapid degradation. Special resin formulations are available for these purposes, some of which are specifically designed as adhesives and others that are suitable for substrate bonding and saturation of fibers simultaneously.

If the composite element is bonded onto a concrete substrate, the efficacy of the method depends on the combined action of the entire system with emphasis on the integrity of the bond and the interface layers. The composite-adhesive/resin-concrete system must be considered as a complete system, and material aspects of each of the constituents and interactions between them and the external environment can have a significant effect on overall efficiency and durability. The external reinforcement can be fabricated in three generic ways:

- Adhesive bonding of a prefabricated element;
- Wet layup of fabric; and
- Resin infusion.

Of these methods, pre-manufactured elements show the highest degree of uniformity and quality control, since processing is done under controlled conditions. The composite strip/plate/panel is prefabricated manually or by automated processes (i.e. pultrusion) and then bonded to the concrete surface using an adhesive under pressure. Application is rapid, but the efficiency is predicated on the use of an appropriate adhesive and the achievement of a good bond between the concrete substrate and the adherent. Care must be taken to ensure that the adhesive is chosen to match as closely as possible both concrete and composite in regards to their elastic moduli and coefficients of thermal expansion, while providing an interlayer to reduce mismatch induced stresses. Commercially available strips are currently fabricated using unidirectional carbon fiber reinforcement, which is pultruded to preset thickness and widths. While this ensures uniformity of the material, preset dimensions often restrict the use of prefabricated material on structures with a more complex geometry.

As in other industries, the wet layup process is perhaps the most used currently and gives the maximum flexibility for field applications. Moreover, it is probably the least costly alternative. However, it presents the most variability and necessitates the use of excessive resin and could result in wrinkling or shear deformation of the fabric used, decreasing its designed efficiency. The process entails application of resin to the concrete substrate followed by the impregnation of layers of fabric, which are bonded onto the substrate using the resin itself. Both the composite and the bond are formed at the same time in the field. The process affords the maximum flexibility in the field but has the disadvantage of field mixing and fabrication along with a high potential for absorption of moisture and/or inclusions and impurities. Once applied, the composite is left to cure under ambient conditions. At present, both plain weave and unidirectional fabrics are commercially available for rehabilitation means.

The in situ resin infusion method is a fairly new variant and is capable of achieving uniformity and good fabric compaction, while making it easier for the reinforcement to be placed without excessive unintended deformation. However, this scheme is difficult to apply over large areas and necessitates application of a vacuum. In the infusion process, the reinforcing fabric is first formed into a preform, which is attached to the substrate using a vacuum bag. Resin is infused into the fibrous assembly under vacuum to form the composite. As in wet layup, the composite and bond are formed at the same time.

Despite the high potential of composite materials, when compared to conventional building materials like steel and concrete, the physical nature of composites yields a much higher potential for introduction of material defects. In addition, composite materials represent a construction material that is relatively new to the civil industry. Consequently, contractors and field workers are still unfamiliar with the appropriate material handling, storage and installation procedures involved. Processing of composite materials, unless performed by highly automated processes like pultrusion or filament winding, typically necessitates a certain degree of human involvement, providing room for errors, such as non-uniformity or matrix flaws, to name only a few. Other examples include air pockets, debonding, fiber misalignment or poor resin quality. As shown by several researchers, the above-mentioned defects in composite materials are capable of reducing performance and long-term durability of composite materials [8, 9, 10, 11].

Structural rehabilitation methods have already encountered several of the previously addressed material flaws, which have led to a substantial amount of material degradation as well as

deterioration of the entire rehabilitation scheme. A typical example is shown in Figure 2.4, where moisture, propagating from inside the concrete, has become entrapped at the concrete/composite interface. The result was loss of intimate bond over a large area in the externally strengthened deck slab. Here, encapsulation of an entire area without incorporation of ventilation gaps has restricted the escape of moisture.

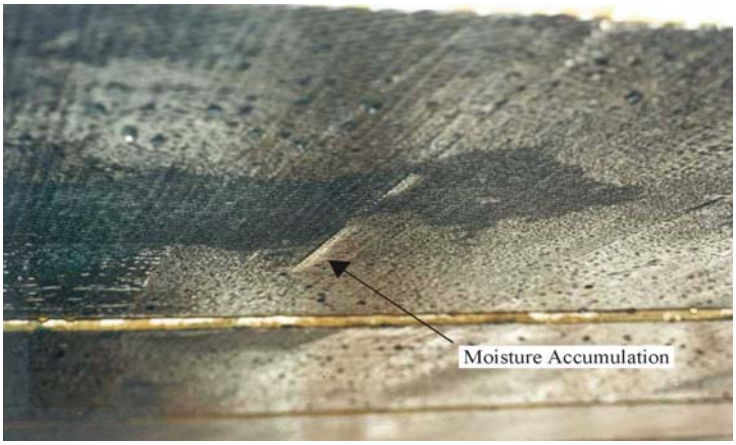

Figure 2.4: Delamination due to entrapped moisture

This report discusses the typical appearance, identification, characterization and effect of defects in structurally rehabilitated members. This chapter focuses on defect identification in composite materials, based on knowledge and results acquired from numerous research investigations conducted by the aerospace industry. This knowledge is projected onto common structural rehabilitation methods to provide a basis for identification of defects and assessment of their criticality in the external strengthening of concrete components. Subsequent sections will focus on defect detection, criticality, and their effect on structural systems.

While a range of materials can be used for external strengthening, this assessment will focus on composites using the wet lay-up process and external bonding of prefabricated strips. Since use of prepreg in structural rehabilitation has been rare, mainly due to the need for cure at elevated temperature and the difficulty to obtain adequate bond without the use of additional resin, it will not be included in the further discussion. Apart from the installation process, material quality, site and material preparation, and service conditions will be addressed. These stages are schematically shown in Figure 2.5. They will be discussed in further detail in the following sections of this report.

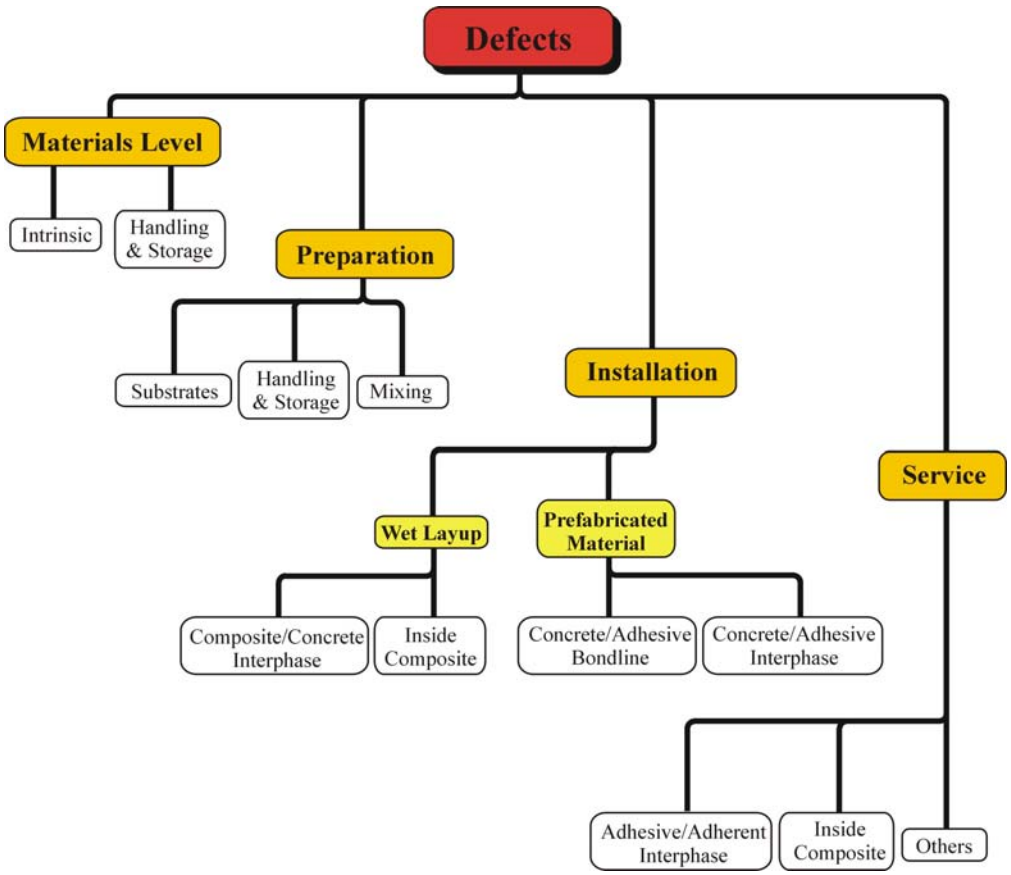

Figure 2.5: Schematic diagram of defect-initiating stages

2.2 DEFECTS IN COMPOSITE MATERIALS

The performance of composite materials depends on the successful incorporation of high strength and stiffness fibers in a surrounding matrix material. While fibers are the main contributors to strength and stiffness, the matrix serves as a medium for transferring stresses between adjacent fibers. Thus, an ideal unidirectional fiber reinforced composite material would have straight fibers running exactly parallel to each other, with fibers completely embedded in a strongly adhering, uniform matrix material. However, due to several factors, uniformity of the material may be disturbed. Such imperfections can occur in the fiber material, the matrix, and at the interface between both materials.

If two materials are bonded together to form a composite (e.g. two composite strips), high quality of the interface is crucial, since it ensures stress transfer between layers. Bonding can be achieved using a resin system identical to that used for fiber infiltration or by application of special adhesives. These materials are preferably high-viscosity polymeric systems, particularly in cases where one material shows a significant amount of surface irregularities (i.e. when bonding composites to concrete).

Apart from knowledge on common defect types encountered in composite materials, their initiating factors (why and when is a defect introduced) must be studied. For most applications, two distinct stages can be identified:

- Defects produced during manufacture; and
- In-service damage.

A large body of research has already been conducted by the aerospace industry, a sector where high material uniformity and performance are an absolute necessity [9, 10, 11, 12, 13, 14, 15]. In the following discussion, results of the extensive knowledge from the aerospace and marine industry are used to provide a basis for defect identification and assessment for the specific application under consideration in this document. Due care is taken, however, to assure applicability and appropriateness for the materials set and processing conditions that would be used in a civil engineering context.

Depending on size, defects can be classified as either microscopic or macroscopic. Microscopic defects include material flaws such as hollow, cracked or otherwise damaged or degraded fibers; variation in fiber diameter; fiber-matrix debonds; and/or non-uniform and poor fiber wet-out. Macroscopic defects are mostly related to matrix voids, misorientation, wrinkling or shearing of fabric, and delamination or separation of reinforcing fabric layers.

2.2.1 Microscopic defects

It has been shown that microscopic defects on fibers occur even in the best laminates and that their effect on material performance is mostly negligible. Consequently, it has been suggested that, while causing slight reductions in material strength, this micro-defect should be regarded as a material property [12]. However, effects of environmental exposure induced fiber degradation, fiber-matrix bond non-uniformity, and non-uniformity in wet-out can be significant and cannot be neglected. Most of these effects can be avoided through the judicious and appropriate selection of constituent materials (fiber and resin) and adherence to rigid processing standards.

The use of prefabricated components is one means of ensuring a reasonable level of quality control and assurance. Classification of defects in wet layup systems, however, is more complicated. Here, the ratio of defective material over good material seems more deterministic towards defect criticality than the actual type of flaw encountered. As such, the isolated local existence of microscopic traces of contaminants such as moisture may be significantly less important for durability than the larger agglomeration of inclusions or global effects of moisture or solvent uptake.

2.2.2 Macroscopic defects

At the macroscopic level, defects are often associated with certain structural features. For example, voids and kinking of fibers is more likely to occur in concave regions, since the laminate must be forced into this shape, resulting in poor material consolidation [12]. Other researchers have suggested further distinguishing the initiating factors of defects [13], as follows:

- Fibers
- Matrix and fiber-matrix bond
- Stacking or layup
- In-service defects

2.2.3 Sources of defects

Generally, it may be assumed that the manufacturer controls quality of constituent materials (fibers, resin system components) to a sufficient degree. Nevertheless, poor manufacturing, handling or storage of the material during production/transportation can result in fiber damage, distorted alignment of fibers within the fabric, contaminations or surface moisture accumulation. Small debris, dirt, or other objects that adhere to single fiber bundles typically contaminate fibrous reinforcement [13].

While resin systems are less susceptible to physical damage, the vast majority of systems can be degraded by impurities. Contaminations in resins occur in form of foreign chemicals, moisture or fine particles, altering the chemical consistency and reactivity of resins. Furthermore, their limited shelf life provides the chance of using overaged material that has lower reactivity along with an increase of viscosity to a point where processing becomes virtually impossible. Also, the fiber-matrix bond is substantially lower if the resin system lacks reactivity or if contaminations are deposited on the fiber surface.

Prefabricated material designed for installation in the field typically possesses a higher degree of material uniformity. Cutting of fabric and/or tensioning of individual tows in unidirectional pultruded elements, infiltration, and cure of the part are performed by automated processes in a controlled environment. Hence, most of the previously addressed material flaws can be ruled out in this form of material. It can thus be assumed that these materials possess a relatively low amount of internal defects. Nevertheless, handling damage remains as a potential initiator for material flaws.

Another important aspect in material quality is related to moisture accumulation. Resin systems are capable of moisture absorption, generally resulting in inferior material properties, including loss in shear strength, reduction in modulus, and depression in the level of glass transition temperature. Further, moisture absorption can cause significant physical and chemical changes in the resin, leading to irreversible changes through hydrolysis, saponification, and other such phenomena. While the strength and modulus of carbon fibers is not influenced by moisture, a significant decrease in bond strength in the composite can occur if moisture is accumulated on their surface. In contrast, both glass and aramid fibers can be severely degraded by the presence of moisture next to the bare fiber. Material properties can further be influenced by storage conditions. Resins and fibrous material should therefore be stored in a cool and dry environment, to prevent moisture accumulation and unintended gel.

One of the main reasons for variations in material properties is the manufacturing process, i.e. the procedure used to develop the desired combination of resin and fibers to form the composite material. Since a small degree of human involvement always remains, even the most automated processes are susceptible to human error. Naturally, composite material defects occur more

frequently in parts manufactured by hand layup than in most other automatically processed components. Common types of defects include porosity, voids (air pockets), incorrect fiber orientation, resin richness/poorness, poor mixing, incorrect cure, inclusions and dirt, and wrong stacking sequences and delaminations [9, 10, 11, 12, 13].

Air pockets typically become entrapped when stacking multiple sheets of lamina and must be removed via the use of rollers. Although this provides a means to remove most of the entrapped air, small amounts always remain inside the matrix. Porosity, a microscopic defect, can also be caused by volatiles given off during the curing cycle. In regions where porosity shows a high occurrence, these microscopic defects may join together to form a large void [13].

In-service defects have drawn the attention of many researchers, especially in the aerospace field [14, 15]. High-localized loading, such as impact of an object, causes one of the most common in-service defects. The exposure to runway debris often induces subsurface delaminations that are not visible on the surface yet significantly reduce material performance. Material defects induced during manufacturing, such as voids or excess resin often weaken the plane between two layers of fibrous reinforcement. Under high loading conditions, interlaminar cracks can form. Furthermore, moisture penetration remains critical even in the cured state. Over time, water and other liquids can penetrate the material and accumulate in porous matrix regions.

Similar to the composite material itself, quality and performance of adhesive bonds can be influenced by a number of material flaws. Depending on the substrate material, adhesives must be chosen to match the surface structure. The two main phases involved in adhesive bonding are:

- Adhesive
- Adhesive/adherent interface

Similar to the matrix in composite materials, porosity, voids, incorrect or incomplete curing and application of incorrect amounts can be found in the application of polymeric adhesives. Moreover, the adhesive/adherent interfaces can experience weak bonding due to chemical deposits or material inclusions. Here, adherent refers to both prefabricated- as well as substrate material. Sufficient abrasion followed by cleaning and, in the case of a concrete substrate, application of adequate surface primers, often results in a high-quality bond. During service, moisture penetration can lower the material properties and cause the loss of bond, resulting in separation of the bonded materials.

2.3 DEFECTS IN STRUCTURAL REHABILITATION

During rehabilitation of structural elements, defects may be induced at different stages of the process. A structurally significant defect can be defined as a material flaw which, within the lifetime of a structure, reduces its load carrying capabilities to a level less than or equal to the design values. Once a defect has been induced, elimination may become difficult, if not impossible. Furthermore, criticality can vary significantly among defects, depending on their type, location, density and size. The following discussion describes those defects most likely to be encountered during structural renewal of concrete structures using FRP composites.

Examples from defects already encountered in rehabilitated structures will be described and evaluated. While most defects can be related to a specific stage of the rehabilitation process, some may be induced at several, if not all, stages of the process. As indicated in the preceding discussion, the following four stages were chosen for closer evaluation:

- Incoming raw or constituent materials,
- Site preparation and on site processing,
- Installation in the field, and
- Service

2.3.1 Incoming raw or constituent materials

Incoming raw materials can be of inferior quality and unsuitable for structural applications. Quality control should be performed in order to detect such defects before the materials are used in the field. Generally, resin, fabric, preimpregnated material (prepreg), and prefabricated material are considered as the primary components. In this section potential defects of each material are listed, illustrated, and discussed.

2.3.1.1 Resin system

Generally, any variation from the manufacturer's specifications should be reported and considered carefully. While many resin systems are commercially available, they generally cannot be used interchangeably. If the resin system is not suitable for the desired purpose, it must not be used. Material variations caused by improper storage or production, such as chemical inconsistency or impurities, are typically inspected visually on a pass/no-pass basis, typically through viscosity tests. More sophisticated techniques of material testing are mostly unavailable in the field, since they generally require laboratory equipment. Consequently, control has to be performed in compliance with a specification sheet, as commonly supplied with most resin systems. While this may be used for some aspects, such as shelf life, it does not provide any information on impurities or moisture absorption during storage.

2.3.1.1.1 Overaged material

Resin, hardener, catalyst or additives may be beyond their specified shelf life. Most cans bear a label, showing the date of expiration of the contents (Figure 2.6). Typically, resin shelf life ranges from 3 to 8 months. If stored in warm environments, resin tends to pre-cure inside the container, thus decreasing shelf life. Although reactive agents have not been introduced to the resin, the constituents slowly cure, as the material is stored. If expired, resins should not be used. An overaged resin system shows lower reactivity, resulting in lower strength and elastic modulus. Also, viscosity increases with time, leading to difficulties during fiber infiltration. These properties can be checked through use of viscosity tests and differential scanning calorimetry (DSC).

Figure 2.6: Resin label

2.3.1.1.2 Contamination/inclusions

Resin inclusions may be present in the form of small particles, such as dirt, sand, etc. If worked into the fabric, fibers may be damaged. Also, chemical consistency may be altered, depending on the type of inclusion. If oils or silicones are mixed within the resin, they may serve as potential initiators for debonding or delamination. These material flaws can be detected through viscosity tests, since additions cause an increase in viscosity. Moisture can be detected through DSC or differential mechanical thermal analysis (DMTA) of cured materials. In extreme cases, Fourier Transform Infrared (FTIR) spectroscopy can be used to assess the state of the resin system itself.

2.3.1.1.3 Moisture entrapment

Improper storage of sealed containers over extended periods of time may induce moisture to the resin, leading to poor reactivity and incomplete cure. Also, resealing of containers may result in moisture contamination of the remaining resin. If large quantities of resin have been stored in a humid environment, a DSC or FTIR test may be used to check for increased moisture content. Although time consuming due to additional off-field laboratory time, it can ascertain the quality of the resin and prevent long-term effects. Introduction of moisture into resin can lead to premature gelation, degradation through saponification, hydrolysis or other chemical reactions.

2.3.1.2 Fibrous material

Fibers are supplied in different forms with varying fibrous assembly geometries (unidirectional and multidirectional) to provide strength in one or multiple directions. For most rehabilitation applications, unidirectional or a woven fabric is preferable.

Supplied on rolls, damage to fibers may not be detected until immediately prior to installation. The primary quality control objectives for fibers are:

- Mechanical properties, and
- Bond to matrix.

2.3.1.2.1 Incorrect fiber type

Prior to installation, fiber type, structure and weave geometry must be inspected. The material must meet the design specifications (type, strength and stiffness properties) in all aspects. If the material appears different in geometry, it most likely possesses strength and stiffness properties that vary from those required. Although this control process is visual and rather unsophisticated, it requires the installer to have basic knowledge of fiber geometry and appearance of different fiber types.

2.3.1.2.2 Kinked or wavy bundles

Fibers inside a fabric may be kinked or wavy, as shown in Figure 2.7. If kinked, fibers may easily break during handling or installation. Wavy fiber bundles do not run in the principle loading direction; hence they are not capable of resisting equally high loads along this direction. As a result, adjacent, straight fiber bundles have to account for higher stresses (stress concentrations). Also, a loss in stiffness is likely to be encountered.

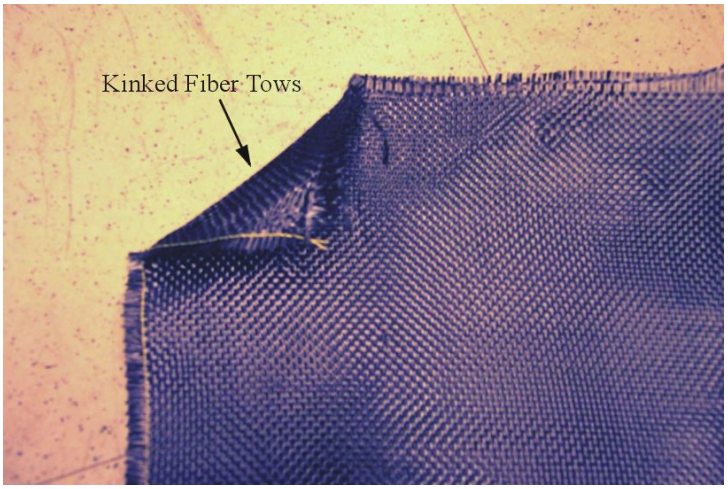

Figure 2.7**:** Kinked fibers

2.3.1.2.3 Broken fibers

While a single broken fiber is difficult to detect, broken fiber strands (Figure 2.8) are more critical and should be noticed. Although each fiber bundle contains a

large number of fiber discontinuities (due to the manufacturing process), these discontinuities differ in location throughout a bundle. Therefore, stress concentrations from one broken fiber may be easily adopted by adjacent fibers. In case of a ruptured bundle, however, stress concentrations are significantly higher and weaken the fabric to an enormous extent.

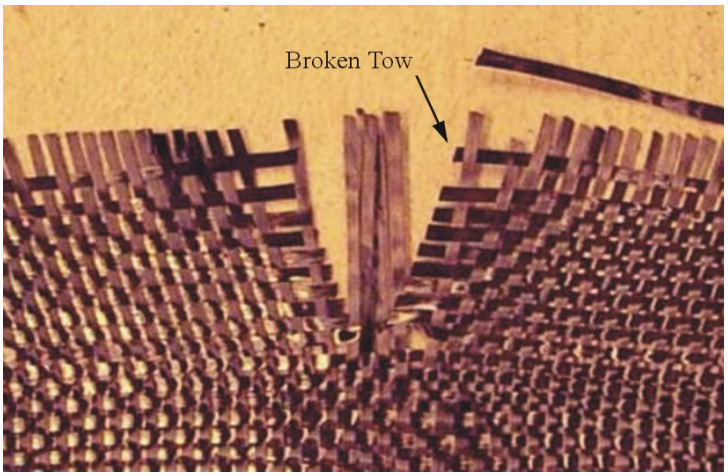

Figure 2.8**:** Broken fiber tows

2.3.1.2.4 Contamination/inclusions

The fiber surface may contain impurities in form of chemicals or small objects, as depicted in Figure 2.9, which can harm both fiber and bond strength. While carbon fibers are rather inert to chemicals, glass fibers are highly susceptible to alkali attack. Sizing chemistry, a measure for resin/fabric bond capability, can be affected by certain chemicals and thus reduce bond strength. Small objects are likely to be trapped near the fiber surface to form a void and serve as a potential debond. In case of sharp-edged inclusions, fibers may be severely damaged upon infiltration.

2.3.1.2.5 Fabric wrinkles

During processing and handling of fabric, fiber wrinkles may be induced. Shown exaggerated in Figure 2.10, such wrinkles should be straightened as much as possible without further disturbing fabric uniformity, before the fabric is infiltrated. On severely wrinkled material, fiber damage may occur. If a fabric has a wrinkle running along its entire width, strength and stiffness reduction may be a concern, especially if the wrinkle is not smoothed out during fabrication of the composite, resulting in air entrapment, fiber misalignment, local zones of weakness, and points of crack/delamination initiation.

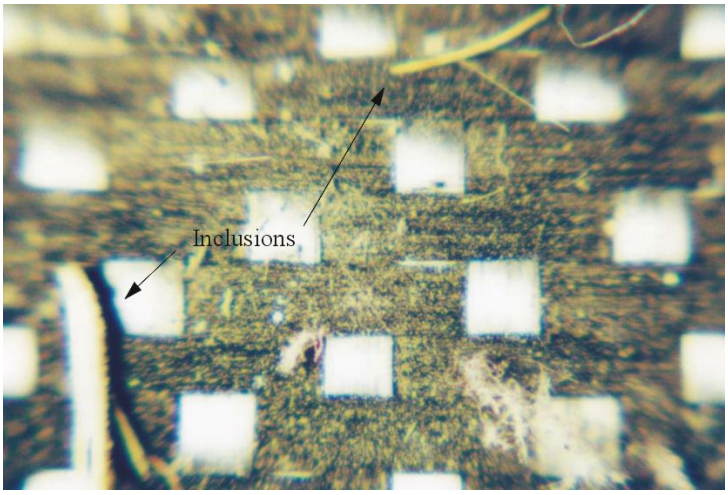

Figure 2.9: Fabric inclusions

Figure 2.10: Wrinkled fabric

2.3.1.2.6 Sheared fabric

If woven fabrics are exposed to shear forces during handling, fiber alignment can change to an undesirable off-axis direction. As such, a 0/90 fabric may end up as a 15/75, similar to the fabric shown in Figure 2.11. As a result, fibers no longer run along the principal axis and cannot develop their full potential in strength and stiffness.

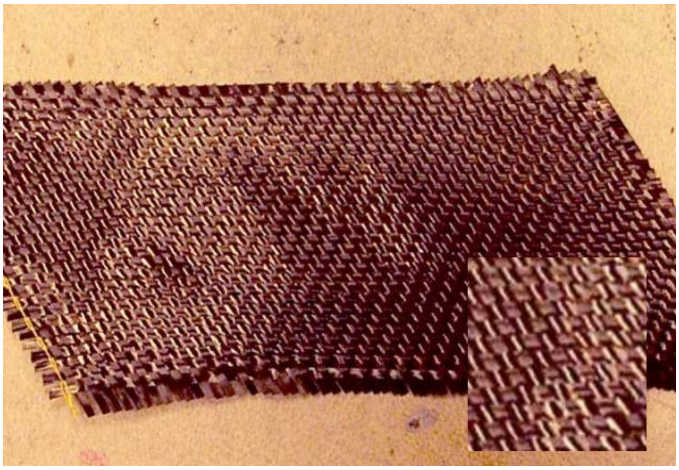

Figure 2.11: Sheared fabric

2.3.1.2.7 Damage to free edges

During handling of fabric rolls, damage to free edges is likely to occur. Because a fabric structure does not exhibit the same integrity around the edges as inside the woven area, edges are also more likely to decompose during resin infiltration. Material such as that shown in Figure 2.12 utilizes additional rows of stitching along the material edges that are effective in preventing such decomposition. However, if the stitching is damaged or missing, as shown on the left, the affected portion must be discarded. In case of multiaxial fabrics, the removal or damage of tows can cause change in the local reinforcement ratio.

Figure 2.12: Damaged edges

2.3.1.2.8 Loose fibers

Pullout of single fibers or fiber bundles (Figure 2.13) may occur during processing and handling in the field. Loose material does not exhibit the same intermediate contact to nearby fibers and is more likely to be sheared during resin infiltration. Furthermore, resin rich areas tend to form in these regions, resulting in low stress transfer capabilities between adjacent fiber strands.

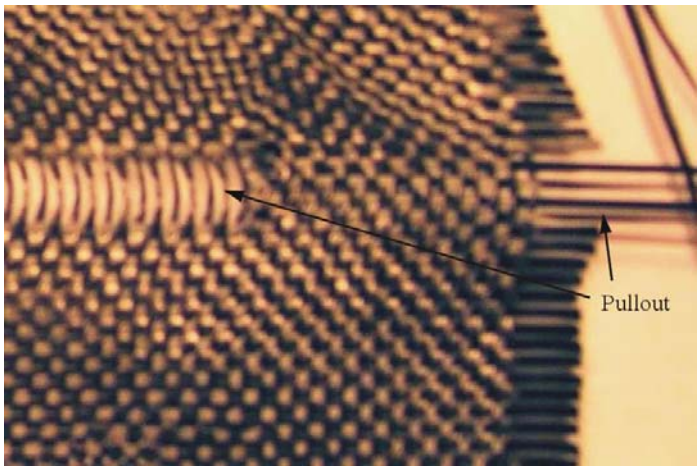

Figure 2.13: Fiber pullout

2.3.1.2.9 Fiber gaps

Separation of fiber tows within a woven fabric or unidirectional tape can be experienced in form of gaps (Figure 2.14). Such gaps will disturb fiber integrity, lower strength and stiffness, promote resin richness and serve as locations of low crack propagation resistance.

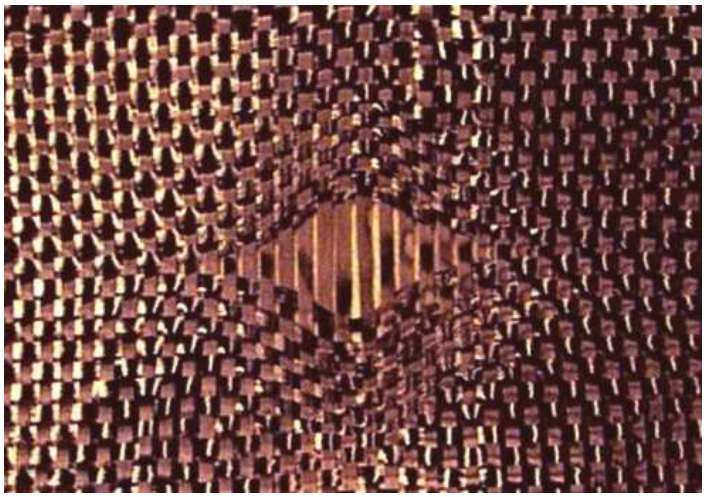

Figure 2.14: Large fiber gap

2.3.1.2.10 Moisture entrapment

Similar to resins, fibers may accumulate surface moisture if exposed to humidity for an extended period. Overnight storage should be performed under stable temperatures and in a moisture-controlled environment. If moisture is apparent, fabric should be discarded. Most fibers do not absorb moisture. However, surface moisture will lower bond strength to the resin matrix and present risk of large area delamination.

2.3.1.3 Prefabricated material

For some applications, prefabricated composite strips are preferred over wet lay-up of fabric. Manufactured under controlled conditions, prefabricated material is less likely to experience material strength degradation due to voids, non-uniform impregnation, or moisture entrapment. A special adhesive is chosen to bond the reinforcement to the prepared concrete substrate. In most cases, long uniform strips are used to serve as additional flexural or shear reinforcement. These are commonly made via the pultrusion process. On more complex members, such as T-girders, the use of prefabricated material is likely to be limited due to the requirement of exact conformance with specific geometric configurations. Although L- and U-shaped sections are commercially available, their suitability must be confirmed for each individual member prior to attempting installation. A slight deviation in chamfer or web dimensions along the girder length may therefore not allow the use of identically prefabricated parts. Nevertheless, prefabricated material has been used successfully in concrete rehabilitation.

2.3.1.3.1 Voids and process-induced defects

Since prefabricated material is manufactured under controlled conditions, void content may be considered low. In most cases, quality control by the supplier determines whether a part is acceptable or should be discarded. In addition, specification sheets of prefabricated material are based on average results and account for a typical void content.

2.3.1.3.2 Transportation/handling damage

Damage to prefabricated material may be induced during storage, transportation or handling. Typical defects include splitting, delamination, matrix cracking, scratched surfaces, etc. Once the material has left the processing facility, the installer must determine whether it has experienced additional damage and make assessments towards the suitability for installation. Figure 2.15 shows typical composite strips with delamination of several layers (top) as well as longitudinal splitting (bottom). It must be emphasized, however, that these forms of material damage are not a common occurrence.

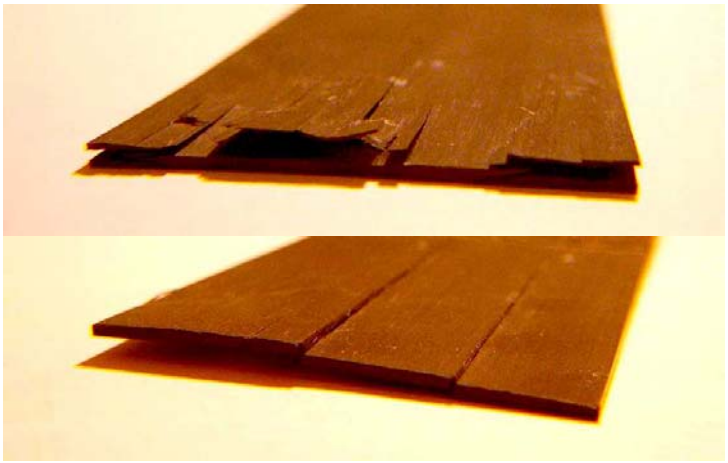

Figure 2.15: Damaged prefabricated material

2.3.2 Site preparation and on site processing

Any successful rehabilitation measure demands proper preparation of the structural element. This includes surface preparation of the concrete to a desired degree (such as sandblasting), storage of fiber and resin constituent materials, and mixing of the resin system. On-site processing, if performed incorrectly, contains a high potential for flaw introduction. It further necessitates assessments in regard to the integrity and bond-capability of the concrete substrate. In some cases, cracked or split concrete sections may contain wide cracks that must be injected with resin prior to application of the composite strengthening system. Defects induced by preparation and site processing are discussed in this section.

2.3.2.1 Resin system

2.3.2.1.1 Storage

Improper storage of the resin system, as well as the hardener/catalyst, can lead to significant moisture absorption. If stored under inappropriate conditions, such as extreme cold, heat or humidity, resin properties may change dramatically with time. In addition, as discussed previously, shelf life must be monitored to assure sufficient reactivity and viscosity.

2.3.2.1.2 Stoichiometry

Resin and hardener/catalyst must be compatible and of adequate mechanical and chemical properties for the job at stake. For all resin systems, the hardener/catalyst ratio must be determined very carefully to prevent premature gelling or loss of matrix strength.

2.3.2.1.3 Mixing

During mixing, several defects may be introduced to the system, and consequently, the laminate itself. Firstly, if using rotary mixers, air can be drawn into the resin and remain as small air bubbles, leading to laminate porosity. In some cases, this porosity may later result in the formation of air bubbles of much larger diameter (mm range). A high number of roller passes are thus required to remove porosity from laminates that have been infiltrated with air-rich resin systems, since it is known that in the range from zero to 5%, each 1% increase in void content decreases interlaminar shear strength by about 10% [16]. Consequently, mixing must be performed at a slow rate and without drawing an excessive amount of air into the matrix.

In contrast, a low degree of mixing can result in chemical inconsistency, meaning that some regions contain high percentages of reactant, while others may contain no reactant at all, schematically illustrated in Figure 2.16. As a result, matrix strength and adhesion are low. Due to lower levels of crosslinking there may be enhanced susceptibility to environmental degradation in areas of low polymer chain linkage. Secondly, the efficacy of the resin system depends on the appropriate use of mix ratio. Errors in mix ratio can result in undercure or no cure, premature gelling and even degradation due to excessive exotherm.

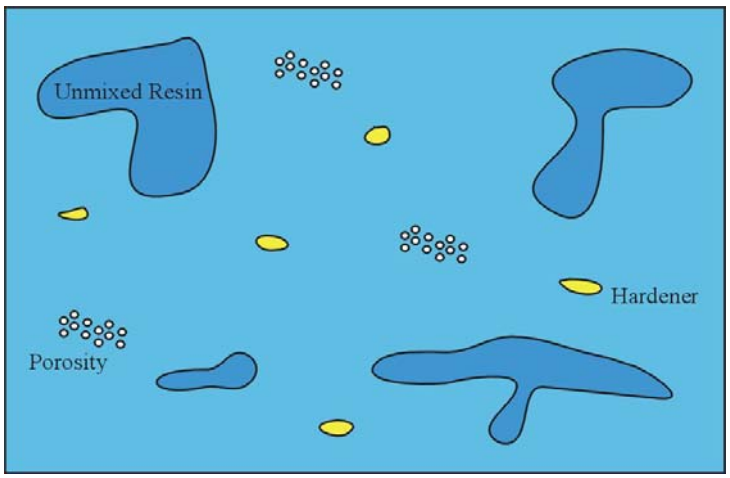

Figure 2.16: Results of incorrect mixing

2.3.2.2 Fibrous material

Like resin, fibers are susceptible to moisture accumulation; however, accumulated moisture does not alter the performance of individual fiber tows. Instead, the bond to the surrounding matrix is severely weakened. Since fibers can be directly exposed to the environment, i.e., through torn plastic packaging, conditions must be monitored more closely than in the case of a sealed resin container. If visual detection shows a significant

amount of moisture accumulation on the fiber surface, they must be discarded. When a moist fabric is infiltrated, it will experience a weak bond to the surrounding matrix. Debonding and subsequent delamination are likely to be the result.

2.3.2.3 Concrete Substrate

To obtain adequate force transfer between the retrofit material and the concrete substrate, concrete preparation is essential. This includes thorough surface preparation to a specified degree and filling of concrete cracks. Large, deep cracks propagating into the concrete may contain water that can destroy the composite-concrete interface bond and should therefore be injected prior to rehabilitation (Figure 2.17). Cracks propagating at shallow depth can promote failure in the substrate. As such, the retrofit becomes ineffective.

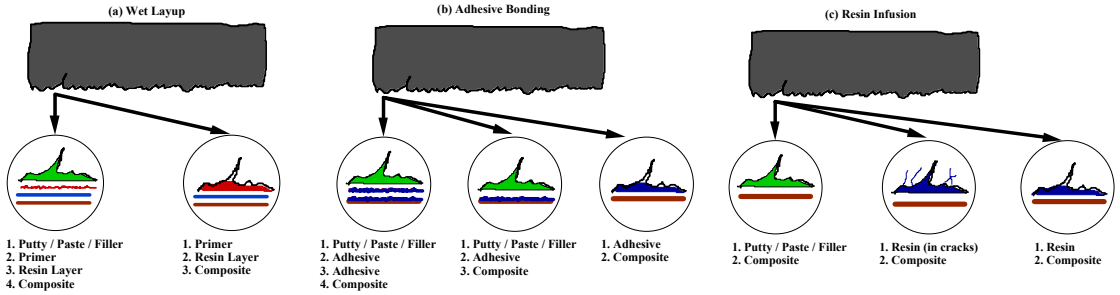

Figure 2.17: Common surface morphologies

2.3.2.3.1 Inadequate primer application

Concrete is a porous material and hence absorbs liquids. Moreover, due to abrasion of cement paste during sandblasting, a large number of small to medium diameter voids become exposed on the concrete surface, as shown in Figure 2.18. Prior to application of the composite overlay, regardless of type, a compatible primer coat should be applied. The role of this primer is to fill voids and quench the absorption so that the surface is prepared for the subsequently applied composite material. If primer coatings are omitted, the saturating resin would otherwise be absorbed to an extent. Also, the primer presents a "bondable" surface. To ensure an intimate bond between composite and concrete, the thickness of the coating should be kept as thin as possible. If excessive amounts of primer are used, low stress transfer capabilities and resin dripping can result (Figure 2.19).

Figure 2.18: Concrete surface irregularities

Figure 2.19: Primer dripping

2.3.2.3.2 Disbonding in marked regions

Marking of areas that require strengthening is generally done using a chalk line. However, care must be taken not to cause separation between the layup and base material by using a marking substance that cannot be penetrated by the resin/adhesive. A typical example is shown in Figure 2.20, where duct tape serves as a "marker line." Here, edge disbonding at the concrete/composite interface was more likely to be encountered.

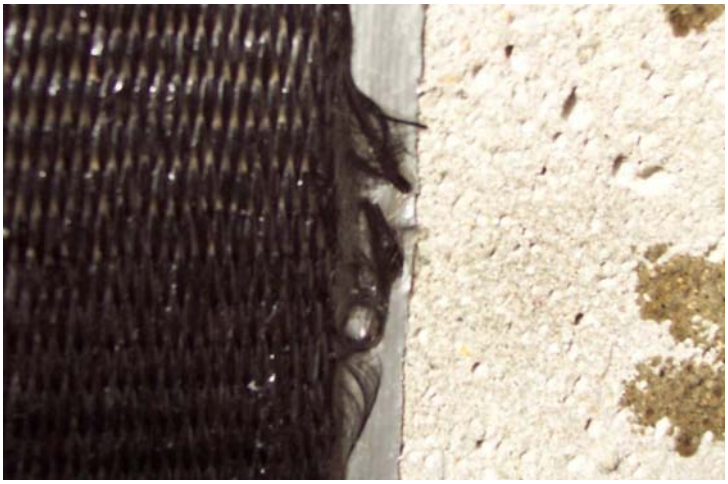

Figure 2.20: Fiber placement over duct tape

2.3.2.3.3 Degradation at imperfections

If the concrete substrate displays a high degree of microcracking at its surface, the composite overlay must bond to an initially weak base material. In extreme cases the poor cover material may need to be completely removed and replaced by appropriate fillers, prior to rehabilitation. Two forms of typical substrate degradation are depicted in Figure 2.21.

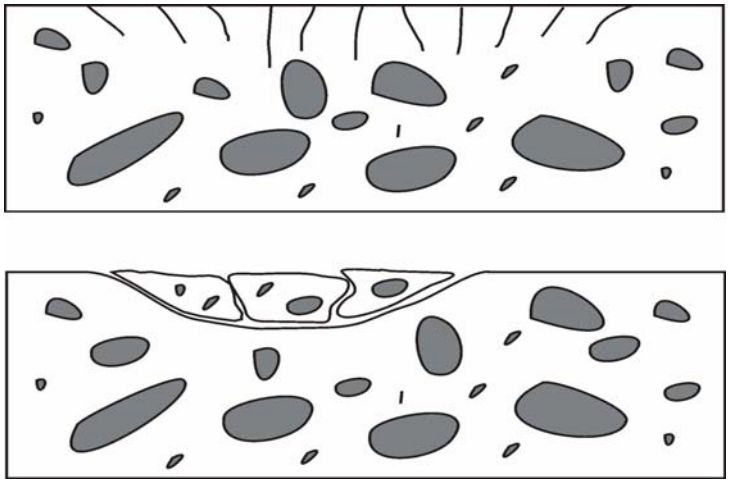

Figure 2.21: Microcracking and spalling of concrete substrate

2.3.2.3.4 Inclusions at imperfections

Naturally, many structures in need of rehabilitation already show a large number of cracks, which may have opened to a significant degree and thus accumulated moisture, dirt or other foreign material over time. By applying a primer coating, inclusions may become permanently encapsulated within the surface to serve as weak spots for future crack initiation and propagation at the interface level (Figure 2.22). As a preventive measure, cracks should be cleaned and injected with appropriate filler materials, depending on the depth and diameter of the crack.

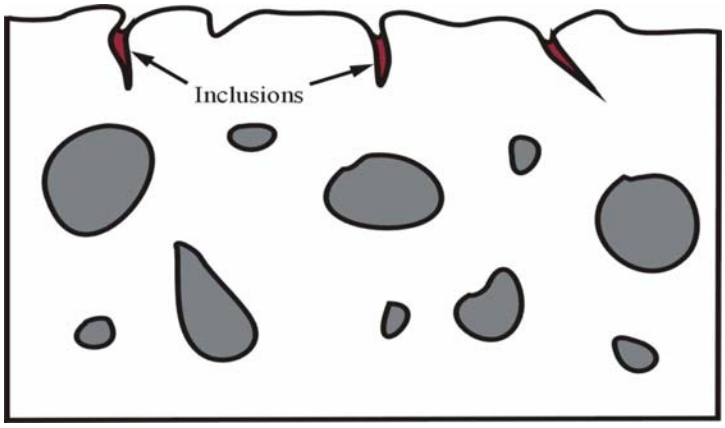

Figure 2.22**:** Inclusions at imperfections

2.3.2.3.5 Inadequate grinding of substrate

To provide a smooth surface for bonding, any irregularities such as form lines or protruding aggregate should be ground down. If a composite laminate is applied to concrete surfaces that contain high spots, as depicted in Figure 2.23, the laminate will tend to form an air pocket. Similarly, large, hollow regions, which may result from high spots in the formwork, must be filled prior to composite application. Figure 2.24 illustrates the effect of composite placement over hollow regions.

2.3.2.3.6 Galvanic corrosion

On spalled or otherwise heavily degraded members, the embedded steel reinforcement may be exposed to the environment. As a result, the composite strengthening system is likely to come into direct contact with the reinforcement (Figure 2.25). Due to the galvanic corrosion potential of carbon fibers, deterioration of the steel as well as the matrix material would be the result [17]. Thus, intimate contact between carbon composites and steel must be prevented,

possible by application of suitable polymeric systems that serve as an insulator (e.g. GFRP, primer coating).

Figure 2.23: Air entrapment over high spots

Figure 2.24: Air entrapment over hollow regions

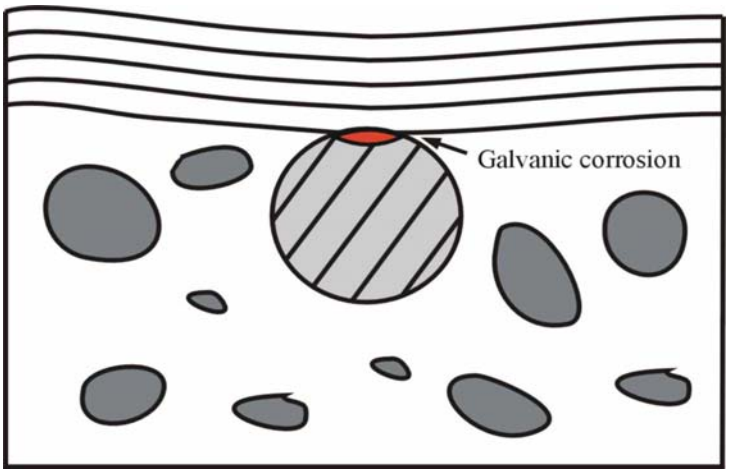

Figure 2.25: Galvanic corrosion

2.3.3 Installation in the field

Among the four main stages of rehabilitation, field installation may be considered the most critical step in regards to quality assurance. A wide range of defects, classifiable from benign to severe can be introduced at this stage. Numerous research studies have been conducted that quantify the possible defects in composite materials. However, most research has been focused on aerospace applications [14, 15].

Environmental conditions and material preparation are key elements to a successful installation of the material. For instance, many resin formulations do not cure at low ambient temperatures (≈ 5°C) and develop significantly lower glass transition temperatures. In addition, a hot environment will cause premature gelling and make handling virtually impossible. Thus, installation must not be allowed to begin or be continued at temperatures below a critical threshold value. Furthermore, surface preparation and application procedures must be followed closely to ensure proper interfacial bond strength as well as complete infiltration of the fibers. In the following discussion, defects most likely to be encountered during installation of rehabilitation systems are addressed.

2.3.3.1 At the composite/concrete interface

2.3.3.1.1 Sagging of infiltrated material

Until the resin has developed adequate tackiness, i.e. turns into a gel, the infiltrated material tends to separate from the concrete, especially in vertical and overhead regions (Figure 2.26). To prevent large-scale debonding, the most susceptible areas must be rolled repeatedly until resin tack can be confirmed. If the material sags there is no bond or intimate contact between the composite and the substrate, thus stress transfer capabilities are severely reduced. Moreover, air pockets promote the accumulation of moisture as a long-term effect.

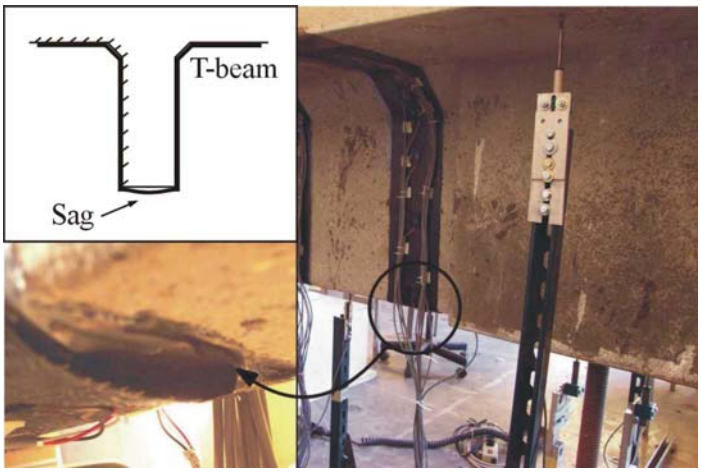

Figure 2.26: Sagging of infiltrated composite material

2.3.3.1.2 Non-uniform concrete/composite interface

Insufficient amounts of resin/adhesive can lead to a weak interfacial bond. While resin-rich regions experience low stress transfer, resin-starved areas tend to favor disbonding of the composite material from the concrete substrate. Figure 2.27 illustrates a typical non-uniform interface thickness.

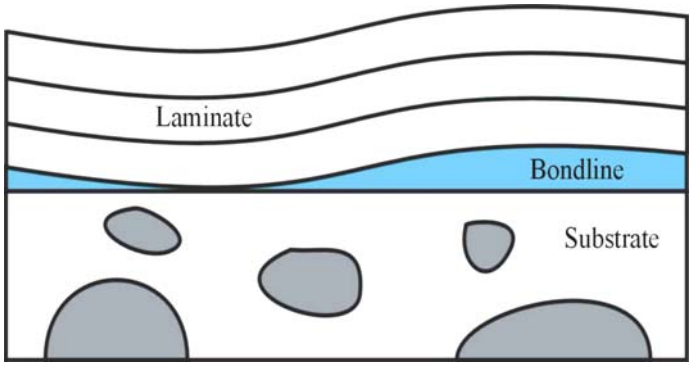

Figure 2.27**:** Resin-rich and resin-starved interface regions

2.3.3.1.3 Porosity

Porosity is termed as the presence of a large number of microscopic air voids, typically in the range of 10μm. It may be caused by volatiles and entrained gasses (air and water vapor) inside the resin/adhesive. While porosity can be considered a normal material property, it serves as a depository for diffused moisture. In certain areas, microvoids may combine to form a large void.

2.3.3.1.4 Voids

Voids are typically caused by air entrapment during the lay-up process. Other factors contributing to void formation are entrapped air from mixing, volatiles/gasses, an insufficient amount of resin applied, and inclusion of foreign particles. Also, if laminate is placed over high spots, which can occur as a result of formwork irregularities, air is likely to become entrapped around it. Thus, careful grinding of irregularities after sandblasting is advisable. Both porosity and voids cause internal stress concentrations. Examples of voids at the concrete/composite interface are shown in Figure 2.28.

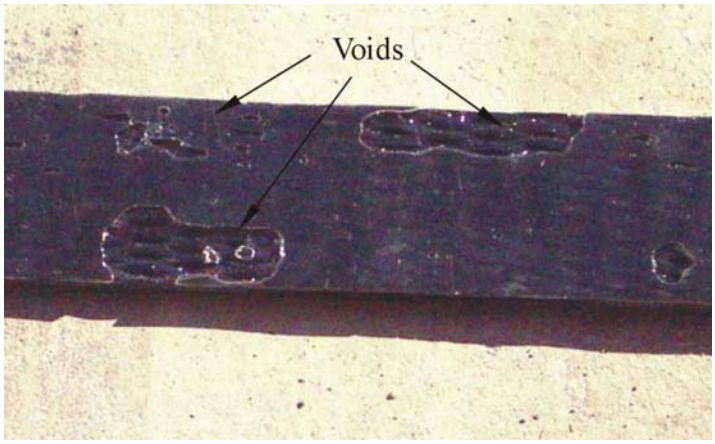

Figure 2.28**:** Typical voids at the concrete/composite interface

2.3.3.2 Intrinsic to the composite material

2.3.3.2.1 Porosity

Similar to porosity at the concrete/composite interface, this flaw can occur inside the composite material. Initiating factors include volatiles given off during resin cure.

2.3.3.2.2 Voids

If multiple layers of fabric are placed on top of each other, air usually becomes entrapped between them. Rollers can be used to 'work out' most of the air. In addition, overlapping of layers promotes the formation of voids, since additional resin is needed to fill the gap formed at the overlap. For instance, voids in unidirectional composites exist as tubular pores, which run along adjacent fiber direction, almost exclusively at the fiber/matrix interface. Figure 2.29 shows the common forms of air entrapment inside the matrix material.

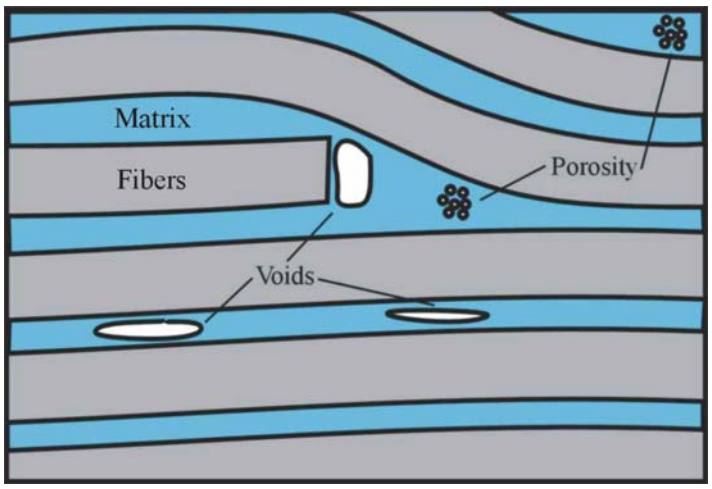

Figure 2.29**:** Voids and porosity inside composite laminates

2.3.3.2.3 Debonding

In the case of moisture accumulation on the fiber surface, deficiencies in bond strength between fibers and the surrounding matrix may occur. Depending on the amount and location of moisture accumulation, this can mean lack of bond formation during cure or debonding of the fibers from the matrix at a later stage. Generally, debonding results in loss of composite strength in transverse tension, interlaminar shear, and impact. Unlike delamination, debonding occurs in localized areas.

2.3.3.2.4 Delamination

Wrinkles, in which air is entrapped between layers, inclusions of non-adherent foreign objects or an inadvertent use of moist material may cause a delamination. In most cases, delamination is present over a fairly large area and severely reduces shear transfer capacity. Figure 2.30 shows certain types of delamination and their initiating factors.

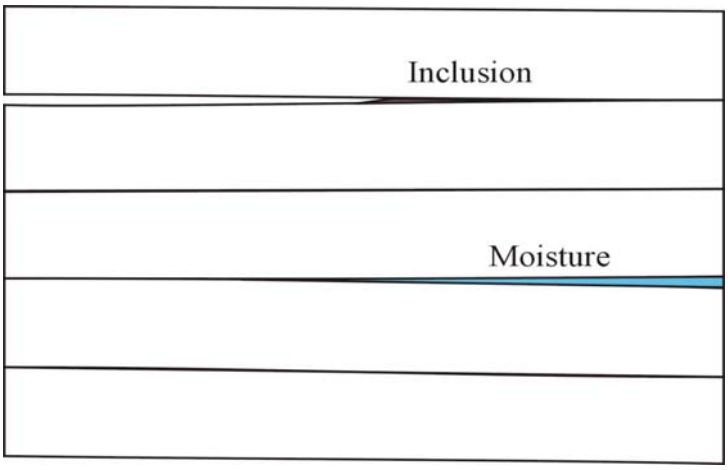

Figure 2.30**:** Delamination in laminates

2.3.3.2.5 Fabric waviness

Performance of a strengthening system is in part dependent on fiber orientation. Fabric waviness in localized regions, as presented in Figure 2.31, can lower the elastic modulus and result in inferior properties (compare Figure 2.2). Waviness originates from improper rolling in opposite directions towards one point of the laminate. Instead, rolling should be performed from mid-length towards both ends of a strengthening strip.

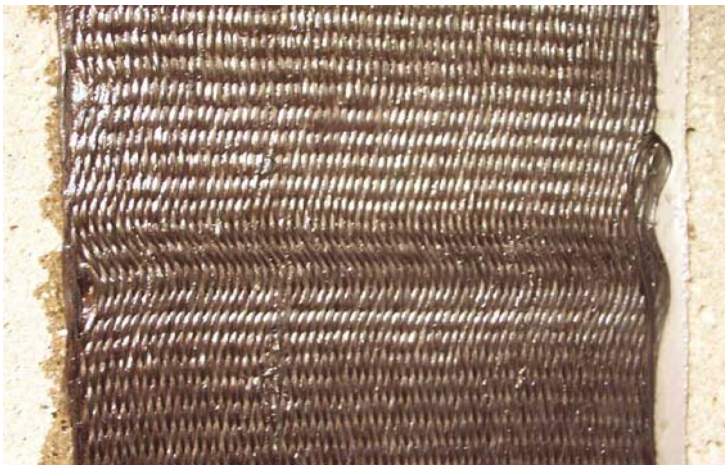

Figure 2.31: Waviness caused by improper rolling

2.3.3.2.6 Resin richness/poorness

Resin rich areas result from the use of excessive amounts of resin during fiber infiltration. Proper rolling/squeezing of the fibers may contribute to lower void volume, higher uniformity, and removal of resin rich areas.

Resin starved areas (resin poorness) are caused by an insufficient amount of resin. Consequently, no interlaminar bond will be present in those areas. Also, resin poor areas serve as a potential initiator for delamination. This material flaw is illustrated in Figure 2.32.

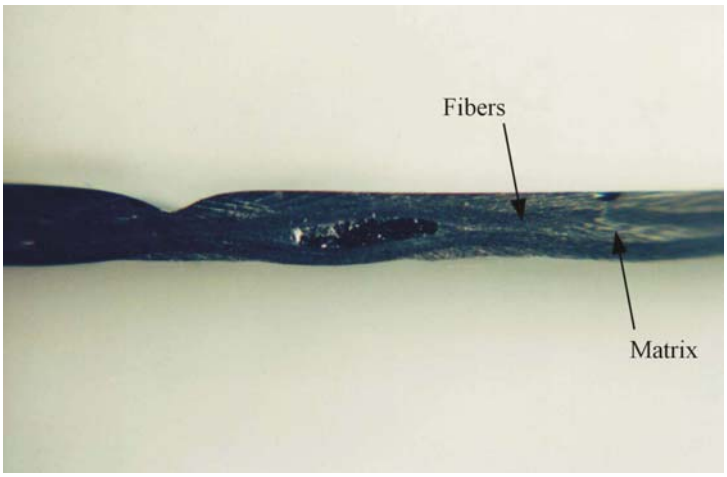

Figure 2.32: Variation in matrix thickness

2.3.3.2.7 Indentations

Although mainly an in-service defect, indentations, presented in Figure 2.33, can occur during installation. Careless handling of prefabricated material can result in deep scratches that propagate into the material and cause damage to fibers. On wet lay-up, indentations can be caused by harsh use of infiltration tools.

2.3.3.2.8 Damaged Edges

Damage to edges mostly occurs in regions where fibers have already been pulled out of the fabric in the dry state. Upon infiltration, the weave loosens and allows fibers to be pulled from the fabric, as shown in Figure 2.34. This will cause reduction in strength and stiffness and increase the likeliness of material separation at the concrete/composite interface.

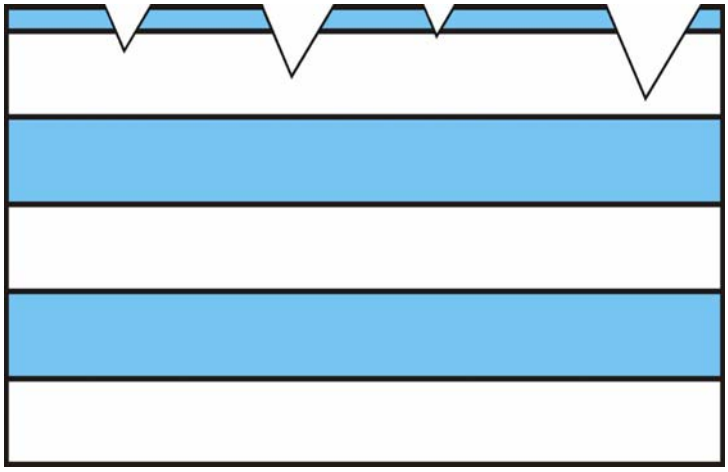

Figure 2.33: Indentations

Figure 2.34: Pullout of loose fiber during infiltration

2.3.3.2.9 Missing layers

The high susceptibility of structural renewal measures to human error allows for the omission of entire layers within a stacking sequence, particularly in more complex applications, where multiple layers are used. Consequently, the occurrence of such a defect will result in strength/stiffness properties of the laminate that will most likely be entirely different from the design values.

2.3.3.3 Prefabricated material

The use of prefabricated material involves two distinct interfaces, the concrete/adhesive interface and the adhesive/adherent interface. The strength of each individual interfacial

zone is dependent on different factors, including surface preparation as well as preparation of the adherent.

2.3.3.3.1 Concrete/adhesive interface

A highly viscous adhesive putty is commonly deposited on the substrate to form a film of approximately 1mm thickness. Prior to combination of substrate and reinforcing strip, a layer of nearly identical thickness is applied to the adherent. Upon combination, both adhesive films are joined and about 50% of the material is ideally removed in the process, resulting in an overall bondline thickness of 1mm. Since the process of putty application is similar to surface priming, defects at the concrete/composite interface can be considered identical to those discussed previously in Section 2.3.3.1.

2.3.3.3.2 Adhesive/adherent interface

Adequate preparation of the prefabricated composite material is essential in obtaining a strong bond. Similar to concrete, surface preparation of prefabricated material is performed to abrade its surface and, ideally, expose some fibers to the surface. However, care must be taken so the fibers will not be severely damaged, i.e. abraded or cut. Bead blasting [18] and solvent wipe have proven to be suitable methods for enhancing mechanical interlock between adhesive and the adherent surface. On certain systems, strips are pre-sanded as part of the manufacturing process, leaving a smooth outer surface and one with a more pronounced fiber texture (Figure 2.35). Apart from preconditioning of the adherent, the adhesive used must be suitable for the composite material, i.e. it must allow for stress transfer and remain functional at a wide temperature range.

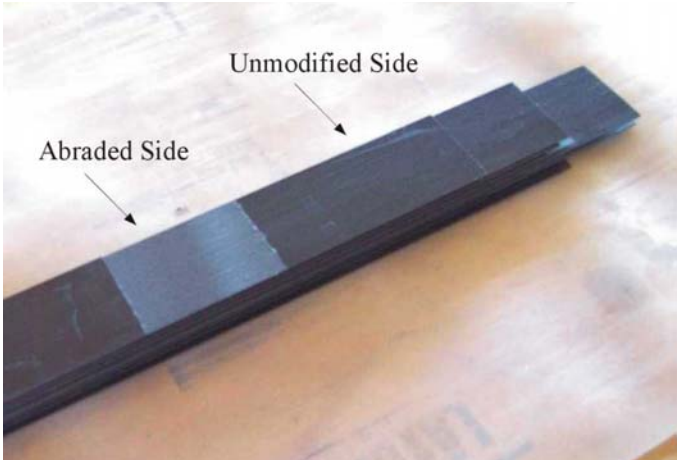

Figure 2.35: Differences in texture of various pultruded strips

Given the fact that prefabricated strips are applied in a cured state, they are less flexible than wet fabric and do not conform to surface irregularities comparatively well. To obtain high uniformity of the adhesive prior to joining, strips are commonly passed through special resin applicators. If this operation is performed at a highly inconsistent rate, it can lead to resin-poor spots, as depicted in Figure 2.36. These must later be filled in by hand to reduce the risk of air entrapment.

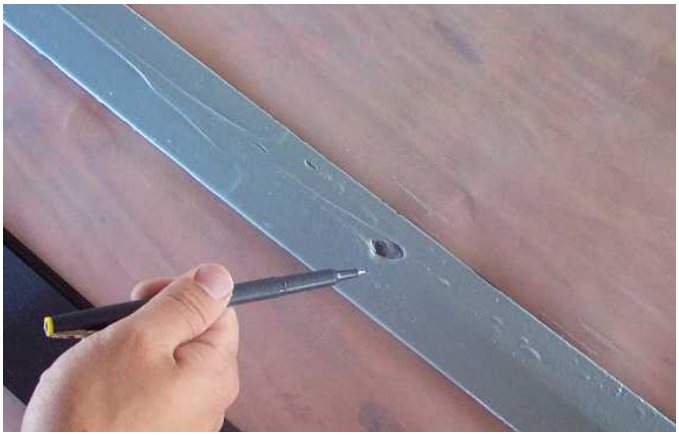

Figure 2.36: Formation of void during putty application

Due to a natural tendency of composite strips to retain their straight orientation, regions of overlapping are usually critical. This includes utilization of grid patterns, which often result in excessive bondline thicknesses, which leads to in a higher load being borne on the adhesive causing its premature failure. If strips are excessively rolled in an attempt to reduce bondline thickness, much of the resin becomes removed from underneath the strip, resulting in resin-poor areas once the composite has returned to its natural orientation. A concave, hollow bondline as shown in Figure 2.37 can be observed. In other areas the ends sag downwards/ outwards, resulting in increased adhesive thickness at ends, which can result in premature peeling or cracking within the adhesive layer itself under load.

While these problems are unique to application of prefabricated strips, other defects include non-uniform concrete/composite interfacial thickness, porosity and voids, as discussed in Sections 2.3.3.1.2, 2.3.3.1.3 and 2.3.3.1.4, respectively.

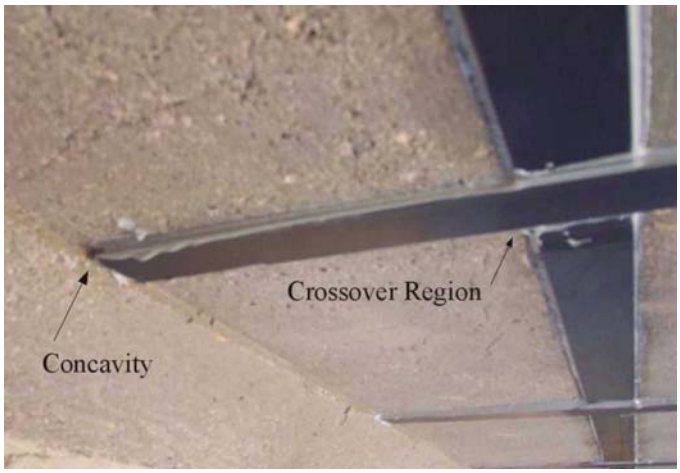

Figure 2.37: Bondline concavity in critical applications

2.3.4 Service

Most in-service defects found in rehabilitated structures may be considered to have long-term effects only, assuming that no significant defects have been induced during the installation process. Service induced damage can be divided into phases:

- Damage initially caused during service
- Growth of existing defects

The latter includes the propagation of existing flaws at the concrete/composite interface or inside the composite. Service loading, fatigue or environmental effects, such as moisture or heat, can cause growth of defects. Damage initially caused during service includes moisture diffusion, both from outside as well as inside the concrete, and impact of objects. Although impact will be rarely encountered in civil structures, occurrences such as hail storms or road debris can induce subsurface delaminations that are often barely visible on the surface. Instead, damage increases with depth and can therefore cause substantial damage to the concrete/composite interface.

2.3.4.1 At the concrete/composite interface

2.3.4.1.1 Penetration of moisture and chemicals

Penetration of moisture and chemicals over time can degrade the interfacial properties by plasticization or other forms of reversible and irreversible changes of the resin/adhesive. This change in material properties results in reduced stiffness of the resin and increases the likeliness of delamination. In general, bonded joints are especially susceptible to damage from aggressive chemicals and moisture.

2.3.4.1.2 Heat damage

The glass transition temperature T_g of each individual resin system, depending on resin type and cure conditions, predetermines maximum service temperatures at which the resin will start to severely degrade. Exposure to high temperatures influences the mechanical properties of most adhesives/resin systems. Under elevated temperatures, polymers may soften and lose their ability to transfer stresses efficiently (Figure 2.38). Under extreme conditions such as exposure to fire, the material completely degrades.

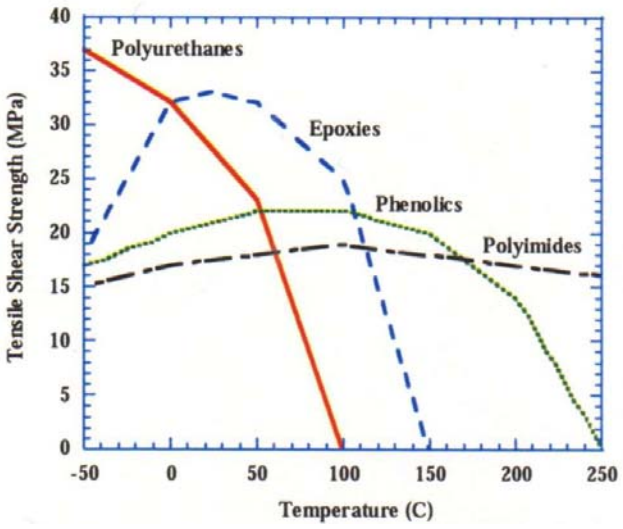

Figure 2.38: Typical working temperature ranges for structural adhesives

2.3.4.2 Inside the composite material

2.3.4.2.1 Penetration of moisture and chemicals

Moisture can be absorbed from the air or can diffuse through the concrete to the concrete/composite interface and ultimately even into the composite itself. These phenomena are promoted by either inadequate or damaged surface coatings (Figure 2.39), which are designed to protect the material from any form of diffusion or a high degree of concrete moisture. To allow evaporation of entrapped moisture inside the concrete, placement of composite sheets over large areas without space for evaporation and/or drainage must be prevented. Instead, gaps providing adequate space for "breathing" must be included at specific intervals. Those regions already containing delaminations, voids or other forms of air entrainment attract moisture and serve as a depository. Figure 2.40 shows moisture accumulation at interlaminar and concrete/composite interface regions.

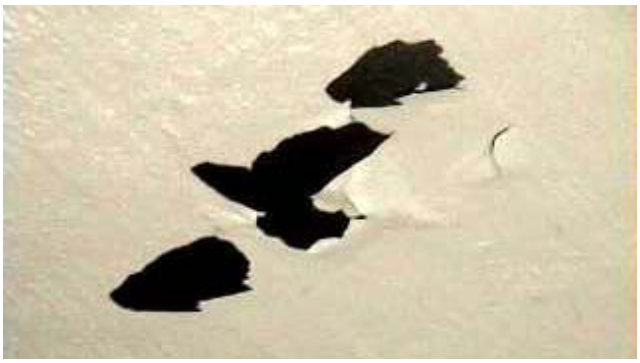

Figure 2.39: Damaged surface coating

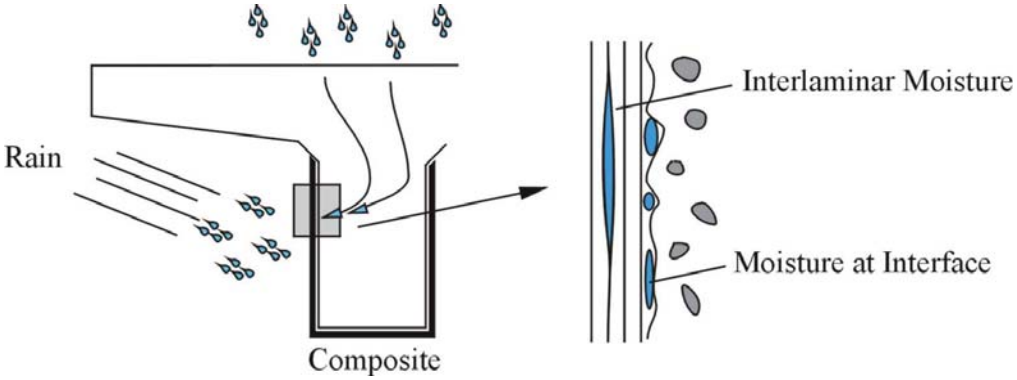

Figure 2.40: Penetration of moisture

2.3.4.2.2 Heat Damage

Unlike the adhesive/resin system, fibers are capable of resisting extremely high temperatures. Nevertheless, degradation of the matrix has a significant effect on mechanical properties since it does not allow for stress transfer between fibers.

2.3.4.2.3 Interlaminar matrix cracking

Most matrix cracking occurs in form of interlaminar cracks (delamination), as opposed to translaminar (perpendicular to the layer direction) or transfibrous (perpendicular to the fiber direction) [12]. Initiating factors can be entrapped air and excess resin, causing sudden changes in direction of load transfer and local stress concentration. Since the transverse tensile strength of a typical composite is much lower than its longitudinal (or fiber direction) tensile strength, such cracks may easily propagate under sustained loading. An example of interlaminar cracking is presented in Figure 2.41.

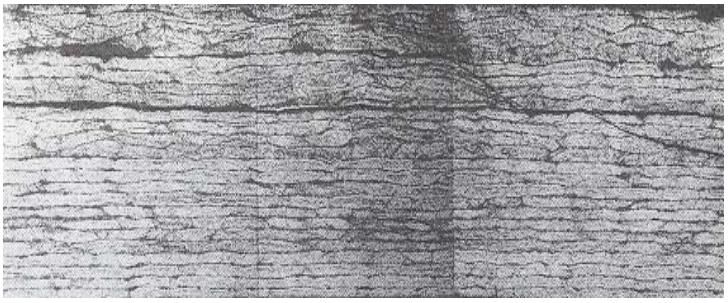

Figure 2.41: Microscopic view of interlaminar cracking

2.3.4.2.4 Surface scratches

Unless they propagate deep into the fibers, scratches can be considered a benign flaw that has a negligible influence on strength and stiffness. However, if scratches are caused by impact of an object, internal damage in forms of subsurface delamination can result. Figure 2.42 displays a severe form of surface damage as found on a bridge after rehabilitation through the application of composites in Sweden.

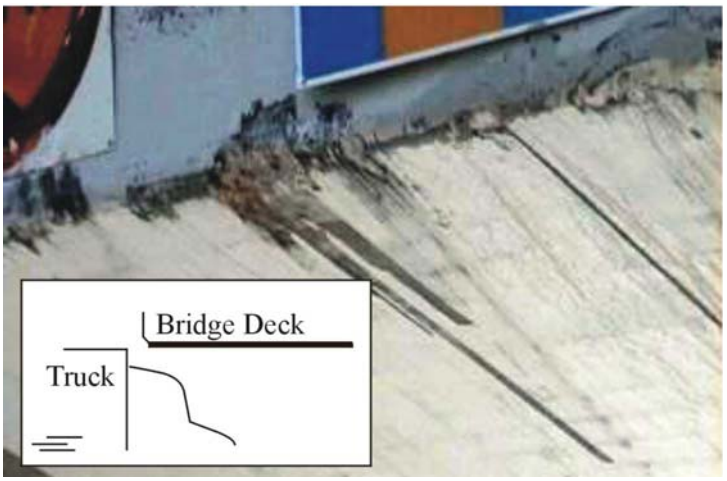

Figure 2.42: Severe form of surface scratching caused by trucks

2.3.4.2.5 Impact damage

Barely visible impact damage (BVID) is considered one of the most critical material flaws that may occur during service of a composite member [14]. If a hard, slow moving object impacts the surface of a composite laminate it may cause only slight damage to the surface, while severe subsurface matrix cracking is likely to occur (Figure 2.43). Road debris or environmental effects (hail, etc.)

are some of the factors that can cause impact damage. It has been shown that little loss of strength is evident if the composite is stressed in tension, whereas extensive local buckling and rapid failure can occur under compressive loading [13].

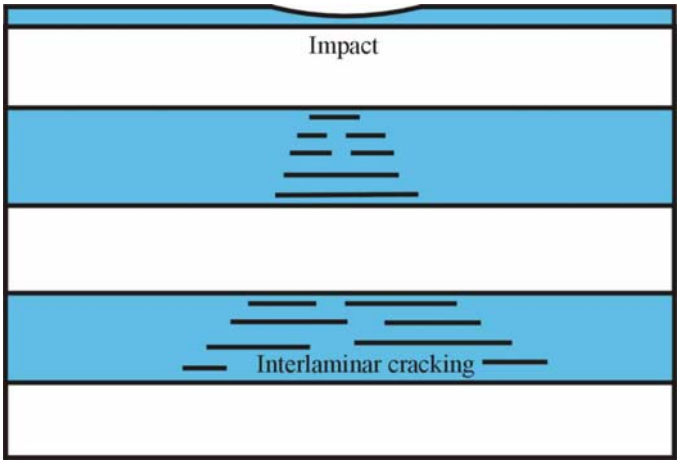

Figure 2.43: Subsurface damage due to impact

2.3.4.3 Other service defects

Other service defects include matrix brittleness due to ultraviolet radiation, exposure to freeze/thaw cycles as well as growth of any existing defect due to service loading or environmental effects. Detailed information on various types of in-service defects in composite materials is presented in the CERF/MDA document [19]. Unprotected composite surfaces lacking adequate protective covers (paint, epoxy coating) are especially susceptible to ultraviolet radiation that causes a steady increase in polymer chain linking. This results in a more brittle matrix behavior and unfavorable mechanical properties.

Growth of existing defects is one of the critical aspects in servicing of rehabilitated structures, since it demands continuous monitoring of composite and concrete/composite interface quality. While many defects may remain constant in size and to some respect, criticality, others may grow quite rapidly under service loading or environmental influences to form flaws that call for immediate repair measures.

2.4 SUMMARY

For concrete rehabilitation, application of fiber reinforced polymer composites continues to grow in popularity. However, the performance and expected lifetime of such rehabilitation measures greatly depend on quality of workmanship and are jeopardized by a wide range of material defects. Prior to installation, potential defects must be known and evaluated upon their likeliness

of occurrence during the individual project. Special attention should be paid to storage, handling and preparation of incoming materials as well as site preparation.

Apart from a well-coordinated installation process, a suitable environment for work with composite materials must be provided. Although a successfully performed installation procedure with low defect occurrence would yield a fairly long service life, harsh environmental conditions can cause rapid deterioration of most composite strengthening systems. Hence, quality monitoring must be performed beyond the installation stage and continued throughout the lifetime of a rehabilitated structure. Tables 2.3 through 2.6 summarize all previously discussed defects by their initiating phase and their potential effects.

While the types of defects to be encountered are mostly known, information on defect criticality and their effect on short/long-term structural performance remain widely unknown. Nevertheless, previous research has shown that defects like localized porosity, surface scratches or single broken fibers do not have a significant effect on material performance. Instead, they should be considered a material property that must be accounted for, especially if processing of composites is performed manually. Assessment of criticality of such "normal" defects will therefore be done on the basis of previous research results, whereas different techniques must be employed to characterize and quantify the effect of defects such as severe debonding, delamination, large voids, tow breakage or moisture accumulation, to name only a few. Thus, the need for further investigation in this field arises.

Chapter 3 will address defect criticality of defects discussed in the previous chapters, categorizing them by criticality with respect to structural performance (strength and stiffness) and short/long-term durability. A comprehensive understanding of defect type, typical appearance and, most importantly, criticality and repair schemes is essential to the installer/inspector and will aid in maintaining rehabilitated structures at their full potential throughout the design-lifetime.

Table 2.3: Defects in raw and constituent materials

	Defect Type	Cause/Description	Potential Effect
Resin	Overaged resin	Expired shelf-life	Low strength and modulus. Potential for incomplete cure & nonuniform impregnation
	Resin inclusions	Dirt and/or chemicals	Change in chemical consistency, voids. Potential effect on cure
	Resin moisture	Inadequate storage/environmental exposure	Change in chemical consistency, voids due to evaporation, resin degradation
Fabric	Incorrect fiber/fabric type	Fiber/resin mismatch, human error	Change in strength and modulus, low fiber/matrix bond (sizing)
	Kinked or wavy fibers	Handling/manufacturing flaw	Fiber breakage, loss in composite properties
	Broken fiber tows	Handling/manufacturing flaw	Stress concentrations
	Fabric contaminations	Environmental exposure/storage	Initiator for debonding and crack propagation
	Fabric wrinkles	Handling/manufacturing flaw	Lower modulus, higher strain at failure, resin-rich encapsulated areas
	Sheared fabric	Handling/manufacturing flaw	Off-axis alignment, lower strength and modulus, resin-rich regions
	Damage to free edges	Handling/manufacturing flaw	Loss of integrity, stress concentrations
	Pull-out of fiber tows	Handling/manufacturing flaw	Resin richness, localized low strength & stiffness
	Fiber gaps	Handling/manufacturing flaw	Resin richness, low crack arresting capability
	Fabric moisture	Inadequate storage/environmental exposure	Reduced fiber/matrix bond, effect on composite performance and durability

Table 2.4: Defects from site and material preparation

	Defect Type	Cause/Description	Potential Effect
Resin System	Moisture absorption	Inadequate storage/environmental exposure	Change in chemical consistency, voids due to evaporation. Potential for incomplete cure & decreased performance levels
	Incorrect stoichiometry	Type or proportions of resin and hardener/catalyst	Inadequate matrix strength/modulus, incomplete and/or nonuniform cure
	Incorrect mixing	Low degree mixing, drawing of air	Partial cure, porosity, nonuniform rheology
Substrate	Inadequate primer coating	Over-, undersaturation of substrate	Low stress transfer capability, potential for poor bond
	Lamination on top of 'marked-out' regions	Placement on duct tape, crayon layer, etc.	Weak or no bond to substrate
	Degraded substrate	Microcracks, spalled concrete	Lower or no composite action
	Inclusions at imperfections	Dirt, moisture or chemicals in concrete cavities	Low bond of primer/putty to substrate
	Galvanic corrosion	Intimate contact of carbon fibers with steel reinforcement	Deterioration of matrix/steel

Table 2.5: Installation defects

		Defect Type	Cause/Description	Potential Effect
Wet Layup	Composite-Concrete Interphase	Concrete cavities	In current practice, concrete cavities are not filled with putty	Stress concentrations
		Sagging of infiltrated fabric	Critical in overhead regions	No composite action, potential moisture entrapment at concrete/composite interface
		Resin-rich/poor concrete/composite interface	Non-uniform primer coating and over-, undersaturation during lay-up	Low stress transfer efficiency
		Porosity and Voids	Porous primer, entrapment of air pockets during lay-up	Low stress transfer, stress concentrations, debond & crack initiation sites
		Highly uneven concrete surface	High degree of sandblasting	Voids or air pockets
	Inside Composite	Porosity and Voids	Air entrainment in resin, entrapment of air pockets during lay-up	Low stress transfer, stress concentrations, decreased performance attributes
		Delamination	Moisture, Inclusions	Low or no stress transfer
		Debonding	Fiber contamination, tubular voids	Low stress transfer (localized), sites for wicking of moisture
		Incorrect stacking sequence	Misplaced fabric, human error	Alteration of strength and stiffness
		Resin-richness/poorness	Non-uniform infiltration	Low crack arresting capability, decreased stress transfer capabilities, locally weak zones
		Indentations	Handling damage	Damaged fibers, stress concentrations
		Missing layers	Human error	Entirely different (and decreased) laminate properties
		Damaged edges	Fiber pull-out during infiltration	Stress concentrations, site for crack initiation
Prefabricated Material		Voids at concrete/adhesive interface	Adhesive applied to highly porous concrete substrate	Stress concentrations, moisture accumulation, local zones of weakness
		Disbonding at adhesive/composite interface	Smooth surface of prefabricated strip	Low stress transfer/inadequate bond strength

Table 2.6: In-service defects

	Defect Type	Cause/Description	Potential Effect
Concrete/ Composite Interface	Penetration of moisture and chemicals	Exposure to aggressive environments	Degradation of adherent layer, plasticization, reduced stiffness, potential for premature failure through peel and/or delamination
	Heat damage	Exposure to sun or fire damage	Softening/degradation of matrix, peel and/or separation from substrate
Composite	Penetration of moisture and chemicals	Exposure to aggressive environments	Plasticization, reduced stiffness, degradation of composite
	Heat damage	Exposure to sun or fire damage	Softening/degradation of matrix
	Matrix Cracking	Interlaminar crack formation	Initiator for delamination and/or splitting
	Surface Scratches	Traffic, hail, etc.	Fiber breakage and initiator for premature local failure
	Impact damage	Traffic, hail, etc.	Delamination

2.5 CHAPTER 2 GLOSSARY[1]

Adherent	A body that is held to another body usually by an adhesive.
Adhesive	Substance capable of holding two materials together by surface attachment. an be a film, paste or liquid.
Bond Strength	The amount of adhesion between two surfaces.
Catalyst	A substance that changes the rate of chemical reaction without itself undergoing permanent change in composition.
Debond[†]	An initially unbonded or nonadhered region between two adherents. Also used to describe a separation at the fiber-matrix interface. In the construction industry, debond and delamination are sometimes used interchangeably when referring to separations at the concrete-composite interface.
Degradation	Deleterious change in physical properties or appearance.
Delamination	Separation of the layers of material in a laminate, either local or covering a wide area.
Disbond	An area within an initially bonded interface between two adherents in which adhesion failure or separation has occurred.
DMTA	Dynamic mechanical thermal analysis. Provides information on presence of solvents, changes in structure and chemical reactions.
DSC	Differential scanning calorimetry. Detects loss of solvents and other volatiles.
Galvanic Corrosion[†]	Galvanic reaction between metals and conductive carbon fibers, resulting in degradation of matrix and metal.
Hydrolysis[†]	Process of degradation that generically includes the splitting of chemical bonds and the addition of water.
Inclusion	Mechanical discontinuity occurring within a material, consisting of a solid, encapsulated material.
Interface	Boundary between two different, physically distinguishable media.
Laminate[†]	A product made by stacking of multiple layers of unidirectional fibers or oriented fiber configurations embedded in a resin matrix.
Porosity[†]	Trapped pockets of air, gas or vacuum within a solid material, typically less than 10μm in diameter.

[1] Based on terminology of ASM Handbook of Composites, Part 1 [20]
[†] Terminology of authors

Pot Life	Time a thermosetting resin retains a viscosity low enough to be used in processing.
Prefabricated Material[††]	Composite material manufactured and cured under controlled factory conditions with a generally high material uniformity and used in cured state in the field.
Prepreg	Ready-to-mold material in sheet form impregnated with resin and stored for use. The resin is partially cured to a B-stage.
Rheology	The study of flow of materials, particularly plastic flow of solids.
Saponification[†]	Specific form of hydrolysis involving alkalis.
Shelf Life	Length of time a material can be stored under specific environmental conditions and continue to meet all applicable specification requirements.
Stoichiometry[†]	Quantitative relationship between constituents in a chemical system.
T_g	Temperature at which increased molecular mobility results in significant changes in the properties of a cured resin system.
Undercure	A condition resulting from the allowance of too little time and/or temperature for adequate hardening.
Vitrification[†]	Process of conversion into a glassy phase.
Voids	Air or gas that has been cured into a laminate or an interface between two adherents. Porosity is an aggregation of microvoids.
Volatiles	Materials, such as water or alcohol, in a resin formulation that are capable of being driven off as vapor at room temperature or at a slightly elevated temperature.

[†] Terminology of authors

2.6 CHAPTER 2 REFERENCES

1. Astrom, B. T., Manufacturing of Polymer Composites, Chapman & Hall, London, 1997.

2. Gutowski, Timothy G., "A Brief Introduction to Composite Materials and Manufacturing Techniques," In Advanced Composites Manufacturing, ed. Timothy G. Gutowski, New York: Wiley, 1997: 5-41.

3. Ali, M. S. M., Oehlers, D. J. and M. A. Bradford, "Shear Peeling of Steel Plates Adhesively Bonded to the Sides of Reinforced Concrete Beams," Proceedings of the Institution of Civil Engineers - Structures and Buildings, V140 (3), 2000: 249-259.

4. Zhang, S., Raoof, M. and L. A. Wood, "Prediction of Peeling Failure of Reinforced Concrete Beams with Externally Bonded Steel Plates," Proceedings of the Institution of Civil Engineers - Structures and Buildings, V110 (3), 1995: 257-268.

5. Triantafillou, Thanasis C., and Costas P. Antonopoulos, "Design of Concrete Flexural Members Strengthened in Shear with FRP," Journal of Composites for Construction, V4 (4), 2000: 198-205.

6. Geng, Z. J., Chajes, M. J., Chou, T. W. and D. Y. C. Pan, "The Retrofitting of Reinforced Concrete Column-to-Beam Connections," Composites Science and Technology, V58 (8), 1998: 1297-1305.

7. Kaliakin, V. N, Chajes, M. J. and T. F. Januszka, "Analysis of Concrete Beams Reinforced with Externally Bonded Woven Composite Fabrics," Composites Part B - Engineering, V27 (3-4), 1996: 235-244.

8. Hawkins, G. F., Johnson, E. and James Nokes, "Typical Manufacturing Flaws in FRP Retrofit Applications," Concrete Repair Bulletin, July/August 1998: 14-17.

9. Bishop, Sarah M., "The Significance of Defects on the Failure of Fibre Composites," Neuilly-sur-Seine, France: North Atlantic Treaty Organization, Advisory Group for Aerospace Research and Development, 1981, iv, 18p.: ill. 30cm.

10. Davies, P. and O. Brunelliere, "Effect of Defects on Interlaminar Fracture of Glass Fibre-Reinforced Polyester Composites," Journal of Material Science Letters, V12 (6), 1993: 427-429.

11. Parslow, Nigel, "An Empirical Appraisal of Defects in Composites, " in Characterization, Analysis and Significance of Defects in Composite Materials, AGARD Conference Proceedings, no. 355, 1993.

12. Purslow, D., "Fractographic Analysis of Failures in CFRP," in Characterization, Analysis and Significance of Defects in Composite Materials, AGARD Conference Proceedings, no 355, 1983.

13. Cawley, P. and R. D Adams, “Defect Types and Non-Destructive Testing Techniques for Composites and Bonded Joints,” Materials Science and Technology, V5, May 1989: 413-425.

14. Potter, R. T., “The Significance of Defects and Damage in Composite Structures,” in Characterization, Analysis and Significance of Defects in Composite Materials, AGARD conference Proceedings, no 355, 1983.

15. Farioli, M., Porro, F., Samanni, G. and V. Wagner, “Advanced Techniques for Composite Primary Structures,” in Characterization, Analysis and Significance of Defects in Composite Materials, AGARD conference Proceedings, no 355, 1983.

16. Ghiorse, S. R., “Effect of Void Content on the Mechanical Properties of Carbon/Epoxy Laminates,” SAMPE Quarterly, January 1993: 54-59.

17. Woo, E. M., Chen, J. S. and C.S. Carter, “Mechanism of Degradation of Polymer Composites by Galvanic Reactions Between Metals and Carbon Fiber,” Polymer Composites, V14 (5), 1993: 395-401.

18. Chajes, M.J., Finch, W.W., Januszka, T.F., Thomson, T.A., “Bond and Force Transfer of Composite Material Plates Bonded to Concrete,” ACI Structural Journal, V93 (2), 1996: 208-217.

19. Karbhari, V.M., Chin J.W. and D. Reynaud, “Gap Analysis for Durability of Composites for use in Civil Infrastructure”. CERF Report, 2001.

20. ASM Society of Materials, ASM Handbook of Composites, Part 1, Materials Park, OH, ASM International, 2000.

3.0 ASSESSMENT OF DEFECT CRITICALITY

3.1 INTRODUCTION

To assess the overall effect of defects on integrity and performance of external rehabilitation using CFRP composites, levels of relative criticality must be assigned to each defect previously described in Chapter 2. Such levels will provide a basis for field engineers to decide whether a specific defect must be viewed critical to the overall performance or rather be classified as an aesthetic imperfection. The basis for such classification can be made through a combination of

- review of past research
- analytical evaluation
- experimental testing

Since the study of the effect of defects in FRP rehabilitated concrete structures is fairly new, there is limited information from previous studies that can be utilized for the present investigation. However, a substantial body of knowledge exists regarding the effect of defects in FRP composites per se, on the basis of which preliminary classification and assessment can be conducted. Further validation can then be derived from selected experiments performed for the express purpose of estimation of defect criticality.

Possibly one of the most influential factors in studying the effect of defects through experimental testing is the modeling of defects. As such, successful and representative modeling demands knowledge of actual defect occurrences, typical installation, and service conditions that may promote initiation of defects, as well as their typical location, and geometry. The latter aspect becomes especially critical for non-geometric defects, such as exposure to heat or moisture. While defects such as broken fiber tows or fiber pullout represent simple geometric alterations, moisture accumulation and heat damage are more difficult to quantify. Further, if defects can exist in several different configurations, i.e. various sizes or shapes, it is desirable to define a single configuration being most representative of all others.

For the purposes of the current investigation defect criticality will be assessed based on five classifications:

1. Aesthetic – these defects are not likely to significantly affect structural response but would result in an unaesthetic appearance. Roughness and unevenness of resin on the surface, or excess adhesive that has been pressed out from between a prefabricated strip and the substrate concrete are examples of this type.

2. QA/QC critical – these defects are generally due to extremely poor QA/QC. These should not occur under normal circumstances unless the crew is absolutely inexperienced. Use of overaged resin (i.e. past shelf life) is an example of this type.

3. Structural performance/integrity – these defects directly affect structural performance and integrity and are likely to cause substantial reduction in performance as compared to the intended levels, even without exposure/load. Lack of bond in large areas is an example of this type

4. Short-term durability – these defects are likely to become critical after short periods of time due to effects of environmental/load exposure. Large voids at the bond-line exposed to substantial water ingress, which could cause premature failure through delamination are examples of this.

5. Long-term durability – these defects are likely to become critical only after prolonged (5+ years) of exposure to environment/load. A high density of very small voids on the bond line or between layers of fabric is an example of this type.

In this chapter a preliminary assessment of defects is provided based on available knowledge on a relative basis. Appendices 1 and 2 cover the use of a fracture mechanics based approach to determine actual effects in terms of fracture energy release rate and thereby provide quantitative assessment of criticality. It is noted that this quantification of defects is still largely unknown and current efforts are being directed towards a comprehensive evaluation.

3.2 ASSESSMENT OF POTENTIALLY CRITICAL DEFECTS

3.2.1 Introduction

Defects in CFRP-rehabilitated concrete components can originate from a number of sources, as discussed in Chapter 2. As the majority of these sources are known, their approximate size, shape, location and likeliness of occurrence can be assessed, particularly for defects that have previously been identified during field inspections. Given the information provided in Chapter 2 as well as information from relevant literature and from tests (Appendices 1 and 2 of this report), subsequent sections will evaluate whether a specific defect should be considered potentially critical.

3.2.2 Establishing defect categories

As mentioned previously, due to the large number of possible defects in CFRP overlays, categorization of defects appears highly desirable. Examples of such categorization include defects related to geometric distortion of dry fabric, stoichiometric alteration or certain bondline defects. For instance, defects like damage of transverse stitching or presence of fiber gaps can be considered similar, as one promotes the other. Herein, loss of transverse stitching allows adjacent fiber tows to move away from each other, resulting in a gap between the two tows.

3.2.3 Criteria for defect selection

In the following, each defect listed in Chapter 2 will be discussed in view of its relevance for further evaluation.

3.2.3.1 Raw and constituent materials

3.2.3.1.1 Overaged resin

The detrimental effects of overaged resins, its hardeners or catalysts becomes apparent in form of a lower reactivity, lower strength as well as lower modulus. Though critical, current in-situ installation procedures used by most contractors specifically address this issue and restrict use of resin systems that have been stored past their design shelf life. Classification: QA/QC critical

3.2.3.1.2 Resin inclusions

Physical contamination of resins through foreign particles require their introduction during mixing, as no other stage of resin storage or installation allows for this defect. However, due to the relatively short mixing duration and immediately following installation of the material, introduction of foreign particles remains a rare incident. Further, inclusion of fine dust or dirt particles of low material strength may be assumed similar and less critical than that or resin porosity or finely distributed voids, regardless of location within the concrete/composite system. Classification: QA/QC critical

3.2.3.1.3 Resin moisture

Although the effects of moisture absorption on mechanical properties of resin systems are widely known, moisture absorption remains one of the most critical aspects in use of FRP materials, especially when encountered in novel applications. Hence, moisture absorption, mainly caused due to improper storage of sealed containers, will be considered a potentially critical defect. Classification: Performance (at high levels) and Short-Term Critical

3.2.3.1.4 Incorrect fabric type

As mentioned previously, adequate material properties as well as material selection are ensured by use of in-situ installation procedures that are followed during preparation and application of the strengthening system. As it is advisable to limit the variety of materials used in the field, mainly due to simplified installation procedures and lower installation time, most contractors utilize only one specific type of fabric at a site. Incorrect selection of fabric can result in substantially lower performance (if fabric is of lower basis weight or of incorrect fiber orientation) or improper wet-out (if it is heavier). Classification: Performance critical

3.2.3.1.5 Kinked or wavy fibers

Given the fabric's structure there is possibility for the fibers to be placed in a wavy or kinked configuration. Based on composite mechanics this will result in changes in properties. Classification: Performance critical

3.2.3.1.6 Broken fiber tows

While broken fibers have previously been classified a microscopic defect, breaking of an entire tow can be expected to severely affect material properties, particularly tensile strength and modulus along the fiber direction. Areas of damage can also result in resin rich zones or voids leading to longer term effects. Classification: Performance and long-term durability critical

3.2.3.1.7 Fabric contamination

Similar to the physical contamination of resin constituents during or prior to mixing, fabric contamination must be rated as a rather unlikely defect. This is mostly based on the cutting and handling of fabric prior to installation. Prior to use, fabric is stored on a roll with only limited exposure to the environment. During the infiltration process, the material is transported through a feeding mechanism into a resin bath while automatically measuring the amount of material removed from the roll, or is infiltrated by hand using rollers and manual implements. Subsequently, the wet fabric is spooled directly onto a second roll from which it may be unrolled and placed in the desired locations along the structure. Hence, presupposing storage conditions that are mostly free of dust or other physical contamination, foreign particles are given minimal opportunity to settle onto the fabric surface. Classification: QA/QC critical

3.2.3.1.8 Fabric wrinkles

See fabric waviness. Classification: Performance critical

3.2.3.1.9 Sheared fabric

Shearing of fabric can result in fiber misorientation and in resin rich areas or voids. Classification: Performance and long-term durability critical

3.2.3.1.10 Damage to free edges

Damage of the free edge of the fabric is often encountered during field installation. The likely result of damaged or missing transverse stitching is separation of individual tows in combination with a flattening effect, as fibers are not restricted in their movement. This may lead to resin-rich areas and local waviness. While the transverse stitching does not affect tensile properties of the reinforcing material, above mentioned resin-rich regions are likely to affect bond strength as well as interlaminar properties of the laminate. Thus, damage to free edges will be evaluated based on extent of the damage, i.e., the propagation depth into the material. Classification: Aesthetic, performance and long-term durability critical

3.2.3.1.11 Pullout of fibers

Typically, fiber pullout tends to occur mostly in fabrics of short lengths and low integrity, such as satin weave, as well as along a cutting edge. This causes a loss in performance and resin rich areas and/or voids. Classification: Aesthetic, performance and long-term durability critical

3.2.3.1.12 Fiber gaps

Similar to pullout, free-edges and shearing. Classification: Aesthetic, performance and long-term durability critical

3.2.3.1.13 Fabric moisture

Similar to resins, fibers may accumulate surface moisture if stored under inadequate conditions for extended periods of time. Hence, overnight storage is typically performed under stable conditions, such as moisture-controlled environments. Generally, accumulated surface moisture will lower bond strength and present risk of large delamination, requiring moist fabric to be discarded. It can also cause blistering resulting in a rough surface. Classification: Aesthetic, performance and short-term durability critical

3.2.3.2 Site and material preparation

3.2.3.2.1 Substrate moisture

As discussed earlier, previous studies have shown the detrimental effect of insufficient surface preparation on bond strength between concrete and CFRP overlays. As such, failure to remove the weak cement paste that covers the stronger aggregate particles has shown to cause a significant reduction in fracture energy, i.e. lower bond strength. It can thus be assumed that a film of moisture, formed by condensation in unstable environments, would result in a similar effect. This is further supported by the fact that most installation is initiated early in the day, mainly to extend the pot-life of most resin systems. However, moisture, which may have accumulated during these early hours, cannot dry off sufficiently prior to application of the composite overlay. As a result, a film of moisture becomes entrapped between the concrete and composite material, providing a potential risk for disbonds. Classification: Performance and short-term durability critical

3.2.3.2.2 Incorrect Stoichiometry

Stoichiometric inconsistencies can originate from several sources, such as incompatibility of the resin and hardener system or deviation from the prescribed resin/hardener ratio. Since epoxy resin systems are commonly provided as a two-part system, incompatibility can largely be avoided. Moreover, most contractors utilize only a single system to simplify installation and reduce complexity of the overall rehabilitation procedure.

In contrast, inconsistency in the prescribed resin/hardener ratio can occur due to measuring incorrect quantities of either part of the two-part resin system. As the measuring process is purely manual, it remains susceptible to human error.

The use of excessive amounts of hardener is known to cause premature gelation, which may result in a variety of defects, including resin-rich areas, voids, porosity or fiber misalignment. Classification: QA/QC, Performance and short-term durability critical

3.2.3.2.3 Incorrect mixing

Prior to installation, the two-component resin system should be mixed for a required minimum time, using an electric drill that is equipped with an adequate mixing head. As part of an installation checklist, this procedure is typically followed closely. Furthermore, incorrect mixing can be easily noticed by the non-uniform consistency of the mix, as the bulk resin and hardener show two distinctly different viscosities. A mix of uniform consistency is only obtained after substantial blending. Classification: QA/QC critical

3.2.3.2.4 Inadequate primer

The role of the primer is to provide a "bondable" surface and further quench the absorption so that none of the saturating resin is drawn from the wet composite into the concrete substrate. To ensure an intimate bond, thickness of the primer should be kept as thin as possible, since excessive amounts of primer can result in low stress transfer capabilities as well as dripping, i.e. formation of excessively resin-rich areas. Classification: Structural and short-term durability critical

3.2.3.2.5 Prolonged primer cure

To ensure perfect bond between the concrete substrate and composite material, regardless of system, the primed surface must be partially cured to show good tackiness, i.e. possess properties similar to that of an adhesive. Good initial adhesion between the primer and composite material ensures adequate bond and further reduces the risk of subsequent separation of the two components, often experienced in the form of sagging. However, primer must not cure completely, as this will cause a glossy, non-adhering surface to form. While application of the composite onto a freshly primed surface with no tackiness will promote formation of a disbond, lamination onto a fully cured primer coat must be regarded as a separate defect. Classification: Structural and short-term durability critical

3.2.3.2.6 Moisture on primer

Moisture on a primed surface is likely to form if the surface is exposed to an unstable environment without immediate placement of the composite overlay. As a result, a film of moisture becomes entrapped between the primer and composite material, providing a potential risk for disbonds. It should be noted that this defect is directly linked to prolonged primer cure, as the primer must be exposed

to the environment for a substantial time before moisture accumulation may occur. Classification: Structural and short-term durability critical

3.2.3.2.7 Lamination on marked-out regions

To aid in the correct placement of the wet or prefabricated material onto the structural component, the rehabilitation scheme is marked on the structure in form of a thin chalk line. These chalk lines are utilized to depict an outline of the subsequently placed composite strips. At few locations, chalk lines may intercept and thus become entrapped during application of the reinforcing material. However, the amount of material used for this procedure is extremely limited and may hence be assumed less significant than other anomalies, such as surface irregularities or abrasion material that remains on the concrete surface. Classification: Important but not critical

3.2.3.2.8 Degraded substrate

Substrate degradation is mostly apparent in form of wide cracks or cavities where concrete has spalled off. Typically, surface cracks and small cavities are filled using appropriate materials, such as the BG-02 binder gel. In extreme cases, the cover material may have to be completely removed and replaced by adequate filler materials. In common practice, cavities larger than ¼ inch (~6 mm) are filled such that a generally strong substrate is provided. Classification: Structural and short-term durability critical

3.2.3.2.9 Inclusions at imperfections

Due to substantial cracking, many structures are capable of accumulating a substantial amount of moisture, dirt or other foreign material. Following a proper surface preparation procedure, which includes removal of the weak cement paste as well as cleaning and subsequent filling of large cracks or spalled areas, the encapsulation of foreign material can be minimized. Classification: QA/QC and structural critical

3.2.3.2.10 Galvanic corrosion

As discussed, galvanic corrosion occurs when the composite strengthening system comes in direct contact with the steel reinforcement, presupposing the member has spalled or is otherwise heavily degraded. Intimate contact between the composite and internal reinforcement must be prevented. Classification: Long-term durability critical

3.2.3.3 Field installation

3.2.3.3.1 Concrete cavities

Although many large cavities are filled prior to application of the composite overlay, regions smaller than ¼ inch (~6 mm) may be left unfilled. Hence,

sufficient amounts of primer must be introduced to these regions to prevent formation of a void. Due to the fact that many applications entail rehabilitation of overhead regions, such as slabs, girders, and bridge decks, many cavities may be assumed to remain unfilled.

Given the uncertain distribution of cavities throughout the concrete surface, severity of this defect is expressed in percentage of total rehabilitated area. Classification: QA/QC critical

3.2.3.3.2 Sagging of fabric

Until the resin has developed adequate tackiness, i.e. turns into a gel, the infiltrated material tends to separate from the concrete, especially in vertical and overhead regions. If the material sags, there is no bond; thus the defect experienced can be considered the most severe form of debonding. Classification: Structural and short-term durability critical

3.2.3.3.3 Resin-rich/resin-poor bondline

Non-uniform bondline thickness is generally the result of either insufficient or excessive amounts of resin and/or primer material. While several causes for this defect exist, the geometric anomaly remains identical for all causes, namely an excessively thick or thin layer between concrete and composite material. Classification: Structural and long-term durability critical

3.2.3.3.4 Voids/disbonds at bondline

Voids are typically caused by air entrapment during the layup process. Factors contributing to void formation include entrapped air from mixing, insufficient amounts of resin or inclusion of foreign material. As a disbond results in zero stress transfer, this defect must be considered extremely critical. Classification: Structural and long-term durability critical

3.2.3.3.5 Porosity at bondline

While porosity can be considered a normal material occurrence, it can serve as a depository for diffused moisture and, in certain areas, cause formation of a large void from a number of microvoids. Classification: Structural and short-term durability critical

3.2.3.3.6 Uneven concrete substrate

Surface irregularities, such as protruding aggregate or cement paste and shallow or deep cavities generally promote formation of air pockets and resin-rich areas. Its effect ranges from formation of resin-rich areas to debonding. Classification: QA/QC, structural and long-term durability critical

3.2.3.3.7 Voids/delamination in composite

Due to their detrimental effect on interlaminar shear strength, a mechanism that is essential in bond applications, these are critical. Criticality of durability depends on size. Classification: Structural and durability critical

3.2.3.3.8 Porosity in composite

Porosity at interlaminar regions results in formation of voids and moisture ingress. Classification: Structural and short-term durability critical

3.2.3.3.9 Debonding in composite

Unlike delamination, debonding occurs in localized areas, promoted by moisture accumulation as well as chemical and/or physical contamination on the fiber surface. Good storage and infiltration procedures used in structural rehabilitation can largely prevent introduction of moisture or foreign particles to the reinforcing material. In situations where debonding occurs, it will eventually result in formation of a larger debond, i.e. formation of a void/delamination. Classification: QA/QC, structural and short-term durability critical

3.2.3.3.10 Incorrect stacking sequence

As all aspects of a structural renewal measure are susceptible to human error, particularly in more complex applications, layup of the reinforcing material may be performed using an incorrect stacking sequence, resulting in severe alteration of the design properties. However, due to the unidirectionality of the reinforcing material, layup directions are trivial and normally should not be confused. Classification: QA/QC, structural critical

3.2.3.3.11 Resin richness/resin poorness in laminate

Similar to non-uniformity at the bondline, resin rich/poor regions inside the laminate originate from use of excessive/insufficient amounts of infiltrating resin, respectively. Although the material is fed through an infiltration mechanism that ensures a constant and uniform wet-out of the fabric, non-uniform rolling and/or dripping of resin during layup may result in resin-rich and resin-starved areas. Classification: QA/QC, structural critical

3.2.3.3.12 Indentations

Indentation of fabric or prefabricated strips mostly occurs due to careless handling during installation as well as impact while the structure is in service. Due to the presumably higher severity of impact damage, indentations of constituent materials will not be evaluated as an individual parameter. Severity depends on location and extent. Classification: Aesthetic and structural critical

3.2.3.3.13 Missing layers

In current rehabilitation using CFRP composites, a maximum of two to three layers are utilized to address the performance deficiency of most structural components. Hence, the omission of even a single layer of reinforcing material would represent a severe deficiency in performance. Consequently, installation checklists are used to monitor the type, quantity and location of the reinforcing material. Classification: QA/QC, structural critical

3.2.3.3.14 Damaged edges

Similar to most other handling damage, damage to edges can result from improper infiltration, rough handling of the wet material or improper use of rollers or other application tools. Ultimately, integrity of the infiltrated material may be lost, resulting in excessive mobility of the fibers, especially during the rolling process. As a result, fiber gaps and resin-rich areas are likely to form. Classification: QA/QC, aesthetic and structural critical

3.2.3.3.15 Voids (at interface of concrete/prefabricated strip)

Similar to the wet layup system, voids in the bonder gel can be the result of air entrapment during the adhesion process. As a void results in zero stress transfer, this defect must be considered extremely critical. Prior to adhesion, prefabricated strips are fed through an applicator tool that is designed to deposit an adhesive film of uniform thickness onto the roughened surface. As the application process is manual, feeding rate as well as the amount of bonder gel available in the tool's depository are subject to fluctuation. Hence, voids tend to form within the film, eventually causing air entrapment. When compared to the wet layup system, the high rigidity of the cured composite strips complicates removal of entrapped air by means of subsequent rolling. Classification: QA/QC, structural and long-term durability critical

3.2.3.3.16 Disbond (at interface of concrete/prefabricated strip)

While disbonds in wet layup applications typically result from formation and growth of localized defects such as voids, accumulated moisture or inclusion of foreign particles, systems utilizing prefabricated material allow for an additional cause, namely using the incorrect mating surface of the strip. Upon delivery to the site, composite strips typically show two distinctly different surfaces, one shiny surface, unsuitable for adhesion, and one pre-sanded surface that provides good adhesion properties. Hence, bond strength may be expected to decrease significantly when the material is accidentally bonded to the incorrect side. Classification: QA/QC, structural critical

3.2.3.4 In-service defects

The following in-service defects are discussed for both the wet layup system as well as the installation procedure utilizing prefabricated strips.

3.2.3.4.1 Penetration of moisture and chemicals

Penetration of moisture and chemicals over time can degrade both the interfacial properties as well as the properties of the composite itself, mainly due to plasticization of the resin/adhesive. This change in material properties results in reduced stiffness of the resin and promotes both disbonds and delamination. In order to propagate to the concrete/composite interface, moisture must diffuse through the composite material or from inside the concrete. Hence, moisture inside the composite and at the interface is typically of simultaneous occurrence. Classification: Short- and Long-term durability critical

3.2.3.4.2 Heat damage

Due to the predetermined maximum service temperatures of individual resin systems, matrix degradation caused by high-temperature exposure represents an important aspect of long-term durability. Facilitated by the high temperature fluctuation experienced at many installation sites (rehabilitation work currently entails several applications in the Californian desert), certain resin systems can likely be exposed to temperatures near or beyond their specified glass transition temperature T_g . However, it should be noted that, since CFRP materials are mainly attached to the bottom or side surfaces of structural components and rarely on surfaces that are directly exposed to the sun, duration of extreme temperature exposure remains minimal, seldom exceeding a few hours. Classification: Long-term durability critical

3.2.3.4.3 Matrix cracking

Interlaminar matrix cracking may easily propagate under sustained loading, causing either a delamination or disbond, depending on the specific location. Classification: Long-term durability critical

3.2.3.4.4 Surface scratches

Unless they propagate deep into the fibers, surface scratches can be considered a benign flaw that has a negligible influence on strength and stiffness. Classification: Aesthetic critical

3.2.3.4.5 Impact damage

Barely visible damage is considered one of the most critical material flaws that may be encountered during service of a composite member. If a hard, slow moving object impacts the surface of a composite laminate it may cause only minor damage to the surface while severe subsurface damage can be expected. However, many of the natural or man-made phenomena causing impact to civil structures, including hail, road debris or truck antennae, must be considered high-velocity/low-mass impact situations. Hence, damage should be evaluated based on parameters resembling a low-mass object impacting the rehabilitated surface at moderate to high velocities. Classification: Aesthetic and Structural critical

3.2.4 Defect size and density considerations

Small entrapped voids or surface discontinuities no larger than 6.4 mm (¼ in) diameter are generally not considered to be serious defects, and require no corrective action, unless they occur next to edges or when there are more than 5 such defects in an area of 0.9 m^2 (10 ft^2). Small defects of size between 6.4 and 32 mm (¼ and 1¼ in) diameter should be repaired using low pressure epoxy injection, as long as the defect is local and does not extend through the complete thickness of the laminate in case of multi-ply FRP systems. If any delamination growth is suspected between the FRP plies due to injection, the procedure should be halted and repair undertaken through removal of the area and scarfing.

Minor defects, which include cracking, abrasion, blemishes, chips, and cuts, are those with diameter between 32 and 152 mm (1¼ and 6 in), and frequency of less than 5 per any unit surface area of 3 m (10 ft) length or width (It is noted that in most cases one dimension is set by constraints of design or of available material such as prefabricated strips. Surface area is required to be assessed in continuity). Repair is needed in these cases and the area surrounding the defects to an extent of at least 25 mm (1 in) on all sides should be carefully removed and then patched by adding an FRP patch of the same type of the original laminate and extending at least 25 mm (1 in) on all sides of the removed area.

Large defects (152 mm (6 in) diameter or greater) are generally indications of significant debonding between layers, lack of adhesion to the concrete substrate, or extended moisture entrapment causing resin degradation. They may include peeling and debonding of large areas, and non-local defects that may require full replacement. Large defects should be carefully examined, since they may be symptomatic of either significant short-term degradation or poor quality of materials or installation. If the extent of the defect is large and in areas critical to the structural integrity, it may be advisable to completely remove and re-apply the entire FRP system.

3.3 SUMMARY

Defects previously identified in Chapter 2 have been assessed for criticality based on a general classification scheme. However, it is emphasized that the differentiation is often dependent on location and total area of the defect relative to the overall area of strengthening. Thus a defect which has very little structural criticality for a large structural component could be extremely critical for a small one, especially if it occurs at a highly stressed area. Thus the classification is set as a guideline only, to be used in conjunction with engineering knowledge regarding the specific structure and overall engineering judgment.

4.0 REVIEW AND ASSESSMENT OF NON-DESTRUCTIVE TESTING METHODS

4.1 INTRODUCTION

4.1.1 Rationale of investigation

In Chapter 2 of this report the reader has been provided with the description of a vast array of possible material defects or anomalies, which can be introduced to fiber reinforced polymer (FRP) composite laminates in the course of structural rehabilitation efforts. Given the four predominant stages of rehabilitation – intrinsic materials, site preparation, field installation and service – defects were categorized in accordance to their initiating stage and factors contributing to such defects. The most probable effect on overall integrity of the FRP-concrete system was also discussed. While the preceding discussion served as an essential step towards developing an overall understanding for the *effect of defects* on externally strengthened concrete structures, it solely provided the reader with information on eventual material flaws and installation deficiencies.

In addition, field inspectors must be familiar with possible non-intrusive techniques that allow the in-situ detection of such defects. Here, techniques sought are those that can be applied to the structure subsequent to conclusion of the rehabilitation work, i.e. in service, and should not be confused with quality control techniques outlined in the previous chapter, such as viscosity tests, DSC, DMTA or FTIC inspections. While a number of defects discussed in the previous chapter can be identified and possibly characterized through visual inspection, the majority only occurs inside the composite material, at the concrete/composite interface, or within the concrete substrate. Generally, these discontinuities can neither be identified nor characterized through simple inspection methods, once the composite overlay has been installed and has reached its cured state. Instead, their detection often demands utilization of more sophisticated testing equipment and procedures. Also required is an experienced operator/inspector with extensive experience in composite inspection and interpretation of data extracted from such equipment.

This chapter will provide a state-of-the art review of potential non-destructive testing (NDT) techniques for defect detection in carbon-fiber reinforced polymer (CFRP) materials through review of past and current projects, including industrial applications, research projects, and methods under current industrial development. Both, theoretical and practical aspects of each individual technique will be addressed, including information on equipment, portability, data storage and their capabilities and limitations. Subsequently, these findings will serve to assess the suitability of each individual method towards in-situ inspection of CFRP-rehabilitated concrete components.

From the authors' perspective, an ideal inspection system, if such exists, must meet a variety of criteria, including the following:

- NDT systems must provide the capability of detecting a wide range of material discontinuities without negatively affecting the rehabilitated structure in performance, serviceability or appearance.
- Inspection must be performable in real-time and over reasonably large areas (full-field) without sacrificing the ability of localized inspections (near-field). This requirement may necessitate utilization of more than a single NDT system, as most full-field techniques lack sensitivity to localized defects.
- All equipment must be portable, easy to handle and operable in a variety of positions/arrangements to allow for inspection of overhead and tight regions.
- Data acquired from an NDT system must be representative of the actual defect parameters (type, size, shape, location) at all times with little or no susceptibility to changes in environmental conditions, unless they are well understood and can be accounted for in subsequent data interpretation.

The indisputable benefit of non-destructive testing lies in its capability to detect and, within limits, characterize a range of subsurface material discontinuities, including voids, delamination, fiber breakage or moisture accumulation in existing structures or their components, which otherwise restrict insight on their current material state. Through non-destructive inspection, engineers can obtain valuable information on eventual changes in the state of a material, including the onset of fatigue cracking or growth of formerly microscopic defects towards a critical level.

If operated by qualified personnel, real-time inspection and data interpretation can allow instant assessment of a structure's integrity and serviceability. Hence, once deficient regions are identified in the field, immediate action can be taken to initiate the required repair procedures in order to retain serviceability and safety of the structure. Also, feasible NDT methods should be capable of detecting both global and local flaws to permit rapid scanning of larger areas, while allowing for detailed distinction between good and defective areas on a local level.

CFRP-rehabilitated structures, in particular, do not benefit from extensive research in regards to short- or long-term deterioration, as often induced by harsh and fluctuating environmental conditions. Hence, the civil sector is currently seeking methods to monitor rehabilitated structures non-destructively to allow in-depth investigation towards finding the types of discontinuities that are most frequently encountered as well as their growth and effect on structural performance with time.

Recently, a variety of methods have been studied extensively for use on laminated composite materials [2, 3, 4, 5]. However, applicability of most NDT methodologies to CFRP-rehabilitated concrete structures remains largely uncertain. Unlike the material composition found in most composite aircraft structures, rehabilitated infrastructure components are comprised of a concrete substrate material, a typically non-uniform interfacial region of primer and/or comparable resin paste as well as an anisotropic fiber-reinforced composite laminate. It may be assumed that this constellation of materials limits the applicability of some well-established NDT methods for

aerospace testing, while possibly favoring other techniques that have not yet been focused on extensively.

It is the objective of this discussion to shed light on NDT methods that are potential candidates for inspection of CFRP- rehabilitated infrastructure, with special consideration of the unique material composition, desired sensitivity on a structural level, and several practical aspects desirable for in-situ application.

4.1.2 Non-destructive testing of composites

For centuries, relevant material properties like ultimate strength, yield point or impact resistance have been determined through a number of destructive test methods in order to provide comprehensive information on material behavior. Inarguably, the advantage of a destructive test is that materials can be exposed to a variety of load conditions without the necessity to remain functional upon completion of a test. While this methodology has long served in optimal design of structures, it can rarely be applied to evaluation of civil structures.

Today, the continuously rising demand on civil and transportation infrastructure has led to the need for finding alternative testing techniques, which allow the inspection of existing structures (airplane wings, bridge decks, etc.) without damaging or dismantling individual components. The impetus for such action is largely based on the need to ensure continuous safety and provide means of monitoring their overall 'health'. While much information on a structure's physical condition can be extracted from visual inspections, most internal damage, namely cracking, corrosion, presence or formation of voids as well as moisture accumulation can rarely be identified per se and thus demand more sophisticated methodologies.

In theory, non-destructive testing should provide information on material properties while neither influencing the material in its current state, nor requiring disassembly or any form of modifications that would cause extensive service disruptions, possibly restricting serviceability over extended periods of time. While the term 'destructive' may be applied in a broad context, its onset should be defined as the instant a component undergoes initial forms of permanent, non-reversible modification. These include changes in chemical or molecular structure and stages at which it experiences severe degradation and can no longer serve the original purpose for which it has been designed. This implies that a non-destructively tested component should retain its original strength, stiffness, chemical consistency, and appearance throughout the entire procedure and for a substantial period thereafter. Although literature offers a seemingly endless array of definitions for non-destructive testing, the following was found to provide a suitable foundation for the subsequent discussion:

> *A process that does not result in any damage or change to the material or part under examination and through which the presence of conditions or discontinuities can be detected [6].*

Similar to the multitude of definitions for non-destructive inspection, several abbreviations are commonly used by field inspectors and the non-destructive testing industry. These include non-destructive testing (NDT), non-destructive evaluation (NDE), and non-destructive inspection (NDI). While this terminology is often used interchangeably, distinct differences exist. As may

be noted from Figure 4.1, both NDT and NDI refer to the inspection process itself, i.e. testing of a part in a non-destructive fashion, leading to identification of defects/discontinuities with possible findings on defect type, location, size and shape.

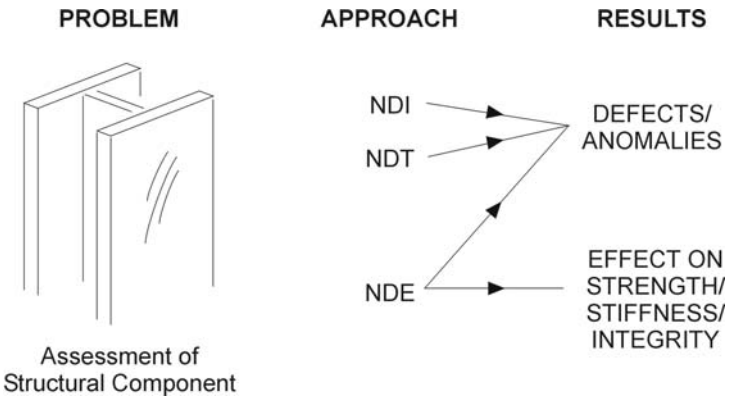

Figure 4.1: Differentiation between common non-destructive terminology

However, NDT and NDI do generally not assess the severity of damage on either a local or global scale. Instead, the effect of damage on system behavior is mostly accomplished through a subsequent evaluation process, as implicated by the term NDE. Here, data collected through testing/inspection is evaluated and interpreted to assess its impact on integrity and performance of the inspected object. Consequently, apart from a systematic methodology for localization and dimensioning of eventual material discontinuities, non-destructive evaluation necessitates an understanding of significance and structural impact of found defects. The mere presence of material discontinuities, introduced during erection, rehabilitation or service of a structure, however, does not imply a reduction of its performance or safety. Thus NDE represents the most challenging task.

In this context, test methods developed to date can be classified into four levels, according to the specificity of the information provided by the individual technique, as depicted in Table 4.1 [7].

Because the majority of methods discussed in the present report are primarily focused at localization and dimensioning of anomalies, they must be categorized as being either Level I or Level II, depending a variety of factors, including system sensitivity, member geometry, environmental conditions, etc.

To perform a non-destructive test, the object is typically exposed to a single form of external media (radiation, stress, temperature, etc.) emitted from the testing equipment, and capable of partially or completely penetrating the material. However, some forms of NDT techniques do not require penetration of the test object to reveal anomalies, such as optical methods. Others utilize sensors that are embedded inside the structure, and hence make use of an alternative testing methodology.

Table 4.1: Designation of NDT levels

Designation	Provided Information
Level I	Methods that only identify presence of anomalies
Level II	Methods that identify presence as well as location of anomalies
Level III	Methods that identify presence and location of anomalies and estimate their severity
Level IV	Methods that identify presence, location, and severity as well as structural impact of anomalies

Techniques that employ sources, which cannot be interpreted by human perception (ultrasound, x-ray, etc.) must employ a suitable detection media coupled to an output device such as a monitor/screen in order to display the recorded information, as schematically depicted in Figure 4.2. Finally, the recorded information can be displayed in a form that is detectable for the inspector. This is imperative, since incorrect interpretation of images can lead to erroneous conclusions about the composition of a material. Hence, apart from choice of method, success of NDT depends largely on experience and expertise of the inspector.

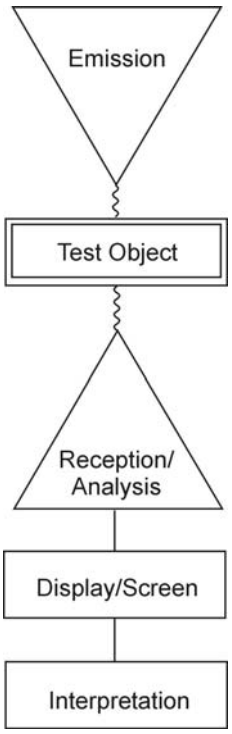

Figure 4.2: Schematic illustration of the NDT methodology

Given the fact that fiber reinforced polymer materials are comprised differently from traditional NDT materials, such as steel, a concise knowledge of the property differences of both materials

with respect to non-destructive testing becomes indispensable. While most NDT techniques have initially been used to locate cracking or other imperfections in metals, they have later proven to be suitable for detection of delamination, moisture or porosity in laminated composite materials. Nevertheless, prior to discussing the various NDT techniques on their suitability for detecting intrinsic material discontinuities, one must be aware of differences between isotropic, ferromagnetic materials, such as steel, and anisotropic, amorphous materials, such as CFRP composites.

Possibly the most important difference between metals and composite materials is the fact that former display a homogeneous structure, whereas composites contain two inherently different constituents, namely fibers and matrix. Consequently, composites are likely to experience different values for wave velocity, thermal conductivity or electromagnetic inductivity along various orientations within the material. Furthermore, they are not ferromagnetic, i.e. they cannot be permanently magnetized, which limits the use of techniques that are based on the principle of electromagnetic induction. Although carbon fibers are known to possess inductive properties, only certain electromagnetic techniques have proven to be feasible inspection tools. Finally, signal attenuation plays an important role in ultrasonic testing of composite materials, since it often results in a rapid reduction of signal strength. Due to a large number of fiber/matrix interfacial regions, ultrasound intensity in composite structures tends to decrease significantly with distance, making testing of thick parts (>1 inch) extremely difficult.

4.1.3 Overview of techniques

Many early discoveries, such as the piezoelectric effect in the 1880's and x-rays in 1895, have formed the basis for most of today's NDT techniques. Over time, additional techniques were developed either independently or based on these general theories, with several modifications to better adapt to material-specific characteristics. Although most techniques may have initially been developed for use in other fields, such as the medical or military industry, they have later proven useful for NDT purposes. Continuous progress in this field, particularly through the use of modern computer software, along with a constant growth in data storage capabilities, has lately allowed an even more successful utilization of these technologies. In particular, application of fast-fourier transform (FFT) functions and computer-assisted tomography (CT) has allowed for more sophisticated presentation and evaluation of test results [8, 9]. In addition, technological improvement has led to an overall increase in sensitivity of most methods.

The majority of current NDT techniques can be assigned to one of the following categories, including:

- Visual Testing (VT)
- Acoustic Impact Testing (AIT)
- Penetrant Testing (PT)
- Ultrasonics (UT)
- Radiographic Testing (RT)
- Thermographic Testing (TIR)
- Magnetic Particle Testing (MT)
- Eddy Current Testing (ET)
- Microwave Testing

- Optical Methods
- Acoustic Emission (AE)
- Ground-Penetrating Radar (GPR)

Moreover, a variety of so-called *data-collection techniques* exist that are not considered traditional NDT methods, including:

- Strain Measurement Techniques
- Modal Analysis
- Rapid Load Testing

Apart from the preceding list, a number of sub-techniques have been developed, which will be discussed in corresponding sections of this report.

Although most of the formerly listed techniques are applicable to CFRP, several methods have limitations due to the distinct material properties of composites. As mentioned earlier, methods utilizing the conductive nature of materials are most commonly applied to inspection of metals. Although carbon fibers are conductive, they are not ferromagnetic. Thus, methods like eddy current testing and microwave inspection are limited in their applicability, while testing via magnetic particles must be considered virtually impossible. Consequently, these techniques will not be discussed in further detail.

As outlined previously, methods can be distinguished based on the amount of area that can undergo simultaneous inspection. In this context it should be noted that a number of the above methods are solely used for localized inspection, including AIT, UT, ET, microwave testing and AE. Others, such as TIR, RT or optical methods may be applied for both near- and full-field assessments.

In common practice, near-field processes serve the localized inspection, in either a randomized fashion or at specific locations where defects are known to exist from a preceding, global NDT inspection. In addition, NDT has been used to assess overall structural integrity, in that data is collected from discrete sensors situated throughout an entire structure. Hence, NDT and data collection methods can be assigned to the former acquisition fields, namely, near-field, full-field, and global, as schematically depicted in Figure 4.3.

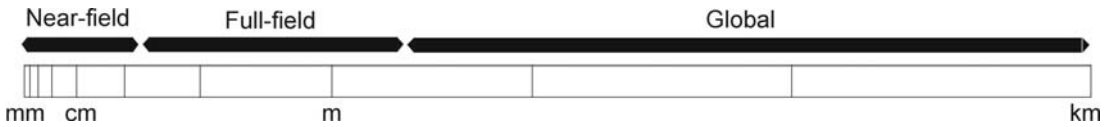

Figure 4.3: Field-of-acquisition for various inspection techniques

As may be expected, testing performed in a near-field manner generally results in highest sensitivity, which generally decreases as the inspection setup is changed towards a more global arrangement. This effect is known to exist for techniques such as thermography or optical methods, both of which have been used successfully in near- and full-field arrangements [10],

[11, 12, 13]. Hence, an increased field of acquisition, as enabled through full-field or global inspection, typically comes at the expense of sensitivity; i.e., the minimum detectable defect size will tend to increase. As may be noted from Figure 4., this decrease in sensitivity is particularly pronounced in global testing, a methodology that, although in wide industrial and experimental use, lacks sensitivity to the degree desired for the current study. Nevertheless, due its frequent use and widespread acceptance, global testing methodologies will be included in subsequent chapters of this report.

4.1.3.1 The electromagnetic spectrum

Many naturally occurring phenomena are based on emission or interaction of electromagnetic radiation. On earth, electromagnetic radiation is present at all times in the form of cosmic radiation, naturally occurring x-rays, heat radiation, visible light and various man-made sources, including radio and radar equipment. Based on the premise that all electromagnetic radiation travels at the speed of light, commonly denoted as c, the various forms of radiation can be distinctly separated by their specific frequency, f. As such, they can also be considered in terms of their specific frequency range, which can be related to wavelength, λ_l, via the relationship

$$\lambda_l = \frac{c}{f} \qquad \textbf{(4-1)}$$

Many forms of electromagnetic radiation build the foundation for non-destructive testing. Hence, a thorough knowledge of the characteristic properties of each type of electromagnetic radiation is indispensable for much of the subsequent discussion. Figure 4.4 illustrates the most common forms of electromagnetic radiation utilized for NDE purposes and their corresponding wave parameters.

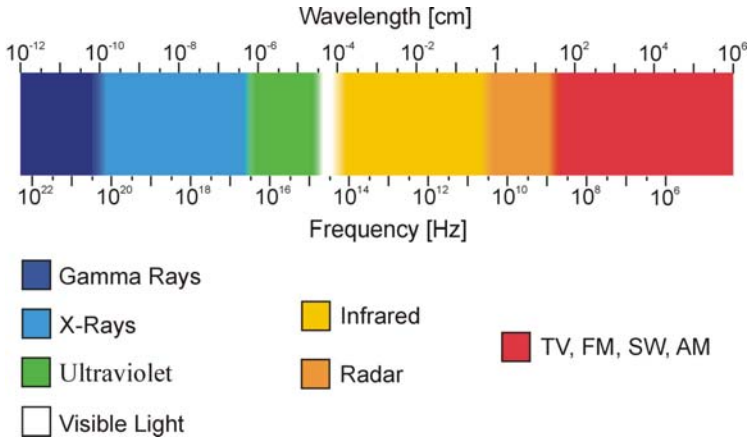

Figure 4.4: The electromagnetic spectrum

4.1.4 NDT applications

Contrary to controlled laboratory conditions, in-situ inspection of materials or structures can pose significantly different demands on an NDT system. In a given environment, a variety of external influences that may complicate the inspection process can oftentimes not be controlled. For instance, large temperature fluctuations tend to alter the efficiency of thermographic imaging or ultrasonic inspection, since most materials undergo slight changes in properties, including wave propagation speed or emissivity [6]. Furthermore, the typically smooth surface texture found on laboratory specimens can differ tremendously from conditions found in the field. As might be expected, NDT techniques are of limited use for structural health monitoring if they are suitable only for laboratory environments. Consequently, a potentially successful inspection method must encompass an array of user modifications in order to adapt to the naturally changing conditions in a field environment.

One of the most important in-situ inspection techniques, if not the most important, is visual inspection. Although one might not be readily aware of the fact that visual inspection is performed at almost any instant during preparation, installation and service monitoring, it provides the basis for all other inspection methods. Without adequate vision and proper judgment of visual perception, none of the previous NDT methods will be useful for defect detection. In many cases, defects like moisture accumulation, delamination, excessive fiber waviness or sagging may easily be identified visually and do not necessitate use of more sophisticated techniques. However, human perception is often insufficient for locating defects that are predominantly found in subsurface locations. Hence, inspection often necessitates additional equipment that is capable of closing the gap between human perception and modern technology. Nevertheless, the importance of visual inspection cannot be overemphasized and remains one of the most powerful NDT tools. For all inspection, visual examination should be the primary initiative before conducting automated measurements.

To date, a limited number of in-situ non-destructive testing has been conducted on CFRP-rehabilitated concrete structures. In contrast, extensive testing has been performed on aircraft composite structures, composite bridge decks and pressurized storage tanks, as these applications have a longer history of industrial use. Nonetheless, a small number of cited works on CFRP-strengthened concrete members appears in the literature, mainly utilizing techniques that are already well established and frequently applied in industrial testing. Examples include ultrasonic inspection of interfacial defects in laboratory environments [14]; thermographic field inspection of carbon fiber column wraps [11]; and stress and temperature effects by electrical resistance measurements [15].

Currently, suitability of other techniques, such as penetrant testing, radiographic imaging or optical methods remain largely unknown. This raises the question whether alternative methods are not being investigated on their potential for this type of inspection simply because other methods have already gained high acceptance and a stage of extensive industrial development. In contrast, methods may have already proven to be unsuitable for in-situ inspection due to safety issues or unjustifiably high cost. Lastly, as mentioned earlier, the unique material constellation found in rehabilitated infrastructure might favor new techniques that have not been previously explored.

From a standpoint of practicality, only techniques that allow portability could be potential candidates for field application. Clearly, in-situ methods must provide rapid testing, both with respect to inspection time as well as data acquisition and interpretation. Ideally, the method should be capable of locating defects on a global level to allow the rapid localization of defects over large areas while retaining relatively high sensitivity to localized discontinuities.

4.1.5 NDT on rehabilitated infrastructure

As addressed in the foregoing section, part thickness plays largely into defining the limitations of an individual NDT methodology. As a result, many techniques are restricted to surface or near-surface inspection. However, this does not imply that they are entirely incapable of revealing any information on subsurface properties. Instead, materials are often capable often revealing significant information about their subsurface nature by application of external stresses. The following paragraphs present a brief review of the particular material and dimensional configurations found in CFRP-rehabilitated concrete components. This will assure familiarity with some important NDE-related parameters, which is indispensable for the subsequent discussion.

For a majority of structural rehabilitation applications, CFRP is applied to a mechanically abraded concrete substrate. As such, the formed hybrid resembles a material of inherently different composition compared to most other NDT materials. Also, a majority of concrete components are of significant thickness, implying the necessity to inspect from only a single side of an individual member. Considering the use of concrete members in civil applications, component thickness rarely falls short of several inches, indicating that so-called “through transmission” techniques are either unsuitable or must be highly energetic to remain applicable.

In addition to former restrictions, which are mainly imposed by the base material, the composite overlay itself entails a number of restricting characteristics. Firstly, the material is oftentimes applied via the wet lay-up process, which tends to result in a composition of inferior quality compared to laminates manufactured under controlled environments or products of higher automation (pultrusion, RTM, etc.). Surface irregularities, lower uniformity, and highly irregular concrete-composite interfacial bondlines are some of the consequences, resulting in additional difficulties during inspection. A generally favorable characteristic of external strengthening systems is the low thickness of the overlaid material. In most applications, laminate thickness remains below 2-3 mm, which might lessen or eliminate several difficulties otherwise linked to inspection of thick composites.

4.1.6 Capabilities and limitations of NDT

To successfully perform non-destructive testing of composite parts, its capabilities and limitations must be well understood and considered when analyzing the soundness of materials. Even though NDT techniques are in theory capable of providing information about specific material properties, they do not give an absolute indication on whether a material will perform well or fail in the near future. This is a common misconception and must be considered when performing NDT. It is thus essential that limitations of each test method be known prior to application [6].

Similarly, sensitivity and depth propagation of the method can significantly affect test results. If parts are extremely thick, attenuation can result in signal loss and restrict the inspection of lower regions of laminates. Due to a minimum detectable defect size that is typically unique to each test method, defects below such a threshold might go undetected. However, this does not indicate that the part is defect-free. It simply means that the inspected regions do not contain defects of equal or larger size than those of smallest detectable dimension. Also, qualification of inspectors to perform a specific type of test plays largely into the validity of the result. If a single method does not provide comprehensive information to characterize a part as mechanically sound, a second, supplementary technique must be employed.

It is the intent of this report to review and discuss a variety of NDT techniques, most of which can be potential candidates for non-destructive inspection and characterization of laminated carbon fiber reinforced composite materials. Later, techniques will be evaluated based on their capability to detect defects that were discussed in Chapter 2 of this report. Techniques known to have significant drawbacks with either CFRP or concrete will be classified as unsuitable. Moreover, a considerable amount of previous work in a field will be valued, since these techniques can be categorized as relatively well established. Also, equipment will most likely be at a higher level of sophistication and more readily available for further practical study, which further yields lower initial equipment cost and higher availability.

Preferably, potential techniques will allow the detection of a variety of defects in both a near-field and a full-field manner. Susceptibility to environmental changes can cause inconsistent results and must be classified as a drawback. Thus, the present report provides the reader with a preliminary assessment of techniques. It should be pointed out that applicability to field use cannot necessarily be derived from this information and must yet be confirmed through further investigation. To date, most research has been conducted on individual CFRP elements that have not been adhesively bonded to concrete substrates. It must be assumed that adhering CFRP to concrete will diminish the suitability of some NDT methods that are otherwise well suited for inspection of composite materials. In contrast, the material composition and specific mechanisms found in rehabilitated infrastructure might favor techniques that have not yet attracted significant interest.

4.1.7 Outline of chapter

To develop an understanding of non-destructive testing and its applicability to inspection of CFRP-rehabilitated structural components, the Chapter 4 will be divided into three categories:

- Methods that have been applied extensively for inspection of CFRP-rehabilitated concrete components (Sections 4.2 and 4.3);

- Methods that are considered ‘traditional’ NDT methods, but have not yet found particular attention in the field of CFRP-rehabilitated infrastructure (Sections 4.4-4.12); and

- Methods that have already been applied to test and subsequently evaluate structures and their current state of performance (Sections 4.13-4.15). Moreover, some of these methods have recently been suggested for inspecting the soundness of CFRP-rehabilitation schemes. However, they are typically not considered NDT techniques, as they mostly serve data-

collection purposes. A subsequent analytical methodology is then applied to evaluate overall structural integrity.

In conclusion, Section 4.16 discusses and subsequently classifies/ranks methods based on the findings of Sections 4.2-4.15. Classification of methods will be provided in tabular format to allow easier comparison of methods and a clear understanding of the relative capabilities and limitations of each individual method. Primary attention will be given to defect-detectability as well as practical aspects, as these are paramount objectives in finding a suitable non-destructive field methodology. Although adequate defect-detectability should be assumed to be of high importance, methods of low flexibility, portability restrictions, extensive complexity or unjustifiably high equipment and service expenses will not be considered significant for further investigation. Only methods that show significant potential in regards to both theoretical and practical aspects will be considered favorable for implementation into NDE concepts for future establishment of structural rehabilitation quality standards.

4.2 VISUAL INSPECTION

4.2.1 Fundamentals and theory

Visual inspection (VT) is used in virtually all fields of construction, including preparation, assembly, and service, making it the most versatile yet simplistic technique. At all stages, personnel use their own judgment as to whether a procedure was followed correctly and if quality standards are being met. It may have been due to its simplicity that VT was the last method to be formally acknowledged as a non-destructive testing technique [6]. While VT typically limits the observer to examine surface discontinuities - unless one inspects transparent or translucent surfaces - the effect of internal defects may sometimes cause deformations or discoloration of the surface, thus indicating a material deficiency. The field of visual testing encompasses a wide range of separate methods, which can be broadly divided into direct and remote techniques (Figure 4.5).

Direct Visual Testing: This form of visual testing is defined as a method where mirrors, telescopes or cameras are utilized. Direct examination is conducted if the observer can obtain access to be within 25 in of the object, and at an angle of no less than 30° to the surface.

Remote Visual Testing: Remote visual testing can be divided into three categories: borescopes, fiberscopes, and video technology. These tools allow for inspection of surfaces that are not directly accessible to the human eye. Use of flexible glass fibers permits the viewer to inspect images in great detail without causing much interference to the object. The incorporation of digital video cameras through the use of solid-state imaging sensors, some of which are known as charge-coupled devices (CCD), allow for the display of images on a monitor. Advanced application for remote inspection via optical fibers will be discussed in more detail in Section 4.12.

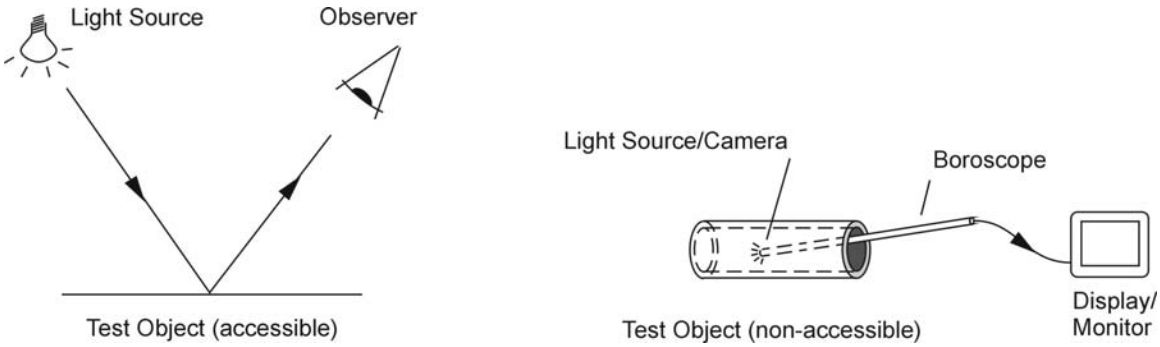

Figure 4.5: Direct and remote visual testing techniques

Independent of method, all NDE techniques eventually rely on the efficiency of the human eye. When using the direct visual method, adequate light intensity must be provided, to retain visual perception of contrast and color, since a certain minimum level of light must be present for the human eye to produce an image. Other factors influencing vision are brightness, surface conditions, temperature, size and shape, and surface texture. As such, cracks are more readily visible on smooth, bright surfaces where the relative difference between shape and color causes this type of discontinuity to stand out from its surroundings.

4.2.2 Instrumentation

4.2.2.1 Direct visual

Clearly, the most important instrument is the human eye itself. As mentioned previously, the eye might need assistance in visualizing objects under difficult conditions, such as low light intensity or disadvantageous surface textures. To enhance visibility, magnifying lenses can be used to obtain a larger image, while auxiliary light sources, such as hand-held flashlights can improve image illumination and contrast. To collect data of examined parts, a multitude of measuring devices is available. The most common tools include calipers, gauges, templates, micrometers and other miscellaneous devices.

4.2.2.2 Remote visual

In situations where the human eye cannot capture an image directly from the object source, remote examination must be performed. Devices used for remote imaging typically provide additional light to areas of low illumination and magnification of extremely small details that are otherwise indistinguishable to the eye. In addition, when the eye cannot obtain an unobstructed view, remote sensing becomes extremely important. For instance, fiber cameras utilize a light guide (fiberoptic bundle) to send light from the source inside an enclosed area to a CCD device for conversion to an electronic signal, which can later be displayed on a screen for further analysis. Also, large-scale examination is performed via use of conventional video cameras, which differ from the previous example in that they utilize a lens instead of a fiberoptic bundle to capture the image and transfer it to the CCD device. Here, remote visual sensing can be

utilized to reduce the field of view, whereas fiberoptic bundles are used for magnification.

Regardless of application, these devices are always used to convert a captured image into a format that is more easily observable and interpretable for the examiner.

4.2.3 Techniques and applications

When performing visual inspection, regardless of its specific type, inspectors are required to have a general understanding of what should be regarded as a material anomaly. Evaluation, as in all comparative techniques, is performed on the basis of comparing two or more objects with respect to their appearance. This includes size, shape, color, surface texture, etc. Hence, sound regions will serve as a baseline to those that may be of inferior quality. As we are familiar through everyday live, inspections are initially performed on a global basis to check for any obvious and outstanding differences. Once an overall baseline has been established, local checks are performed.

Visual inspection is used in virtually all aspects of health monitoring of composite rehabilitated structures. Currently, defectiveness and overall integrity of composite overlays are still assessed by this simple and cost-effective method. If visual inspection reveals certain surface deficiencies, inspectors may be able to comment on subsurface conditions and initiate further investigation using tools of higher sophistication.

4.2.4 Capabilities and limitations

As has been discussed, visual inspection is a fast, convenient and inexpensive method to characterize the appearance of repair schemes in view of global and local soundness, aided through use of a variety of tools, such as magnifying lenses, auxiliary lighting or digital recording devices. One of the main advantages of visual inspection is the real-time acquisition of data and its instantaneous interpretation. Given the extremely low equipment cost, this inspection technique should be regarded as an indispensable precondition for all further investigations. However, access to and illumination of the object or area of interest is a major restriction of this technique. Moreover, it is limited only to the object surface. While obstructed views or acquisition of multiple images simultaneously can be realized though use of recording devices, subsurface conditions of opaque materials cannot be revealed.

Other drawbacks of VT are the high susceptibility to human misperception and the requirement for establishing of a baseline for defects in general, especially under varying conditions (i.e. time of day when inspection is performed, lighting conditions, inspector's past experience, etc.). Consequently, examination procedures must follow inspection codes to ensure comparable results. On the other hand, although a thorough investigation is essential for quality control, overly particular inspection of minor discontinuities can result in a time-consuming inspection procedure.

Summarized, visual inspection can provide rapid information on overall health of a structure and should thus be performed prior to initiating any further inspection processes. However, inspectors should understand its apparent limitations such that assessment does not lead to

erroneous assumptions. Given this knowledge, visual inspection can serve as a highly effective supplementary NDE method.

4.3 ACOUSTIC IMPACT TESTING

4.3.1 Fundamentals and theory

The mechanics of the acoustic impact technique (AIT) are based on the premise that assumes alteration of local stiffness of a laminated material by presence of a defective region [16]. Interestingly, it is one of the few methods that has found successful application at two distinctly different levels of sophistication. In the basic approach, a hard, hand-held object (e.g. coin, miniature impact hammer, etc.) is used to impact the test object, as shown in Figure . In industry, the method is often referred to as the *coin tap test* [16]. Its methodology is based on the fact that if two materials that are bonded together are impacted with a small, hard object, the sound emanated will vary depending on the bond-quality of each tapped region.

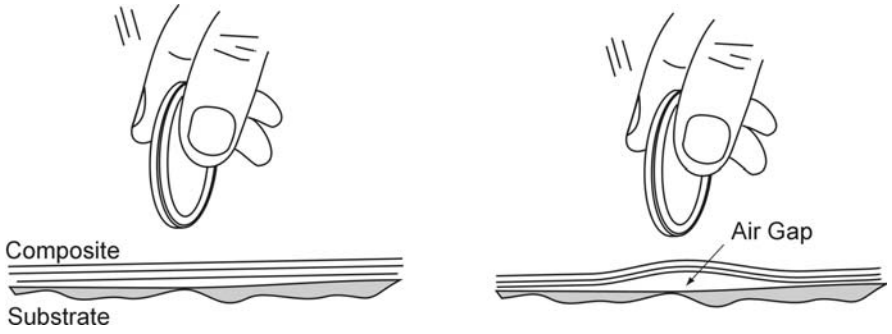

Figure 4.6: Coin-tap test

Over good regions, where there is an intimate bond between either composite or substrate and individual layers of fabric, tapping will cause a “full” sound whereas defective (e.g. unbonded) regions will result in a hollow response. This phenomenon is based on a localized reduction in stiffness above regions of disbonds, causing a difference in frequency excitation [17]. As a result, frequencies over bonded areas are perceptible as low-frequency sound, whereas unbonded areas respond with higher frequencies [16]. While this is true for localized defects, where the debonded region acts like an independent membrane, global softening, a phenomenon that rarely occurs in civil structures containing localized material discontinuities, would result in just the opposite effect.

Although the tap test is a real-time inspection method that provides the inspector with immediate results on subsurface anomalies, its efficiency is largely dependent on experience in signal interpretation. Similar to visual inspection, a persistent baseline must be established that represents characteristics of good signals comparative to those indicative of an anomaly, simply based on their response to impact. Since the method is non-automated, consistency of tapping

force, angle and equipment are potential sources of variation. As such, the most significant drawback of the method has been operator dependency [16].

To enhance the reliability of the AIT method, a more sophisticated form of impact testing can be utilized. Here, the motivation is to obtain more control over impact energy while recording the signal response at a more accurate and consistent level. Although the method is theoretically analogous to the tap procedure, the experimental configuration varies significantly. Both input force and signal response are recorded by means of digitization and subsequent analysis on the basis of fixed evaluation parameters. Thus, variation in signal interpretation can be reduced.

In a generalized setup configuration of the AIT method, the manually induced impact force of the tap test is substituted by a mini-shaker, which is excited in the form of a sinusoidal signal that is delivered from a power amplifier. A gauge is connected to the impacter-head to measure the force amplitude and time duration of the response signal. By further performing a Fourier transform on the force-time history, the frequency content can be obtained [18].

Signal interpretation is derived from the fact that the contact stiffness is reduced in regions of delamination, which will cause a corresponding reduction in force amplitude. Further, a signal collected from a delaminated region is likely to show an overall broadening of the pulse width, i.e. longer pulse duration. A typical graph obtained from good and delaminated regions within a multi-layered carbon-epoxy laminate is shown in Figure 4.7. Given such information, the user can comment on subsurface quality in a more quantitative manner as compared to the coin tap method.

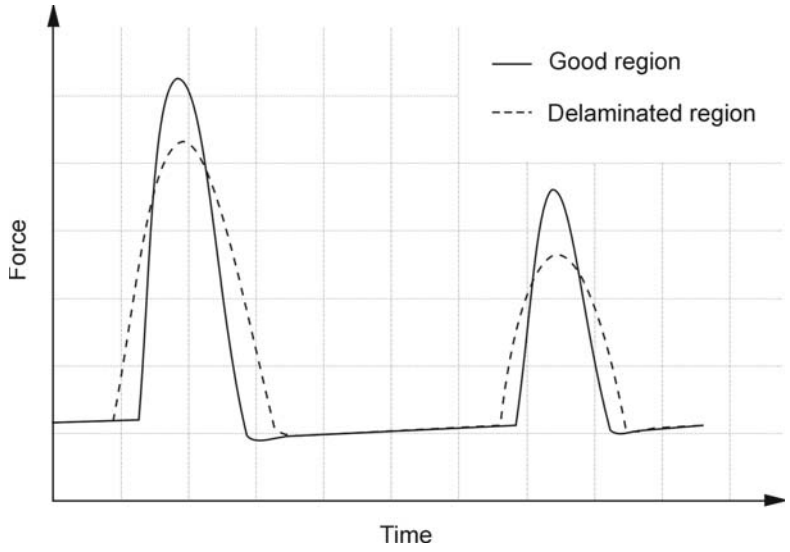

Figure 4.7: Force-time history in AIT testing (arbitrary units)

4.3.2 Instrumentation

Apart from audible perception as well as a suitable object for impacting of local areas, the tap test does not utilize any type of sophisticated instrumentation. In force-time history analyses, however, instruments must allow distinct excitation and acquisition of the corresponding force amplitude. For this, some commercially available products have been used in industry. These include the Mitsui "Woodpecker" advocated by Airbus as well as the WichiTech "RD3" instrumented hammer, a commercially developed apparatus used at Boeing [19]. Both tools operate by using solenoid and hand-wielded hammers to measure the output of an accelerometer embedded in the hammer head (Figure 4.8).

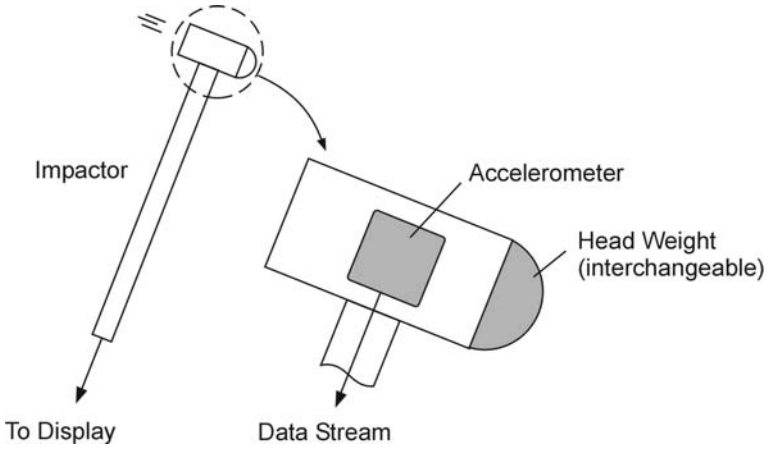

Figure 4.8: Common AIT impact device

4.3.3 Techniques and applications

The simplest and most rapid AIT approach uses audible perception exclusively, not implying that this method is less suitable or must necessarily result in lower accuracy. Experienced personnel may be equally efficient in using a coin to tap surfaces for defects as someone trying to extract and evaluate data from instrumented impact devices. Similar to visual inspection, good hearing and a sense for differentiating between audio signals are prerequisites for the manual form of AIT, since no data is being recorded for subsequent interpretation. Only a very limited number of research investigations have been conducted on manually induced impact response from CFRP-rehabilitated infrastructure components. This might be due to the fact that the method is difficult to instrument unless microphones or accelerometers are used to acquire frequency-time or force/acceleration-time histories. More likely, due to the rapid procedure, it has been around to complement other methods.

Conversely, the instrumented version of AIT has been used extensively on composite components, such as honeycomb panels and graphite fiber reinforced composite laminates [20], [18]. Raju focused on identification of defects in graphite-epoxy and graphite phenolic specimens, manufactured from twelve plies of prepreg (t = 1.9 mm) and six layers of carbon

fabric (t = 1 mm), respectively [20]. Herein, delamination was induced between the 5th and 6th ply of the graphite-epoxy composite. Also, fiber breakage and misalignment, induced during the layup process and located in layers 2 through 5 of the graphite phenolic specimens, were studied. A striker was used to apply an input force at a rate of 3 taps/sec. Results indicated that delamination could be easily identified from differences in pulse duration between good and defective specimens. In contrast, force-time history analysis was insufficient to comment on presence of fiber misalignment and fiber breakage in the six-layered hand layup specimens. Instead, acoustic emission sensors (see Section 4.11) were required to extract multiple frequency components.

Reports from Haque, et al. provide further confirmation for these results [18]. Herein, carbon-epoxy composite specimens comprised of 19-20 layers of carbon prepreg, oriented at various angles were investigated via AIT. The artificially implanted material anomalies included delaminations; impact damage (resulting in a combination of delamination, debonding and matrix cracking); and 90-day moisture exposure.

The test setup was mostly identical to that utilized in Raju [20]. It was shown that AIT is highly sensitive to delamination as localized as 0.254 mm^2, especially if situated close to the part surface. However, adequate quantification of the extent of damage was limited to areas less than 160 mm^2. Beyond that, no further significant change in force-amplitude signal was observed. Similarly, due to the presence of subsurface delamination, regions of impact damage could also be located using the previously described AIT setup. However, AIT did not appear to be sensitive to either moisture-induced damage or shape or position of delamination along the width of specimens.

4.3.4 Capabilities and limitations

In manual tap tests, differentiation between individual acoustic responses represents one of the main challenges of AIT. It remains largely subjective to operator interpretation and may cause considerable confusion, especially if a certain level of ambient noise is experienced at the site. Thus, operator dependency remains one of the major drawbacks of this form of AIT [19]. Furthermore, due to the low sensitivity in human audible sensing, the tapping method lacks sensitivity to small defects, such as porosity or fiber breakage. Nonetheless, it has proven to be quite suitable as a supplementary method to visual or other forms of examination, as it can provide rapid insight to medium to large subsurface deficiencies.

Through the development of specific tapping devices, some of the previous limitations of AIT could be reduced or eliminated. Because of a more controlled tapping force, frequency and incident angle, as well incorporation of force-time history analyzers, data interpretation is no longer susceptible to subjectivity. Also, systems remain fairly compact and thus allow good transportability and handling in field environments. From the earlier discussion, it was also shown that delamination of extremely small size can be detected without the necessity of coupling the detector to the test part. As such, one may easily scan an impactor along the part surface, which further eliminates the risk of eventual chemical incompatibilities between coupling agents and the composite material.

Nonetheless, AIT remains largely a surface inspection method. This, however, may not be of great significance due to the generally low thickness of CFRP used in this kind of application. From the aspect of signal visualization, AIT is currently limited to display force-time or frequency spectra, exclusively. For defect detection, these signals require further interpretation from an experienced inspector. Since no 'mapping' or area-scanning feature is available, AIT testing renders signal interpretation more difficult, particularly for inexperienced personnel.

4.4 PENETRANT METHODS

4.4.1 Fundamentals and theory

Dye penetration has been utilized for a long time to display discontinuities in nonporous solid materials, which can be virtually any metallic or non-metallic material. The basic principle of this method is based on capillary action, a phenomenon that allows liquids to be drawn into tight openings (e.g., cracks, porosity, laps or seams) due the high surface energies, which are present at such surfaces. Any liquid absorbed by these openings is then made visible by means of special chemicals and, if needed, enhanced by external illumination with lamps.

For dye penetrants, good 'wetability' is important to ensure penetration into extremely small surface irregularities. Poor wetability of a liquid occurs when the surface energy of the penetrant is relatively high, such that the difference in energy between the liquid and surface irregularities is not significantly large. In contrast, wetable penetrants have a low surface energy and are absorbed more easily by high-energy surface cracks. An effective way of determining wetability of liquids is measuring of the contact angle between the tangent of the contact point and the surface. A shallow angle represents low energies and therefore good penetration (Figure 4.9). Other important aspects are the dye concentrate and viscosity. While high concentration of dye pigments ensures good visibility, a low viscosity will reduce the amount of time that is required for the penetrant to effectively infiltrate the material. Typically, ultraviolet (UV) 'black' lights are used to visualize regions where penetrant has accumulated [6].

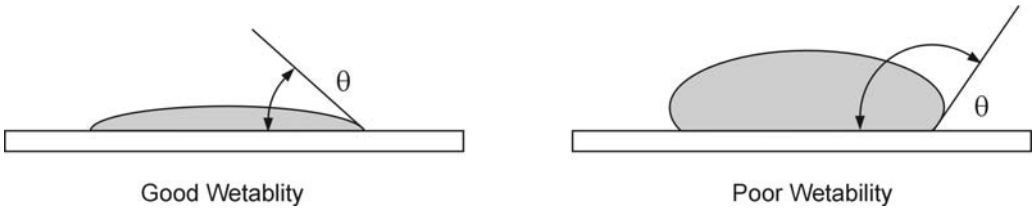

Figure 4.9: Wetability based on contact angle θ

4.4.2 Instrumentation

Penetrant systems can vary significantly in size and complexity. While a laboratory setup consists of multiple stages in an in-line arrangement, portable systems are available for use in the field. Systems typically consist of a precleaner, the penetrant liquid, some form of surface

penetrant removal solution, a developer, and a black light. Since these solutions can be supplied in small quantities, the method can be applied in virtually all in-situ situations.

4.4.3 Techniques and applications

Successful use of penetrant techniques requires the inspector to follow a precise application scheme in order to ensure best visualization and contrast of any possible surface flaws. The application procedure, as shown schematically in Figure 4.10, can be summarized as follows:

- Precleaning and drying of the surface to be inspected
- Application of a suitable penetrant
- Removal of excess penetrant off the inspection surface
- Visualization of penetrant submerged in defects by use of developers
- Interpretation under black light or other comparable methods
- Post-cleaning to remove all surface residues

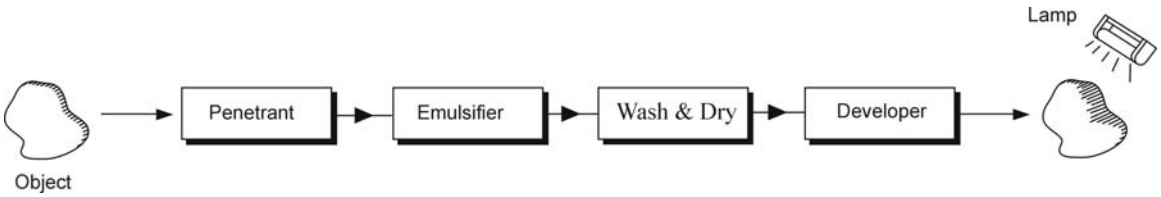

Figure 4.10: Procedural steps in dye penetrant inspection

One essential step in penetrant testing is the thorough cleaning of the material surface. This must be done to ensure the unobstructed entry of penetrant into possible surface openings, which may otherwise be restricted by surface contaminants. Common forms of cleaning include solvents, ultrasonics, alkaline, steam, water and detergent or other chemicals.

On large parts that do not allow immersion in liquid baths, or when hand application becomes too time consuming, penetrants can be sprayed over the entire area to provide complete wetting. Typically, penetrant imaging is used to detect defects in steel components, where crack formation is commonly found in the through-thickness direction and can therefore be detected. In contrast, composite materials tend to respond to impact or fatigue in the form of delamination of interlaminar matrix cracking, both of which are undetectable using PT, as schematically shown in Figure 4.11. This may be the main reason why there has been little effort in utilizing this technique for non-destructive evaluation of laminated composite materials. For steel members, examples of successful applications include detection of leaks in tanks, tubings, welds and other components [21].

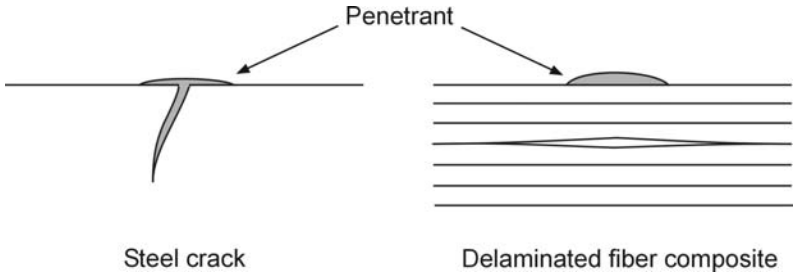

Figure 4.11: Differences in dye penetration between steel and laminates

4.4.4 Capabilities and limitations

Penetrant testing is one of the best methods for locating surface discontinuities in solid, non-permeable materials. The rapid detection along with its simplicity and high rate of coverage makes it a favorable technique for non-destructive inspection. Moreover, no electronic or sophisticated tooling is required. Also, penetrant systems are significantly less expensive compared to most other methods. The cost for a standard system, comprised of penetrant, emulsifier, developer and evaluation tools, i.e., black light, rarely exceeds a few hundred dollars.

Drawbacks of the method are obviously linked to the fact that only defects that reach the surface can be displayed. Delamination and debond of laminate layers are only detectable if they extend to the surface and allow seeping of penetrant into lower regions. Hence, a long but shallow surface scratch might appear to be more critical than a localized impact damage that may well have caused subsurface delamination throughout the laminate. In addition, the length of an external defect can be visualized; however, no information can be given on its depth [21]. Maybe the most significant drawback of penetrant methods is the difficulty of penetrant removal off rough surfaces [21]. It is known that composite materials, especially those processed by wet lay-up, typically show a significant roughness on their exposed surfaces. Consequently, penetrant tends to be trapped over the entire inspection surface, causing distracting background fluorescence upon black light exposure.

Unlike many automated techniques, penetrant inspection uses chemicals to visualize material discontinuities; hence fluids that are flammable or volatile are potentially hazardous due to the likelihood of explosion or fire. If large amounts of substances like benzene or acetone are used, vapors that escape from open containers can ignite.

4.5 ULTRASONICS

4.5.1 Fundamentals and theory

4.5.1.1 Wave properties

In ultrasonic testing (UT), mechanical stress waves are utilized to detect internal material discontinuities. Mechanical waves propagate through material by means of particle oscillation, where motion within a material is carried out by particle motion, which may be visualized as discrete particles of mass connected by springs. Wave propagation is largely dependent on the type of excitation, the mass of the individual particles, and the spring stiffness of their individual connections. A wave, initiated by an external event such as normal or shear forces, travels by vibratory movement that is transmitted from particle to particle. If the springs that connect the particles were infinitely stiff, all particles of the material would start to oscillate at the same instant and the wave would be transmitted at infinite speed. Hence, material elasticity and density play an important role in wave propagation. Elasticity is related to the spring stiffness between particles, while density describes the mass of the individual particles. Naturally, inertial forces restrict particles from being excited by their adjacent counterparts; thus, wave propagation occurs at a material-specific rate, termed as its *wave velocity*. A simple model of particle interaction is shown in Figure 4.12.

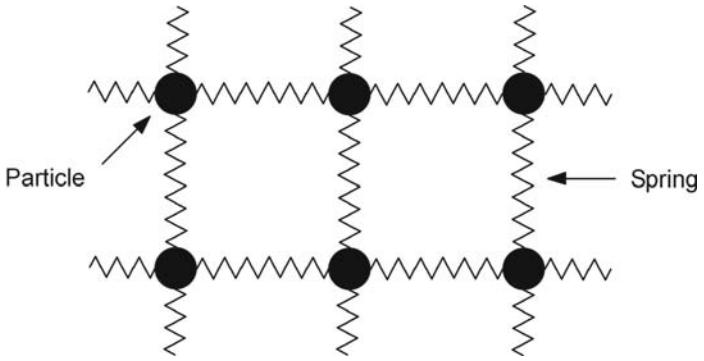

Figure 4.12: Particle interaction model [22]

While the above is applicable to solid materials, liquids or gaseous substances are not necessarily capable of transmitting certain forms of excitation to adjacent particles. Low-viscosity materials are often incapable of transmitting transverse excitations, whereas propagation of compressive forces remains possible. Common waveforms or *modes* that are utilized in ultrasonic testing are *compression waves* (longitudinal waves), *shear waves* (transverse waves), *surface waves* (Rayleigh waves) and *lamb waves* (plate waves). Compression waves are probably the most important form of wave that exists, since they form the waves for transmission of sound through air. Their particle oscillations occur in direction of wave propagation, causing compression of particles. Because solids, liquids,

as well as gasses can resist compressive forces, longitudinal waves can travel in these media.

Particle oscillation in shear waves occurs perpendicular to the direction of propagation, hence the material must be capable of resisting shear forces. Since this is only true for solids and certain liquids (of preferably high viscosity), all gaseous substances are incapable of transmitting shear waves. *Rayleigh-* and *lamb waves* are created when a compressive wave hits an interface and is consequently forced into *mode conversion*, as discussed in Section 4.5.1.2. Both wave types travel in the form of elliptical oscillations along the surface of a material. Lamb waves, however, are more likely to occur in thin materials, such as plates or shells [22, 6]. Examples of the different waveforms are depicted in Figure 4.13.

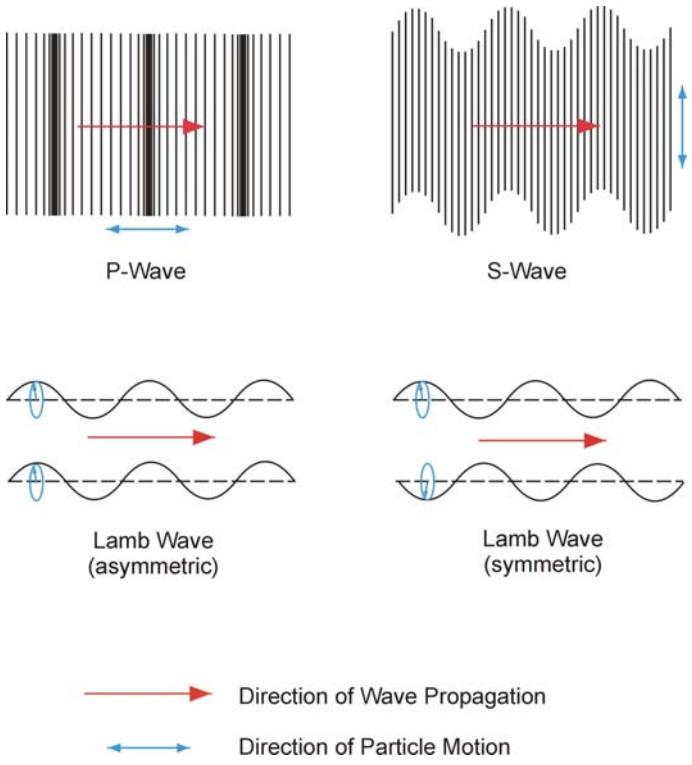

Figure 4.13: Propagation of common wave forms

4.5.1.2 Waves at boundaries

Since no substance extends over infinite space, waves propagating through a material eventually encounter material boundaries. If an incident wave encounters a material boundary, wave propagation is disturbed and wave characteristics are most likely altered. Although of rare occurrence, waves can hit an interface perfectly perpendicular, in which case neither mode conversion nor deviation from the initial propagation path will occur.

Because the wave mode will not be altered, a compressive incident wave will transmit and reflect in the same compressive mode. In most cases, waves will encounter boundaries at some off-perpendicular angle, referred to as the *angle of incidence*. While this angle is taken to be 0° in case of perfectly perpendicular incidence, it can range from 0° to 90° for all other cases. At the boundary, part of the wave will be reflected at an angle equal to the angle of incidence, while some fraction of the wave will transmit into the second medium and *refract* (Figure 4.14). This phenomenon is described by Snell's law, which states:

$$\frac{\sin i^\circ}{V_1} = \frac{\sin r^\circ}{V_2} \qquad \textbf{(4-2)}$$

indicating dependency of the refraction angle on the ratio of wave velocity of the two materials.

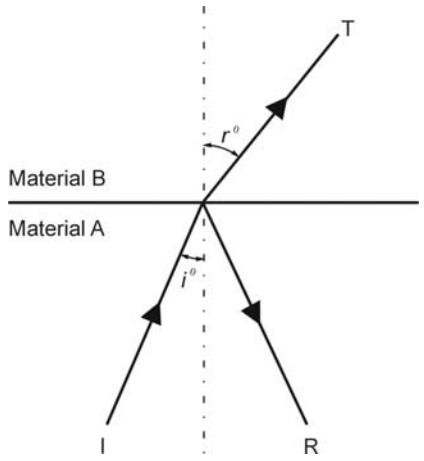

Figure 4.14: Geometric relationship between Incident- (I), Reflected- (R), and Transmitted (T) wave

A second phenomenon encountered at material boundaries is known as mode conversion, defining formation of new wave forms. The two most important material properties affecting mode conversion are the relative density and elasticity of the two materials through which the wave travels. They describe the *acoustic impedance, Z,* of materials, which in turn controls how much energy of the incident wave will be reflected at the boundary and how much is allowed to propagate into the adjacent material.

Although the incident wave may travel by means of particle compression, refracted shear waves can develop if boundaries are hit at angles other than 90º. At incidence angles nearly perpendicular to the surface, this effect is negligible. As the angle deviates more and more from 90°, however, the amplitude of the refracted shear wave begins to increase. With the further increase in angle, the compression wave is refracted along the material boundary, i.e. it never crosses over into the second material. At this point only the refracted shear wave is present. In a similar fashion, the shear wave can be forced to

propagate along the boundary, resulting in its disappearance. This specific type of mode conversion creates Rayleigh and plate waves. They constitute an essential part in long distance UT detection techniques, since they are capable of traveling over far distances with substantially less susceptibility to attenuation. Detailed information on calculation of wave parameters is can be found in the literature [22, 6].

Although the velocity for each of the waveforms discussed in Section 4.5.1.1 can theoretically be calculated, it requires the precise knowledge of all material parameters, including any variation in homogeneity throughout the material. Because this is difficult to obtain, it is more standard to perform a *calibration* procedure in which the timebase of the detector is adjusted against a calibration sample [6]. This, however, presupposes that the user is provided with a material of identical thickness and composition as that under inspection.

4.5.1.3 Defect detection

As mentioned earlier, incident wave fronts experience reflection at the boundaries of differing acoustic impedance. It is this interfacial property that allows the detection of discontinuities in materials. Most defects, such as delamination, moisture, or air pockets constitute a finite volume of air or water, entrapped inside the host material, whose acoustic impedance is significantly different from that of its surroundings. The percentage of acoustic energy that is reflected at a material boundary is given by:

$$R = \frac{Z_2 - Z_1}{Z_2 + Z_1} \qquad \textbf{(4-3)}$$

$$\textbf{with } Z_i = \rho \cdot V_i \qquad \textbf{(4-4)}$$

Here, R is termed the *coefficient of reflection*. Considering the difference in acoustic impedance between epoxy resins (Z_2 = *2.7-3.6 kg/m^{2}s*) and air (Z_1 = *0.0004 kg/m^{2}s*), one learns that the coefficient of reflection at a boundary of these two materials is roughly 1. Hence, due to the large mismatch in acoustic impedance, a nearly perfect reflection can be obtained at a composite/air interface. In a similar fashion, moisure, chemicals and physical inclusions are examples where acoustic mismatch allows their detection. It should be noted that these defects are only detectable as long as a finite volume of air is present between two adjacent plies.

If materials are in intimate contact but completely unbonded so that no tensile or shear forces can be transmitted, an infinitely small volume of air is present that can often not be detected by UT. In these cases, other characteristic features of UT can be enployed to allow detection of these more critical anomalies.

4.5.1.4 Attenuation

Unless a material is perfectly homogeneous, slight variations in material density will cause permanent fluctuations in acoustic impedance in that specific region. While the difference in acoustic impedance can be used to detect discontinuous areas, it can also

cause a disadvantageous effect in most materials, which is experienced in form of scattering or true absorption of the ultrasonic signal. Both of these effects are combined in the term *attenuation*, which causes a more rapid loss in the ultrasonic signal than that caused by pure spreading of a spherical wave.

Generally, attenuation is dependent on the homogeneity of a material. Although metals can be assumed to have high homogeneity, variations in crystalline structure are sufficient to cause noticeable attenuation. Naturally, composite materials contain an almost infinite number of these discontinuities, mostly in form of matrix porosity and fiber-matrix interfacial regions. Moreover, attenuation is not felt equally in all directions in a composite material, since fibers are typically arranged in one or multiple principal directions.

Apart from acoustic impedance, the ratio of particle size to ultrasonic wavelength plays an important role in how the approaching wave front is attenuated. If the material is very coarse and its particle size is comparable to the wavelength, refraction, as described in Section 4.5.1.2, occurs at virtually every boundary. Once the wavelength is significantly longer than the particle size, waves are no longer geometrically divided. Instead, scattering occurs.

In conclusion, when testing anisotropic composite materials, one should give preference to longer wavelengths, i.e. excite the material at lower frequency. However, as the wavelength increases, sensitivity to small defects rapidly decreases, due to the fact that waves are no longer reflected at boundaries but much rather scattered [14]. Hence, frequency selection in UT inspection of laminated composite materials is usually a tradeoff between attenuation and sensitivity.

4.5.2 Instrumentation

A variety of ultrasonic detection devices are available as portable units, consisting of one or more ultrasonic transducers and a control unit. Today, most portable units are no larger than 11 x 6 in (as in Figure 4.15) and encompass the entire palette of controls required for ultrasonic testing, including signal pulsing and detection, amplification and signal display. Most units can be battery operated and allow inspection with high flexibility.

Figure 4.15: Portable UT unit

4.5.2.1 Transducer

An ultrasonic transducer, also referred to as a *probe*, is responsible for emitting and receiving mechanical waves. Its primary function is to convert an electric signal into a mechanical impulse and vice versa. Use of the piezoelectric effect in quartz crystals allows this type of conversion, in which a high voltage spike causes expansion or contraction of the crystal, depending on polarity. Figure 4.16 depicts a schematic of the mode of operation for piezoelectric elements. A transducer can be composed of a single crystal, which can either transmit or receive a signal.

Alternatively, dual transducers combine the possibility of sending and receiving mechanical signals simultaneously. To allow simultaneous inspection of broad areas, a phased array transducer can be used. It incorporates a number of small piezoelectric elements that, under proper excitation, are capable of directing the acoustic beam at various angles. However, these transducers require a more advanced control unit that is capable of sending signals to each of the elements individually, so that acoustic beams can be sent out at predefined angles.

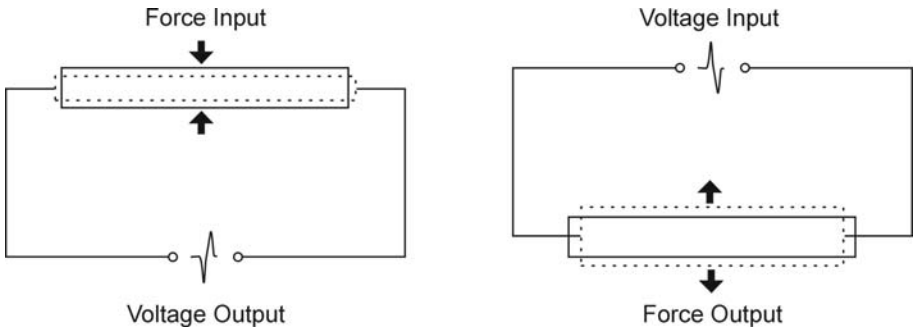

Figure 4.16: Piezoelectric element under mechanical stress (left) and voltage (right)

One of the most important specifications for UT testing is the frequency range at which transducers operate. Each transducer has a predetermined frequency based on its thickness. While each transducer tends to oscillate at its resonant frequency, a range of other frequencies is produced as well, ranging from slightly lower to slightly above the resonant frequency. Also, to adjust to different thicknesses and surface textures of test specimens, transducers are available in various diameters. For inspections that require high accuracy and resolution, a smaller probe is preferable. However, an important tradeoff of small probes is the usually large variations in signal amplitude due to increased sensitivity to surface roughness [23].

A common classification for transducers in UT is based on their excitation frequency. In practice, transducers utilizing excitation frequencies above 10 MHz are classified as high-frequency, while those of frequencies lower than 10 MHz are regarded as low-frequency types.

The transducers shown in Figure 4.17 utilize piezoelectric elements of about 1 inch in diameter and are specifically designed for pulse-echo inspection in conjunction with a *delay line* material. The delay line, which is comprised of material with acoustical properties similar to that of water, is coupled to the transducer wear surface through a thin film of glycerin and attached by means of a retainer ring. The impetus for utilizing the delay material lies in distancing the transducer's piezoelectric elements from the front surface of the inspected part, which enhances near-surface resolution.

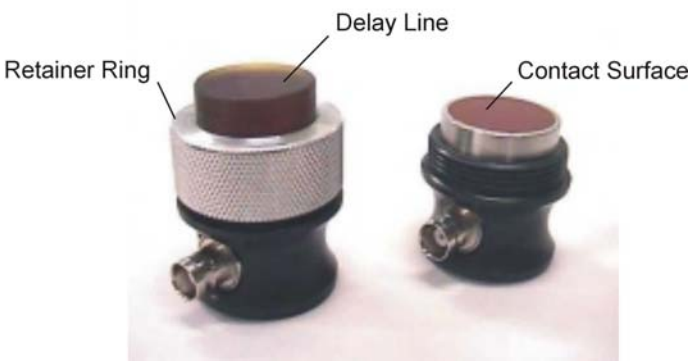

Figure 4.17: Piezoelectric transducers

4.5.2.2 Clock

To force the piezoelectric crystal into mechanical oscillation, a high voltage pulse is supplied at a certain repetition rate. A clock that is incorporated in the UT unit controls this frequency rate. It regulates the frequency of the exerted mechanical excitation, preferably in a range that allows penetration of the material without sacrificing much of the lower end of the sensitivity scale. In most modern systems, the excitation pulse can be generated in either spiked of square form. Generally, the spike pulser will yield better

results when using high frequency transducers (see Section 4.5.2.1), whereas the square pulser generally performs best in combination with lower frequency probes.

4.5.2.3 Receiver/amplifier

The receiver is another component that is incorporated in the UT unit and is responsible for receiving the electrical signal from the transducer. To adjust the signal intensity such that it can be appropriately displayed on a screen, an amplifier is used to regulate the electrical signal.

4.5.2.4 Display

Ultrasonic signals are normally displayed in an x-y coordinate system, with the x-axis linked to a time-base-trigger, while the y-axis is utilized to represent the energy that is received from a mechanical wave at the transducer. In its simplest form, information is displayed in form of an A-scan, where each image represents a spot-scan of the material. In regions where sound waves of high intensity are recorded, as would occur at a shallow discontinuity, peaks are displayed on the screen. Although this method of displaying data is fast, it simply provides a momentary spot image that is typically not recorded for further evaluation.

A more sophisticated image can be acquired when performing B-scans. This method displays a cross-sectional view of the component by successively recording A-scans as the transducer is moved along a path over the test piece. Hence, a spot-image is recorded synchronously as the probe is moved over the specimen. The brightness of each location is dependent on the intensity of the received signal.

If cross-sectional scanning is performed in a continuous grid pattern, a plan image or C-scan is obtained. C-scans are currently the most well suited method for fast and comprehensive testing of materials. Through modern systems and a variety of digital adjustments, as well as the possibility to transfer all acquired information to a personal computer (PC), much information can be derived from a modern ultrasonic scan. Examples of typical A-, B-, and C-scans are shown in Figure 4.18.

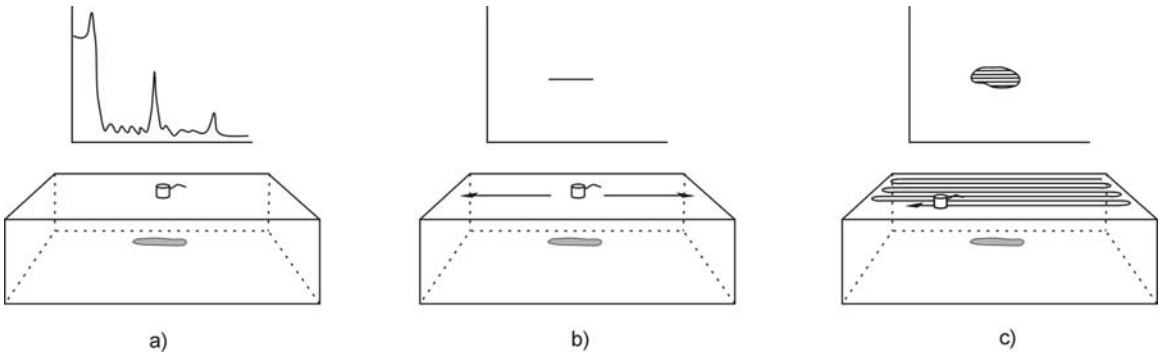

Figure 4.18: Idealized A-Scan (a), B-scan (b) and C-scan (c) of delamination

In the left image, the transducer resides in a fixed location on the part, and the graph obtained depicts the intensity of the received signal on its vertical axis, while time-of-flight is graphed along the horizontal axis. Reading the signal from left to right, the user obtains three distinct energy peaks that represent reflections off the front- defect- and backwall surface, respectively.

In Figure 4.18 b), the transducer is swept along a straight line while successively recording A-scan data at preset time increments. From their relative intensity, changes in the A-scan profile can be transformed into various levels of grayscale. Due to the continuous stream of data, B-scans impose a significantly higher demand on recording and storage capability of the ultrasonic system.

Finally, Figure 4.18 c) shows a 'mapped' image of the subsurface anomaly, which is more or less a combination of B-scans, each taken from a slightly different section of the part. As these sections are recombined into one image, the defect perimeter is visualized.

4.5.3 Techniques and applications

Ultrasonic inspection is one of the most frequently used NDE methods today. It has found excessive use in the medical field as well as the civil and aerospace industry. Most industrial applications aim at crack detection in airplane wing skins, defect detection on composite laminates, or thickness measurements.

4.5.3.1 Immersion testing

Immersion testing is performed to ensure good and continuous *coupling* between the transducers and test piece. Although the impedance mismatch between water and most solid materials is of considerable magnitude, it has proven to transmit the sound waves much more efficiently than air. Furthermore, water immersion allows for a wide spectrum of incidence angles since the transducer must simply be tilted to the right angle without the need for wedges that connect the transducer surface to the surface of the test piece. An obvious disadvantage of this method is the need to immerse parts into a tank for inspection. Since this cannot be done with entire structures, water immersion is not suitable for structural inspection.

4.5.3.2 Contact vs. non-contact methods

Alternatively to immersion techniques, the transducer can be coupled to the test piece in a variety of other ways. To achieve adequate energy transfer and to minimize the acoustic impedance mismatch between the transducer and composite material, viscous gels, waxes or water jets (squirters) are commonly used as coupling agents. Although these forms of coupling allow for more flexibility compared to immersion testing, the user remains relatively restricted due to the requirement of continuous the presence of a thin film between probe and sample surface.

Lately, the need to provide a means of non-contact inspection has arisen, since this method promises a decrease in inspection time as well as a broader range of applications.

The main advantage of air-coupled inspection lies where the inspected material or its subsequent processing is incompatible with the coupling media. Moreover, a near surface delamination may become filled by low-viscosity couplants and therefore be missed during inspection. However, the large mismatch in impedance between air and solids has been a limitation for such forms of testing [22]. It is known that, in comparison to water coupling, signal reductions of up to 140 dB are experienced [24]. Recently, through the use of electrostatic transducers with broader bandwidth, successful studies have been conducted using air-coupled techniques on composite laminate structures [25, 26]. In the following section, a number of UT procedures from previous investigations are presented and evaluated towards their applicability to NDE of rehabilitated structures.

4.5.3.3 Through-transmission testing

In this form of testing, two transducers are positioned on either side of the inspected part. Due to a shadowing effect caused by internal material discontinuities, signals of different magnitude can be recorded on the opposite side of the test piece. This method has proven to be unsuitable for NDE of structures, since high attenuation, linked to the large thicknesses of most structural components, rarely allows adequate transmission of ultrasonic signals.

4.5.3.4 Pulse-echo testing

4.5.3.4.1 Theory

In pulse-echo testing, access to only one side of the test piece is required, since this method evaluates the echo of mechanical waves as they are reflected off interfaces inside the composite laminate. Such interfaces can be the front surface where the transducer is placed, the back surface of the composite strip, and any internal defects of adequate size and orientation. Two forms of probes are commonly used in this technique, namely single and dual-crystal transducers.

In the standard compression wave technique, ultrasonic energy is directed either perpendicular or near perpendicular into the test piece, such that an adequate amount of energy is transmitted into the test material. Unless air-coupled transducers can be used, a couplant that is compatible with the test material must be employed to ensure wave energy transfer. The time base of the UT display must be calibrated to at least one times the full scale to display the entire thickness of the test piece, as depicted in Figure 4.19.

In a perfect material, an A-scan image will show two peaks, which originate from the front surface and the far surface, assuming both are near perpendicular to the transducer. Two important features of the signal obtained from an A-scan are separation of peaks and signal clarity. Utilization of too low frequencies (directly related to large wavelengths) can cause interference between signals reflected off the front and rear surfaces of an object, a problem that is faced most frequently in thin materials. Again, a tradeoff between the excitation frequency and the

attenuative properties of the material must be considered. Also, the clarity of the recorded peaks will be mostly dependent on the material attenuation as well as the surface smoothness.

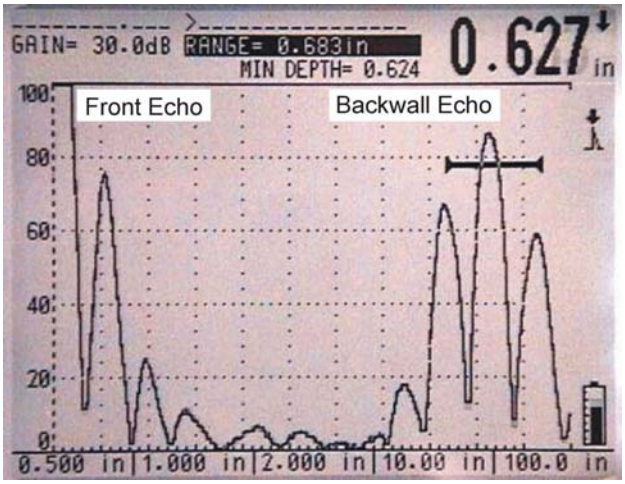

Figure 4.19: Calibration of display to 1x specimen thickness

If the incident wave front encounters a delamination that is smaller than the transducer width, parts of the wave will be reflected back to the probe while parts of it will continue to travel towards the far surface. Depending on the magnitude and location of the intermediate and far-surface peaks, estimates about size and depth of internal defects can be made.

In cases where the direction of the face of the propagating crack is not near perpendicular to the direction of wave travel, reflections will most likely be directed away from the transducer. Thus, no signal will be received and no predictions about internal defects can be made. Also, if the defect size is much smaller than the probe diameter, the signal intensity from a defect may be much smaller compared to that of the material interfaces. In this case, it will be necessary to increase the equipment gain to display any internal defects on the screen. In situations where defects propagate parallel to the direction of wave travel, as shown in Figure 4.20, only a weak signal will be reflected off the defect, making an estimate impossible.

With particular focus on bondline inspection between the concrete and composites, the usually highly attenuating concrete surface diminishes most of the incident wave front and can contribute significantly to signal scattering. Consequently, noise instead of a clear backwall reflection will be recorded.

4.5.3.4.2 Applications

Successful applications of the pulse-echo technique have been reported in the literature [14, 27, 23]. Kundu, et al. can be named as one of the few references that discuss the detection of delamination between concrete and CFRP plates [14]. In this study, a GCFRP plate, manufactured from three layers of [0/90] fabric was attached to a concrete substrate by means of adhesive bonding. The plate measured 3.66 mm in thickness, resulting in a total thickness of adhesive and plate of 4.56 mm. The artificially induced defect was in form of an air pocket of roughly 50 mm diameter located near the center of the concrete/composite interface.

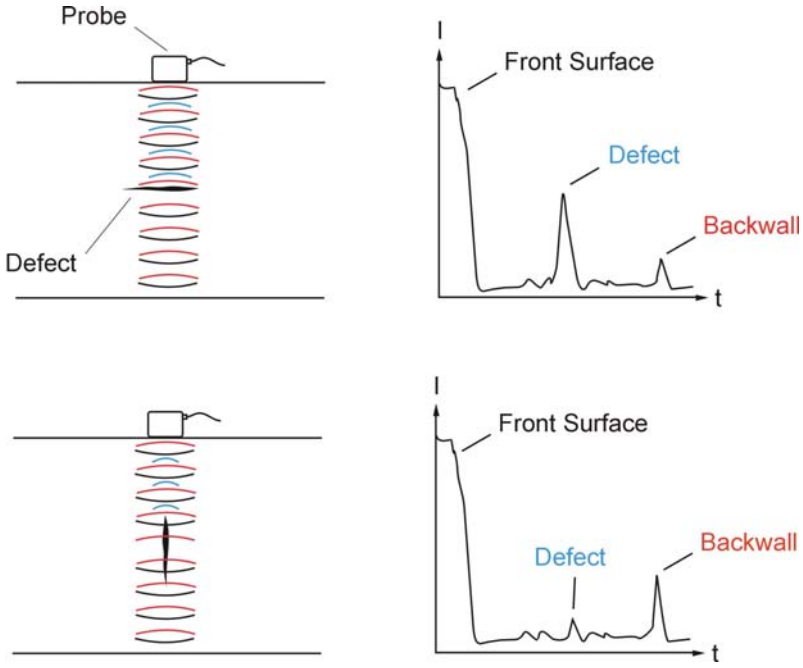

Figure 4.20: Reflection of stress waves off internal discontinuities

Due to the negative effect of attenuation, low frequency excitation below 1 MHz had to be used in this study. It was found that at low frequencies, penetration deep into the material could be accomplished. Pulses reflected off the front and rear surface were not well separated, however. Upon increasing the frequency to 5 MHz, attenuation reached levels at which almost no material penetration was possible.

Such findings led to utilization of resonance properties of composite laminate. Due to destructive interference at multiples of the ultrasonic wavelength, a sharp drop in voltage amplitude vs. frequency response can be observed. If the apparatus is adjusted, such that this drop occurs in good regions of the material, any change in material constitution, as would be caused by a delamination or

voids, will result in a shift or disappearance of this peak. From this, the observer can conclude a material discontinuity. Even though this technique has shown potential in finding defects, little is known about its sensitivity to size or type of the particular anomaly. Further, any slight variation in plate thickness would also cause a change in resonance properties. As a result, false conclusions could be drawn.

One of the major difficulties in bond inspection via UT lies in the necessity to obtain clean back wall echoes from the interface where two materials are joined. To obtain a reflective signal of sufficient amplitude, the incident wave front must be reflected at a preferably flat interface. This, however, is rarely provided by concrete morphology, particularly in situations where surface roughness is considered advantageous for enhancing mechanical interlock. As a result, the incident wave front encounters a surface morphology that causes severe signal scatter resulting in a considerable amount of background noise (Figure 4.21).

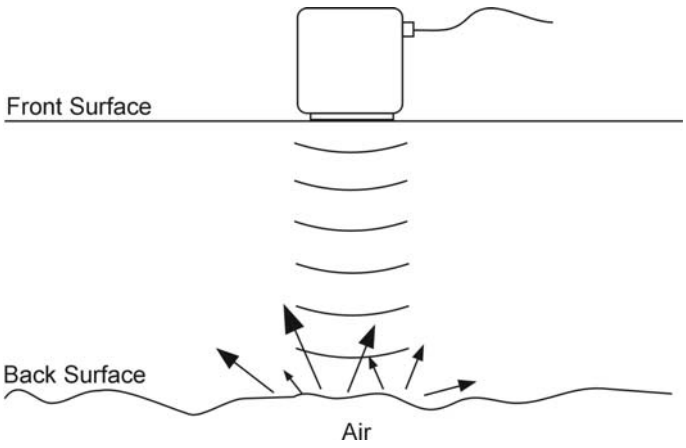

Figure 4.21: Signal scatter due to uneven surface morphology

Scarponi and Briotti conducted experiments on low-velocity impacted CFRP plates as they are typically found in aerospace applications [27]. The NDE system was comprised of 5 and 15 MHz probes for emission and reception of the ultrasonic waves. Test results showed a successful use of even the high frequency 15 MHz probes that were able to detect both the size and depth of the impact damage. While this is in contradiction to Kundu et al. [14], the extremely high uniformity and consequently low attenuation of the aerospace CFRP components may have allowed the use of short wavelengths. This is a promising result for the use of high-frequency UT on prefabricated strips, nonetheless, its applicability to wet lay-up should be reviewed more skeptically.

Summarized, normal incidence pulse echo inspection has limited applicability to concrete-bonded CFRP composites due to the high attenuating properties, lack of

adequate resolution of reflected peaks, and the generally tedious procedure for large-area scanning.

4.5.3.5 Plate and lamb wave testing

4.5.3.5.1 Theory

Unlike propagation of normal incidence waves, lamb waves travel parallel to the test surface and have an elliptical particle motion. They are also referred to as *plate waves* or *guided waves*, indicating the possibility of predetermining their direction of travel. Lamb waves can solely be generated in materials that have thicknesses of only a few wavelengths, indicating their applicability to thin, plate-like objects. As a result, they have been used extensively for studying the wave propagation of thin composite laminates [2, 23, 28, 24].

To initiate lamb waves in a thin material, the incidence angle must be adjusted according to the specific frequency and material thickness. For use on composite materials, these angles are typically within the range of 17 to 25° [14]. Waves can be transferred into the test material by means of using perplex wedges or through air coupling. They can propagate at symmetric and asymmetric modes, commonly denoted as *S* and *A*, respectively. In the symmetric mode, energy is transferred in a similar manner to that of a compressive wave where the midplane of the plate remains stationary. In contrast, shearing motion is predominant in asymmetrical propagation lamb waves, resulting in a flexural motion of the entire plate [29].

Interestingly, attenuation properties are significantly different between symmetric and asymmetric lamb waves. As such, the *A*-mode attenuates roughly eight times greater than the *S*-mode. Hence, the *S*-mode appears more attractive for large-area inspection [2]. Compared to normal incidence pulse echo, lamb waves are capable of traveling for significantly longer distances, often up to several meters. As a result, the path between two angled probes, placed at a fixed distance from each other, can be inspected rapidly using this technique. It can thus be concluded that lamb wave testing is more suitable for in-situ inspection of large areas than the more commonly used pulse-echo technique.

Regarding sensitivity, the two methods can be viewed as complementary to each other. This is based on the fact that sensitivity of the lamb wave method reaches a maximum in regions where defects are situated closest to the surface. In contrast, the normal incidence method is highly sensitive to delaminated regions located deeper in the material, assuming its material composition is fairly uniform. Fortunately, most UT equipment can be utilized for both normal incidence and lamb wave tests. Figure 4.22 illustrates the difference in test setup between normal incidence and guided wave testing.

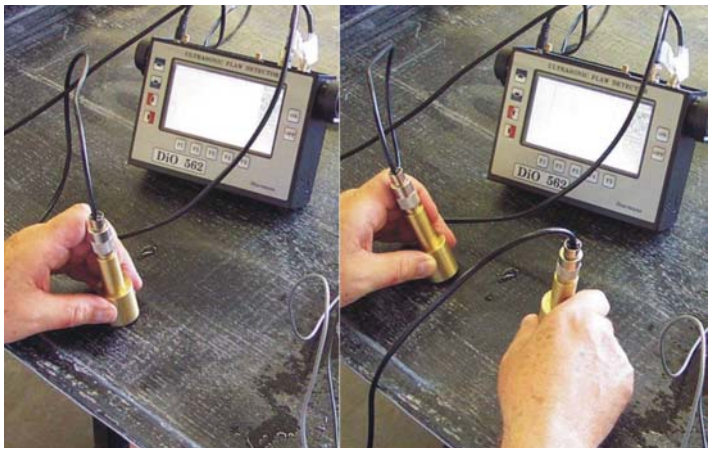

Figure 4.22: Test setup for normal incidence (left) and guided wave testing (right)

4.5.3.5.2 Applications

Over the past years ultrasonic lamb wave testing has been utilized extensively, including inspection of adhesively bonded joints, delamination, porosity and fiber misalignment [30, 14, 24]. Furthermore, studies on the detectability of impact and thermal damage have shown promising results [31]. Such studies have shown several significant advantages of lamb waves over normal incidence testing for detection of a wide range of defects. These include an increased sensitivity to near surface defects, as they are naturally found in composites comprised of only a few layers, which makes lamb wave testing especially favorable for the current discussion.

Since flaw detection through the use of lamb waves is not based on their reflection off surfaces but much rather their alteration through the presence of defects, two transducers must be employed for testing. In a typical test setup, transducers are positioned at a fixed distance apart and at identical angles from the vertical axis. For inspection of longer distances, the surface of the test object is located in the defocus position, indicating that the axes of both transducers coincide below the test surface. If the defocus position is selected, the emitted signal that is reflected directly off the test surface cannot reach the receiving transducer. Instead, a *leaky* signal, which the wave emits as it travels along the plate, can be picked up by a second transducer and used for further interpretation.

Signal interpretation can generally be performed using one of the following three methods. First, the attenuation caused by travel through a defective region can be interpreted. This is generally performed via amplitude monitoring of the received signal. It has been shown that determination of delamination depth is possible solely based on a drop in signal amplitude [23]. One example of such a drop in signal is caused when an incident lamb wave encounters a delamination situated near the surface, which results in separation of the wave. Most of the energy is attracted by thicker sections of the laminate (Figure 4.23). Consequently, if the

wave signal were picked up just above a shallow delamination, a significant decrease in amplitude would be noticed. Second, reflections of *S*-modes, caused by interference of the incident lamb wave with defect boundaries, can be used to comment on possible material discontinuities. Lastly, mode conversions can potentially provide information on the presence of defects. Similar to C-scan imaging in normal incidence UT, the results obtained from lamb wave analysis are displayed via so-called L-scans.

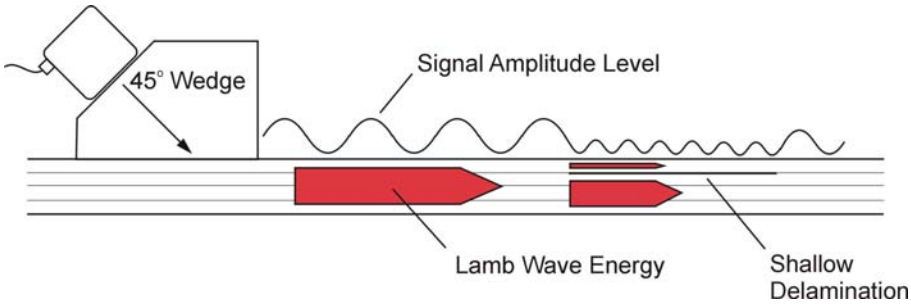

Figure 4.23: Lamb wave interaction near delaminations

4.5.4 Capabilities and limitations

Without question, UT has been the most frequently utilized method over the past decades. It has found wide acceptance in aerospace and manufacturing industry in general, mainly for use in quality control of welds or discontinuities in metallic or laminated composite parts. The method is capable of detecting a wide range of defects, including shallow and deep delamination in thin to medium laminates, porosity, and effects of environmental influences such as moisture accumulation or impact damage.

Due to the continuous development of ultrasonic devices, the method can be classified as extremely portable with a wide variety of test equipment being readily available. Use of computer-aided signal filtering (DAC, TVG, and CSC) has been shown to decrease sensitivity towards material variations, which makes the method even more applicable for field inspection.

Although coupling to the test surface remains a delicate issue for field use, development of new transducers has lately opened advanced possibilities for air-coupled inspection [26]. Furthermore, UT allows part inspection from only one side, making it potentially suitable for defect detection in rehabilitated concrete structures. Using these techniques, most defects can be characterized in size and depth. Based on numerous sources, UT has been assessed as being one of the most versatile and promising NDE techniques available today [23, 32].

However, no single nondestructive testing method can be considered a panacea. UT signal interpretation is largely influenced by a number of variables, including defect orientation, ambient temperature, attenuation, surface conditions and choice of couplant. As mentioned earlier, the orientation of a defect relative to the direction of wave propagation is crucial to detectability. Although complementary methods are available to detect defects of multiple

orientations, this can result in a time consuming inspection process. The same is true for inspection of large areas, especially when using spot scans obtained from pulse-echo testing.

When applied to composite laminates, a limitation called the *shadowing effect* is often experienced. If examined from only one side, delaminations that occur near the surface may obscure those located deeper in the composite, a phenomenon that is commonly experienced in impacted specimens [33]. Also, reproducibility of the UT method is significantly reduced. The high attenuation caused by an almost infinite number of interfacial boundaries restricts the use of high frequency testing that is needed for adequate sensitivity. In many cases, the signal is not capable of penetrating deep into the material because of disadvantageous surface conditions.

For in-situ inspection, environmental conditions can cause further variance of the results. Since temperature affects the velocity of sound in most materials, erroneous depth readings or refraction angles can be obtained. Thus, the possibility of changes in temperature must be considered when first calibrating the equipment. A specifically critical aspect for detection via UT is a so-called *cold* or *kissing bond*. These are regions where two materials are in intimate contact but do not possess any strength at their interface to resist tension or shear forces. This form of debond is not detectable via pulse echo UT since the encapsulated volume at the interface is of such infinitesimal size that virtually no acoustic impedance mismatch exists.

Concerning signal interpretation, the various forms of ultrasonic scans, namely A-, B-, and C-scans, allow for a multitude of visualization options. However, it should be noted that C-scans can only be generated if the probe is scanned over a fixed x-y coordinate system in which the system receives distinct information on probe location at each instance in time. The cost for these systems is often extremely high (in excess of $100,000) and demands equipment of significantly higher sophistication, including continuous acquisition and storage of each data point along the x-y area scan. A much more cost efficient A-scan unit ($7,000 to $15,000) can generally perform identical inspection routines as the C-scan setup. However, it necessitates manual scanning of the entire area including real-time signal interpretation, which demands the permanent attention of the inspector throughout the entire testing procedure.

Summarized, UT is capable of detecting a large number of material defects and has proven to be applicable for in-situ inspection for many years. Although certain difficulties arise when applied to composite materials, especially on those processed via manual lay-up, it must be considered a potential candidate.

4.6 RADIOGRAPHIC TESTING

4.6.1 Fundamentals and theory

Radiographic testing (RT) dates back to the discovery of x- and γ-rays in the late 19th century, which has led to tremendous advances in the field of medical examination as well as scientific testing. In general, radiographic imaging involves three components, including a radiation-emitting source, the specimen to be examined, and a recording device such as a suitable film or digitizing system. While radiographic films are typically covered with an emulsion that is

chemically changed through ionization as radiation interacts with it, digital recording devices represent more convenient means of radiographic detection.

In theoretical terms, radiographic energy is a form of electromagnetic radiation of extremely short wavelengths, where higher energy levels correspond to shorter wavelengths [34]. The important characteristic of radiation lies in the ability to penetrate most opaque materials while retaining a high percentage of its energy to produce an image on the opposite side of the test specimen. In the past, three main forms of radiation have been applied to nondestructive testing namely x-rays, γ-rays and neutrons.

X-rays are produced in a vacuum tube where high-speed electrons are focused at a target material, usually made of tungsten, and forced to interact with it. Such interaction results in the release of quantum energy, or *photons*, which are capable of penetrating solid matter. This ability to penetrate matter is related to the extremely short wavelength of electromagnetic radiation of x-rays, which is in the range from 10^{-6} to 10^{-10} cm (see Figure 4.4). The applied voltage, typically expressed in kilovolts (kV) is the main governing factor for energy of the radiation. Most commercially applied units operate in the range of 100 to 400 kV [6]. For inspection purposes, an increase of radiation energy will cause shorter wavelengths and an increase in material penetration.

Unlike x-rays, γ-rays are emitted by unstable radioactive isotopes, which possess a so-called *half-life*. While the energy level of individual isotopes, such as cesium, iridium or radium, is unique to each material and remains a constant, intensity will decay with time. Since exposure is a function of intensity and time, the level required for adequate penetration of a material will not be achievable once a certain time period has passed. Thus, the isotope must be discarded and exchanged for a new source.

Neutrons, the sub-atomic particles, are not considered electromagnetic radiation. Instead, they are released by *particle sources* that can be in the form of nuclear reactors, particle accelerators, or man-made radioactive materials. While reactors are highly regulated devices with limited access, particle accelerators have been available for laboratory testing and are quite small in size. Lastly, radioactive isotopes, such as californium-252, have been developed for small, simple and reliable operation [34].

While all success in radiographic imaging is governed by the capability of penetrating the test material, the penetrability of each of the previous forms of radiation is dependent on different parameters. For example, x-rays are not capable of penetrating high-density materials, which is why lead jackets are commonly used to shield humans from the emitted rays.

Material discontinuities can be detected via differences in absorption or attenuation rates as photons pass through the atomic structure of the test material. Similar to radiographic imaging of the human skeleton in medical x-ray, regions of higher material density typically allow for lower penetration of photons than their surroundings. Consequently, lighter appearances on the recording media will indicate the presence of more dense materials along the beam path. As such, porosity or other gaseous inclusions show as dark spots or lines. While a clear relationship between mass attenuation coefficient and material density does exist for photon penetration, no such relationship can be derived for inspection with neutron sources. Instead, a unique

characteristic is their high sensitivity to the presence of hydrogen, which has proven to be efficient in detection of corroded regions in structural joints [34].

As for other NDE methods, the sensitivity of RT is in part dependent on the orientation of an internal material discontinuity. Using the example of a long, thin crack propagating in the through-thickness direction of a composite laminate, the most favorable orientation is such that the photon ray must penetrate the maximum distance of the crack. Hence, if a crack were arranged near perpendicular to the incident radiation, penetration through the defective region would only take place over an infinitesimally short distance. Accordingly, little attenuation, scattering or absorption would result and the recorded image would most likely reveal no meaningful information. As such, sensitivity of the RT method is distinctly different from UT, where defects are best detectable at near perpendicular orientations.

4.6.2 Instrumentation

Mainly, instrumentation is composed of the emitting source and a suitable recording medium that can be in form of a conventional film or, more recently, a digital imaging system. As discussed earlier, neutron particle machines are extremely difficult to obtain; nevertheless, their mode of operation should be discussed briefly.

4.6.2.1 X-ray machines

Typically, photon-emitting units are categorized by their energy level. Equipment with energies up to 125 kV is considered low energy, guns consuming between 125 to 400 kV are classified as medium energy, and all other with radiation energies above 400 kV are commonly referred to as high-energy. Up to the medium energy range, small and lightweight units are available for field inspection. Because of stray radiation, lead sheathing is normally required. Apart from safety precautions, little preparation is needed for inspection or equipment assembly. While most stationary units can be run continuously, many portable systems are operated with duty cycles, meaning they require a cool down phase in-between long exposure times [6]. Figure 4.24 shows a schematic detail of a typical x-ray tube as it is found in most conventional x-ray unit.

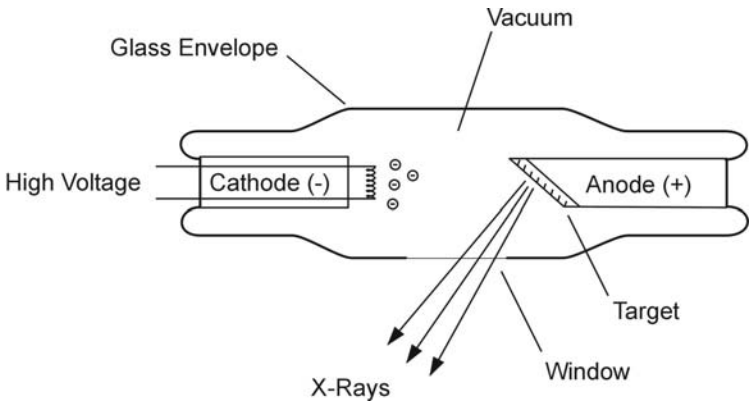

Figure 4.24: Schematic view of x-ray tube

4.6.2.2 Gamma ray machines

Exposure devices using gamma rays use isotopes that are permanently encapsulated inside a protective casing. For exposure, the radiographer cranks the source material out of its casing for a predetermined amount of time. Upon complete exposure, the source is returned into the casing for safe storage (Figure 4.25).

One significant disadvantage of γ-ray sources is their fixed energy level, whereas x-ray energy is a function of the applied voltage. Since most tubes are manufactured for operation at a certain kilo-voltage range, various thicknesses can be tested using the same x-ray unit. Also, the contrast of the obtained image can be more effectively manipulated by use of x-ray units [6].

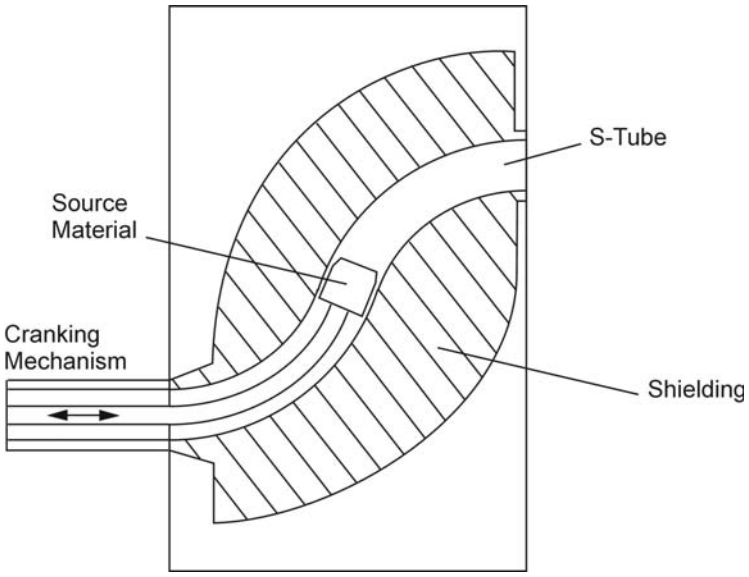

Figure 4.25: Schematic view of gamma ray machine

4.6.2.3 Neutron particle machines

Available units for neutron radiography in the field are those comprised of accelerator guns. Such units are more restricted in terms of portability, since power and control mostly requires additional trailers or heavy equipment. Nevertheless, it offers the possibility of neutron inspection if desired as a supplementary method [34].

4.6.2.4 Radiographic film

To visualize attenuation and absorption of photons as they pass through the test specimen, radiographic film is still most commonly used. If properly developed, it serves as a permanent record of all discontinuities that are present along the beam path. Films consist of thin cellulose or polyester bases coated with silver halide crystals that undergo

chemical changes when exposed to radiation or light. The grain size of the chemical emulsion has a significant effect on exposure rate as well as the resolution detail. Therefore, the film type must be matched with the radiation source and the expected minimum flaw size. Similar to photography, a radiographic film must be processed once it has been exposed. The steps involved in processing are developing, stopping, fixing, washing and drying. Viewing of the fully developed films is obtained via use of high-intensity illuminators in a preferably dark environment. Such conditions help improve contrast of the image and aids in a more detailed interpretation.

4.6.2.5 Real-time imaging

Real-time imaging, also referred to as *radioscopy*, offers considerable time advantages, especially in cases where in-situ interpretation is indispensable. This method produces an instantaneous image of the radiographed section on a screen or other suitable device. It works with all forms of radiation, including x-ray, γ, or neutron radiation. An important difference between conventional and real-time imaging is the fact that dynamic inspection of the object can be performed, whereas radiographic film is only capable of capturing a static image. Also, images obtained from radioscopy are displayed as positives. In contrast, radiography only allows the inspection of a negative image. Furthermore, the electronic signal obtained from radioscopy can be digitally processed to enhance image quality and eliminate noise and other unwanted information. A drawback of real-time imaging is the requirement of higher-energy sources, since a relatively short exposure time must be used to deliver successive images to the recording device [34]. This, in turn, imposes a much higher demand on safety regulations and radiation shielding.

4.6.3 Techniques and applications

While conventional radiography is still commonly used for straightforward medical evaluation, other, more sophisticated techniques have found their application in the nondestructive field. This can be linked to two facts. First, structural components are not susceptible to alteration of their atomic structure in such a way that long-term damage or deterioration may occur. Thus, they can be exposed to higher levels of electromagnetic energy and longer exposure times. Moreover, project specific conditions such as dimensions and geometry are highly variable, whereas conditions in human radiology are mostly constant. To accommodate various material configurations, thicknesses, and inspection details, a number of specialized techniques have been developed. These include methods that, unlike traditional transmission x-ray, do not require access to both sides of the specimen, as discussed in Section 4.6.3.1.

In recent years, RT has found a considerable interest for NDE of composites; however, it has not yet been utilized nearly as extensively as other methods. The main reason might be high safety regulations and cost, which are significant drawbacks of the technique. Nevertheless, several promising projects have utilized RT, indicating a high potential of this method, especially for inspections where high detail of thick members is desired.

4.6.3.1 Compton backscatter

This specific application of radiography utilizes a portion of the attenuated radiation as it passes through a material. As mentioned earlier, radiation can be attenuated by absorption or scattering. The latter can occur in the form of *Compton scattering*, a process in which photons in the 0.1-3.0 MV-range interact with the orbital electrons of the test material. This interaction causes photons to be reflected into different directions with a usually lower wavelength [6].

One highly useful application of Compton backscattering is the inspection of multiple delaminations in impact-damaged composite laminates [35]. The technique is especially suitable for this form of defect since it is capable of visualizing defects at multiple depths. Also, delaminations oriented parallel to the laminate can be identified. Unlike transmission x-ray, Compton backscatter detects a variation in material density in terms of scattering characteristics. Hence, thin delaminations can be detected. This was shown on 2.3 mm-thin carbon-epoxy laminates using a 100 kV x-ray tube with scanning resolution of 0.02 mm [33].

Despite this excellent resolution, Compton scans are susceptible to contamination and blur from a number of sources. These include voltage fluctuations, scanning fixture vibrations, and irregularities in fiber/matrix distribution. The latter indicates the extreme sensitivity to signal noise if Compton backscattering is applied to materials that generally do not possess a high material uniformity, as may be expected in externally bonded laminates manufactured by the wet lay-up process.

4.6.3.2 Computed tomography

Through digitization of radiographic images at a large number of varying angles, a three-dimensional representation of the test object can be produced. One such method that is commonly used in medical evaluation is computed tomography (CT). In this method, where access to both sides of the specimen is required, the part under inspection is placed between the source and the recording device while being rotated about different axes. Individual images are stored in a computer and reconstructed to form a three-dimensional image [34]. Recently, engineering applications of CT have increased substantially [36], [37].

In general, CT is a volumetric method, i.e. any feature to be detected must have adequate volume. Consequently, disbonds that are in intimate contact cannot be sensed using this technique. CT has been used for detection of common material flaws in adhesive bonds of a T-spar to panel section in an aerospace application [37]. Results were compared to those from conventional UT data. Although both methods were capable of indicating the defective regions in size and location, UT could not provide cross-sectional information on the cause. Tests on other specimens proved high applicability of CT to detection of resin-rich and resin-starved areas as well as fiber misalignment. Nonetheless, it must be emphasized that the cost of this method is significantly higher than that of other methods. CT should therefore be preferred in manufacturing control rather than for in-situ testing.

4.6.4 Safety considerations

An important aspect of radiation is that, as materials are penetrated, it ionizes matter by knocking electrons out of their orbit, thereby changing their electrical balance. Unless adequate precautions are taken to block radiation, such ionization eventually causes alterations in the human tissue. Furthermore, lack of human perceptibility to these forms of radiation makes RT extremely dangerous when operated in-situ, particularly if done so by inexperienced personnel. Damage to human cells is mainly dependent on the amount of radiation that has been absorbed during exposure.

The three essential safety parameters in radiographic testing are time, distance, and shielding. Generally, shorter exposure times are most favorable. Also, farther distances to the area of testing are preferable, since exposure decreases with distance by an inverse-square relationship. Lastly, shielding through the use of lead protectors can block most of the electromagnetic radiation. One should be aware of these indispensable safety precautions before considering radiographic inspection as a potential in-situ NDE method.

4.6.5 Capabilities and limitations

One of the most outstanding advantages of radiographic testing is the extreme accuracy and sensitivity that can be obtained. Most types of defects can be detected, including porosity and matrix cracks. Further, no surface contact is required; hence almost any geometric configuration can be inspected. This also holds true for maximum thickness, where RT allows for a broad range that encompasses both thin membranes as well as solid concrete members. Since radiographic imaging has been used for many decades, equipment is readily available and most of the capabilities and limitations are well understood.

In an adequate laboratory environment, most of the safety hazards related to radiography can be eliminated, leaving little chance for damage to humans. Also, the energy levels required for operating RT equipment are more readily available in stationary testing. In contrast, in-situ inspection requires a mobile energy resource to be situated in the field, while the largely uncontrollable environmental factors and variable site conditions tend to impose significantly higher risks of operation. The safety precautions stringent to RT typically come at a higher cost and can disqualify the technique based on unjustifiably high expenses, which may further go to the expense of flexibility and rapidness of an in-situ method. Summarized, safety and energy supply remain as two of the main drawbacks that must be taken into consideration, as they are important factors for both contractors and inspectors.

Nevertheless, if these factors can be controlled, the excellent sensitivity and resolvability of RT imaging can result in a highly transparent inspection of solid components and possibly provide the most comprehensive information among all formerly discussed NDT techniques. Undoubtedly, the method provides the most exhaustive information on defects of extremely small size, which makes it preferable for certain well-controllable inspection environments.

4.7 THERMOGRAPHIC TESTING

4.7.1 Fundamentals and theory

In a general sense, thermography entails measurement and graphing of isothermal contours on the surface of an object [38], in that it displays the effects of temperature differences in materials caused by presence of internal discontinuities. In theory, all heat transfer within a material as well as transfer from one material to another is related to conversion of heat energy. Herein, different methods of thermography are used, which can be classified as either *passive* or *active*.

The passive form of thermography monitors anomalies in temperature profiles of a part under normal environmental or operating conditions. Examples of passive inspection are thermographs of a roof structure or operating machinery, since both components store internal energy and are thus capable of radiating thermal signals without the need for external excitation. The former examples differ insofar as structural components obtain energy predominantly from ambient sources, such as the sun, whereas operating machinery develops heat by means of internal friction. Because a quantitative assessment of the heat emitted from these sources is oftentimes not possible, passive thermography is mostly qualitative in that it is used to simply pinpoint anomalies [39].

In contrast, active thermography uses external heat sources to induce energy into the specimen and thereby characterize defects on a more qualitative basis. For a majority of sources, duration, magnitude and frequency of the electromagnetic wave are known entities that can be controlled and adjusted by the user. Lately, a variety of techniques has become available for active thermography, which will be discussed Sections 4.7.3.1 through 4.7.3.3.

4.7.1.1 Forms of energy transfer

Heat can be transferred by one of three modes: *conduction*, *convection*, and *radiation*. Which mode is predominant mainly depends on the medium in which the energy transfer is taking place. As such, transfer in solids primarily occurs in the form of conduction, where two adjacent molecules transfer thermal energy between themselves. Fourier's law describes how much heat is transferred and is expressed by:

$$Q = \frac{k}{t \cdot A \cdot \Delta T} \qquad \textbf{(4-5)}$$

In the above equation, k describes a material's *thermal conductivity*. Materials with a high k-value, such as metals, are efficient conductors of heat energy, i.e. heat flow through the material occurs fairly rapidly. Composites, in contrast, are relatively poor conductors. This property comes as an advantage to thermographic inspection, since differences in the heat pattern, which are representative of anomalies, approach thermal equilibrium at a relatively slow rate. Hence, discontinuities can be distinguished over a longer period, leaving more time for inspection and data acquisition. Furthermore, a higher contrast can be obtained in materials of higher thickness.

Convection primarily occurs by subsequent mixing of molecules and is thus mainly present by the interaction of liquids or gases. This is important in thermographic imaging, since water or wind forces acting on a surface can significantly affect its temperature.

Radiation is inherently different from both previous forms of energy transfer in that it is a form of electromagnetic radiation. So-called *infrared* radiation (IR) possesses certain characteristics that are similar to those of light or x-rays, although it is of significantly lower frequency and hence longer wavelength. As indicated in Figure 4.4, the spectrum of infrared radiation ranges from roughly 10^{-4} to 1 cm in wavelength. Hence, IR is comprised of waves exhibiting much lower energy compared to x- or gamma radiation; this allows application with virtually no safety restrictions. In addition, IR-sources required for development of infrared radiation show a much lower energy demand. While x-ray equipment is operated in the kV range, IR-radiation can be generated from only a few volts.

Similar to conduction, radiation is governed by a thermodynamic relationship, given as:

$$Q = \sigma \cdot \varepsilon \cdot T^4 \qquad \textbf{(4-6)}$$

Radiation, governed largely by its material specific parameter ε, denoted as *emissivity*, may be viewed as one of the main parameters in thermographic imaging. When electromagnetic radiation is given off by an external heat source and allowed to interact with a surface, it can be reflected, transmitted or absorbed. Here, the corresponding parameters are denoted as *R'*, *T'* and *A'*, respectively. Due to conservation of energy, the total energy present can be divided into these three components:

$$\textbf{R' + T' + A' = 1} \qquad \textbf{(4-7)}$$

with their sum being equal to 100%. Since most materials that are inspected via IR are opaque, the transmitted part can be omitted from the equation, leaving only those fractions that are either reflected or absorbed. If $R' = 1$, the surface reflects all the energy, almost acting like a heat mirror, and no assessments about the internal material properties can be made. Although no such material exists, most metals approach a value of 1. On the other hand, emissive objects with $A' \cong 1$ reveal most about their internal temperature composition.

For most nonmetals, such as composite materials, emissivity lies in the range between 0.8-1 (it can reach values as high as 0.98 for pure graphite [39]) indicating their suitability for thermographic inspection. Generally, it is not recommended to make IR measurements on materials with emissivities below 50% [6]. One must further be aware of the fact that emissivity of a material can be affected by various environmental factors. As such, surface condition, temperature and angle of view are parameters that must be monitored carefully to ensure consistency of results [6, 39].

4.7.1.2 IR transmission

To allow monitoring of the emitted IR radiation, it must be effectively transmitted from the test surface to the detecting unit. In most applications, radiation must pass through the atmosphere, which happens to be fairly transparent to IR radiation. The simple fact that a medium is transparent to light does not indicate that the same holds true for IR. In fact, heat radiation is most effectively transmitted in one of two wavebands, 2-6 μm and 8-14 μm. Between these ranges, air allows only limited transmission of infrared radiation. Since recording devices are typically in the form of a camera, lens material as well as CCD devices have to be matched such that they allows transmission/reception of thermal radiation.

4.7.1.3 Defect detection

Although CFRP materials consist of two distinctly different phases, a properly laminated composite material will have relatively uniform thermal characteristics. Once a disbond, delamination or other anomaly has been introduced, the thermal pattern within the composite will be altered. As with other NDE methods, the sensitivity of thermographic inspection has its limitations when it comes to the type and size of a defect in particular. Because different materials possess different values of thermal conductivity, regions such as disbonds or air inclusions tend to build up heat, thus indicating the location and size of the flaw.

Figure 4.26 shows a comparison between thermal patterns in steel and composite materials. Assuming equal magnitude and duration of the heat imposed onto both samples, the composite sample will conduct heat at a slower rate; i.e., thermal energy does not spread as rapidly throughout the part as it would in the case of a steel sample of comparable dimensions. Also, as may be seen, heat propagation will occur more rapidly along the fiber direction. The significantly higher conductivity of carbon facilitates more rapid heat propagation compared to the transverse direction.

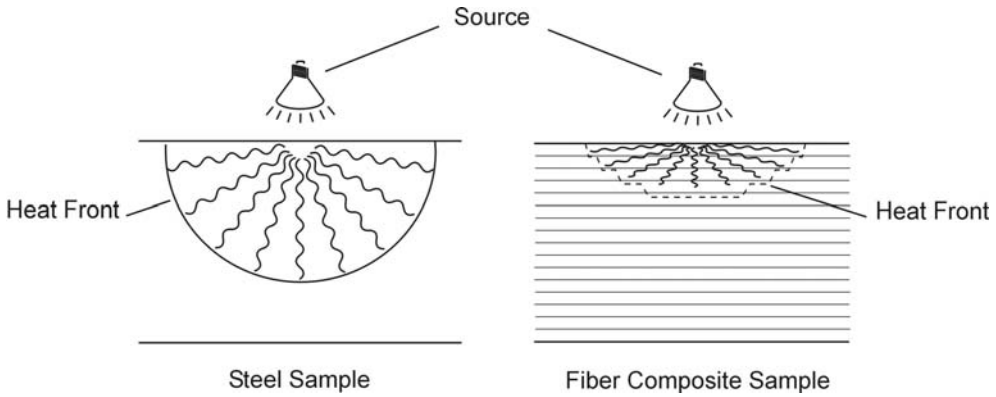

Figure 4.26: Thermal conduction in (a) steel; and (b) composite samples

4.7.2 Instrumentation

A complete thermographic imaging system for active thermographic inspection is typically comprised of a thermal stimulation system (air guns, heat lamps, etc.), an IR camera and an image and analysis system (display, TV, etc.). In passive thermography, however, ambient or internal heat sources substitute for an external heating device.

4.7.2.1 Stimulation devices

Thermal perturbations can be deployed in two forms, either by cooling the specimen or by heating it. Which device is given preference is mainly dependent on the specific application as well as the material's thermal properties. Examples of cooling devices are liquid nitrogen spray or cool water jets. High-powered lamps, photographic flashes, laser beams or heat guns/air jets, typically perform external heating. The main desirable characteristics of these devices are consistency and reproducibility. These parameters are important to conduct continuously representative tests over longer time periods without experiencing loss in heat energy that might yield different results. Herein, the level of automation is of extreme importance, as non-uniform heating will lead to heat buildup, which may later be interpreted as an imbedded material flaw.

Consequently, heat intensity, distance to the source, exposure time, and the heating/inspection intervals must be held consistent. While this is most successfully done using a fully automated system, manual heating assemblies can also make use of features that ensure a more uniform and reproducible introduction of heat into the part. One such example is the semi-automated heating tool as shown in Figure 4.27. Although manually operated, an integrated driving mechanism allows movement over the part surface at near-constant velocity and distance. By altering wheel diameter and velocity, this tool can adjust to a range of material and test conditions.

Figure 4.27: Semi-automated heating device

Depending on the emissivity of the material under investigation, the duration of the heat (or cooling) pulse must be adjusted. Materials with high emissivity generally require longer exposure times compared to materials that show high conductivity/low emissivity. A calibration procedure might be required to adjust the impulse duration to obtain the most insight to the material properties.

4.7.2.2 IR cameras

The primary function of IR cameras is the conversion of radiant infrared energy into a detectable electric signal. An essential parameter is described by the minimum measurable temperature difference, which is directly related to the sensitivity of the detection device. Most modern cameras are capable of detecting temperature differences as small as 0.1°K (0.18°F) [10]. On more advanced units, temperature gradients in the milli-kelvin range can be discriminated. Many of the modern devices are similar to conventional CCD chips, since they form video images directly from on-chip electronics. Resolution is fairly high and is typically in the range of 752×582 pixels. To capture rapid changes in surface radiation at a sufficient detail, cameras are commonly operated at a minimum of 30 frames per second. For special applications, where short heat pulses are used for external heating, frame rates of up to 60 frames per second or more might be preferred.

Cooling mechanisms are often used on these cameras to enhance detectivity by reducing ambient electromagnetic noise to an acceptable level. This can be performed by use of *cryogenics* or through thermoelectric elements, which cool down when an electric current is applied to two dissimilar metals. The cost for portable infrared cameras typically ranges from $25,000 to $70,000, depending on the sensitivity and resolution of the CCD unit.

Users should be aware of the fact that lenses for IR cameras are substantially different from those used for conventional video recording. Whereas conventional lenses are transparent to visible light, IR lenses are manufactured from germanium, silicone or zinc selenide, which are opaque to visible light. However, these materials are highly effective in transmitting infrared radiation, as discussed in Section 4.7.1.2. As shown in Figure 4.28, the overall dimensions of IR cameras are mostly comparable to those of conventional video camcorders, which makes them highly preferable for environments that require high mobility and flexibility.

4.7.2.3 Analysis systems

As most IR cameras are not equipped with integral imaging systems, image display and data analysis must be performed utilizing a remote system. Such remote analysis systems are comprised of an electronic unit that converts the electric signals of the IR cameras into a thermal image. A number of controls are available to adjust for thermal level, range, emissivity and other parameters [6]. The processed data is most conveniently imaged on a liquid crystal display (LCD) in either grayscale or color to allow rapid visualization of critical areas and to further identify those that may require a more detailed inspection.

Figure 4.28: IR camera

While grayscale provides sufficient detail, color imaging should be preferred for in-situ applications where difficult lighting conditions may otherwise hinder correct interpretation. A number of different color palettes can be selected to display various radiometric parameters. Typically, the display selects a series of distinct colors, each covering a specific window or range of the total frequency band. The use of computer programs further enables the user to perform a number of on-screen modifications and allows the export of data into spreadsheets for further analysis. Examples of a typical computer analysis system and a hand-held LCD unit are shown in Figure 4.29 and Figure 4.30, respectively.

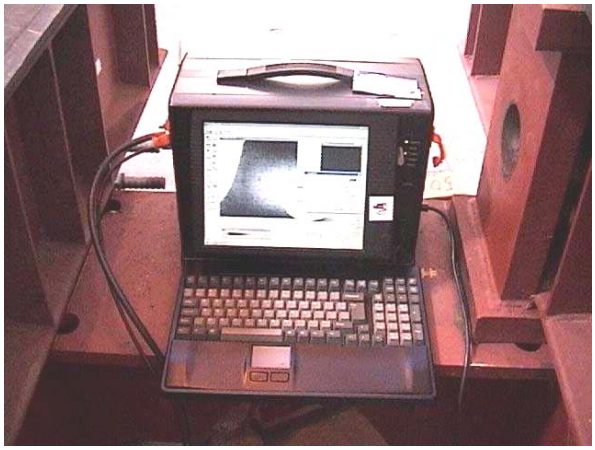

Figure 4.29: Portable IR analysis system

Figure 4.30: Hand-held LCD screen

4.7.3 Techniques and applications

Due to the advantageous thermal properties of composite materials, thermographic NDT has found extensive use over the past decades [10, 40, 11, 41]. As with ultrasonics, a variety of thermographic methods have been developed to suit individual material and geometric configurations. As discussed earlier, thermal testing can be either passive or active, depending on the availability of an ambient source and overall dimensions of the structure to be inspected. In most cases, passive thermographic testing is given preference on large projects, such as detection of heat-loss in sections of an entire building [42].

While passive testing of large areas can provide insight on variations in thermal diffusivity, the results are mostly qualitative and relevant only for evaluation on a structural level. For quantitative inspection, i.e. detection and characterization of defects, an alternate methodology must be followed. If magnitude and duration of individual heat pulses are known, a more exact study on internal properties can be pursued. Hence, active methods are generally preferred for NDE of composites, as duration and energy of the heat pulse are more easily adjustable. In the following sections, some of the most frequently applied methods are reviewed and discussed.

4.7.3.1 Pulsed thermography

Pulsed thermography can be considered the foremost thermal stimulation technique [39]. Herein, a heat pulse of relatively short duration, exerted from a conventional lamp, heat gun, strobe light or laser beam, is directed at the test surface (Figure 4.31), causing a thermal front to propagate into the material by means of diffusion. The corresponding thermal image of this process is depicted in Figure 4.32. As may be noted, heat generated by the strobe light appears in white, indicating a high level of intensity.

Figure 4.31: Thermal stimulation using a hand-held source

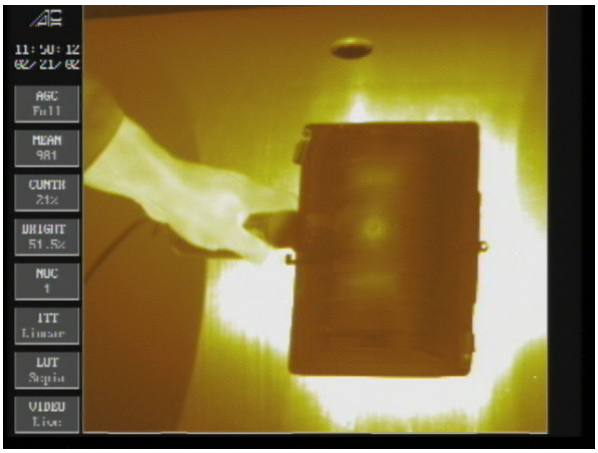

Figure 4.32: IR image of thermal stimulation

Upon completion of the thermal stimulation, a temperature decay curve of the specimen surface is continuously monitored and recorded by one or multiple external recording devices. Presence of any subsurface anomalies will alter the rate of diffusion with respect to the surrounding area. As such, entrapped pockets of air tend to retain heat longer and serve as so-called *hot spots*. This phenomenon is mainly due to the low thermal conductivity of air as well as the comparatively high heat flow rate in the surrounding material.

As discussed in Section 4.7.1.3, areas of low thermal conductivity will inhibit rapid heat flow through the material and thus restrict loss of thermal energy during the cooling cycle. An example of such thermal energy buildup in a filament-wound CFRP shell is illustrated in Figure 4.33. During specific instances of the cooling cycle, both helical and localized regions of higher intensity could be identified, serving as possible indicators for

resin buildup in regions of tape overlap and air entrapment in-between winding cycles performed at various orientations.

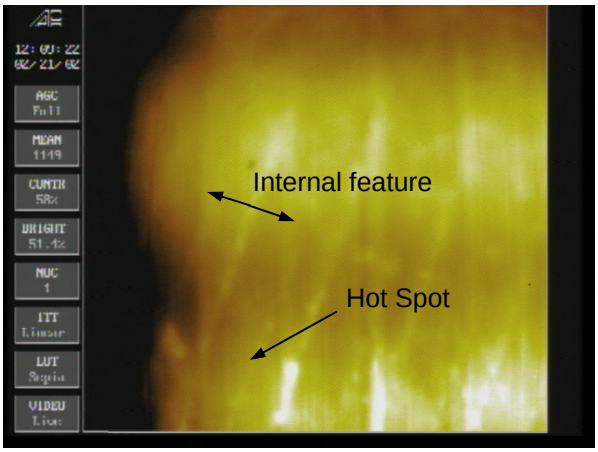

Figure 4.33: IR image of thermal gradient caused by internal anomalies

Although differences in thermal conductivity apply to composite materials and metals alike, the low emissivity of latter often restricts imaging of thermographic contours altogether (Section 4.7.1.1). Due to the rapid flow of thermal energy through metallic bodies, duration of the heat pulse is mainly governed by the conductivity of the material. Herein, metals require only short pulses of a few milliseconds whereas composites may necessitate exposure times of up to several seconds. If long exposure times were to be used on metals, the rapid propagation of thermal energy would overwhelm most of the information given off by localized internal anomalies.

For anisotropic materials and laminated composites in particular, it should further be noted that conductivity varies significantly among the various configurations, mainly depending on the specific fiber type, layup sequence as well as fiber, resin, and air contents. As such, glass fiber reinforced polymer (GFRP) composites generally show a low conductivity, whereas certain graphite fibers can have conductivity comparable to metals, as may be seen in Table 4.2. Hence, to capture the temperature decay of CFRP to the desired detail, higher frame rates may be required.

Table 4.2: Thermal conductivity of various materials

SUBSTANCE	THERMAL CONDUCTIVITY, k [W/m-°C]
Carbon Fibers (longitudinal)	84
Carbon Fibers (transverse)	0.84
Epoxy Resin	0.18
CFRP (transverse, $V_f = 65\%$)	0.72
Steel (20°C)	36-54[†]
Concrete (20°C)	1.37

[†] depending on carbon-content

Alternative to monitoring the temperature decay curve on the heated side of a component, one may chose to allow transmission of heat through a part and capture the heat signature on the far surface. In this arrangement, heat flow through a part will be restricted in regions of low *k*-values (voids, porosity, volatiles or water), resulting in a region of lower temperature to be noted in the heat-contour image. Since this arrangement requires access to both sides of a part, applicability of through-transmission is mainly restricted to parts of minimal thickness. On structural components, through-transmission would typically require dismantling or may not be possible at all. The general test setup employed in both test arrangements along with a characteristic image obtained from each test setup are shown in Figure 4.34.

The use of pulsed thermography for inspection of CFRP materials has been well documented in the literature, including studies by Hawkins, Jones and Berger, and Maldague [11, 40, 43].

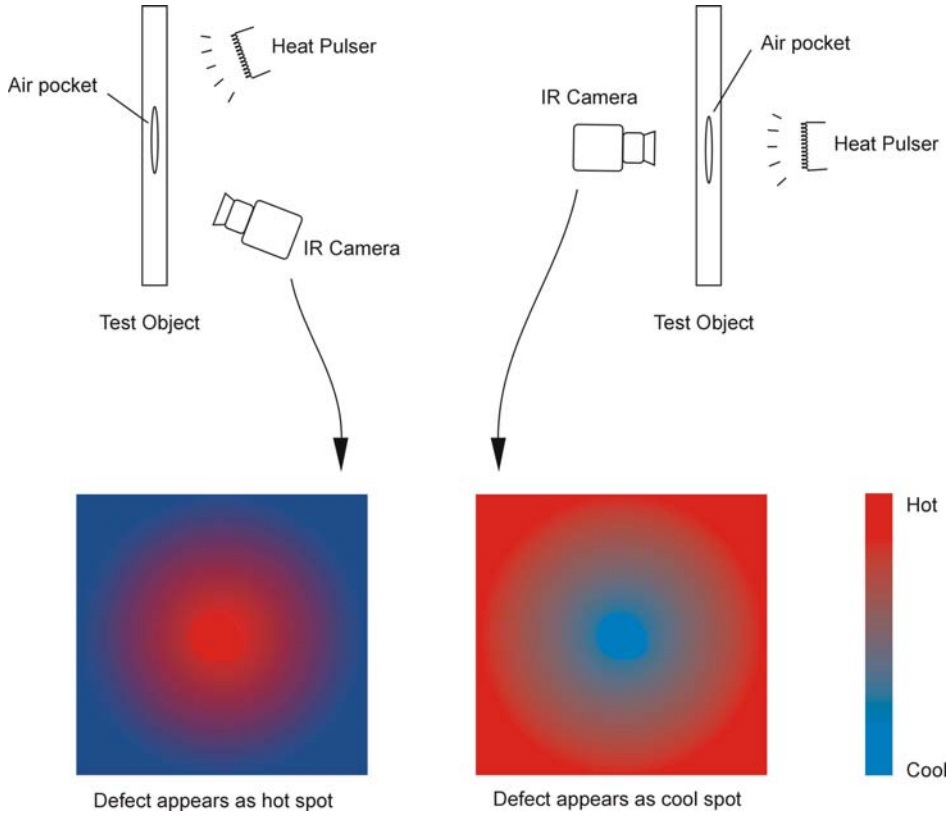

Figure 4.34: Qualitative representation of one-sided (left) and through-transmission IR testing (right)

Hawkins investigated the detectability of debonds on composite overwraps for circular concrete columns in an in-situ environment. In this study, the heat source consisted of 12 quartz lamps, having 500 watt/lamp, mounted on a semicircular frame. A distance of 100 mm to the test surface was kept constant while the fixture was descended from the top of

the column at a speed of about 70 mm/sec. Roughly 15 seconds after heating, IR images were captured. In order to ensure a damage-free inspection process, surface temperature of the composite never exceeded 40°C. It was shown that debonded regions in form of entrapped air pockets of about 100 mm in diameter could be identified using this method.

Reports on impact damage have shown that IR imaging is an effective tool for detection of barely visible impact damage [40]. The inspection was carried out on 0.25 in thick CFRP samples that had suffered a range of impact delamination. Tests were conducted using a quartz halogen lamp as the heat source and a camera in the 8-11 μm wavelength band as the receiving unit.

Inspection in both through-transmission and one-sided modes showed a large effect of the test mode on thermal contrast, and thus, detectability of damage. As such, increasing depth and decreasing flaw size yielded a decay in detectability for the one-sided inspection mode. For small flaws, the contrast approached zero, even at shallower depths. A comparison of this method to ultrasonic inspection and eddy current testing (to be discussed in Section 4.8), showed that IR pulse inspection was capable of revealing impact damage to a degree equivalent to that obtained from other methods.

The main advantages of pulsed IR testing are the ease of deployment for in-situ inspection and the relatively short inspection time due to surface-wide heating and monitoring [43]. Difficulties may arise in the computation of thermal contrast for which temperature differences between good and defective regions must be obtained. This, however, demands *a priori* knowledge on which areas are defect free [39].

4.7.3.2 Lock-in thermography

Modulated infrared thermography, commonly referred to as *lock-in thermography*, is increasingly being used for evaluation of CFRP materials. Lock-in refers to the need for synchronization of both the input (modulated heating) and the recorded signal. The technique is generally based on the submission of specimens to sinusoidal temperature stimulation (Figure 4.35). Such stimulation causes an oscillating temperature field inside the specimen, which can be recorded remotely through IR capturing devices. Sine-modulated external heating can be performed using a laser source such that both the amplitude and the phase of the signal become available. Since both parameters differ between good and defective regions of the laminate, conclusions on internal discontinuities can be drawn [44].

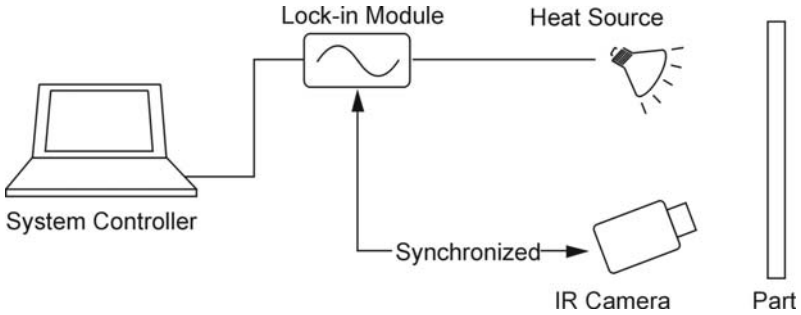

Figure 4.35: Modulated heating in lock-in thermography

In addition to the standard IR testing equipment, lock-in thermography requires use of a lock-in module that drives the heat source and is controlled by a system controller. During inspection, IR recording of the oscillating surface temperature is synchronized with the modulation frequency and multiple images are taken per modulation cycle. These signal values are captured in the lock-in system and used to calculate the phase difference between object and heat source.

Successful application of this technique is reported by Bai and Wong [44]. They inspected specimens with 30 layers of CFRP lamina (totaling approximately 4.2 mm in thickness), containing various artificially implanted layers of Teflon film. Defect size ranged from 1 to 11 mm in diameter at depths between 0.28 and 2.8 mm. Both, the heat source and the IR camera were positioned on identical sides of the specimens at a distance of 0.5 and 0.6 m, respectively. The heat modulation frequency was varied over a predefined range to evaluate its effect on defect detectability.

It was found that, depending on defect size and depth, a "blind frequency" exists at which no distinct phase difference is apparent. Optimum frequencies also exist that are most suitable for displaying defects of a certain size and depth. While large defects could be detected throughout the entire depth range, phase differences of defects ranging from 1 to 6 mm in diameter were not sufficient for detection. However, because differences between the thermal properties of Teflon and CFRP are less pronounced than between air and CFRP, the detectivity of this specific application can be considered as conservative.

Summarized, lock-in thermography is capable of performing inspection of near surface defects in composite laminates to a satisfactory degree.

4.7.3.3 Vibrothermography

Instead of using an external heat source, vibrothermographic imaging uses the effect of externally induced mechanical vibrations to release heat energy inside the test object, as shown in Figure 4.36. Even in the elastic range, heat is emitted by dissipation of mechanical energy through nonconservative micromechanical deformation processes such as dislocation motion, impurity diffusion, and other complex atomic activity [38].

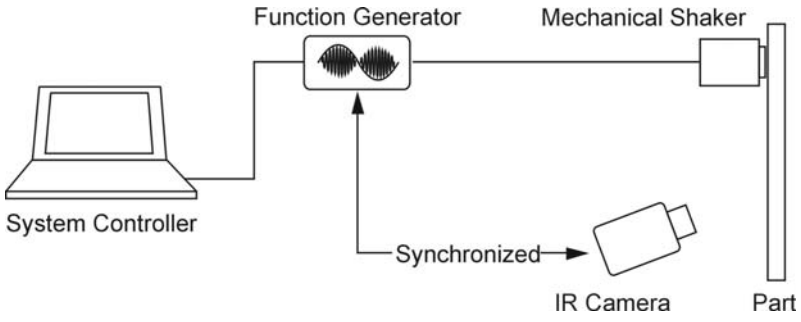

Figure 4.36: Vibrothermographic testing

For polymeric composite materials, it has been shown that viscoelastic dissipative hysteresis dominates heat generation [45]. It may be assumed that these dissipative mechanisms remain below a level that would be considered destructive testing of the material. When excited, the presence of stress concentrations at flawed regions in the material will cause a disturbance in the vibration mode shapes and thus be observable in the heat pattern. Using conventional real-time IR imaging, thermal gradients on the part surface can be recorded and interpreted.

The most important parameters in vibrothermography are the amplitude and frequency of the mechanical excitation. To fulfill the definition of nondestructive testing, the amplitude of stress/strain levels must be limited to roughly one third of that equivalent to failure of the material under inspection. For most situations, such amplitude levels are sufficient to produce observable heat patterns [38].

A trial and error procedure is often followed to determine the frequency at which thermal patterns develop. Since most of the energy-dissipating mechanisms are frequency dependent, a steady increase of frequency throughout the predetermined frequency band is practiced. The typical excitation frequencies range from 0 to 25 kHz, while most heat patterns in composite materials are created in the range between 5 and 30 kHz. It has been found that formation of thermal patterns is highly sensitive to the applied frequency. As such, variations of ±0.5 kHz from the resonant frequency can cause thermal gradients to appear or vanish [38]. Hence, a gradual increase in excitation frequency over the entire frequency band is essential in finding the most suitable test condition.

Apart from the equipment listed in Section 4.7.2, vibrothermographic testing requires utilization of mechanical shakers. For high frequency excitation, electromagnetic coils or piezoelectric transducers are commonly used. Further, a suitable couplant is required to efficiently transfer mechanical energy from the excitation device to the part surface.

Reports on experimental evaluation of vibrothermography for detecting delamination in CFRP strips are given by Rantala et al. [46]. Instead of using constant excitation amplitude, lock-in amplitude modulation, as discussed in Section 4.7.3.2, was utilized. To generate sufficient hysteresis energy per time while ensuring purely non-destructive test conditions, high excitation frequencies were chosen. This enabled the examiner to keep the amplitude below the critical level or one-third the failure stress, as mentioned earlier. In contrast, improved depth range was obtained via the use of low-frequency amplitude modulation.

Unlike lock-in or pulsed thermography, vibrothermographic inspection provides more insight into the mechanical state of the material, because thermal patterns are directly related to mechanical stress, while those of techniques discussed in Sections 4.7.3.1 and 4.7.3.2 are based on differences in thermal conductivity. Compared to other IR techniques, vibrothermography can detect defects such as closed cracks or delaminated regions (cold bonds), which are not detectable by pulsed IR or lock-in thermography. Also, the method has proven to be highly suitable for in-situ inspection, provided that the mechanical excitation can be achieved.

4.7.4 Capabilities and limitations

Independent of its specific form, thermographic imaging has significant advantages over many other NDE techniques, primarily due to the fact that it provides a quick and more comprehensive insight to material properties. Due to the capability of covering large areas at relatively short duration, thermography can be applied in both near- and full-field. The high sensitivity of modern recording equipment (±0.1°K temperature difference) provides spatial resolution with such detail that thermal imaging is often prioritized over visual inspection [6]. An example of the extremely high sensitivity of modern IR cameras may be seen in Figure 4.37, showing the heat gradient induced from a human fingerprint on the surface of a CFRP shell structure. The duration of heat introduction was only about one second.

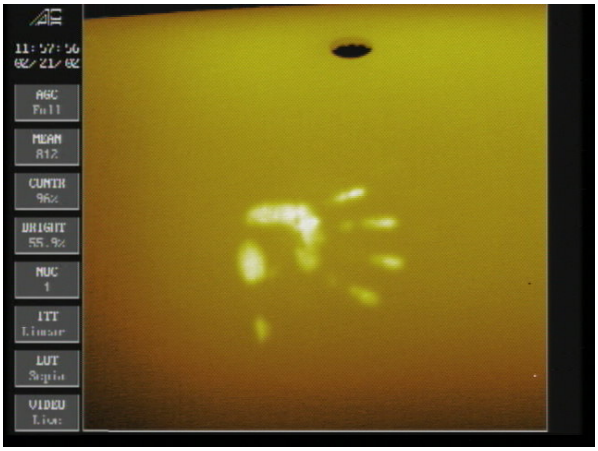

Figure 4.37: Fingerprint on a CFRP shell

Being a non-contact technique, it allows inspection of highly complex geometric configurations. The high portability of a complete thermographic system of less than 2.5 kg (~5 lb.) gives further support to thermography as a suitable field inspection method.

Although difficulties can arise using reflective or highly conductive materials, composites are nearly ideal for thermographic imaging. Their high coefficient of emission of about 1, in combination with typically low values of thermal conductivity, allows for high contrast imaging of thermal gradients. Also, in vibrothermographic examination, their high loss angle (or damping of elastic waves) provides an efficient conversion from mechanical to thermal energy [46].

Nevertheless, thermography has its limitations with respect to depth range and defect characterization. Since only the surface of an object can be viewed thermally, internal defects must be of sufficient magnitude to affect heat transfer at the surface. As discussed previously, small defects at considerable depth can rarely be identified. Moreover, assessment of the defect type depends largely on the experience of the inspector, because thermal patterns simply reveal

regions of stress concentrations, which can originate from a variety of different defects, such as porosity, voids, fiber breakage, etc.

Under field conditions, a number of environmental effects may further complicate inspection with infrared sensors. Because all thermal mapping is dependent on fluctuation in surface heat patterns, any rapid variation in ambient temperature may restrict the use of thermographic imaging. Factors like rapid changes in sun intensity, precipitation or wind can possibly influence heat patterns to a degree that will result in erroneous IR readings. Thus, to provide stable test conditions, adequate protection from random ambient radiation must be provided at all times during testing.

4.8 EDDY CURRENT TESTING

4.8.1 Fundamentals and theory

Due to their non-magnetic nature, composite materials are largely unsuitable for magnetic inspection techniques. Specifically, the use of magnetic particles, a method that finds extensive use in NDE of metallic substances, cannot be applied to composites. Nevertheless, carbon-epoxy composite materials are suitable for inspection via electromagnetic induction, since carbon allows for transport of electrons among atoms. Although the material itself cannot be magnetized, it is amenable to magnetic lines emitted from electromagnetic coils or other similar induction devices.

The inductive nature of carbon fibers has been utilized for NDE of composites by development of the eddy current testing (ET) method. Eddy currents are produced when a coil circuit, driven by an alternating electrical current, is brought in close proximity to the test specimen. The alternating magnetic field that is caused by the driving coil induces a voltage into the test specimen. As a result, electrons in the material under investigation are forced to circulate in an eddy-like pattern, while the circular currents themselves form a magnetic flux field that can be picked up by either the driving coil or a second, separately placed coil (Figure 4.38). Alterations in current flow through the pickup coil can then be related to a number of material anomalies [6]. While induction of magnetic flux does not require contact between the coil and the test material, induction is highly sensitive to the lift-off (spacing between the sample and coil) and the angle between the induction coil and the test surface [47].

Performance of the ET method greatly relies on the electrical conductivity of the test material. Conductivity describes the ability of the material's atoms to conduct electricity, whereas resistivity, the opposite of conductivity, describes its ability to resist electric flow. How well a material conducts is solely governed by the number of electrons present in the outer shell of the atom. Materials with a high number of outer-shell electrons, such as seven or eight, are *insulators* and cannot develop electric flux. For carbon, two electrons are present in the outer shell, which classifies it as a *conductor*. Any material of such atomic composition is capable of transporting electrons among its atoms. While electrical conductivity can be assumed as a constant value depending on the specific material composition, it can be influenced by variations in temperature as well as the frequency of the driving coil [6].

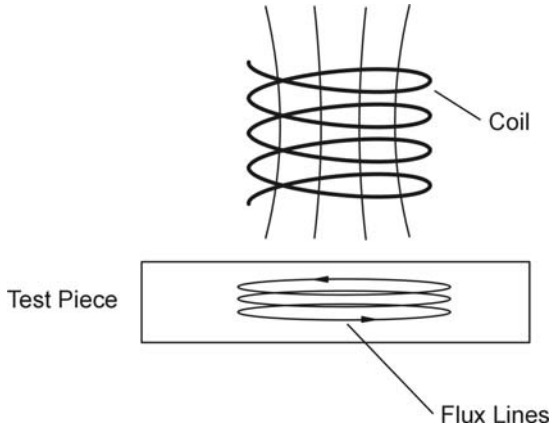

Figure 4.38: Induction of electromagnetic flux

Unless the test material is interspersed with boundaries or discontinuities, eddy currents flow in circular patterns. Upon encountering a material anomaly, the eddy current flow is likely to be altered, which corresponds to a change in the current flow in the pickup coil. Although a number of material defects can be detected using eddy currents, the size and orientation of the defects are the governing factors for detectability. In order to be noticed, the defect must be of considerable size such that it can cause a detectable change in the current flowing through the pickup coil. Since flux lines travel in circular paths, defects oriented tangential to the line pattern are more difficult to detect than those that are located perpendicular, as depicted in Figure 4.39.

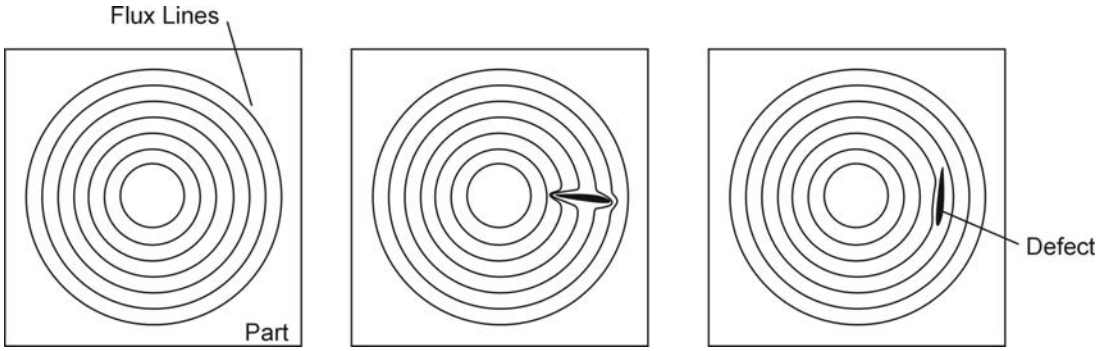

Figure 4.39: Flux patterns near material anomalies

Similar to other NDE methods, ET entails specific performance criteria that define its suitability for non-destructive evaluation purposes. These include sensitivity, penetration and resolution. While the highest sensitivity in near surface regions can be achieved in materials with high electrical conductivity, penetration decays rapidly with increasing depth. This is due to secondary flux, in which the flux lines developed in the test material cause cancellation of the primary flux induced via the driving coil. Due to a low resistivity (i.e. high conductivity), this phenomenon is particularly pronounced in most metallic substances, such as iron and steel.

Since the driving coil utilizes an alternating current to induce the magnetic flux, its driving frequency can be adjusted to obtain the best results. Commonly, frequency ranges between 50 Hz and 10 MHz are used [6]. As in ultrasonic testing, an increase in frequency results in increased sensitivity to small discontinuities, while penetration into the material is significantly reduced. As a rule of thumb, the coil diameter defines the maximum penetration depth, while it also governs the minimum equivalent defect size detectable [6].

In CRFP materials, fibers are the only conductive component. Hence, only defects that are directly related to damage or disorientation of fibers can be sensed by this method. Depending on the specific type of CFRP, its electrical resistivity can vary between 3,300 to 10,000 μΩ-cm in direction parallel to the fibers and 140,000 to 50,000,000 μΩ-cm in the transverse direction [47]. This implies a much higher penetration depth for CFRP as compared to most metals, which have resistivity values that range from 16 to 60 μΩ-cm [6]. However, it requires much higher excitation frequencies to provide sufficient interaction between the eddy fields and the material. As a result, special coil arrangements may often be required.

4.8.2 Instrumentation

The test equipment for eddy current testing is generally comprised of an alternating current (AC) generator and processing unit as well as a coil of variable size and arrangement. Modern instruments are compact in size and light enough so they can be easily transported.

4.8.2.1 AC generators and processing circuitry

The generator of most standard units drives the coil at only one frequency, which necessitates that the unit is matched to the specific application in terms of material type, dimensions and flaw to be detected. Common adjustments that can be made on a standard unit include frequency, gain (amplification of output signal), gates, filters, etc. A high-resolution display can be used to display important information simultaneous and convenient for the operator.

A significant advance of ET has been the introduction of multi-frequency units. Due to the fact that pickup coils are sensitive to a multitude of frequencies, signals from more than one source often combine to form a signal that becomes difficult to interpret. By using more than one frequency at a time, undesirable frequencies can be filtered out. Examples for this are inspections of non-metallic materials that are in close contact to a metallic surface. Such material combination often results in erroneous interpretation if using single frequency instruments. Other aspects of multi-frequency instruments include reduction of inspection time by simultaneous operation in two or more inspection modes, and near surface inspection at high frequency while penetrating deeper into the material by using a second, lower frequency [6].

4.8.2.2 Coils

Coils constitute an important element of the eddy current system since their size and arrangement is predominant in fitting the test object. While large coils provide means for scanning large areas at one time, they sacrifice sensitivity to small defects and are often

unable to pinpoint local material deficiencies. Conversely, the use of extremely small probes can result in a tedious and time-consuming inspection process.

The three main categories of coils are surface coils, encircling coils and internal coils. Only the former type will be addressed in this discussion, as encircling and internal coils are not suitable for external inspection of structural components.

4.8.2.2.1 Bobbin wound probes

A majority of coils used for surface inspection are made of wire wound around a hollow core and are commonly referred to as 'bobbin wound'. They are designed to be held perpendicular to the test surface and are highly sensitive to surface cracks and discontinuities that are oriented perpendicular to the test surface [6].

4.8.2.2.2 Gap probes

Also known as 'horseshoe' probes, these probes consist of a U-shaped ferrite core surrounded by a pair of coils around each end. Unlike bobbin wound probes, these probes induce flux lines that propagate from opposite poles of the U-shape. This mode of propagation yields higher sensitivity to planar discontinuities while being relatively insensitive to defects that lie perpendicular to the surface. As shown in Figure 4.40, these two types are coils can be used together to cover a wider range of possible defects.

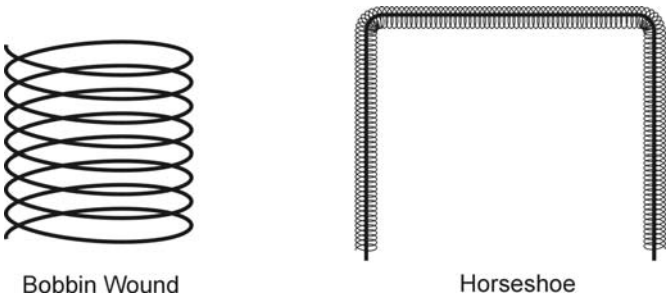

Figure 4.40: Major coil types in ET

4.8.3 Techniques and applications

Despite the fact that ET cannot be considered one of the predominant methods for NDE of CFRP materials, a number of research projects have proven its applicability. Oftentimes, it is used as a complementary method to confirm the results of other, more established test methods, such as radiographic or ultrasonic testing.

Experimental investigation of eddy current tests on CFRP has been conducted by several researchers [47, 48, 49, 50]. To obtain a comparison between results from ET and UT, Lane et al. investigated CFRP samples in a $[0/90]_s$ stacking sequence under influence of impact, tensile

failure as well as simulated delamination [47]. Results showed that ET is not capable of detecting separation of composite plies, which was attributed to the absence of fiber damage. In contrast, fiber breakage as a result of impact damage was detectable, even though low energy impact required UT as a complementary method. Finally, tension tests were performed to study the effect of deliberate fiber failure on eddy current signals. It was found that there is good correlation between visual fiber damage and signals obtained from the ET system. It was concluded that, unless fiber fracture was the predominant failure mode, ET distinguishes itself as more suitable in terms of discriminations than detection of damage.

Similar results were obtained by Degtyar and Pearson [48]. They investigated 0.25 in thick filament-wound graphite/epoxy rocket tubes for the detectability of impact damage. Initially, UT measurements were obtained to provide a baseline for comparison. A 0.375 in radius coil, operated at a single frequency of 2 MHz, was utilized to scan the 4x4 in specimens that were previously impacted at various energy levels. Results showed little variation in impedance of the pickup coil with only slight deviations over regions where fiber damage had presumably occurred. This presumption was later confirmed by baking off the matrix and deplying the laminate layer by layer. It was concluded that ET provides complementary information on damage in impacted CFRP specimens but should not be chosen as the primary inspection method.

Further studies are reported by Gros et al. [50] who investigated ET and UT upon their suitability for detecting delamination in 0.04 in thick quasi-isotropic CFRP plates. Unlike the typical modeling approaches used in other NDE-studies, delamination was initiated by causing interlaminar ply separation between -45° and 90° plies under application of uniform tension. It should be emphasized that this form of delamination is inherently different from delamination induced by nonbonding material such as Teflon sheets, since delamination caused by tensile loading is not necessarily restricted to separation of plies, but can further result in damage or rupture of fibers. Although the sensitivity of ET in detecting delamination was shown to be lower than in UT tests, most defective regions could be located and characterized to a certain extent. Whether ET signals were caused by interlaminar ply failure or fiber rupture in the vicinity of delamination was not clearly addressed.

4.8.4 Capabilities and limitations

Although most effort in the arena of eddy current inspection has focused on metallic components, its use on CFRP has recently found increasing attention. Similar to ultrasonic testing, ET systems have steadily become more compact in size and have reached a high level of sophistication in terms of data acquisition and operation modes. Even though spot checks are usually performed manually, probes can theoretically be incorporated in an area scan unit, which can feed data into secondary processing devices such as a laptop. As a purely nondestructive method, no solvents, couplants or other substances must be applied to the surface in order to take measurements. The non-ferromagnetic nature of composite materials further aids in obtaining deeper penetration into the material. During in-situ inspections, results are usually available in real time, such that assessments on serviceability can be made instantaneously.

As outlined in the previous discussion, ET entails characteristics that allow only very specific inspection of CFRP composites. The fact that magnetic flux can only develop in regions of high

fiber density presents one of the most significant limitations of ET. Although fiber damage can be characterized in most cases, damage related to matrix cracking or nonconductive material inclusions, such as sand or oils, remain largely undetected. In applications where reliability is mainly governed by the tensile properties of the composite, the method provides suitable information on serviceability, since tension members experience failure primarily by fiber rupture. In bond applications, however, interply separation is more critical than fiber rupture, since fiber rupture is rarely experienced in externally bonded strengthening schemes.

In conclusion, ET may be capable of providing supplementary information on localized damage where fiber damage is either predominant or has been caused as a result of a secondary damage mode (impact, ply separation in tension, etc.). It should not be considered a method that can provide comprehensive insight on composite, and in particular, bond strength of composite systems.

4.9 MICROWAVE TESTING

Like infrared and x-radiation, microwaves are a form of electromagnetic radiation characterized by a distinct frequency band. Traditionally, the microwave domain is considered to encompass electromagnetic frequencies roughly between 300 MHz and 300 GHz. In the electromagnetic spectrum shown in Figure 4.4, this yields wavelengths of 10^{2} to about 10^{-1} cm [51]. As may be seen, this region coincides with that classified as 'radar'. In fact, the entire range of individual frequencies, including TV, radar, and FM radio are regarded parts of the microwave frequency band. In the lower end of this range, the spatial resolution of microwaves is thus in the order of 1 mm, which indicates their ability to discern closely spaced material features.

The imaging capabilities of microwaves is based on transmitting highly directed electromagnetic waves into a dielectric material and using the information of magnitude and phase to create images of the specimen [52]. Since penetration of microwaves into conducting materials can be considered minimal, they are commonly applied only to non-conducting materials. As discussed in earlier sections, carbon fibers classify as conductors; hence, there is a significant restriction in using microwaves as a transparent medium, especially in examination of relatively thick components. However, microwave NDE has found application in thick non-conductive composites such as GCFRP plates with thicknesses of up to 100 mm [52].

While microwave NDE has not found appreciable attention in the civil sector, a more pronounced body of work has been established in the more specified field of radar testing, with particular focus on ground-penetrating radar (GPR), to be discussed in Section 4.14. Although it has been shown that applicability of microwave NDE to carbon-epoxy laminates is limited, this report will provide a detailed review on the use of GPR towards characterization of civil infrastructure. Since radar has already found implementation into field methodologies, the authors feel that this review serves a more comprehensive understanding of radar technology and can thus aid in assessing its apparent limitations in NDE of CFRP-rehabilitated components.

4.10 OPTICAL METHODS

4.10.1 Fundamentals and theory

The field of optical testing entails a large variety of individual sub-methodologies that allow detection of almost infinitesimal surface deflections through formation of fringe patterns on the surface of an object. Limited by the wavelength of light, displacements of fractions of 1 μm can theoretically be measured [53]. Some of the most frequently applied methods include moiré interferometry, holography, and shearography.

Basic optical methods, such as geometrical moiré, utilize superposition of two gratings to cause formation of fringe patterns [54]. Similar to lines on a contour map, lines formed by moiré interference correspond to regions of equal displacement relative to a fixed reference point. Depending on the number and frequency of fringes in an area, one can derive the magnitude of in-plane displacement and corresponding strain in the material. Figure 4.41 illustrates fringe patterns resulting from superposition of a stationary (vertical) grating with a rotated (a) and horizontally strained grating (b), respectively. If the point of zero rotation and zero translation is defined to be located at fringe N_0 for the left and right image, respectively, each adjacent fringe is representative of a specific incremental rotation/translation. The absolute value of these displacements depends on the spacing between individual lines on the grating, denoted as *pitch*, which is the main factor governing the sensitivity of optical methods.

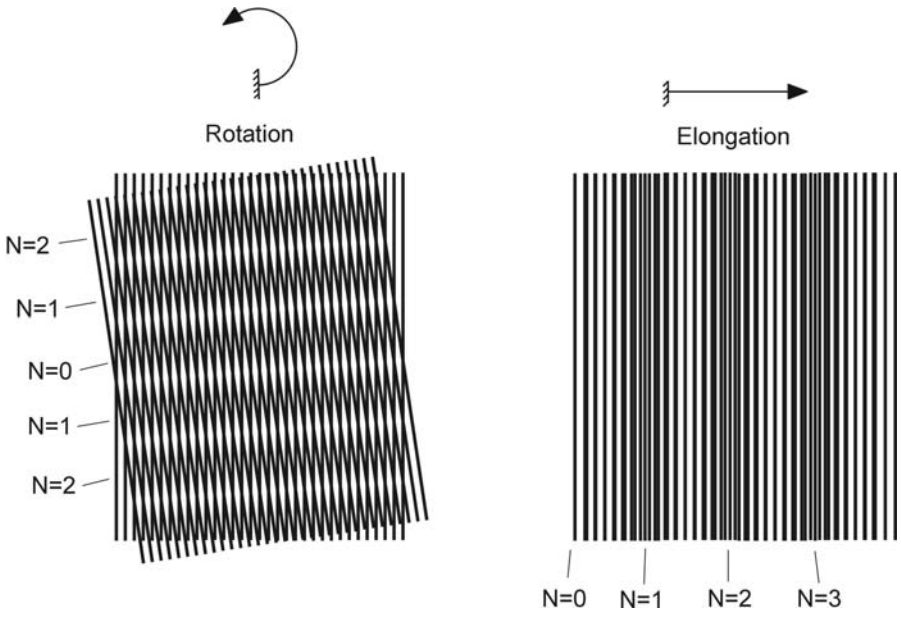

Figure 4.41: Moiré fringes caused by (a) Rotation and (b) Translation

In geometrical moiré, sensitivity soon reaches its limitations due to the maximum number of lines that can be physically situated on a unit length of material. To obtain a significantly larger

line frequency, the principle of optical interference of *coherent* light can be employed. As illustrated in Figure 4.42, interference of two coherent light beams results in regions of constructive and destructive interference, i.e. regions of presence and absence of light. If two of such gratings are superimposed, interference patterns of extremely high detail will result.

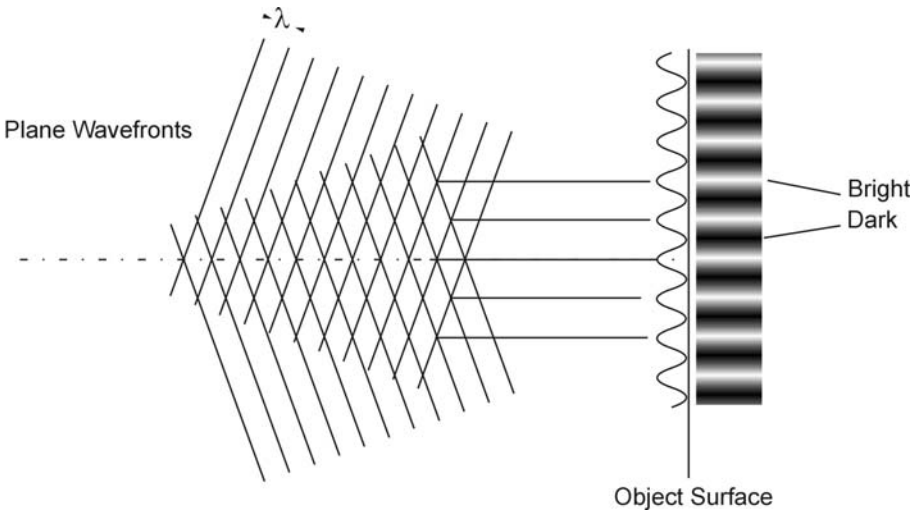

Figure 4.42: Interference of coherent light beams

To investigate displacement or strain on an object surface, a *specimen grating* must be attached directly to the object itself. In most cases, this is done with a special adhesive that is chemically formulated to provide full strain compatibility with the test object without causing a chemical or reinforcing effect to the object itself. A second grating, commonly known as the *master grating*, is situated between the specimen and the observing/recording medium.

During testing, a superimposed image of both gratings is recorded at distinct time instances. Preferably, these are instances of varying load levels, to allow interpretation of minute differences between the individual images. In all tests, one desires to relate the fringe arrangement to the actual displacements/strains in the material. While displacements and strains become readily available from the number of fringes over a certain area, stresses can also be obtained, assuming that material properties are known. Since most material anomalies induce stress concentrations to the host material, strain in such regions will deviate from that of a sound area. In many cases, strain patterns can be interpreted to detect material flaws, even if they are located inside the material [55, 56, 57].

As may be seen from Figure 4.41 b), the resulting fringe patterns only reveal information on the displacement and strain of the object in a single direction. Since the grating is oriented parallel to the y-axis, any object deformation along this axis would not cause alteration in the fringe patterns. To overcome this drawback, a cross grating can be applied to the specimen. However, this also necessitates two separate master gratings, oriented along the two principal axes.

Unlike all of the previously discussed methods, optical techniques require a stress to be imposed onto the material such that fringe patterns can be obtained. Hence, optical methods are inherently different from classical NDE techniques in that they necessitate application of an external or internal load, which can be of either a mechanical or a thermal nature. For evaluation of adhesive bonds, it has been shown that detectability is often more pronounced under thermal loading [56]. Other methods of external excitation include vibration, microwave or impact. For optical methods to remain truly nondestructive, the level of loading must not be taken to a level at which permanent deformation can be expected. Due to the high sensitivity set forth by the nature of light, minute strain levels are often sufficient to display most anomalies.

For defect analysis, advanced optical measurement techniques allow the continuous recording and evaluation of data via digital equipment, which have led to an increased interest in this form of NDE testing. In earlier applications, results could not be obtained in real time due to limitations imposed by the development process inherent to photographic films. Lately, digital acquisition has led to the ability of real-time imaging and more rapid quality assessment. This development has also increased the attractiveness of optical testing for in-situ applications. Particularly, the development of lasers has contributed significantly to the broad utilization of optical techniques. The fact that lasers emit *collimated*, coherent light makes them particularly useful for optical measurements. As such, lasers have found particular attention in speckle interferometry, a method mostly suited for out-of-plane measurement.

As opposed to the more sophisticated optical methods, geometrical moiré has found limited implementation into automated processes. In most applications, interferometric methods are given preference, mostly due to their extremely high sensitivity. In the following sections, only processes that show particular potential for incorporation into automated and rapid processes will be discussed in more detail.

4.10.1.1 Moiré interferometry

Interferometry combines methodologies of geometrical moiré with a more complex setup, thus allowing even higher resolution and flexibility. Since gratings in moiré interferometry are formed by optical interference of laser light, it provides whole-field patterns of high spatial resolution with a sensitivity of 2.4 fringes per μm [58].

In moiré interferometry, the master grating is formed by the interference of two coherent light beams that obliquely illuminate the specimen at two complimentary angles α. These beams typically originate from a single remote laser source whose beam is separated by means of beam splitters and broadened/redirected by beam expanders and several mirrors. Due to coherence, the beams generate walls of constructive and destructive interference, which results in a virtual grating in the zone of their intersection [58]. Although the interference of these walls is not visible in space, it can be made visible once the waves intersect an object and are reflected off its surface. Hence, the specimen grating is physical while the master grating is created virtually through light beam interference. A conventional setup for interferometry measurements is depicted in Figure 4.43.

As outlined in the previous discussion, complete full-field strain analysis requires two gratings with lines oriented perpendicular to each other. Such a setup can be obtained from two beam-pairs, while a cross grid substitutes for the formerly utilized linear specimen grating. Hence, one may obtain strain profiles in two orthogonal directions.

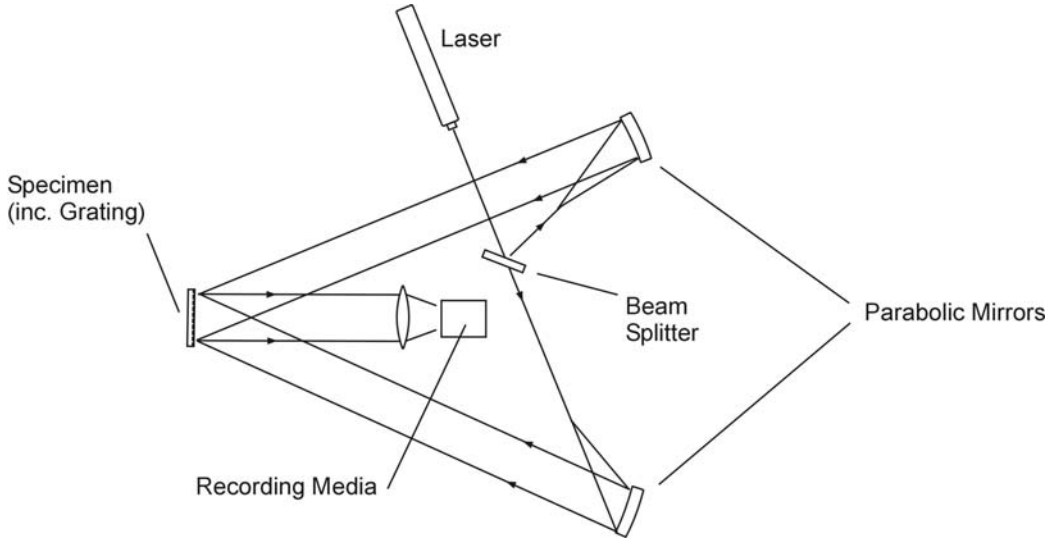

Figure 4.43: Setup for moiré interferometry

4.10.1.2 Holography

Compared to moiré interferometry, holographic interferometry (Figure 4.44) utilizes a slightly different test setup, which provides the possibility of creating perfect three-dimensional images from a body. Instead of causing interference of two beams in close proximity to the object to form a virtual grating, a reference beam is aimed directly at the recording media, while a second beam illuminates the test object. The preferably white surface of the object causes reflection of the scattered light waves towards the recording device where interference of the two beams occurs. In real time holography, results can be obtained instantaneously by looking at the image of the unstressed object superimposed on the stressed object [59].

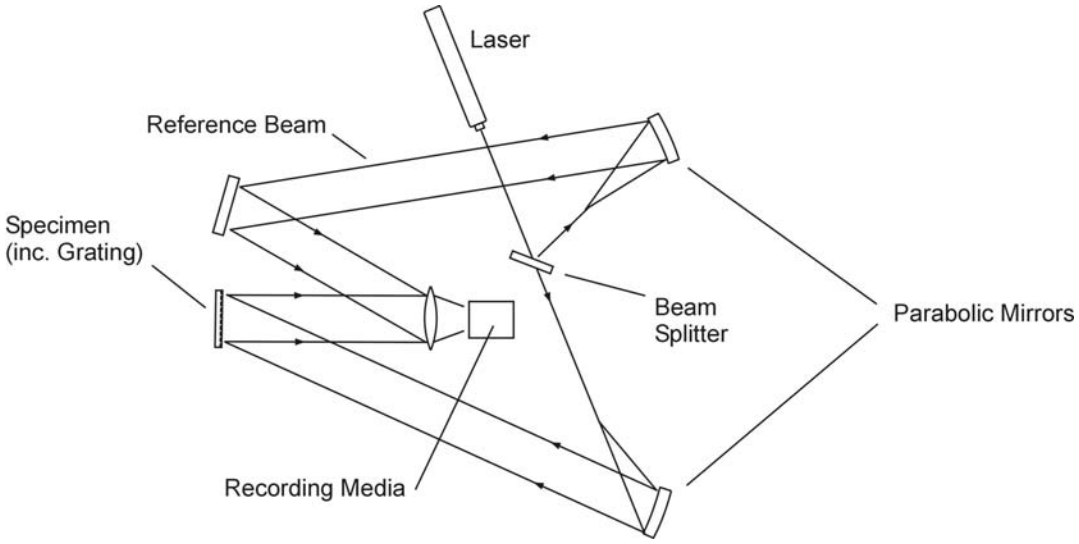

Figure 4.44: Test setup employed in holography

A significant advantage of this method lies in the fact that it does not necessitate a specimen grating, which might become undesirable especially due to practical or aesthetic restrictions. However, holographic testing has stringent stability requirements that are often difficult to assure in the field. Thus, this technique has mostly found application in laboratory experiments [59].

4.10.1.3 Shearography

Following the introduction of the laser, its *speckle effect* caused a considerable amount of disappointment for many years. A cause of this effect is the minute roughness of any surface that is not ideal specular, and it is experienced in the form of a grainy structure on any object surface that is illuminated by coherent laser light [53]. As in the previously discussed optical methods, scattering of coherent light from a single broadened laser source causes points of interference in the image plane in form of speckles. Recently, the potentials of this phenomenon have been employed in form of shearographic imaging of surface strain fields.

The key to object study in electronic shearography is a birefringent crystal that serves as a shearing device. This shearing crystal brings two nonparallel beams scattered from two separate points on the object surface to become nearly colinear [56]. As in sections 4.10.1.1 and 4.10.1.2, images taken at two different time instances display a slight alteration in intensity distribution and are thus related to surface strains. As a result of image subtraction, their differences can be visualized.

Shearography has certain distinct advantages over moiré interferometry and holography, which are summarized as follows [56, 55]:

- It employs a simpler optical setup.

- Since no reference beam is required, it alleviates the stringent environmental stability typically necessitated in holography.
- It provides a wider and more controllable range of sensitivity.
- It measures displacement-derivatives, which are directly related to strain, whereas interferometry and holography measure absolute displacements.

Similar to moiré interferometry and holography, flaw detection in shearography is based on the comparison of two states of deformation in the test object. While it is ideal to impose stresses similar to those found under service conditions, these sometimes induce intolerable rigid-body motion, causing decorrelation of the speckles in the two images resulting in degradation of fringe quality [56]. A number of loading techniques are known that normally do not produce the intolerable rigid-body motions, including pressurization, thermal stressing, vibrational excitation or impact stressing. The schematic setup of shearography is depicted in Figure 4.45.

4.10.2 Instrumentation

Depending on the optical method and the individual setup, a range of components is needed to complete an optical imaging system. However, most setups are comprised of an illuminating system, a set of beam splitters/expanders, mirrors and lenses, as well as the recording medium. In the following sections, the vital components will be discussed briefly.

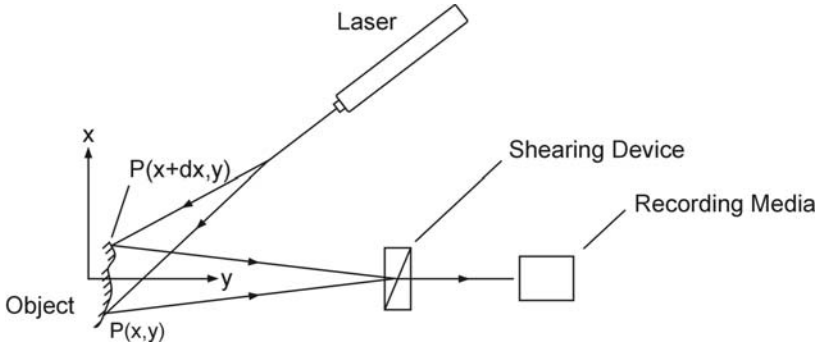

Figure 4.45: Setup for shearographic imaging

4.10.2.1 Light sources

An important variable of light sources for technical applications is their bandwidth, which describes the range of wavelengths that are emitted from a source. In conventional helium-neon or argon-ion lasers, the bandwidth lies in the order of 10^{-6} nm (10^{-15} m), constituting an extremely small range of dominant frequencies. Consequently, the output is comprised of a single wavelength of 632 nm, 514.5 nm or 488.0 nm, for red, green and blue-green lasers, respectively. Secondly, laser light is said to have high *spatial* and *temporal coherence*. These characteristics relate to the fact that waves are created in the laser at almost the same instant in time as well as at the same point in space. Lastly, the

laser output beam is so well directed that it can be considered a perfect point source, whereas most other sources are extended sources due to their significantly broader emissions [58].

Today, laser sources are readily available and particularly tailored for many applications in research and industry. Although lasers are much more expensive than conventional light sources, they offer unsurpassed possibilities for optical testing. For use in mobile units, small laser diodes have been developed that run at about 50 mW and are capable of covering areas of up to 400x400 mm^2, provided that the system is not operated in direct sunlight, since this can greatly reduce fringe contrast [60].

4.10.2.2 Prisms and partial mirrors

To reduce the complexity of an optical setup, it is preferable to utilize only a limited number of light sources. Hence, in most systems, beams are split and redirected at various locations along their path. To separate a coherent beam, the incident light wave is directed at a very thin film deposited on the surface of a glass body, which acts as a semi-transparent medium. As a result, specific amounts of the incident light wave are both reflected and refracted. The ratio of both values depends mainly on the thickness of the coating. One concern in utilizing beam separation lies in the consequent reduction of light intensity with formation of a new branch. However, most laser sources provide sufficient energy to allow splitting of one beam into multiple beams.

Through laws of reflection and refraction, the exact direction of emergence of an incident beam can be prescribed [53]. For small angle refraction, wedges are typically used, while prisms provide stronger refractive characteristics for large angle changes (Figure 4.46). Being a semi-transparent mirror, beam splitters are essential. These partial mirrors have become an integral part in almost every system where two beams are caused to interfere.

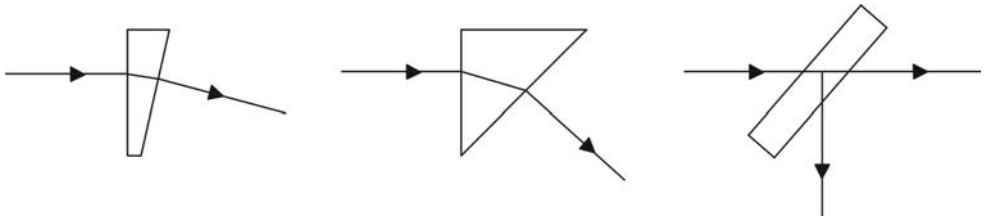

Figure 4.46: Common methods for beam modification: wedge (left); prism (middle); beam splitter (right)

4.10.2.3 Recording media

Generally, two forms of recording media are available for storage of optical data. As in conventional photography, perturbation of fringe patterns can be permanently recorded on photographic film that is exposed prior and after an incremental load has been applied to the test specimen. Although it provides high resolution and a permanently recorded image, one significant disadvantage of this process is its incapability of real time

imaging. This drawback has been overcome by the introduction of digital CCD equipment, which allows continuous recording of fringe patterns. Data is successively fed into a frame grabber that can be integrated into most modern computer systems. This enables the inspector to perform both on-site analysis as well as post-test analysis for detailed observation.

When laterally sheared images are forced to interfere with one another, each pixel of the CCD device acts as a separate strain gauge, indicating output capabilities of up to 250,000 real-time adjacent strain gauges [13].

4.10.3 Techniques and applications

As outlined in the previous discussion, shearography can be clearly identified as an optical method that offers the most potential for actual in-situ applications. Although interferometry and holography are suitable methods for laboratory testing, their stringent stability requirements imposed on the optical system can seldom be met in field applications. As a result, the subsequent discussion on previous experimental work will be focused on shearography exclusively.

Despite being a fairly young technique, shearography has already received considerable industrial acceptance for nondestructive inspection. Examples include testing of automotive tires and evaluation of pressure vessels, adhesive bonds, and composite panels for the aerospace industry [56]. For on-aircraft use, portable systems are already in use worldwide [13].

Hung demonstrated inspection of a composite filament wound pressure vessel by means of internal pressurization as well as core debonds on a Boeing 747 wing flap [56]. Along the perimeter of the vessel, four fringe patterns were obtained at 90° increments that led to the detection of impact damage in several regions. The wing flap was made of 0.072 in thick graphite skin bonded to a honeycomb core of about 2 in thickness. Under the external vacuum imposed by a suction cup, debonds were detected. The rate of inspection for this specific application was reported to be 0.5 sq. ft in less than 10 seconds.

Gregory addressed the current applications of shearography to inspection for aircraft and space structures and, in particular, inspection of CFRP sandwich panels containing ventilated Nomex cores [13]. The components were comprised of ten carbon fiber layers with the disbond size ranging from 6.35 mm (1/4 in) up to 10 mm (5/8 in) diameter. Hot air emitted from a heat gun was used as the stressing medium, raising the surface temperature by only 3-4ºC. During an overall inspection period of only 30 seconds, disbonds of all sizes were detected.

Particularly in the civil sector, shearography must be considered a novice technique that has not yet experienced similar industrial widespread or acceptance as ultrasonics or thermographic imaging. Moreover, most experimental work and field inspections are performed under controlled laboratory environments, which are often inherently different from those encountered in the field. Confirmation of the applicability to civil environments thus remains an objective of future research.

4.10.4 Capabilities and limitations

Shearography is a whole-field non-contact method which, although fairly recently developed, has already gained significant acceptance as an NDE method. Depending on the intensity and broadness of the incident laser beam, large areas can be inspected simultaneously, which results in a less time consuming process. Currently, test units that incorporate a CCD camera, a shearing device and a laser diode are only about 200x60x80 cu mm in size and weigh less than 1 kg [60]. Hence, they are mobile and can be easily set up in the field.

A significant prerequisite for shearographic imaging, and in fact for most other optical methods, is the fact that a component must be loaded to allow the recording of displacement derivatives. While this imposes certain flexibility restrictions, it ensures that the structure is inspected under real-life conditions in that it is exposed to one or multiple actual loading situations. It further dictates that only those defects of sufficient dimension to cause stress concentrations in the material will be sensed. One may further argue that those defects that are not imposing stress concentrations into the composite or the adhesive bondline may very well be classified negligible in terms of their criticality. Hence, the technique is able to differentiate between relevant and cosmetic defects [13]. Nevertheless, for a comprehensive characterization of all defects, regardless of criticality, a second complementary method should be utilized.

As outlined above, optical methods are limited to surface inspection. This fact limits defect detectability to those anomalies that are of sufficient size or shallowness to induce stress concentrations into the surface. While this is a significant drawback for inspection of thick composites, it is less critical in thin or honeycomb composite structures with a more flexible core material. Nevertheless, experience in signal interpretation is indispensable for characterization of subsurface defects. In addition, even though regions of increased strain may be identifiable, their characterization with respect to defect type can be of more difficulty.

4.11 ACOUSTIC EMISSION

4.11.1 Fundamentals and theory

Acoustic Emission (AE) has been applied extensively to provide real-time information on damage progression in mechanically loaded components [61, 62, 63]. Similar to optical methods, AE is a *passive method*, whereas most other NDE techniques are considered *active*[†]. In fact, acoustic emission cannot be considered truly non-destructive, since acoustic signals are only emitted if a permanent, non-reversible deformation occurs inside the material. As such, only non-reversible processes that are often linked to a gradually progressing material degradation can be detected using AE. Nonetheless, acoustic emission has found wide acceptance for industrial use, such as pressure vessels and tanks [6], hybrid CFRP-concrete columns [62], as well as bridge stay cables [63].

[†] *Active* refers to the emission of some form of energy, whereas *passive* methods draw all signal energy from externally applied loading, in either mechanical or thermal form.

As a material is stressed, energy is first released in regions where stresses are sufficiently high to cause new, permanent deformation. This deformation can occur on the atomic level as well as on a macroscopic scale, and since it is more likely to occur in regions of material anomalies, AE signals are commonly first emitted from defective regions with deficient integrity. Once a signal is given off, it propagates in the form of high-energy stress waves, similar to those found in ultrasonic testing. Through the use of adequate sensors (transducers) a wave of mechanical energy can be recorded and electronically amplified for further analysis by suitable AE equipment.

Under most loading conditions, regions of discontinuous composition tend to experience some form of stress concentration. In these regions energy is stored in form of a high local stress field. In fiber composites, these stress concentrations can reach levels as high as nine times the average full-field stress. When the material cracks at internal discontinuities, a new surface is formed and the stored elastic energy is released in the form of heat and a short pulse of elastic and kinetic energy that travels from the defect and disperses into the material. Although the frequency spectra of stress waves theoretically ranges from a few hertz to 1000kHz and higher, experience has shown that transducers operating between 100-500kHz provide sufficiently high sensitivity to most relevant AE events [6].

Once the acoustic signal has been emitted from a source inside the material, a process that typically lasts no longer than a few millionths of a second, it propagates in all directions. Velocity and directionality of propagation are material-specific, as discussed in Section 4.5.1.1. In many aspects, wave propagation in acoustic emission follows the same physical laws as those prescribed for ultrasonics. As such, high frequency signals tend to experience attenuation in form of dispersion (geometric spreading), reflection (scatter) and absorption. Composite materials contain a large number of interfacial boundaries at which signal scattering and absorption can reduce signal intensity and impose difficulties in obtaining a clear and distinguishable signal. On the other hand, waves tend to propagate along the fiber direction, making composite materials more preferable for signal detection over relatively long distances [63].

Once an acoustic signal has propagated from its source to reach the object surface, piezoelectric probes can be used to convert the mechanical stress waves into an electrical signal, assuming that the wave has not attenuated to a level below the sensitivity of the transducer. Herein, good contact between the surface and the probe is essential in obtaining a high amplitude signal. Acoustic couplants are typically in form of a gel-like substance that is applied to the sensor face as a thin film. Subsequently, the sensor is pressed against the surface and securely held in place with adhesives or similar means. This ensures a low impedance gradient between the test object and sensor surface, as this is essential for most of the wave energy to be transmitted to the transducer surface instead of being reflected back into the bulk material.

All electronic signals collected from the piezoelectric crystal in the transducer are transformed into a voltage level, which is proportional to the amplitude of mechanical excitation. In other words, the output voltage amplitude varies linearly with the input motion amplitude [6]. Once a mechanical wave arrives at the transducer surface, causing deformation to its piezoelectric crystal, a short voltage spike is sent to an electronic acquisition device, which filters and amplifies the signal to reduce low frequency background noise and to obtain a voltage level that

is optimum for the circuitry of the AE instrument. In order to solely collect information representative of significant events, the user can preset a voltage threshold by which the system ignores events that fall below the specified voltage amplitude.

Signals are characterized by their four main parameters, namely amplitude, duration, energy and counts. Each constitutes a specific characteristic of the incoming signal where the correct interpretation of one or more of these parameters is dependent on the experience and analytical skill of the inspector. Because data is continuously streaming to the memory of the AE system, a multitude of analytical graphs can be displayed in real time.

Difficulties in AE testing arise from the fact that discrete bursts can originate from a variety of sources. This aspect is especially critical in hybrid structures where two or more materials are forced to interact, because signals can be initiated in either material or at their joint interfaces. With respect to CFRP-concrete hybrid structures, a number of AE energy sources are known, including cracking, plastic deformation, friction of aggregate interlock, mortar/aggregate debonding in concrete, fiber/matrix debonding, matrix cracking, delamination, and fiber breakage in composite laminates [62]. If both materials are joined, debonding must be considered as a further signal source.

Apparent damage in materials is often deduced from the presence of the *Kaiser* and *Felicity* effect, which are related to the appearance of AE signals in successive loading and unloading [62]. A material that experiences the Felicity effect is said to emit acoustic signals at loads below that of the previous stress level. Conversely, the Kaiser effect postulates the absence of any signal until the previous load is exceeded. A qualitative representation of this is depicted in Figure 4.47.

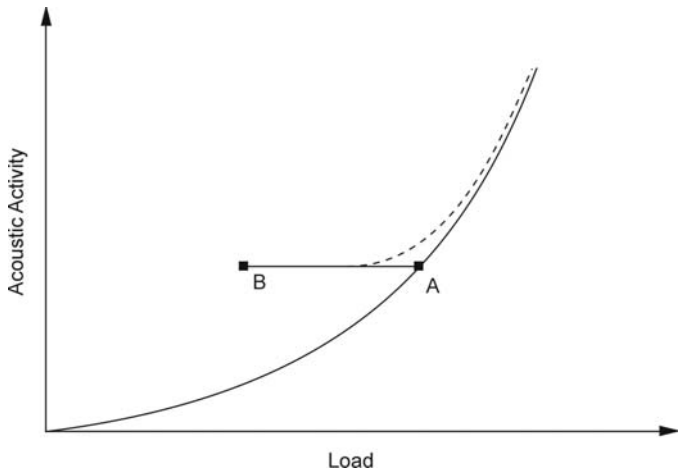

Figure 4.47: Graphical representation of the Felicity and Kaiser effect

As the material is loaded, the number of total acoustic events increases from zero up to point A. During a short unloading phase (A to B), no further acoustic signals are emitted. Upon reloading, materials following the dashed line begin to emit acoustic signals at a load below that

of the previous level and are thus said to experience the Felicity effect. Conversely, the solid line returning to point A with a subsequent increase in acoustic events represents materials governed by the Kaiser effect.

From previous studies, it has been shown that concrete experiences the Kaiser effect to load levels up to 75-85% of its ultimate strength [62]. In contrast, fibrous composites are known to emit AE signals at significantly lower stress levels than those encountered during previous cycles and are thus governed by the Felicity effect.

4.11.2 Instrumentation

AE inspection systems envelop a fairly small number of components that are all highly mobile and simple to operate. As most other computer assisted testing methods, software and acquisition devices can be incorporated into most modern computer systems, which makes AE highly favorable for use in the field. Transducers used for signal capturing are generally identical to those discussed in Section 4.5 and will therefore not be further addressed here. Nonetheless, it should be pointed out that transducers are commonly selected based on their natural frequency of vibration, since it determines the frequency range in which they are most easily excited.

Apart from the transducers, typical systems are comprised of one signal preamplifier per channel as well as a central AE unit that records and analyzes the incoming data stream.

4.11.2.1 Preamplifiers

Preamplifiers, as shown in Figure 4.48, are used in most systems having transducers that do not already have preamplifiers incorporated in them. A typical voltage spike produced by a piezoelectric crystal is of insufficient amplitude for the acquisition system to record. Thus, a preamplifier is used to boost the signal to about 40-60 dB, depending on individual test conditions.

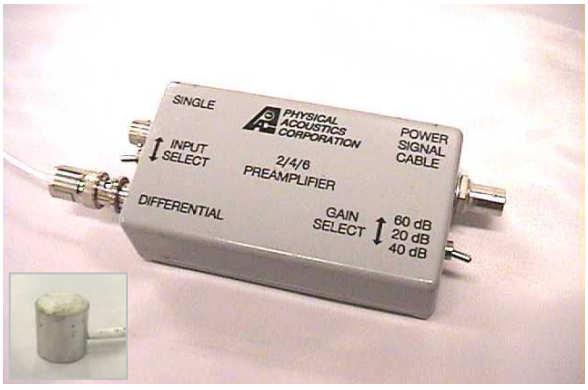

Figure 4.48: AE preamplifier and transducer sample (inset)

4.11.2.2 Software and data display

Data display in AE is inherently different from other NDE techniques. Rather than displaying visual images, the numerical data is graphed. Most software packages provide the user with a number of possible graphs to display during testing such that acoustic activity can be monitored in real time. The most common graphs are amplitude-time, energy-time or event-time (Figure 4.49).

Figure 4.49: AE data acquisition system

4.11.3 Techniques and applications

Because AE tests do not provide the inspector with visual information comparable to that obtained from radiography or thermographic imaging, other characteristics unique to AE must be employed. Problems mostly arise from the fact that it is often not possible to predict the type, shape or exact location of a defect by simple acquisition of acoustic wave signals.

Difficulty in signal interpretation is even more pronounced in testing of composite materials, where anisotropy causes wave fronts to disperse at different velocities depending on its specific lay up sequence. In unidirectional composites, however, fibers often act as wave guides such that signals can travel over longer distances [63]. On the other hand, if sensors are positioned at a distance from the signal source and perpendicular to the fiber direction, strong signal decay is almost unavoidable.

Prior to testing, the system setup, encompassing preamplifier setting and positioning of transducers must be checked by inducing an artificial acoustic event. Such calibration is most commonly performed via a simple pencil lead break (Figure 4.50) in which the tip of a pencil is broken near the region of an expected defect. Since frequencies produced by fracturing of the

lead tip are similar to those encountered from internal material fracture, system sensitivity can be adjusted to an acceptable amplitude threshold.

Apart from the four main signal parameters listed in Section 4.11.1, signal frequency provides valuable information on the signal source type. Experiments have shown that the frequency content of AE signals can be associated with particular forms of damage [64, 65]. Frequency separation can be advantageous in determining the cause of failure in composite materials, since fibers and matrix possess significantly different material properties. For CFRP, frequencies in the 90-180 kHz region are proposed to be representative of matrix cracking, 180-310 kHz for fiber pullout, while higher frequencies correspond to fiber fracture [65].

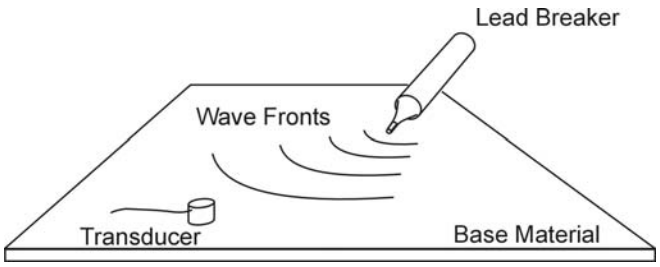

Figure 4.50: The lead-break test

Since an acoustic signal can originate from anywhere in the material, source location is AE is difficult. However, information on source location can be provided through the attachment of multiple sensors and comparing the arrival times of one specific event. While this is a feasible method in isotropic materials, a variation in wave velocity restricts source location to quasi-isotropic composites.

Examples of previous AE experiments include investigation of glass- and graphite-epoxy dog bone specimens in static and fatigue loading and tests to study the cracking mechanism in concrete [66, 67, 68].

Damage progression monitoring by Lorenzo, et al. showed that fiber fracture could be clearly identified from other acoustic activity, while matrix cracking could not be clearly distinguished [66]. Further, fatigue tests indicated that most of the acoustic signals are emitted within 90 to 98 percent of the fatigue life of the composite, which is promising in terms of long term failure monitoring of CFRP composites.

Investigation by Rizzo, et al. was aimed at introduction of AE as a permanent monitoring system for CFRP bridge stay cables [63]. Cables of varying diameter and average length of about 5650 mm were exposed to dynamic fatigue tests and monitored with two AE transducers positioned at each end. Results showed that, despite their enormous length, CFRP cables are excellent waveguides exhibiting relatively low attenuation.

Lastly, Mirmiran, et al. evaluated acoustic emission towards applicability for monitoring of hybrid CFRP-concrete columns [62]. Columns measured roughly 150 mm in diameter and were

encapsulated by bonded and unbonded GCFRP shells. Cyclic compression tests showed a significant Felicity effect for both bonded and unbonded shells with even a slight increase in the energy level during the unloading phase. Overall, the signal activity was more pronounced for unbonded shells, which was attributed to friction developed at the core-shell interface.

4.11.4 Capabilities and limitations

Compared to other NDE methods, the significantly different nature of acoustic emission testing implies certain advantages and disadvantages. First, the rather simplistic setup of an AE monitoring system allows on-line life monitoring of existing structures. In anisotropic materials, such as CFRP cables, AE has already been proposed as a permanently installed health monitoring system [63].

Second, the method allows global monitoring without altering the setup parameters. As such, no repetitive inspection routines have to be performed, which represent a source for errors, assuming that inspection personnel as well as routines may be altered or changed over time.

Also, since AE systems are favorable for long-term monitoring, they offer the possibility of incorporation into remote data acquisition systems from which data can be transmitted to numerous receivers simultaneously. Remote sensing can be especially advantageous in structures with a high public demand, such as bridges, dams or high-rise buildings. In case of an earthquake or fire, serviceability can thus be assured more rapidly.

Limitations in AE testing arise from a number of factors. Primarily, meaningful AE testing can only be performed on members that undergo some sort of material degradation, which separates the method from most other NDE techniques as not being truly nondestructive. In addition, signal emission is a unique occurrence that is not repeatable once the material has permanently deformed. Also, if signals are acquired, they can originate from a number of sources, including friction at interfaces [62]. As such, the AE signal-time history must be monitored and recorded continuously throughout a structure's lifetime, which demands the incorporation of a system immediately following its erection. If testing is initiated at a later stage, damage that may have previously occurred will most likely go undetected.

Apart from these practical aspects, signal interpretation is far more difficult than in most other techniques. Due to difficulties in matching the frequency response of the transducer with the frequency content of the various AE signals, spectral analysis can be considered an ineffective tool for source determination [62]. In initially cracked components, signals can originate from newly developing damage as well as from friction at already existing fracture surfaces. Their exact distinction is a highly difficult task. Also, size, shape and type of defects can often not be clearly identified, and because the acquired data is not mapped in ways similar to UT or thermography, much is dependent on the inspectors' experience.

Summarized, acoustic emission should be regarded as a potential method for early failure detection and health monitoring of new or existing structures. However, it should not be considered to be of high potential for providing comprehensive insight on the presence and progression of internal defects.

4.12 GROUND-PENETRATING RADAR

4.12.1 Fundamentals and theory

In many aspects, the concept of ground-penetrating radar inspection is similar to that employed in air traffic control. In principle, an electromagnetic wave of variable frequency (500 MHz to about 1.5 GHz) is emitted from an antenna and directed at either a stationary or moving object. As the emitted signal encounters the object surface, part of it is reflected back and can be used to calculate location and, in the case of a moving object, velocity [69].

In structural inspection, the object of interest resides at a fixed position in space; hence measurements of dynamic movement are not of primary importance. Instead, the electromagnetic wave, which is capable of penetrating materials like concrete, wood or masonry, can provide information on internal material discontinuities. While radar has long been applied to problems such as measurement of sea-ice thickness, profiling of lakes and rivers or geological surveying of the lunar surface, it has recently found application in detecting delamination in concrete bridge decks, caused by corrosion of the reinforcing steel and moisture in masonry structures [70, 71].

Within the electromagnetic spectrum (Figure 4.4), radar can be located adjacent to the infrared spectrum, indicating an average decrease in frequency of about three orders of magnitude. Because of its electromagnetic nature, extremely high frequencies are stringent for obtaining short wavelengths. For instance, excitation frequencies in the order of 1 GHz yield wavelengths of about 30 cm.

In principle, the propagation of the signal is affected by the dielectric properties of the propagation medium, so that its attenuation and reflected components vary accordingly [72]. As the method relies on reflection of wave fronts from within the host material, theoretic assumptions regarding the laws of penetration and reflection, as discussed in Section 4.5.1.2 to 4.5.1.4 remain valid. Moreover, the general methodology of testing is mostly identical to that of ultrasonics. As such, a single antenna can be used to transmit and receive a signal as it is reflected off interfaces in the material. However, the detectability of radar systems is dictated by differences in dielectric material properties instead of variation in acoustic impedance.

Similar to acoustics, the coefficient of reflection for electromagnetic waves is as given in Equation 4-3, assuming the acoustic impedance's Z_1 and Z_2 are substituted with the electromagnetic impedance Z_e, denoted as follows:

$$Z_e = \sqrt{\frac{\mu_0}{\varepsilon_0 \cdot \varepsilon_r}} \qquad \textbf{(4-8)}$$

As before, reflection and refraction of the incident wave will occur as the wave encounters an interface between two inherently different materials. As radar travels through the host material, its propagation velocity is described as follows:

$$v = \frac{c}{\sqrt{\varepsilon_r \mu_r}} \qquad \textbf{(4-9)}$$

indicating the strong dependence on the relative dielectric constant, ε_r, as well as the relative magnetic permeability, μ_r.

Further similarity between radar and ultrasonics can be noted by signal attenuation. Whereas attenuation in ultrasonics is primarily governed by a high impedance gradient at interfaces, magnetic permeability and conductivity of the propagation medium predicate signal decay in radar inspection. It may be assumed that these fundamental differences impose new or alternative requirements onto the overall testing methodology of radar inspection.

First, the stringent coupling requirements imposed on ultrasonic testing can be named as one of the most significant differences. Herein, one must consider that differences in electromagnetic impedance, which in turn dictate energy reflection at interfaces, are solely influenced by the relative dielectric constant, ε_r, of individual materials (see Equation 4-8). Assuming a commonly encountered interface of air/concrete, these materials have relative dielectric constants of $\varepsilon_r = 1$ and $\varepsilon_r = 6\text{-}12$, respectively [70]. From Equation 4-8, one finds that roughly 50% of the energy is transmitted into the material, which eliminates the need to physically couple the antenna to the concrete substrate. Consequently, a variation of test setups can be used, some of which are shown in Figure 4.51. The illustrations depict typical measurement as performed in localizing internal steel reinforcement and zones of high moisture and chloride content in reinforced concrete slabs.

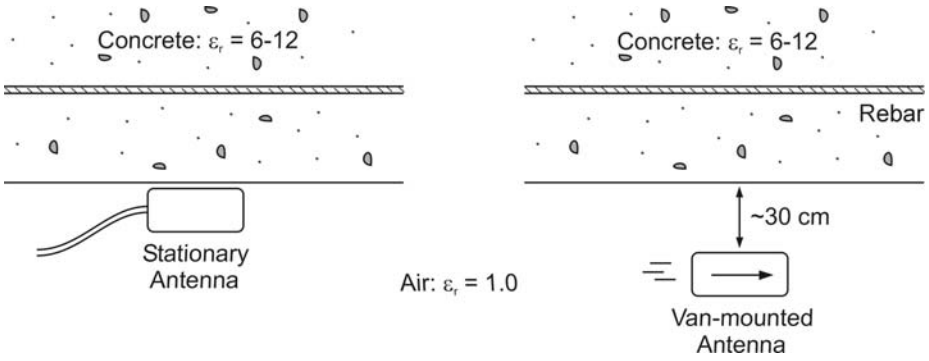

Figure 4.51: Various employable GPR setups

Second, only a limited range of materials allows inspection via penetrating radar. As such, applicability is generally limited to materials that are good electrical resistors, including sand, soil, water or concrete [72]. In conductive materials, i.e. steel or salt water, the rapid signal decay restricts deep penetration of the electromagnetic signal. Although ocean mapping is performed in a conductive medium and should therefore be assumed to be problematic, the unusually long wavelengths contribute significantly to lower attenuation of the signal.

4.12.2 Instrumentation

As implied by the extensive use of radar equipment in the modernized world, these systems represent a well-established and highly specialized field. The primary components found in a radar system are a waveform generator, a single transducer comprised of an emitting and receiving antenna, a signal processor, and a data storage/display unit.

4.12.2.1 Generator

Waveform generators are used to transmit either a continuous or pulsed sinusoidal excitation signal to the antenna, and subsequently into the test material. To adapt to a variety of test conditions, generators can cause excitation over the full frequency range. Depending on the test approach, the transmitted frequency can be kept constant or swept within preset limits, as further described in Section 4.14.3. Relatively low energy consumption permits these units to be operated on a conventional 12 volt DC automotive battery; however, this adds significantly to the weight of the system [70]. Hence, these systems are restricted in their portability, as the total weight of a typical system may be about 25 to 30 kg.

4.12.2.2 Antennae

Configuration and layout of the antenna is largely influenced by the specific application. The most commonly applied configuration is that of a 'bowtie' dipole, providing a diverging beam that is most preferable when performing surface contact inspection. Alternatively, 'horn' antennas with a more focused beam, usually driven at 1 GHz, have been developed for special applications. Here, the beam is of a more focused configuration, which allows for testing at increased distances. Horn antennas have found use in vehicle-mounted surveying of highway and bridge decks, where the antenna resides at a constant distance of about 30 cm above the surface [70].

4.12.2.3 Display

Typically, the signal that is received by the secondary antenna can be visualized using a standard oscilloscope. Herein, the intensity of the reflected signal can be assigned levels of a grayscale, such that internal discontinuities can be visualized. As with most equipment, modern GPR devices encompass a number of signal modifications, such as variable gain, filtering, or waveform rectification, which significantly enhance signal interpretation.

4.12.3 Techniques and applications

A number of different approaches have been found most suitable for structural applications, including frequency modulation, synthetic pulse-radar and pulse (impulse) systems. While all of the former methods are applicable to structural inspection, pulsed systems have found the greatest practical acceptance and the most commercially available equipment [70]. This is due in part to the low power output and consequent elimination of safety concerns typically found in systems of higher energy consumption. To adapt systems to dimensions found in structural

applications, frequencies ranging from 500 MHz to about 1.5 GHz are most suitable. At 1 GHz, concrete members of 40 cm thickness exhibit the most efficient inspection.

To date, the most widely reported structural applications relate to assessment of concrete bridge decks to detect delamination caused by the uppermost surface of reinforcing steel. Moreover, methods have been developed that identify delamination of asphalt surfacing. The best results are typically obtained for regions within 50 mm of the concrete surface. Moreover, voids and regions of moisture uptake have been located using GPR.

Comprehensive background information on GPR inspection can be found in reports by Lim [69], Bungey and Millard [70], Colla et al. [72], and Shaw and Berström [73].

4.12.4 Capabilities and limitations

The recent development of ground radar penetration for inspection of concrete civil infrastructure has yielded substantial benefits in the rapid localization and quality assessment of defects in concrete components. These include misplacement of reinforcement, severe moisture uptake, and discrete air-filled voids. Moreover, inspection via radar enables the user to often de-couple the equipment from the structure under inspection, which allows for a more rapid inspection process without the time-consuming coupling processes. Nonetheless, a number of significant drawbacks must be emphasized.

Foremost among them is that the principal structural applications are related to dimensioning and localizing of major components and internal features, such as rebar and air voids [70]. Because relative changes in the dielectric constant are a precondition for detectability, accurate sizing of most internal features, including dry air voids and cracks, becomes highly challenging.

In addition, features located in close proximity to the surface are difficult to detect. As most transducers are operated in the lower GHz-range, signal reflection off the front surface will occupy a depth of about 100 mm, causing strong interference with signals originating from shallow depths. This imposes a strong limitation to radar inspection of CFRP-rehabilitated components, since most defects are located within a few millimeters of the front surface.

Moreover, given the fact that no application of GPR to carbon-epoxy composites can be found in the literature, little is known about the detection-potential of radar in these materials. This may be primarily due to the relatively high conductivity of carbon fibers (i.e. low dielectric constant), which restricts their inspection via radar altogether.

In conclusion, GPR has proven adequate for locating and, within limits, sizing of internal discontinuities of conventional reinforced concrete components. Due to the limited background on its applicability to composites, plus restrictions imposed by the high conductivity of the material and generally shallow inspection depth, one may conclude that GPR is unfavorable for the inspection of CFRP-rehabilitated concrete members.

4.13 STRAIN MEASUREMENT TECHNIQUES

4.13.1 Fundamentals and theory

Traditionally, surface mounted electrical resistance strain gauges are used in a wide field of applications for monitoring material deformations, both internally and externally. Consisting of a thin electrical wire with a predetermined electrical resistance, these gauges are specifically designed to provide highly accurate strain readings (as low as 10^{-6}) while ensuring full strain compatibility with the host material. They are bonded to the test object by means of a thin adhesive film and usually require protection from the surrounding environment through adequate coatings or covers.

As the base material strains, the thin wire of the gauge is forced to elongate, corresponding to a fixed rise in resistance gradient/unit extension, commonly measured in voltage/microstrain (με). Although this method remains in wide use for most laboratory testing, it provides only localized information and lacks insight on strain at multiple locations along the entire dimension of a member. In order to provide the user with a more comprehensive strain profile, a high number of individual gauges would be advantageous, though at the expense of an increased logistical effort. For most applications, strain gauges are surface-mounted. Internal applications have mostly been restricted to investigation of rebar in reinforced concrete. Especially due to their relatively high surface area and the demand for protective coatings, electrical resistance strain gauges have not found wide acceptance for use inside laminated composite materials.

Lately, embedded optical fibers have been introduced to overcome the apparent shortcomings of conventional strain gauges. Optical fibers are manufactured from a transparent *core* that is capable of transmitting light waves over large distances. To provide guidance as the light beam (emitted from either a broadband diode or laser source) progresses through the fiber, a *cladding* is applied to cover the core surface, thus acting as a reflector. As a result, any portion of the light beam that does not travel parallel to the core axis is reflected at the fiber/cladding interface and forced to continue its path inside the fiber. To permit incorporation of optical fibers in a variety of harsh environments, a protective polyimide coating surrounds the core and cladding, resulting in a total fiber diameter of only about 250 μm. As such, fibers are significantly smaller than conventional strain gauges and can be embedded into a variety of materials with significantly lower influence on mechanical behavior (Figure 4.52).

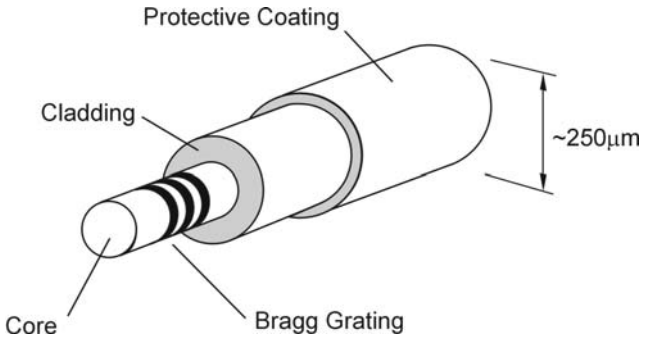

Figure 4.52: Composition of an optical fiber

The most significant advantage of fiber optics has been realized with the introduction of fiber-optic Bragg gratings (FBG). Due to the inherent properties of coherent light, portions of an incident beam traveling though the fiber can be reflected at a grating that essentially acts as a wavelength selective mirror [74]. These gratings are similar to those in optical interferometry (see Section 4.10), in that they function by means of destructive and constructive interference of coherent light. As the material strains, the grating on the fiber surface is caused to deform, which results in a small change in spatial period. Hence, the frequency content of the reflected signal shifts accordingly.

It has been shown that sensors give a linear shift in wavelength in response to linear strain of the Bragg grating, assuming that strain levels are within the elastic deformation limit of the fibers [74]. This is preferable, since it allows for linear correlation between the measured shift in frequency and elongation of the structural component containing the optical fiber.

Because light can be emitted over a large frequency range, the previous feature enables the user to apply *multiplexing*, a technique that allows measurement of strain at various locations along a single optical fiber. Essentially, a signal of known frequency content is emitted into the fiber and any signal reflected off a grating is recorded and analyzed. Using a frequency modulated continuous wave signal (FMCW), up to 20 gratings can be included along a single fiber [74]. Since each individual grating can be designed such that it only reflects a specific wavelength and a small derivative thereof, signal frequency content can be easily separated using optical spectrum analyzers (OSA). Subsequently, through known velocity-time relationships, the recorded information can be related to the position of a grating along the fiber.

4.13.2 Instrumentation

As with optical methods, a laser source must provide coherent light to send a signal of specified wavelength into the fiber core. A light signal is launched from a broadband source that is responsible for modulating the frequencies. A photodetector is incorporated in the same unit as the laser beam and analyzes the incoming reflected signal of each of the FBG sensors.

4.13.3 Techniques and applications

To date, most effort for the introduction of fiber optics to civil applications has been focused on new and more comprehensive strain measurement techniques that were formerly difficult to accomplish using conventional electrical resistance strain gauges. Special attention has hereby been paid to investigation of interlaminar fracture behavior of composite materials [74, 75, 76]. Since optical fibers can be fully embedded in the surrounding host material without experiencing significant long-term degradation, their incorporation into the concrete-composite bondline and composite matrixes has been studied.

Due to the fact that most material anomalies in loaded components yield induction of some form of stress concentration, strain anomalies are likely to be indicative of such defects. Particularly in composite-wrapped concrete components, optical strain gauges have proven to reveal the physical condition change to a greater detail than surface mounted gauges [74]. Herein, both optical and conventional surface mounted gauges were used to monitor the behavior of composite-wrapped concrete cylinders under compressive loading.

Results indicated that deformation of the concrete core was in most instances larger than that indicated by surface measurements. Also, since the optical fibers were embedded directly inside the adhesive layer, a loss of stress transfer between the concrete core and composite layer could be detected at an early stage. However, it was shown that different embedding directions of fibers inside the composite might influence the mechanical properties. As such, the largest reduction in flexural strength was observed when the fibers were positioned transverse to the load bearing direction.

Chan, et al. reported the use of optical strain gages for the monitoring of strain development along the concrete-composite interface for notched GFRP-strengthened beams in three-point bending [75]. Results showed similar trends as those outlined in reference Chan, et al., in that the strain measured at the interface deviated noticeably from that at the surface [75]. Embedded optical fibers allowed detection of interfacial debonding between the concrete and the composite at load levels that were about 20% less than those of visible separation of the two components.

4.13.4 Capabilities and limitations

Similar to acoustic emission equipment, optical fiber technology allows for long-term monitoring of structures with minimal effort, assuming the monitoring system is already incorporated into the design prior to erection of the structure. In rehabilitation, the full potential of optical fibers can be exploited if they are embedded into the concrete-composite bondline to monitor the strain distribution and indicate eventual long-term degradation. Unlike most electrical systems, especially those relying on line resistance, optical fibers are immune to interference from electromagnetic or radio frequency related noise [77]. Further, they are extremely small and can thus be incorporated into materials to provide the first ‘smart’ structures. Through multiplexing, the amount of foreign material that is introduced by such a monitoring system can also be greatly reduced.

Despite significant advantages over conventional strain gauges, the current use of optical fibers in monitoring remains highly limited. Although they represent a potential alternative to conventional strain gauges, most equipment for optical strain measurement has not yet been fully developed, a factor of particular importance for in-situ applicability. Moreover, the appreciable advantage offered by multiplexing comes at a price. If FBG’s are spaced in too close proximity, *spectral shadowing* can occur, meaning that the recorded signals are not sufficiently spaced apart to be separated by the optical receiver. For most experiments, a distance of up to 40 in was required to ensure proper system functionality. Consequently, a considerably long ‘dead-zone’ exists from which no strain information can be extracted, which must be regarded a limiting factor for application of multiplexing in small- to medium-scale structures. In addition, if a fiber ruptures during service, the signal of all subsequently placed FBG’s is lost and with it all means of data acquisition [75].

In conclusion, the high potential of optical fibers for detection of material anomalies has not yet been fully investigated or developed. Although it has been shown that the methodology is potentially capable of detecting initiation and progression of stress transfer deficiencies at concrete/composite interfaces, little is known about its potential for flaw detection at stringent service levels. Compared to most manually operated NDE techniques, optical strain measurements lack flexibility, since the FBG locations cannot be changed once the fibers have

been permanently embedded. As such, the method is highly localized, immobile and does not provide full-field information.

4.14 MODAL ANALYSIS

4.14.1 Fundamentals and theory

In most concrete structures, damage can often be associated with certain forms of material degradation, primarily present in form of moisture absorption, excessive spalling, concrete cracking and corrosion of internal steel reinforcement. As a result of the consequent change in material properties, the mass and stiffness of a structure are likely to be altered as well. Hence, it can be assumed that, as a structure undergoes certain forms of degradation, its vibration characteristics will change.

For many years, modal analysis has been used to investigate vibration characteristics of mechanical components, including aerospace components and rotational machinery. Lately, the field of modal testing has been extended towards testing of existing structures to comment on serviceability and loss in performance through eventual degradation of individual components [78, 79, 80]. As mentioned above, a gradual change in material performance, promoted by the progression of the above-mentioned factors, will most likely result in changes in the variation characteristics. Herein, modal frequencies, mode shapes and damping properties of structural components, such as bridge superstructures, are of paramount interest. These can be extracted through modal testing, which has proven suitable for in-situ testing of structures, even on the large scale. In the following section, the methodology employed in modal testing will be outlined and discussed.

To excite a structure for modal measurements, two methods of excitation can be chosen, namely input-output (*active excitation*) and output only (*ambient noise*). Input-output methods of excitation involve a contact procedure in which a forcing function is introduced to initiate vibration of the structure. Typical forms of excitation entail impact hammers, drop weights, shakers or displacement-release. As may be noted from the previous examples, the waveforms used in modal analysis can be of various natures, including harmonic and random input, as well as impulsive excitation [78]. Output only excitation is present as long as the structure is in service and under some form of external excitation, e.g. vehicular traffic or wind loads [81, 82].

In field testing, dynamic properties are extracted by placing a number of motion sensors at predetermined locations along the structure. To suit the need for full-motion recording, triaxial accelerometers are commonly given preference [78]. The objective of placing sensors in multiple locations is to attain a sufficient amount of frequency response functions (FRF), such that individual modes can be identified from the modal test. Herein, the highest measurable mode depends largely on the optimal placement of accelerometers; i.e., the extraction of higher modes demands a higher number of accelerometers.

As the structure is excited, acceleration data is streamed to a recording device where the frequency response functions are stored. Following computational analysis, which is commonly performed by software incorporated in laptops, frequency and damping ratios for each mode of

interest can be calculated. A schematic of the general modal testing field examination is depicted in Figure 4.53. The illustration shows vibratory motion of a two-span bridge superstructure in its first mode of longitudinal bending (Mode I).

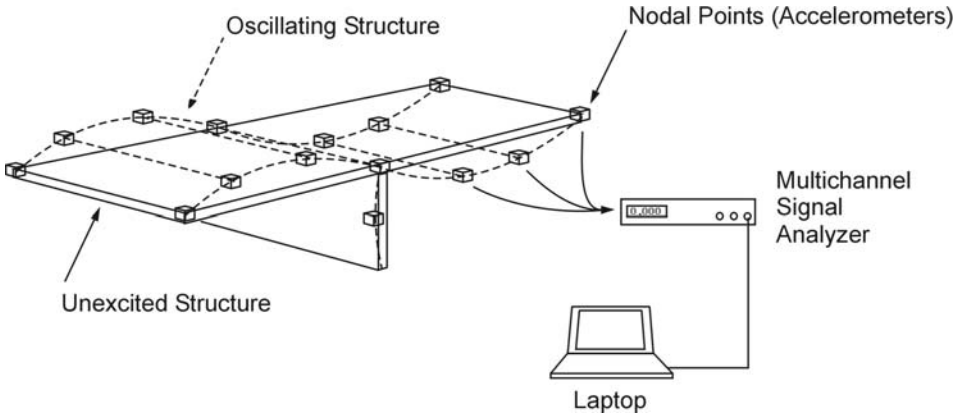

Figure 4.53: Modal testing of large-scale structural components

As previously discussed, damage/deterioration of structural components can be related to changes in dynamic properties [79]. Hence, to comment on the probable deterioration of structural components, vibration properties must be monitored in successive intervals and compared to the properties of the initially sound structure. Given the fact that most structures were erected prior to implementation of modal analysis into civil testing methodologies, an experimental baseline of dynamic properties (i.e., vibration behavior of the sound, undamaged structure) is often not made available to engineers. Instead, finite element models are commonly utilized to mimic the vibration properties to such detail that the model can be assumed representative of the original structure. By successively comparing the FEM baseline model with data extracted from field experiments, engineers are given a means to comment on the overall performance of the structure.

4.14.2 Instrumentation

For active excitation, modal analysis systems are typically comprised of a single excitation mechanism, a multitude of individual transducers to acquire the parameters of interest, and an analyzer to extract the desired frequency response information [83]. Data from the accelerometers is collected and processed by multi-channel signal analyzers, from where it can be conveniently transferred to PC's or laptops for further analysis.

In passive excitation, ambient vibration serves as a substitute for the loading mechanism. Apart from portability restrictions set forth by massive impact devices, modal analysis equipment is typically located in compact units, which provide increased mobility as well as protection from harsh environmental influences.

4.14.2.1 Excitation sources

In order to record data and information about the vibration characteristics of a structure, an excitation mechanism is necessary. For input-output excitation, several different systems are available, including impact hammers, drop weight impactors and shakers. Since no single method is superior to another, preference is dependent on individual site conditions and the consent of the tester. Important in the choice of impact equipment is the magnitude of its weight, since this is the governing factor for producing acceptable signal-to-noise ratios [78]. Also, the size of the system and accessibility of the structure are of importance, as they largely influence the weight and portability of the exciter. Alternative to force-excitation, the structure may be excited by means of displacement-release. However, this method is often difficult to realize in the field. Moreover, it has been shown that it might possibly limit the range of available modes for extraction [81]. Some of the most common excitation sources employed in modal testing are shown in Figure 4.54.

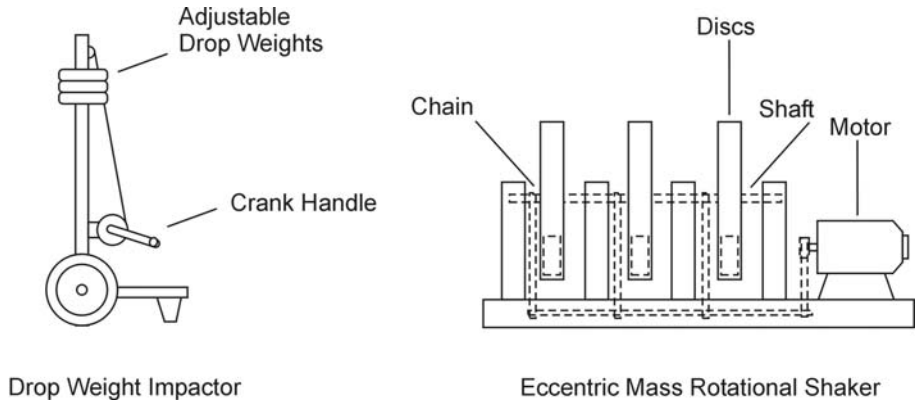

Figure 4.54: Various excitation sources

4.14.2.2 Transducers

Among the various types of transducers, the piezoelectric type is typically given preference in modal testing [83]. Depending on the desired quantity measured, two inherently different types of transducers can be used in modal testing – force transducers and accelerometers. In the force transducer, force from an external vibration is transferred through a casing directly into the piezoelectric crystal, which then generates an electric charge corresponding to the magnitude of deflection. Because the force must be transferred through the casing into which the crystal is installed, cross-sensitivity from the shear of transverse loading represents a source for erroneous readings.

Accelerometers utilize a slightly different configuration, in which the piezoelectric crystal is located between the casing and an additional seismic mass, acting as an inertia force. Thus, within a certain frequency range, the transducer records the acceleration of the body it is attached to. In this type of configuration, the lowest resonant frequency of

the transducer is of particular interest, since this defines the working range of an accelerometer [83]. Figure 4.55 shows an example of a typical accelerometer, which is most commonly used for modal testing of large structures.

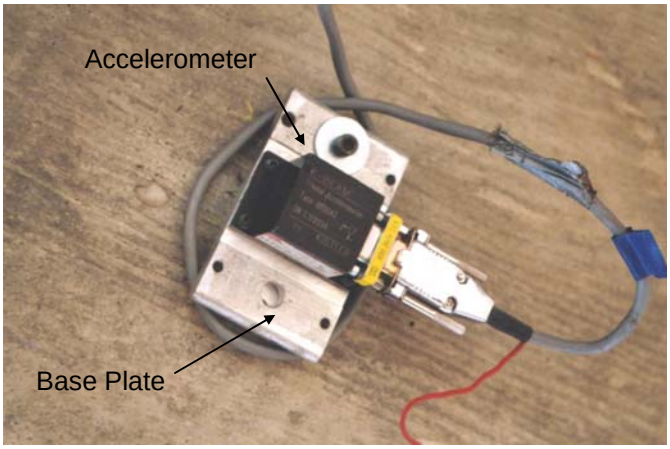

Figure 4.55: Piezoelectric transducer on base plate

4.14.2.3 Data processing

As the structure undergoes vibration, data continuously streams from each of the various accelerometers into a central signal-analyzing unit (Figure 4.56). Upon acquiring an adequate number of excitations of an acceptable signal level, this data is transferred to a stationary or portable computer that extracts the damped natural frequency and damping ratios for each of the individual modes of the structure. Depending on the number of accelerometer points, the individual modeshapes can be displayed to a greater detail. Utilization of a high number of transducers is particularly important if one seeks to extract higher modes of vibration, as these contain a much larger number of nodes.

Figure 4.56: Portable acquisition unit

4.14.3 Techniques and applications

Driven by the continuous deterioration of today's civil infrastructure, modal analysis has already attracted considerable attention as a means for monitoring and characterizing the onset and progression of global structural damage [78, 80]. Consequently, this has led to the development of methodologies for stationary and in-situ documentation of changes in the modal parameters of structures, as found in the literature [78, 79, 80, 84].

While mostly applied to measure levels of deterioration in conventional reinforced concrete structures, recent projects have been aimed at investigating the efficiency of CFRP-rehabilitation schemes. Herein, it was assumed that the global stiffening, induced by the external bonding of pultruded CFRP strips or in-situ-processed composites, would yield changes in modal characteristic that can be extracted from such tests.

In the civil sector, modal analysis has found highest acceptance in the investigation of long-term deterioration, i.e., the loss in structural performance of medium- to large-scale structures. Often, these structures already display a significant degree of visible damage, such as flexural and transverse cracking, along with consequent discoloration caused by the corrosion of the internal steel reinforcement.

The general test methodology employed in modal analysis of large structures is discussed by Bolton et al. [78]. Herein, they investigated a concrete box-girder overcrossing consisting of two spans, each of about 120 ft in length. The entire structure was modeled using a total of 30 nodal response points, yielding an average spacing between transducers of approximately 20 ft. Modal test data were collected incrementally in several data sets using a portable instrumentation setup consisting of five to seven individual accelerometers.

The test employed an impact hammer with variable tip weight so as to adjust for the needed impulse levels that were required to excite the structure and develop acceptable signal-to-noise ratios. The resulting excitation pulse contained frequencies of 100 Hz or less with a duration of approximately 10 to 15 milliseconds, causing acceleration extremes ranging from 0.003 to about 0.025g. The system sensitivity is typically adequate to sense these levels of excitation.

To comment on eventual deterioration of the structure, two 3-day modal field tests were performed at an interval of roughly one year. Surprisingly, modal parameters extracted from the second field test yielded an increase in modal frequency, i.e. a stiffening of the structure, which is contradictory to the expected decrease in modal frequency. These unexpected changes were attributed to differences in environmental conditions, as the first test was performed under moist conditions, yielding a higher structural mass and consequently lower modal frequency.

4.14.4 Capabilities and limitations

Traditionally, modal analysis has been used to analyze damage in small- and medium-scale components, most of which show high material homogeneity and clearly defined boundary conditions. Unlike these former approaches, modal analysis of civil structures brings upon new and challenging difficulties, mainly due to the unusually high material-variability, environmental instability and procedural variations related to collection, extraction and interpretation of in-situ

data streams. Herein, unknown boundary conditions of large-scale structures, promoted by the presence of considerable deterioration near abutments, and the large environmental fluctuations may be considered predominant factors. Quite often, these factors contribute to high variability and sometimes inconclusive test results. As previous research has shown, variations in the structural mass, as a result of moisture uptake, can result in significant signal scatter between successive field tests [78]. This, in turn, may lead to erroneous interpretations, such as loss in stiffness and consequent internal structural damage.

In view of the present discussion, modal analysis presents further drawbacks. Foremost among these, one should critically assess the maximum obtainable sensitivity of modal testing of large structural components. On structures often exceeding several hundred feet, it may be concluded that signals generated at discontinuities in or below the CFRP material are of insignificant size to contribute to the overall modal response. Moreover, an almost infinite number of internal discontinuities inherent to the concrete substrate (moisture, voids, internal reinforcement) will contribute to background noise, most likely resulting in a shadowing of any such signal.

Apart from former sensitivity-related aspects, the user is confronted with a variety of practical concerns. First, modal analysis entails considerable limitations in terms of real-time data acquisition capability. Although the data stream is collected and permanently stored in the field, analysis and the rather complex interpretation of the collected waveforms must often be performed off-site. Hence, no instantaneous assessment can be given on the current state of structural integrity. Second, identification of changes in modal response necessitates precise knowledge of a baseline model, which can only be provided through complex FEM analysis. Alternatively, the relative change in modal response may be obtained from two or more successive field tests, which imposes a significant time delay, as one may not draw any conclusions on structural integrity until after the second test.

Given the above, it remains doubtful as to whether modal data can display changes in vibration characteristics to such high detail that it allows the inspector to comment on changes in the quality of externally bonded rehabilitation schemes, particularly in situations where these are of highly localized occurrence. Hence, it is concluded that modal analysis remains a tool of global structural analysis and shows little feasibility for detection of localized damage in externally bonded CFRP composites.

4.15 RAPID LOAD TESTING

4.15.1 Fundamentals and theory

Prior to erection, structures are designed based on certain predefined maximum permissible levels of loading and deflection. A structure is considered to be in good or serviceable condition as long as these limiting criteria are not exceeded under service load levels. With progressing age, individual components are likely to experience distinct forms of material degradation, such as fatigue cracking, moisture absorption, or creep, directly affecting the overall performance of the structural system. In most cases, material degradation can be linked to a reduction in stiffness [78]; hence members will become more flexible once they show significant levels of one or more of the above degradations. Since load-deflection behavior of individual members,

such as transverse girders, can be directly related to their stiffness, one may conclude that a component, which shows sufficient levels of degradation, is likely to exceed its preset levels of deflection. In a general sense, the principle of rapid load testing is based on this methodology.

Often, material composition and geometry are not known to a sufficient degree, which restricts the feasibility of analytical approaches and necessitates the use of alternative methodologies. One such methodology is the rather simplistic approach of applying an experimental loading condition that, within limits, simulates the real-life situation given at a distinct location within the structural system. Thus, experimental testing can provide a more representative and meaningful evaluation of the structure.

Although modeling of most real-life loading conditions requires replication of a uniform downward pressure, loads are mainly induced at a single point, and the corresponding deflections are measured at various locations along the member. Loads are commonly applied via hydraulic jacks in combination with a load cell to monitor the applied levels of loading. For any given structure, the critical load levels are typically defined as 85% of its factored design load, excluding any loads induced by self-weight or test equipment [85]. At numerous locations, linear variable differential transformers (LVDT) serve for deflection measurement. In addition, material strain, crack growth and rotation are commonly also of interest. These parameters can be instrumented via the use of electrical resistance strain gauges, extensometers and inclinometers, respectively.

Depending on load magnitude and specific test conditions, a suitable test setup must be chosen. To complement testing at both ground and elevated levels, a number of different load application methods are typically utilized. Because high levels of loading are induced at an isolated location, reaction forces must be directed into a multitude of suitable supports, which can be provided in form of other members, situated in close vicinity to the test member, or through ground fixation by means of steel chains. Regardless of the force transfer mechanism, distribution of the induced hydraulic reaction force is paramount, as it reduces the risk of failure in secondary components of the structure. Illustrations of some of the most frequently employed loading schemes are depicted in Figure 4.57.

In early load testing procedures, loads were applied statically for about 24 hours, after which the first deflection reading was taken. A second measurement followed roughly 24 hours after removal of the load to supply information on the deflection recovery capability of the structure. In rapid load testing, the duration can be significantly shorter, while its cyclic nature is considered a suitable substitute for the 24-hour sustained load of earlier applications [85].

Similar to modal testing, the principle of defect detection in rapid load testing is manifested by a stiffness reduction principle. It is assumed that a sound structural component retains its initial stiffness as long as no material deficiencies are introduced. With the onset of material degradation, stiffness is likely to be reduced. As a result, one may conclude that material degradation has occurred simply based on an increase of deflection under identical levels of externally applied load. However, this presumes that such variations are of sufficient magnitude to be sensed by the load testing system. Thus, if defects develop or progress in locations of structural irrelevance, they are likely to go undetected.

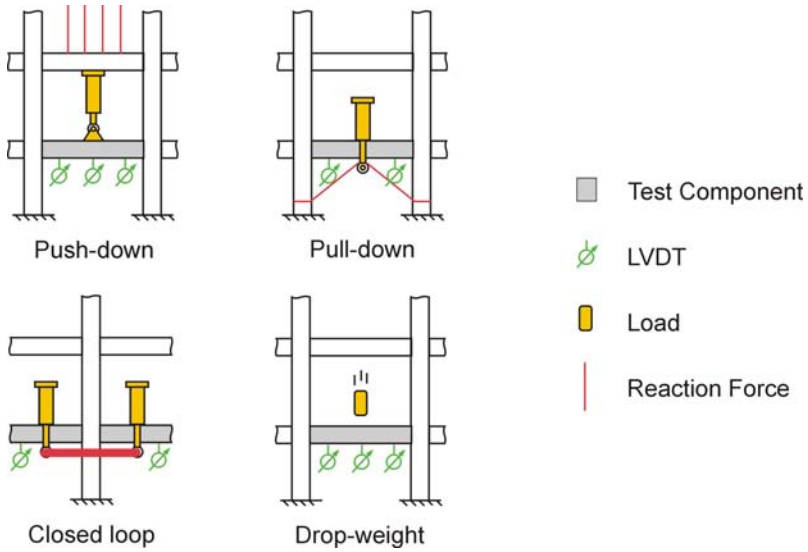

Figure 4.57: Common loading-mechanisms in Rapid Load Testing [85]

4.15.2 Instrumentation

Systems for rapid load testing are similar to those used for structural testing in many laboratories. Complete systems encompass one or several hydraulic actuators, typically capable of developing extremely high loads. Such high capabilities are required to produce the forces required to induce noticeable deflections in structural members. To monitor the corresponding deflection of the member under investigation, a number of deflection, rotation and strain measurement devices are used. Lastly, data acquisition systems store all information provided by the actuator and measuring devices.

4.15.2.1 Hydraulic actuator and pump

Hydraulic systems provide efficient means to develop the usually high forces required in load testing. A typical system is comprised of a pump, controlling the flow of hydraulic oil, and a telescopic actuator (Figure 4.58). Both components are connected by two pressure hoses that allow hydraulic oil to flow to and from the piston inside the actuator. Pressure regulators allow the exact control of oil flow, such that the load can be increased and decreased at a desired rate. A load cell is typically installed between the actuator and the component to allow continuous monitoring of the applied force.

4.15.2.2 Measuring devices

Deflection measurements are commonly performed by use of highly sensitive devices, such as strain gauges or extensometers. As mentioned earlier, electrical resistance strain gauges provide sensitivities as low as 1 με, whereas the recommended minimum measurable value of extensometers lies at about 50 με [85]. While strain gauges find use mostly for monitoring of crack growth phenomena, LVDT's provide sufficient sensitivity for most load-testing applications. Due to their small dimensions, they often require a

supporting fixture, such as a tripod, to be located at an elevated height. With increasing deformation of the extensometer shaft, an electronic signal is delivered to a data acquisition unit for recording and further evaluation.

Figure 4.58: Hydraulic jacks

4.15.2.3 Data acquisition

To perform measurements at various locations throughout a structure, a large number of strain and deflection devices are required. This implies that the recording system must supply adequate capabilities to accommodate the incoming data stream. Since each device occupies a separate channel for data storage, large data acquisition bays (Figure 4.59) are commonly used. From there, data is swept onto computers for permanent storage and evaluation.

4.15.3 Techniques and applications

Numerous case studies and commercial projects have been conducted, which are discussed in great detail by Mettemeyer and Nanni [85]. Most tests were aimed at evaluation of concrete structures that had undergone external strengthening by means of bonded steel and CFRP plates. Since the use of CFRP for external strengthening of structures has not yet been accepted as a standard practice, rapid load testing has been used to validate and 'proof' test their performance.

According to the methods outlined in Section 4.15.1, loads were applied in various locations, including pushdown, closed loop, vehicle, and dropped weight. In the testing of individual rehabilitated components, the loads were limited to levels not exceeding 85% of the factored design moments, which resulted in a linear response for all load levels and configurations. In all cases, a stiffening effect of the strengthened member could be observed.

Figure 4.59: Multi-channel data acquisition bay

4.15.4 Capabilities and limitations

Rapid load testing has proven to be a useful tool in the evaluation of post-strengthened structural components [85]. Based on the variation in stiffness (and consequently deflection) under cyclic loading, the efficacy of the rehabilitation method can be assessed. If the induced loads are limited in such ways that they do not exceed a linear load-deflection range, the method can be assumed to be of a non-destructive nature without causing reduction in the performance to the individual members or the structure as a whole. Because much of the equipment utilized in rapid load testing is commercially available and currently employed in many structural-testing facilities, familiarity with the equipment and methodology of the technique can be assumed.

Problems for non-destructive evaluation, especially on a local scale, can arise insofar as the system is highly capable of capturing a multitude of local effects and combining them into a single response, while the individual initiators may not be clearly distinguishable. Such local initiators include, but are not limited to, concrete cracking, debonding at the concrete-composite interface, fiber rupture, and moisture absorption. As such, a distinct separation between the individual defects, assuming a noted reduction in stiffness, becomes virtually impossible. Also, the true non-destructive characteristics of rapid load testing may be limited to a level at which the defects in composites have already exceeded acceptable limits. In other words, defects in CFRP composites or the interfacial regions between the CFRP and concrete may not be of sufficient magnitude to alter the load-deflection response acquired during a rapid load testing procedure. Currently, this area has not been investigated and thus remains subject to further research.

Summarized, the method is likely to lack sensitivity to small defects as well as the capability to provide characterization in terms of size, location and magnitude of individual flaws. Hence, in comparison to most of the previously discussed NDE methods, rapid load testing shows severe limitations for defect detection in CFRP strengthening systems.

4.16 DISCUSSION AND CLASSIFICATION

4.16.1 Introduction of a classification methodology

Hitherto, the reader has been given a general review of NDT techniques and a number of data-collection methods, most of which have already been implemented into industrial inspection procedures or which are currently used for numerous experimental research applications. The individual techniques have been discussed in terms of basic methodology, instrumentation, recent applications, and capabilities and limitations. It has been shown that successful application of techniques is largely dependent on a variety of test parameters, such as material composition, dimension and surface texture of the test object, test conditions, and means of data acquisition/interpretation. Hence, to comment on the applicability of individual NDT methods in view of the present discussion, the former characteristics of such methods must be reviewed and classified with special consideration of their applicability to CFRP-rehabilitated structural components.

As mentioned, a limited body of work discussing NDT of CFRP-rehabilitated components has been made available. This body of work serves well in assessing the suitability of a few established NDT techniques; however, most traditional and recent methods must be classified on an alternative basis. Primarily, techniques that have proven to be applicable for investigating CFRP must be rated higher than those having little to no history in nondestructive evaluation of composites. As mentioned earlier, a suitable method must satisfy two preconditions:

- It must possess characteristics that strongly encourage its use on CFRP overlays, i.e. provide adequate detectability, preferably supported by previous research conducted in the composites sector; and
- It must utilize equipment which meets the practical necessities imposed by in-situ NDT, i.e. be suitable for inspecting a variety of geometric configurations and be operable in a number of different field environments.

In review, defect detectability entails system sensitivity, transparency, and reproducibility, all being factors of paramount importance. Conversely, practical aspects are related to portability, system complexity, flexibility, and equipment availability and cost. Thus it is imperative that the individual requirements be given relative levels of importance.

Most important, non-destructive testing techniques must allow the inspector to obtain information from inside the composite material or concrete/composite interfacial regions to such a detail that predictions on the overall integrity of the composite/concrete system can be made. While this does not imply a global assessment on structural safety, defect type, location, and size should be obtainable from a potential technique. Although practical aspects can have a profound

effect on efficiency, safety, and equipment and labor expenses, only systems yielding high detectability can be considered feasible.

Undoubtedly, methods not capable of providing the desired level of sensitivity and comprehensiveness are to be disregarded, regardless of their practical merits. Hence, compared to practical aspects, defect detectability will generally be assigned a higher level of importance. Nonetheless, if stringent safety requirements or unjustifiably high cost imply practical limitations, the former ranking scheme will be revised and adjusted accordingly. However, stringent practical limitations will not result in immediate exclusion of the method as in the case of insufficient detectability. Figure 4.60 depicts the individual steps of the previous ranking rationale in more detail. Although adherence to the ranking procedure should not be considered stringent in every aspect, it provides insight to the general rationale.

As may be seen, Figure 4.60 entails information given in Table 4.3 as well as individual graphs of Table 4.4 to comment on detectability and practicality, respectively. In the following, the rationale for obtaining this information will be presented. Because detectability and practicality each encompass a number of subcomponents, which can be of considerable relevance for an individual technique, these will be discussed in further detail. Components of the classification scheme include the following:

1. Defect Detectability
   - Range of detectable defect types
   - Minimum detectable defect size
   - Range of detection depth

2. Practicality
   - System type [near-field/full-field/global]
   - System portability
   - Coupling requirements
   - Real-time data acquisition
   - Ease of interpretation
   - Possible service inflictions
   - Initial and servicing cost of equipment
   - Level of sophistication

Ideally, it would be preferable to obtain defect detectability from a number of field or laboratory experiments. However, for most techniques, such information has not yet been made available. Moreover, the presence of a concrete substrate can cause substantial signal interference in form of scattering or absorption. Due to this limited knowledge, the classification matrix shown in Table 4.3 must, at present, be considered mostly qualitative. Although minimum detectable size and depth penetration will later be of profound importance, it is extremely difficult to assess at this point.

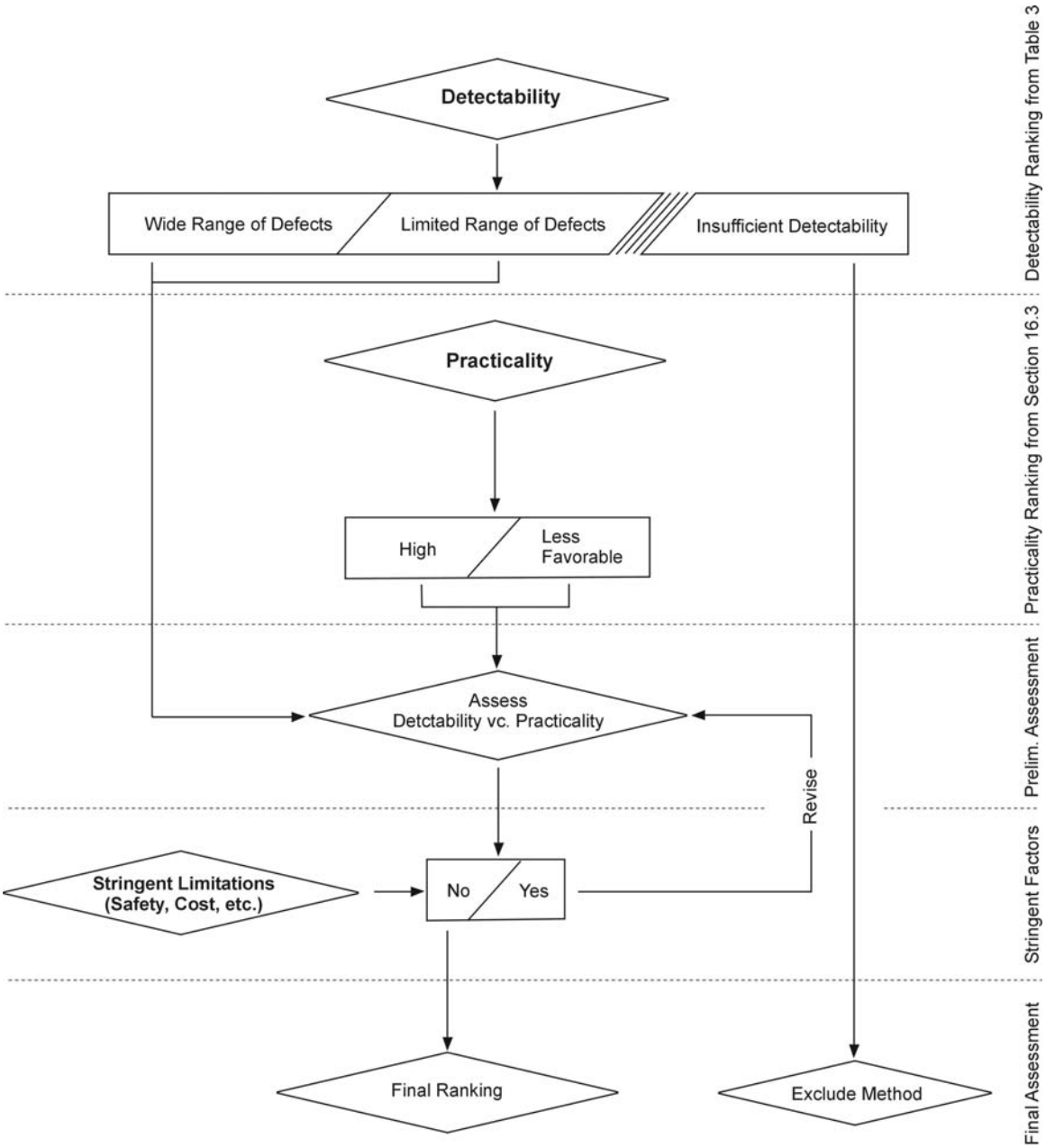

Figure 4.60: Flowchart for ranking assessment

4.16.2 Detectability matrix

The detectability matrix (DM) is presented in Table 4.3. Only a limited number of defects were chosen for assessment purposes, most of which can be considered to be of likely occurrence in laminated composite materials. Those omitted are mostly related specifically to FRP-rehabilitation, e.g. high spots, substrate degradation, etc., and hence cannot be assessed at this point. Further, the reader should differentiate sharply between defects that cannot be identified (⇩) and those of which detectability is currently unknown (-). The DM differentiates between

unknown and *unidentifiable* in such a manner that the former does not necessarily imply the unsuitability of a method towards the specific type of defect. Rather, the method has not yet been investigated upon its sensitivity to this type of defect; hence no assessment can be given. On the other hand, unidentifiable defects are those for which insensitivity has already been proven. Furthermore, the capability of localizing and sizing of a specific form of defect is addressed.

As may be noted, the capability of techniques to detect the presence of defects does not necessarily imply the ability of localization and sizing. Excellent examples of this are acoustic emission and optical fiber measurements. Although signals of internal material fracture and/or friction can be sensed by both methods, exact localization and sizing, the former being especially critical for AE, pose extreme difficulties. As was discussed, the material anisotropy of CFRP makes localization via AE measurements even more inconclusive. Hence, only methods bearing indices 'L' and 'S' show adequate means of defect characterization.

4.16.3 Practicality matrices

Irrespective of previous application to CFRP-rehabilitated structural components, most of the above methods have found use in one or multiple fields of engineering. Hence, much information can be given on equipment and overall system complexity, as well as the detection methodology of each individual technique. Although practicality entails a number of individual aspects, experience gained through past applications often reveals the eventual difficulties in system setup, data acquisition, interpretation, portability issues, etc. Such background knowledge thus builds the basis for the subsequent practicality assessment.

A template for the practicality matrix (PM) is shown in Figure 4.61. To aid the reader in comparing individual methods, the matrix displays information in a graphical format. Individual aspects are assigned columns of various heights, with longer columns representing a more preferable situation while implicit limitations are indicated by a short column height. This may be particularly helpful since the overall practicality must be considered a combination of its individual components. Hence, from comparing the overall column heights, one may quickly discern unsuitable methods from those yielding high practicality.

In addition, the PM includes a short list of some of the most outstanding advantages and/or disadvantages of each individual method. Similar to the detectability matrix, three distinct levels of practicality are used in the ranking scheme. It should be noted that certain parameters cannot be ranked and are thus classified as 'not applicable.' In cases where one method may be applied in different forms (e.g. A-scan versus C-scan) dotted lines are used to indicate a range of practicality variation. In such cases, a footnote will provide further information of why such variability must be granted. In the following sections, a brief introduction to each of the individual practicality parameters is given.

Table 4.3: Detectability classification matrix

NDE METHODS	DEFECT TYPES							
	Delamination	**Voids**	**Moisture**	**Resin Thickness Irregularities**	**Fiber Waviness**	**Fiber Breakage**	**Porosity**	**Matrix Cracking**
Visual Testing (VT)	⇨$_{L}$	⇩	⇩	⇩	⇨$_{L,S}$	⇩	⇩	⇩
Acoustic Impact Testing (AIT)	⇧$_{L}$	⇨$_{L}$	⇩	⇩	⇨$_{L}$	⇨$_{L}$	⇩	⇩
Penetrant Testing (PT)	⇩	⇩	⇩	⇩	⇩	⇨$_{L,S}$	⇩	⇨$_{L,S}$
Ultrasonics (UT)	⇧$_{L,S}$	⇨$_{L}$	⇨$_{L}$	-	-	⇩	⇩	⇩
Radiographic Testing (RT)	⇧$_{L,S}$	⇧$_{L,S}$	⇨$_{L,S}$	⇧$_{L,S}$	⇧$_{L,S}$	⇧$_{L,S}$	⇧$_{L,S}$	⇧$_{L,S}$
Thermographic Testing (TIR)	⇧$_{L,S}$	⇨$_{L,S}$	⇨$_{L}$	-	-	-	-	⇩
Eddy Current Testing (ET)	⇩	⇩	-	⇩	⇧$_{L}$	⇧$_{L}$	⇩	⇩
Optical Methods (Shearography)	⇧$_{L,S}$	⇧$_{L,S}$	-	-	⇧$_{L,S}$	⇧$_{L,S}$	-	-
Acoustic Emission (AE)	⇨	⇩	⇩	⇩	⇩	⇧	⇩	⇧
Ground Penetrating Radar (GPR)	-	-	-	-	-	-	-	-
Strain Measurement Techniques (Optical Fibers)	⇨$_{L}$	⇩	⇩	⇨$_{L}$	⇨$_{L}$	⇩	⇩	⇩
Modal Analysis	-	-	-	⇩	⇩	-	⇩	⇩
Rapid Load Testing	-	-	-	⇩	-	-	⇩	⇩

⇧ Generally Detectable ⇨ Limited Detectability ⇩ Not Detectable - Detectability Unknown

Indices: L = Allows localization
S = Allows accurate sizing

Note: Microwave Testing has been omitted from this table as its general methodology has been outlined through discussing ground-penetrating radar (GPR) in Section 4.12.

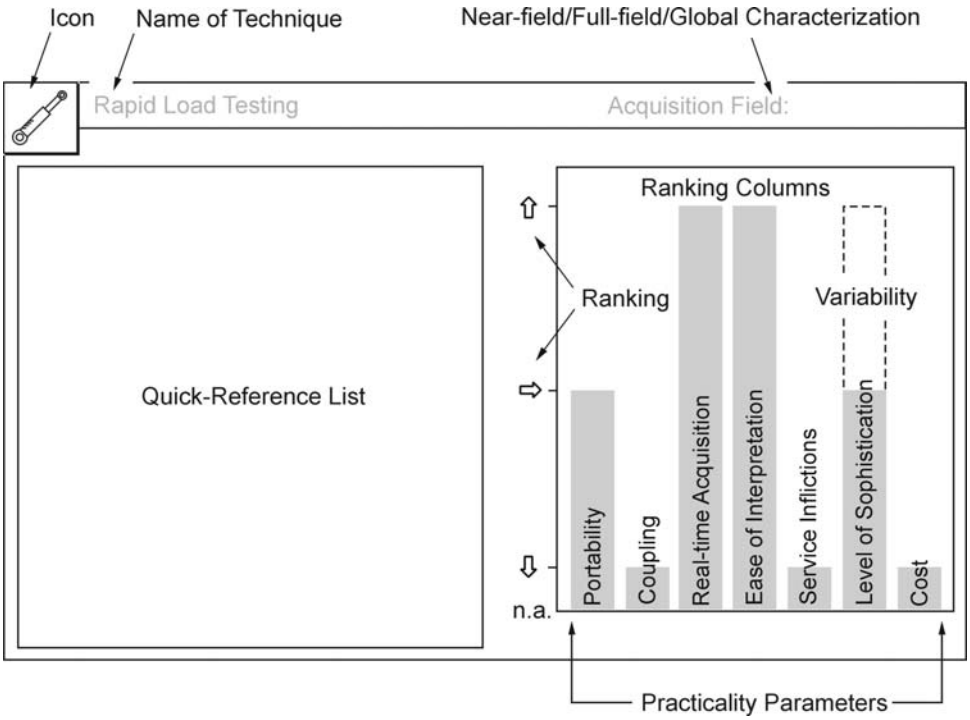

Figure 4.61: Practicality matrix

4.16.3.1 System type

NDE systems can be assigned to one of three general system types, namely near-field, full-field and global. The profound difference between these system types is given by their field-of-view. As such, a global system is preferably used to obtain information on a structural level, while near- and full-field techniques serve a more localized and detailed analysis in regions where the presence of defects is known or expected to be of particularly high occurrence. While global methods can provide rapid insight to large discontinuities and overall structural deficiency, they typically lack the sensitivity to localized defects. Conversely, local NDE systems are given preference once defects have already been located on a global level, as they provide enhanced sensitivity to minute anomalies. As discussed, a suitable combination of the two can provide a means for rapid inspection on the structural level with subsequent near-field capabilities for a more detailed inspection.

4.16.3.2 Portability

As with all field inspection, portability and ease of handling of the test equipment and related tooling is of paramount importance. During local inspection, equipment must be easily transportable from one location to the next, preferably by a single person. Quite often, bulky equipment restricts the applicability of a technique simply because inspectors cannot handle, adjust or even assemble the individual components in the field.

For global methods, which may allow users to inspect entire parts of a structure from a single location, portability, as outlined above, will be of less significance. Nevertheless, global methods must be portable insofar as the equipment is of manageable size and weight to be transported to and from the site. Generally, the portability of global testing equipment entails any factors restricting its removal from a laboratory environment, such as a high power source, environmental sensitivity, etc.

4.16.3.3 Coupling

Intimate contact requirements can impose great limitations on the overall efficiency of an NDE method. The necessity to provide permanent coupling between the part and the inspection tool often results in a slow and sometimes messy inspection procedure, especially in cases where gels or chemicals are applied to the test surface. Further immediate- and long-term effects of couplants and chemicals on the integrity of CFRP laminates have not yet been established. Thus, to ensure a more efficient scanning process, it is preferable to operate all equipment in a non-coupled arrangement, i.e., such that data can be acquired without intimate contact with the structure.

4.16.3.4 Real-time acquisition

To allow in-situ interpretation, data acquisition must be realizable in real-time; i.e., the inspection must be able to extract all information during or directly following completion of a testing cycle. Herein, difficulties typically arise in cases where a method requires a massive computational effort or development of exposed films in a laboratory environment. In most cases, the use of digital systems in combination with modern laptop computers can facilitate faster acquisition times and a more efficient computation process.

4.16.3.5 Ease of interpretation

Upon completion of the acquisition process, the user is typically presented with a plot or image, showing a systematic representation of the collected data in a tabular, graphical, or other suitable format. Ideally, graphical images show the inspected part in two-dimensional view with information superimposed in the desired format (e.g., temperature contours in IR testing, strain profiles in shearography, etc.). These ‘mapped’ images are most convenient to interpret, as the observer can best correlate between the displayed image and the test part. In contrast, information provided in x-y coordinate systems (e.g., A-scan, AIT force-time history plot) are more difficult to interpret and require a more fundamental knowledge of the technique.

4.16.3.6 Service inflictions

During inspection, the serviceability of the structure should not be influenced to a significant degree; i.e., inspection teams should not be required to disrupt traffic or shut down entire lanes of a bridge. Typically, infliction with traffic is required due to one of two reasons. First, the test setup may require simultaneous access to one or multiple traffic lanes, such that inspectors would be exposed to a significant safety hazard if traffic were not disrupted. Second, ongoing traffic may induce vibration to the structure that,

while preferable for passive methods, may result in background noise and/or erroneous readings for a number of active methods. Hence, methods that are immune to either of the two formerly mentioned conditions are most preferable.

4.16.3.7 Level of sophistication

Sophistication is mainly dictated by the amount of previous research and practical work conducted in a specific area. Although a method can be rather simplistic, a long history of industrial and experimental application ensures familiarity, reproducibility and higher efficiency during inspection. Further, equipment is likely to be more readily available and obtainable at a lower cost. As such, sophistication is profoundly different from the level of complexity, which mostly relates to how exhaustive and detailed the given information is. However, high complexity does not necessarily imply a high level of industrial establishment.

4.16.3.8 Cost

Equipment cost is mostly regulated by two factors, namely complexity and extent of industrial use. In most instances, complexity may be assumed to be the governing factor; however, widespread industrial use often leads to a significant reduction of equipment and instrumentation cost.

Table 4.4: Practicality matrices

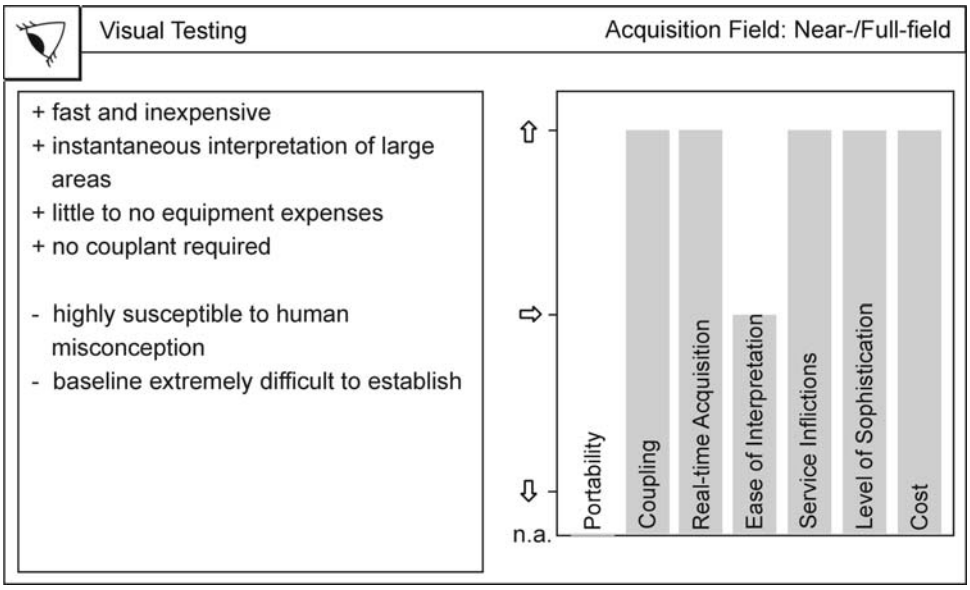

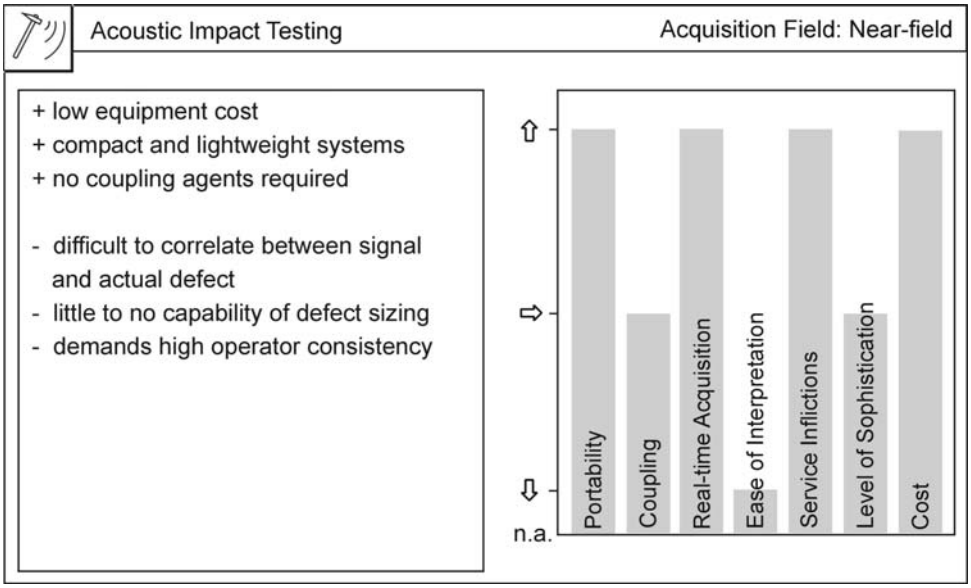

Table 4.4 (continued): Practicality matrices

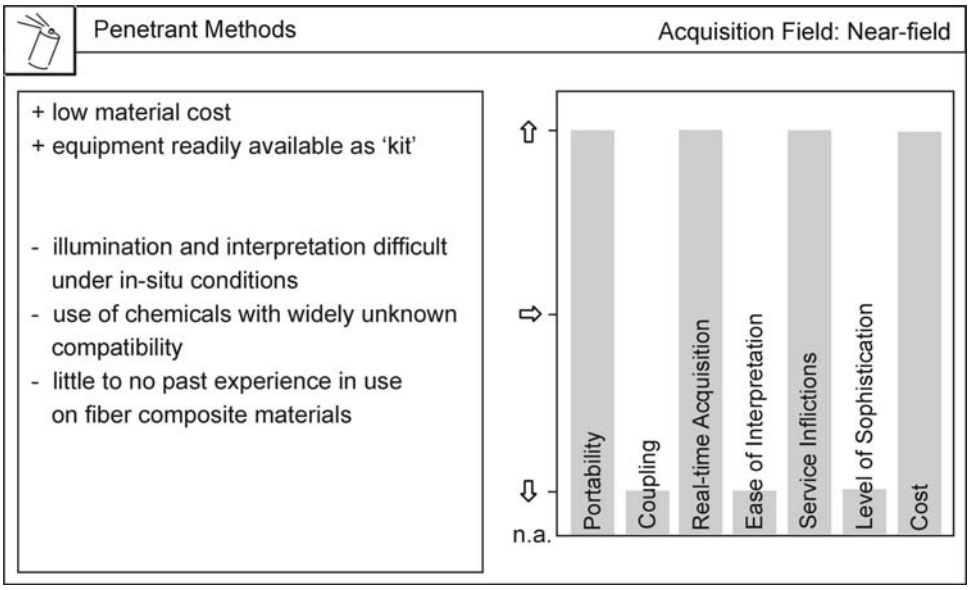

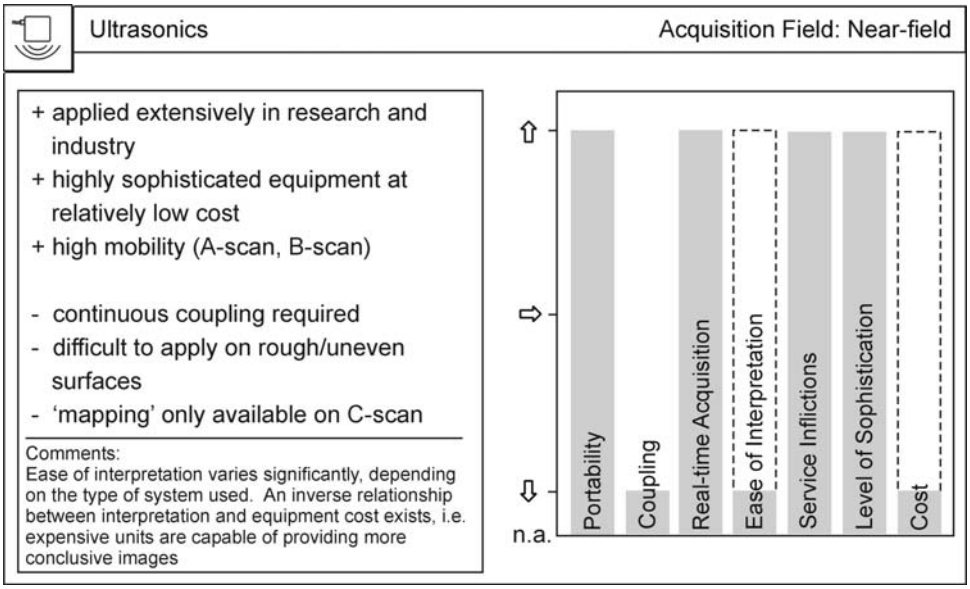

Table 4.4 (continued): Practicality matrices

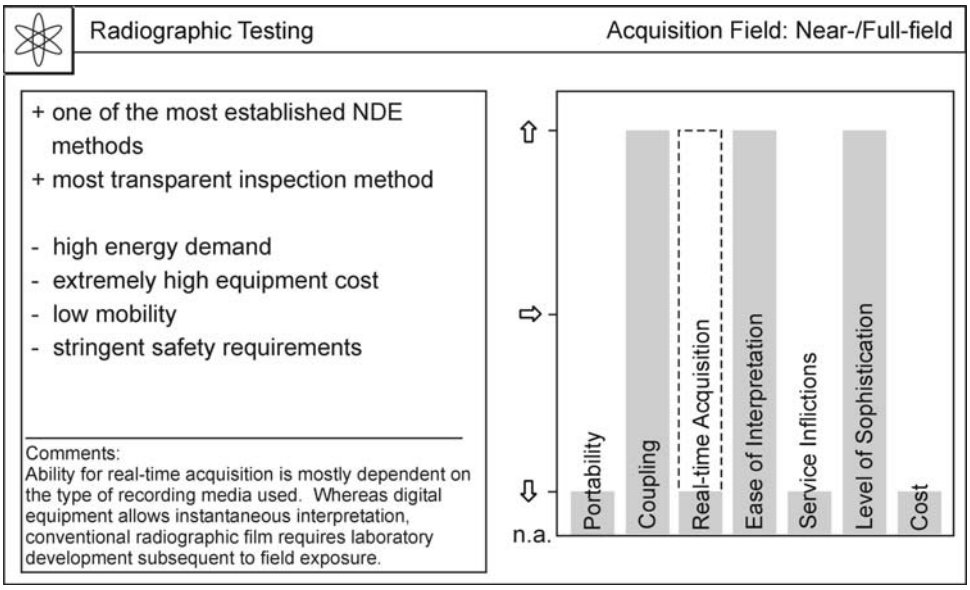

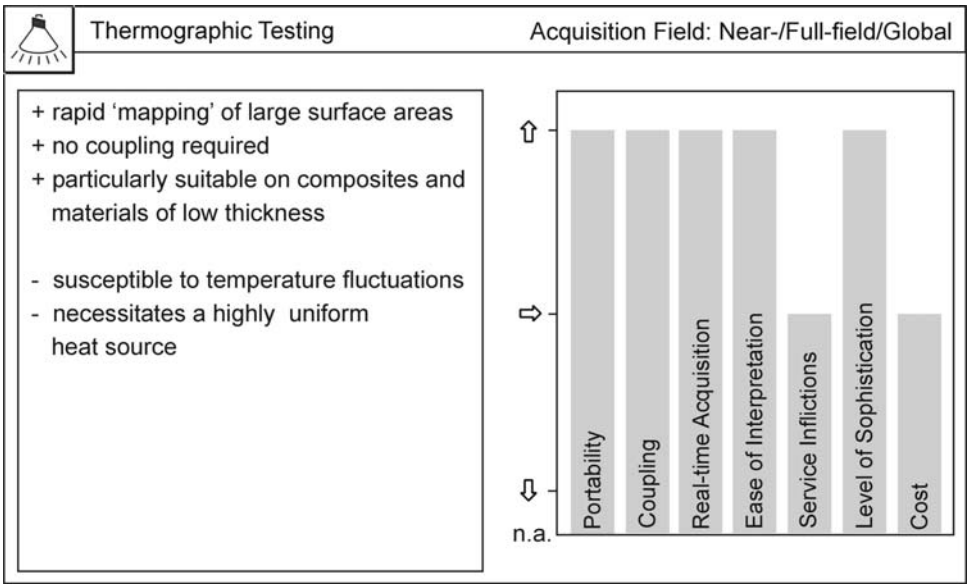

Table 4.4 (continued): Practicality matrices

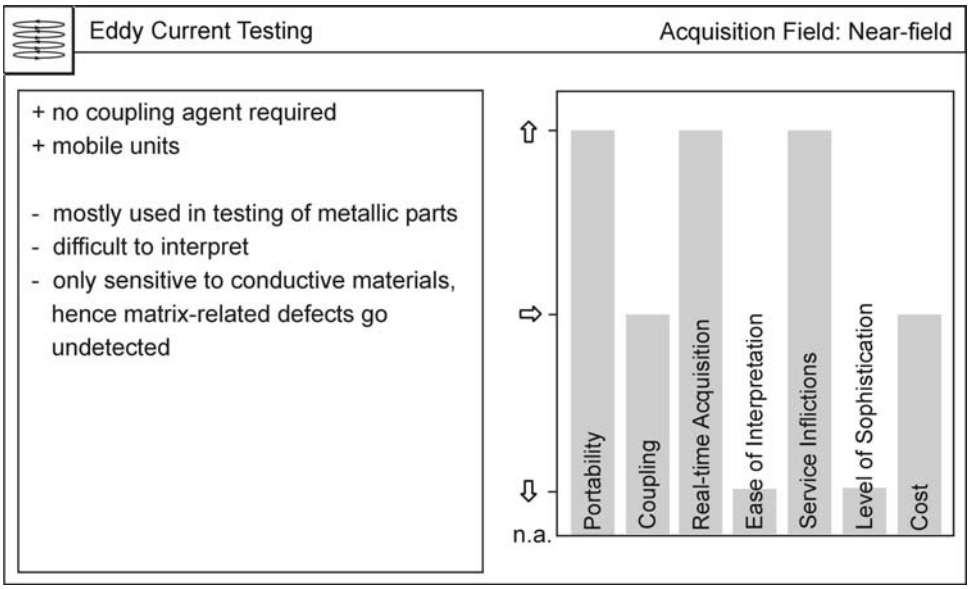

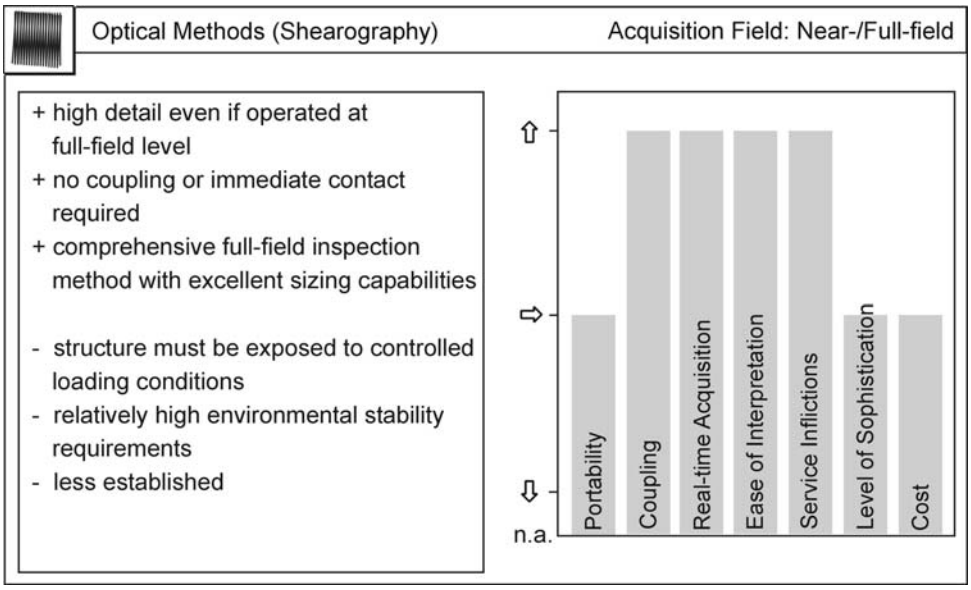

Table 4.4 (continued): Practicality matrices

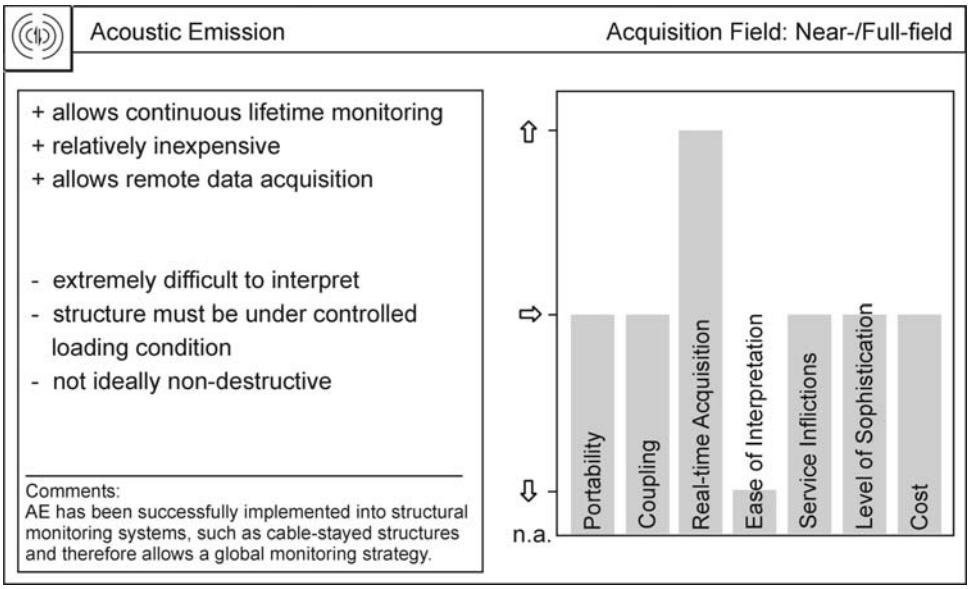

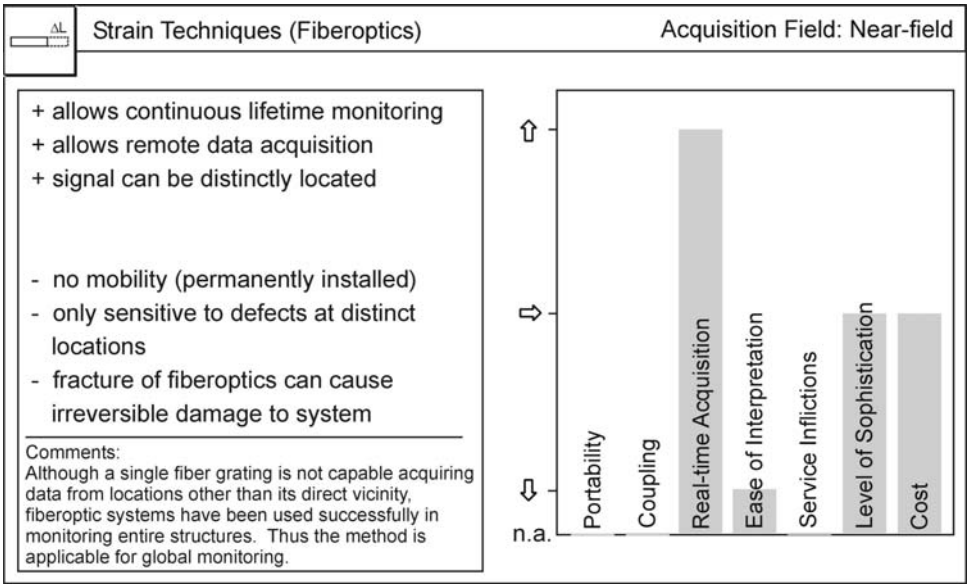

Table 4.4 (continued): Practicality matrices

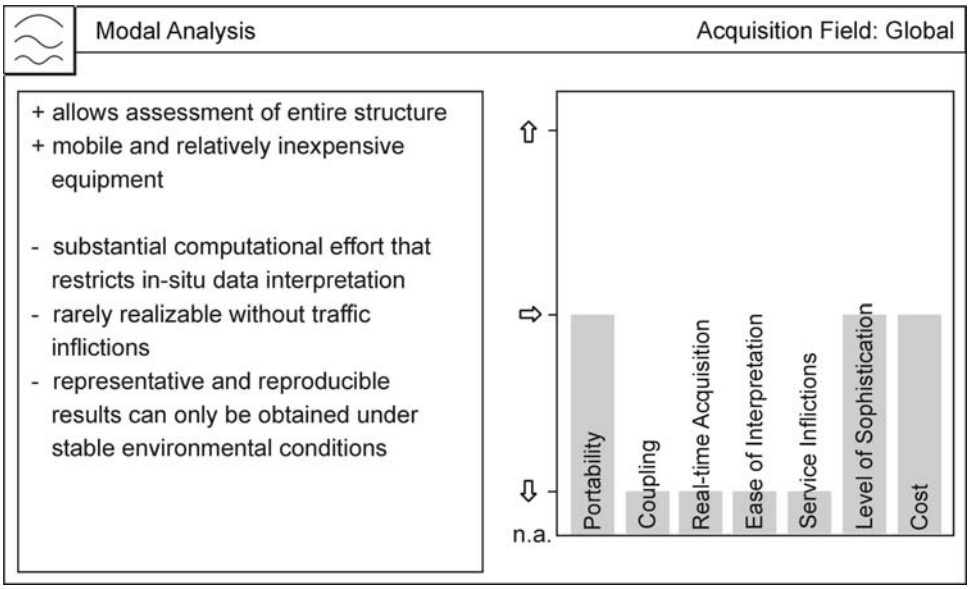

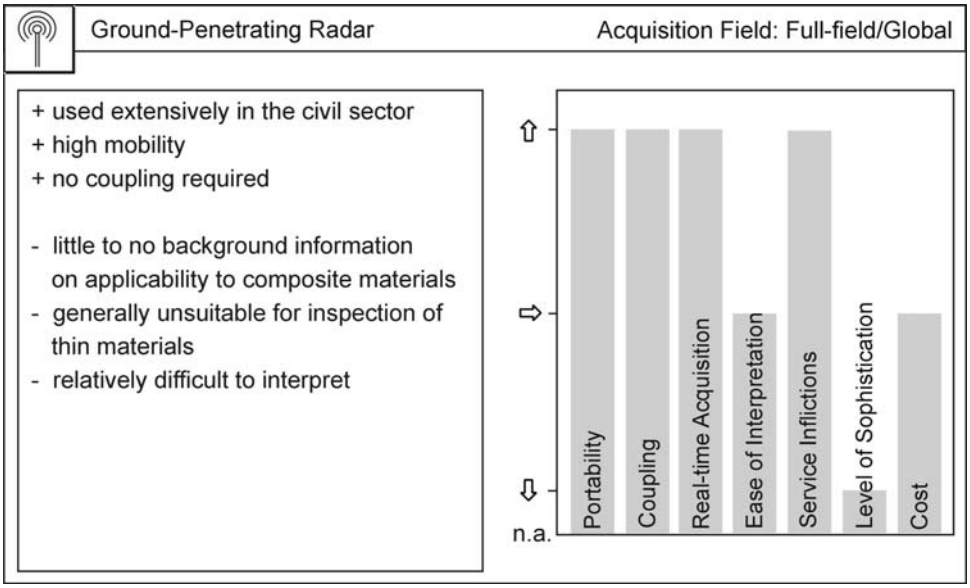

Table 4.4 (continued): Practicality matrices

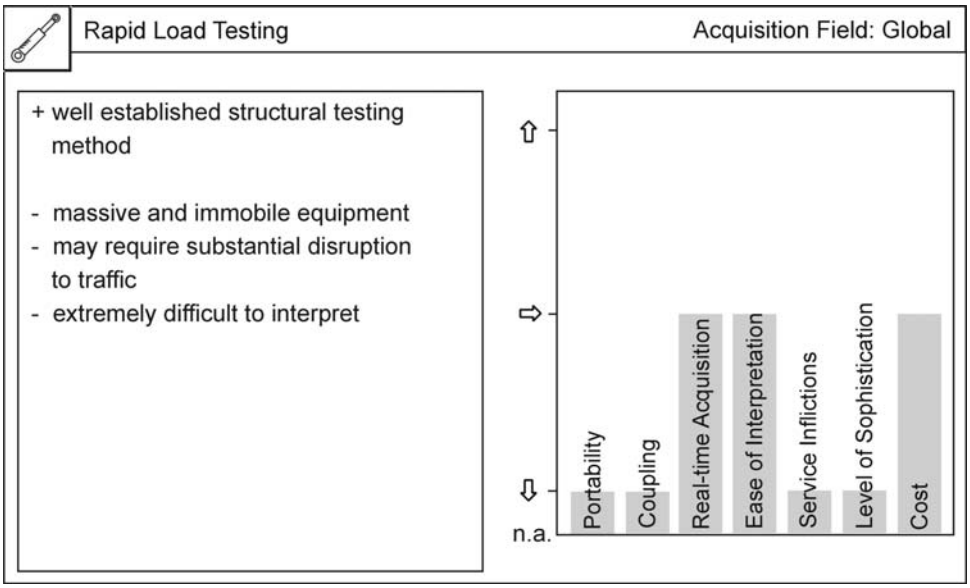

4.16.4 Ranking matrix

Taking the previous classifications into consideration, the final ranking matrix (RM) may now be assembled, as shown in Table 4.5. As outlined, it entails all of the discussed methods, ranked according to a combination of detectability, practicality, and eventual stringent limitations, as outlined in Figure 4.60. First, selected methods will be classified as *primary* choices, as they show superior applicability over the remaining field. This superiority is mostly expressed in terms of defect detectability but can extend significantly into the practicality regime. As formerly mentioned, the primary category must include techniques applicable in both full-field and near-field inspection. Again, the basic methodology proposed by the authors is to first inspect a structure for defects on a full-field scale with subsequent detailed analysis of any discontinuous regions.

Second, a subset of *conditional* choices will be given. Their applicability largely depends on the specific inspection objective and/or site conditions. As mentioned in Section 4.1, a majority of defects found in CFRP are of relatively small dimension and thus give preference to near- and full-field inspection techniques. However, if a global assessment on structural integrity must be established, near- and full-field methods are mostly inappropriate choices. Further, in well-controlled environments, practical drawbacks may be less pronounced and enable the use of methods that require a more complex test setup.

Third, a number of methods will be classified as *supplementary* to those of primary choice. Supplementary methods should be applicable in the near- to full-field range, portable and inexpensive, yet provide information on material properties that cannot be extracted from the two primary methods.

Lastly, the RM will address methods that were shown to have significantly lower applicability and should hence be *excluded* from the list of viable methodologies. Such inapplicability is implied by either the high uncertainty and/or profound insensitivity towards a large number of defects, significant restrictions in practicality, or certain stringent limitations that extend beyond the issues addressed by the DM and PM matrices. Prior to presentation of the RM, the rationale will again be outlined in a systematic manner, so as to provide the reader with conclusive information on why certain decisions were made.

4.16.4.1 Primary methods

Primary methods must combine a generally high defect-sensitivity with capabilities of locating and, ideally, sizing of each individual defect. As may be seen from Table 4.3, this precondition is satisfied, within limitations, by ultrasonics, thermography, shearography, and radiographic imaging. While the latter is undoubtedly the most transparent of all methods, its stringent safety requirements, due to the utilization of aggressive x- or γ-radiation, may often restrict a flexible use in field environments. Hence, thermography, optical methods and ultrasonics remain as possible methods. It should be pointed out that ultrasonics is largely restricted to localized inspection, while thermography and optical methods can be applied in both the near- and full-field range.

While the stringent requirement of external loading in optical testing appears to add to the complexity of the inspection procedure, it should be considered that service load levels might often be of sufficient magnitude to expose a majority of the internal deficient regions. In contrast, defects located in regions of negligible strain levels are likely to go undetected. Nevertheless, optical methods have been shown to provide strain patterns of excellent geometric clarity.

Presently, the sensitivity of both methods to a variety of defects remains largely unknown. This is in part due to the fact that a majority of past research work has been focused on inspection of a very limited range of defects, most of which were either delamination, impact-related damage or voids of rather significant magnitude. Hence, both methods are given equal potential and must be subject to future investigation.

4.16.4.2 Conditional methods

Considering the characteristics of radiographic testing and modal analysis discussed in previous sections, their drawbacks for safe, economical and, in the latter case, detailed analysis of defects have become apparent. Nevertheless, if site conditions allow the use of radiographic equipment (i.e., supply a source capable of providing the several kilovolts required for operation and further allow its safe use) the high transparency can most certainly be of considerable advantage.

Alternatively, as supported by numerous reports, the impact of material degradation on the global structural response can most successfully be monitored using modal data [7]. As the evaluation of global behavior remains one the primary objectives in structural testing, modal analysis must be considered a viable, though conditional, method.

4.16.4.3 Supplementary methods

Traditionally, visual and acoustic impact testing have been the methods of choice to perform fast and preliminary inspections on composite materials. To date, similar methodology has been followed for rapid in-situ quality assessment of CFRP overlays. This is mostly dictated by the fact neither method demands extensive background knowledge on material properties, operation of equipment or signal interpretation. As such, visual inspection precedes virtually all automated test procedures. Hence, instead of treating VT as a separate NDE technique, it should much rather be considered a precondition for all further inspection, simply due to its simplicity and extreme flexibility.

Moreover, VT and AIT are both inexpensive and have proven to detect defects that are often of primary interest, namely medium to large delamination, considerable moisture accumulation, and severe fiber misalignment. Hence, both methods are proposed to serve as additional tools in assessing the quality of CFRP overlays. Nevertheless, it should be emphasized that neither method possesses adequate detectability necessitated for a comprehensive quality assessment.

4.16.4.4 Excluded methods

The majority of the remaining techniques have been excluded due to their typically low detectability (as shown in Table 4.3). Included are penetrant and eddy current techniques. Although fiberoptic sensors and acoustic emission systems have proven suitable lifetime monitoring systems for new and existing structures, the data from such systems often lacks sufficient interpretability. As such, localization and sizing of defects through mere detection of stress concentrations or acoustic activity at a surface fracture remains difficult. In existing structures, sensors cannot be situated at the concrete/composite interface or at interlaminar locations, which are the regions of high interest.

Table 4.5: Ranking matrix

Ranking	Method	Comments
PRIMARY METHODS	Thermography (TIR) † Shearography † Ultrasonics (UT) ††	† Both methods are proposed for near- and full-field monitoring, however, one may yield higher applicability over the other, which must be confirmed through future experimental investigation. †† Ultrasonics must be considered applicable for near-field inspection, exclusively. It's extensive background and range of instrumentation makes it especially favorable
CONDITIONAL METHODS	Radiographic Testing (RT) Modal Analysis	Applicability of these methods is largely dependent on site conditions and detail of inspection. For highly detailed inspection in controlled environments (i.e. access to adequate power supply, no concern of safety) RT remains a favorable technique. In contrary, for changes in structural response through material degradation, modal analysis provides most conclusive results.
INITIAL QUALITATIVE METHODS	Visual Testing (VT) Acoustic Impact Testing (AIT)	These methods are proposed as supplementary, mostly due to their general ease of use and extremely high flexibility. Moreover, they can be applied in simplistic form and do not necessitate extensive background knowledge in theory and/or application of the technique. The reader should be reminded, however, that neither method is of such transparency or level of sophistication that is could be considered solely for comprehensive in-situ inspection.
EXCLUDED METHODS	Penetrant Testing [1] Eddy Current Testing (ET) [2] Acoustic Emission (AE) [3] Strain Measurement Techniques (Fiberoptics) [4] Ground-Penetrating Radar (GPR) [5] Rapid Load Testing [6]	Quick-Reference List: Low detectability [1,2,4,5,6] Presumed inadequate for defect localization [3,6,8] Presumed inadequate for defect sizing [3,4,5,6]

4.17 CONCLUSIONS

As CFRP composites continue to gain acceptance in structural rehabilitation of deteriorating infrastructure, the need for comprehensive and rapid in-situ quality assessment has arisen. Due to the inevitable presence of material-, installation-, and service-induced defects, many rehabilitation schemes are likely to undergo deterioration to a level where they become ineffective, if their defects go undetected and are not restricted from further propagation at an early stage. At present, field methodologies include the rather simplistic inspection through visual inspection or surface tapping. Though applicable, these methods are largely inadequate in assessing the overall 'health' of rehabilitation schemes. Hence, alternative means for early detection and characterization of such defects must be developed.

From the preceding discussion it has been shown that non-destructive testing methodologies, as currently applied to CFRP-rehabilitated components, are often insufficient in providing field inspectors and engineers with comprehensive information on bond, material, and geometrical deficiencies located within the concrete/composite hybrid. These include visual inspection and acoustic impact testing, the latter commonly practiced in form of a 'coin tap' test. Given this insufficiency, the authors have evaluated a multitude of alternative non-destructive inspection methods for their potential for in-situ quality assessment of CFRP-rehabilitated structures. Apart from methodologies currently applied in the civil sector, a variety of so-called 'traditional' NDE techniques, plus several accepted 'state-of-the-art' techniques, were discussed. This investigation was aimed at identifying a limited number of primary NDE methods that appear most suitable for in-situ testing of CFRP-rehabilitated infrastructure.

It has been shown that the suitability of field techniques often demands rapid and comprehensive detection of defects, while placing importance on factors like mobility, flexibility and ease of interpretation. Finally, primary NDE methods should be complementary to each other; i.e., inspection should be initiated on a full-field level with subsequent detailed inspection utilizing a more sensitive near-field technique.

This chapter has addressed fundamental theory, common means of instrumentation, recent application to CFRP composites, and capabilities and limitations of each individual NDE technique. Subsequently, the methods were classified according to a predefined ranking scheme. Herein, detectability was given paramount importance. However, some methods appeared to impose such stringent requirements on site, loading, or environmental conditions that they were excluded solely on these premises. Ultimately, three methods were identified to be particularly suitable, given their most favorable combination of detectability and practicality:

- Ultrasonics,
- Thermography, and
- Shearography

Of these methods thermography was identified as a potential technique for future implementation and further study.

In addition, two methods are identified as being the first line of inspection due to their low cost and simplicity of use:

- Visual testing, and
- Acoustic impact testing

It should be noted, however, that these methods are qualitative only and do not provide quantitative assessment of defects. Further, while these are extremely useful in rapidly pinpointing the location of a defect, they may not be able to differentiate between different defects nor to provide quantitative evaluation of criticality.

Despite the widespread use of non-destructive testing methodologies in the field of laminated composite materials, most experimental work has been aimed solely at inspecting 'traditional' laminates, including thin plates or sandwich structures, as they are commonly utilized in the aerospace sector. Only limited work has been presented in the field of concrete-composite hybrid components. The reader should thus be reminded that the findings presented in this report are based predominantly on results of experimental work performed on the 'traditional' composites. The detectability and practicality of each method as it applies to in-situ inspection of CFRP-rehabilitated infrastructure must be evaluated and confirmed through further investigation.

4.18 ANNOTATION

Λ	=	Spatial period of optical fiber grating
A	=	Area normal to heat flow [m^2]
A'	=	Absorbed energy component
c	=	Speed of light = $2.9979*10^8$ [m/s]
C_c	=	Speed of compression wave [m/s]
C_s	=	Speed of shear wave [m/s]
D	=	Diameter of transducer [mm]
E	=	Young's modulus of elasticity [N/mm^2]
f	=	Frequency [Hz]
G	=	Shear modulus [N/mm^2]
$i°$	=	Angle of incidence
k	=	Thermal conductivity [W/m^2-°C]
N	=	Moiré fringe order
n_{eff}	=	Refractive index of optical fiber core
p	=	Pitch of grating [mm]
Q	=	Heat energy [W]
R	=	Coefficient of reflection [%]
$r°$	=	Angle of refraction
R'	=	Reflected energy component
T	=	Absolute temperature [°C]
t	=	Material thickness [m]
T'	=	Transmitted energy component
u	=	Component of deflection [mm]
V_1	=	Velocity in medium 1 [m/s]
V_2	=	Velocity in medium 2 [m/s]
V_c	=	Compression wave velocity [m/s]
V_f	=	Fiber volume fraction [%]
V_s	=	Shear wave velocity [m/s]

Z = Acoustic impedance [kg/m^{2}s]

Z_1 = Acoustic impedance in material 1 [kg/m^{2}s]

Z_2 = Acoustic impedance in material 2 [kg/m^{2}s]

Z_e = Electromagnetic impedance

ΔT = Temperature difference [°C]

$\Delta\lambda_B$ = Change in reflective wavelength

K_ε = Theoretical gauge constant, determined experimentally [86]

δ = Standard depth of penetration [mm]

ε = Emissivity

ε_0 = Dielectric permittivity of free space = $8.854*10^{-12}$ [Fm^{-1}]

ε_r = Relative dielectric constant

ε_x = Strain component in x-direction

ε_y = Strain component in y-direction

ϕ = Half the angle between propagation axes of two laser beams

γ_{xy} = Shear strain component

λ = Wavelength [m]

λ_1 = Wavelength of light [m]

λ_B = Reflective wavelength of optical fiber [m]

μ_0 = Magnetic permeability of free space

μ_r = Relative permeability

$\mu\varepsilon$ = Microstrain [10^{-6}]

ν = Poisson's ratio

θ = Angle of beam spread [deg]

ρ = Material density [kg/m^3]

ρ_e = Electrical resistivity [μΩ-cm]

σ = Stefan-Boltzmann constant = $1.38*10^{-23}$ [JK^{-1}]

ξ_0 = Coefficient of thermo-optic component and thermal expansion = $6*10^{-6}$ [°C^{-1}] (nominal)

4.19 CHAPTER 4 APPENDIX

In this section some of the most essential formulations in NDE are provided. They serve towards a more thorough understanding of some of the previously discussed methods. In Section 4.19.5, numerous important material parameters for NDE inspection are given. It must be understood that these values have been obtained from specific references. In most cases, minute changes in material composition will likely alter these values by a significant degree. These include changes in fiber volume fraction in CFRP composites, temperature fluctuation, moisture absorption, or variation in concrete aggregate size.

While a comprehensive theoretical discussion of most techniques would go beyond the scope of this report, the authors refer to literature, in which a complete background theory for most methods can be obtained [6, 39, 34, 53, 83].

4.19.1 Ultrasonics

As discussed in Section 4.5.1.1, different waveforms can be generated and transferred through a material. The most common form of waves are P- and S- waves. The velocity for a compressive wave for a material is given as:

$$V_c = \sqrt{\frac{E}{\rho} \cdot \frac{1-\upsilon}{(1+\upsilon)\cdot(1-2\cdot\upsilon)}} \qquad \textbf{(4-10)}$$

The shear wave velocity can be calculated from:

$$V_s = \sqrt{\frac{E}{\rho} \cdot \frac{1}{2\cdot(1+\upsilon)}} \qquad \textbf{(4-11)}$$

or alternatively:

$$V_s = \sqrt{\frac{G}{\rho}} \qquad \textbf{(4-12)}$$

In close vicinity (near field), the diameter of the beam and transducer crystal can be assumed to be of equal size [6]. Beyond a certain distance, the beam is likely to spread out like a cone, where beam spread is governed by the following equation:

$$\sin\frac{\theta}{2} = \frac{1.22\lambda}{D} \qquad \textbf{(4-13)}$$

4.19.2 Eddy current testing

An exponential decay of eddy current is experienced below the surface of the material that is penetrated. The standard depth of penetration is defined as the depth at which the eddy current strength has reduced by 37% relative to the initial surface strength [50]. Depending on the frequency of the induction coil, this value is given as:

$$\delta = 25 \cdot \sqrt{\frac{\rho_e}{f \cdot \mu_r}} \qquad \textbf{(4-14)}$$

where δ is in units of [mm].

4.19.3 Optical methods

In conventional geometrical moiré, the relative displacement between the specimen and the master grating can be found from:

$$u = N \cdot p \qquad \textbf{(4-15)}$$

From the stress-strain relationship of materials one obtains the three strain components:

$$\varepsilon_x = p \frac{\partial N_x}{\partial x} \qquad \textbf{(4-16)}$$

$$\varepsilon_y = p \frac{\partial N_y}{\partial y} \qquad \textbf{(4-17)}$$

$$\gamma_{xy} = p\left(\frac{\partial N_x}{\partial x} + \frac{\partial N_y}{\partial y} \right) \qquad \textbf{(4-18)}$$

In moiré interferometry, the intersection of two laser beams at an angle 2ϕ produces a reference grating. The distance between adjacent fringes, i.e., the fringe spacing of the grating is given by:

$$D = \frac{\lambda_l}{2} \cdot \sin\phi \qquad \textbf{(4-19)}$$

4.19.4 Strain measurement techniques

Strain variation in optical fiber measurements is derived from the shift in the wavelength arriving at the optical sensor. According to Bragg's law, the reflective wavelength can be expressed as:

$$\lambda_B = 2 \cdot n_{eff} \cdot \Lambda \qquad \textbf{(4-20)}$$

By considering effects arising from thermal expansion and mechanical strain, the expansion of the optical fiber can be calculated from:

$$\Delta\lambda_B = K_\varepsilon \cdot \varepsilon_l + \lambda_B \cdot \xi_0 \cdot \Delta T \qquad \textbf{(4-21)}$$

4.19.5 Material constants for NDE testing

Table 4.A.1: Material constants in NDE

Material Property	Air	Water	Steel	CFRP*	Concrete
Density, ρ [kg/m^3]	1.275	1,000	7,800	1,620	1,900-2,300
P-Wave Speed, C_c [m/s]	330	1,483	5,900	- [3]	3,600- 4,500
S-Wave Speed, C_s [m/s]	- [2]	- [2]	3,230	- [3]	- [3]
Thermal Conductivity, k [W/m-°C]	0.026	0.65	54	$\frac{54.4}{0.72}$	1.37
Electrical Resistivity, ρ_e [$\mu\Omega$cm]	∞	10^5-10^8	45	$\frac{3.3\cdot10^3\text{-}10^4}{1.5\cdot10^5\text{-}5\cdot10^7}$	10^5-10^7
Relative Permeability, μ_r [ ]	1.0	1.0	100	- [3]	- [3]
Emissivity, ε [ ]	- [2]	0.99	0.35/0.16 [1]	0.8-1.0	0.92

* Values for CFRP are dependent on fiber direction. Top values give properties parallel to fibers and bottom values give that in transverse direction

[1]Alloy/Polished [2]Not applicable [3]Not made available

4.20 CHAPTER 4 GLOSSARY

A-scan	Ultrasonic data representation using instantaneous data that is displayed on a horizontal baseline (distance or time of flight) versus a vertical deflection (amplitude).
Adherent	A body that is held to another body usually by an adhesive.
Adhesive	Substance capable of holding two materials together by surface attachment. Can be a film, paste of liquid.
Attenuation	Factor representing a decrease in signal intensity with distance. Expressed in decibels (dB) per unit distance.
Black light	Electromagnetic radiation in the range of 315-400 nm.
Bond strength	The amount of adhesion between two surfaces.
Boroscope	Industrial scope that transmits images from inaccessible regions for visual inspection. They can be flexible or rigid in nature.
B-scan	Ultrasonic data representations along a line scan that represent one particular cross-section of a part. Interior features can be displayed in their approximate length.
BVID	Barely visible impact damage.
Capillary action	Movement of liquids within the spaces of a porous material due to forces of adhesion, cohesion, and surface tension.
Catalyst	A substance that changes the rate of chemical reaction without itself undergoing permanent change in composition.
CCD	Charge coupled device, used to obtain electronic signals in modern video cameras.
Coherence	Multiple events (i.e. emission of light rays) that occur at an identical time instant (temporal coherence) while originating from the same location in space (spatial coherence).
Cold bond	Separation within a material or at the interface between two adjacent materials which are in intimate contact but possess no capability of stress transfer.
Collimated light	Plane wave front comprised of coherent light.
Compression wave	A wave in which the direction of particle motion coincides with direction of wave propagation.
Conduction	Heat transfer through interaction of atoms and molecules, mostly encountered in solids.
Convection	Heat transfer in fluids by mixing of molecules.

Cryogenics	Chemicals used to obtain extremely low temperatures at around -180°C (i.e. liquid nitrogen).
CSC	Curved-surface-correction feature applied in ultrasonic test units for sound path correction when inspecting around the circumference of a curved surface.
C-scan	Ultrasonic data representation that provides a plan view of material constitution, including internal discontinuities.
DAC	Distance amplitude correction in ultrasonic units that automatically adjusts amplitude in regions of varying signal intensity.
Debond	An initially unbonded or nonadhered region between two adherents. Also used to describe a separation at the fiber-matrix interface. In the construction industry, debond and delamination are sometimes used interchangeably when referring to separations at the concrete-composite interface.
Decibel (dB)	Logarithmic scale expressing relative amplitude or intensity of ultrasonic signals.
Degradation	Deleterious change in physical properties or appearance.
Delamination	Separation of the layers of material in a laminate, either local or covering a wide area.
Delay line	Column of material such as Plexiglas that behaves similar to a water path and allows a shift of the initial ultrasonic pulse.
Disbond	An area within an initially bonded interface between two adherents in which adhesion failure or separation has occurred.
DMTA	Dynamic mechanical thermal analysis. Provides information on presence of solvents, changes in structure and chemical reactions.
DSC	Differential scanning calorimetry. Detects loss of solvents and other volatiles.
Dye penetrant	Visible or fluorescent solution that seeps into porous surfaces.
Electrical conductivity	Readability of a material to allow flow of electric current.
Emissivity	Ability to radiate energy relative to a perfect radiator (blackbody) with values ranging from zero to one.
Emulsifier	Liquid that interacts with an oily substance to make it water-soluble.
Ferromagnetic	Materials that are strongly attracted to a magnet and can become magnetized, such as iron.
Fiberscope	Device that delivers light through a fiberoptic bundle to a CCD unit that converts it into an electric signal.

Galvanic corrosion	Galvanic reaction between metals and conductive carbon fibers, resulting in degradation of matrix and metal.
Half-life	Measure of the average lifetime of a radioactive substance, where one half-life represents the time required for one half of any given quantity of the substance to decay.
Heat mirror	A perfect light reflector with extremely low emissivity.
Hydrolysis	Process of degradation that generically includes the splitting of chemical bonds and the addition of water.
Hybrid	The combination of two materials of different origin or composition.
Inclusion	Mechanical discontinuity occurring within a material, consisting of a solid, encapsulated material.
Interface	Boundary between two different, physically distinguishable media.
Kissing bond	See *cold bond*
Lamb wave	Surface waves that travel between two parallel surfaces by means of elliptical particle motion, such as inside a plate.
Laminate	A product made by stacking of multiple layers of unidirectional fibers or oriented fiber configurations embedded in a resin matrix.
Longitudinal wave	See *compression wave*
LVDT	Linear variable differential transformer
Mode conversion	Phenomenon where wave modes are altered due to refraction at material boundaries.
NDE	Non-destructive evaluation. Methodology encompassing the use of non-destructive testing (NDT) techniques with subsequent assessment on severity in view of performance or integrity of an entire structure or components thereof.
NDI	Non-destructive inspection, often synonymous to *NDT*.
NDT	Non-destructive testing. A process that does not result in any damage or change to the material or part under examination and through which the presence of conditions or discontinuities can be detected.
Photons	Particles composing light and other forms of electromagnetic radiation, possessing no mass or charge.
Piezoelectric crystal	Material that transforms electrical energy into mechanical energy and vice versa.
Pitch	Distance between adjacent lines of a grating.
Plate wave	See *lamb wave*

Porosity	Trapped pockets of air, gas or vacuum within a solid material, typically less than 10μm in diameter.
Pot life	Time a thermosetting resin retains a viscosity low enough to be used in processing.
Prefabricated material	Composite material manufactured and cured under controlled factory conditions with a generally high material uniformity and used in cured state in the field.
Prepreg	Ready-to-mold material in sheet form impregnated with resin and stored for use. The resin is partially cured at a B-stage.
Probe	See *transducer*
P-wave	See *compression wave*
Quasi-isotropic	Laminate, whose extensional stiffness properties behave like those of an isotropic material.
Radiation	Transfer of heat energy in form of electromagnetic waves.
Rayleigh wave	Surface waves that travel predominantly in media with only a single surface.
Reproducibility	Ability to obtain identical test results under repeated testing.
Rheology	The study of flow of materials, particularly plastic flow of solids.
Saponification	Specific form of hydrolysis involving alkalis.
Sensitivity	Measure of the smallest feature inside a material that produces a discernible signal.
Shear wave	A wave in which the direction of particle motion is perpendicular to the direction of wave propagation.
Shelf life	Length of time a material can be stored under specific environmental conditions and continue to meet all applicable specification requirements.
Stoichiometry	Quantitative relationship between constitutions in a chemical system.
S-wave	See *shear wave*
Thermal conductivity	Rate at which heat flows through a body.
Transducer	Device used to produce mechanical stress waves.
Transverse wave	See *shear wave*
T_g	Temperature at which increased molecular mobility results in significant changes in the properties of a cured resin system.

TVG	Time-varied-gain feature in ultrasonic test units that corrects for distance/amplitude variations due to attenuation or beam spreading.
Undercure	A condition resulting from the allowance of too little time and/or temperature for adequate hardening.
Vitrification	Process of conversion into a glassy phase.
Voids	Air or gas that has been cured into a laminate or an interface between two adherents. Porosity is an aggregation of microvoids.
Volatiles	Materials, such as water or alcohol, in a resin formulation that are capable of being driven off a vapor at room temperature or at a slightly elevated temperature.
Wetability	The ability of a liquid to adhere to a surface.

4.21 CHAPTER 4 REFERENCES

1. Chapter 1 of this report.

2. Birt, E.A., *Damage Detection in Carbon-Fibre Composites Using Ultrasonic Lamb Waves.* Insight, 1998. **40**(5): p. 335-339.

3. Wong, B.S., et al., *Thermographic Evaluation of Defects in Composite Materials.* Insight, 1999. **41**(8): p. 504-509.

4. Grimberg, R., et al., *Eddy Current Holography Evaluation of Delamination in Carbon-Epoxy Composites.* Insight, 2001. **43**(4): p. 260-264.

5. Zhang, Y., et al., *Damage Growth Investigation in a Random Fiber Composite Beam by Moiré Interferometry.* Journal of Composite Materials, 1998. **32**(7): p. 664-678.

6. Hellier, C.J., *Handbook of Nondestructive Evaluation*. 2001, New York: McGraw-Hill.

7. Stubbs, N., et al., *A global non-destructive Damage Assessment Methodology for Civil Engineering Structures.* International Journal of Systems Science, 2000. **31**(11): p. 1361-1373.

8. Green, J.R.E., *Advanced NDE Techniques for Manufacturing and Construction Application*, in *Nondestructive Testing and Evaluation for Manufacturing and Construction*, H.L.M. dos Reis, Editor. 1990, Hemisphere Publishing Corporation: New York. p. 1-16.

9. Bartlett, S.W. and J. Duke, J. C., *Nondestructive Evaluation of Complex Geometry Advanced Material Components*, in *Nondestructive Testing and Evaluation for Manufacturing and Construction*, H.L.M. dos Reis, Editor. 1990, Hemisphere Publishing Corporation: New York. p. 17-25.

10. Connolly, M.P., *The Measurement of Porosity in Composite Materials Using Infrared Thermography.* Journal of Reinforced Plastics and Composites, 1992. **11**(12): p. 1367-1375.

11. Hawkins, G.F., E. Johnson, and J. Nokes, *Typical Manufacturing Flaws in FRP Retrofit Applications.* Concrete Repair Bulletin, 1998: p. 14-17.

12. Hertwig, M., T. Flemming, and R. Usinger, *Speckle Interferometry for Detection of Subsurface Damage in Fibre-reinforced Composites.* Measurement Science and Technology, 1994. **5**: p. 100-104.

13. Gregory, R., *Laser Shearography Inspection for Aircraft and Space Structures.* Insight, 2001. **43**(3): p. 150-154.

14. Kundu, T., et al., *C-Scan and L-Scan Generated Images of the Concrete/GFRP Composite Interface.* NDT & E International, 1999. **32**: p. 61-69.

15. Mei, Z.M. and D.D.L. Chung, *Effects of Temperature and Stress on the Interface Between Concrete and Its Carbon Fiber Epoxy-Matrix Composite Retrofit, Studied by Electrical Resistance Measurement.* Cement and Concrete Research, 2000. **30**: p. 799-802.

16. Cawley, P. and R.D. Adams, *The Mechanics of the Coin-tap Method of Non-destructive Testing.* Journal of Sound and Vibration, 1988. **122**: p. 299-316.

17. Mackie, R.I. and A.E. Vardy, *Applying the Coin-Tap Test to Adhesives in Civil Engineering: A Numerical Study.* International Journal of Adhesion and Adhesives, 1990. **10**(3): p. 215-220.

18. Haque, A. and R.P. K, *Sensitivity of the Acoustic Impact Technique in Characterizing Defects/Damage in Laminated Composites.* Journal of Reinforced Plastics and Composites, 1995. **14**: p. 280-296.

19. Wu, H. and M. Siegel, *Correlation of Accelerometer and Microphone Data in the "Coin Tap Test".* IEEE Transactions on Instrumentation and Measurement, 2000. **49**(3): p. 493-497.

20. Raju, P.K., J.R. Patel, and U.K. Vaidya, *Characterization of Defects in Graphite Fiber Based Composite Structures Using the Acoustic Impact Technique (AIT).* Journal of Testing and Evaluation, 1993. **21**(5): p. 377-395.

21. McMaster, R.C., ed. *Nondestructive Testing Handbook*. Vol. 2: Liquid Penetrant Tests. 1982, American Society for Metals: Metals Park, OH.

22. Krautkrämer, J. and H. Krautkrämer, *Ultrasonic Testing of Materials*. 4 ed. 1990, Berlin: Springer-Verlag. 675.

23. Tan, K.S., et al., *Comparison of Lamb Waves and Pulse Echo in Detection of Near-Surface Defects in Laminate Plates.* NDT & E International, 1995. **28**(4): p. 215-223.

24. Lanza di Scalea, F., M. Bonomo, and D. Tuzzeo, *Ultrasonic Guided Wave Inspection of Bonded Lap Joints: Noncontact Method and Photoelastic Visualization.* Research in Nondestructive Evaluation, 2001. **13**: p. 1-19.

25. Castaings, M. and B. Hosten, *Lamb and SH Waves Generated and Detected by Air-Coupled Ultrasonic Transducers in Composite Material Plates.* NDT & E International, 2001. **34**: p. 249-258.

26. Buckley, J., *Principles and Applications of Air-coupled Ultrasonics.* Insight, 1998. **40**(11): p. 755-759.

27. Scarponi, C. and G. Briotti, *Ultrasonic Technique for the Evaluation of Delaminations on CFRP, GFRP, KFRP Composite Materials.* Composites: Part B 31, 2000: p. 237-243.

28. Maslov, K. and T. Kundu, *Selection of Lamb Modes for Detecting Internal Defects in Composite Laminates.* Ultrasonics, 1997. **35**: p. 141-150.

29. Dewhurst, R.J. and B.A. Williams. *A Study of Lamb Wave Interaction with Defects in Sheet Materials Using a Differential Fibre-Optic Beam Deflection Technique*. in *Seventh International Symposium on Nondestructive Characterization of Materials*. 1995. Prague, Czech Republic: Transtec Publishing.

30. Lowe, M.J.S. and P. Cawley, *The Applicability of Plate Wave Techniques for the Inspection of Adhesive and Diffusion Bonded Joints.* Journal of Nondestructive Evaluation, 1994. **13**: p. 185-200.

31. Seale, M., B.T. Smith, and W.H. Prosser, *Lamb Wave Assessment of Fatigue and Thermal Damage in Composites.* Journal of the Acoustical Society of America, 1998. **103**(5, Pt. 1): p. 2416-2424.

32. Jones, T.S. and G. Lubin, *Nondestructive Evaluation Methods for Composites*, in *Handbook of Composites*, S.T. Peters, Editor. 1998, Chapman & Hall: London. p. 838-856.

33. Kim, N. and J.D. Achenbach, *Quantitative Characterization of Multiple Delaminations in Laminated Composites Using the Compton Backscatter Technique.* Journal of Nondestructive Evaluation, 1998. **17**(2): p. 53-65.

34. Bray, D.E. and R.K. Stanley, *Nondestructive Evaluation : A Tool in Design, Manufacturing, and Service*. 1997, Boca Raton: CRC Press. 586.

35. Poranski, C.F., E.C. Greenawald, and Y.S. Ham. *X-Ray Backscatter Tomography: NDT Potential and Limitations*. in *Seventh International Symposium on Nondestructive Characterization of Materials*. 1995. Prague, Czech Republic: Transtec Publishing.

36. Demeis, R., *CAT Scanning Composites.* Aerospace America, 1991. **29**(2): p. 44-45.

37. Bossi, R.H. and G.E. Georgeson, *Composite Structure Development Decisions Using X-ray CT Measurements.* Materials Evaluation, 1995. **53**(10): p. 1198-1203.

38. Henneke II, E.G., *Vibrothermography Applied to Polymer Matrix Composites*, in *Manual on Experimental Methods for Mechanical Testing of Composites*, C.H. Jenkins, Editor. 1998, The Fairmont Press: Lilburn, USA. p. 213-221.

39. Maldague, X.P.V., *Theory and Practice of Infrared Technology for Nondestructive Testing*. Wiley Series in Microwave and Optical Engineering, ed. K. Chang. 2001, New York: John Wiley & Sons, Inc. 684.

40. Jones, T. and H. Berger, *Thermographic Detection of Impact Damage in Graphite-Epoxy Composites.* Materials Evaluation, 1992. **50**(12): p. 1446-1453.

41. Brady, R.P., et al., *Thermal Image Analysis for the In-Situ NDE of Composites.* Journal of Composites Technology and Research, 1999. **21**(3): p. 141-146.

42. Titman, D.J., *Application of Thermography in Non-Destructive Testing of Structures.* NDT&E International, 2001. **34**: p. 149-154.

43. Maldague, X. and S. Marinetti, *Pulse Phase Infrared Thermography.* Journal of Applied Physics, 1996. **79**(5): p. 2694-2698.

44. Bai, W. and B.S. Wong, *Evaluation of Defects in Composite Plates under Convective Environments Using Lock-in Thermography.* Measurement Science and Technology, 2001. **12**: p. 142-150.

45. Lin, S.S., *Frequency Dependent Heat Generation During Vibrothermographic Testing of Composite Materials*. 1987, Virginia Polytechnic Inst. and State Univ.: Blacksburg, VA.

46. Rantala, J., D. Wu, and G. Busse. *Lock-In Vibrothermography Applied for Nondestructive Evaluation of Polymer Materials*. in *Seventh International Symposium on Nondestructive Characterization of Materials*. 1995. Prague, Czech Republic: Transtec Publishing.

47. Lane, S.S., et al., *Eddy Current Inspection of Graphite/Epoxy Laminates.* Journal of Reinforced Plastics and Composites, 1991. **10**(2): p. 158-166.

48. Degtyar, A.D. and L.H. Pearson. *Ultrasonic and Eddy Current Characterization of Impact Damage in Graphite/Epoxy Rocket Motor Cases*. in *Review of Progress in Quantitative Nondestructive Evaluation*. 2000. Montreal, Canada: AIP.

49. Valleau, A.R., *Eddy Current Nondestructive Testing of Graphite Composite Materials.* Materials Evaluation, 1990. **48**(2): p. 230-239.

50. Gros, X.E., O. K, and K. Takahashi, *Eddy Current, Ultrasonic C-Scan and Scanning Acoustic Microscopy Testing of Delaminated Quasi-Isotropic CFRP Materials.* Journal of Reinforced Plastics and Composites, 1998. **17**(5): p. 389-405.

51. Ida, N., *Microwave NDT*. Developments in Electromagnetic Theory and Applications, ed. G.F. Roach. Vol. 10. 1992, Dordrecht, The Netherlands: Kluwer Academic Publishers.

52. Zoughi, R., S. Ganchev, and G.W. Carriveau. *Overview of Microwave NDE Applied to Thick Composites*. in *Seventh International Symposium on Nondestructive Characterization of Materials*. 1995. Prague, Czech Republic: Transtec Publications.

53. Cloud, G., *Optical Methods of Engineering Analysis*. 1998, Cambridge: Cambridge University Press. 503.

54. Parks, V.J., *Geometric Moiré*, in *Manual on Experimental Methods for Mechanical Testing of Composites*, C.H. Jenkins, Editor. 1998, The Fairmont Press, Inc.: Lilburn, USA. p. 137-146.

55. Hung, Y.Y., et al., *Evaluating the Soundness of Bonding using Shearography.* Composite Structures, 2000. **50**: p. 353-362.

56. Hung, Y.Y., *Computerized Shearography and It's Application for Nondestructive Evaluation of Composites*, in *Manual on Experimental Methods for Mechanical Testing of Composites*, C.H. Jenkins, Editor. 1998, The Fairmont Press: Lilburn, USA. p. 161-174.

57. Zanetta, P., et al., *Holographic Detection of Defects in Composites.* Optics & Laser Technology, 1993. **25**(2): p. 97-102.

58. Post, D., B. Han, and P. Ifju, *High Sensitivity Moiré : Experimental Analysis for Mechanics and Materials*. 1994, New York: Springer Verlag. 444.

59. Gryzagoridis, J., *Holographic Nondestructive Testing*, in *Nondestructive Testing and Evaluation for Manufacturing and Construction*, H.L.M. dos Reis, Editor. 1990, Hemisphere Publishing Corporation: New York. p. 451-462.

60. Steinchen, W., et al., *Non-destructive Testing of Aerospace Composite Materials using Digital Shearography.* Proceedings of the Institution of Mechanical Engineers Part G - Journal of Aerospace Engineering, 1998. **212**(NG1): p. 21-30.

61. Mizutani, Y., et al., *Fracture Mechanism Characterization in Cross-Ply Carbon-Fiber Composites Using Acoustic Emission Analysis.* NDT & E International, 2000. **33**: p. 101-110.

62. Mirmiran, A., M. Shahawy, and H. El Echary, *Acoustic Emission Monitoring of Hybrid FRP-concrete Columns.* Journal of Engineering Mechanics, 1999. **125**(8): p. 899-905.

63. Rizzo, P. and F. Lanza di Scalea, *Acoustic Emission Monitoring of Carbon-fiber-reinforced-polymer Bridge Stay Cables in Large-scale Testing.* Experimental Mechanics, 2001. **41**(3): p. 282-290.

64. Bohse, J., *Acoustic Emission Characteristics of Micro-failure Processes in Polymer Lends and Composites.* Composites Science and Technology, 2000. **60**: p. 1213-1226.

65. De Groot, P.J., P.A.M. Wijnen, and R.B.F. Jansen, *Real-time Frequency Determination of Acoustic Emission for Different Fracture Mechanisms in Carbon/Epoxy Composites.* Composites Science and Technology, 1995. **55**: p. 405-412.

66. Lorenzo, L. and H.T. Hahn, *Static and Fatigue Fracture Monitoring in Unidirectional Composites by Acoustic Emission*, in *Nondestructive Testing and Evaluation for Manufacturing and Construction*, H.L.M. dos Reis, Editor. 1990, Hemisphere Publishing Corporation: New York. p. 67-85.

67. Ohtsu, M., T. Okamoto, and S. Yuyama, *Moment Tensor Analysis of Acoustic Emission for Cracking Mechanisms in Concrete.* ACI Structural Journal, 1998. **95**(2): p. 87-95.

68. Ohtsu, M., M. Shigeishi, and Y. Sakata, *Nondestructive Evaluation of Defects in Concrete by Quantitative Acoustic Emission and Ultrasonics.* Ultrasonics, 1998. **35**: p. 187-195.

69. Lim, M.K., *Impulse Radar Applications.* Concrete International, 2001. **23**(8): p. 64-68.

70. Bungey, J.H. and S.G. Millard, *Radar Inspection of Structures.* Proceedings of the Institution of Civil Engineers - Structures and Buildings, 1993. **99**(2): p. 173-186.

71. Bindi, L., G. Lenzi, and A. Saisi, *NDE of Masonry Structures: Use of Radar Tests for the Characterization of Stone Masonries.* NDT & E International, 1998. **31**(6): p. 411-419.

72. Colla, C., et al., *Comparison of Laboratory and Simulated Data for Radar Image Interpretation.* NDT & E International, 1998. **31**(6): p. 439-444.

73. Shaw, P. and J. Bergström, *In-Situ Testing of Reinforced Concrete Structures using Stress Waves and High-Frequency Ground Penetrating Radar.* Insight, 2000. **42**(7): p. 454-457.

74. Lau, K., et al., *Strain Monitoring in Composite-Strengthened Concrete Structures Using Optical Fibre Sensors.* Composites: Part B, 2001. **32**: p. 33-45.

75. Chan, P.K.C., et al., *Multi-Point Strain Measurement of Composite-Bonded Concrete Materials with a RF-Band FMCW Multiplexed FBG Sensor Array.* Sensors and Actuators, 2000. **87**: p. 19-25.

76. Uskokovic, P.S., et al., *Delamination Detection in Woven Composite Laminates with Embedded Optical Fibers.* Advanced Engineering Materials, 2001. **3**(7): p. 492-496.

77. Unknown, *Installation, Use and Repair of Fiber Optic Sensors*. 2001, University of Toronto: Ontario.

78. Bolton, R., et al., *Documentation of Changes in Modal Properties of a Concrete Box-girder Bridge due to Environmental and Internal Conditions.* Computer-Aided Civil and Infrastructure Engineering, 2001. **16**: p. 42-57.

79. Sanders, D.R., Y.I. Kim, and N. Stubbs, *Nondestructive Evaluation of Damage in Composite Structures Using Modal Parameters.* Experimental Mechanics, 1992. **32**(3): p. 240-251.

80. Ndambi, J.M., et al., *Comparison of Techniques for Modal Analysis of Concrete Structures.* Engineering Structures, 2000. **22**: p. 1159-1166.

81. Salawu, O.C. and C. Williams, *Review of Full-Scale Dynamic Testing of Bridge Structures.* Engineering Structures, 1995. **17**(2): p. 113-121.

82. Peeters, B., J. Maeck, and G. De Roeck, *Vibration-based Damage Detection in Civil Engineering: Excitation Sources and Temperature Effects.* Smart Materials and Structures, 2001. **10**: p. 518-527.

83. Ewins, D.J., *Modal Testing: Theory and Practice*. Mechanical Engineering Research Studies, ed. J.B. Roberts. 1984, Taunton, Somerset, England: Research Studies Press, Ltd. 269.

84. Hermans, L. and H. Van Der Auweraer, *Modal Testing and Analysis of Structures under Operational Conditions: Industrial Applications.* Mechanical Systems and Signal Processing, 1999. **13**(2): p. 193-216.

85. Mettemeyer, M. and A. Nanni, *Guidelines for Rapid Load Testing of Concrete Structural Members*. 2001, University of Missouri, Rolla.

86. Saouma, V.E., et al., *Application of Fiber Bragg Grating in Local and Remote Infrastructure Health Monitoring.* Materials and Structures, 1998. **31**: p. 259-266.

5.0 USE OF DYNAMIC TESTING AS A METHOD OF NDT

5.1 INTRODUCTION

With the degradation of civil infrastructure in the United States, a significant need exists to repair or replace civil structures – in particular, bridge systems – prior to failure. Many existing reinforced concrete bridges were designed in accordance with older design codes, where load demands were less than current loading specifications. The prospect of replacing every outdated bridge across the country is an unfeasible alternative because of the high cost, time of construction, and interference with traffic. Thus, structural health monitoring of bridges and bridge life management is a rapidly developing field of interest for many researchers.

Structural health monitoring methods provide a means to evaluate the remaining useful life of the structure. Knowledge of a structure's useful life allows for the development of a systematic repair or replacement strategy for civil structures, maximizing the performance of the structure. Inherent in the structural health monitoring strategy is a nondestructive evaluation technique to evaluate the condition and behavior of the structural system in its current state. Most nondestructive testing techniques available, however, are localized methods (such as ultrasonic testing, acoustic emission, magnetic field methods, radiography, eddy-current methods, and thermal field methods), which require the vicinity of damage be known a priori [1]. While these local nondestructive testing (NDT) methods prove useful for the interrogation of structures and characterization of damage once the area of damage has been identified, methods for global nondestructive evaluation are necessary for large civil structures primarily because of the impractical nature of applying local nondestructive evaluation (NDE) techniques to examine civil structures. The need for global NDE methods has led to an increased interest in the examination of the dynamic characteristics of a structure.

Information related to the vibration properties of structure – in particular, the modal properties – can be useful in improving monitoring, analysis and design procedures, assessing design codes, monitoring the in-service behavior of structures, and evaluating the safety of the structure [8]. Here, modal parameters refer to natural frequencies, mode shapes, which are often used as a measure of structural change over a period of time or after a repair or a major event such as an earthquake, blast, etc. By developing an effective procedure to acquire the modal properties of a structure, an analysis of the global capacity of the structure is possible, based on the premise that modal parameters directly correspond to the mechanical properties, i.e., stiffness and mass of a structure. An evaluation of the modal parameters of a structure at periodic time intervals allows for monitoring of changes in the mechanical properties, thus providing a means to measure the change in capacity of a structure as damage accumulates over time.

5.1.1 History of modal testing

In this section a brief history of dynamic testing is provided as a precursor to the development of dynamic testing practices and procedures currently available. Dynamic testing of structures has been used in a qualitative and intuitive manner since ancient times, when changes in the acoustics were observed to detect some change in the performance or quality of a tool [1]. In modern times, the increasing observation of fatigue failures in structures prompted the need to monitor the behavior of structures as damage accumulated due to cyclic or repeated loadings.

Formal vibration evaluation procedures emerged during and following World War II, primarily due to observations of failures in structures, which were significantly different from the expected failure mechanisms due to static loading. Initially, vibration tests were simulated with the intent of evaluating the performance of a system under stress induced by vibration from a field environment [14]. Typical systems included gun mounts, warheads, shipping containers, and automotive or aircraft components. The objective of the first dynamic or vibration tests was to ensure the operability of the system or structure under harsh environments where systems were subject to dynamic loading in field conditions. As technology has advanced with improvements and increased capacity of computers, data acquisition systems, and the performance of sensors, so too has the versatility of dynamic testing methods in evaluation of a system's survivability, performance, identification, and reliability [14].

Modal testing of structures relies heavily on the accuracy of the tools available for data acquisition and methods of excitation available to vibrate the structure. Early excitation methods involved machines utilizing rotating eccentric weights, with electrodynamic vibration machines emerging in the 1950's. In addition, the development of electrohydraulic machines provided a method of inducing vibrations into a structure by moving a piston using fluid pressure. Information regarding the function, limitations, and capabilities of electrodynamic and electrohydraulic shakers is provided in Section 5.3.1.2. Improvements in electrodynamic and electrohydraulic oscillators continued through the 1960's with the introduction of high current, solid state electronics along with improvements in materials, leading to stiffer, more durable armatures and test fixtures [14].

Use of electrodynamic and electrohydraulic shakers is relatively straightforward, since the oscillators introduce a single frequency sinusoidal wave into the system with the amplitude of the input sine wave corresponding to the input vibration level and the amplitude of the response sine wave corresponding to the response acceleration level [14]. In order to simulate realistic conditions where multiple frequencies are excited during operation, impulse excitation and ambient excitation methods have been developed, with the general classification being input-output methods and output-only methods, respectively. Input-output methods indicate the force or excitation level input to the structure is known; and output-only methods indicate the modal parameters are extracted from the vibration response of a system from an unknown input level and source.

Associated with increased improvements in the dynamic test procedure is the development of data acquisition equipment and data processing methods. Modern data acquisition systems began with the use of accelerometers in the 1950's. Accelerometers now include integral charge amplifiers such that a majority of the signal conditioning occurs within the device [14]. Whereas

in the past large quantities of data were used to process modal models, which are effective descriptions of linear systems, the emphasis on linear behavior for vibration response was alleviated with the use of fast Fourier transforms (FFT) and frequency domain averaging to acquire power spectra and transfer functions and therefore, modal frequencies and mode shapes.

5.1.2 Chapter overview

With the degradation of civil infrastructure, particularly in reinforced concrete bridge structures built in the 1960's, a practical nondestructive damage detection tool is necessary for the assessment of bridges. Ideally the nondestructive methodology would not interrupt daily public activities nor disrupt "business as usual" on highways and roadways connecting cities and businesses. Modal testing is the primary experimental procedure of a complete damage detection methodology, which serves as the tool to acquire the vibration properties of a structure (i.e., accelerations, velocities, displacements, frequency response functions, modal parameters), in order to determine and evaluate the condition and durability of the structure. The implementation of a modal testing procedure in conjunction with an analysis via a damage detection algorithm utilizing modal parameters provides a methodology for global non-destructive evaluation of civil structures. In addition, the nondestructive damage technique is applicable for evaluation of as-built and rehabilitated structures. The reasons for the use of modal testing on civil structures, specifically on bridges, are listed below.

Modal testing:

- Determines the modal properties, which include the frequencies, mode shapes and damping properties of the bridge;
- Assesses the changes in dynamic properties over a period of time to determine the changes in the mechanical properties of the bridge structure;
- Quantifies the effectiveness of a rehabilitation or change to the bridge structure;
- Provides a means to correlate a finite element model of the structure with the measured results from the real structure for purposes of systems identification [7];
- Assesses the integrity of a structure for higher loading levels due to a change of use, higher environmental loading, or an increase in allowable loading [8]; and
- Provides a means for continuous monitoring of the structure to detect levels of degradation and locations for local inspection and repair.

This chapter explains the major components of modal testing and modal analysis as it applies to bridges. First the theoretical development for modal testing is explained. Of particular importance is the development of the frequency response functions (FRF's), since the extraction of modal properties of the structure (i.e., natural frequency, damping properties, mode shapes) relies on the FRF's.

Second, methods of excitation for bridges are categorized into input-output methods and output-only methods for modal testing. Input-output methods of excitation involve a contact procedure such that a forcing function is introduced to vibrate the bridge structure. Input-output techniques include the use of an impact hammer, drop weight, shaker, or displacement-release procedure to excite the structure.

Output only methods, typically described as ambient excitation methods, utilize the service level conditions of the structure in order to excite the structure. Sources of "natural" vibration include vehicular traffic, wind, pedestrian traffic, ocean waves, and micro-earthquakes [1, 4, 8].

There is no single method of excitation superior to all others; rather the experimenter must decide the method of excitation that is most suitable for the modal testing of a particular bridge structure and the constraints presented by the structure in the field. A comparative study of the advantages and disadvantages for the various excitation techniques is also provided.

Third, the testing procedure is described with an overview of the types of transducers available for use on modal tests. Associated with the selection of sensors used for data acquisition procedures is the optimal placement of the sensors in order to minimize their quantity and ensure sufficient resolution exists to characterize the system.

Finally, methods for extraction of modal parameters from measured frequency response functions are briefly reviewed and explained. The selection of an appropriate experimental modal analysis procedure to extract the vibration properties of a structure is dependent on the type of modal test being conducted, i.e., whether an output-only procedure is specified or if forced excitation methods are employed.

5.2 THEORETICAL BASIS

For a fundamental understanding of modal testing and insight into the development of damage detection algorithms, the theoretical basis for modal testing and extraction of modal properties must be understood. The following section provides a theoretical overview of modal testing.

A detailed review of the development of the equations of motion (spatial model), theoretical modal analysis (modal model), and the solution to the equations of motion for a given excitation (response model) for both the single degree of freedom (SDOF) and multi-degree of freedom (MDOF) systems is available in a number of structural dynamics textbooks [5, 10, 11, 12].

5.2.1 Spatial model

There are three distinct components in the theoretical analysis for a vibrating structure. The first is development of the spatial model, which involves providing a mathematical description of the mass, stiffness, and damping of the structure by means of the equations of motion. Developing the equations of motion for a structure typically involves utilizing Newton's 2nd law and D'Alembert's principle, which provides for dynamic equilibrium at each time instant when inertia forces are included. Energy-based procedures involving Hamilton's principle, Lagrange's equations, or the principle of virtual work, are also available for developing the equations of

motion for a structure. The generalized equation of motion for an *N*-degree-of-freedom system is provided below in matrix form.

$$\mathbf{m}\ddot{\mathbf{u}} + \mathbf{c}\dot{\mathbf{u}} + \mathbf{k}\mathbf{u} = \mathbf{p}(\mathbf{t}) \qquad \textbf{(5-1)}$$

where **m**, **c**, and **k** are the mass, damping, and stiffness matrices, respectively, with each matrix having dimensions *N* x *N*. The vector, **p(t)**, describes the externally applied dynamic forces with dimension *N* x 1. $\ddot{\mathbf{u}}, \dot{\mathbf{u}}$, and **u** are the acceleration, velocity, and displacement response vectors of the structure each having dimension *n* x 1. The matrix form of the equations of motion represents *N* coupled, ordinary differential equations describing the spatial model of the structure.

5.2.2 Modal model

A theoretical modal analysis is performed to describe the structure as a set of vibration modes via its natural frequencies and mode shapes. This is the modal model of the structure, which describes the structure without any external excitation or forces (free vibration). Since the natural modes characterize the response of a structure under free vibration, the mode shapes and natural frequencies for a classically damped system are evaluated by solving the following matrix eigenvalue problem for the scalar $\lambda_n\ (= \omega_n^2)$ and vector mode shape $\boldsymbol{\varphi}_n$.

$$\left[\mathbf{k} - \lambda_n\ \mathbf{m}\right]\boldsymbol{\varphi}_n = \mathbf{0} \qquad \textbf{(5-2)}$$

where λ_n, is the nth eigenvalue equal to the square of the nth natural frequency, ω_n^2; and $\boldsymbol{\varphi}_n$ is the nth mode shape vector. Two possible solutions exist for the above equation, one being the trivial solution, $\boldsymbol{\varphi}_n = \mathbf{0}$, which is not useful since the result implies no motion. Nontrivial solutions occur when the following equation is true.

$$\det\left|\mathbf{k} - \lambda_n\ \mathbf{m}\right| = 0 \qquad \textbf{(5-3)}$$

The characteristic equation evaluated from the determinate above has *N* real and positive roots for λ_n (n = 1, 2,…, N) from which the nth natural frequency, ω_n (n = 1, 2,…, N), is calculated. Upon evaluating the natural frequency, Equation (5-2) is employed to evaluate the associated eigenvector or mode shape, $\boldsymbol{\varphi}_n$. The process of calculating natural frequencies and mode shapes assumes the structure is linear and the damping matrix, **c**, is proportional to its mass, **m**, and stiffness, **k**, matrices (i.e. Rayleigh damping). Development of the damping matrix, **c**, from individual structural elements is not a practical consideration since the damping properties of materials are not well defined, nor is the energy dissipated by friction, opening and closing of microcracks, and other similar mechanisms accounted for [10]. For bridge structures, the assumption of proportional damping is a valid idealization if similar damping mechanisms are distributed throughout the structure [10]. Proportional damping is unacceptable when the system to be analyzed consists of two or more parts with significantly different levels of damping, i.e. a soil-structure system or structure-fluid system.

Solving the eigenvalue problem yields a set of N undamped natural frequencies, ω_n and associated mode shapes $\boldsymbol{\varphi}_n$ for $n = 1, 2, \ldots, N$. The corresponding mode shape vectors, $\boldsymbol{\varphi}_n$, are assembled into an $N \times N$ modal matrix, $\boldsymbol{\Phi}$ as shown below.

$$\boldsymbol{\Phi} = \left[\boldsymbol{\varphi}_1\ \boldsymbol{\varphi}_2 \ldots \boldsymbol{\varphi}_n \ldots \boldsymbol{\varphi}_N\right] \tag{5-4}$$

These mode shapes possess orthogonality properties with respect to the structure's physical properties such that the following $N \times N$, square, diagonal matrices result:

$$\mathbf{K} \equiv \boldsymbol{\Phi}^{\mathrm{T}}\mathbf{k}\boldsymbol{\Phi} \ \text{ and } \ \mathbf{M} \equiv \boldsymbol{\Phi}^{\mathrm{T}}\mathbf{m}\boldsymbol{\Phi} \tag{5-5}$$

where $\mathbf{K}$ is the modal stiffness matrix with diagonal elements $K_{nn} = \boldsymbol{\varphi}_n^T\mathbf{k}\boldsymbol{\varphi}_n$; and $\mathbf{M}$ is the modal mass matrix with diagonal elements $M_{nn} = \boldsymbol{\varphi}_n^T\mathbf{m}\boldsymbol{\varphi}_n$. The assumption of proportional damping implies that the damping matrix is also orthogonal and can similarly be defined as a modal damping matrix, $\mathbf{C} \equiv \boldsymbol{\Phi}^{\mathrm{T}}\mathbf{c}\boldsymbol{\Phi}$, with diagonal elements $C_{nn} = \boldsymbol{\varphi}_n^T\mathbf{c}\boldsymbol{\varphi}_n$.

The orthogonality of modes asserts the following conditions for natural modes corresponding to different natural frequencies. When $\omega_n \neq \omega_r$:

$$K_{nr} = \boldsymbol{\phi}_n^T\mathbf{k}\boldsymbol{\phi}_r = 0 \quad M_{nr} = \boldsymbol{\phi}_n^T\mathbf{m}\boldsymbol{\phi}_r = 0 \quad C_{nr} = \boldsymbol{\phi}_n^T\mathbf{c}\boldsymbol{\phi}_r = 0 \tag{5-6}$$

Therefore, the off-diagonal terms in the modal mass, modal stiffness, and modal damping matrices are zero. The orthogonality of modes physically implies that the work done by the n^{th} mode inertia forces in going through the r^{th} mode displacements is zero or that the work done by equivalent static forces associated with displacements in the n^{th} mode in going through the r^{th} mode displacements is zero [10].

As mentioned previously, the equations of motion describing the spatial model of a structure are coupled, and thus impractical to evaluate for multi-degree of freedom systems. In order to uncouple the equations of motion, the modal model is developed by utilizing the orthogonality properties of the linear system. The displacement vector, $\mathbf{u}(t)$, is expanded into modal space such that:

$$\mathbf{u}(t) = \boldsymbol{\Phi}\mathbf{q}(t) \tag{5-7}$$

where $\mathbf{q}(t)$ is the vector of modal coordinates.

The matrix transformation and orthogonality characteristics result in the conversion from the physical space to the modal space [20]. Substituting Equation (5-7) into Equation (5-1) and premultiplying each component by $\boldsymbol{\Phi}^T$ and applying orthogonality conditions results in an uncoupled system of equations for N single degree of freedom systems in modal space.

$$\mathbf{M}\ddot{\mathbf{q}} + \mathbf{C}\dot{\mathbf{q}} + \mathbf{K}\mathbf{q} = \boldsymbol{\Phi}^{\mathrm{T}}\mathbf{p}(t) = \mathbf{P}(t) \tag{5-8}$$

where **M** is a diagonal matrix of generalized modal masses M_{nn}; **C** is a diagonal matrix with generalized damping terms, C_{nn}, for proportional damping; **K** is a diagonal matrix of generalized modal stiffnesses, K_{nn}; **P**(t) is a column vector of the generalized modal forces $P_n(t)$; and **q** is a column vector of generalized modal coordinates, $q_n(t)$. For the case where each point has an independent excitation force, the following equation is true:

$$M_{nn}\ddot{q}_n + C_{nn}\dot{q}_n + K_{nn}q_n = \sum_{r=1}^{N}\phi_{rm}p_r(t) \qquad \textbf{(5-9)}$$

5.2.3 Response model

The response model provides a description of how a structure responds to a given excitation. For a bridge structure, the excitation source is typically a single point input or an ambient excitation involving random vibrations. In the following section, the response model for a single point excitation and for random vibrations is developed. For identification of a theoretical model of the structure, it is convenient to present the result in the frequency domain, since the output of a modal test is typically given as a function of the frequency. The response model of the structure is merely the solution of the equations of motion under a given excitation and is presented as a function of time or frequency in the form of frequency response functions (FRF's).

5.2.3.1 Single point excitation

For a single point excitation, where the excitation occurs at the i^{th} location and all other forces are zero, Equation (5-9) becomes:

$$M_{nn}\ddot{q}_n + C_{nn}\dot{q}_n + K_{nn}q_n = \phi_{in}p_i(t) \qquad \textbf{(5-10)}$$

The above equation shows that the n^{th} mode is not excited if the i^{th} point or the location of the input is a node point, such that $\phi_{in} = 0$ [20]. During the modal test of a bridge structure, the location of the input excitation must be selected away from the vibration nodes of the desired mode shapes.

Methods for solving the 2^{nd} order ordinary differential equation (ODE) given by Equation (5-10) include the use of a Fourier transform to convert the equation from the time domain to the frequency domain and solving for the frequency response function. Other methods are available in standard mathematical texts such as in Grossman [21].

One method of solving the 2^{nd} order ODE is by the use of phasors [20]. Phasors provide a convenient methodology for solving time-harmonic problems in steady state without having to solve directly a differential equation. Using phasors equates time dependent terms to an exponential representation, which converts an ODE in the time domain to an algebraic equation in the frequency domain. As part of the solution process, $p_i(t)$ and $q_n(t)$ are assumed to be phasors expressed as the following exponentials:

$$p_i(t) = p_i e^{j\omega t} \textbf{ and } q_n(t) = \overline{B}_n e^{j\omega t} \qquad \textbf{(5-11)}$$

where ω is the frequency of the excitation; and $j = \sqrt{-1}$; $\overline{B}_n$ is a complex quantity containing both magnitude and phase information. Substitution of Equation (5-11) into Equation (5-10) results in a standard single degree of freedom, forced vibration response:

$$\overline{B}_n = \frac{\phi_{in} p_i}{K_{nn} - M_{nn}\omega^2 + jC_{nn}\omega} \qquad \textbf{(5-12)}$$

The modal model for displacement at a location *p* is acquired by substituting Equation (5-12) into Equation (5-11) and subsequently substituting Equation (5-11) into Equation (5-8), resulting in the following:

$$u_p(t) = \sum_{n=1}^{N}\left[\frac{\phi_{pn}\phi_{in}}{K_{nn} - M_{nn}\omega^2 + jC_{nn}\omega}\right] p_i e^{j\omega t} = H_{pi}(\omega) p_i e^{j\omega t} \qquad \textbf{(5-13)}$$

where $H_{pi}(\omega)$ is the receptance frequency response function (FRF) defined below,

$$H_{pi}(\omega) = \sum_{n=1}^{N}\left[\frac{\phi_{pn}\phi_{in}}{K_{nn} - M_{nn}\omega^2 + jC_{nn}\omega}\right] = \frac{U_p(\omega)}{p_i(\omega)} \qquad \textbf{(5-14)}$$

where $U_p(\omega)$ is the frequency spectrum of the response $u_p(t)$ at location *p*; and $p_i(\omega)$ is the frequency spectrum of the input time history $p_i(t)$. $H_{pi}(\omega)$ is the response at location *p* due to a unit excitation at the i^{th} location which has frequency ω. If *p* and *i* are different, $H_{pi}(\omega)$ is a transfer receptance. When *p = i,* $H_{pp}(\omega)$ is a driving-point receptance. From Equation (5-14), it is observed that the receptance FRF contains information regarding natural frequencies, modal damping, and mode shape.

Although the receptance FRF is convenient for displacement measurements, experimental modal analysis procedures typically measure velocity or acceleration. Therefore, if the response velocity is selected as the output quantity, the corresponding frequency domain FRF is called mobility, $Y_{pi}(\omega)$. The mobility, $Y_{pi}(\omega)$ relates the output velocity frequency spectrum, $V_p(\omega)$ for location *p* due to an input force frequency spectrum $p_i(\omega)$ at location *i*. The mobility is related to the receptance FRF by:

$$Y_{pi}(\omega) = j\omega H_{pi}(\omega) = \frac{V_p(\omega)}{p_i(\omega)} \qquad \textbf{(5-15)}$$

Similarly, if the output quantity is the response acceleration, the corresponding FRF is called accelerance or inertance. The accelerance, $A_{pi}(\omega)$, relates the output acceleration frequency response $a_p(\omega)$ at location *p* to input excitation frequency spectrum $p_i(\omega)$ at location *i*. The accelerance is related to the mobility and the receptance by:

$$A_{pi}(\omega) = j\omega Y_{pi}(\omega) = -\omega^2 H_{pi}(\omega) = \frac{a_p(\omega)}{p_i(\omega)} \qquad \textbf{(5-16)}$$

5.2.3.2 Random vibrations

Background. Acquisition of FRFs from random vibrations to a structure requires additional formulations and parameters as opposed to a single source excitation because the excitation and response are both characterized by random processes. As part of the approach to analyze random vibrations and responses, two sets of parameters are introduced and defined to describe random signals. The first set of parameters is classified as correlation functions, which are defined in the time domain. The second set is spectral densities, which are in the frequency domain.

Consider a typical random vibration parameter, *f(t)*, shown in Figure 5.1(a), which is assumed ergodic. An ergodic function is a type of random process, which requires a single sample to portray all the statistical properties required for its definition. The autocorrelation function, $R_{ff}(\tau)$, which is a type of correlation function, is introduced and defined as the expected or average value of the product $[f(t)\cdot f(t+\tau)]$, evaluated in the time domain. The autocorrelation function is a real and even function of time and is denoted as follows:

$$R_{ff}(\tau) = E\left[f(t)\cdot f(t+\tau)\right] \qquad \textbf{(5-17)}$$

The autocorrelation function takes the form shown in Figure 5.1(b), and is used to transform the original random signal such that the requirements for evaluation via a Fourier Transform[2] is possible. The result of the Fourier transform of the autocorrelation function results in the auto- or power spectral density (PSD), $S_{ff}(\omega)$, which is a type of spectral density and is given as follows:

$$S_{ff}(\omega) = \tfrac{1}{2\pi}\int_{-\infty}^{\infty} R_{ff}(\tau)e^{-i\omega t}\,d\tau \qquad \textbf{(5-18)}$$

The auto-spectral density is a real and even function of frequency, and provides a description of the frequency function of the random signal, *f(t)*. An example plot is included in Figure 5.1(c).

[2] The Fourier Transform decomposes or separates a waveform or function into sinusoids of different frequency which sum to the original waveform, i.e. conversion of a function from the time domain to the frequency domain. The Fourier transform of a function, *f(t)*, is given by $F(\omega) = \tfrac{1}{2\pi}\int_{-\infty}^{\infty} f(t)\exp(-i\omega t)dt$.

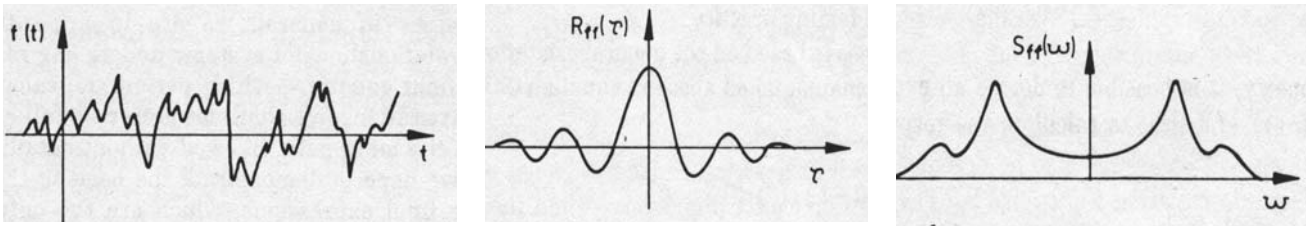

(a) Time History (b) Autocorrelation Function (c) Auto or Power Spectral Density

Figure 5.1: Random signals [5]

Similarly, an additional pair of correlation and spectral density functions are developed for a pair of random vibration parameters, *f(t)* and *x(t)*, to produce the cross correlation and cross spectral density functions. The cross correlation function, $R_{xf}(\tau)$, is defined as follows:

$$R_{xf}(\tau) = E\left[x(t) \cdot f(t+\tau)\right] \qquad \textbf{(5-19)}$$

Fourier transform of the cross correlation function results in the cross spectral density (CSD):

$$S_{xf}(\omega) = \tfrac{1}{2\pi} \int_{-\infty}^{\infty} R_{xf}(\tau) e^{-i\omega t} d\tau \qquad \textbf{(5-20)}$$

Cross correlation functions are real, but not always even, functions of time; while, cross spectral densities, unlike their counterpart of auto spectral densities, are usually complex functions of frequency with the following particular conjugate property:

$$S_{xf}(\omega) = S_{fx}^{*}(\omega) \qquad \textbf{(5-21)}$$

With an understanding of the correlation functions and spectral densities involved in analyzing random vibrations, the input-output relationships for systems undergoing random vibrations become the primary focus. Given an understanding of how FRFs are acquired for the modal test procedure, the general mathematical process for FRF development is provided without algebraic detail.

FRF Development. Given that a force *p(t)* varying arbitrarily with time can be represented by a sequence of infinitesimally short impulses, the response of a linear dynamic system to a single impulse at time t' and magnitude $p(t')$ is provided as the following unit impulse response function [10]:

$$du(t) = [p(t')dt']h(t-t') \qquad \textbf{(5-22)}$$

where *du(t)* denotes the differential displacement response of the system in the time domain, *t*; $p(t')$ is the magnitude of the impulse at time t'; and $h(t-t')$ is the unit impulse response function. Thus the response of the system at time *t* is the sum of the responses to all impulses up to that time.

$$u(t) = \int_{-\infty}^{\infty} h(t-t')p(t')dt' \qquad \textbf{(5-23)}$$

Using the above property, known as the convolution integral, an expression for the response at time *t*, *u(t)*, and the response at time $t+\tau$ is derived. Subsequently the response autocorrelation function, $R_{uu}(\tau)$ is given as follows:

$$R_{uu}(\tau) = E\left[u(t)\cdot u(t+\tau)\right] \qquad \textbf{(5-24)}$$

Manipulation of the above expression can result in a description of the response autocorrelation in terms of the corresponding property of the excitation, $R_{pp}(\tau)$; however the result is complicated and an unusable triple integral. Nonetheless, Equation (5-24) can be transformed to the frequency domain, which results in the following convenient form:

$$S_{uu}(\omega) = \left|H\left(\omega\right)\right|^2 S_{pp}(\omega) \qquad \textbf{(5-25)}$$

where S_{uu} is the response PSD; S_{pp} is the excitation PSD; $H(\omega)$ is the receptance FRF.

Although it appears well-suited for FRF determination, the above equation does not provide a full description of the random vibration conditions, nor could it be used to determine the FRF from measurements of excitation and response since phase information is omitted from the formulation. Therefore, a second equation, the cross correlation between the excitation and the response, is required and presented in the frequency domain form:

$$S_{pu}(\omega) = H\left(\omega\right)S_{pp}(\omega) \;\; \textbf{or} \;\; S_{uu}(\omega) = H\left(\omega\right)S_{up}(\omega) \qquad \textbf{(5-26)}$$

The analysis performed in this section is limited to a single excitation parameter; however, several responses can be considered by repeated application of Equations (5-25) and (5-26). The analysis can be extended to a situation where several excitations are applied simultaneously, regardless of their correlation with each other. This level of analysis requires the autospectra of the individual excitations, and also the cross spectra which connect one with the others, resulting in a matrix formulation as follows:

$$[\mathbf{S}_{pu}(\omega)] = [\mathbf{H}\left(\omega\right)][\mathbf{S}_{pp}(\omega)] \qquad \textbf{(5-27)}$$

Here the brackets denote matrices.

Equation (5-26) provides the basis for determining a system's FRF properties from a random vibration or ambient excitation test. A convenient formula for determining the FRF is available from estimates of the relevant spectral densities:

$$H(\omega) = \frac{S_{pu}(\omega)}{S_{pp}(\omega)}\text{, usually identified as } H_1(\omega)\text{, or} \qquad \textbf{(5-28)}$$

$$H(\omega) = \frac{S_{uu}(\omega)}{S_{up}(\omega)}\text{, usually identified as } H_2(\omega) \qquad \textbf{(5-29)}$$

The three equations, Equations (5-28), (5-29), and (5-25) present an opportunity to check the quality of calculations made using measured data.

5.3 METHODS OF EXCITATION

5.3.1 Input-output methods

The input-output method for a bridge typically involves introducing an impulse or displacement release procedure and subsequently measuring the free vibration response of the structure [1]. In the following section, forced excitation methods applicable to bridge structures are examined with an emphasis on their advantages and disadvantages. In general, input-output excitation techniques are advantageous as compared to output-only methods, since they are able to suppress the effects of extraneous noise in the measured structural response [8].

5.3.1.1 Impact hammer and drop weight impactor

An impact excitation requires a contact between the bridge and a mass, which provides a forced-pulse excitation of the bridge [4]. The impulse hammer is usually built-up with an impactor and various tips, which help to control the frequency and force range of the impulse [5], as shown in Figure 5.2. The use of the impact hammer is advantageous because of its portability and ease of operation; however, it is difficult to achieve consistent input because of the manual nature of the impact, specifically it's variability in force due to height and inconsistency of the contact point during impact.

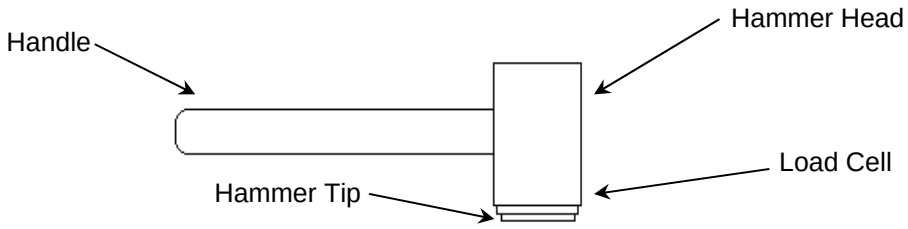

Figure 5.2: Impact hammer

As a resolution for the inconsistencies of the input, some researchers implement a drop weight impactor [1, 3, 4]. The drop weight device involves the use of weights, a damper, a load cell, and a soft interface between the bridge and load cell, as shown in Figure 5.3. The drop weight system uses a pulley system to raise and release the load repeatedly from the same height, thus providing a consistent excitation into the structure for accurate measurements from impact to impact [4].

The variation of the impulse into the structure is controlled by altering the mass of the impact device and/or by changing the height of the release point for a drop weight impactor. Although impact excitation by hammer and/or drop weight is a convenient and efficient means for vibration testing of a bridge, the method is susceptible to input noise because of the short duration of the pulse compared to the length of recording time [8].

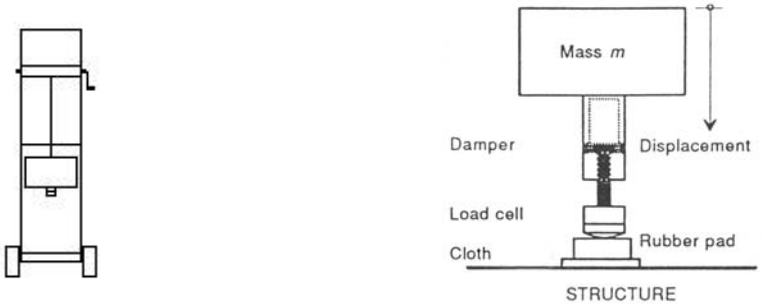

(a) Impactor Frame (b) Impactor Contact-point [4]

Figure 5.3: Drop weight impactor

A limitation on the forced impulse excitation method is its restriction to shorter span bridges because of the potential for local damage at the point of contact, which may occur when large force levels are applied [8]. Green suggests limiting impact hammers to bridges with spans of less than 30 meters, since greater masses are required for longer spans, and the portability of the impact device becomes compromised [4]. However, Bolton, et al. have successfully implemented a modal test procedure to examine changes in modal properties of a concrete box girder bridge with spans greater than 30 m [15].

5.3.1.2 Shaker

Another method of forced vibration testing of a bridge is through the use of shakers or vibrators, which generally stay in contact with the bridge through the testing period [8]. Shakers are often composed of eccentric rotating masses or are electrohydraulic. They are used for broadband testing, where the structure is excited with a signal containing energy over a wide range of frequencies simultaneously [7]. Shakers are versatile in the range of forces input into the structure as well as in the type of excitation. The maximum forces can range from 5 kN to 90 kN with sinusoidal excitation, sine sweep excitation, or random excitation over the frequency range of interest [4]. The most effective excitation method with a shaker for the acquisition of modal properties is the transient type, which include sine sweep, random burst, and triggered random excitations [4, 6]. Once the

impulse is introduced to the structures, the free vibration response is measured and modal properties are extracted [1].

The eccentric rotating mass shaker is a reaction type mechanical vibration machine, which generates a vibration force by using a rotating shaft carrying a mass whose center of gravity is displaced from the center of rotation of the shaft [8]. A constant force is applied to the structure for a given mass, rotating mass and out of balance displacement. The shaker can have more than one rotating mass, as shown in Figure 5.4, which gives the particular advantage of generating forces in more than one direction.

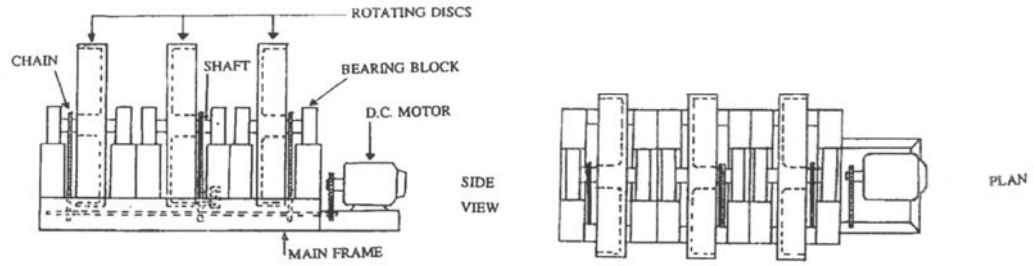

Figure 5.4: Eccentric rotating mass shaker [8]

The electrohydraulic vibrator generates forces through the countering motion induced by the high-pressure flow of liquid [8]. The electrohydraulic shaker is comprised of a servo-controlled hydraulic actuator, which controls the motion of an attached mass (see Figure 5.5). The weight of the mass can be varied to control the different levels of excitation into the structure. The electrohydraulic shaker offers the advantage of being able to excite higher modes of the structure, as well as excite the structure in bending or torsion [8]. In addition other benefits include the capability of introducing a static preload and complex waveforms to the bridge [8].

Figure 5.5: Electrohydraulic shaker[3]

[3] Photo available at www.hotektech.com courtesy of Hotek Technologies, Tacoma Washington.

Although shakers are advantageous in the types and variability of the excitation to the test bridge, disadvantages often outweigh the capabilities they present. In particular, the shaker device is often large and requires a significant amount of labor and equipment to set up and place. In addition to being cumbersome, the devices are expensive compared to testing with impact hammers or drop weights. Electrodynamic shakers have difficulty producing lower frequency excitation and are limited in the force levels that can be generated while servo hydraulic shakers can provide higher force levels, but have difficulties producing excitations at frequencies above 100 Hz [13].

5.3.1.3 Displacement-release

The displacement-release method of excitation for modal testing requires imposing an initial, static displacement on the bridge structure by means of a cable or a large mass, as shown in Figure 5.6. The structure is released and undergoes free-vibration. This step-release is perhaps the simplest form of excitation; however, the method is disadvantageous because of the safety issues associated with using large masses [4]. In addition, it is often difficult to implement in the field [8]. Typically the response of the structure to a displacement-release excitation is governed by modes that most closely resemble the initially deformed shape of the structure, possibly limiting the range of available modes for extraction [8].

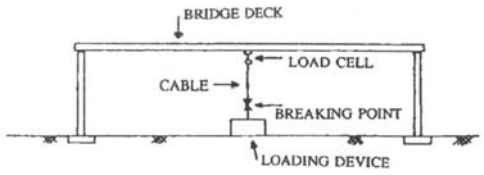

Figure 5.6: Displacement-release of structure [8]

5.3.2 Output-only excitation

Ambient excitation or output-only methods measure the response of the structure under its normal operating conditions [13]. As compared to input-output excitation techniques, the measurement of the structural response is performed while the structure is in service (no lane closures needed), is cost effective (essentially no cost for the excitation source), and is available for the continuous monitoring of the bridge structure [1, 4, 8]. In addition, ambient vibration testing is also applicable to long span bridges [4]. Further, locations of bridge structures such as the center traffic lane or locations over water may be inaccessible for input-output excitation methods.

Sources for ambient vibration methods include vehicular traffic, wind, pedestrian traffic, ocean waves, and low seismic activity [1, 4, 8, 13]. Several assumptions for ambient excitation test methods are necessary since the input is unknown. First, the excitation forces are assumed to be a stationary random process, having a flat frequency spectrum, thus implying that the vibration

response of the bridge contains all the normal modes [8]. Furthermore, this eliminates concern that input-output excitation methods may have with input noise. Second, the output-only excitation methods assume that the recorded response of the structure alone is sufficient for extraction of modal parameters. While the method is certainly cost effective and implemented without disruption of traffic, ambient excitations are of unknown amplitude and often are unable to achieve high frequency excitations. Nevertheless, the development and maturation of acquisition systems and modal extraction techniques have helped to mitigate the disadvantages associated with ambient vibration techniques [1].

5.3.3 Comparison of excitation techniques

A concern with ambient vibration test methods is the ability to extract modal parameters from the response data and still attain adequate correlation to force excitation modal test methods. Farrar and James performed a systems identification comparison on a bridge, examining results from ambient excitation measurements and forced vibration testing using a hydraulic shaker [22]. The results of the ambient and forced vibration tests showed good correlation. Resonant frequencies measured from the forced vibration tests were found to be 1.44% to 4.37% higher than the ambient excitations. The higher frequencies from the forced vibration tests were attributed to the reduced mass of the system that resulted when bridge traffic was closed during the forced vibration tests.

A study by Bolton, et al. compared the modal parameters extracted from single-input multiple output (SIMO) tests, using a drop weight impactor and output-only (vehicular traffic) excitation techniques for a reinforced concrete highway bridge [3]. The forced excitation and ambient modal tests were conducted on a reinforced-concrete, two span bridge for purposes of comparing excitation techniques and two methods for extraction of modal properties. The first method utilized frequency domain transmissibility functions between a reference acceleration and other response accelerations. The transmissibility function is the ratio of the cross-spectrum density and the auto spectrum density [3]. The second method was the Ibrahim time domain (ITD) technique, a methodology for extracting modal parameters directly from decaying time or impulse response functions [3]. The authors found good correlation between the forced and output-only testing techniques for the natural frequencies and mode shapes extracted from each test method. Table 5.1 shows a comparison of modal frequency results from the respective tests.

Table 5.1: Comparison of modal frequencies [3]

Extraction Method	**Mode**				
	1 (Hz)	**2 (Hz)**	**3 (Hz)**	**4 (Hz)**	**5 (Hz)**
SIMO	10.06	12.75	14.63	16.53	21.06
Transmissibility	10.06	12.75	14.63	16.50	21.06
ITD	10.04	12.63	14.27	16.95	21.12

If the excitation techniques for the input-output and output-only test methods are shown to have good correlation, selection of the excitation method may be determined based on the conditions available at the bridge and most suitable configuration for data acquisition. The following tables provide summaries of the advantages and disadvantages of the different excitation techniques available for use on bridge structures. No single technique is superior to the others; rather it is at the discretion of the tester to select the method of excitation most suitable for the conditions in the field.

Table 5.2: Input-output techniques

Input-Output	Advantage	Disadvantage
Impact Hammer	▪ Cost Effective [6] ▪ Portable ▪ Easy Operation [6]	▪ Poor signal to noise ratio[6] ▪ High sensitivity to nonlinearities [6] ▪ Lack of control over frequency content[6]
Drop Weight Impactor	▪ Mass normalized mode shapes [1] ▪ Cost Effective ▪ Low (< 1 Hz) frequency modes [1] with up to 20 Hz modes observed in field [3] ▪ Can control amplitude of input [1]	▪ Not viable for continuous monitoring [1] ▪ Susceptible to input noise [8]
Shaker	▪ Mass normalized mode shapes [1] ▪ Capable of higher frequency excitations (1.5 to 100 Hz) [8, 13] ▪ Can apply a static preload to the test structure [8]	▪ Expensive [1, 4] ▪ Difficult to excite frequencies below 1 Hz [2, 8] ▪ Heavy weight makes it difficult to install and move [4]
Displacement-Release	▪ Simple and effective in determining damping [8]	▪ Response dominated by modes most resembling the deformed shape [8] ▪ Difficult to implement [4, 8] ▪ Safety hazard in releasing large masses [4] and potential damage to structure

Table 5.3: Output-only techniques

Output-Only	Advantage	Disadvantage
Ambient Excitation	▪ Capable of continuous monitoring [1] ▪ Cost-effective, excitation source is essentially free [1] ▪ Applicable for long span bridges [4]	▪ Difficult to extract damping properties [8] ▪ Uncontrolled amplitude input into the structure [1, 8] ▪ Limited to low frequency excitation (<1 Hz) [1, 2] ▪ Difficult to excite the lateral modes of a bridge, which are of interest for seismic studies [13].

5.4 MODAL TESTING PROCEDURE

Modal testing on a bridge presents unique challenges, since the testing procedure is implemented outside of a controlled laboratory environment. Regardless of the location or obstacles existing during the test period, the goal of modal testing is to acquire sets of Frequency Response Functions (FRFs) that serve the purpose of analysis and extraction of the properties of the structure for all required modes of the bridge [7]. The modal testing methodology includes the selection of the transducers and their placement. Following the selection of the excitation methodology, the ability to identify and separate the different modes of the structure is critical in determining the modal properties of the structure.

5.4.1 Transducers

A variety of transducers is available for modal testing on a bridge structure. The response of the structure can be defined by displacement, velocity, or acceleration [7]. The most commonly used transducer types for modal testing of bridges include accelerometers, velocity, and displacement transducers. Selection of the transducer type is determined such that the mass of the transducer does not interfere with the response of the structure, and the transducer provides the type of data required for structural assessment [7]. Typically, for large civil structures such as bridges, the mass of the transducer is not a concern, but rather care should be used to determine that the transducer does not distort the response of the structure. Transducers should measure the acceleration, velocity, or displacement response of the structure directly for convenient conversion into the frequency domain. This section provides an overview of sensors applicable for the measurement of the structural response during dynamic testing of bridge structures.

5.4.1.1 Accelerometer

Accelerometers are the most common and applicable of transducers for use during modal testing of bridge structures, since they are capable of operation over a wide range of frequencies and are easy to install [4]. There are several different types of accelerometers available for modal testing of bridge structures. Accelerometers capable of measurements of +/- 5G are adequate for modal testing of bridge structures, since the maximum accelerations observed during a modal test of a reinforced concrete bridge structure is typically 0.5G [4].

Piezoelectric Accelerometer [7]. The piezoelectric accelerometer is comprised of a base and case, a center post, an annular section of piezoelectric ceramic, and an annular seismic mass element (see Figure 5.7). The base of the accelerometer is attached to the structure such that the seismic mass within the accelerometer undergoes the equivalent motion of the structure during excitation. The excitation force travels through the piezoelectric crystal, which deforms due to the excitation force. There is a change produced in the crystal proportional to the deformation that is directly related to the acceleration of the seismic mass and ultimately the response of the structure.

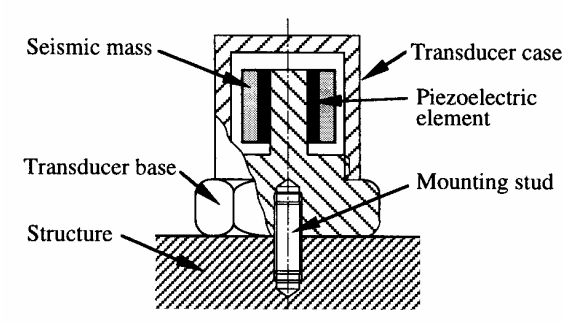

Figure 5.7: Piezoelectric accelerometer [7]

Piezoresistive and Capacitance Accelerometers [7]. Other types of accelerometers available for use on bridges are piezoresistive and capacitance accelerometers. In the piezoresistive accelerometer, semiconductor flexure elements supporting a seismic mass form part of an active Wheatstone bridge. As the structure displaces due to the excitation force, the Wheatstone bridge becomes unbalanced and the differential output (proportional to the applied strain) relates to the measure of acceleration. Figure 5.8 displays a layout example of a piezoresistive accelerometer.

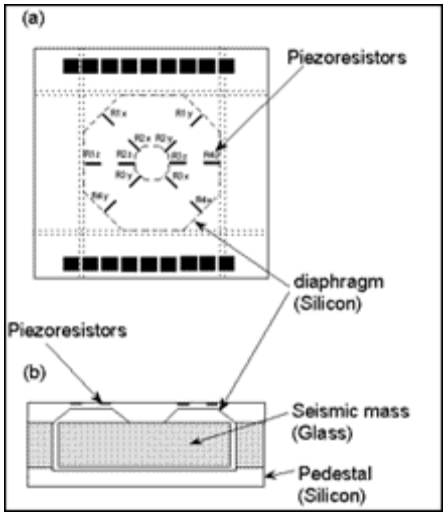

Figure 5.8: Piezoresistive accelerometers[4]

Similarly, in a capacitive-type accelerometer, the measuring elements form a capacitive half-bridge versus the Wheatstone bridge in the piezoresistive accelerometer. When the structure moves as a result of the excitation, the capacitive bridge becomes unbalanced, thus being able to measure the differential output relating directly to the acceleration

[4] Figure available at www.sensorsmag.com, courtesy of Fujikura Ltd., Tokyo, Japan

response on the bridge. An example of a capacitance accelerometer is shown in Figure 5.9.

Figure 5.9: Capacitance accelerometer[5]

5.4.1.2 Velocity transducer [7]

A velocity transducer uses a laser velocimeter, which is an optical system that measures the instantaneous velocity of a point (or points) on the structure. The basic laser Doppler velocimeter (LDV) operates by measuring the velocity of a point addressed by a focused laser beam using the Doppler shift between the incident light and scattered light returning to the measuring point using an interferometer [24]. One advantage associated with the velocity transducer is that the transducer is a non-contact device, which is capable of measuring the response of the bridge by the use of mirrors at locations that are difficult to access. The disadvantages associated with the cost of the laser and signal processing equipment and the time required for set-up configuration, however, outweigh the advantages for field modal testing of bridges.

A natural extension of the LDV is the scanning laser Doppler velocimeter, which incorporates a dynamic feature in the location mechanism, such that the laser beam moves from one measurement site to the next [5]. Ideally, the faster the scanning takes place, the shorter the measurement time. The speed is limited, however, by the physical limitations inside the transducer, such as the inertia of the mirrors, which must be moved in order to bring about the desired change of direction of the beam [5].

The velocity transducer is a developing technology for the response measurement of bridge structures. In its current state, however, the use of a laser Doppler velocimeter for a modal test performed in the field introduces complexities in the set-up and increases cost in measuring several locations for response.

5.4.1.3 Displacement transducer [4, 7]

The third type of transducer is the displacement transducer. Displacement transducers are an alternative to using accelerometers for the global response measurement of the bridge during a modal test. Unfortunately, displacement transducers require an inertial platform, which is typically unavailable or difficult to install in the field. The

[5] Figure available at www.sensorsmag.com courtesy of Kistler Instruments Corporation, Amherst, NY.

potentiometer is the simplest form of a displacement transducer, but it is limited to low frequency vibrations and large displacement applications. An example of a potentiometer is shown in Figure 5.10.

Figure 5.10: Potentiometer[6]

Another type of displacement transducer is the linear variable differential transformer (LVDT), as shown in Figure 5.11. The LVDT contains a free moving magnetic core connecting the magnetic flux between a surrounding primary coil and two secondary coils. When the magnetic coil moves away from its central position, the voltage in one of the secondary coils increases while the other decreases. This results in a linearly varying differential voltage output, which is utilized to determine the response of the structure. An LVDT requires the use of a push-rod in order to decouple the lateral motion and connection to the structure. Although the LVDT may be applicable on large civil structures, its convenience is questionable because of the calibration required for each transducer location.

Figure 5.11: Linear variable displacement transducer[7]

Alternatively, laser optical range sensors are available for measuring large displacements; however, just as in the case of velocity transducers, the cost of equipment and coordination of a configuration for the measuring technique makes it an unfeasible option for modal testing of bridge structures.

[6] Figure available at www.omega.com courtesy of Omega Engineering, Inc.
[7] Figure available at www.omega.com, courtesy of Omega Engineering, Inc.

5.4.2 Sensor placement

The determination of sensor location and quantity has often been dependent on engineering judgment and experience without any formal relationships developed between the desired mode shapes and the sensor placement. A number of researchers have investigated the optimal placement of sensors for large flexible structures for the aerospace industry [16]; however, few methodologies have been proven for nondestructive evaluation and health monitoring of bridge structures, nor have the economic ramifications of using an alternative quantity and location of sensors been thoroughly investigated to date [9]. In this section two techniques for optimal sensor placement for modal testing of bridge structures are examined.

Sensor (transducer) location and placement during modal testing of a bridge is a function of the cost and number of mode shapes to be acquired. Optimization of the number and placement of sensors provides a cost savings in terms of time reduction for the test set-up, data acquisition, modal analysis, and interruption of traffic [9]. The objective of placing sensors in multiple locations is to attain a sufficient amount of frequency response functions such that individual modes are identified from the modal test [4]. For bridge systems, the allocation of sensors for sufficient resolution of the vibration properties is a critical aspect of the modal test strategy due to the large size of the bridge structure and restrictions on accessibility to locations on the structure. Furthermore, the experimental setup time and time for data analysis increase as the number of sensors increases; consequently, the time needed to divert traffic from the bridge area increases as well as the number of FRF's required and the duration of the total test procedure [9].

5.4.2.1 Sensor optimization by Shannon's sampling theorem

Shannon's sampling theorem states that a signal is correctly represented by a set of samples that are assigned with a certain periodicity, T, if it is possible to reconstruct the original signal in the time domain [9]. The primary concept here is that all the information contained in the original signal is also contained in sample values that are taken at equally spaced intervals. According to Shannon's sampling theorem, if a signal does not contain a component with a frequency greater than or equal to f_{max}, the signal is completely determined by the set of its values at regularly spaced intervals of values $T = 1/2 \cdot f_{max}$, where the sampling rate must satisfy the inequality $f_s > 2 f_{max}$ where $f_s = 1/T$; the minimum of this sampling rate is referred to as the Nyquist sampling rate [9]. By extending Shannon's Sampling Method into the spatial domain from the time domain and applying the Nyquist sampling rate, Stubbs and Park developed the following rules for optimal placement of sensors [9]:

1. Select the highest mode to be measured.
2. Estimate $\frac{\lambda_{WL}}{2}$ for that mode, where λ_{WL} is the wavelength of the mode.
3. Place a sensor at each node of the mode.

4. Place two additional sensors within the $\frac{\lambda_{WL}}{2}$ span, with each sensor being $\frac{\lambda_{WL}}{6}$ spacing form each node.

The rules for sensor placement are applied in both the longitudinal and transverse directions of the bridge: determine the highest desired mode in the transverse direction, and follow the developed rules; then repeat the method in the longitudinal direction.

5.4.2.2 Kinetic energy optimization technique (EOT)

Heo, et al. derived a technique for optimal transducer placement for health monitoring of a bridge structure by maximization of the modal kinetic energy. The energy optimization technique described by Heo, et al. is a modification of Kammer's effective independence method (EIM) based on the spatial independence concept [16]. It searches for sensor configurations that maximize the rank of the measured modal matrix $[\Phi_s^T \Phi_s]$, where rank indicates the number of linearly independent rows in a matrix [25].

Here, the principle of the Fisher information matrix, considered an "extended design matrix", is introduced, whose i^{th} row consists of independent variables for the i^{th} data point [23]. The components of the inverse of the Fisher information matrix are proportional to the variances of the least squares estimates of the model parameters [23]. Consequently, maximizing the Fisher information matrix minimizes the variances of the model parameters leading to an optimal design. Therefore, the Fisher information matrix (**Q**), as implemented by Heo et al., is maximized such that the covariance matrix (**Co**) between the displacement vector in the modal coordinate (**q**) and the estimated modal displacement $\left(\overline{\mathbf{q}}\right)$ is minimized:

$$Min(\mathbf{Co}) = E\left[\left(\mathbf{q}-\overline{\mathbf{q}}\right)\left(\mathbf{q}-\overline{\mathbf{q}}\right)^T\right] \qquad \textbf{(5-30)}$$

$$Max(\mathbf{Q}) = Max\left\{\left[\mathbf{\Phi}_s^T \mathbf{\Phi}_S\right]\right\} \qquad \textbf{(5-31)}$$

where E indicates the expected value; and $\mathbf{\Phi}_s$ represents a reduced set of the mathematical mode shapes corresponding to the target modes.

In an attempt to improve the signal to noise ratio for mode shape identification of bridge structures, Heo, et al. prescribe a modified form of the EI method first by introducing the energy optimization technique (EOT) [16].

The implementation of the procedure requires selection of an initial configuration for the sensors. The distribution of the kinetic energy is described by the definition of modal mass from the measured mode shape vectors, $\mathbf{\Phi}$.

$$\mathbf{KE} = \mathbf{\Phi}^T \mathbf{m} \mathbf{\Phi} \qquad \textbf{(5-32)}$$

Utilizing the Cholesky decomposition, the system mass matrix, **m**, is placed into upper and lower triangular Cholesky factors, with the kinetic energy now equal to [16]:

$$\mathbf{KE} = \mathbf{\Psi}^T \mathbf{\Psi} \tag{5-33}$$

where $\mathbf{\Psi} = \mathbf{U\Phi}$ *and* $\mathbf{m} = \mathbf{LU}$. The matrix **L** and **U** denote the lower and upper triangular Cholesky factor. The projections of the mode shapes on the reduced sensor locations are denoted by $\overline{\mathbf{\Phi}}$ and $\overline{\mathbf{\Psi}}$. Likewise, the energy of the reduced sensor configuration is given by:

$$\overline{\mathbf{KE}} = \overline{\mathbf{\Psi}}^T \overline{\mathbf{\Psi}} \tag{5-34}$$

The objective of the transducer placement is to find a configuration that maximizes the measured kinetic energy of the structure. Reduction of the number of sensors ceases when a rank deficiency of the energy matrix occurs. The problem is solved by the following iterative procedure where the eigenvalues, Λ and eigenvectors, $\boldsymbol{\psi}$ of the energy matrix are first extracted by applying the traditional algebraic eigenvalue formulation:

$$\overline{\mathbf{KE}}\boldsymbol{\psi} = \boldsymbol{\psi}\Lambda \tag{5-35}$$

Then fractional contributions of the remaining transducers are assembled into the EOT vector:

$$\mathbf{EOT} = \sum_{i=1\ldots m} \left[\overline{\mathbf{\Psi}}\boldsymbol{\psi}\Lambda^{-1/2} \right]^2 \tag{5-36}$$

The transducer location with the minimal contribution to the **EOT** vector is removed from the configuration, and its contribution to the kinetic energy matrix, $\overline{\mathbf{KE}}$, is also removed. A check for rank deficiency is performed, resulting in the following possible outcomes: 1) removal of the transducer results in a rank deficiency which implies the sensor cannot be removed; or 2) no rank deficiency occurs and the transducer location is removed. The process is repeated until reaching the required number of transducers.

Similar to Stubbs and Park's method for optimal transducer placement and location, Heo's method provides information regarding sensor optimization based on the premise that the data generated from the modal test is capable of being processed to evaluate the health of a bridge structure. In terms of health monitoring of structures and conducting modal tests over various intervals of time, questions arise pertaining to how changes in mode shapes due to accumulated damage affect sensor locations, since the optimal placement and quantity of sensors is based on a model or on pre-damage measured mode shapes of the structure. Heo et al. observed that changes in mode shapes shown in bridge modal test data are not significant enough to warrant a re-optimization of sensor locations and quantity [16].

5.4.3 Identification of dynamic properties

The extraction of modal parameters from the FRFs acquired from the modal test data aims to identify, by curve fit, the constants to develop a mathematical model of the test data. The modal analysis procedure is dependent on the curve-fit technique selected to approximate the test data and determine the coefficients for a theoretical FRF, which correlates with the test data. Many techniques are available, which predominately operate on the response characteristics of the frequency domain [5].

During the modal testing process, the identification of dynamic properties is usually a self-contained analysis accompanying the data acquisition system. Even a limited understanding of what modal analysis identification techniques are available assists in determining the type of procedure most appropriate for the extraction process. The following are a set of criteria that ought to be considered when selecting a procedure for the identification of dynamic properties from the acquired frequency response functions from the modal test.

- Experimental modal analysis techniques are divided into two groups: 1) methods applicable for the frequency domain, and 2) methods applicable for the time domain. Depending on the selected domain for the response of the structure, the appropriate method can be extracted. In addition to division by domain, the algorithms for identification of modal properties can be further divided into the input and output categories.

- For forced excitation techniques, a modal analysis technique that can analyze several FRFs simultaneously is appropriate, with responses taken at various locations on the bridge, but using one excitation point [7]. These methods are identified as single-input multiple-output (SIMO) techniques.

- If all the FRFs are to be analyzed simultaneously from various excitation locations and response locations, then a technique capable multi-input multi-output (MIMO) is appropriate.

For bridge structures the most fully developed method for modal testing are input-output techniques utilizing a contact excitation in the form of an impulse load via an impact hammer or drop-weight hammer. The application of output-only methods for large scale dynamic testing is particularly attractive, however, since the methods allow for continuous monitoring of the structure while still in service.

Numerous techniques for extraction of modal parameters for both input-output and output-only methods are available. Some examples of experimental modal analysis techniques include the following:

- Peak picking of the auto- and cross-powers of the measured response selects peaks in the spectra to acquire estimates of the resonance frequencies, and thus operational deflection shapes are obtained [17];

- The natural excitation technique (NExT) essentially involves applying time domain curve-fitting algorithms to cross-correlation measurements made between various response

measurements on an ambiently excited structure to estimate the resonant frequencies and modal damping [22];

- The nonlinear least squares curve-fit approach is a general multi-degree-of-freedom curve-fit approach utilizing weight factors at each frequency point of interest and minimizing the curve fit error by differentiation [5]; and

- Descriptions of transmissibility functions and the Ibrahim Time Domain (ITD) technique were described briefly in section 5.3.3 of this report [3, 4, 18].

5.5 SUMMARY

The identification of modal parameters of a bridge structure is the main objective of the modal test procedure and the first component of a complete nondestructive damage detection technique for large civil structures. The modal test consists of the following phases, which are necessary for successful identification of modal properties of a bridge structure:

- Understanding of the theoretical basis of modal testing and development of the frequency response functions;

- Selection and placement of transducers to be used on the structure for an accurate and sufficient amount of data collection;

- Selection of the method of excitation considering location and available accessibility to the bridge; and

- Identification of dynamic properties by experimental modal analysis.

Once the dynamic properties of the bridge structure (i.e., natural frequencies, damping properties and mode shapes) are identified, a system identification procedure and damage detection algorithm is implemented for completion of the nondestructive damage detection technique. It is important to emphasize that modal testing alone is not a nondestructive evaluation method but rather a tool to extract the modal parameters of a bridge structure for use as part of verification of an analysis model, as in Huang, et al. and Farrar, et al., or in conjunction with a vibration based damage detection approach as in the damage index method approach developed by Stubbs, et al. [18, 22, 19].

5.6 CHAPTER 5 REFERENCES

1. Farrar, C.R. and Sohn, H. "Condition/Damage Monitoring Methodologies." Invited Talk, *The Consortium of Organizations for Strong Motion Observation Systems (COSMOS) Workshop,* Emeryville, CA November 14-15, 2001. LA-UR-01-6573

2. Peeters, B., Maeck, J., and De Roeck, G. "Vibration-based Damage Detection in Civil Engineering: Excitation Sources and Temperature Effects." Smart Materials and Structures. Volume 10. pp. 518-527. 2001

3. Bolton, et al., "A Comparison of Modal Properties Derived from Forced And Output-Only Measurements for a Reinforced Concrete Highway Bridge." Proceedings of the 18th International Modal Analysis Conference, San Antonio, Texas.

4. Green, M. F., "Modal Test Methods For Bridges: A Review." Proceedings of the 13th International Modal Analysis Conference, Nashville, Tennessee. Volume 1. pp. 552-558.

5. Ewins, D. J. Modal Testing: Theory, Practice and Application. Research Studies Press, Ltd. Second Edition. 2000.

6. Reynolds, P. and Pavic, A., "Impulse Hammer vs. Shaker Excitation for the Modal Testing of Building Floors." Experimental Techniques. Structural Testing Series: Part 7. pp. 39-44. May/June 2000.

7. Maia, N. M. M. and Silva, J. M. M. editors. Theoretical and Experimental Modal Analysis. Research Studies Press, Ltd. 1997.

8. Salawu, O. S. and Williams, C. "Review of Full-Scale Dynamic Testing of Bridge Structures." Engineering Structures. Volume 17, No. 2. pp. 113-121. 1995.

9. Stubbs, N. and Park, S. "Optimization of Sensor Placement for Mode Shapes Via Shannon's Sampling Theorem." Microcomputers in Civil Engineering. Volume 11. pp. 411-419. 1996.

10. Chopra, A. K. Dynamics of Structures: Theory and Applications to Earthquake Engineering. Prentice Hall, Inc. 1995.

11. Clough, R. W. and Penzien, J. Dynamics of Structures. McGraw-Hill Book Company. 1975.

12. Rao, S. S. Mechanical Vibrations. Third Edition. Addison-Wesley. 1995.

13. Farrar, C.R., Duffey, T. A., Cornwell, P. J. and Doebling, S. W. "Excitation Methods for Bridge Structures." Proceedings of the 17th International Modal Analysis Conference, Kissimmee, Florida. Volume 1. pp. 1063-1068.

14. Hunter, N. F. "Vibration Testing: Reviewing the State of the Art – Prospects and Challenges." Structural Dynamics @ 2000: current status and future directions. Research Studies Press Ltd. 2001. pp. 175-192.

15. Bolton, R., Stubbs, N., Park, S. and Sikorsky, C. "Documentation of Changes in Modal Properties of a Concrete Box Girder Bridge Due to Environmental and Internal Conditions." Computer-Aided Civil and Infrastructure Engineering. Vol. 16, No. 1. January, 2001. pp. 42-57.

16. Heo, G., Wang, M.L., and Satpathi, D. "Optimal Transducer Placement for Health Monitoring of Long Span Bridge." Soil Dynamics and Earthquake Engineering. Vol. 16. 1997. pp. 495-502.

17. Hermans, L. and Van der Auweraer, H. "Modal Testing and Analysis of Structures Under Operational Conditions: Industrial Applications." Mechanical Systems and Signal Processing. Vol 13, No. 2. 1999. pp. 193-216.

18. Huang, C.S., Yang, Y.B., Lu, L.Y., and Chen, C.H. "Dynamic Testing and System Identification of a Multi-Span Highway Bridge." Earthquake Engineering and Structural Dynamics. Vol. 28. 1999. pp. 857-878.

19. Stubbs, N., Park, S., Sikorsky, C., and Choi, S. "A Global Non-destructive Damage Assessment Methodology for Civil Engineering Structures." International Journal of Systems Science. Vol. 31. No. 11. 2000. pp. 1361-1373.

20. McConnell, K.G. "Modal Testing." Philosophical Transactions of the Royal Society of London Series A-Mathematical, Physical, and Engineering Sciences. Vol. 359. No. 1778. 2001. pp. 11-28.

21. Grossman, S. I. Multivariable Calculus, Linear Algebra, and Differential Equations. Third Edition. Saunders College Publishing. 1995.

22. Farrar, C.R. and James III, G.H. "System Identification from Ambient Vibration Measurements on a Bridge." Journal of Sound and Vibration. Vol. 205. No. 1. 1997. pp. 1-18.

23. Atkinson, A.C. and Donev, A.N. Optimal Experimental Designs. Oxford Science Series Vol. 8. Oxford: Clarendon Press. 1992

24. Stanbridge, A.B. and Ewins, D.J. "Modal Testing Using a Scanning Laser Doppler Vibrometer." Mechanical Systems and Signal Processing. Vol. 13. No. 2. 1999. pp. 255-270.

25. Strang, Gilbert. Linear Algebra and Its Applications. Third Edition. Saunders College Publishers, Harcourt Brace Jovanovich College Publishers. 1988.

6.0 REVIEW OF DAMAGE DETECTION TECHNIQUES

6.1 INTRODUCTION

6.1.1 Background

Structural health monitoring is a critical application for determining a structure's ability to provide adequate service, evaluating the necessity for maintenance, and assessing the need for repair or replacement of a component or the entire structure. A proficient structural health monitoring system is capable of determining and evaluating the serviceability of the structure, the reliability, and the remaining functionality of the structure in terms of durability [26]. The concept of structural health monitoring is analogous to human health management as described by Aktan, et al. [27], where health management undergoes the sequence of periodic physical examination, preventive intervention, and surgery and recovery. Similarly, structural health monitoring requires periodic investigation during service/operation, occasional maintenance, and repair-retrofit or replacement as deemed necessary by the inspection. A necessary component in the sequence of structural health monitoring activities is an efficient nondestructive evaluation (NDE) technique, which supplies an adequate amount of information to determine the functionality of the structure for its intended design objective.

The development and implementation of a structural health monitoring system utilizing the vibration characteristics of a structure is the focus of a number of researchers [26, 27, 34, 43, 44, 59]. Common to each overview and general plan for structural health monitoring and assessment is a requirement for a robust damage detection algorithm, which is capable of identifying, locating and evaluating damage in the structure. In essence, the final goal of a structural health monitoring strategy is to determine the amount of damage a structure is able to tolerate before the damage level reaches a critical stage. Therefore, structural health monitoring is the process of implementing a damage detection strategy for identification and evaluation of structures [28].

"Monitoring" implies that an evaluation is performed on a property or aspect of the structural system over a specified duration. A damage detection algorithm for structural systems identifies alterations of a specific property or aspect of the structure in question. For the effective use of a damage detection algorithm, the definition of damage is an important component, since this is the indicator of the performance of a structure in its current state. Farrar, et al. provide a general definition for damage as changes introduced into a system that adversely affect its current or future performance [29]. For the purposes of a structural system, the interpretation of damage is limited to changes in the material and/or geometric properties of the structural system, including changes to the boundary conditions and system connectivity [29].

Vibration based monitoring of structures is predominant and attractive in the area of structural health monitoring, since each structure possesses a unique vibration structure and the testing procedure allows for an evaluation of a large global structure in a time efficient manner. The

motivation behind most vibration based damage detection strategies is the correlation of a structure's dynamic properties (i.e., natural frequencies, mode shapes, and damping properties) with the mechanical properties of the structure. Hence, damage to a structure causes changes in the structure's stiffness, mass or energy dissipative characteristics and those alterations can be detected in variations of its dynamic properties via modal testing [29].

6.1.2 Paradigm for structural health monitoring

The planning, implementation, and analysis or decision making processes involved in an overall scheme for structural health monitoring are often categorized by researchers into separate divisions to provide a general framework for the structural health monitoring process. A number of paradigms are available generalizing the activities and components of the structural health monitoring strategy. Aktan, et al. and Farrar, et al. provide two contemporary approaches to the sequence of structural health monitoring [27, 30, 31, 28, 29]. These paradigms are valuable in providing a perspective on the diversity and breadth involved in the structural health monitoring process and are reviewed briefly below.

Aktan, et al. describe critical issues for the execution and acceptance of an effective structural health monitoring technique, including a discussion of sociological and political issues related to the acceptance of a structural health monitoring strategy [27]. The technical aspects of structural health monitoring are described as three primary components. First, the experimental arts involve experimental methods for structural identification and condition assessment of the structure [27, 30]. Structural identification according to Aktan, et al. is defined as methods for analytically conceptualizing, modeling, designing experiments for measuring, and quantifying behavior as well as the phenomena affecting it, in order to make engineering decisions [30]. Specifically, structural identification is related to procedures for quantifying the parameters of an analytical model given experimental information. These experimental procedures typically involve a modal analysis procedure that satisfies basic assumptions of linearity, observation, and constancy in order to provide direct quantitative information about the structure.

Second, the analytical aspects involved with condition assessment of a structure emphasize the numerical modeling of a structure, typically through a finite element analysis (FEA). According to Aktan, et al., the numerical modeling of a structure for condition assessment is to use discrete geometric models taking advantage of any heuristic knowledge base as opposed to just numerical or nonparametric models [31]. The analytical aspects also require the use of experimental data from modal testing so as to calibrate the model. Here the experimental and analytical components are correlated in the systems identification process by information technology such as model calibration, data integration, and parametric studies [27].

With the implementation of experimental and analytical procedures for system identification, components of the decision-making process are employed so as to establish clearly defined performance criteria in order to evaluate changes in the condition of the system. Condition indicators describe changes in the global and local mechanical characteristics of a structure. With the understanding that changes in an index should relate to changes in the state-of-force, distribution of strain energy, and load distribution of the structure, one can understand the influence of these factors on overall system reliability. These condition indices are typically the final measure provided by damage detection methods, which are the primary focus of this report.

Figure 6.1 provides a schematic of the generalized monitoring procedure as described by Aktan, et al. [27, 30, 31].

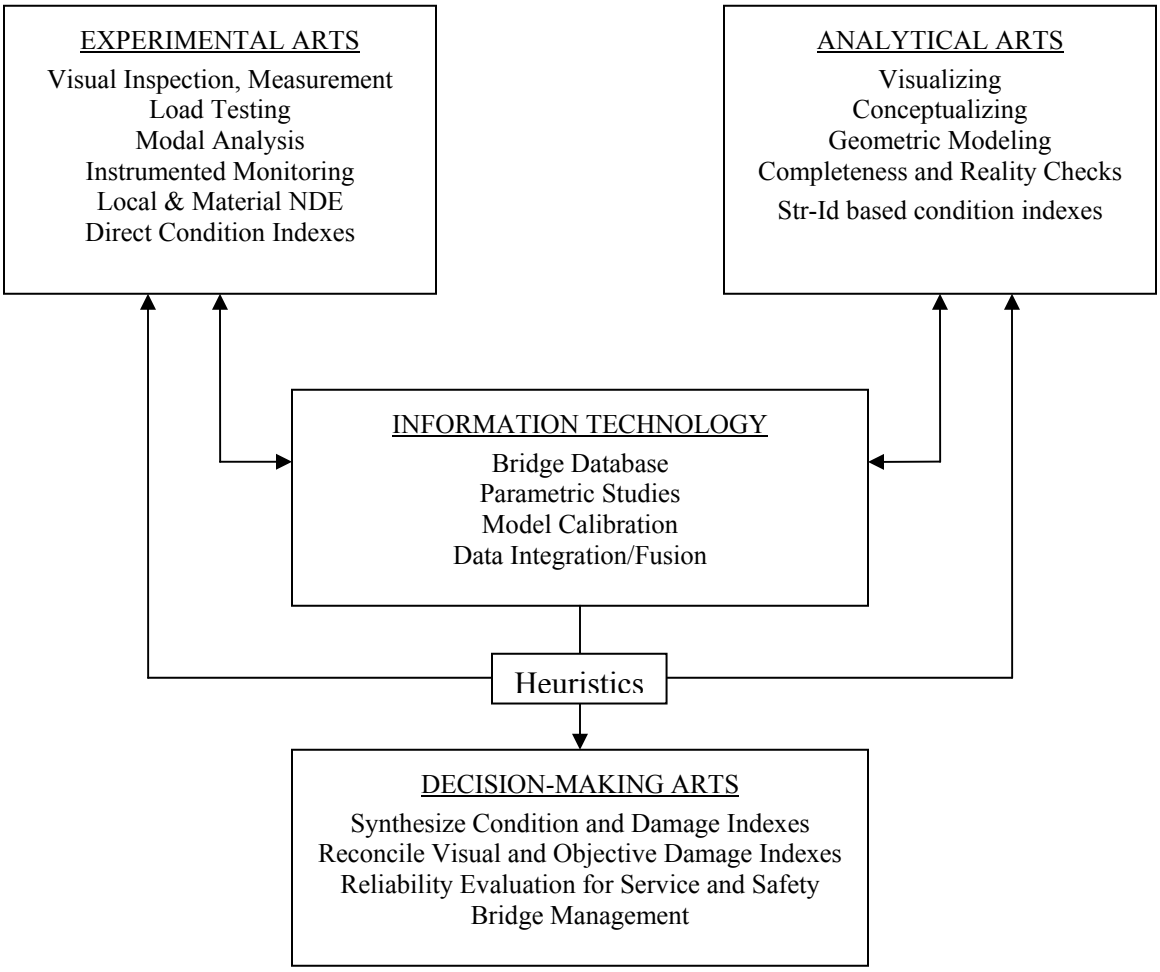

Figure 6.1: Schematic of structural health monitoring system by Aktan, et al. [27]

Aktan, et al., similar to the majority of researchers, describe an approach to structural health monitoring using the vibration properties of a structure in conjunction with a finite element model for system identification and evaluation of damage. Farrar, et al., provide a broader description of a structural health monitoring technique with a classification system for each aspect of the monitoring strategy [29]. They describe the structural health monitoring strategy in four divisions: (1) operational evaluation, (2) data acquisition and cleansing, (3) feature selection, and (4) statistical model development. Depending on the structural system, its constraints, and desired level of sophistication, the selection of methodologies and experimental procedures may vary in a structural health monitoring system.

The operational evaluation and data acquisition sections of the program require an understanding of the structure and its anticipated dynamic behavior. Specifically, a definition for damage to the system and understanding of the operational and environmental conditions limiting the data acquisition system are necessary. The operational evaluation customizes the structural health monitoring strategy to accommodate and/or take advantage of any unique characteristics exhibited by the structure. The operational evaluation begins to set limitations on what is monitored and how the monitoring is to take place.

During the data acquisition and cleansing, details and procedures for experimental investigation are planned and performed. Here, consideration is made in regards to the type of sensors, location of sensors, number of sensors, and defining the data acquisition/storage/transmittal hardware [29]. Included in the data acquisition process is the normalization of data in the presence of variability during the operation and environment in order to facilitate the comparison of measured data. Data cleansing is the process of selectively choosing data to accept or reject for the feature selection process.

The feature selection process is the determination and identification of data features, which distinguish between damaged and undamaged structures [28]. Farrar, et al., state that condensation of data is a necessity for structures where long term monitoring is desired with comparisons to several data sets. Selecting a feature of the structure for damage detection is typically application-specific and may involve more than one feature, in which case a feature vector is developed to evaluate the structure. Ideally feature vectors are of low order and can be placed in a variety of combinations. For example, a feature vector may contain the first three resonant frequencies of the system, time of measurement, and a temperature reading of the system [28]. Past experience with damaged structures and/or numerical simulation of a damaged system's response is often the basis for feature selection. Some common features used in vibration based damage detection are basic modal parameters (natural frequencies and mode shape vectors), mode-shape curvature changes, dynamically measured flexibility, and updating of structural model parameters (mass, stiffness, damping).

Development of a statistical model is the final component of Farrar's monitoring paradigm, which is used to enhance the damage detection process. A statistical model provides information on whether changes in the features for damage detection are statistically significant [28]. Algorithms for statistical models fall into three categories:

(1) Group classification, placing features into 'undamaged' or 'damaged' categories;

(2) Analysis of outliers to determine if a significant change from previously observed features occurs; and

(3) Regression analysis, which is the process of correlating data features with particular types, locations, or extents of damage [28].

Figure 6.2 provides a summary and overview of the overall structural health monitoring strategy by Farrar, et al. [28].

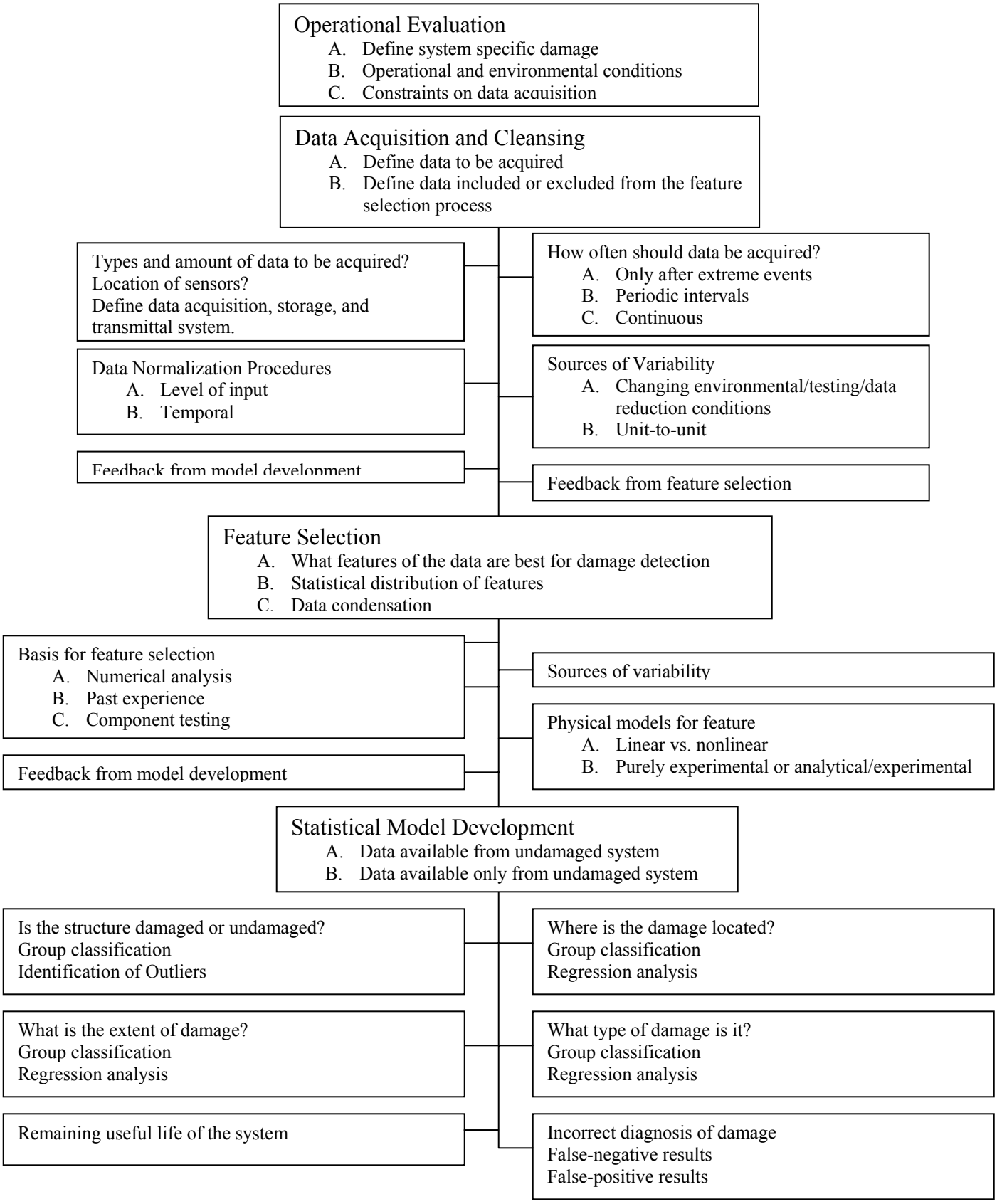

Figure 6.2: Structural health monitoring paradigm by Farrar, et al. [28]

In the two paradigms presented by Farrar, et al. and Aktan, et al., the primary objective of the structural health monitoring process is to acquire sufficient information such that a decision regarding the most effective measure for the structure is determined, i.e., no action, repair, or replacement [28, 27]. The validity of an NDE methodology is predicated on the ability to identify local areas of damage and translate the information to the global performance of the structure. The global performance of the structure can be defined as the residual strength of the structure, the remaining useful life in terms of time, or the probability of failure of the system. Aktan, et al. suggests evaluation of the bridge reliability through the use of condition indicators or damage indices, whereas Farrar, et al. recommends utilizing the damage indicators or features as part of statistical models to identify, locate, quantify and determine the remaining useful life of the structure [27, 29].

Evaluation of the remaining useful life requires an integrated disciplinary approach in order to understand rates of deterioration of structural components and incorporating this information for a prediction of the performance level of the structure with respect to time. Although the potential exists for a prediction of a structure's remaining useful life, the prediction is without merit unless there is sufficient capability to evaluate the structure in real time and provide a validation of the analytical findings. In the Figure 6.3 a simplified schematic, incorporating the experimental evaluation and sequence typical of a vibration based damage detection approach, is provided.

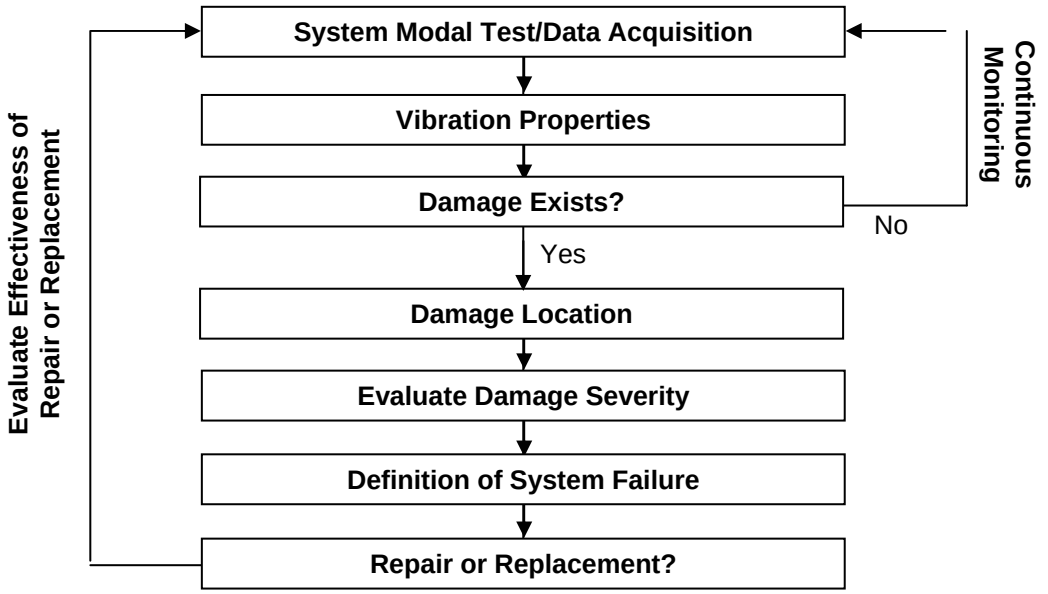

Figure 6.3: Schematic of vibration-based damage detection

The following sections emphasize damage detection algorithms specifically employing vibration properties of the structures such as accelerations, velocities, displacements, frequency response functions, etc. or derived modal parameters such as frequencies or mode shapes to characterize

changes in the structural system due to damage. Vibration properties are attractive for evaluation of large civil structures because of the potential for characterizing localized damaged regions from a single dynamic test of the structure. In accordance with the frameworks previously described for structural health monitoring, this chapter examines current literature in the area of damage detection or what is referred to by Aktan, et al. as condition indicators, or by Farrar, et al. as the feature component of the structural health monitoring paradigm [27, 28]. The categorization of damage detection algorithms is provided in Section 6.1.3, followed by an overview of the chapter in Section 6.1.4.

6.1.3 Vibration based nondestructive damage detection

For civil structures, a global NDE technique utilizing the vibration characteristics of a structure proves to be the most effective method because of the size and the impractical nature of using localized nondestructive testing (NDT) methods such as ultrasonics and acoustic emission [26]. Ideally, a localized NDE technique is utilized upon identification of a damage location, so as to determine the specific nature of the damage. The global nondestructive examination technique utilizing vibration properties involves the following features:

(1) Modal testing for the acquisition of modal parameters (i.e., natural frequencies, mode shapes, and damping properties) or other features (i.e., time histories, FRF's, etc.);

(2) A damage detection algorithm to identify damage in the structure, it's location, and severity;

(3) Prediction of system's remaining useful life; and

(4) Decision rules for evaluating the need for repair and/or replacement.

Of particular importance is the damage detection procedure, since the accuracy of the algorithm and its effectiveness establishes the quality of the nondestructive evaluation technique.

The damage detection procedure selected to assess damage on a structural system is vital to the quality of a structural health monitoring system. Any nondestructive damage detection technique can be classified according to the following four categories [32]:

Level 1: Identify that damage has occurred.

Level 2: Identify that damage has occurred and determine the location of damage.

Level 3: Identify that damage has occurred, locate the damage, and estimate its severity.

Level 4: Identify that damage has occurred, locate the damage, estimate its severity, and evaluate the impact of damage on the structure or estimate the remaining useful life of the structure.

With the classification of nondestructive damage detection methods, several challenges exist for the development of a comprehensive solution to damage detection. The general idea of a

damage detection algorithm is to utilize the response characteristics of a structure and evaluate the state of the structure; however, damage is typically a local occurrence, which requires higher frequency modes to detect its presence [33]. From a testing perspective, the lower frequency modes of a civil structure, which are less sensitive to the local changes, are readily available and easier to access [33]. It is difficult to evaluate the reliability of a small portion of a large civil structure, thereby reducing the vibration-based damage detection problem to some form of pattern recognition problem [28,33]. In addition, the presence of signal noise and incomplete measurements from real applications often result in inaccuracies and poor resolution in the damage detection techniques.

Although not specifically addressed in this report, another issue of significance is the unavailability of baseline parameters of a majority of existing structures; (i.e., information regarding the initial condition or undamaged state of a structure is not accessible for comparison of pre- and post-damaged states) [34]. The absence of an initial measurement becomes significant for existing deteriorating structures, since most damage detection methodologies are dependent on a comparison between the undamaged state and the current state of the structure to evaluate changes to a parameter of a structure, e.g., a change in stiffness.

As a resolution to this problem, Stubbs and Kim provide a system identification approach to determine baseline modal parameters from as-built plans and field inspections of structures in conjunction with existing system identification approaches [35], more detail is provided in Section 6.3.2. Often researchers rely on an experimentally updated finite element model to simulate the undamaged state of a structure.

Those damage detection methods displaying the ability to perform according to their intended level of inspection in the presence of the previously mentioned constraints are considered robust and effective. For summary purposes, the often identified constraints impeding the damage detection procedure are listed below and arranged with respect to the stage of the structural health monitoring process as described in Section 6.1.2:

Table 6.1: Constraints in structural damage detection

Occurrence	Constraints
Experimental Evaluation / Vibration Testing	• Incomplete measurements • Presence of signal noise
Analysis / Modeling	• Modeling errors
Decision Making	• Complex structures • Structures without baseline measurements

6.1.4 Chapter overview

In the following chapter a literature review of damage detection procedures is provided, examining methodologies applicable for global nondestructive damage evaluation of structures

with an emphasis on those methods utilizing vibration characteristics or measurements of a structure to detect, locate, and estimate the severity of damage in the structure. Included in this chapter is a strategy for structural health monitoring of fiber reinforced polymer (FRP) rehabilitated structures, detailing the role of a global nondestructive damage detection methodology. Methods are categorized according to their selected feature for damage detection (i.e., frequencies, mode shapes, FRF's, etc.) or the procedures to characterize damage within the structure (i.e., optimization methods, genetic algorithms, artificial neural networks, etc.).

Past literature reviews include Doebling, et al. who conducted an extensive literature review with brief summaries of damage detection techniques using changes in measured structural vibration response and the applications of these techniques to various types of engineering structures [36]. Salawu specifically examines techniques using natural frequency as a parameter in structural assessment, including limitations of using natural frequencies such as the influence of temperature, humidity and condition of the structure, e.g., temperature of the bridge deck soffit [37].

Vibration based damage detection is a broad field with both global and local methodologies for application to structures in aerospace, mechanical, and civil engineering [33]. Critical issues contributing to the success of a damage detection methodology arise in the steps in acquiring the modal parameters of a structure (such as excitation and measurement considerations), the type and location of the sensors, and signal processing [33]. Issues related to the acquisition of vibration properties are not addressed specifically in this review; but rather, the emphasis of this study is placed on current damage detection algorithms utilizing the quantities measured during vibration testing. Reviews addressing dynamic testing of structures for acquisition of vibration properties are available in Chapter 5 of this report and in the references at the end of Chapter 6 [38, 4, 20, 41, 8, 43].

A recurring theme in the literature addressing damage detection algorithms is the ability of the methodology to perform in the presence of measurement noise and incomplete measurements, i.e., in the presence of signal noise or when only the first three modes of vibration of a structure are available. This report includes no comparison of damage detection methods utilizing a standard set of experimental data; however, since signal noise and incomplete measurements are common occurrences in field-measured properties or during the data acquisition process, a methodology validated using field-measured data is considered robust.

The amount of literature detailing a new methodology for damage detection using vibration properties has increased significantly since the early 1990's. Evidence of such growth is observed in conference proceedings of the International Modal Analysis Conference, the proceedings of SPIE-The International Society for Optical Engineering, and the International Workshop on Structural Health Monitoring. This review of damage detection methods provides an explanation on a selected feature for damage detection, followed by a summary of current damage detection techniques characteristic of that feature. The following chapter is divided into categories according to methodology, such as stiffness matrix optimization or genetic algorithms to evaluate the vibration response of a structure or according to a specific modal parameter, such as measured resonant frequencies or mode shapes. Independent of the feature selected for analysis, the damage detection methodologies identified in this chapter utilize a measured vibration response of the structure, be it a modal parameter, time history, frequency response

function, etc. Table 6.2 provides a summary of features applied for damage detection algorithms utilizing vibration properties examined in this chapter.

Table 6.2: Summary of damage detection categories and methods

Category		Methodology
Modal Parameters	Natural Frequencies	• Frequency changes • Residual force optimization
	Mode Shapes	• Mode shape changes • Modal strain energy • Mode shape derivatives
Matrix Methods	Stiffness-based	• Optimization techniques • Model updating
	Flexibility-based	• Dynamically measured flexibility
Machine Learning	Genetic Algorithm	• Stiffness parameter optimization • Minimization of the objective function
	Artificial Neural Network	• Back propagation network training • Time delay neural network • Neural network systems identification with neural network damage detection
Other Techniques		• Time history analysis • Evaluation of FRFs

Section 6.7 presents an outline of the integration of a global nondestructive damage detection methodology into a strategy for health monitoring of FRP rehabilitated structures. As part of the evaluation and comparison, the damage detection methods reviewed in this chapter are classified according to feature and listed with positive and negative aspects associated with health monitoring of structures and FRP rehabilitated structures.

6.2 FREQUENCY BASED METHODS

The most common and earliest approaches for damage detection use resonant frequencies of the structure to evaluate the existence of damage. Frequency based methods are developed on the premise that resonant frequency shifts occur as the structure experiences some change in its structural properties. Most damage detection methods assume that changes in the frequencies of the structure are due to damage and independent of environmental conditions. In general, changes in frequencies are unable to provide spatial information regarding damage in a structure [44]; thus damage detection methods relying solely on changes in frequency are typically Level 1 methods.

Frequency information alone does not provide reliable results, especially because several combinations of damage in the structure can produce the same changes in the natural frequencies. The magnitude of damage is indicated only in a qualitative sense [56]. Resonant frequencies depend on the global properties of a system and are often used in conjunction with frequency domain identification procedures to improve the level of damage detection, i.e., find the location and magnitude of stiffness degradation [56].

For applications to large civil engineering structures the low sensitivity of frequency shifts to damage requires either very precise measurements of frequency change or large levels of damage. An exception occurs at higher modal frequencies where the modes are associated with local responses. However, the practical limitations involved with the excitation and identification of the resonant frequencies associated with these local modes, caused in part by high modal density and low participation factors, can make them difficult to identify.

In the following section, several damage detection methods utilizing resonant frequencies are reviewed with an emphasis on those methods applying additional techniques to improve the level of damage detection in the structure.

6.2.1 Changes in frequency

Bicanic and Chen present a method for damage identification using only a limited number of natural frequencies to identify, locate, and determine the extent of damage in the structure [45]. The major premise is that any local or distributed changes in stiffness result in changes in the modal parameters. The development of the damage identification procedure involves a characteristic equation for the relative stiffness change in a structure. Although, the formulation requires that only natural frequencies be measured from pre- and post-damage states of the structure, baseline mode shapes are required to determine spatial information regarding damage. Once natural frequency measurements of the post-damage state of the structure is acquired, the change in mode shape vector is expressed as the linear combination of the original eigenvectors and frequencies, allowing for computation of the damaged mode shape vector.

$$\Delta\boldsymbol{\varphi}_i = \sum_{k=1,k\neq i}^{N} \frac{\boldsymbol{\varphi}_k^T \Delta\mathbf{K}\boldsymbol{\varphi}_i + \boldsymbol{\varphi}_k^T \Delta\mathbf{K}\Delta\boldsymbol{\varphi}_i}{\lambda_i^* - \lambda_k}\boldsymbol{\varphi}_k = \sum_{k=1,k\neq i}^{NC} C_{ik}\boldsymbol{\varphi}_k \qquad \textbf{(6-1)}$$

$$C_{ik} = \frac{\boldsymbol{\varphi}_k^T \Delta\mathbf{K}\boldsymbol{\varphi}_i + \boldsymbol{\varphi}_k^T \Delta\mathbf{K}\Delta\boldsymbol{\varphi}_i}{\lambda_i^* - \lambda_k} \qquad \textbf{(6-2)}$$

where quantities denoted with superscript * refer to their respective terms for the damaged structure; C_{ik}, is the mode participation factor; N, is converted to NC to denote the number of original mode shapes available; $\mathbf{K}$ is the global system stiffness matrix; $\Delta\mathbf{K}$ is the change in the global system stiffness matrix; $\Delta\boldsymbol{\varphi} = \boldsymbol{\varphi}_i^* - \boldsymbol{\varphi}_i$, is the change in mode shape; and λ_i and $\boldsymbol{\varphi}_i$ are respectively the i^{th} eigenvalue and the corresponding mode shape for the original structure. The above expression provides an evaluation of the change in mode shapes with only post-damage natural frequencies required.

Evaluation of the mode participation factor is the critical component of this damage detection algorithm, since the change in mode shapes correspond to changes in stiffness, which determines the damage state of the system. The following generalized equation is presented relating modal participation factors and scalar damage indicators. In order to solve for scalar damage parameters, α_j, and mode participation factors, C_{ik}, numerical methods are employed [45].

$$\sum_{j=1}^{NE} a_{kji}\alpha_j + \sum_{j=1}^{NE}\sum_{l=1,l\neq i}^{NC} a_{kjl}C_{il}\alpha_j - \left(\lambda_i^* - \lambda_k\right)C_{ik} = 0 \qquad \textbf{(6-3)}$$

where α_j, is the scalar damage indicator for the j^{th} element; *NE* is the number of elements in the structure; and a_{kji} is the eigenmode-stiffness sensitivity coefficients, which are defined in general form as, $a_{kji} = \boldsymbol{\varphi}_k^T \mathbf{K}_j \boldsymbol{\varphi}_i$.

The damage identification procedure using natural frequencies presented by Bicanic and Chen is a methodology, which if valid in field applications or real structures, would prove significantly advantageous since spatial information and severity of damage is determined with the knowledge of post-damage frequencies alone, assuming the pre-damage natural frequencies of the structure and mode shapes are known. However, Bicanic and Chen show that in the presence of signal noise, the methodology performs poorly for numerical examples with noise levels of 0.5% to 2.0%, showing results overestimating or underestimating damage severity, as well as resulting in false positive indications of damage.

Contursi, Williams, and Messina present a structural damage detection methodology based on changes in the natural frequencies of the structure, on the premise that natural frequencies are least contaminated by measurement noise and provide good accuracy during measurement [47]. The approach is based on the MDLAC developed by Messina, et al. [46, 47, 48, 49]. A statistical evaluation program for damage location at a single site is developed then extended for multiple sites. The location of damage at a single site is determine by the damage localization assurance criteria (DLAC).

$$DLAC(j) = \frac{\left|\left\{\Delta\mathbf{f}\right\}^T \cdot \left\{\delta\mathbf{f}_j\right\}\right|^2}{\left(\left\{\Delta\mathbf{f}\right\}^T \cdot \left\{\Delta\mathbf{f}\right\}\right)\cdot\left(\left\{\delta\mathbf{f}\right\}^T \cdot \left\{\delta\mathbf{f}\right\}\right)} \qquad \textbf{(6-4)}$$

where $\left\{\Delta\mathbf{f}\right\}$ is the measured frequency change vector for a structure having a single defect of unknown size or location; and $\left\{\delta\mathbf{f}_j\right\}$ is the theoretical frequency change vector for damage of a known size at location *j*.

The formulation requires that damage of a specific size at a specific location results in frequency changes which are unique to the damage scenario. Thus, when the DLAC approaches or equals a value of 1, a match between the patterns of frequency changes exist and damage in the structure is indicated by the theoretical model. A DLAC value equal to 0 implies no correlation exists between frequencies. The highest DLAC value corresponds to the predicted damage site. The

DLAC criterion is a statistical measure to discriminate between patterns for potential damage sites.

Determination of the theoretical frequency change vector, $\{\delta \mathbf{f}_j\}$, requires that variations of the theoretical frequency for each damage size and location combination be evaluated for the given structure. Possible combinations of damage size and location are enormous for most civil structures and subsequently involve extensive calculations to evaluate the damage type and location at a single location. Furthermore the DLAC becomes a reliable statistical measure when 10 to 15 modes of the structure are available [49]. Acquisition of 10 modes for large civil structures in the field is typically unfeasible; thus the damage detection methodology is susceptible to the limited number of distinct vibration modes available in large, complex structures.

Messina, et al. modify the formulation of the DLAC criterion to detect damage at multiple locations by calculating the sensitivity of the frequencies according to the following equation:

$$\frac{\partial f_k}{\partial D_j} = \frac{1}{8 \cdot \pi^2 \cdot f_k^0} \cdot \frac{\{\boldsymbol{\varphi}_k^0\}^T \left[\mathbf{K}_j^0\right] \{\boldsymbol{\varphi}_k^0\}}{\{\boldsymbol{\varphi}_k^0\}^T \left[\mathbf{M}^0\right] \{\boldsymbol{\varphi}_k^0\}} \qquad \textbf{(6-5)}$$

where $\{\boldsymbol{\varphi}_k^0\}$ represents the kth mode shape vector; $\left[\mathbf{K}_j^0\right]$ is the stiffness matrix of the j^{th} element within the global stiffness matrix; and $\left[\mathbf{M}^0\right]$ is the global mass matrix. The superscript zero indicates quantities for the undamaged state of the structure.

For identification of multiple damage locations, evaluating mode shapes from an analytical model is necessary, since spatial information of the damage is required. A stiffness reduction factor, D_j, is incorporated into the formulation such that when D_j equals 1 no damage exists in the element and when D_j equals 0 the element is completely lost. In addition, the multiple location damage detection procedure requires an analytical model of the structure. The MDLAC by Messina, et al. is provided below, assuming that corresponding reductions in natural frequencies can be written as a linear combination of the sensitivities.

$$MDLAC(\{\delta \mathbf{D}\}) = \frac{\left|\{\Delta \mathbf{f}\}^T - \{\delta \mathbf{f}(\{\delta \mathbf{D}\})\}\right|^2}{\left(\{\Delta \mathbf{f}\}^T \cdot \{\Delta \mathbf{f}\}\right) \cdot \left(\{\delta \mathbf{f}(\{\delta \mathbf{D}\})\}^T \cdot \{\delta \mathbf{f}(\{\delta \mathbf{D}\})\}\right)} \qquad \textbf{(6-6)}$$

where $\{\delta \mathbf{D}\}$ is a vector of changes in the stiffness reduction factor describing the combination of size and location of damage at one or more sites; and $\{\delta \mathbf{f}\}$ is the vector containing the analytical predictions of frequency changes.

Similar to the single location damage detection criterion, the MDLAC is obtained by searching for the vector $\{\delta \mathbf{D}\}$ maximizing the MDLAC value. Since the size of $\Delta \mathbf{f}$ is dependent on the

number of modes and $\{\delta\mathbf{D}\}$ is dependent on the number of possible damage sites, the analysis becomes computationally expensive, since all elements in the model are potential damage sites with varying damage sizes.

The use of the MDLAC assumes that damage in an element corresponds with a homogeneous reduction of stiffness and assumes that the occurrence of damage does not change the mass of the structure. The basic underlying concept in the MDLAC is that damage at a particular location causes changes in natural frequencies larger than undamaged locations and these changes are detectable via a pattern recognition principle.

In order to alleviate some of the extensive computational aspects of the MDLAC, Messina, et al. suggest limiting the search for damage to probable locations, implying that possible damage locations need to be known beforehand, further reducing the confidence in the level of damage detection capability and localization, essentially discounting any benefits provided by the frequency based technique. As previously mentioned, the methodology assumes that 10 to 15 distinct vibration modes are attainable from the vibration testing of the structure.

Numerical applications to a 2-d, 6 bay truss structure and 3-d steel frame offshore oil platform showed that the methodology is able to locate damage successfully although severity estimates are unreliable. Laboratory validation was conducted on an aluminum rod test structure with a non-updated model of the finite element structure to simulate a real routine monitoring with minimum effort. Damage was simulated by reducing cross sections of the members; however, for a small structure it is observed that the assumption of constant mass is no longer applicable and adversely affects the MDLAC. The method was observed to adequately locate damage from the laboratory experiment.

Hassiotis formulates an optimization algorithm on the basis that damage results in localized changes in the stiffness matrix [56]. In order to find the magnitude of the damage, measurements of the natural frequency are used to determine a set of equations to resolve the stiffness matrix of the structure. The classical eigenvalue problem in structural dynamics, shown below, is used to find the eigenvalue sensitivities to the stiffness matrix, **K**.

$$\left(\mathbf{K} - \lambda_i \mathbf{M}\right)\phi_i = \mathbf{0} \qquad \textbf{(6-7)}$$

where **K** is the global stiffness matrix; λ_i is the eigenvalue equal to the square of the natural frequency, ω_i; **M** is the diagonal mass matrix of the structure; and ϕ_i is the eigenvector or corresponding mode shape.

Application of the eigenvalue problem to evaluate the stiffness properties typically results in an underdetermined set of equations, which is optimized using a set of optimality criterion. The damage detection algorithm presented by Hassiotis is extended from an earlier work with Jeong by employing an optimization criterion based on the impulse response measurements as provided by the Markov parameters [57]. Markov parameters of a continuous system are the impulse response sequence of the system and obtained from the measured impulse-response of a continuous structure or from the pulse response of a discrete system.

The optimization problem is formulated as the following minimization problem for the residuals of the eigenvalue problem:

$$\begin{aligned} &\text{minimize} \quad \tfrac{1}{2}\delta\mathbf{k}^T\mathbf{Q}\delta\mathbf{k} + \delta\mathbf{k}^T\mathbf{c} \\ &\text{subject to} \quad \mathbf{D}\delta\mathbf{k} = \delta\lambda \quad \text{and} \quad \delta\mathbf{k} \le 0 \end{aligned} \tag{6-8}$$

where $\delta\mathbf{k}$ is a vector of element stiffness changes; $\mathbf{c}$ is a vector in linear terms of quadratic optimization; $\delta\lambda$ is a vector of changes in eigenvalue; and $\mathbf{D}$ is a matrix relating changes in stiffness to changes in eigenvalues.

Hassiotis introduces Markov parameters for determination of light to severe damage in any number of members in the structure, whereas the previous formulation in Jeong assumes the structure has not changed significantly due to damage.

$\mathbf{Q}$ is a weighting matrix in quadratic optimization, defined as:

$$\mathbf{Q}(p,k) = \sum_{i=1}^{s}\sum_{j=1}^{l}\mathbf{T}_k(i,j)\mathbf{T}_p(i,j) \tag{6-9}$$

for the optimization problem with the matrix $\mathbf{T}$ defining the Markov parameter as a relationship between the measurement locations and force input locations with the elements of the stiffness matrix.

The algorithm is applied to locate damage in a 10-story two-bay steel frame, via a numerical simulation with damage induced by decreasing stiffness in elements. The Markov parameters and frequency values serve as the input data of the identification algorithm. Successful identification of damage in multiple locations is observed using 12 measured natural frequencies. However, severity estimations are unreliable. The methodology is highly dependent on the number of sensors and locations; i.e., a large number of data must be available in order to detect a large number of damage locations, leaving the methodology susceptible to reduced measurements from the field. In addition, the problem of noise in measurements was investigated with erroneous identification of location and magnitude for noise having a coefficient of variation above 0.8%.

Ray and Tian propose a method for enhancing modal sensitivity to damage using feed back control to address the unattractive features of frequency measurements for damage detection, specifically because a significant amount of damage is required before a shift in modal frequencies becomes detectable [50, 51, 52]. The primary focus of the methodology by Ray and Tian is to accentuate the sensitivity of frequency shifts to damage occurring in the structure, such that modal frequencies become a viable measure for damage detection, particularly for smart structures, i.e., those capable of self-excitation, self-sensing, and closed-loop vibration control. The method reverses the control problem; instead of using a control law to make the system insensitive to changes in the system parameters; the sensitivity is magnified in a predictable manner by feedback control.

As an illustration of the methodology, consider the sensitivity of natural frequency, $\omega_n = \sqrt{\frac{k}{m}}$ for a single degree of freedom system to small changes in stiffness, *k* and mass, *m*:

$$\frac{\partial \omega_n}{\partial k} = \frac{\omega_n}{2k}, \quad \frac{\partial \omega_n}{\partial m} = -\frac{\omega_n}{2m} \tag{6-10}$$

where ∂ denotes a change in the respective parameter. By applying feedback control, the closed-loop natural frequency is dependent on the control gain, *K*, resulting in a closed loop frequency, $\omega_{n_{cl}} = \sqrt{\frac{k+K}{m}}$. Thus the sensitivities are functions of the control gain, *K*:

$$\frac{\partial \omega_{n_{cl}}}{\partial k} = \frac{\omega_n}{2(k+K)}, \quad \frac{\partial \omega_{n_{cl}}}{\partial m} = -\frac{\omega_{n_{cl}}}{2m} \tag{6-11}$$

The above sensitivity expression shows that a negative or decrease in gain, -*K*, enhances sensitivity to changes in stiffness, while a positive or increase in gain, +*K* enhances sensitivity to changes in mass. The methodology is applied to a numerical simulation of a cantilevered beam with sensitivity of modal frequencies to damage increased by a factor of 60 for the first mode and a factor 5 for the third mode, as compared to the unmodified sensitivity analysis showing a maximum frequency shift of 5% for severe damage and never exceeding 0.5% for modest damage. The method is able to detect damage; however, sensitivity to damage is dependent on the location of the actuator and sensor and the mode of vibration collected.

6.3 METHODS UTILIZING MODE SHAPES

Analyzing changes in mode shapes is another category that has received a tremendous amount of attention for purposes of damage detection. Mode shapes provide an advantage over a feature such as frequency since they are spatially defined quantities. Thus identification of damage using mode shapes implies that the locations of damage are realized. However, mode shapes are difficult to measure and a large number of measurement locations may be required to accurately characterize mode shape vectors and to provide sufficient resolution for determining the damage location [44].

Theoretically, the comparisons of mode shapes (i.e., undamaged and damaged) possess spatial information, which is useful in identifying the existence and location of damage in a structure. Predominant methods employing mode shapes compare measured mode shapes directly, or they measure the properties of mode shapes such as curvature or modal strain energy to enhance sensitivity to damage detection and localization.

6.3.1 Mode shape changes

Salawu presents a method for damage detection utilizing natural frequencies to determine the existence of damage and qualitatively determine the severity of damage globally, and then employs mode shapes for identification and localization of damage [62]. The global assessment

component of Salawu's integrity index method is identified as the global integrity index, denoted GI, which is a function of natural frequency alone. Salawu assumes that mass remains constant in the formulation and changes are attributed to a reduction or increase in the global structural stiffness. The expression for the global index is:

$$GI = f(\omega) = \sum \left[a_r \left(\omega_{Dr} / \omega_{Or} \right) \right] \qquad \textbf{(6-12)}$$

where *GI* is the global integrity index as a function of frequency; *r* is the mode number; a_r is the weighting factor for mode, *r* ; and the subscripts *D* and *O* refer to the damaged and undamaged structures respectively.

Salawu recommends using a minimum of three mode shapes for the methodology. Weighting factors a_r are structure dependent with the following effective participation factors assigned for large civil engineering structures: mode 1 – 70%; mode 2 – 20%; other modes – 10%.

If the number of available modes exceeds three, the modes most sensitive to damage are selected on the basis of the modal sensitivity value (MSV) function in the following equation:

$$MSV\left(\{\phi_A\}_r, \{\phi_B\}_r\right) = \frac{\dfrac{\left\{\sum\left(\phi_{Bir}\right)^2\right\}^{0.5}}{\lambda_{Br}} - \dfrac{\left\{\sum\left(\phi_{Air}\right)^2\right\}^{0.5}}{\lambda_{Ar}}}{\dfrac{\left\{\sum\left(\phi_{Air}\right)^2\right\}^{0.5}}{\lambda_{Ar}}} \qquad \textbf{(6-13)}$$

where the summation is from 1 to *n* (number of measurement points); (ϕ_{Air}) is the element of the r[th] mode shape vector at measurement point *i* for data set *A;* and λ_{Ar} is the eigenvalue (natural frequency squared) of mode *r* for data set *A*. Subscripts *A* and *B* refer to the undamaged and damaged structures, respectively.

The MSV for all modes (for a particular damage case) are normalized such that the mode showing least correlation has an MSV value of 100. Salawu states that an MSV value close to 100 is an indicator of damage; however, the effect of measurement noise and modeling errors are not considered.

Following a global evaluation of the structure based on frequencies, Salawu develops the local integrity indices (LI) in order to detect localized defects and locate damage areas. The LI index operates as a function of frequency and mode shapes as damage locators at measurement point, *i*. Ratios of the squares of the modal amplitudes are used to compute LI_i while the absolute difference of LI_i from unity is used to infer the damage site.

$$LI_i = \sum \left[a_r \left(\frac{\omega_{Dr}}{\omega_{Or}} \right) \left(\frac{\left(\phi_{Dir}\right)^2}{\left(\phi_{Oir}\right)^2} \right) \right] \qquad \textbf{(6-14)}$$

where (ϕ_{Dir}) and (ϕ_{Oir}) are elements of the r^{th} mode shape vector at measurement point *i* for the damage and undamaged structures, respectively.

The existence of damage in a structure results in $|LI_i - 1| > 0$ for all *I*; whereas $|LI_i - 1| = 0$ signifies no change in the structural integrity. However, values of $|LI_i - 1|$ for points most likely to be the damage locations would be much greater than those for other points. Therefore, for identification of single damage locations, values of $|LI_i - 1|$ are normalized such that the point with the largest values has a value of 100. If multiple damage locations are desired, the process is repeated, excluding the previously identified point(s).

Salawu provides applications of the methodology to numerical, laboratory, and field data [63]. The laboratory experiment was conducted on a steel I-beam with progressive levels of damage. Frequency results, as often stated in literature, are not sensitive to damage and large changes in frequency occur only when the damage is large. The LI index is shown to adequately locate damage near the vicinity of sensors during the laboratory experiment. In addition, a reinforced concrete highway bridge was evaluated before and after repairs to the bridge, with decreases in frequencies observed before and after the repair in the range of –1% to –3%, indicating that the improvement to the structure was insignificant. The LI index was used to identify the locations of the repair from the sensors in close proximity. However, no effort is made to determine if the local index is at a significant level other than that the highest values are the most likely damage locations; here a statistical model may prove useful in particular for multiple damage locations.

The author does not discuss the impact of signal noise and reduced measurements; however, a field application is provided displaying the ability to identify and locate a change on a real structure. The integrity index method has not been demonstrated for damage detection on a real structure nor has the issue of baseline modal parameters been addressed.

6.3.2 Mode shape derivatives

Abdo and Hori provide a numerical study of structural damage detection for purposes of determining the feasibility of using changes in rotation of mode shapes of a structure [64]. With the premise that the rotation of mode shapes will become a measurable quantity in the future, Abdo and Hori compare the changes in the displacement mode, the strain mode, and the frequency changes to identify and locate damage. Numerical simulations are conducted for the first four modes of a beam and a steel plate. Indicators for damage in a truss element and beam element are derived with the damage located and detected by discontinuities in the derivatives of the mode shapes. A study is performed on the feasibility of using changes in rotation of mode shapes with the assumption that rotations of modes shapes will be measured directly from the structure and not analytically derived from field measured displacement mode shapes.

It is shown that the curvatures of mode shapes suffer a discontinuity at locations of damage and thus approximating the moment, M as $K\kappa^0(x_d)$, the curvature change in a beam element is evaluated as:

$$[\kappa] \approx \left(\frac{K}{K - \Delta K} - 1 \right) \left| \kappa^0 (x_d) \right| \qquad \textbf{(6-15)}$$

where $[\kappa]$ is the amount of curvature discontinuity; $K = EI$ is the bending stiffness of the beam element; E is Young's modulus; I, is the moment of inertia; ΔK is the change in stiffness; and $\kappa^0(x_d)$ is the curvature for an undamaged beam at location, x_d.

The primary emphasis is to show that the derivative of the mode shape provides an improved indicator for damage compared to the displacement modes. Abdo and Hori show accurate detection and localization of damage in the plate structure using numerical simulations, by observing that localization of the rotation of mode shapes occurs at the damaged region and approximate zero values beyond the damaged location make the methodology effective and accurate. In addition, the lower modes of the structure are shown to be sufficient to detect damage at multiple locations of the plate in the numerical example.

6.3.3 Modal strain energy

Law, et al. propose a method based on modal strain energy to detect damage at the element level with particular attention to incomplete and noisy measured modal data [72, 73, 74]. Three stages are involved with the approach: (1) expansion of modal data to estimate modal parameters at unmeasured degrees of freedom; (2) localization of the damage domain using the elemental energy quotient difference to identify a group of elements forming a possible damage domain, thus reducing the problem size; and (3) damage quantification based on the sensitivity of the modal frequency.

Law, et al. combine the following three components in order to develop the damage detection approach. First, measured modal data is expanded to match the finite element model. Second, the modal strain energy of each element normalized with its potential energy is used to locate the damage domain. Third, the measured modal frequency changes are then employed to determine the magnitude of damage using a sensitivity-based method. Here damage is assumed to affect only the stiffness matrix; i.e., damage in a structure results in the reduction of a design parameter, such as the elastic modulus or sectional area of a member. Damping is ignored in the formulation.

Damage detection and localization of the structure is developed with the assumption that damage to the structure results in small changes in modal frequencies, λ_i, and mode shape vector, Φ_i. The perturbation in the system due to damage is represented in the stiffness matrix as $\mathbf{K}^{\mathrm{d}}$, the i^{th} modal eigenvalue λ_i^d, and the i^{th} mode shape $\mathbf{\Phi}_i^d$ as follows:

$$\begin{aligned} \mathbf{K}^d &= \mathbf{K} + \sum_{j=1}^{L} \Delta \mathbf{K}_j = \mathbf{K} + \sum_{j=1}^{L} \alpha_j \mathbf{K}_j \quad \left(-1 < \alpha_j \le 0\right) \\ \mathbf{\Phi}_i^d &= \mathbf{\Phi}_i + \Delta \mathbf{\Phi}_i; \;\; \lambda_i^d = \lambda_i + \Delta \lambda_i \end{aligned} \qquad \textbf{(6-16)}$$

where α_j is a stiffness reduction factor of the j^{th} element of the stiffness matrix; and L is the total number of elements in the system.

Since the damaged and undamaged systems experience the same energy inputs, the difference in total energy of the two systems, Π_d and Π_u, respectively, is zero:

$$\Pi_d - \Pi_u = 0 \tag{6-17}$$

For damage localization, the energy content within each j^{th} element is assumed unchanged:

$$\Pi = \left(\text{Kinetic Energy}\right)_j + \left(\text{Potential Energy}\right)_j \tag{6-18}$$

The physical interpretation of the above formulation indicates that an increase in elemental modal strain energy results in a reduction in the elemental kinetic energy. Thus the ratio of the modal strain energy to the kinetic energy shows increased sensitivity to damage as compared to elemental modal strain energy alone. Here this ratio is denoted as the modal strain energy coefficient (MSE), and its change between damage and undamaged states is used as an indicator for damage localization, MSECR.

$$MSECR_{ij} = \frac{\left| MSE_{ij}^{d} - MSE_{ij} \right|}{MSE_{ij}} \tag{6-19}$$

where $MSE_{ij} = \Phi_i^T \mathbf{K}_j \Phi_i$ and $MSE_{ij}^{d} = \Phi_i^{d^T} \mathbf{K}_j \Phi_i^{d}$ are the elemental modal strain energy of the undamaged and damaged structures, assuming the stiffness matrix of the undamaged element is an adequate approximation of the damaged elemental stiffness matrix.

Here it may prove advantageous to provide a statistical model so that the user of the technique may be able to determine if the *MSECR* is statistically significant compared to modal strain energy ratios of the other elements. Nonetheless, the authors suggest that high values of the *MSECR* relative to other locations are considered indicative of a damaged location. Furthermore, if more than one measured mode is available, the $MSECR_{ij}$ is calculated for all modes and $MSECR_j$ of the j^{th} element is defined as the average of the summation of all $MSECR_{ij}$ normalized with respect to the maximum of $MSECR_{ij}$ for each mode as:

$$MSECR_j = \frac{1}{m} \sum_{i=1}^{m} \frac{MSECR_{ij}}{MSECR_{i,\max}} \tag{6-20}$$

As a component of the Law, et al. damage detection strategy, a mode shape expansion procedure is presented such that a limited number of measured DOF's are expanded to the full dimension of the finite element model, with the model expansion preserving the connectivity of the structure in the final expanded mode shape.

If a small change in the stiffness of the structure occurs, each perturbed mode shape is assumed as a linear combination of the original mode shapes:

$$\mathbf{\Phi}_d = \begin{bmatrix} \mathbf{\Phi}_{dc} \\ \mathbf{\Phi}_{df} \end{bmatrix} = \mathbf{\Phi}_u \mathbf{Z} \tag{6-21}$$

where $\mathbf{\Phi}_d$ and $\mathbf{\Phi}_u$ are the matrices of damaged and undamaged mode shape vectors, respectively; the subscript *c* denotes master DOFs of the experimental model; the subscript *f* indicates the number of additional DOFs to be expanded to from the measured mode shape; and **Z** is a transformation matrix. The cross orthogonality of the damaged and undamaged mode shapes is expressed as follows:

$$\mathbf{\Phi}_u^T \mathbf{M} \mathbf{\Phi}_d = \mathbf{Z} \qquad \textbf{(6-22)}$$

Therefore, when small local damage occurs, **Z** is approximately the identity matrix. The transformation matrix is obtained using the following expression:

$$\mathbf{Z} = \left(\mathbf{\Phi}_{uc}^T \mathbf{\Phi}_{uc} + \mathbf{WI}\right)^{-1} \left(\mathbf{\Phi}_{uc}^T \mathbf{\Phi}_{dc} + \mathbf{WI}\right) \qquad \textbf{(6-23)}$$

where $\mathbf{\Phi}_{uc}$ is the measured modal matrix of the undamaged structure; $\mathbf{\Phi}_{dc}$ is the measured modal matrix of the damaged structure; and **W** is the weight coefficient.

If a modal analysis model is reliable and accurate, less weight is given to the analytical information by setting the weight **W** less than 1.0. Additional weight is given to the analytical model with values of **W** greater than 1.0.

Substituting the definition of **Z** into the modal mass relationship yields the additional expansion required to complete the damaged mode shape and thus the modal expansion of measured data:

$$\mathbf{\Phi}_{df} = \mathbf{\Phi}_{uf} \mathbf{Z} \qquad \textbf{(6-24)}$$

Damage quantification can be expressed in the following system of equations:

$$\begin{Bmatrix} MSEC_{i1} \\ MSEC_{i2} \\ \cdots \\ MSEC_{iJ} \end{Bmatrix} = \begin{bmatrix} \beta_{11} & \beta_{12} & \cdots & \beta_{1q} \\ \beta_{21} & \beta_{22} & \cdots & \beta_{2q} \\ \cdots & \cdots & \cdots & \cdots \\ \beta_{J1} & \beta_{J2} & \cdots & \beta_{Jq} \end{bmatrix} \begin{Bmatrix} \alpha_1 \\ \alpha_2 \\ \cdots \\ \alpha_q \end{Bmatrix} \quad \beta_{st} = -2 \sum_{r=1}^{n} \Phi_i^T \mathbf{K}_s \frac{\Phi_r^T \mathbf{K}_t \Phi_i}{\lambda_r - \lambda_i} \Phi_r \quad \left(r \neq i\right) \qquad \textbf{(6-25)}$$

where $MSEC_{ij} = \Phi_i^{d^T} \mathbf{K}_j \Phi_i^d - \Phi_i^T \mathbf{K}_j \Phi_i$ is the modal strain energy difference between the damaged and undamaged structure; *q* is the number of identified damage locations; and β_{st} is the element sensitivity coefficient of MSEC to damage. Solving the system of equations with expanded mode shapes provides the severity estimation of damage in the structure.

The modal strain energy method by Shi and Law is applied to a numerical simulation of a fixed-fixed beam. The methodology is able to identify damage locations accurately in the fixed-fixed beam with the MSECR value changing sequentially as a 5% and 7% signal noise is introduced. The magnitudes of damage are identified correctly with the number of analytical mode shapes greatly affecting the severity estimate, requiring 20 analytical modes in the beam application. The influence of noise in the severity estimates results in errors ranging from 0 to 30%. The

methodology is experimentally applied to a two-story steel plane frame structure, with damage simulated by the loosening of semi-rigid joints in two locations. Both locations were identified with the first two mode shapes and mode shape expansion with 15 analytical modes, with unverified severity estimations for the loosened joints.

In the effort by Stubbs, et al. to develop a Level 4 global NDE technique, a damage detection algorithm utilizing changes in modal strain energy is applied in conjunction with an overall methodology to continuously monitor the safety or reliability of civil structures [34, 35]. The prescribed methodology combines a modal-based damage detection algorithm, analyzing the changes in the modal strain energy of the structure before and after the occurrence of damage. It uses a procedure to estimate the system's reliability in order to describe the performance of the structure. The damage detection algorithm alone is sufficient to describe a Level 3 global NDE technique capable of identifying, locating, and estimating severity of the damage. The addition of the reliability analysis provides additional insight into the probability of failure of the structure and potentially into the remaining useful life of the structure. Particular attention is warranted to the Stubbs, et al. damage identification approach, since it is potentially the most developed approach available for damage detection procedures, with a number of publications from outside researchers evaluating the validity and applicability of this approach [65, 66, 67, 68].

The damage detection algorithm as developed and updated by Stubbs, et al. detects changes in the modal strain energy to identify and locate damage where the modal parameters, specifically natural frequencies and mode shapes, are used to identify the modal stiffness properties of the as-built and existing structures [34]. As mentioned previously, one of the difficulties associated with damage localization is that damage is typically a local phenomenon, making it difficult to determine the integrity of a small portion of the structure when only a few modal parameters are available [34]. To overcome this challenge, Stubbs converts the damage localization problem into a statistical pattern recognition problem where physical world data is transformed into the pattern space. Accordingly, the physical world data is depicted as the dynamic response of the structure, and the pattern space represents the modal parameters of the structures. The feature space contains indicators, which are a function of pre- and post-damaged modal parameters of the structure. Damage in this application is defined as a loss of stiffness.

This section provides an account of the theoretical development of the damage index method with examination of the assumptions and limitations from its formulation. Detailed examinations into the different components for the global nondestructive damage detection technique are presented. There are three primary components of the global NDE methodology outlined by Stubbs, et al. [34]:

1. Damage Index Method – identifies and locates damage in the structure, Level 2.

2. Damage Severity – evaluates the existing damage and determines the stiffness capacity available in each element, Level 3.

3. Evaluate Structural System Reliability – application of elemental changes in stiffness to structural reliability concepts to evaluate the probability of system failure.

In developing the damage index method, Stubbs prescribes the formulation with consideration for the following objectives: (1) The damage detection algorithm accurately localizes damage; and (2) The damage detection algorithm uses a minimum number of modal parameters.

With damage defined as a loss of stiffness in the structure, the i^{th} modal stiffness, K_i, for a linear undamaged structure is given by the following:

$$K_i = \Phi_i^T C \Phi_i \qquad \textbf{(6-26)}$$

where Φ_i is the i^{th} modal vector; and C is the system stiffness matrix. The contribution of the j^{th} element of the system stiffness matrix to the i^{th} modal stiffness is given as:

$$K_{ij} = \Phi_i^T C_j \Phi_i \qquad \textbf{(6-27)}$$

Thus, the fraction of the i^{th} mode concentrated in the j^{th} member (which is also called the modal sensitivity for the i^{th} mode in the j^{th} location) is as follows:

$$F_{ij} = \frac{K_{ij}}{K_i} \qquad \textbf{(6-28)}$$

Similarly, the damaged structure (denoted with an asterisk) has the following modal sensitivity definition:

$$F_{ij}^{*} = \frac{K^{*}_{ij}}{K^{*}_{i}} = F_{ij}\left(1 + \sum_{k=1}^{NE} A_{ik}\alpha_k + HOT\right) \qquad \textbf{(6-29)}$$

where $K^{*}_{ij} = \Phi_i^{*T} C_j^{*} \Phi_i^{*}$ and $K^{*}_{i} = \Phi_i^{*T} C^{*} \Phi^{*}_{i}$; A_{ik} is the set of coefficients associated with mode, i at location, k; α_k is the fraction of damage at location k in the structure; and HOT represents higher order terms.

Thus far in the development of the damage index method, no significant assumptions are made outside of the general framework of structural dynamics. By utilizing the modal strain energy, Stubbs defines a measure of sensitivity of one specific location of the structure to the total modal strain energy of the structure for an individual mode shape. This development is considered advantageous, since individual mode shapes of the structure have been identified for use in a damage detection algorithm without the need for resolving all or a large portion of mode shapes from the experimental modal analysis.

The system stiffness matrices are separated into material and geometric components as shown below:

$$C_j = E_j C_{j0} \qquad \textbf{(6-30)}$$

$$C_j^{*} = E_j^{*} C_{j0}^{*} \qquad \textbf{(6-31)}$$

where scalars E_j and E_j^* are parameters representing material properties for the undamaged and damaged j^{th} member of the structure, respectively. The matrix C_{j0} involves geometric quantities and possibly terms containing Poisson's ratio.

The ratio of modal sensitivities given below compares the relative modal stiffness changes of a damaged structure to an undamaged structure for a specific location:

$$\frac{F_{ij}^*}{F_{ij}} = \frac{K_i}{K_{ij}} \cdot \frac{K_{ij}^*}{K_i^*} = \left(\frac{K_{ij}^*}{K_{ij}}\right) \cdot \left(\frac{K_i}{K_i^*}\right) \qquad \textbf{(6-32)}$$

Stubbs and Kim provide the following observations regarding the characteristics of their damage detection algorithm [35]: 1) an equation per elemental location of the structure is available for each mode; 2) as the region of interest for the damage detection decreases in size, the number of equations grows significantly; and 3) a method for determining the linear coefficients A_{ik} and the higher order terms is necessary in order to proceed with the derivation.

On the basis of experimental observation, Stubbs and Kim make the most critical assumption or simplification at this stage of the derivation to avoid evaluating the linear coefficients A_{ik} and higher order terms [35]. The authors recognize that the geometry of an undamaged location is unaffected when damage occurs elsewhere in the structure. In addition, experimental test results indicate that the relative modal deformations are large after indicating the presence of damage (loss in stiffness) [35]. Given these observations, the fractional change in modal strain energy, F_{ij}, in an element is assumed unchanged before and after the occurrence of damage, which is represented by the following relationship, $F_{ij}^* = F_{ij}$.

According to Stubbs and Kim, this approximation is valid for simultaneous structural damage at multiple locations and at a damage level up to 30%, implying the unchanged sensitivity assumption following the occurrence of damage and the algorithm are no longer applicable for damage scenarios where the severity exceeds 30% [35]. Manipulation of the sensitivity relationship results in the following expression:

$$1 = \frac{F_{kj}^*}{F_{kj}} = \frac{K_{ij}^* \big/ K_i^*}{K_{ij} \big/ K_i} \qquad \textbf{(6-33)}$$

Substituting the definitions of the undamaged and damaged stiffness relationships yields the following equation:

$$\beta_{ij} = \frac{E_j}{E_j^*} = \frac{\Phi_i^{*T} C_{jo}^* \Phi^*{}_i}{\Phi_i^T C_{jo} \Phi_{\ i}} \cdot \frac{K_i}{K_i^*} \qquad \textbf{(6-34)}$$

where β_{ij} is the localized damage indicator relating the change in modal strain energy for element j to the i^{th} mode. For a specific quantity of measured mode shapes, N, the damage index, β_j, is written as follows:

$$\beta_j = \frac{E_j}{E_j^*} = \frac{\sum_{i=1}^{N} \Phi_i^{*T} C_{jo}^* \Phi^*{}_i \cdot K_i}{\sum_{i=1}^{N} \Phi_i^T C_{jo} \Phi_{\ i} \cdot K_i^*} \qquad \textbf{(6-35)}$$

The definition of the damage indices β_{ij} and β_j possess quantities on the right hand side, which are either available or can be approximated from experimental measurements and the geometry of the structure, C_{jo}. In addition, if the structure is discretized into a large number of small elements, it is reasonable to assume there is no single component dominating the modal sensitivity, i.e., the modal sensitivity for the damaged and undamaged structures is small:

$$F_{ij} << 1 \ \textbf{and} \ F_{ij}^* << 1 \qquad \textbf{(6-36)}$$

β_j provides a positive and initial indicator for the existence and location of damage when $\beta_j > 1$. However, obvious difficulties in the algorithm occur if the i^{th} member or element is located at or near a node of the i^{th} mode, resulting in a zero in the denominator of the damage index β_j and providing a false-positive reading of damage in the structure. In order to alleviate the problem of a false-positive result, unity is added to both the numerator and denominator. Although there appears to be no rigorous formulation for the addition of unity, successful implementation of the damage index is observed [65, 66, 69].

$$1 = \frac{F_{kj}^* + 1}{F_{kj} + 1} = \frac{\left(K_{ij}^* + K_i^*\right) K_i}{\left(K_{ij} + K_i\right) K_i^*} \qquad \textbf{(6-37)}$$

Substituting the definitions for K_{ij}^* and K_{ij} results in the following indicator of damage for a single mode of the structure:

$$\beta_j = \frac{\left(\Phi_i^{*T} C_{jo}^* \Phi_i^* + \left(1/E_j^*\right) \sum_{k=1}^{NE} \Phi_i^{*T} E_k^* C_{ko} \Phi_i^*\right)}{\left(\Phi_i^T C_{jo} \Phi_i + \left(1/E_j\right) \sum_{k=1}^{NE} \Phi_i^T E_k C_{ko} \Phi_i\right)} \cdot \frac{K_i}{K_i^*} \qquad \textbf{(6-38)}$$

$$\beta_j \approx \frac{\left(\Phi_i^{*T} C_{jo}^* \Phi_i^* + \sum_{k=1}^{NE} \Phi_i^{*T} E_k^* C_{ko} \Phi_i^*\right)}{\left(\Phi_i^T C_{jo} \Phi_i + \sum_{k=1}^{NE} \Phi_i^T E_k C_{ko} \Phi_i\right)} \cdot \frac{K_i}{K_i^*} \qquad \textbf{(6-39)}$$

The conventional form of the damage index method when several modes are know is provided below:

$$\beta_j = \frac{\sum_{i=1}^{NM}\left\{\left(\Phi_i^{*T} C_{jo}^{*} \Phi_i^{*} + \sum_{k=1}^{NE} \Phi_i^{*T} E_k^{*} C_{ko} \Phi_i^{*}\right) K_i\right\}}{\sum_{i=1}^{NM}\left\{\left(\Phi_i^{T} C_{jo} \Phi_i + \sum_{k=1}^{NE} \Phi_i^{T} E_k C_{ko} \Phi_i\right) K_i^{*}\right\}} \qquad \textbf{(6-40)}$$

The advantages and convenience presented by the final formulation of the damage index method in the equation above is two fold: (1) Losses in stiffness, or damage, is identified and located as a function of the pre-damaged and post-damaged mode shapes of the structure, Φ_i and Φ_i^*; (2) The remaining terms are available from the geometry of the structure as long as $K_i^* \approx \Phi_i^{*T} C \Phi_i^*$, implying the structure continues to behave linearly after damage occurs.

Although the final formulation of the damage index, β_j, is adequate to indicate and locate damage on the structure, an additional statistical criterion is established using hypothesis testing with damage index, β, considered a random variable, whose mean is zero regardless of the actual distribution of β, and thus creating a normalized damage indicator:

$$Z_j = \frac{\beta_j - \overline{\beta}}{\sigma_\beta} \qquad \textbf{(6-41)}$$

where Z_j is the normalized damage indicator; $\overline{\beta}$ is the mean of the damage indicator, β_j; and σ_β is the standard deviation of the damage indicator, β_j.

For each element of the structure, one of two possibilities exists for the member: 1) the element is damaged; or 2) the element is undamaged. For example, if a 98% confidence level is desired then damage exists at an element when $Z_j \geq 2$. If $Z_j < 2$, then there is no damage to element j.

Damage Severity Estimation. The application of a set of statistical criteria for damage detection is one of the advantages that differentiate the damage index method from other global damage detection strategies. Imbedded in the damage detection algorithm is an estimate for the severity of damage in the structural element or member. A fractional change in stiffness, α_j, of an element, j, is described by the following equation:

$$\alpha_j = \frac{E_j^* - E_j}{E_j} = \frac{\Phi_i^T C_{jo} \Phi_i}{\Phi_i^{*T} C_{jo}^{*} \Phi_i^{*}} \cdot \frac{K_i^*}{K_i} = \frac{1}{\beta_j} - 1 \qquad \textbf{(6-42)}$$

where α_j is the fractional change in stiffness of an element, j.

Some of the limitations and characteristics of the above equation are a function of the assumptions made during the development of the damage index method. In general, the above severity estimation results in an overestimation of the severity of damage in a structure because of the assumption that the structure continues to behave linearly after the occurrence of damage, i.e., $K_i^* \approx \Phi_i^{*T} C \Phi_i^*$ when in actuality $|C| > |C^*|$ [35].

Furthermore, since the damage index method assumes that the fraction of modal strain energy is equivalent before and after damage occurs, a limitation on its ability to accurately locate and identify damage exists at magnitudes greater than 30% [35]. This limitation becomes a point of concern, particularly if damage scenarios exceeding losses in stiffness greater than 30% occur and are not detectable from a visual inspection of the location.

Nonetheless, if damage does not exist in the structure according to the results of the damage index method, then $\alpha_j = 0$. If damage does exist, $\alpha_j < 0$ with α_j approaching –1 as the stiffness capacity is lost [34].

For purposes of understanding and evaluating the impact of damage in a structure, a technique for analyzing the failure probability of a system is employed using structural reliability concepts. Analogous to the damage detection methodology, where the definition of damage is defined as a loss in stiffness, evaluation of system failure requires a definition for failure. Failure of the system is defined here as geometric instability of the structure as a whole, where s is the redundancy of the structure and the structure fails when $s+1$ components fail [70].

Park, et al. identify structures as being classified into three categories: 1) Series Systems, where the failure of any element leads to failure of the system; 2) Parallel Systems, where the combined failure of each and every element of the system results in failure of the system; and 3) Hybrid Systems, for systems not obeying the definitions of a "series" or "parallel" system where failure of "some", "few", or "most" of the elements constitutes failure of the system [70]. Bridge structures are typically classified as hybrid systems, since most real structures are statically indeterminate. A hybrid system is described as a series system of parallel failure modes [34]. For an individual failure mode, a statistical correlation between the demand on the elements of a structure or the capacity of the elements to resist the demand is possible.

Assuming that the safety margins of basic elements are correlated, a random safety margin, g_i, is established in the context of basic reliability theory for a structure having M failure elements [34]:

$$g_i = R_i - \sum_{j=1}^{NL} a_{ij} S_j \qquad \textbf{(6-43)}$$

where R_i is the random resistance of an element, i; S_j is the applied j^{th} load on the structure; A_{ij} is the influence coefficient dependent on the geometry, redundancy and material properties of the structure; and NL is the number of applied loads.

For a given failure mode j, let elements k, l, m, n, and o be the components for the failure mode, such that the probability of failure for mode j is as follows:

$$P_j = P\{[g_k \le 0] \cap [g_l \le 0] \cap [g_m \le 0] \cap [g_n \le 0] \cap [g_o \le 0]\} \qquad \textbf{(6-44)}$$

The material of the structure is the assumed to be the same throughout, thus allowing a correlation between the resistances, R_i. Furthermore, the random safety margins, g_i, are also correlated because of the common existence of loads, S_j. The probability of failure of a mode is

simplified into the following, assuming the safety margins of each and every mode of failure are correlated [34]:

$$P_j \approx Min\{p_k, p_l, p_n, p_o\} \quad \textbf{(6-45)}$$

The above equation is a conservative, upper bound expression for the probability of failure of a parallel system. After establishing the complete correlation among modes, the definition for the safety of a structure is determined. P_j establishes the failure probability of a single failure mode, j. According to Park, et al., if F_i is the event where failure mode, i, occurs, and P_i is the probability of the event occurring, then failure of the system is denoted by the following [70]:

$$P_{system} = P\left[\bigcup_{i=1}^{NM} F_i\right] \quad \textbf{(6-46)}$$

where NM is all possible failure modes of the structures.

Since correlation between failure modes is established, the lower bound of the failure probability of a series system is represented by the equation below:

$$P_{system} = Max\left[P_1, P_2, P_3, ..., P_{NM}\right] \quad \textbf{(6-47)}$$

One of the challenges with the above equation for P_{system} is the requirement to identify all the possible failure modes of the structure, which in itself is a daunting task in addition to damage detection. Therefore, Stubbs, et al. suggest using mathematical induction to alleviate the need for identifying a large amount of failure modes [34]. Assuming a knowledge of the component failure probabilities, a_i, the probabilities are arranged in descending order of magnitude with $a_1 > a_2 > a_3 > ... > a_n$. With the reordering of the failure probabilities, it is observed that for a series system the lower bound of the failure probability is $P_{system} = a_1$. In addition if the redundancy of the structure is one, then the probability of failure of that mode is $P_{system} = a_2$. For a structure with a redundancy of two, the probability of failure of that mode is $P_{system} = a_3$. Therefore, by mathematical induction, if a structure has a redundancy, s, the system probability of failure is given as $P_{system} = a_{s+1}$.

Per the observations from the mathematical induction by Stubbs, et al., a rule is developed for estimation of the system probability of failure with the sequence of failure of the components in a mode unknown [34]:

If the failure probabilities of the elements are rearranged in order of descending magnitude $a_1 > a_2 > a_3 > ... > a_n$ and if the redundancy of the structure (or substructure) is s, an estimate of the failure probability of the system is given by $P_{system} = a_{s+1}$.

The system probability of failure is now available for evaluation utilizing the fractional changes in stiffness or severity of damage provided in the damage index method. The classification of this global NDE method as a Level 4 is debatable because of the assumptions used in the reliability analysis and the quality of information available from the probability estimations.

In developing the rules for the structural reliability a rigorous solution may prove to supply a more accurate prediction of reliability versus the mathematical induction procedure by Stubbs, et al., where several assumptions allow for conservative estimates of the probability of system failure. Furthermore, the reliability analysis provides information relating the current state of damage to the current failure probability of the structure.

According to Rytter, the Level 4 definition of a global NDE technique describes the impact of damage as a prediction of the remaining life of the structure, which implicitly involves a durability assessment in terms of a structure's capability to accumulate damage before the damage becomes critical [32]. Implementation of the strategy as well as comparisons of the technique for field bridge data is available with field verification of the procedure [65, 66, 69].

The damage index method has been applied to field measured modal parameters showing the ability to locate, detect, and estimate the severity of damage in the structure. Predicted damage locations from the damage index method were verified from a visual inspection of existing cracks on a deteriorating reinforced concrete bridge structure as part of the validation of the method [69].

Kim and Stubbs return to the general problem of utilizing changes in dynamic modal parameters of structures to detect, locate, and estimate the severity of damage [71]. In particular, the modal strain energy procedure developed by Stubbs and Kim [35] is improved for better localization and severity estimation by eliminating several assumptions and limitations imposed in the previous derivations.

Eigenvalues of the pre- and post-damage multi-degree-of-freedom structure λ_i and λ_i^* can be related in the following forms:

$$\lambda_i^* = \lambda_i + d\lambda_i = \frac{\left(K_i + dK_i\right)}{\left(M_i + dM_i\right)} \qquad \textbf{(6-48)}$$

where K_i and M_i are the i^{th} modal stiffness and i^{th} modal mass of the undamaged system respectively; and $d\lambda_i$, dK_i, and dM_i are the change in the i^{th} eigenvalue, the change in the i^{th} modal stiffness, and the i^{th} modal mass, respectively. The sensitivity matrices are similarly defined as:

$$F_{ij}^* = F_{ij} + dF_{ij} \qquad \textbf{(6-49)}$$

where F_{ij}^* and F_{ij} are the respective damaged and undamaged stiffness matrices; $F_{ij} = \frac{K_{ij}}{K_i}$ is the undamaged modal sensitivity expressed as the fraction of modal energy of the i^{th} mode and the j^{th} member; $K_{ij} = \Phi_i^T C_j \Phi_i$ is the contribution of the j^{th} member to the ith modal stiffness; C_j is the contribution of the j^{th} member to the system stiffness matrix, C; and Φ_i is the i^{th} mode vector.

The fractional change of modal energy at the j^{th} member for the i^{th} mode is represented by dF_{ij}, which is acquired as follows:

$$dF_{ij} = \frac{K_{ij}}{K_i}\left[\frac{dK_{ij}}{K_{ij}} - \frac{dK_i}{K_i}\right] \qquad \textbf{(6-50)}$$

where dK_{ij} represents the fractional change in K_{ij}. It is observed that $K_i >> K_{ij}$ and thus the fraction of modal energy is reduced to the following equation:

$$dF_{ij} \cong \frac{dK_{ij}}{K_i} \qquad \textbf{(6-51)}$$

As compared to previous formulations, the sensitivity of the modal stiffness is not assumed to remain the same for pre- and post-damaged structures; furthermore, the shift in the reference axis is no longer necessary to develop the damage index. The fraction of modal energy is then modified and expressed in terms of parameters representing material stiffness properties of the individual elements for the damage and undamaged structure respectively, E_j^* and E_j; and geometric quantities (and possibly Poisson's ratio) of the structure, C_{jo}.

$$\frac{dK_{ij}}{K_i} \cong \frac{\gamma_{ij}}{\gamma_i}\frac{dE_j}{E_j} + \frac{d\gamma_{ij}}{\gamma_i} \qquad \textbf{(6-52)}$$

where $\gamma_{ij} = \Phi_i^T C_{j0} \Phi_i$ and $\gamma_{ij}^* = \Phi_i^{*T} C_{j0} \Phi_i^*$; $d\gamma_{ij} = \gamma_{ij}^* - \gamma_{ij}$, and $\gamma_i = \sum_{k=1}^{ne} \Phi_i^T C_{k0} \Phi_i$; and *ne* is the number of elements. The fractional changes in modal stiffness are approximately related to the fractional changes in modal properties:

$$\frac{dK_{ij}}{K_i} \cong g_i(\lambda, \Phi) = \frac{d\lambda_i}{\lambda_i} + \frac{dM_i}{M_i}\left(1 + \frac{d\lambda_i}{\lambda_i}\right) \qquad \textbf{(6-53)}$$

where $g_i(\lambda, \Phi)$ is the dimensionless factor representing the systematic change in modal parameters of the i^{th} mode due to the damage.

With the sensitivities, stiffness and modal mass quantities expressed as linear relationships between damaged and undamaged states of the structure, a new damage index for *nm*, the number of modes, at the j^{th} location is given by:

$$\beta_j = \frac{E_j}{E_j^*} = \frac{\sum_{i=1}^{nm} \gamma_{ij}^*}{\sum_{i=1}^{nm} \gamma_i \, g_i(\lambda, \Phi) + \gamma_{ij}} \qquad \textbf{(6-54)}$$

Once damage is located, the severity is estimated from:

$$\alpha_j = \frac{dE_j}{E_j^*} = \frac{1}{\beta_j} - 1, \quad \alpha_j \geq -1 \qquad \textbf{(6-55)}$$

where damage severity is indicated as the reduction in stiffness in the *j*th member if $\alpha_i < 0$.

The above formulation provides information in terms of location and severity of damage from changes in mode shapes of structures. The current formulation presents the following advantages: (1) damage can be located and sized using a few modes; (2) damage can be located and sized without solving a system of equations; and (3) damage can be located and sized in structures containing many members. A numerical simulation on a two span continuous beam is conducted to demonstrate the improvement over the previous versions of the damage index, with improvements shown in accuracy of the severity estimation and reduction of false-positive indications of damage. No examples related to field data or demonstrations on bridge structures are currently available.

6.4 STIFFNESS AND FLEXIBILITY BASED METHODS

Another category of damage detection methods utilizes dynamic measurements to determine the system matrices of a structure to characterize damage in a structure. Assembly and evaluation of the system matrices provides inherent advantages of being able to locate and estimate the severity of damage by a comparison of damaged and undamaged matrices of the system. However, the problem of incomplete measurements or inability to identify all modes of the structure results in partial population of the system matrices. As with a majority of damage detection methods the realization of a stiffness reduction factor for elements of the structure are critical in terms of determining location and severity of damage. In the following section, methods utilizing system matrices are examined, in particular the stiffness matrix or flexibility matrix of the system utilizing vibration measurements of the structure.

6.4.1 Matrix update methods

Matrix updating procedures are a developing area for structural damage detection. In general these methods are either sensitivity-based matrix updating techniques, optimal matrix update procedures, or control-based algorithms. The data used to develop the finite element model (FEM) matrices are either the modal parameters or frequency response functions of the structure. The identification of modal parameters is mathematically derived; however, the computation becomes complicated for large and modally complex structures. Due to the inability of acquiring all modes of large structures from field vibration measurements, an approximation of the stiffness or flexibility matrices of a structure is available at best.

Optimal matrix update methods, seeking to determine system property matrices, such as the stiffness matrix, using measured test data, are used extensively in FEM refinement and damage detection. Changes in the system matrices are associated with the overall health of the system, where a stiffness reduction is often associated with damage. The objective for optimization of the stiffness matrix is to adequately populate the matrix under the guide of some objective

function with a constraint set defined, based on preserving characteristics of the system matrix, such as symmetry, sparsity (the zero/nonzero pattern of the matrix), and positivity.

Typically matrix update problems vary in terms of the iterative refinement process to converge to an approximate stiffness matrix of the system. Optimization of the stiffness matrix addresses the issue of reduced measurements for structural damage detection by completing the stiffness matrix of a system based on constraints established according to characteristics of the system matrices and satisfaction of the classical eigenvalue problem from structural dynamics.

A successful matrix optimization procedure is intended as a Level 3 damage detection methodology, since spatial information and damage severity information become available if the stiffness matrix and its subsequent changes due to damage are resolved. Matrix update methods generally vary among the following three considerations [36]: (1) Objective function to be minimized; (2) Constraints placed on the problem; (3) Numerical scheme used to implement the optimization.

Abdalla, et al. propose implementing alternating projection algorithms to provide improved optimal matrix updates for damage detection purposes [53]. In particular, the emphasis is placed on providing theoretical foundations, the formulation of the alternating projection method, and a justification of their convergence and properties. Included is a directional alternating projection damage detection algorithm, which results in enhanced convergence. Abdalla, et al. assume that the number of measured mode shapes is the same as the analytical eigenvectors, which introduces the possibility of erroneous results since accurate population of the damaged stiffness matrix requires *all* associated mode shapes and frequencies of the system.

The alternating projection method is used to solve an optimization problem with defined constraints to the optimization. The algorithm requires iterating until the intersection of all constraints is nonzero, i.e., find a matrix $\mathbf{K}_\mathbf{d}^*$ where $\mathbf{C}_1 \cap \mathbf{C}_2 \cap \mathbf{C}_3 \cap \ldots \cap \mathbf{C}_n \neq \mathbf{0}$. Where it is important that constraint sets $\mathbf{C}_i$, are convex, i.e., any two points (matrices) that belong to a set define a line segment that is fully contained in the set. Convexity implies that the optimization problem and feasibility problem have unique solutions. In order to preserve structural connectivity for more accurate damage detection, the following optimal matrix update problem is solved:

$$\underset{\mathbf{K}_\mathbf{d}^*}{\text{minimize}} \left\| \mathbf{K}_\mathbf{d}^* - \mathbf{K} \right\| \qquad \textbf{(6-56)}$$

where $\|\bullet\|$ denotes the Frobenius norm[+]; $\mathbf{K}_\mathbf{d}$ is the stiffness matrix of the damaged structure and $\mathbf{K}_\mathbf{d}^*$ is the solution matrix representing the optimally modified stiffness matrix; and $\mathbf{K}$ is the analytical stiffness matrix. The optimization problem is subject to the following constraints:

$$\mathbf{K}_\mathbf{d}^* \in \mathbf{C}_1 \cap \mathbf{C}_2 \cap \mathbf{C}_3 \textbf{ and } \mathbf{K}_\mathbf{d}^* \in \mathbf{C}_4 \qquad \textbf{(6-57)}$$

[+] The Frobenius norm of a matrix, A is defined as follows $\|A\| = \left[\sum_{i,j} A_{ij}^2 \right]^{\frac{1}{2}} = \left[tr\left(AA^T \right) \right]^{\frac{1}{2}}$

where $\cap$ is the set intersection operation. $\mathbf{C}_1 = \{\mathbf{K}_d : \mathbf{K}_d \geq \mathbf{0}\}$ ensures a positive definite matrix; $\mathbf{C}_2 = \{\mathbf{K}_d : \mathbf{K}_d = \mathbf{K}_d^T\}$ introduces a constraint keeping the solution matrix symmetric; and $\mathbf{C}_3 = \{\mathbf{K}_d : \mathbf{K}_d \text{ is } \mathbf{K} - \text{sparse}\}$ ensures that $\mathbf{K}_d$ is **K**-sparse if $\mathbf{K}_d$ has the zero/nonzero pattern of the analytical stiffness matrix.

$\mathbf{C}_4 = \{\mathbf{K}_d : \mathbf{K}_d\mathbf{V}_d = \mathbf{M}\mathbf{V}_d\mathbf{\Omega}_d^2\}$ provides for a $\mathbf{K}_d^*$ such that the eigenvalue problem is satisfied, where **M** is the mass matrix, $\mathbf{V}_d$ is the measured mode shape matrix, and $\mathbf{\Omega}_d$ is the measured natural frequency matrix. The fourth constraint, $\mathbf{C}_4$ does not intersect the other constraints such that flexibility is introduced in terms of satisfaction of the eigenvalue problem, since the presence of signal noise may lead to a solution that does not satisfy the eigenvalue problem. The methodology is applied to experimental data from a NASA eight bay truss with damage inflicted by the removal of truss members. The matrix optimization technique is able to able to predict damage locations; however errors in severity estimation are observed between 5% and 30%.

Escobar, et al. propose a transformation matrix method for damage detection, with damage defined as a loss of stiffness [54]. The methodology is based on the transformation matrix that reduces the global stiffness matrix of a structure to a condensed state with only the primary degrees of freedom, which correspond to the rigid body movements of the slabs on different floors of a building. The methodology is able to identify, locate, and estimate severity of damage in a structure by considering the contribution of elements to the overall performance of the structure.

The methodology assumes that an analytical stiffness matrix represents the undamaged state of the structure with the damaged global stiffness matrix acquired by a matrix update technique using the matrix of measured frequencies, Ω_d, and the matrix of mode shape vectors, Φ_d by Baruch and Bar-Itzhack[55], shown below:

$$\text{minimize } \left\| M^{-\frac{1}{2}}\left(K_d^* - K\right)M^{-\frac{1}{2}} \right\| \qquad \textbf{(6-58)}$$

$$\text{subject to } K_d^*\Phi_d = M\Phi_d\Omega_d^2, \quad K_d^* = K_d^{*T}$$

where K is the analytical stiffness matrix; K_d^* is the optimally modified stiffness matrix; M is the system mass matrix; and $\|\bullet\|$ again denotes the Frobenius norm. A closed form solution to the minimization problem is available and given below:

$$\begin{aligned} K_d^* &= K - KXX^TM - MXX^TK + MXX^TKXX^TM + MX\Omega_d^2X^TM \\ \text{where, } X &= \Omega_d\left(\Omega_d^TM\Omega_d\right)^{-\frac{1}{2}} \end{aligned} \qquad \textbf{(6-59)}$$

The Baruch-Bar Itzhack formula provides a matrix update that is consistent with the measured modal data, although structural connectivity of the stiffness matrix is not ensured. Assuming the undamaged and damaged stiffness matrices of the structure are available, the damage detection algorithm by Escobar, et al. computes the transformation matrices of the structure to condense the stiffness matrices such that only those degrees of freedom associated with rigid body

movements of the slabs are used for the damage identification process [54]. This modifies the computationally expensive procedure to a reduced set of degrees of freedom of the structure.

The damage detection algorithm was applied to numerical simulations of a ten-story office building with vibration parameters acquired from earthquake acceleration data from the Mexico City earthquake on Sept. 19, 1985. Numerical simulations show accurate identification of damage location and severity as compared to nonlinear analyses. In addition the authors examined the effect of noise and reduced measurements on the damage detection process. As noise levels increased from 0% to 1%, 3%, and 5%, a general increase in the estimated damage magnitude was also observed.

Initially 10 measurements were used to attain the stiffness matrix of the structure, analyses were conducted with reduced measurements of 50%, 70%, and 90% of the 10 mode shapes. It was found that for accurate damage location, 80% of the 10 mode shapes were required. The identified magnitudes of the damage were observed to decrease as the number of mode shapes decrease.

The adjustment of the stiffness matrix is based on the difference of the undamaged stiffness matrix; consequently as fewer modes are included, the use of Baruch and Bar-Itzhack's methodology to determine the damaged stiffness matrix resulted in a result close to the original stiffness matrix. Therefore, fewer damaged elements are identified during the damage detection process. The damage detection algorithm presented by Escobar, et al. relies on an accurate analytical model to develop the undamaged stiffness matrix and the availability of a procedure for acquiring the stiffness matrix of a damaged structure.

6.4.2 Stiffness evaluation in state space

Sivico, et al. present a Level 3 global damage detection methodology for civil structures with damage indicated by changes or reductions in stiffness and damping parameters of the structural elements [58]. The damage detection algorithm utilizes the state-space representation of the time domain structural response to evaluate stiffness and damping parameters of a structure. The eigensystem realization algorithm is used for systems identification, which provides a discrete state-space representation of the structure. In addition, a method for the linear transformation to convert the arbitrary state-space representation of the structure to the physical coordinate system of the structure is necessary to implement the global damage detection methodology.

Beginning with the equations for an *n* degree of freedom (DOF) structure:

$$\mathbf{M}\ddot{\mathbf{q}} + \mathbf{D}\dot{\mathbf{q}} + \mathbf{K}\mathbf{q} = \mathbf{0} \qquad \textbf{(6-60)}$$

where **M**, **D**, and **K** are the mass, damping, and stiffness matrices, respectively; and **q**(t) is the displacement of *n* DOF of the structure. Conversion to the state-space is facilitated by representing the displacement and velocity vectors of the structure with $\mathbf{x}_1 = \mathbf{q}$ and $\mathbf{x}_2 = \dot{\mathbf{q}}$.

$$\begin{bmatrix} \dot{\mathbf{x}}_1 \\ \dot{\mathbf{x}}_2 \end{bmatrix} = \begin{bmatrix} \mathbf{0} & \mathbf{I} \\ -\mathbf{M}^{-1}\mathbf{K} & -\mathbf{M}^{-1}\mathbf{D} \end{bmatrix} \begin{bmatrix} \mathbf{x}_1 \\ \mathbf{x}_2 \end{bmatrix} \Leftrightarrow \dot{\mathbf{x}} = \mathbf{A}\mathbf{x} \qquad \textbf{(6-61)}$$

Sivico, et al. explain the global stiffness, mass, and damping matrices are a result of individual element contributions for the undamaged system and can be expressed as follows:

$$\mathbf{M} = \sum_{i=1}^{n} \mathbf{M}_i \qquad \mathbf{D} = \sum_{i=1}^{n} \mathbf{D}_i \qquad \mathbf{K} = \sum_{i=1}^{n} \mathbf{K}_i \tag{6-62}$$

where $\mathbf{M}_i$, $\mathbf{D}_i$, and $\mathbf{K}_i$ are the contributions from the i^{th} mass, damping, and stiffness element matrices.

Here, mass is assumed to be an unchanging characteristic of the structure as damage occurs. The presence of damage in the methodology is recognized by a reduction factor on the individual element contributions to the global system matrices. Damage is assumed to cause a reduction in the stiffness and/or damping contribution of an individual element, with the objective of the methodology being to evaluate the reduction factors a_i and b_i. If accurate evaluation of the reduction factors is possible, then indications of damage, locations, and severities are available from the algorithm. The equations incorporating reduction factors in the stiffness and damping matrix formulation are given below:

$$\mathbf{D}_d = \mathbf{D} + \sum_{i=1}^{d} a_i \mathbf{D}_i = \sum_{i=1}^{d} (1 + a_i)\mathbf{D}_i \tag{6-63}$$

$$\mathbf{K}_d = \mathbf{K} + \sum_{i=1}^{k} b_i \mathbf{K}_i = \sum_{i=1}^{k} (1 + b_i)\mathbf{K}_i \tag{6-64}$$

where the subscript *d* indicates the matrices are associated with the damaged state of the structure.

Without consideration for computational costs, the damage detection methodology proposed by Sivico, et al. is theoretically capable of localizing and estimating damage severity at any scale, depending on the level of discretization of the structure during the modeling phase. The state-space representation of the damaged structure is provided below:

$$\begin{bmatrix} \dot{\mathbf{x}}_1 \\ \dot{\mathbf{x}}_2 \end{bmatrix} = \begin{bmatrix} \mathbf{0} & \mathbf{I} \\ -\mathbf{M}^{-1} \sum_{i=1}^{k} (1 + b_i)\mathbf{K}_i & -\mathbf{M}^{-1} \sum_{i=1}^{d} (1 + a_i)\mathbf{D}_i \end{bmatrix} \begin{bmatrix} \mathbf{x}_1 \\ \mathbf{x}_2 \end{bmatrix} \Leftrightarrow \dot{\mathbf{x}} = \mathbf{A}_d \mathbf{x} \tag{6-65}$$

The matrices $\mathbf{A}$ and $\mathbf{A}_d$ are determined from a systems identification procedure. Matrix $\mathbf{A}$ is subtracted from matrix $\mathbf{A}_d$ to isolate the component of the stiffness directly related to the damaged state of the structure. The methodology is reduced to a comparison of the difference in stiffness and damping matrices in state-space.

$$\mathbf{A}_d - \mathbf{A} = \begin{bmatrix} \mathbf{0} & \mathbf{0} \\ -\mathbf{M}^{-1} \sum_{i=1}^{k} b_i \mathbf{K}_i & -\mathbf{M}^{-1} \sum_{i=1}^{d} a_i \mathbf{D}_i \end{bmatrix} \tag{6-66}$$

Since mass is assumed to remain constant with the occurrence of damage in the structure, the sub matrices in the lower part of $[\mathbf{A}_d - \mathbf{A}]$ can be pre-multiplied by $[-\mathbf{M}^{-1}]$, resulting in the following relationships within the matrix for stiffness and damping:

$$\tilde{\mathbf{K}} = \sum_{i=1}^{k} b_i \mathbf{K}_i \qquad \tilde{\mathbf{D}} = \sum_{i=1}^{d} a_i \mathbf{D}_i \qquad \textbf{(6-67)}$$

Converting the summations into matrix vector equations produces the following system of equations:

$$\begin{bmatrix} K_{1_{11}} & K_{2_{11}} & \cdots & K_{n_{11}} \\ \cdots & \cdots & \cdots & \cdots \\ K_{1_{1n}} & K_{2_{1n}} & \cdots & K_{n_{1n}} \\ K_{1_{21}} & K_{2_{21}} & \cdots & K_{n_{21}} \\ \cdots & \cdots & \cdots & \cdots \\ K_{1_{2n}} & K_{2_{2n}} & \cdots & K_{n_{2n}} \\ \cdots & \cdots & \cdots & \cdots \\ K_{1_{n1}} & K_{2_{n1}} & \cdots & K_{n_{n1}} \\ \cdots & \cdots & \cdots & \cdots \\ K_{1_{nn}} & K_{2_{nn}} & \cdots & K_{n_{nn}} \end{bmatrix} \begin{bmatrix} b_1 \\ b_2 \\ \cdots \\ b_n \end{bmatrix} = \begin{bmatrix} \tilde{K}_{11} \\ \cdots \\ \tilde{K}_{1n} \\ \tilde{K}_{21} \\ \cdots \\ \tilde{K}_{2n} \\ \cdots \\ \tilde{K}_{n1} \\ \cdots \\ \tilde{K}_{nn} \end{bmatrix} \Leftrightarrow \hat{\mathbf{K}}\vec{\mathbf{b}} = \tilde{\mathbf{k}} \qquad \textbf{(6-68)}$$

where $\hat{\mathbf{K}}$ according to the formulation is composed of undamaged element stiffness values of the structure associated with the vector of damage reduction factors $\vec{\mathbf{b}}$. $\tilde{\mathbf{k}}$ is the known resultant for the subtraction of $\mathbf{A}$ from $\mathbf{A}_d$. Subsequently $\vec{\mathbf{b}}$ is determined from matrix operations with $\vec{\mathbf{b}} = \hat{\mathbf{K}}^{\dagger}\tilde{\mathbf{k}}$, where $\hat{\mathbf{K}}^{\dagger}$ is the pseudo inverse of the vector-matrix, $\hat{\mathbf{K}}$.

Similarly the damping reduction factors $\vec{\mathbf{a}} = \hat{\mathbf{D}}^{\dagger}\tilde{\mathbf{d}}$ are developed and evaluated. The method is capable of determining the location and severity by determination of the reduction factors $\vec{\mathbf{a}}$ and $\vec{\mathbf{b}}$. However, the system identification procedure, not described here, introduces a level of uncertainty, where any reduction factor less than 10% is not applicable, i.e., the damage detection algorithm has a minimum detectable reduction in stiffness and/or damping of 10%.

The damage detection algorithm presented by Sivico, et al. details an approach utilizing the state-space representation of the structure [58]. The transformation from state-space to the physical coordinates of the structure requires having the same amount of actuators as DOFs or identification of multiple single-input systems, which are combined into a multi-input state space representation. Furthermore, the algorithm requires a representation of the as-built or baseline of the structure, since a comparison of two states of the structure is necessary in order to detect and evaluate damage.

Applications of the methodology are examined with numerical simulations, with any stiffness or damping reduction factors less than 10% neglected, due to the uncertainty in the systems identification procedure. Damage localization and severity estimation on a simple mass-spring-damper model and three-bar truss were successful, although damage cases with stiffness or damping changes greater than 50% were simulated.

6.4.3 Dynamically measured flexibility

As the stiffness matrix is used for detection of damage in the system, the system's dynamically measured flexibility matrix can also be used as an indicator of damage. As with the stiffness matrix development, the measurement of the flexibility matrix is approximate because of the inability to acquire all the mode shapes of a structure.

Application of the flexibility matrix presents several advantages versus dynamically measured stiffness. First, flexibility matrices are attainable from modes and mode shapes that are determined from a mode identification procedure [59, 60]. Second, most updating damage detection algorithms incorporate an iterative refinement process for which the fastest converging solutions are typically high eigenvalues. In stiffness-based approaches, the high eigenvalues correspond to high frequency modes, which are difficult to acquire for large civil structures; however, in flexibility based methods the high eigenvalues correspond to dominant low frequency modes of the structure, rather than unmeasured high frequency components [59]. Because the flexibility matrix demonstrates an inverse relationship to the squares of the natural frequencies, the measured flexibility matrix is more sensitive to changes in the lower frequency modes of the structure.

Park and Reich develop a flexibility-based approach using the partitioned flexibility equation in order to detect changes in substructural characteristics by identifying changes in the measured global flexibilities before and after damage [59, 60]. As previously mentioned, methods utilizing measured flexibility matrices are limited to approximations because of the unavailability of higher modes and thus the inability to measure the complete flexibility or stiffness matrices for a given structure. Although, no definition of damage is explicitly stated, the definition of damage implicit in the procedure by Park and Reich, and apparent in the applications, is that damage is indicated by a loss of stiffness or an increase in flexibility. The formulation by Park and Reich first provides a procedure for evaluating the global flexibility matrix of the structure from experimentally acquired modal parameters. Subsequently, localized damage detection scenarios are formulated for localized flexibility of a structure in three different generalized coordinates, which are localized or substructural displacement, elemental deformation basis, and elemental strain basis [59, 60].

Utilizing the theoretical concepts in structural dynamics, Park and Reich develop the equation of motion using the discrete energy functional of a linear damped structure; the equation of motion is derived taking the first variation of the energy of the system:

$$\mathbf{M}_g\ddot{\mathbf{u}}_g + \mathbf{C}_g\dot{\mathbf{u}}_g + \mathbf{K}_g\mathbf{u}_g = \mathbf{f}_g \qquad \textbf{(6-69)}$$

where $\mathbf{M}_g$ is the mass matrix of the assembled structure; $\mathbf{C}_g$ is the assembled damping matrix; $\mathbf{K}_g$ is the assembled stiffness matrix; $\boldsymbol{u}_g, \dot{\boldsymbol{u}}_g, \ddot{\boldsymbol{u}}_g$ are the displacement, velocity, and acceleration vectors, respectively; and $\mathbf{f}_g$ is the applied force vector.

Assembly of the global stiffness matrix, $\mathbf{K}_g$, is composed of stiffness matrices of substructures partitioned from the complete structure [24].

The response of the structure to the applied force vector is given in the frequency domain with the frequency response function (FRF) by applying a Fourier transform to the force and displacement components. This results in the following frequency domain output, $\overline{\mathbf{u}_g}$:

$$\overline{\mathbf{u}_g} = \mathbf{H}_g(\omega)\overline{\mathbf{f}_g} = \left(\mathbf{K}_g + j\omega\mathbf{C}_g - \omega^2\mathbf{M}_g\right)^{-1}\overline{\mathbf{f}_g} \qquad \textbf{(6-70)}$$

where $\mathbf{H}_g(\omega)$, the transmittance function, is called the "global" FRF. According to Park and Reich, the mass normalized "global" flexibility matrix, $\mathbf{F}_g$ is defined as follows:

$$\mathbf{F}_g = \mathbf{\Phi}\ \mathbf{\Lambda}^{-1}\mathbf{\Phi}^T,\ \mathbf{\Phi}^T\mathbf{M}_g\mathbf{\Phi} = 1,\ \mathbf{\Phi}^T\mathbf{K}_g\mathbf{\Phi} = \mathbf{\Lambda} \qquad \textbf{(6-71)}$$

The above expressions are applicable to an analytical model and serve as a background to the development of the damage detection methodology using localized flexibilities. In actuality, the measured global flexibility matrix is significantly smaller in size relative to the analytical expression and is given below:

$$\mathbf{F}_{gm} = \mathbf{\Phi}_m\mathbf{\Lambda}_m^{-1}\mathbf{\Phi}_m^T \qquad \textbf{(6-72)}$$

where *m* indicates the measured mode and mode shape.

The global flexibilities alone are insufficient for damage localization, since they are unable to model elemental changes in flexibility and the infinite number of load paths that occur in multiply-connected or continuum structures tends to "smear" elemental flexibility changes as strain energy can pass from one location to another through a number of different paths [60]. Thus the substructural flexibilities are required for accurate characterization of damage. Park and Reich utilize a general partitioned flexibility method to establish a relationship between the global and substructural flexibilities [61].

The localization of damage using the global flexibility matrix, $\mathbf{F_g}$, requires resolving the localized flexibilities for the elements of the structure. These are determined by relating the global FRF, $\mathbf{H}_g(\omega)$, to the substructural FRF, $\mathbf{H}(\omega)$ via the following relationship:

$$\mathbf{H}(\omega) = \mathbf{L}\mathbf{H}_g(\omega)\mathbf{L}^T = \mathbf{L}\left(\mathbf{K}_g + j\omega\mathbf{C}_g - \omega^2\mathbf{M}_g\right)^{-1}\mathbf{L}^T \qquad \textbf{(6-73)}$$

where **L** is the Boolean assembly matrix relating global and substructural displacements.

The combined result of the substructural FRFs and the relationship between the global FRFs and substructural FRFs leads to the following, which is used for damage detection purposes by comparing the localized flexibility of the undamaged state of the structure to its current state. For the quasistatic limit, where $\omega \to 0$, the following equation results, allowing for a calculation of the substructural flexibility, **F**, by an iterative procedure:

$$\mathbf{L}\mathbf{F}_g\mathbf{L}^T = \mathbf{F}\left\{\mathbf{I} - \mathbf{B}\mathbf{F}_B^{-1}\left[\mathbf{I} - \mathbf{L}_b\mathbf{F}_L\mathbf{L}_b^T\mathbf{F}_b^{-1}\mathbf{F}_B^{-1}\right]\mathbf{B}^T\mathbf{F}\right\}$$
$$\mathbf{F} = \mathbf{K}^+, \quad \mathbf{F}_B = (\mathbf{B}^T\mathbf{F}\mathbf{B}), \quad \mathbf{F}_L = \left(\mathbf{L}_b^T\mathbf{F}_B^{-1}\mathbf{L}_b\right)^{-1}, \quad \mathbf{L}_b = \mathbf{B}^T\mathbf{L} \tag{6-74}$$

where the symbol (+) indicates a generalized inverse; **B** is a constraint projection matrix; and **I** is the identity matrix.

The above formulation is the substructural displacement based flexibility. A deformation-basis flexibility is attainable by partitioning of substructural displacements into deformational and rigid parts. The result is an equation relating global flexibility to deformation-basis substructural flexibility:

$$\mathbf{T}\mathbf{L}\mathbf{F}_g\mathbf{L}^T\mathbf{T}^T = \mathbf{P}_v^T\mathbf{F}_v\mathbf{P}_v$$
$$\mathbf{F}_v = \mathbf{K}_v^+, \quad \mathbf{P}_v = \mathbf{I} - \mathbf{B}_v\left[\mathbf{B}_v^T\mathbf{F}_v\mathbf{B}_v\right]^{-1}\mathbf{B}_v^T\mathbf{F}_v \tag{6-75}$$

where **T** is a matrix relating the relative rigid body deformations between two nodes; and *v* is used to denote the deformation-basis derivation for the respective matrices.

The final formulation is for the strain-basis flexibility, where the strain output is related to the substructural displacement. The result is a similar formulation as the displacement and deformation based substructural flexibilities:

$$\mathbf{D}\mathbf{L}\mathbf{F}_g\mathbf{L}^T\mathbf{D}^T = \mathbf{P}_s^T\mathbf{F}_s\mathbf{P}_s$$
$$\mathbf{F}_s = \mathbf{K}_s^+, \quad \mathrm{P}_s = \mathbf{I} - \mathbf{B}_s\left[\mathbf{B}_s^T\mathbf{F}_s\mathbf{B}_s\right]^{-1}\mathbf{B}_s^T\mathbf{F}_s \tag{6-76}$$

where **D** is the discrete strain-displacement relation matrix which can be derived from finite element shape functions; and *s* is used to denote the strain-based formulation of the substructural flexibility.

Application of the three damage detection methods was applied to a numerical simulation of a plane ladder using beam elements, with reductions in the bending rigidity imposed. The strain basis and deformation-basis approaches accurately identified the location of damage, with the strain basis providing the closest damage severity estimates. The strain-basis flexibility was applied to a beam model of a ten-story structure using three modes; the predicted damage location was verified on the real structure, but no information regarding the quantification of damage was provided. In addition, the methodology was applied to the I-40 modal test data, with the correct location identified with the strain basis flexibility; however little detail is provided as to the damage scenario and the severity estimation [65, 66].

6.5 MACHINE LEARNING TECHNIQUES

Machine learning is the development of computing systems, or expert systems, with learning capability [75]. Computational intelligence methods such as neural networks and genetic algorithms are attractive processes in the area of structural damage detection because of their

effectiveness and robustness in coping with uncertainty, insufficient information, and noise [75]. Machine learning techniques were developed as a remedy to four major problems in expert systems: brittleness, lack of metaknowledge, knowledge acquisition, and validation [76].

Expert systems enable the manipulation of knowledge in a certain domain, particularly in dialogue form, by searching for answer recommendations to problems of a qualitative nature [76]. The primary development of each system is the knowledge base employed to develop the appropriate decision rules, which are intended to simulate the expert's way of thinking. Knowledge acquisition, or the transfer of knowledge from the source of domain expertise to the knowledge base, is an art and is considered the most difficult component of machine learning techniques.

Machine learning systems are classified in the following general categories [76]:

1. *Interactive knowledge acquisition*; programs learn new interface rules by means of user interaction.

2. *Learning by being told*; adaptation of knowledge from the source and its conversion into a usable form for the learning system.

3. *Learning from examples, or inductive learning, or concept learning*; a set of examples is used as input, and the learning system induces a higher-level concept description in the form of trees and decision rules.

4. *Learning from observations, or conceptual clustering, or concept formation*; establishment of new theories that account for given facts; requires a significant amount of inference as compared to other categories.

5. *Theory-driven learning;* involves learning a general concept description with the guidance of elaborate domain theory.

6. *Learning by discovery*; problem solving procedure in which the system attempts to find and understand some regularities in its environment.

The application of machine learning techniques to structural damage detection is typically observed under the classification of inductive learning, or learning by examples. Specifically, artificial neural networks and genetic algorithms are used for the characterization of damage in vibration based damage detection of structures.

6.5.1 Artificial neural networks

Artificial neural networks (ANN) are a functional abstraction of the biologic neural structures of the central nervous system [79]. ANN's are versatile for problems that are too complex to be modeled and solved by classical mathematics and traditional processes, because they are powerful pattern recognizers and classifiers. The topology of an ANN model consists of a number of simple processing elements, called nodes or neurons that are interconnected to each other. Interconnection weights that represent the information stored in the system are assumed to

quantify the strength of the interconnections; these weights establish the inherent abilities associated with an ANN [83].

Before an ANN is applied, the ANN needs to learn or be trained from an existing training set consisting of pairs of input-output elements. The majority of ANNs applied to structural damage detection employ the simple error back propagation (BP) training algorithm, which is based on a gradient-descent optimization technique [79].

The BP is an error-correcting learning procedure that generalizes the delta rule[Δ] to multi-layer feed forward neural networks with hidden units between the input and output units [75]. The multilayer feed forward networks with hidden units are able to learn in more complicated learning domains than those lacking hidden units.

The training of a neural network, or the learning procedure, is to update the weights of the links connecting the nodes (neurons) and to minimize the average squared system error between the desired and computed outputs. This error function in the form of sum squares of errors between the actual outputs from the training set and the computed outputs is minimized iteratively. The learning or training rule specifies how the weights are modified in each iteration [75].

ANN's operate as black box, model free, and adaptive tools to capture and learn significant structures in data. Artificial neural networks are attractive because damage detection algorithms are vulnerable to inaccuracies in the presence of imprecise or incomplete measured data [77]. However, damage detection methods utilizing ANNs are highly dependent on the examples used to train the network. Figure 6.4 provides a schematic of the application of structural damage detection utilizing neural networks. The measured vibration property is input into the trained network and is filtered through hidden layers resulting in output nodes, which characterize the state of damage.

In this section several structural damage detection methods employing ANNs are reviewed.

Zang and Imregun implement the use of neural networks with frequency response functions (FRFs) as input to the neural network to characterize damage in the structure [80, 81]. A specific problem addressed in the approach is that the size of FRF data, which is determined by the number of spatial response locations and the number of spectral lines, is too large for neural network applications for representative engineering problems. The direct use of such data leads to neural networks with a very large number of input nodes, which results in a large number of connections. This ultimately leads to an impractical neural network in terms of training and convergence stability.

Zang and Imregun impose a principal component analysis, which is a linear data compression technique achieving dimensionality reduction, to the FRFs for feasible application to neural networks [80]. The authors use a back propagation neural network with the principal components of the FRF as input to identify the existence of damage.

[Δ] the delta rule is defined as the amount of learning representing the difference between the desired and computed outputs.

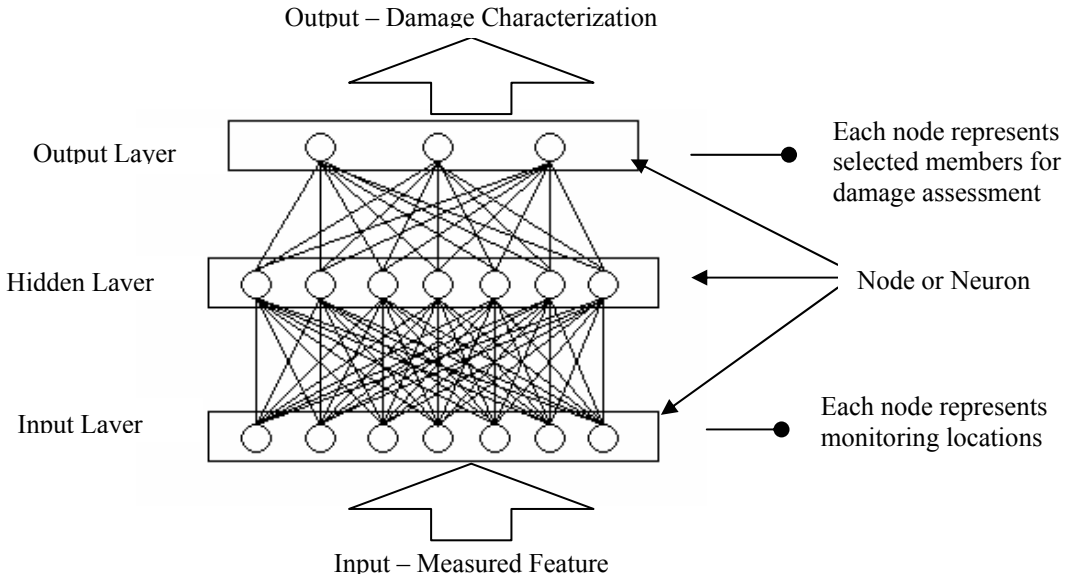

Figure 6.4: Artificial neural network damage detection

Application of the damage detection strategy was conducted on a railway wheel, with damage detected, even after a 5% random noise is introduced to the structures. The procedure was also applied to a space antenna with various modifications to the neural network for damage identification.

It was observed that using too many principal components did not necessarily yield better results, since there was an increased susceptibility to signal noise. Furthermore, the extension of the methodology to damage location is more difficult, since it requires an increase in the number of input nodes and subsequently more output nodes will be required, contradicting the intent of the data FRF reduction via principal component analysis.

Barai and Pandey compare two types of neural networks for damage detection of steel truss bridge structures [82]. One network is a traditional neural network (TNN) consisting of an input layer, output layer, and a number of hidden layers with the back propagation method used as the training algorithm for the neural network. The other network is the time-delay neural network (TDNN), which is a class of spatiotemporal neural networks.

A TDNN assumes that its output depends on its current and previous inputs. TDNNs use spatial representation of temporal sequences on their input layers. In these networks the size of the input buffer is fixed, and the data entry is controlled by a time stepping arrangement. TDNNs are specifically employed to deal with patterns that may vary over time and that require a period of time to be presented. The performance of the two neural networks was evaluated with an application to a numerically modeled steel truss bridge structure. With various cases representing reduction in the available input nodes, the TDNN was shown to perform better in the presence of incomplete information. The trained TNNs and TDNNs were able to identify the damaged member with reasonable estimates of the cross-sectional areas of all members.

Hung and Kao develop an ANN based the nondestructive damage detection approach with two primary components [83]. The first is a system identification approach using a neural systems identification network (NSIN) to acquire the undamaged and damaged states of the structure. The inputs into the NSIN are relative displacement, velocity, acceleration, and external excitations. The outputs of the NSIN are relative displacements, velocities and accelerations. Accordingly, the approximation by the NSIN in a discrete linear system is analogous to identifying the mass, damping, and stiffness coefficients in the equation of motion.

However, determining the systems dynamic characteristics from the optimal weight of the approximating neural network is arduous because of the non-uniqueness of the optimal weights, and also since the values of the network weights are not directly related to the system's physical properties. Therefore, Hung and Kao develop the partial derivative form of the ANN, such that the NSIN results in partial derivatives of the outputs.

The second component is the ANN or neural damage detection network (NDDN) used to identify the location and extent of the structural damage. The NDDN is trained to recognize the partial derivatives of the outputs with respect to the inputs of NSINs that identify the structure in undamaged as well as various damaged states by assuming that some a priori information about the system is available. The output of the NSIN is used as the input to the NDDN.

Numerical simulation of the approach is conducted using a single degree of freedom structure and a five-story shear building to demonstrate the feasibility of the approach. Damage in the applications is defined as a decrease in stiffness or damping. The application to the five-story shear building shows good correlation between the predicted stiffness loss and location as compared to the numerically simulated damage. The methodology is also observed to be able to detect damage scenarios for which it has not been specifically trained.

6.5.2 Genetic algorithms

Genetic algorithms (GA) have been introduced for solution of optimization problems as an effective means for exploring a large complex space in an adaptive way, with general rules following biological evolution mechanisms of reproduction, crossover, and mutation [75]. GA is a search method based on Darwin's theory of evolution and survival of the fittest. Darwin's theory of natural selection is that "…any being, if it vary slightly in any manner profitable to itself…will have a better chance of surviving" [78]. Solution of an optimization problem by GA requires five components [75]:

(1) *Encoding.* This is the process in which the decision variables of the optimization problem are assigned in a string of binary digits (1's and 0's) called a chromosome; i.e., if there are m decision variables and each decision variable is encoded in an n-digit binary number, then a chromosome is a string of $n \times m$ binary digits.

(2) *Evaluation or objective function*. The objective function evaluates the given decision variables and returns a value. The value of the chromosome's objective function determines the fitness of that chromosome. The fitness value establishes the probability that a chromosome will be selected as a parent and will reproduce, i.e., generate new chromosomes.

(3) Initialization of the population. An appropriate initialization methodology for the chromosome population is selected depending on the application. Typically, initialization of the chromosome population is a random process.

(4) A set of operators to perform evolution between two consecutive chromosome populations. GA simulates the process of natural selection for parent selection, selecting chromosomes to create a new generation, where the fittest members reproduce most often. Following the parent selection, the crossover process is applied to recombine two chromosomes and generate two new chromosomes when a random value associated to this pair is greater than a predefined crossover rate. The crossover operation is followed by a one-point mutation, which alters one bit in the string (chromosome) when a random value between 0 and 1, associated to that bit is greater than the predefined mutation rate.

(5) Working parameters. The working parameters are a set of predefined parameters, which guide the GA, such as the length of the decision variable encoded as a binary string; the number of chromosomes generated and operated in each generation; the crossover rate; mutation rate; and the stopping criterion. The crossover and mutation rates are assigned as real numbers between 0 and 1. The stopping criterion is a predefined number such as the number of iterations or a tolerance value for the objective function.

A flow chart of the genetic search procedure is shown in Figure 6.5, followed by a review of several damage detection methodologies using GA as the search algorithm for optimization of the defined objective function.

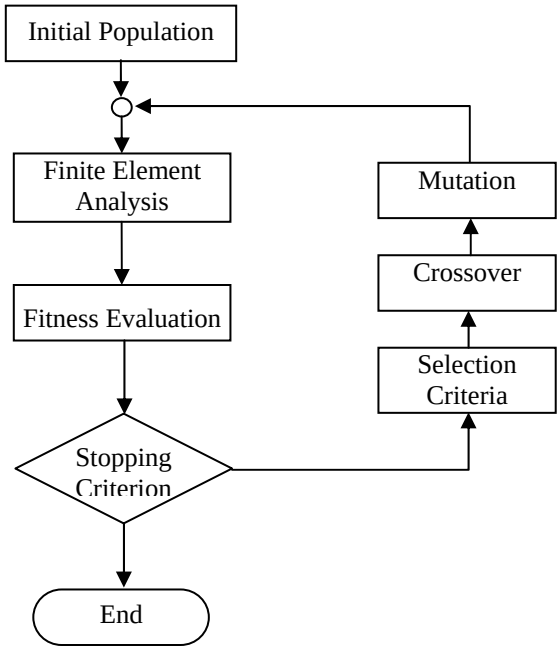

Figure 6.5: Flowchart of optimization by genetic algorithm [84]

Chou and Ghaboussi utilize static displacement measurements for structural damage detection posed as an optimization problem solving for unknown stiffness variables of the structure [78]. GA is employed here to find the best-fit solution of the unknown stiffness parameters. The optimization problem for single and multiple loading conditions is shown below:

$$\mathbf{As} = \mathbf{p} - \mathbf{a} \qquad \begin{bmatrix} \mathbf{A}_1 \\ \mathbf{A}_2 \\ \vdots \\ \mathbf{A}_{nlc} \end{bmatrix} \mathbf{s} = \begin{Bmatrix} (\mathbf{p}-\mathbf{a})_1 \\ (\mathbf{p}-\mathbf{a})_2 \\ \vdots \\ (\mathbf{p}-\mathbf{a})_{nlc} \end{Bmatrix} \tag{6-77}$$

where **A** is the matrix of element force components; **p** is the load vector; and **a** is the element force component times a known stiffness variable.

The above formulation cannot be solved directly since the number of unknowns is greater than the number of equations. Also, matrix **A** cannot be fully populated due to an insufficient number of measured displacements. Chou and Ghaboussi propose two methods implementing GA to evaluate the unknown stiffness parameters of the structure. The first method uses the difference between measured displacements and the computed displacements, which is minimized using GA; the fitness function is shown below:

$$f = \left[\sum_j \prod_i \left(1 + \left| \frac{u_{ij} - u_{ij}^m}{u_{ij}^m} \right| \right)^{p_1} \right]^{-p_2} \tag{6-78}$$

where the superscript m, denotes the measured response; u_{ij} is the displacement at the i^{th} degree of freedom under the j^{th} load condition, and it is computed from the finite element model; u_{ij}^m is the corresponding measured displacement; and p_1 and p_2 are used to magnify differences among the strings. Chou and Ghaboussi select $p_1 = p_2 = 2$.

The second method was developed to avoid solving the system of equation in finite element analyses needed for the fitness evaluation in the first method. Here, the unmeasured displacement and material properties are encoded in GA strings and allow the correct values of the unmeasured displacements to evolve during the process of GA. The entire displacement vector becomes available, with both measured and unmeasured displacements decoded from the GA. The displacement vector is used to determine a residual force vector **R**:

$$\mathbf{R} = \mathbf{Ku} - \mathbf{p} \tag{6-79}$$

which is used to determine the fitness function shown below:

$$f = \left[\sum_j \prod_i \left(1 + \left| \frac{u_{ij} - u_{ij}^m}{u_{ij}^m} \right| \right)^{p_1} \left(1 + \frac{|R_{ij}|}{\|p_j\|_2} \right)^{p_2} \right]^{-p_3} \tag{6-80}$$

where R_{ij} is the computed residual force at the i^{th} degree of freedom in the j^{th} load condition; $\|p_j\|_2$ is the Euclidean norm of the j^{th} load; and p_1, p_2, and p_3, are used to magnify differences among the strings. Chou and Ghaboussi select $p_1 = p_2 = p_3 = 2$.

Application of the method is conducted for numerically simulated damage on a plane truss structure. The application shows the ability to identify and detect damage, with the second proposed methodology shown to be more robust when multiple damage locations occur. A second application is provided for numerically simulated damage on a plane truss bridge structure. The effect of noise on the methodologies affects the severity estimation of damage by increasing the scatter; however, the damage location is still correctly identified.

Mares and Surace formulate an objective function for GA, using stiffness reduction factors as parameters. The objective function incorporates a residual forces vector, which is formulated considering the stiffness of the damaged structure as opposed to the stiffness of the undamaged structure. The residual force is determined as a sum of three parts: 1) the identification error, **e**; 2) the residue vector associated with the structural damage $\mathbf{R}'$; and 3) the vector associated with an inaccurate mathematical model of the undamaged structure, **f**.

$$\begin{aligned}\mathbf{R}^{err} &= \left[\left(\mathbf{K}+\Delta\mathbf{K}\right)-\hat{\lambda}_d\mathbf{M}\right]\hat{\mathbf{\Phi}}_d \\ &= \left[\left(\mathbf{K}_d+\sum_{i=1}^{m}\alpha_i\mathbf{K}_i+\Delta\mathbf{K}\right)-\hat{\lambda}_d\mathbf{M}\right]\hat{\mathbf{\Phi}}_d \\ &= \left[\mathbf{K}_d-\hat{\lambda}_d\mathbf{M}\right]\hat{\mathbf{\Phi}}_d+\sum_{i=1}^{m}\alpha_i\mathbf{K}_i\hat{\mathbf{\Phi}}_d+\Delta\mathbf{K}\hat{\mathbf{\Phi}}_d=\mathbf{e}+\mathbf{R}'+\mathbf{f}\end{aligned} \qquad \textbf{(6-81)}$$

where $\mathbf{R}^{\mathbf{err}}$ is the residual force in terms of the identification, damage, and modeling; **K** is the original stiffness matrix; $\Delta\mathbf{K}$ is the error in the original stiffness matrix; **M** is the system mass matrix; $\hat{\lambda}_d$ and $\hat{\mathbf{\Phi}}_d$ are the eigenvalue and eigenvector including the identification error; and α_i are the stiffness reduction factors.

Mares and Surace question the assumption of the traditional method of residual force vectors that the residual forces can be applied to detect damage as long as the uncertainties of the identification error is not large. As part of the optimization problem using GA, the objective function is defined considering the residual force term differentiating the errors in modeling, damage, and identification. The objective function to be maximized is provided below:

$$J_{obj}\left(\beta_1^*,...,\beta_i^*,...\right)=\frac{c_1}{\sum_{j=1}^{r}\mathbf{R}_j^*\left(\beta_1^*,...,\beta_i^*,...\right)^T\mathbf{R}_j^*\left(\beta_1^*,...,\beta_i^*,...\right)+c_2} \qquad \textbf{(6-82)}$$

where c_1 represents a constant used to control the value of the objective function; c_2 represents a constraint used to build a well defined function for the ideal case; r represents the number of modes taken into consideration; and $\mathbf{R}_j^*$ is the generalized residual force for each mode j, given by:

$$\mathbf{R}_j^* = \sum_{i=1}^{m} \beta_i^* \mathbf{K}_i \mathbf{\Phi}_{dj} - \lambda_{dj} \mathbf{M} \mathbf{\Phi}_{dj} = \mathbf{K}^* \Phi_{dj} - \lambda_{dj} \mathbf{M} \mathbf{\Phi}_{dj} \qquad \textbf{(6-83)}$$

β_i^* is a set of parameters that are allowed to evolve during the GA optimization procedure. If the model is absent of initial errors and the identified eigenvalues and eigenvectors are not affected by experimental errors, when each of the structural parameters β_i^* has the same values as the counterpart in its set of parameters β_i from the damaged case, the generalized residual force becomes zero and the objective function is maximized.

A numerical simulation of a five bay truss structure and cantilever beam is conducted to evaluate the methodology in the presence of noise and reduced measurements. The best results for damage detection and quantification require a minimum of 10 modes for the truss and 8 modes for the beam, with the damage detection procedure compromised with a decrease in the number of the modes. Introduction of noise at 5% reduces the precision of damage detection, although the location is identified.

Hao and Xia present a structural damage detection approach minimizing the objective function using a genetic algorithm with real number encoding [85]. The objective function of the algorithm compares changes of the measured modal parameters, namely frequencies and mode shapes, from the undamaged and damaged structure with those of the analytical model before and after updating. Versatility is achieved in the methodology since a precise model of the structure is not necessary. The damage detection strategy compares the measured vibration data before and after damage and updates a finite element model of the structure such that its changes in vibration properties are approximately equal to the changes observed in the measured vibration data due to structural damage. The objective function of the GA is to minimize:

$$\begin{aligned} J &= \left\| W \left\{ \Delta V^A \left(\{\alpha\} \right) - \Delta V^E \right\} \right\|^2 \\ &= \left\{ \Delta V^A \left(\{\alpha\} \right) - \Delta V^E \right\}^{\mathrm{T}} \mathbf{W}^2 \left\{ \Delta V^A \left(\{\alpha\} \right) - \Delta V^E \right\} \end{aligned} \qquad \textbf{(6-84)}$$

where $\|\bullet\|$ denotes the Frobenius norm; **W** is a diagonal positive definite matrix of the weight for each term; ΔV represents changes in the vibration data; $\{\alpha\}$ is a vector of stiffness reduction factors; and the superscripts *A* and *E* represent the analytical and experimental data, respectively.

Modifications to the objective function are conducted in terms of the modal parameter used. Hao and Xia implement the objective functions for frequency measurements, mode shapes, and a combination of frequencies and mode shapes for purposes of damage detection. The goal is to estimate the stiffness reduction factor for each element, $\{\alpha\}$, so that the objective function is minimized. In GA, however, the aim is to always increase the fitness; so the minimization problem is converted into a maximization problem by defining the fitness as a large number subtracted by the initial objective function.

The damage detection method was applied to a laboratory tested aluminum cantilever beam and frame. Damage was introduced to the structure by a saw cut at one location for a severe damage

case. There was successful identification of damage location; however, false-positive indications of damage were observed due to measurement noise and nonlinearity.

Although not addressed by the authors, the stiffness reduction factor tends to underestimate the severity of the damaged element showing a stiffness reduction of approximately 50% while the section was weakened 93.75%. In the frame examples, multiple damage locations are introduced to the structure. The combined use of frequency and mode shape measurements provide for damage localization; however, the methodology is highly dependent on the weights per contribution of the frequency and mode shape measurements. The methodology is unable to accurately estimate damage severity in the structure.

6.6 OTHER METHODS

6.6.1 Time history analysis

Fugate, et al. present a damage detection methodology implementing statistical process control methods to vibration-based damage detection methods [86]. Development of a statistical model is effective in analyzing extracted features to determine if a statistically significant change in the behavior of the structure has occurred. Here statistical process control (SPC) is applied to vibration measurements by determining the distribution with associated mean, μ, and variance, σ^2, of acceleration measurements. The idea is that as the structure is damaged the mean, the variance, or both may change. The implementation of SPC provides a framework for monitoring future acceleration measurements and for identifying new data that is inconsistent with past data. The damage detection strategy requires the use of quality control charts to monitor the mean, the variance or some other function of the acceleration measurements.

Assuming the mean and standard deviation are known, a control chart is constructed with a line at the mean, μ, and with two more lines representing the upper and lower control limits, $\mu + k\sigma$ and $\mu - k\sigma$, respectively. The number k is selected such that when the structure is in good condition a large percentage of observations lie within the control limits. However, in practice acceleration measurements are typically autocorrelated; thus the implementation of an autoregressive[+] model (AR) to the time history data is implemented in order to develop control charts from the residuals of the fitted AR model. If the fitted AR model is approximately correct, the residuals from the fit are sufficiently uncorrelated with no systematic pattern.

For autocorrelated data, an X-bar control chart is appropriate to determine if any significant changes in the structure have occurred. The X-bar control chart requires the formation of subgroups of size, n; the sample mean within each subgroup is then calculated and charted. The centerline of this control chart is the mean, μ, with the standard deviation of the charted values equal to $\sigma/\sqrt{n}$. The control limits are placed at $\mu \pm k\sigma/\sqrt{n}$.

[+] Autoregressive (AR) models are used to model a stationary time series. The current value of the time series is a linear combination of the p most recent past values of itself plus an error term, which incorporates everything new in the series at time t that is not explained by the past values. In simple terms, AR models utilize the statistical properties of the past behavior of a variable at some time, t, to predict its behavior in the future.

The vibration damage detection problem is presented in the context of statistical pattern recognition to evaluate the occurrence of some change in the structure [86]. However, the methodology presented is limited to evaluating whether or not a change in the behavior of the structure has occurred. Whether or not that change in the vibration properties is due to damage or other change in the structure and environment (i.e., change in mass, boundary condition, weather, etc.) is indiscernible. The location of damage is not identified, nor is the severity of damage determined. The appeal of SPC is realized in long term health monitoring; as the feature of interest is selected, future observations can be monitored to see if the feature distribution has exhibited any significant change to warrant an inspection. The methodology is applied to a laboratory tested reinforced concrete column with outliers occurring as the structure is damaged.

6.6.2 Frequency response function based damage detection

As part of the frequency response function (FRF) curvature method utilizing modal parameters, Sampaio, et al. provide the definition of damage as a change in stiffness, where damage is generally measured from changes to one of its dynamic properties of mass, stiffness, or damping [87]. Sampaio, et al. assume damage to be a first order approximation, such that the mass of the structure remains unchanged and thus is a negligible dynamic property of the structure. In addition, changes to damping characteristics of the structure from damage are also ignored. The assumptions specified for the FRF curvature method are intended to observe the structural behavior through the stiffness parameters of the FRF's.

The FRF curvature method presented by Sampaio, et al. is an extension of the mode shape curvature method by Pandy, et al. [88] to all frequencies in the measurement range, i.e., using FRF data instead of limiting observations to mode shapes. A central difference approximation is applied to determine the curvature for each frequency by the following equation:

$$\alpha''(\omega)_{i,j} = \frac{\alpha(\omega)_{i+1,j} - 2\alpha(\omega)_{i,j} + \alpha(\omega)_{i-1,j}}{h^2} \qquad \textbf{(6-85)}$$

where $\alpha_{i,j}$ is the receptance FRF measured at location i for a force input at location j; and h is the distance between measured points $i+1$ and $i-1$.

The absolute difference between the FRF curvature of the damaged and undamaged structure at location i along the chosen frequency range is calculated, for an applied force at point j, by:

$$\Delta\alpha''_{i,j} = \sum_{\omega} \left| \alpha''_d(\omega)_{i,j} - \alpha''(\omega)_{i,j} \right| \qquad \textbf{(6-86)}$$

For several force location cases, the FRF curvature differences are summed directly:

$$S_i = \sum_j \Delta\alpha''_{i,j} \qquad \textbf{(6-87)}$$

The FRF curvature method proposed by Sampaio, et al. utilizes the mode shape curvature method combined with a summation approach for multiple force locations. There are no

significant differences between the FRF curvature method and mode shape curvature method in terms of method of formulation. The primary advantage of the FRF curvature method is that once the FRF's are evaluated via a Fourier transform from the time history response record, individual modes are not required to determine the presence of damage in the system. However, the authors observe a decrease in reliability of detecting damage and estimating damage severity as the range of frequencies is increased in the damage detection process.

Several laboratory-controlled examples are used to generate data and provide a comparison at a simplified level to mode shape based methods for damage detection. In accordance with the work performed by Farrar and Jaruegui on the I-40 bridge over the Rio Grande, an analysis is performed on the bridge deck data [65, 66]. In summary the FRF method was unable to detect damage for the first three damage levels, although damage was identified for the most severe damage scenario.

6.7 MONITORING OF FRP REHABILITATED BRIDGE STRUCTURES

Development of NDE methods capable of accurately locating and quantifying damage in bridge structures arise from the need to maintain and manage a worldwide investment of trillions of dollars in civil infrastructure, which is increasingly compromised by deficiencies in bridge infrastructure related to wear, environmental deterioration and aging structural components, as well as increased traffic loads and changing traffic patterns [89]. In the United States, for example, an estimated 35% of all bridges on the federal inventory are judged to be structurally deficient or functionally obsolete and require repair, strengthening, widening or replacement [89].

Renewal of aging and deteriorating civil infrastructure using fiber reinforced polymer (FRP) composites is rapidly developing into a viable, cost effective option, with applications ranging from seismic retrofit of columns to the strengthening of girders and slabs. Fiber reinforced polymer composites provide advantages in terms of (1) high stiffness-to-weight ratios, (2) enhanced fatigue life, (3) corrosion resistance, and (4) ease of fabrication [89]. Nonetheless issues pertaining to quality control and overall durability of FRP remain, especially as related to their capacity for sustained performance under extreme and changing environmental conditions subject to load. The implementation of a global NDE methodology such as vibration based damage detection provides a means to assess the influence of factors contributing to deterioration of FRP rehabilitated structures as well as repairs or retrofit schemes implemented on structures.

6.7.1 Strategy for health monitoring of FRP rehabilitated bridge systems

Health monitoring of FRP rehabilitated bridge structures requires three levels of interrogation: the materials level, the components level, and the systems level [90]. The materials level of investigation involves standardized tests of composite materials used for quality assurance and durability estimation by means of tension tests, tests for interlaminar shear strength by short beam method, three point bending for flexural properties, moisture absorption, and determination of glass transition temperature with materials exposed to various environmental conditions.

The components level inspection assesses defects and their respective effects on the rehabilitation and influence on the performance of the rehabilitated bridge structure. Here local NDE methods are employed such as ultrasonic testing, thermography, and shearography in conjunction with a visual inspection and acoustic impact or "tap" testing of the FRP rehabilitation.

At the systems level, a global NDE procedure is utilized to evaluate the overall structural capacity and identify local damage areas for the components level inspection. The objective of the systems level inspection is three-fold:

(1) Evaluate the global structure to determine the current performance level of the structure and the effectiveness of rehabilitation;

(2) Identify locations and estimate the severity of damage for purposes of further interrogation using local NDE techniques; and

(3) Validate global system performance prediction, where the prediction is based upon results of the components and materials level investigation.

The systems level phase of the health monitoring strategy is essential in incorporating the impact of materials degradation and defects in the performance of the FRP rehabilitated bridge structure and determining the existing state of the bridge relative to predictions. The illustration in Figure 6.6 provides a synopsis of the integration of a global damage detection procedure into the health monitoring of FRP rehabilitated structures.

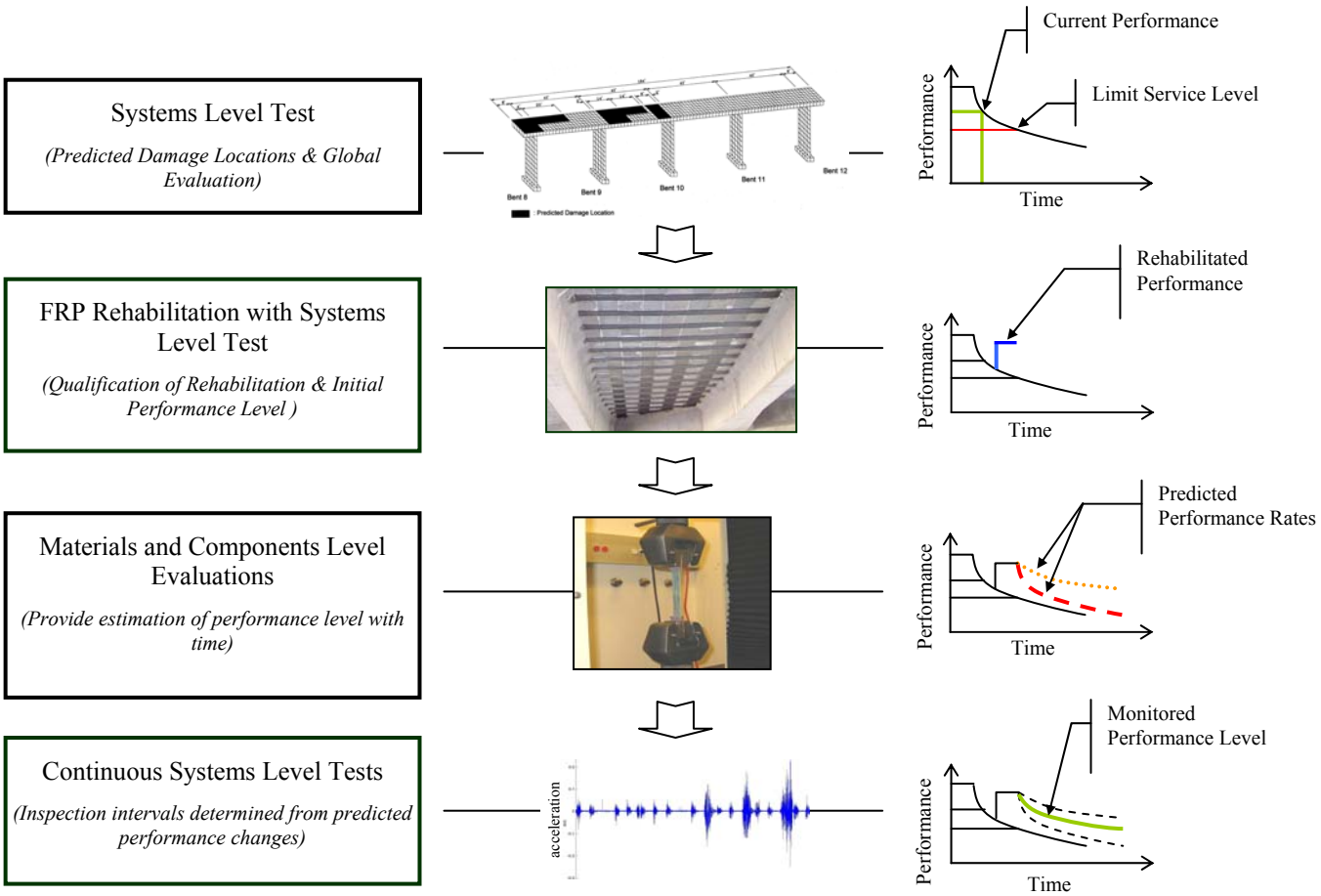

Figure 6.6: Strategy for health monitoring of FRP rehabilitated structures

6.7.2 Damage detection methods for FRP rehabilitated bridge systems

Evaluation of FRP rehabilitated structures requires three separate analyses at the systems, components, and materials level. Since this chapter emphasizes the global nondestructive damage evaluation methodologies available for health monitoring of bridge structures, an evaluation of damage detection methods has been presented to determine which procedures qualify as potential systems level methodologies for monitoring of FRP rehabilitated bridge systems. Attractive features of a systems level inspection of an FRP rehabilitated structure are congruent with the requirements for damage detection procedures intended for most structures.

It is useful to understand the general verification procedure for a global damage detection strategy in particular the applications. As shown in Figure 6.7, verification of a damage detection strategy occurs in three stages with an intended structure and proposed level of damage detection: 1) a numerically simulated model with signal noise and reduced measurements; 2) a laboratory experiment with signal noise and reduced measurements, and 3) field validation on a real structure.

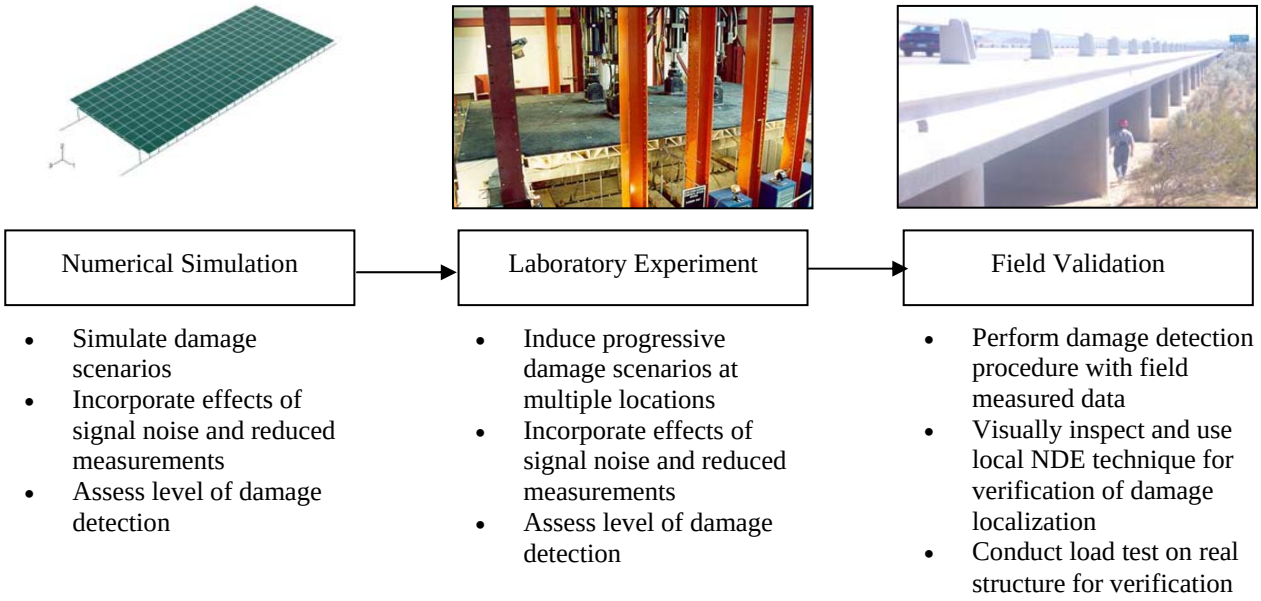

Figure 6.7: Sequential validation of global NDE procedure

Unfortunately, most proposed damage detection strategies rarely display these three stages of validation, and few contain field applications reflecting the intended level of nondestructive evaluation (i.e., Level 1, 2, 3, or 4). In Table 6.3 the advantages and disadvantages of features for damage detection reviewed in this chapter are summarized. These global NDE algorithms are developed with the intent to identify changes in a system regardless of improvement or degradation. Since degradation is a more critical aspect to the safety of structures, the severity of damage is typically estimated by defining damage as a loss in stiffness, with the inherent assumption that damage affecting the performance of a structure is realized by losses in stiffness.

Table 6.3: Advantages and disadvantages of damage detection strategies

Technique	Advantage	Disadvantage
Frequencies	• Capable of damage identification • Simplest derived modal parameter	• No spatial information provided by frequency measurements • Qualitative damage severity estimation • Low sensitivity to damage
Mode Shapes	• Contains spatially related information, thus damage location is readily available	• Large number of measurement locations required to accurately characterize mode shapes
Matrix Update Methods (Matrix Optimization)	• Resolving system matrix provides damage location and severity	• Most precise solution is an approximation since all modes of a structure cannot be measured
Artificial Neural Networks	• Able to solve complex problems difficult to model and explain by classical mathematics • Flexibility available in feature used for damage detection	• Uncertainty in assigning weights to connections between layers • Training of networks requires prior knowledge of damage mechanisms in the system • Potential convergence instability with large quantities of data
Genetic Algorithms	• Capable of solving large complex problems for optimal solutions • Optimization begins from a population unlike traditional methods which initiate from a single point • Operates in the presence of uncertainty and insufficient information	• Dependent on validity of the objective function • Appropriate size of population, crossover rate, and mutation rate not clearly defined for structural problems

6.7.2.1 Damage detection summaries

In this section the damage detection methods reviewed in this chapter are compared in Tables 6.4 through 6.9. They show the positive and negative aspects during the validation portion of each method, (i.e., whether consideration for signal noise or reduced measurements exists, use of field measured data, classification level of the global damage detection procedure, etc.).

Although no specific damage detection procedure displays a significant advantage, it is observed that those methods utilizing mode shapes are the most developed in terms of displaying the ability to identify, locate, and estimate the severity of damage. In particular, the method by Stubbs, et al. is arguably the most developed methodology available for damage detection with several field applications verified and third party reviews conducted on the quality of the methodology [34, 35, 65, 66, 67]. In addition, it is the only reviewed methodology that applies a statistical model to determine if its

condition indicator or damage index is statistically significant, in addition to estimating the reliability or probability of failure of the system. However, given its applications and advantages, the minimum required amount of measurements and the effect of signal noise are not addressed; nor has the application of the system reliability evaluation procedure been validated on real structures.

It is important to note that a number of methodologies reviewed in this chapter demonstrate the ability to identify, locate, and estimate the severity of damage in structures using numerical simulations. However, the absence of field validations and impacts on their performance due to signal noise limits their potential for damage detection of FRP rehabilitated bridge structures. Machine learning techniques continue to receive a significant amount of research in the area of structural damage detection, also showing ability to identify, locate, and estimate damage severity. Training of the network or the quantity of input information necessary for GA and ANN, however, are still unresolved issues with no methods demonstrating robustness with field measured data.

Table 6.4: Frequency based damage detection methodologies

Damage Detection Method	Positive Aspects	Negative Aspects
Bicanic and Chen [45]	• Back calculation of mode shapes • Frequencies only for damage localization	• Unable to identify or locate damage with signal noise levels of 0.5% and 2.0% • No validation with field structure • No examination with reduced measurements
Contursi, Williams, and Messina [46, 47, 48, 49]	• Capable of damage identification and localization with frequencies alone	• Requires 10 to 15 modes for accurate damage detection • Computationally expensive • No examination of signal noise • No validation with field structure
Hassiotis [56, 57]	• Only frequencies required to evaluate stiffness matrix of the system • Capable of damage identification and localization • Able to identify damage with 0.8% signal noise	• Unable to determine damage severity of structure • Stiffness matrix remains incomplete • Dependent on the number of sensors and sensor locations (i.e., requires large amount of data for improved accuracy) • No validation with real structures
Ray and Tian [50]	• Increased frequency sensitivity to damage by change in control gain • Capable of damage identification	• Tailored to smart structures, not applicable to existing structures • Sensitivity to damage dependent on vicinity of sensor and actuator • No validation with real structures

Table 6.5: Damage detection utilizing mode shapes

Damage Detection Method	Positive Aspects	Negative Aspects
Law, Shi, and Zhang [72, 73, 74]	• Capable of identifying, locating, and quantifying damage • Contains modal expansion procedure addressing reduced measurements • Able to expand additional modes from 2-3 experimentally measured modes	• Presence of signal noise results in severity estimate errors from 0% to 30%. • No field evaluation on bridge structure
Stubbs [34, 35]	• Capable of identifying, locating, and quantifying damage • Applies statistical model (hypothesis testing) to differentiate between damaged and undamaged areas • Damage characterization using individual mode shapes • Field application and verification of methodology on reinforced concrete bridge structures • Procedure for acquiring baseline modal properties of existing structure • Method for evaluation of system reliability • Most developed and applied damage detection procedure	• Dependent on experimentally calibrated numerical model • Valid only for damage severity levels up to 30% • Effect of signal noise or not explicitly addressed • No definition of required minimum number of mode shapes for accurate damage characterization
Kim and Stubbs [71]	• Capable of identifying, locating, and quantifying damage • Able to use individual mode shapes • Damage located and sized without need to solve system of equations • Improved approximation of damage severity compared to previous method	• No field validation studies • Presence of signal noise not addressed • No definition as to minimum number of mode shapes for accurate damage characterization

Table 6.6: System matrix based damage detection methodologies

Damage Detection Method	Positive Aspects	Negative Aspects
Abdalla et al. [53]	• Capable of identifying and locating damage	• Unreliable severity estimations with errors between 5% and 30% • Presence of signal noise not addressed • Susceptible to inaccuracies with reduced measurements • No field validation studies
Escobar [54]	• Transformation to rigid body modes reduces computational costs • Capable of identifying, locating, and quantifying damage	• Increases in signal noise results in increase of severity estimate • Accurate damage detection requires a minimum of 8 modes • Decrease in damage severity estimate with decrease in number of measured modes • Assumes stiffness matrix of structure is readily available from analytical model • No field evaluation studies
Sivico [58]	• Capable of identifying, locating, and quantifying damage • Evaluates changes in damping	• Computationally expensive • Minimum detectable reduction in stiffness and/or damping is 10% • Number of actuators or multiple single input systems must be same as degrees of freedom in problem • No field evaluation studies
Park and Reich	• Capable of damage identification, localization and quantification • Flexibility determined directly from modal identification procedure, no addition computation necessary • Identification and localization of damage using field data • High eigenvalues in flexibility base methods correspond to dominate, measurable low frequency modes • Greater sensitivity to damage	• Does not address the effects of signal noise and reduced measurements • No severity validation provided from field data application

Table 6.7: Damage detection utilizing artificial neural networks

Damage Detection Method	Positive Aspects	Negative Aspects
Zang and Imgruen [80, 81]	• Capable of identifying and locating damage • Damage localization in the presence of 5% signal noise • FRF data reduction to reduce computational costs	• Unable to estimate damage severity • Increasing the number of principal components in analysis does not improve results because of increased susceptibility to signal noise
Barai and Pandey [82]	• Capable of damage identification • TDNN procedure capable of identification with incomplete information • Application to numerically simulated steel bridge	• Incapable of damage localization or severity estimation
Hung and Kao [83]	• Use neural network for system identification approach to acquire characteristics of undamaged and damaged states of structure • Capable of damage identification and localization • Able to detect damage scenarios for which specific training has not been implemented	• Systems identification requires displacement, velocity, and acceleration in addition to quantification of input source • In capable of severity estimation • Signal noise and reduce measurements not addressed

Table 6.8: Damage detection utilizing genetic algorithms

Damage Detection Method	Positive Aspects	Negative Aspects
Chou and Ghaboussi [78]	• Capable of damage identification and localization • Does not require solving system of equations in finite element method • Uses measured displacements without the need for additional processing	• Increase in signal noise increase scatter of severity estimation • No application to real structures
Mares and Surace [84]	• Capable of damage identification, localization and quantification • Successful damage identification and localization in 5% signal noise	• Damage severity estimation requires 8-10 modes of structure • No application to real structures
Hao and Xia [85]	• Flexibility in terms of accuracy of FEM • Capable of damage identification, localization, and quantification	• Signal noise in measurements results in false-positive indications • Underestimates damage severity • Weighting factors for contribution of frequencies and mode shape measurements not clearly defined

Table 6.9: Other damage detection methodologies

Damage Detection Method	Positive Aspects	Negative Aspects
Fugate (Time History Analysis) [86]	• Uses time history data to determine damage presence, requires no additional processing • Statistics used as indicators of change to structure	• Incapable of damage localization or severity estimation • Does not detect damage, rather identifies only a change in the structural behavior
Sampaio, et al. [87]	• Uses FRF data directly from structure's dynamic test	• Decrease in reliability of damage identification, localization and severity estimation as range of frequencies is increased • Low sensitivity to damage

6.8 SUMMARY

In this chapter an overview of current damage detection algorithms has been presented in the context of health monitoring of structural systems. Damage detection methods are presented examining changes in modal parameters, specifically natural frequencies and mode shapes. In addition, optimization methods for the stiffness matrix of the structure are investigated and a methodology for dynamically measured flexibility matrix is also reviewed. Due to the complexity of large civil structures and the susceptibility of measured modal data to signal noise, damage detection algorithms in the form of optimization problems and decision-making programs have evolved, employing machine learning techniques, namely genetic algorithms and artificial neural networks.

Other available methods include examination of time histories and frequency response functions, which avoid the need for experimental modal analysis to extract modal parameters from vibration test data. The shear volume of damage detection algorithms makes it difficult to include all literature addressing damage detection of structural systems using vibration properties. The intent of this chapter has been to provide an overview of the current and developing damage detection algorithms available and provide a schematic for how a global nondestructive damage detection procedure is integrated with a structural health monitoring approach for FRP rehabilitated bridge structures.

Depending on the vibration properties and tools available for structural health monitoring, appropriate damage detection is critical to the level and quality of evaluation conducted on the structure. Important considerations when selecting damage detection methodologies are the following:

(1) Level of damage detection desired: Level 1, Level 2, Level 3, or Level 4. Currently no damage detection methodologies have been observed in the literature that incorporate a strategy for evaluation of the remaining useful life of a structure.

(2) Demonstrated capability of the damage detection level via numerical simulation in the presence of signal noise and reduced measurements.

(3) Demonstrated capability of the damage detection level via experimental validation in the laboratory in the presence of signal noise and reduced measurements.

(4) Validation of the damage detection algorithm to field data of large civil structures.

Certainly no one damage detection algorithm suits the needs of all structures; rather it would behoove the user to select a methodology based on the above four criteria. The abundance of damage detection algorithms available and uncertainty involved in applications necessitates comparisons of methodologies to a standardized set of vibration data to qualify the damage detection method for use on a specific type of structure.

For instance, damage detection methodologies for use on reinforced concrete bridge structures are validated from a blind test using field measured vibration data for various damage scenarios on the bridge structure, similar to the work by Farrar and Jauregui [65, 66]. The following criteria are established as a quality indicator of the damage detection method:

> Category 1: Level of damage detection according to the baseline vibration data without the introduction of signal noise and the effect of reduced measurements: Level 0, 1, 2, 3, or 4 is assigned.
>
> Category 2: Level of damage detection using base line vibration data in the presence of signal noise. Signal noise introduced into the data is evaluated at various levels (i.e., 1%, 5%, and 10%) for a fixed number of measurements. The signal noise level is noted with the level of damage detection provided, e.g., Level 0, 1, 2, 3, or 4 at 5% signal noise.
>
> Category 3: Level of damage detection with reduced measurements. This category is more relevant to damage detection algorithms utilizing changes in modal properties or where a large number of measurements are required. Here the methodology is evaluated based on a fixed number of measurements, e.g., 3, 5, 10. The quantity of measurements is established based on the number of measurements typically available from field measurements of a structure.

Table 6.10 provides an example of the categorization described above, where the number of measurements are reduced and analyzed in conjunction with the presence of signal noise in the structure. For each combination of measurement number and signal noise presence, a level of damage detection capability is assigned.

Table 6.10: Comparison of damage detection methods

Damage Detection Method	Number of Measured Modes											
	3				5				10			
	0%	1%	3%	5%	0%	1%	3%	5%	0%	1%	3%	5%
Method A	2	1	0	0	3	2	1	1	3	3	3	2
Method B	2	2	1	1	3	3	2	2	3	3	3	3

6.9 CHAPTER 6 REFERENCES

26. Sikorsky, C. "Development of a Health Monitoring System for Civil Structures Using a Level IV Non-Destructive Damage Evaluation Method." Structural Health Monitoring 2000. Proceedings of the 2nd International Workshop on Structural Health Monitoring, Stanford University, Stanford, CA. September 8-10, 1999. pp. 68-81.

27. Aktan, A.E., Catbas, F.N., Grimmelsman, K.A., and Tsikos, C.J. "Issues in Infrastructure Health Monitoring for Management." Journal of Engineering Mechanics, Vol. 126, No. 7, July 2000. pp. 711-724.

28. Farrar, C.R., Doebling, S.W., and Nix, D.A. "Vibration-based Structural Damage Identification." Philosophical Transactions: Mathematical, Physical, & Engineering Sciences. Vol. 359. No. 1778. 2001. pp. 131-149.

29. Farrar, C.R., Duffey, T.A., Doebling, S.W., and Nix, D.A. "A Statistical Pattern Recognition Paradigm for Vibration-Based Structural Health Monitoring." Proceedings of the 2nd International Workshop on Structural Health Monitoring, Stanford, CA. Sept. 8-10, 1999. pp. 764-773.

30. Aktan, A.E., Farhey, D.N., Helmicki, A.J., Brown, D.L., Hunt, V.J., Lee, K-L. and Levi, A. "Structural Identification for Condition Assessment: Experimental Arts." Journal of Structural Engineering. Vol. 123. No. 12. December, 1997. pp. 1674-1684.

31. Aktan, E., Catbas, N., Turer, A, and Zhang, Z. "Structural Identification: Analytical Aspects." Journal of Structural Engineering. Vol. 124, No.7. July, 1998. pp. 817-829.

32. Rytter, A. "Vibration based inspection of civil engineering structures." Ph.D. Thesis, Department of Building Technology and Structural Engineering, Aalborg University, Denmark. 1993.

33. Farrar, C.R. and Doebling, S.W. "An Overview of Modal-based Damage Identification Methods." Los Alamos National Laboratory Report No. LA-UR-97-2468.

34. Stubbs. N., Park, S., Sikorsky, C., and Choi, S. "A Global Non-Destructive Damage Assessment Methodology for Civil Engineering Structures." International Journal of Systems Science. Vol. 31. No. 11. 2000. pp. 1361-1373.

35. Stubbs, N. and Kim, J-T. "Damage Localization in Structures without Baseline Modal Parameters." AIAA Journal. Vol. 34. No. 8. August, 1996. pp. 1644-1649.

36. Doebling, S.W., Farrar, C.R., Prime, M.B., and Shevit, D.W. "Damage Identification and Health Monitoring of Structural and Mechanical Systems from Changes in Their Vibration Characteristics: A Literature Review." Los Alamos National Laboratory. LA-13070-MS. Issued: May 1996.

37. Salawu, O.S. "Detection of Structural Damage Through Changes in Frequency: A Review." Engineering Structures. Vol. 19. No. 9. 1997. pp. 718-723.

38. Lee, L.S. and Karbhari, V.K. "Dynamic Testing of Bridge Structures." In progress.

39. Green, M. F., "Modal Test Methods For Bridges: A Review." Proceedings of the 13th International Modal Analysis Conference, Nashville, Tennessee. Volume 1. 1995. pp. 552-558.

40. McConnell, K.G. "Modal Testing." Philosophical Transactions of the Royal Society of London Series A-Mathematical, Physical, and Engineering Sciences. Vol. 359. No. 1778. 2001. pp. 11-28.

41. Pickrel, C. R. "A Practical Approach to Modal Pretest Design." Mechanical Systems and Signal Processing. Vol. 13, Issue 2. 1999. pp. 271-295.

42. Salawu, O.S. and Williams, C. "Review of Full-Scale Dynamic Testing of Bridge Structures." Engineering Structures. Volume 17, No. 2. pp. 113-121. 1995.

43. Salawu, O.S. "Assessment of Bridges: Use of Dynamic Testing." Canadian Journal of Civil Engineering. Vol. 24. 1997. pp. 218-228.

44. Farrar, C.R., Doebling, S.W., and Duffey, T.A. "Vibration-Based Damage Detection." LANL report

45. Bicanic, N and Chen, H. "Damage Identification in Framed Structures Using Natural Frequencies." International Journal for Numerical Methods in Engineering. Vol. 40. 1997. pp. 4451-4468.

46. Williams, E.J., Messina, A, and Payne, B.S. "A Frequency-Change Correlation Approach to Damage Detection." Proceedings of the 15th International Modal Analysis Conference, Orlando, Florida. 1997. pp. 652-657.

47. Messina, A., Contursi, T., and Williams, E.J. "Multiple Damage Evaluation Using Natural Frequency Changes." Proceedings of the 15th International Modal Analysis Conference, Orlando, Florida. 1997. pp. 652-657.

48. Contursi, T., Messina, A., and Williams, E.J. "A Multiple Damage Location Assurance Criterion Based on Natural Frequency Changes." Journal of Vibration Control. Vol. 4. No. 5. 1998. pp. 619-633.

49. Messina, A, Williams, E.J., and Contursi, T. "Structural Damage Detection by a Sensitivity and Statistical-Based Method." Journal of Sound and Vibration. Vol. 216. No. 5. 1998. pp. 791-808.

50. Ray, L.R. and Tian, L. "Damage Detection in Smart Structures Through Sensitivity Enhancing Feedback Control." Journal of Sound and Vibration. Vol. 227. No.5. 1999. pp. 987-1002.

51. Adams, R.D., Cawley, P., Pye, C.J., and Stone, B.J. "A Vibration Technique for Non-destructively Assessing the Integrity of Structures." Journal of Mechanical Engineering Science. Vol. 20. 1978. pp. 93-100.

52. Swamidas, A.S.J and Chen Y. "Monitoring Crack Growth Through Change of Modal Parameters." Journal of Sound and Vibration. Vol. 186. 1995. pp. 325-343.

53. Abdalla, M.O., Grigoriadis, K.M., and Zimmerman, D.C. "Enhanced Structural Damage Detection Using Alternating Projection Methods." AIAA Journal. Vol.46, No. 7. July, 1998. pp. 1305-1311.

54. Escobar, J.A., Sosa, J.J., and Gomez, R. "Damage Detection in Framed Buildings." Canadian Journal of Civil Engineering. Vol. 28. No. 1. 2001. pp. 35-47.

55. Baruch, M. and Bar-Itzhack, I.Y. "Optimal Weighted Orthogonalization of Measured Modes." AIAA Journal. Vol. 16, No. 4.

56. Hassiotis, S. "Identification of Damage Using Natural Frequencies and Markov Parameters." Computers and Structures. Vol. 74. 2000. pp. 365-373.

57. Hassiotis, S. and Jeong, J.D. "Identification of Stiffness Reductions Using Natural Frequencies." Journal of Engineering Mechanics. Vol. 121. No. 10. October, 1995. pp. 1106-1113.

58. Sivico, J. V., Rao, V. S. and Koval, L. R. "Health monitoring of bridge like structures using state variable models." SPIE Vol. 3043, 1997. pp. 156-168.

59. Park, K.C. and Reich, G.W. "Structural Damage Detection Using Localized Flexibilities." Journal of Intelligent Material Systems and Structures. Vol. 9. November, 1998. pp. 911-919.

60. Experimental Application of a Structural Health Monitoring Methodology. Park and Reich

61. Park, K.C. and Felippa, C.A. "A Variational Framework for Solution Method Developments in Structural Mechanics." Journal of Applied Mechanics. Vol. 65, No. 1. pp. 242-249.

62. Salawu, O.S. "An Integrity Index Method for Structural Assessment of Engineering Structures Using Modal Testing." Insight. Vol. 39. No. 1. January 1997. pp. 33-37.

63. Salawu, O.S. "Non-Destructive Assessment of Structures Using the Integrity Index Method Applied to a Concrete Highway Bridge." Insight. Vol. 37. No. 11. November, 1995. pp. 875-878.

64. Abdo, M.A.B. and Hori, M. "A Numerical Study of Structural Damage Detection Using Changes in the Rotation of Mode Shapes." Journal of Sound and Vibration. Vol. 251, Issue 2. 2002. pp. 227-239.

65. Farrar, C.R. and Jauregui, D.A. "Comparative Study of Damage Identification Algorithms Applied to Bridge: Part I. Experiment." Smart Materials & Structures. Vol. 7. 1998. pp. 704-719.

66. Farrar, C.R. and Jauregui, D.A. "Comparative Study of Damage Identification Algorithms Applied to Bridge: Part II. Numerical Study." Smart Materials & Structures. Vol. 7. 1998. pp. 720-731.

67. Wang, M.L., Xu, F.L., and Lloyd, G.M "A Systematic Numerical Analysis of the Damage Index Method used for Bridge Diagnostics." Smart Structures and Materials 2000: Smart Systems for Bridges, Structures, and Highways. Proceedings of SPIE. Vol. 3988. 2000. pp. 154-164.

68. Cornwell, P., Doebling, S.W., and Farrar, C.R. "Application of the Strain Energy Damage Detection Method to Plate-like Structures." Journal of Sound and Vibration. Vol. 224. No. 2. pp. 359-374.

69. Park, S., Stubbs, N., Bolton, R., and Choi, S. "Field verification of Damage Index Method in a Concrete Box Girder Bridge via Visual Inspection." Computer Aided Civil and Infrastructure Engineering. Vol. 16. 2001. pp. 58-70.

70. Park, S., Stubbs, N., and Sikorsky, C. "Linkage of Nondestructive Damage Evaluation to Structural System Reliability." Smart Structures and Materials 1997: Smart Systems for Bridges, Structures, and Highways. Proceedings of the SPIE. Vol. 3043. 1997. pp. 234-245

71. Kim, J.-T. and Stubbs, N. "Improved Damage Identification Method Based on Modal Information." Journal of Sound and Vibration. Vol. 252. No. 2. 2002. pp. 223-238.

72. Law, S.S., Shi, Z.Y., and Zhang, L.M. "Structural Damage Detection From Incomplete and Noisy Modal Test Data." Journal of Engineering Mechanics. Vol. 124. No. 11. November, 1998. pp. 1280-1288.

73. Shi, Z.Y., Law, S.S., and Zhang, L.M. "Structural Damage Detection From Modal Strain Energy Change." Journal of Engineering Mechanics. Vol. 126. No. 12. December, 2000. pp. 1216-1223.

74. Shi, Z.Y., Law, S.S., and Zhang, L.M. "Structural Damage Localization From Modal Strain Energy Change." Journal of Sound and Vibration. Vol. 218. No. 5. 1998. pp. 825-844.

75. Adeli, H., Hung, S. Machine Learning – Neural Networks, Genetic Algorithms, and Fuzzy Systems. John Wiley & Sons. 1995.

76. Melhem, H.G. and Nagaraja, S. "Machine Learning and Its Application to Civil Engineering Systems." Civil Engineering Systems. Vol. 13. 1996. pp. 259-279.

77. Barai, S.V. and Pandey, P.C. "Performance of the Generalized Delta Rule in Structural Damage Detection." Engineering Applications of Artificial Intelligence. Vol. 8. No. 2. 1995. pp. 211-221.

78. Chou, J.-H. and Ghaboussi, J. "Genetic Algorithm in Structural Damage Detection." Computers and Structures. Vol. 79. No. 14. 2001. pp. 1335-1353.

79. Adeli, H. "Neural Networks in Civil Engineering: 1989-2000." Computer-Aided Civil and Infrastructure Engineering. Vol. 16. 2001. pp. 126-142.

80. Zang, C. and Imregun, M. "Structural Damage Detection Using Artificial Neural Networks and Measured FRF Data Reduced Via Principal Component Projection." Journal of Sound and Vibration. Vol. 242. No. 5. 2001.

81. Zang, C. and Imregun, M. "Combined Neural Network and Reduced FRF Techniques for Slight Damage Detection Using Measured Response Data." Archive of Applied Mechanics. Vol. 71. 2001. pp. 525-536.

82. Barai, S.V. and Pandey, P.C. "Time-delay Neural Networks in Damage Detection of Railway Bridges." Advances in Engineering Software. Vol. 28. 1997. pp. 1-10.

83. Hung, S-L. and Kao, C.Y. "Structural Damage Detection Using the Optimal Weights of the Approximating Artificial Neural Networks." Earthquake Engineering and Structural Dynamics. Vol. 31. 2002. pp. 217-234.

84. Mares, C. and Surace, C. "An Application of Genetic Algorithms to Identify Damage in Elastic Structures." Journal of Sound and Vibration. Vol. 195. No. 2. 1996. pp. 195-215.

85. Hao, H. and Xia, Y. "Vibration-based Damage Detection of Structures by Genetic Algorithm." Journal of Computing in Civil Engineering. Vol. 16. No. 3. July, 2002. pp. 222-229.

86. Fugate, M.L., Sohn, H., and Farrar, C.R. "Vibration-Based Damage Detection Using Statistical Process Control." Mechanical Systems and Signal Processing. Vol. 15, No. 4. 2001. pp. 707-721.

87. Sampaio, R.P.C., Maia, N. M. M., and Silva, J. M. M. "Damage Detection Using the FRF Curvature Method." Journal of Sound and Vibration. Vol. 226. No. 5. 1999. pp. 1029-1042.

88. Pandey, A. K., Biswas, M., and Samman, M.M. "Damage Detection from Changes in Curvature Mode Shapes." Journal of Sound and Vibration. Vol. 145. No. 2. 1991. pp. 321-332.

89. Karbhari, V.M and Zhao, L. "Use of Composites for 21st Century Civil Infrastructure." Computer Methods in Applied Mechanics and Engineering. Vol. 285. 2000. pp. 433-454.

90. Lee, L.S., Karbhari, V.M, and Sikorsky, C. "Field Monitoring and Degradation Assessment of FRP Bridge Rehabilitation Using Level IV NDE Techniques." First International Workshop on Structural Health Monitoring of Civil Engineering Structures, Proceedings. Sept. 19-20, 2002.

7.0 DYNAMIC TESTING DEMONSTRATION CASE STUDY

7.1 INTRODUCTION

This chapter presents a case study pertaining to the use of the Damage Index Method for the identification of changes in the response of an FRP strengthened bridge. The chapter also provides details pertaining to the use of modal testing as a means of nondestructive evaluation.

7.1.1 Description of the bridge

The bridge selected for rehabilitation was built in 1964. The Byron Road Bridge is a 340-foot long, five-span, two-lane highway bridge spanning a canal that is part of the California Aqueduct System. The bridge superstructure consists of five, cast-in-place, continuous, reinforced concrete T-girders, monolithically connected to the bents. The five spans have lengths of 58, 75, 75, 75, and 58 feet, respectively. The 6-1/4 inch thick, reinforced concrete deck spans transversely between the 7.25 foot, center-to-center spaced girders. Expansion is provided in Span #3 in the form of a hinge, whereas the abutments are a fixed diaphragm.

It should also be noted that the bridge was retrofitted in the past decade to resist larger magnitude earthquakes. As part of the retrofit, the top two inches of the concrete deck were removed and replaced with a polymer concrete overlay of equivalent thickness. Unfortunately, cores taken from the bridge deck indicate that the deck may not have been cleaned properly prior to the application of the polymer concrete. Therefore, the structural integrity of the concrete deck and polymer overlay is questionable.

7.1.2 Problem

In the spring of 1998 this bridge experienced punching shear failures in Span #1 and #4 of the bridge superstructure (see example in Figure 7.1). At several other locations in the same region, punching failure was imminent. The punching failures were concentrated in the deck regions where evenly spaced cracks in both the longitudinal and transverse directions were visible on the bridge soffit as shown in Figure 7.2. These cracks showed large amounts of efflorescence, indicating water penetration through the deck. The punching failures occurred approximately three feet from the bridge centerline, which locates them under the left wheel load of the southbound traffic lane, a strong indicator that local wheel loads contributed to the observed failure conditions.

The punching shear cone was approximately fifteen inches in diameter and featured very steep, close to vertical failure planes, not the typically observed inclination of 45° or less. These observations were more indicative of a punching shear failure plane forming along existing transverse and longitudinal flexure cracks, which seemed to be on a five to six inch grid pattern corresponding to the 5.5 inch reinforcement spacing of the #5 deck reinforcement along the

bottom soffit in the transverse direction. In the longitudinal direction, only the bottom reinforcement existed in the deck slab with six #5 bars evenly spaced over the center four feet of the deck between girders. Longitudinal reinforcement was spaced at approximately 9.6 inches, whereas the transverse deck reinforcement was spaced at approximately 5.5 inches.

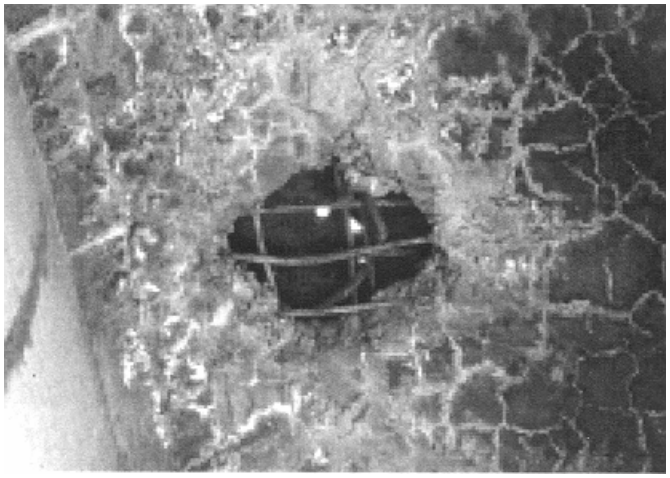

Figure 7.1: Punching shear in deck

Figure 7.2: Typical cracking and damage visible on deck soffit

Detailed analytical investigations showed that the transverse spanning decks first cracked in longitudinal bending along the transverse soffit reinforcement, since longitudinally very little flexural capacity existed and transverse cracks could open widely. Thus the effective width in the transverse direction was limited to the spacing between the transverse cracks, resulting in significant flexure and shear overloads. As a consequence, longitudinal cracks developed and spread along the entire deck length due to the moving nature of the wheel loads. Finally, the

local shear capacity was exceeded over a shear area limited by the existing flexural cracks in both directions, as shown schematically in Figure 7.3. An example from the actual soffit emphasizing the pattern is shown in Figure 7.4. Results from an analysis performed by Seible and Karbhari to verify this failure scenario are shown in Table 7.1 [5].

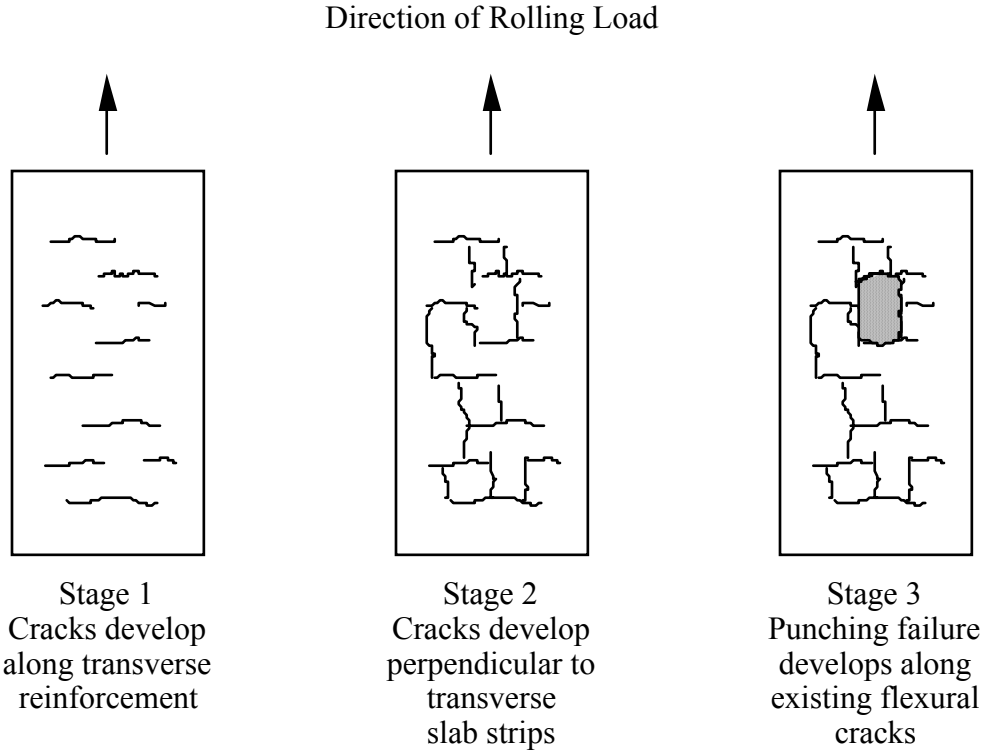

Figure 7.3: Schematic of failure progression

In addition to signs of distress shown in the deck, cracking was also seen in girders, predominantly in the vertical direction. An example of crack patterns on a girder is shown schematically in Figure 7.5. In general, the cracks did not extend through the bottom of the girders, and very little damage was seen on the bottom face of the girders, with the exception of honeycombing apparent in some areas from poor initial construction.

To reverse the effects of deterioration and strengthen the bridge, a rehabilitation scheme using fiber reinforced polymer (FRP) composites was developed by the University of California – San Diego [5]. Based on detailed analysis for punching shear, a pattern of external FRP reinforcement in both the longitudinal and transverse directions of deck soffits was submitted for DWR approval and was then installed by a contractor. However, during the application of the FRP reinforcement, DWR engineers on-site made changes to the prescribed reinforcement pattern. Examples of the use of both impregnated unidirectional fabric and adhesively bonded pultruded strips are shown in Figures 7.6 and 7.7.

Figure 7.4: Crack pattern in soffit showing Stage 3 cracking

Table 7.1: Summary of deck failure mechanisms [5]

Failure Mechanism	Capacity	Demand	Acceptance
Deck Cracking (kN.mm/mm)	13.8	13.3-20.0	NO
Deck Moment Capacity (kN.mm)	22370	20562	OK
Deck Shear Capacity (kN)	30.3	46.3	NO
Punching Shear (kN)	84.1	92.5	NO

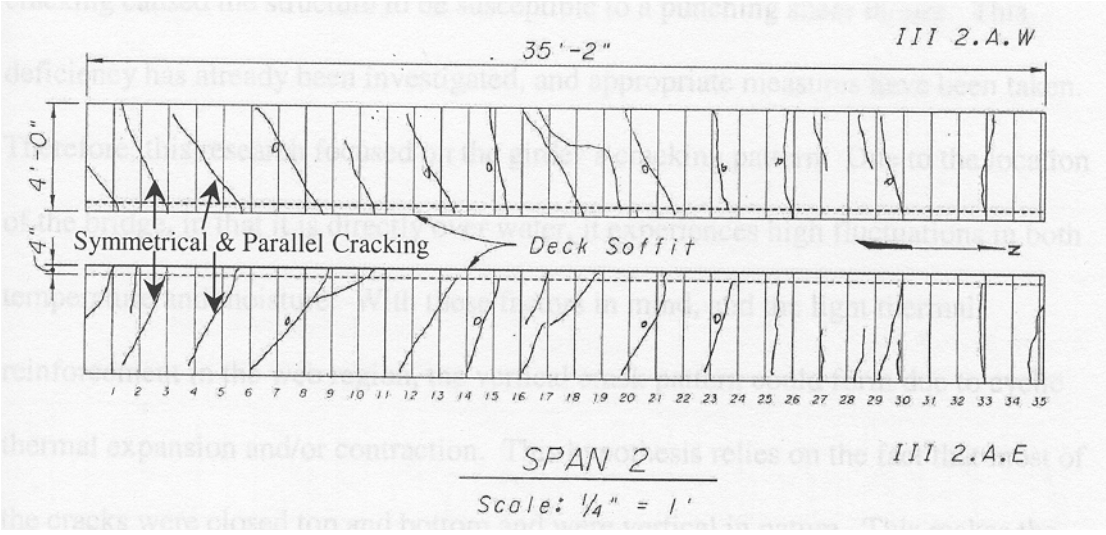

Figure 7.5: Schematic of crack patterns in a typical girder (Center Girder of Span 2 from Pier 2 to Mid Span)

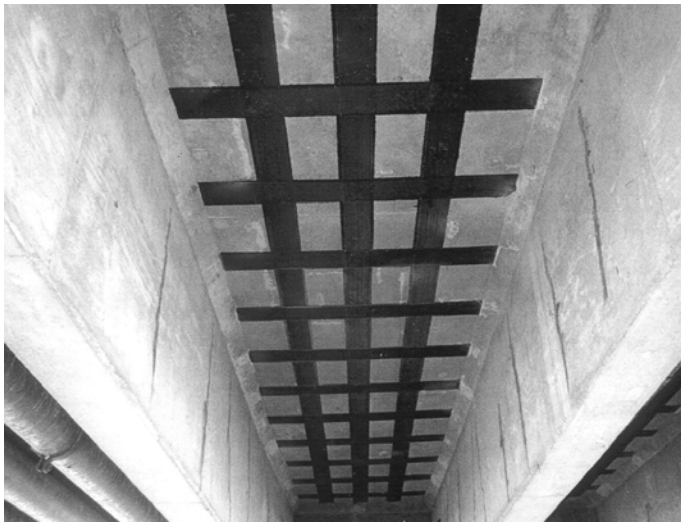

Figure 7.6: Example of strengthening through the use of field impregnated (wet layup) unidirectional fabric

Figure 7.7: Example of strengthening through the use of adhesively bonded pultruded strips

The objective of this chapter is to summarize the sequence of dynamic vibrational tests performed on the Byron Road Bridge to determine the potential changes in the stiffness properties of the bridge, to evaluate the impact of those changes on the strength of the bridge, and to show the sensitivity of the technique in assessing defects and damage. The change in stiffness properties was evaluated for each span of the bridge, as well as for the entire bridge. First, the analytical procedures used to evaluate the structural capacity of the bridge are presented. Second, a description of the process used to extract the necessary modal parameters from the bridge is provided. Third, the results from the dynamic tests conducted at intervals are provided, along with a short discussion of these results. Lastly, several chapter appendices are

included which provide additional information from each and every test performed in the study. Appendix 5 includes notes recorded during the field inspections that followed these tests.

7.2 DESCRIPTION OF ANALYTICAL PROCEDURES

A significant amount of research has been conducted in the area of nondestructive damage evaluation (NDE) using the dynamic properties of a structure [2]. Each of the NDE techniques developed to date can be classified into one of four categories as defined by Rytter [4]:

> Level I Methods, which only identify if damage has occurred;
>
> Level II Methods, which identify if damage has occurred and simultaneously determines the location of the damage;
>
> Level III Methods, which identify if damage has occurred, determines the location of the damage, and estimates the severity of the damage; and
>
> Level IV Methods, which identify, locate, estimate the magnitude of the damage, and evaluate the impact of the damage on the structure.

For this work, damage is defined in terms of a loss of element or global stiffness. This case study utilized a Level IV NDE Method to evaluate the bridge [8]. More specifically, a four-step process was utilized to evaluate the bridge, including a systems identification scheme, an analytical procedure to compute the loss of stiffness, and an approach to link structural demand to the damage indicators. In the last step, structural capacity was evaluated using California bridge specifications [1].

7.2.1 Theory of system identification scheme

The rationale behind the development of the effective values of model parameters can be explained with the aid of Figure 7.8. Suppose a flawed (i.e., damaged) structure (Figure 7.8a) is given with field-measured mode shapes Φ_i^* and eigenfrequencies ω_i^*. Assume that the magnitude of the flaw is small in comparison to a flawless structure.

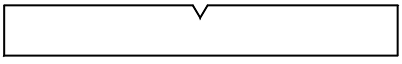

(a) Flawed structure: Φ_i^* , ω_i^*

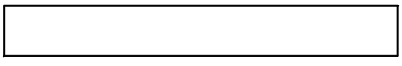

(b) Estimate of flawless structure: Φ_i , ω_i^*

Figure 7.8: Flawed structure and estimate of flawless structure

Suppose that an estimate of the flawless structure can be identified, as shown in Figure 7.8b, using only the frequency information from the flawed structure. Then the identified model with the effective parameters (Figure 7.8b) will have eigenfrequencies close to ω_i^* (in, for example, the least square sense) of the flawed model (Figure 7.8a); but the mode shapes of the two structures will be different in the neighborhood of the flaw. It is also reasonable to assume that the identified elastic properties of the flawless structure are close to those of the flawed structure. The differences in the mode shapes of the identified structure and the measured mode shapes of the existing structure can then be exploited to localize the flaw.

Here, a system identification methodology to identify effective elastic properties of a structure is outlined [7]. Consider a linear skeletal structure with *NE* members and *N* nodes. Suppose k_j^* is the unknown stiffness of the j^{th} member of the structure for which *M* eigenvalues are known. Also, suppose k_j is a known stiffness of the j^{th} member of a FE model for which the corresponding set of *M* eigenvalues are known. Then, relative to the FE model, the fractional stiffness change of the j^{th} member of the structure, α_j, and the stiffnesses are related according to the following equation:

$$k_j^* = k_j\left(1+\alpha_j\right) \tag{7-1}$$

Similarly the fractional mass change of the j^{th} member of the structure, β_j, and the masses are related according to the following equation:

$$m_j^* = m_j\left(1+\beta_j\right) \tag{7-2}$$

The fractional stiffness change and the fractional mass change of *NE* members may be obtained using the following equation [6]:

$$\mathbf{Z} = \mathbf{F}\boldsymbol{\alpha} - \mathbf{G}\boldsymbol{\beta} \tag{7-3}$$

where $\boldsymbol{\alpha}$ is a $NE \times 1$ matrix containing the fractional changes in stiffness between the FE model and the structure; $\boldsymbol{\beta}$ is a $NE \times 1$ matrix containing the fractional changes in mass between the FE model and the structure; **Z** is a $M \times 1$ matrix containing the fractional changes in eigenvalues between the two systems; **F** is a $M \times NE$ stiffness sensitivity matrix relating the fractional changes in stiffnesses to the fractional changes in eigenvalues; and **G** is a $M \times NE$ mass sensitivity matrix relating the fractional changes in masses to the fractional changes in eigenvalues.

The $M \times NE$, **F** matrix can be determined as follows: first, *M* eigenvalues are numerically generated from the initial FE model; second, the stiffness of the first member of the FE model is modified by a known amount; third, the corresponding set of *M* eigenvalues are numerically generated for the modified FE model; fourth, the fractional changes between the *M* initial eigenvalues and *M* eigenvalues of the modified structure are computed; fifth, each component of the first column of the **F** matrix (i.e., the $M \times 1$, **F** matrix) is computed by dividing the fractional changes in each eigenvalue by the magnitude of the modification at member one; and finally, the

$M \times NE$, **F** matrix is generated by repeating the entire procedures for all *NE* members. The $M \times NE$, **G** matrix can be determined in similar manner.

Using the above rationale as a basis, the following 7-step algorithm is proposed to identify a given structure:

1) Select a target structure (e.g. a post-damage state of the structure) for which sufficient eigenfrequencies that can be used to identify the associated flawless structure are available. (Note that the mode shapes of the damaged structure in defining the target structure are ignored.)
2) Select an initial FE model of the structure, utilizing all possible knowledge about the design and construction of the structure.
3) As outlined above, compute the sensitivity matrices of the FE model.
4) As outlined above, compute the fractional changes in eigenvalues between the FE model and the target structure.
5) Solve Equation 3 to estimate fractional changes in mass and stiffness.
6) Update the FE model using the results in Step 5 and Equations 1 and 2.
7) Repeat steps 4~6 until $Z \cong 0$ which indicates that the effective parameters of the structure have been identified.

7.2.2 Analytical evaluation of stiffness properties

In this case study two methods were utilized to evaluate the stiffness changes of the structure: 1) successive system identification, and 2) a direct sensitivity approach [6]. The successive system identification approach consisted of the following steps:

1) Develop a finite element model of the structure including soil-structure interaction;
2) Identify mass and stiffness properties pertaining to the structure at a baseline instant of time;
3) Identify mass and stiffness properties pertaining to the structure at the point of time under consideration; and
4) Determine changes in the stiffness properties of the structure.

The direct sensitivity approach for estimating the changes in the spans included the following steps:

1) Assume that the changes in modal properties are solely attributed to changes in stiffness;
2) Define the average change in stiffness of a single span as the unknown variable (i.e., a_1, a_2, a_3, a_4, a_5);
3) Develop a stiffness-sensitivity matrix (F_{ij}) for the decks of the five spans using the finite element model of the identified structure;
4) Develop fractional changes in eigenvalues (i.e., z_1, z_2, z_3, z_4, z_5) using data; and
5) Compute stiffness changes in deck spans for a five-month time interval using the equation: $\mathbf{Fa} = \mathbf{z}$; where, **F** is the sensitivity matrix, **z** is a matrix containing the fractional changes in eigenvalues, and **a** is a matrix containing the fractional stiffness changes in the spans.

7.2.3 Linking structural demand to the damage indicators

While this technique could locate and quantify damage severity, some means was required to relate this damage information to either structural demand or capacity. In other words, could the bridge continue to support the legal load, given the presence of the damage? Relying on previous work in the area of continuum damage mechanics, a theoretical link between damage indicators and structural demand was formulated.

Let A_0 be the initial area of the undamaged member. After that section has incurred some damage, a certain part of the section is cracked or "lost" [3]. Let us denote the lost area as A. It is important to note the difference between local damage characteristics that can be detected visually, as opposed to an analytical expression for damage. A local damage characteristic such as a crack or delamination can be identified visually. However, that damage characteristic will also cause some change in the dynamic characteristics of the bridge. The analytical expression for damage developed here is an average damage indicator for the area in question. Therefore, this analytical expression for damage can be used to locate a visible sign of damage, or more importantly warn of impending damage that has yet to manifest itself.

Thus, the value $A_0 - A$ can be interpreted as the actual area (or material) of the section. For the case of isotropic damage, cracks and voids are equally distributed in all directions. The damage indicator can be taken as a scalar. Here we define the damage indicator as ω using the following expression:

$$\omega = \frac{A}{A_0} \quad where \quad 0 \le \omega \le 1 \tag{7-4}$$

For an undamaged material, ω = 0, and ω = 1 when the structure has lost all capacity and failed.

In order to determine structural demand, let us subject the section to uniaxial tension or an actual stress σ_a:

$$\sigma_a = \frac{P}{A_0 - A} = \frac{P}{A_0(1-\omega)} = \frac{\sigma}{(1-\omega)} \tag{7-5}$$

where σ is the nominal stress and σ_a is the stress related to the damaged area.

The underlying assumption here is that the strain response of the body is modified by damage only through the actual stress. We also assume that the rate of damage growth is determined primarily by the level of actual stress [3]. Based on these assumptions, the elastic strain of a damaged material is:

$$\varepsilon = \frac{\sigma_a}{E'} = \frac{\sigma}{E(1-\omega)} \tag{7-6}$$

where E' represents the damaged modulus. Reformulating Equation (6) yields:

$$\psi = (1-\omega) = \frac{1}{E}\frac{d\sigma}{d\varepsilon} = \frac{E^{'}}{E} \qquad \textbf{(7-7)}$$

Based on this formulation, damage may be estimated by measuring the elastic response. In previous work, Stubbs et al. demonstrated that relative to the FE model, the fractional stiffness change of the j^{th} member of the structure, α_j, and the stiffnesses are related according to Equation (7-1) from Section 7.2.1 [8]:

$$k_j^* = k_j(1+\alpha_j) \quad for \quad -1.0 \le a \le 0.0 \qquad \textbf{(7-1)}$$

where k_j^* represents the stiffness of the damaged member and k_j is the original undamaged member. It should be noted that for $\alpha = 0$ no damage is present. Therefore:

$$1+\alpha = \frac{k_j^*}{k_j} = \frac{c_j E_j^* I_j^* / L_j^3}{c_j E_j I_j / L_j^3} = \frac{E_j^* I_j^*}{E_j I_j} \qquad \textbf{(7-8)}$$

If we accept the notion that damage is not due to gross changes in geometric properties, then the length (L) of the damaged and undamaged members are numerically equivalent. Note also that if a large section of the bridge had disappeared, similar to a punching shear failure, a visual inspection would be sufficient to locate the damage and therefore no need would exist for an inspection using an NDE technique such as the one presented here.

Therefore, we can reduce Equation (7-8) to:

$$1 + \alpha = \frac{E_j^* I_j^*}{E_j I_j} \qquad \textbf{(7-9)}$$

Substituting Equation (7-7) into Equation (7-9) yields:

$$1+\alpha = \frac{E_j^* I_j^*}{E_j I_j} = (1-\omega) \qquad \textbf{(7-10a)}$$

or

$$\alpha = -\omega \qquad \textbf{(7-10b)}$$

Based on this argument, we may conclude the damage indicator ω, as defined in damage mechanics is the same as the damage severity estimation determined from this modal based non-destructive damage detection scheme [3]. Therefore, the estimation of damage severity (α) may be used to compute the actual load a "damaged" structure experiences. For example, the flexural stress in an undamaged beam element is given by:

$$\sigma = \frac{Mc}{I} \qquad \textbf{(7-11)}$$

and for a damaged element, the flexural stress is determined by substituting Equation (7-11) into (7-5) to yield:

$$\sigma_a = \frac{Mc}{I(1+\alpha)} = \frac{\sigma}{(1+\alpha)} \quad where\ -1.0 \le \alpha \le 0.0 \qquad \textbf{(7-12)}$$

7.2.4 Analytical evaluation of stiffness properties

From the Caltrans Bridge Design Specifications, the dead load moment demand for the bridge deck slab is given by [1]:

$$M_{DL} = \frac{0.8\, w\, S^2}{8} \qquad \textbf{(7-13)}$$

where w is the distributed dead load and S is the effective span distance. Utilizing Equation (7-12) and (7-13) for a damaged member, the flexural moment due to dead load (M^*_{DL}) can be given by:

$$M^*_{DL} = \frac{0.8\, w\, S^2}{8(1+\alpha)} \qquad \textbf{(7-14)}$$

Similar equations can be formulated to determine the live load demand for a damaged structural element (M^*_{LL}):

$$M^*_{LL} = \frac{1.3(S+2)P}{32(1+\alpha)} \qquad \textbf{(7-15)}$$

where P = 16 kips for an HS-20 loading. Note also that Equation (7-15) includes a 30% increase for impact loads. The load combination, Grp(1), used to design the bridge is defined as:

$$Grp(1)^* = 1.3\left[M^*_{DL} + \frac{5}{3}M^*_{LL}\right] \qquad \textbf{(7-16)}$$

A ratio of demand to capacity (D/C) is computed to quickly identify where demand exceeds capacity in flexure as shown in Equation (7-17):

$$\frac{D}{C} = \frac{Grp(1)^*}{\varphi M_u} \qquad \textbf{(7-17)}$$

where the ultimate moment capacity $M_u = [A_s f_y (d - 0.5*a)]$ and $\phi = 0.9$. A demand to capacity ratio of unity or less is deemed acceptable. Note also, that in accordance with Article 3.24.4 of the current design specification, slabs designed for bending moment per the specification are considered acceptable in shear [1].

7.3 SUMMARY OF MODAL ANALYSIS

7.3.1 Description of finite element model

A finite element (FE) model for the Byron Road Bridge was developed to create a baseline model of the bridge. Development of the finite element model as a first step is necessary for at least two reasons. First, a theoretical modal analysis can be performed to determine the theoretical eigenfrequencies and eigenvectors. Second, the instrumentation layout for the modal test can be optimized once the theoretical modal parameters are known.

The schematic of the FE model is shown in Figure 7.9. A total of 4,502 nodes and 3,140 elements were used to model the bridge. As shown in the figure, the concrete deck and girders were modeled using 8-node linear brick elements. The intermediate diaphragms were modeled using 4-node linear shell elements. The internal hinge located in Span #3 was modeled by releasing the moment in the transverse direction. The substructure consisted of two abutments, four piers, and soil-structure interaction. The bents and piers were modeled using 8-node brick elements. The abutments at both ends were also modeled using brick elements. The soil-structure interaction beneath abutments, bents, and piers was modeled using linear elastic spring elements.

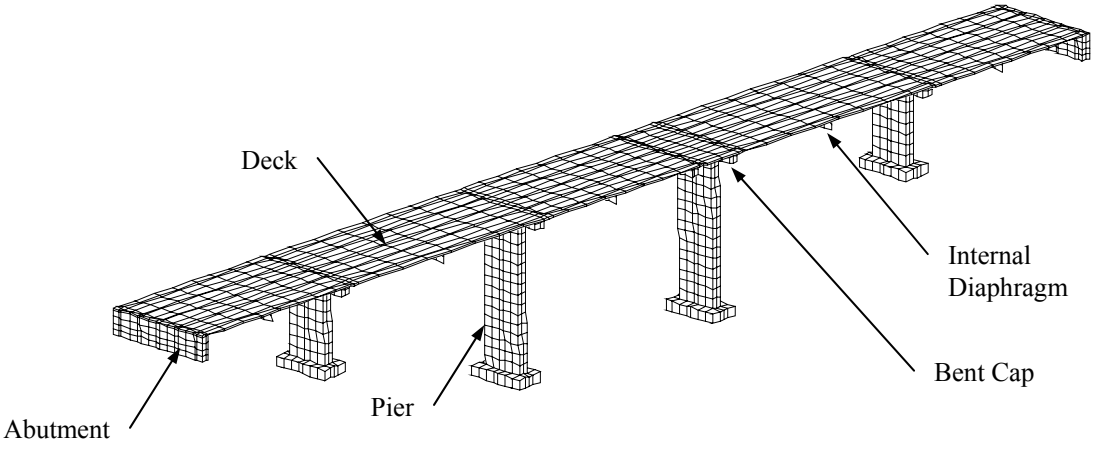

Figure 7.9: Schematic of the finite element model

The damage detection model is shown in Figure 7.10. Here the bridge superstructure was divided into 230 elements to aid in the detection and localization of damage.

It should be noted these elements extended across the width of the deck due to the instrumentation locations. Had data been acquired along a third row midway between the N1 and S1 lines, then the number of damage elements could be doubled. While this data would have helped reduce the area of potential damage, additional resources would have been required to

collect this data, as well. Therefore, a decision had to be made between the data needed and the cost to acquire that data.

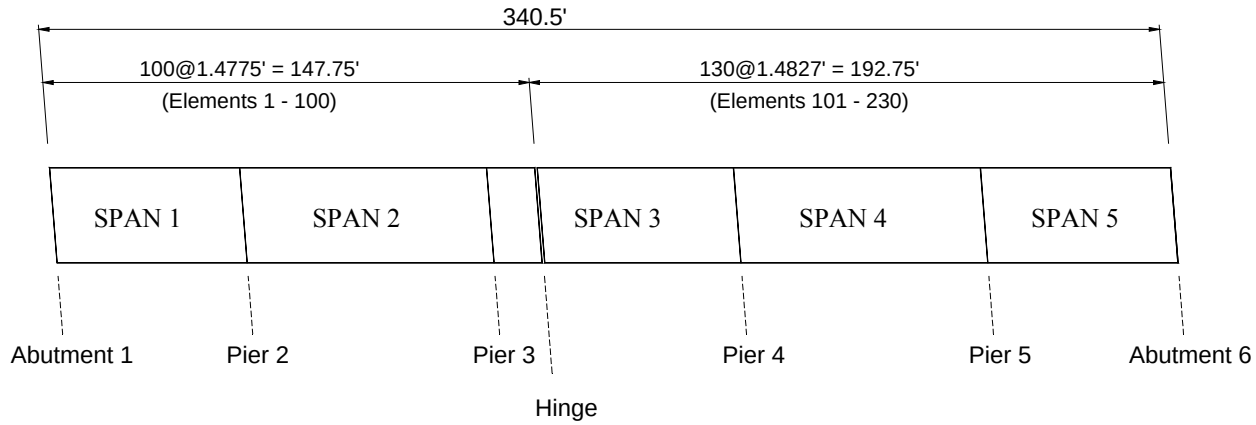

Figure 7.10: Damage detection model

7.3.2 Equipment and sensor layout for modal test

The equipment and sensor layout was identical for all forced excitation tests performed on this bridge. An impact device was used to excite the bridge rather than relying on traffic excitation, since traffic control was required to mount the sensors on the bridge deck. Due to the Aqueduct below, mounting sensors on the bridge soffit and collecting output only data generated by traffic crossing the bridge would have posed significant logistical problems. Kistler 8390A2 triaxial accelerometers were used for all acceleration measurements. These devices were attached directly to response points in orientations matching global Cartesian response directions.

Data from the accelerometers and impact hammer were acquired and processed on a 16-channel SigLab 20-42 DSP analyzer manufactured by DSP Technologies. Time data were transferred to a laptop computer for further analysis. The modal parameters were extracted from the time histories using ME'Scope, a commercially available modal analysis software package.

The sensor layout for the field test is shown in Figure 7.11. Data were collected at forty-four (44) sensor locations on the bridge. Sensors S1-S22 were located on the downstream side of the bridge and N1-N22 were on the upstream side. In addition, data were collected at deck locations above the piers to help identify mode shapes.

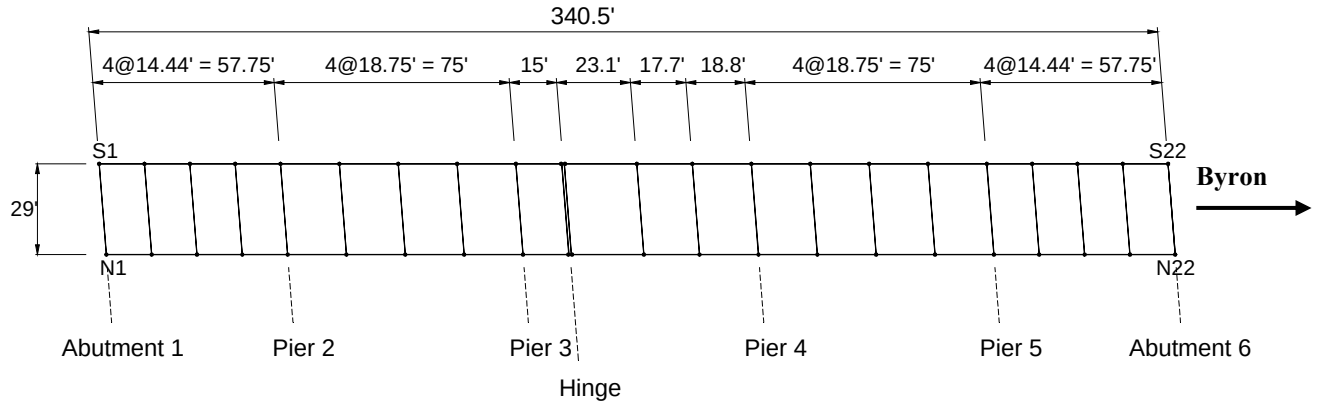

Figure 7.11: Sensor locations

7.4 RESULTS

7.4.1 Overview

Results using the analytical procedures described in Section 7.2 and the modal parameters collected as input (Section 7.3) are presented in this section. The Chapter 7 Appendices 1 – 4 contain the results of the modal analyses and subsequent system identification results. Chapter 7 Appendix 5 is a record of the visual inspections performed in concert with the dynamic field tests.

Modal tests (i.e., field tests) were performed at four times, referenced as T1 (prior to rehabilitation), T2 (about 6 months after T1), T3 (about 1 year after T1) and T4 (about 2 years after T1). Chapter 7 Appendix 1 presents information from modal testing at T1 as follows:

- The experimental frequencies and mode shapes from the T1 test are summarized in Table A1.1 and Figure A1.1.
- The initial values for the parameters of the finite element model are listed in Table A1.2.
- The stiffness-frequency sensitivity matrix of the structure is summarized in Table A1.3. This shows the sensitivity of the structural stiffness to the frequency change. It should be noted these sensitivities were obtained using the structural model defined by the parameters in Table A1.2.
- The mass-sensitivity matrix is tabulated in Table A1.4.
- Table A1.5 shows the rate of convergence of the iterative scheme as the initial finite element model is updated.

- The properties corresponding to the converged model are listed in Table A1.6.

- A measure of the quality of the mode shapes of the finite element model and the field mode shapes is provided in Table A1.7. It should be noted that a MAC value equal to 1.0 is indicative of a strong correlation between the theoretical and experimental mode shapes.

- Figure A1.2 shows the damage localization results using the first bending mode.

Analogous results for the modal analysis and system identification of the structure using the test data from T2, T3 and T4 are shown in Chapter 7 Appendices 2, 3, and 4, respectively.

7.4.2 System identification results

The effective moduli of the entire bridge superstructure between T1 and T4, using the successive systems identification technique are listed in Table 7.2. The trend is a relative increase in stiffness of the deck up to 7.5 percent relative to the T1 reading. Note also the effective decrease for the T4 results, which indicates the strength of the bridge has reverted back to its condition as in T1.

Table 7.2: Results using successive system identification

	T1	T2	T3	T4
Effective Modulus of Superstructure (ksi)	1333	1394	1433	1329
Percent Change from T1	-	+4.6	+7.5	-0.3

7.4.3 Effective span stiffness

The individual deck spans to be investigated in the direct sensitivity approach are identified in Figure 7.10. Also, Figure 7.10 delineates the elements of the sensitivity matrix associated with the deck portion of each span. The fractional changes in eigenvalues for this approach are listed in Table 7.3. The relative stiffness increases by span using the sensitivity approach are summarized in Table 7.4. Note that while the system identification results in Table 7.2 show an increase in stiffness properties through T3, the fractional eigenvalue changes shown in Table 7.3 indicate a decrease in structural stiffness began in T3. This demonstrates the importance of utilizing both mode shape and frequency information to detect and locate damage. As demonstrated by other researchers, frequency data alone is not sufficient to locate and quantify damage.

The fractional loss of stiffness, as related to the baseline (i.e., as-built bridge) is tabulated in Table 7.4. Chapter 7 Appendix Figure A2.3 shows the damage severity, for significant amounts of damage, expressed as a fractional loss of stiffness from the T2 data. The term “significant” is taken here to include a stiffness loss of 40% or greater. The damage severity is plotted as a function of each row of sensors and quantifies specific locations relative to Abutment #1. Similar plots are shown in Figures A3.2 and A4.2 for the T3 and T4 tests. In order to identify a

trend in the data, results from Figures A2.3, A3.3 and A4.3 are plotted in Figure 7.12. This figure indicates a significant amount of damage present in Spans #1 and #2 of the bridge.

Table 7.3: Fractional eigenvalue changes relative to baseline structure

Mode	Fractional Eigenvalue Changes				
	Baseline	**T1**	**T2**	**T3**	**T4**
1	0	-0.1142	-0.0780	-0.0843	-0.1560
2	0	-0.0076	-0.0022	0.0389	-0.0460
3	0	-0.0481	-0.0042	0.0666	-0.1019
4	0	0.1709	0.2080	0.6438	0.3832

Table 7.4: Fractional stiffness loss relative to baseline structure by span

Span	Baseline	Average Fractional Stiffness Loss			
		T1	T2	T3	T4
1	0	-0.0404	-0.0221	-0.0039	-0.0682
2	0	-0.2409	-0.1315	-0.0230	-0.4062
3	0	-0.1180	-0.0644	-0.0113	-0.1989
4	0	-0.1616	-0.0882	-0.0154	-0.2726
5	0	-0.032	-0.0175	-0.0031	-0.0542

– = decrease in stiffness
+ = increase in stiffness

Finally, using the values from Table 7.4 and the technique developed in Section 7.2.3, the capacity of the slab in T1 prior to the rehabilitation and then again in T4 are evaluated. The bridge was rated for HS-20 truck loads with 30% impact. The ability of the slab to resist these loads was evaluated and the results are shown in Table 7.5 and 7.6. In Table 7.6, the steel reinforcement (A_s) was modified to include the equivalent FRP reinforcement added. Table 7.7 shows the results of the evaluation of girder capacity using the T4 results.

Table 7.5: Summary of slab demand / capacity – T1

Span	**α**	**A_s (in^2)**	**S (feet)**	**Group(1) Loads**	**ϕM_u (ft-kips/LF)**	**D/C**
as-built	0.000	0.62	6.68	12.70	13.16	0.96
1	0.040	0.62	6.68	13.23	13.16	1.00
2	0.241	0.62	6.68	16.73	13.16	1.27
3	0.118	0.62	6.68	14.40	13.16	1.09
4	0.162	0.62	6.68	15.15	13.16	1.15
5	0.032	0.62	6.68	13.12	13.16	1.00

Table 7.6: Summary of slab demand / capacity – T4

Span	α	A_s [1] (in^2)	S (feet)	Group(1) Loads	ϕM_u (ft-kips/LF)	D/C (<1.0)
as-built	0.000	0.62	6.68	12.70	13.16	0.96
1	0.068	0.78	6.68	13.62	16.51	0.83
2	0.406	0.78	6.68	21.38	16.51	1.29
3	0.199	0.78	6.68	15.85	16.51	0.96
4	0.273	0.78	6.68	17.47	16.51	1.06
5	0.054	0.78	6.68	13.42	16.51	0.81

[1] effective steel reinforcement

Table 7.7: Summary of girder demand / capacity – T4

Span	α	A_s (in^2)	S (feet)	Group(1) Loads	ϕM_u (ft-kips)	D/C (<1.0)
as-built	0.000	9.36	56.0	1403	2065	0.68
as-built	0.000	9.36	72.0	2038	2065	0.99
1	0.068	9.36	56.0	1505	2065	0.73
2	0.406	9.36	72.0	**3431**	2065	**1.66**
3	0.199	9.36	72.0	**2544**	2065	**1.23**
4	0.273	9.36	72.0	**2804**	2065	**1.36**
5	0.054	9.36	56.0	1483	2065	0.72

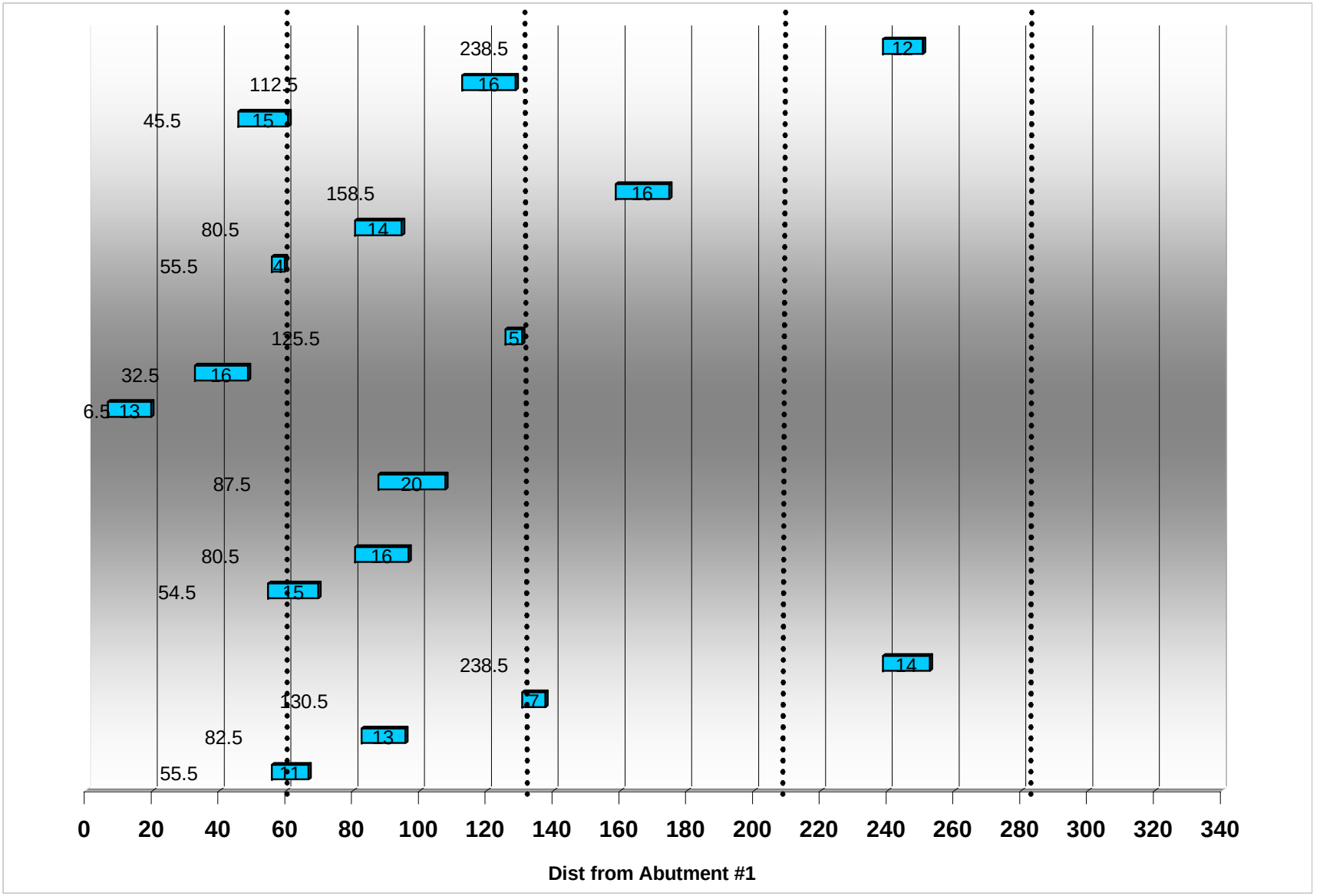

Figure 7.12: Summary of damage locations identified between T1 and T4

7.5 DISCUSSION OF RESULTS

Based on a review of theses results, several statements can be made regarding the condition of the bridge and its ability to support legal loads. First, the experimental frequencies increase between T1 and T3, which indicates a relative increase in stiffness. The T4 test results indicate a decrease in stiffness. This statement is supported by the results in Tables 7.3 and 7.4.

Second, the primary weak link in the system continues to be the girders, which have not been strengthened. Table 7.7 shows demand/capacity (D/C) ratios exceeding 1.0 for certain spans of the bridge, more specifically Spans 2, 3 and 4.

Third, while the overall structural stiffness may have declined between T3 and T4, the results in Table 7.6 indicate the deck slab is able to support the HS-20 load, with the exception of Span #2. The demand/capacity ratio for Span #2 approaches 1.3. It should be noted that the fractional stiffness losses, shown in Table 7.4 are used to compute the demand/capacity ratios. These losses are an average value for the span and are also influenced by single "outlier" values. For example, both rows of sensors were indicating damage in Span #2 as shown in Figures A4.2 and A4.3, which was not the case for the other spans. Note also that the damage indicator (z) in Figure A1.2 approached 5.0 for certain elements; that condition did appear until the T4 results (See Figure A4.2). While there was no indication of immediate collapse, these results should be taken as an indication of a potentially severe problem and not ignored.

It is noted that the results of the analysis were corroborated by visual investigation of the girders and deck soffits. For example, visual inspection of Span #1 and #2 in January 2002 identified patterns of distress and damage growth that corroborated the damage localization results shown in Figure A4.3. Examples of patterns of distress and of damage growth through the time periods of investigation are discussed in Chapter 7, Appendix 5. This case study shows the extreme sensitivity of the method in detecting even isolated defects/damage. It is noted that the sensitivity also depends on sensor placement and mesh size of FEA used in the damage detection step.

Lastly, it is important to note that using frequency data only, the results in Table 7.2 indicated an increase in stiffness after the rehabilitation was completed. However, the results of the damage evaluation using the mode shapes indicated the presence of damage. See Figures A2.2 and A3.2. This observation demonstrates the importance of utilizing the mode shapes to identify and locate damage in a structure and not relying on frequency data only.

7.6 CHAPTER 7 REFERENCES

1. Caltrans (2000). *Bridge Design Specifications*. LFD Version, State of California, Department of Transportation, Sacramento, CA.

2. Farrar, C., and D. Jauregui (1996). "Damage Detection Algorithms Applied to Experimental and Numerical Modal Data from the I-40 Bridge." Report No. LA13074-MS, Los Alamos National Laboratory, Los Alamos, New Mexico.

3. Kachanov, L.M. (1986). *Introduction to Continuum Damage Mechanics***,** Martinus Nijhoff Publishers, Dordrecht, The Netherlands.

4. Rytter, A. (1993). *Vibrational Based Inspection of Civil Engineering Structures*. Ph.D. Thesis, University of Aalborg, Aalborg, Denmark.

5. Seible, F. and V. Karbhari (1998). "Byron Road Rehabilitation Project", Report to the California Department of Water Resources. Report No. SSRP 98/10, University of California San Diego, August.

6. Stubbs, N. and R. Osegueda (1990). "Global Non-destructive Damage Evaluation in Solids." *The International Journal of Analytical and Experimental Modal Analysis*, Vol. 5 (2), pp. 67-79

7. Stubbs, N. and J.T. Kim (1996). "Damage localization in structures without baseline modal parameters." *AIAA Journal*, Vol. 34, pp. 1644-1649

8. Stubbs, N., Park, S., Sikorsky C., and S. Choi (2000). "A Global Non-destructive Damage Assessment Methodology for Civil Engineering Structures." *International Journal of Systems Science*, Vol 31 (11), pp. 1361-1372.

7.7 CHAPTER 7 APPENDICES

APPENDIX 7-1: IDENTIFICATION OF THE EXISTING STRUCTURE AS OF T1

A1.1 Summary of Modal Test

Table 7.A1.1: Measured frequencies

Mode	Frequency (Hz)
1	3.950
2	4.428
3	6.007
4	6.788

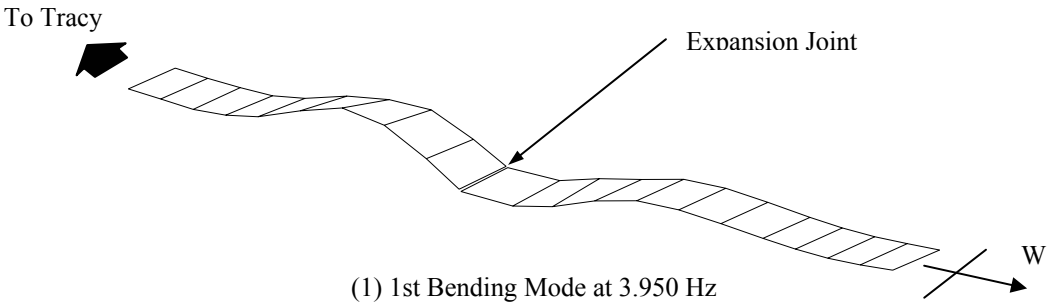

(1) 1st Bending Mode at 3.950 Hz

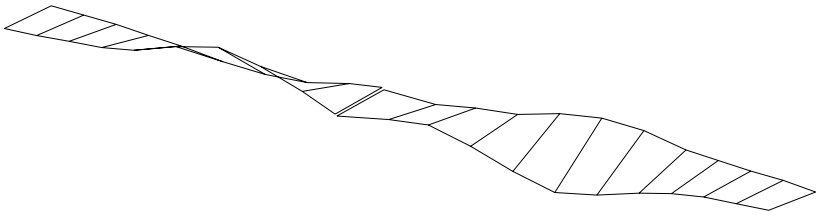

(2) 1st Torsional Mode at 4.428 Hz

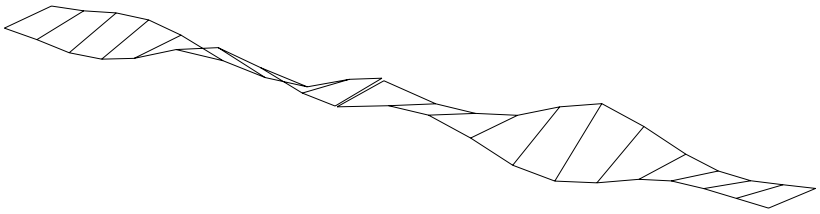

(3) 2nd Torsional Mode at 6.007 Hz

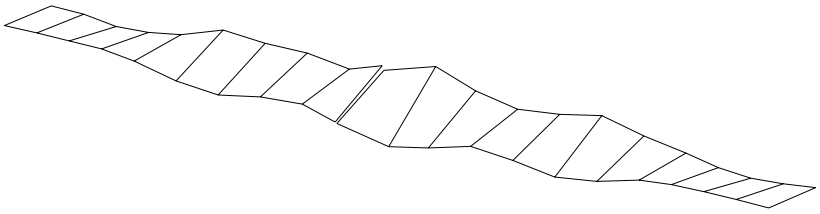

(4) 3rd Torsional Mode at 6.788 Hz

Figure 7.A1.1: Extracted mode shapes (T1)

A1.2 System Identification

Table 7.A1.2: Initial values of material properties of FE model

	Deck and Piers	Springs for Soil-Structure Interaction	
		Pier	Abutment
E (lb/ft2)	360 x 106 (2500 ksi)	-	-
ρ (lb·s2/ft4)	4.7	-	-
k (lb/ft)		32.40 x 106	14.17 x 106

Table 7.A1.3: Stiffness Sensitivity Matrix F

Mode	Deck and Piers	Springs for Soil-Structure Interaction
1	0.9789	0.0252
2	0.8707	0.1489
3	0.9822	0.0208
4	0.9743	0.0300

Table 7.A1.4: Mass Sensitivity Matrix G

Mode	Deck and Piers
1	0.9092
2	0.9089
3	0.9091
4	0.9091

Table 7.A1.5: System identification

Mode	Frequency of Initial FE model	Updated Frequencies (Hz)			Frequency of Target Structure	Error (%)	
		Iter. 1	Iter. 3	Iter. 5		Initial	Final
1	5.707	4.194	4.196	4.197	3.950	44.5	6.2
2	5.889	4.428	4.442	4.445	4.428	33.0	0.4
3	8.376	6.154	6.156	6.157	6.007	39.4	2.5
4	8.520	6.269	6.272	6.273	6.788	25.5	7.6

Table 7.A1.6: Identified material properties of FE model (baseline)

	Deck and Piers	Springs for Soil-Structure Interaction	
		Pier	Abutment
E (lb/ft2)	191.96 x 106 (1333 ksi)	-	-
ρ (lb·s2/ft4)	4.68	-	-
k (lb/ft)		28.62 x 106	12.52 x 106

Table 7.A1.7: Modal assurance criteria (measured vs. FE model)

Mode	1/FE	2/FE	3/FE	4/FE
1/M	0.9657	0.0259	0.0024	0.0001
2/M	0.0026	0.8582	0.5674	0.0050
3/M	0.0069	0.8305	0.8896	0.0013
4/M	0.0002	0.0076	0.0000	0.9072

Note: M ≡ Measured Mode; FE ≡ Finite Element Modes

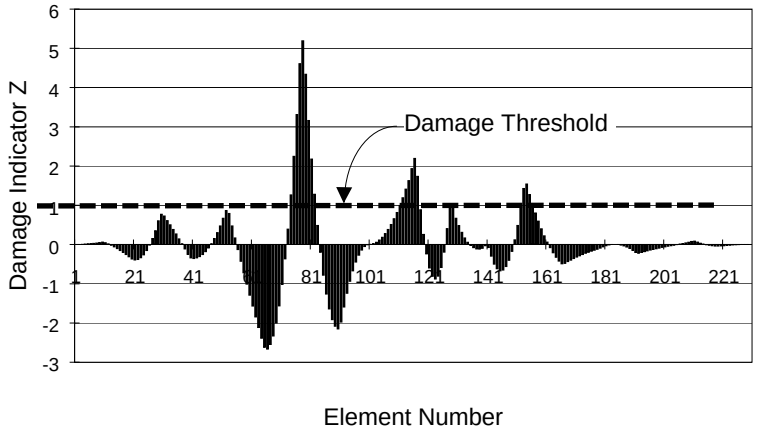

(a) Result using the measurements along sensors S1 - S22

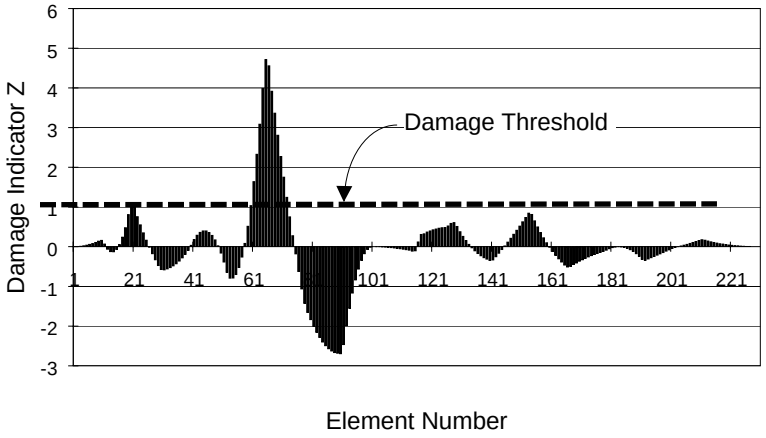

(b) Result using the measurements along sensors N1 - N22

Figure 7.A1.2: Damage localization results using the first bending mode

APPENDIX 7-2: IDENTIFICATION OF THE EXISTING STRUCTURE AS OF T2

A2.1 Summary of Modal Test

Table 7.A2.1: Measured frequencies

Mode	Frequency (Hz)
1	4.030
2	4.440
3	6.144
4	6.895

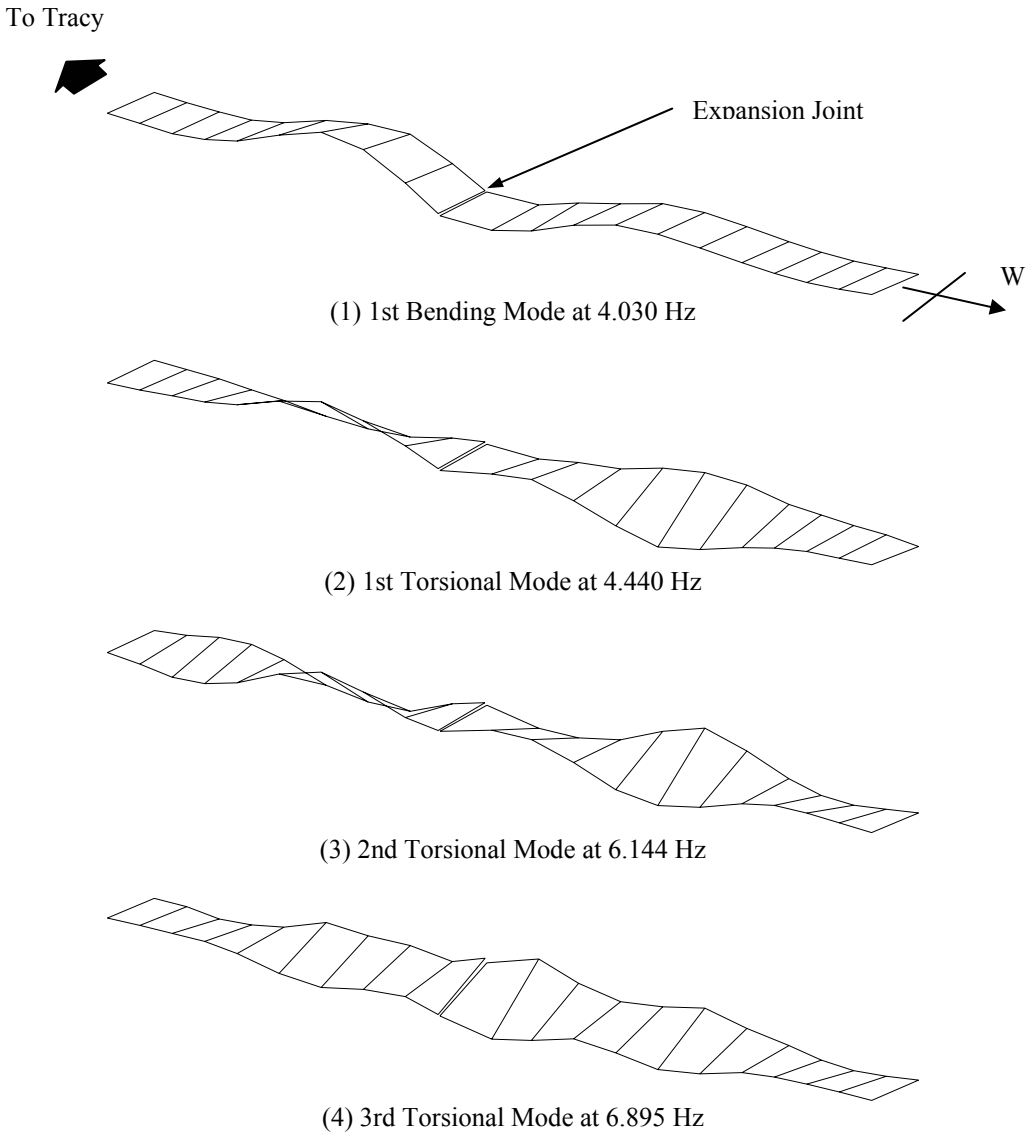

Figure 7.A2.1: Extracted mode shapes (T2)

A2.2 System Identification

Table 7.A2.2: System identification

Mode	Frequency of Initial	Updated Frequencies (Hz)			Frequency of Target	Error (%)	
	FE model	Iter. 1	Iter. 2	Iter. 3	Structure	Initial	Final
1	5.719	4.282	4.280	4.279	4.030	41.9	6.2
2	5.902	4.475	4.461	4.459	4.440	32.9	0.4
3	8.395	6.284	6.280	6.279	6.144	36.6	2.2
4	8.539	6.397	6.392	6.392	6.895	23.8	7.3

Table 7.A2.3: Identified material properties of FE model (baseline)

	Deck and Piers	Springs for Soil-Structure Interaction	
		Pier	Abutment
E (lb/ft2)	200.78 x 106 (1394 ksi)	-	-
ρ (lb·s2/ft4)	4.68	-	-
k (lb/ft)		21.48 x 106	9.394 x 106

Table 7.A2.4: Modal assurance criteria (measured vs. FE model)

Mode	1/FE	2/FE	3/FE	4/FE
1/M	0.9571	0.0571	0.0007	0.0006
2/M	0.0025	0.8420	0.6169	0.0110
3/M	0.0120	0.7886	0.9378	0.0000
4/M	0.0000	0.0163	0.0248	0.9038

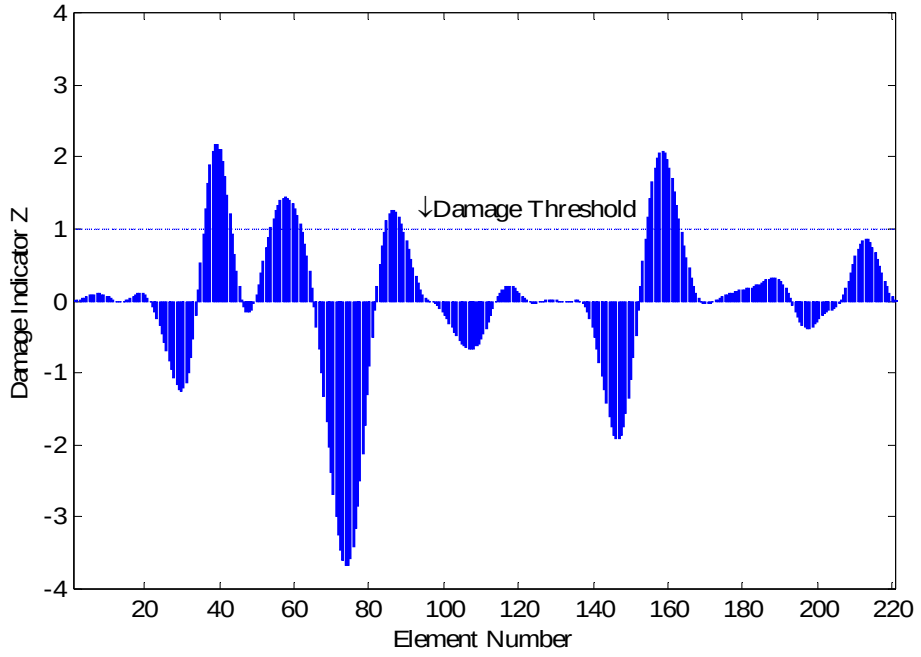

(a) Results using measurements along Sensors S1-S22

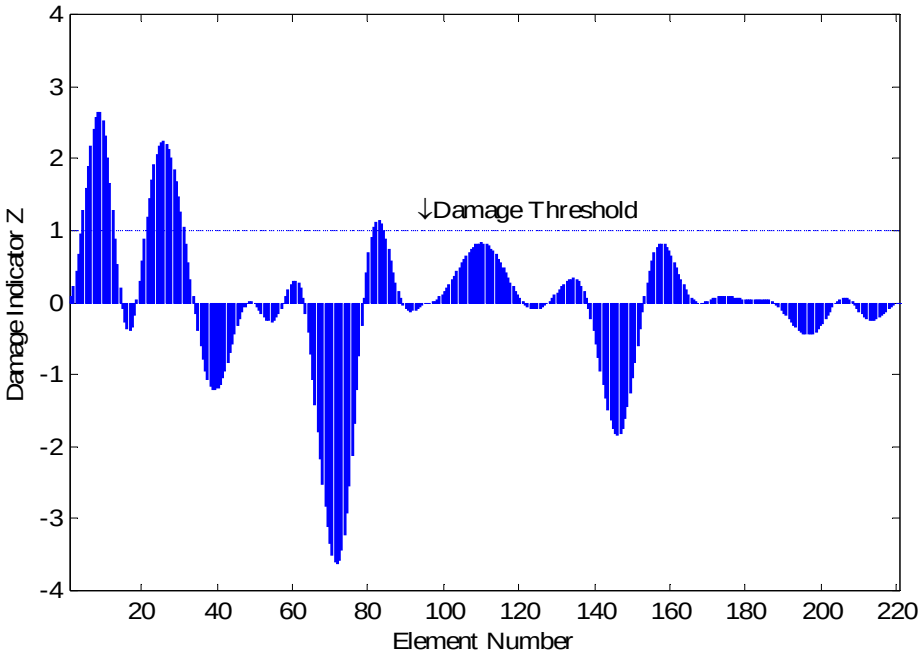

(b) Results using measurements along Sensors N1-N22

Figure 7.A2.2: Damage localization results using first bending mode: T2 (T1 is used as the baseline)

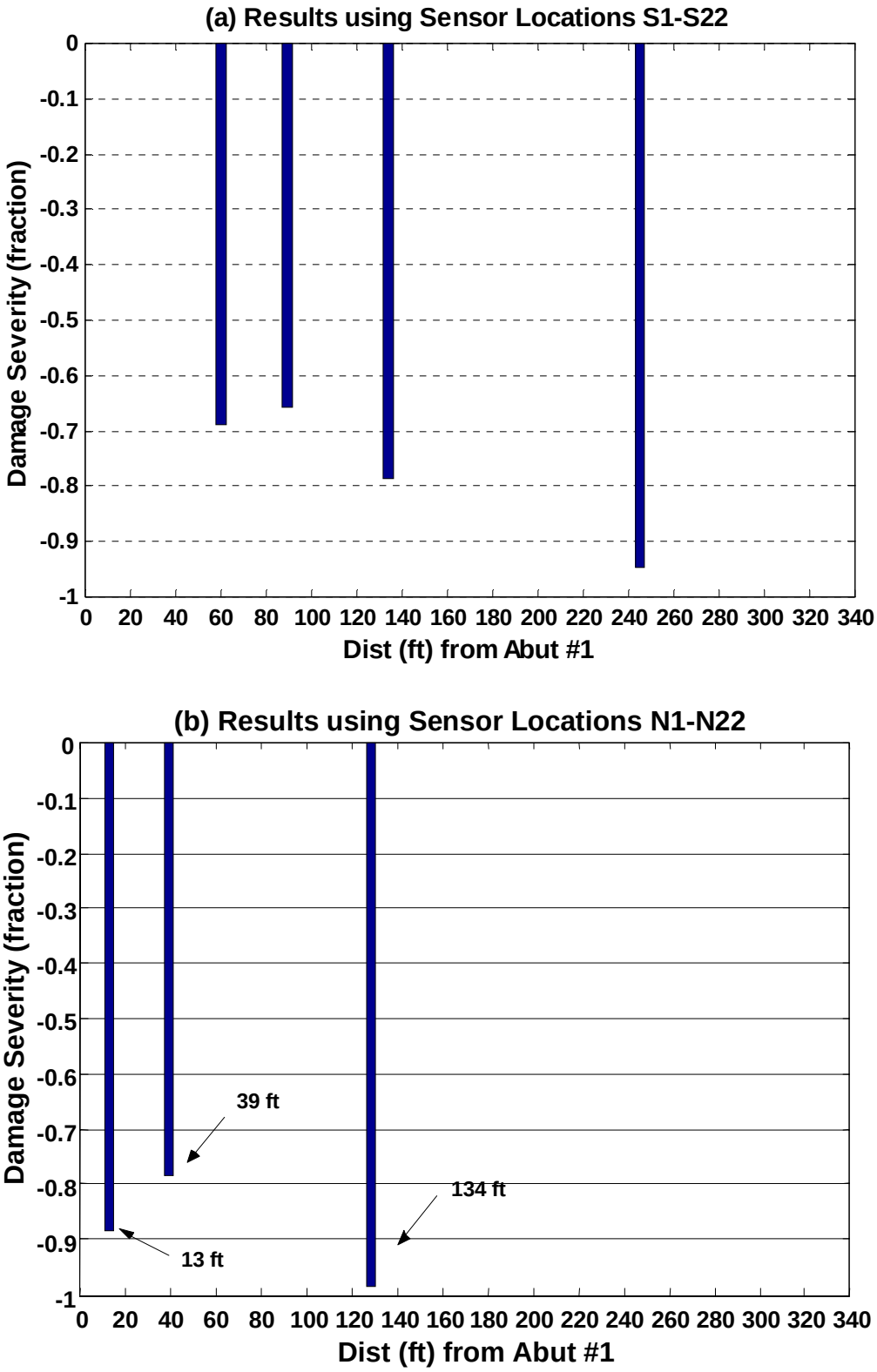

Figure 7.A2.3: Damage severity results using all modes: T2

APPENDIX 7-3: IDENTIFICATION OF THE EXISTING STRUCTURE AS OF T3

A3.1 Summary of Modal Test

Table 7.A3.1: Measured frequencies

Mode	Frequency (Hz)
1	4.072
2	4.501
3	6.249
4	6.985

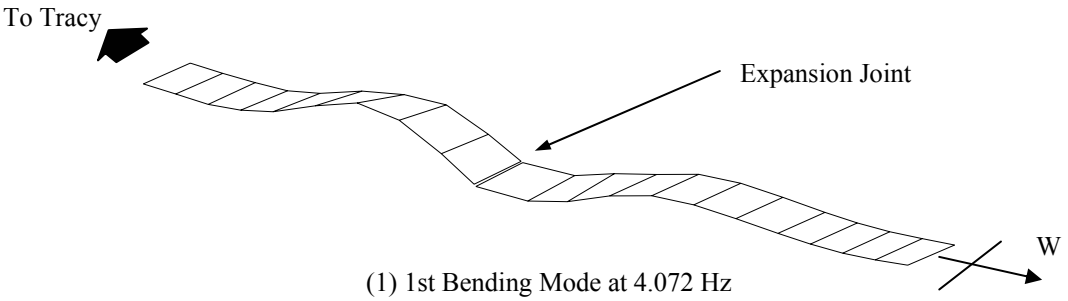

(1) 1st Bending Mode at 4.072 Hz

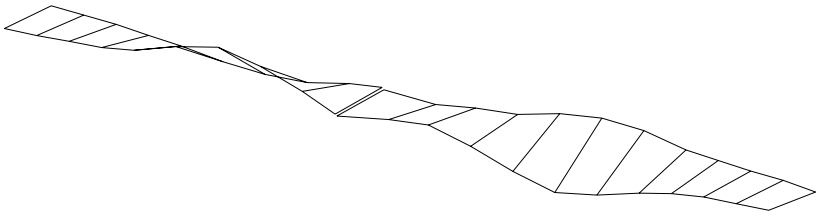

(2) 1st Torsional Mode at 4.501 Hz

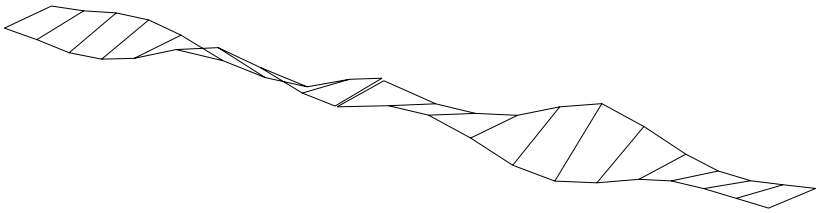

(3) 2nd Torsional Mode at 6.249 Hz

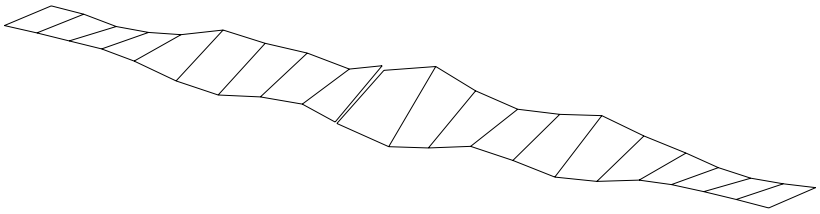

(4) 3rd Torsional Mode at 6.985 Hz

Figure 7.A3.1: Extracted mode shapes (T3)

A3.2 System Identification

Table 7.A3.2: System identification

Mode	Frequency of Initial FE model	Updated Frequencies (Hz)			Frequency of Target Structure	Error (%)	
		Iter. 1	Iter. 2	Iter. 3		Initial	Final
1	5.719	4.341	4.338	4.337	4.072	40.4	6.5
2	5.902	4.534	4.521	4.519	4.501	31.1	0.4
3	8.395	6.369	6.365	6.365	6.249	34.3	1.9
4	8.539	6.484	6.479	6.478	6.985	22.2	7.3

Table 7.A3.3: Identified material properties of FE model (baseline)

	Deck and Piers	Springs for Soil-Structure Interaction	
		Pier	Abutment
E (lb/ft2)	206.28 x 106 (1433 ksi)	-	-
ρ (lb·s2/ft4)	4.68	-	-
k (lb/ft)		22.06 x 106	9.65 x 106

Table 7.A3.4: Modal assurance criteria (measured vs. FE model)

Mode	1/FE	2/FE	3/FE	4/FE
1/M	0.9609	0.0147	0.0007	0.0016
2/M	0.0077	0.9041	0.7909	0.0074
3/M	0.0000	0.5441	0.9041	0.0035
4/M	0.0003	0.0057	0.0004	0.9116

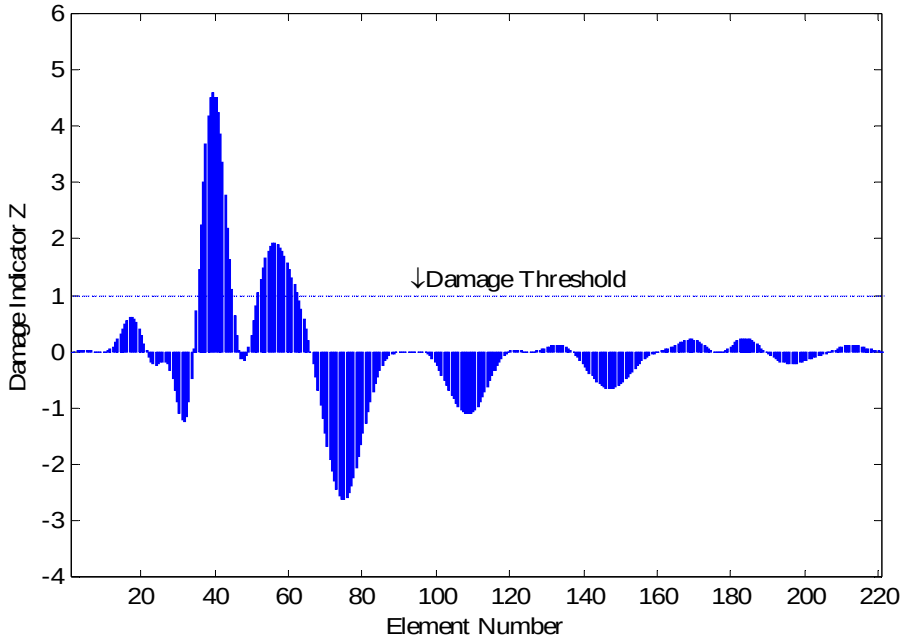

(a) Results using measurements along Sensors S1-S22

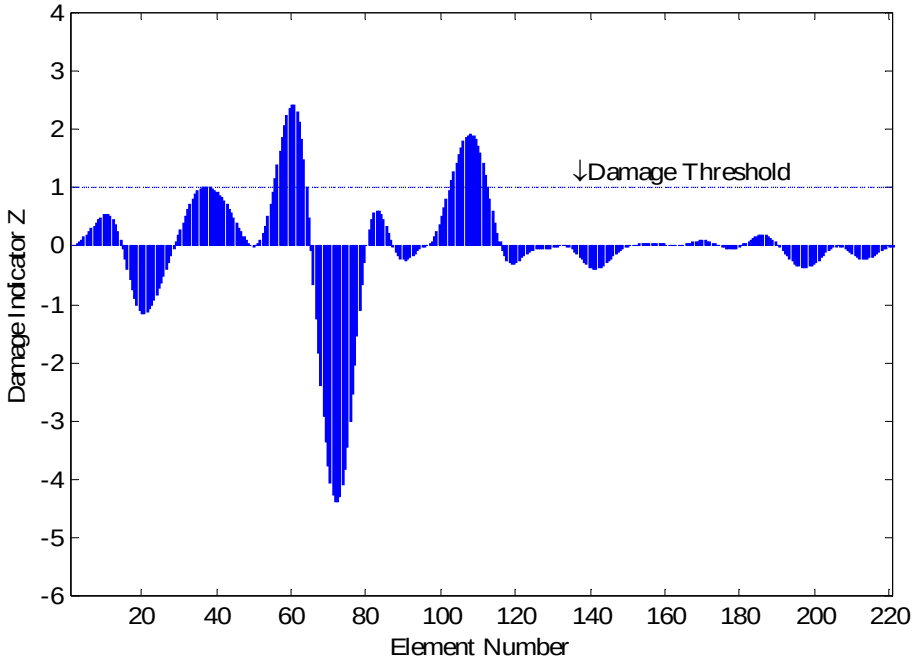

(b) Results using measurements along Sensors N1-N22

Figure 7.A3.2: Damage localization results using first bending mode: T3 (using T1 as the baseline)

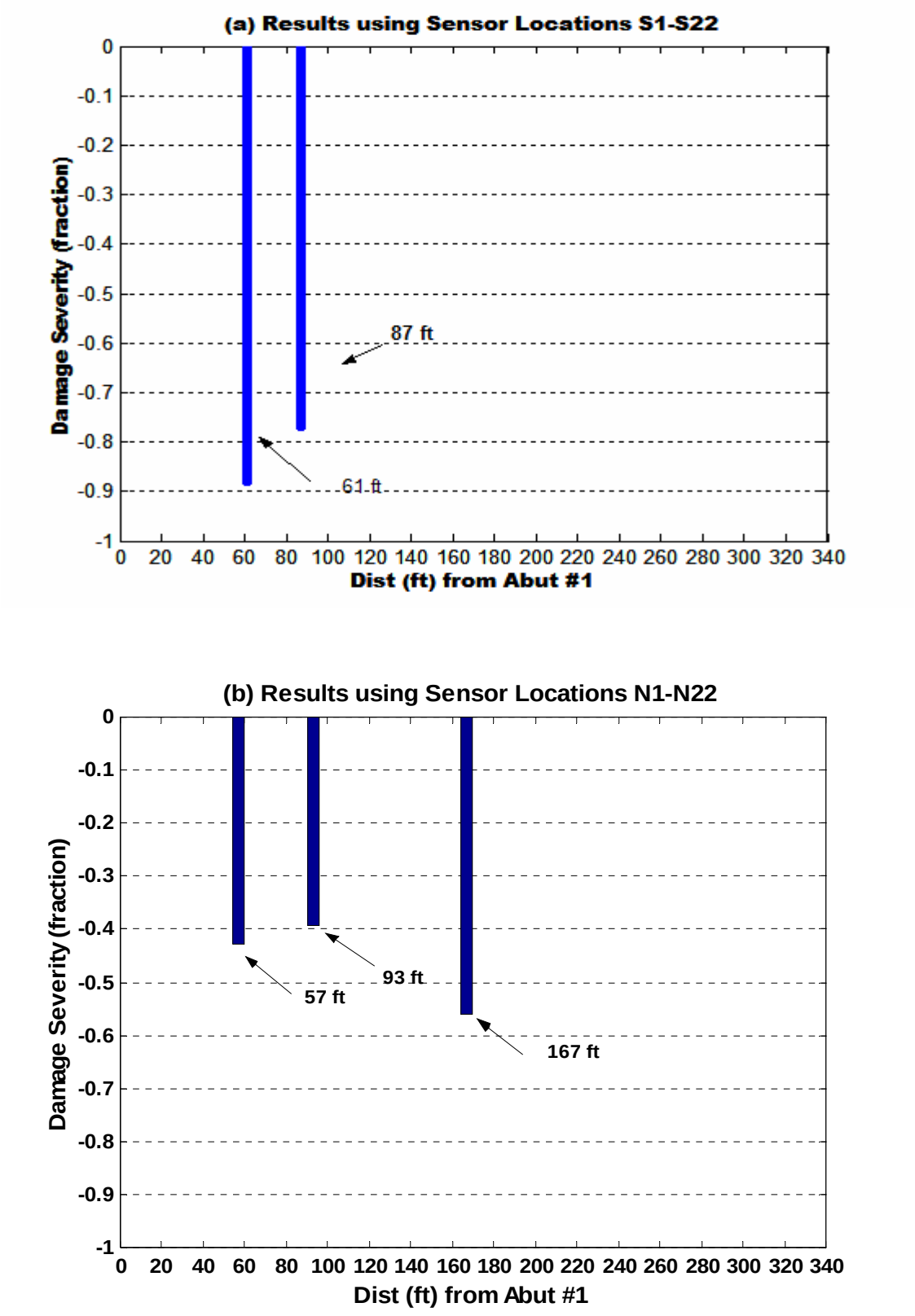

Figure 7.A3.3: T3 damage severity results using all modes

APPENDIX 7-4: IDENTIFICATION OF THE EXISTING STRUCTURE AS OF T4

A4.1 Summary of Modal Test

Table 7.A4.1: Measured frequencies

Mode	Frequency (Hz)
1	3.95
2	4.38
3	6.00
4	6.72

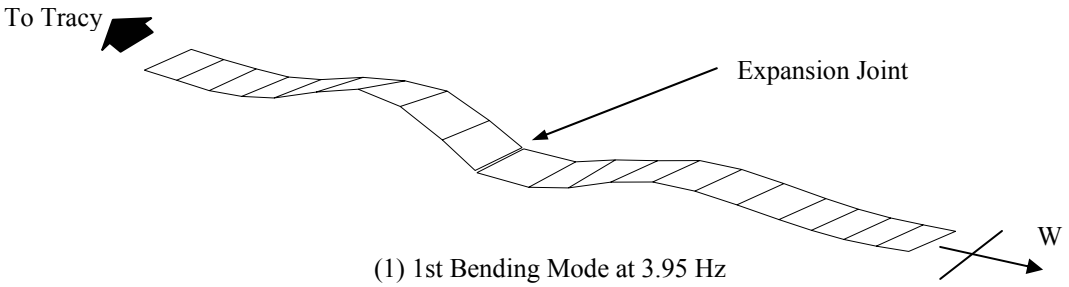

(1) 1st Bending Mode at 3.95 Hz

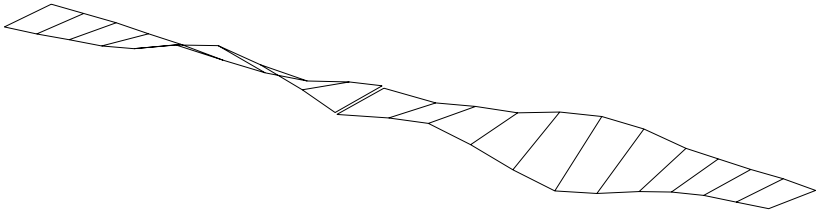

(2) 1st Torsional Mode at 4.38 Hz

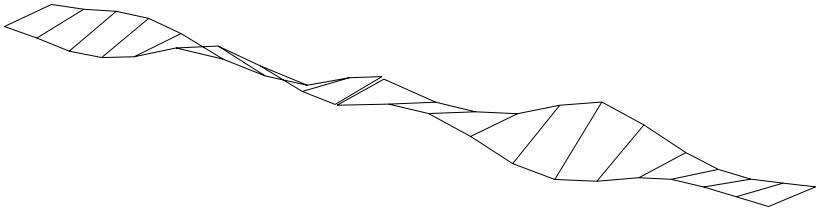

(3) 2nd Torsional Mode at 6.00 Hz

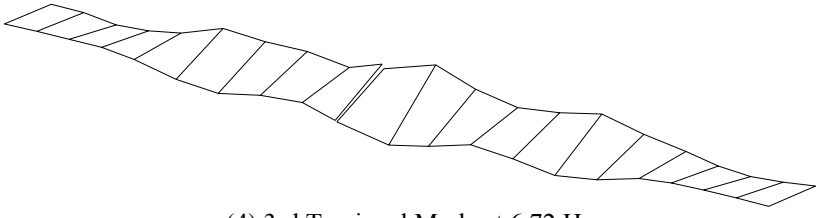

(4) 3rd Torsional Mode at 6.72 Hz

Figure 7.A4.1: Extracted mode shapes (T4)

A4.2. System Identification

Table 7.A4.2: System identification

Mode	Frequency of Initial FE model	Updated Frequencies (Hz)			Frequency of Target Structure	Error (%)	
		Iter. 1	Iter. 2	Iter. 3		Initial	Final
1	3.95	3.95	3.95	3.95	3.95	004	0.0
2	4.43	4.38	4.38	4.38	4.38	1.14	0.0
3	6.01	6.00	6.00	6.00	6.00	0.17	0.0
4	6.79	6.92	6.92	6.92	6.72	0.74	2.96

Table 7.A4.3: Identified material properties of FE model (baseline)

	Deck and Piers	Springs for Soil-Structure Interaction	
		Pier	Abutment
E (lb/ft2)	191.38 x 106 (1329 ksi)	-	-
ρ (lb·s2/ft4)	4.68	-	-
k (lb/ft)		24.70 x 106	10.77 x 106

Table 7.A4.4: Modal assurance criteria (measured vs. FE model)

Mode	1/FE	2/FE	3/FE	4/FE
1/M	0.9609	0.0147	0.0007	0.0016
2/M	0.0077	0.9041	0.7909	0.0074
3/M	0.0000	0.5441	0.9041	0.0035
4/M	0.0003	0.0057	0.0004	0.9116

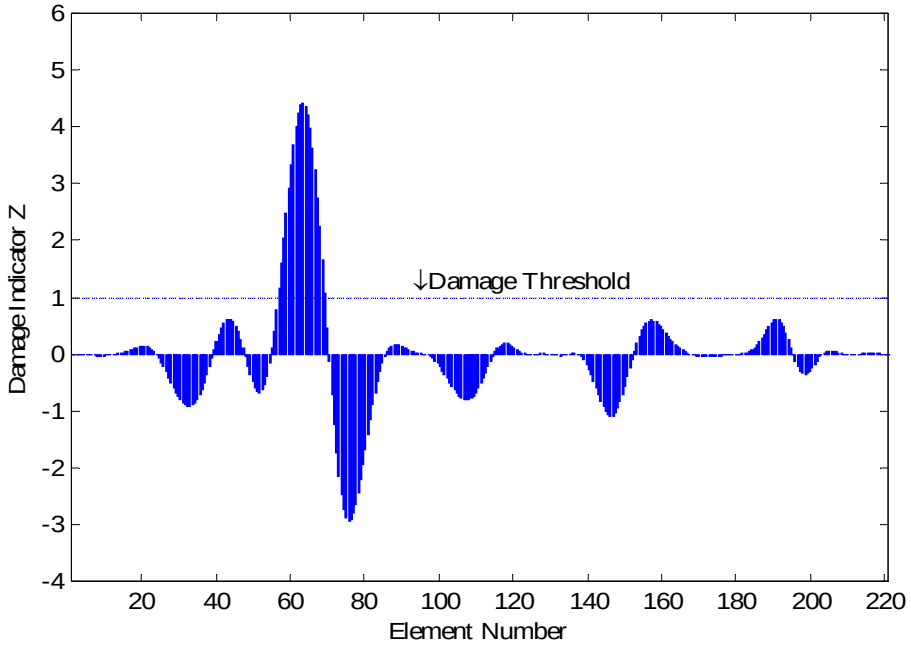

(a) Results using measurements along Sensors S1-S22

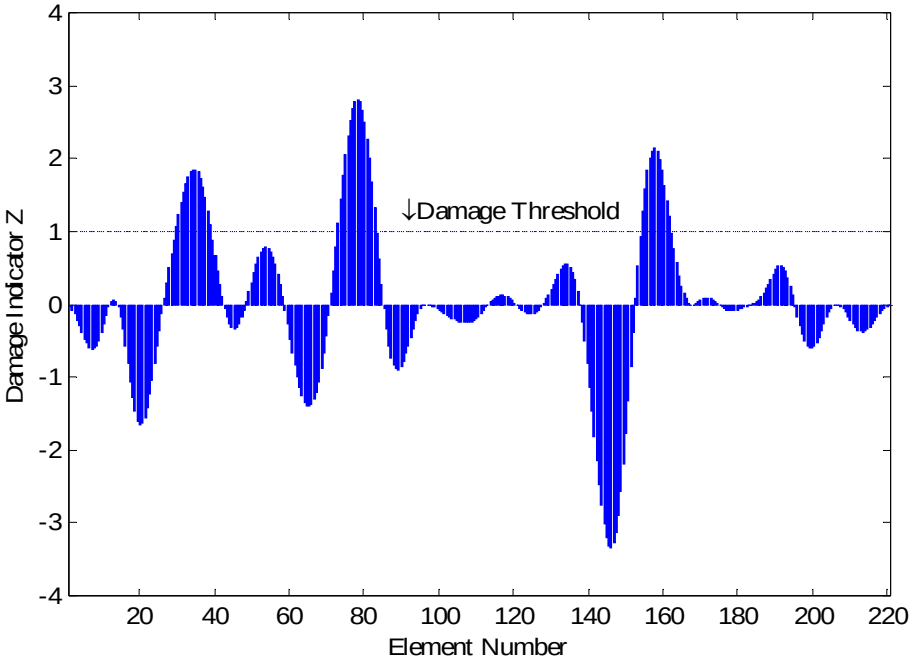

(b) Results using measurements along Sensors N1-N22

Figure 7.A4.2: Damage localization results using first bending mode: T4 (using T1 as the baseline)

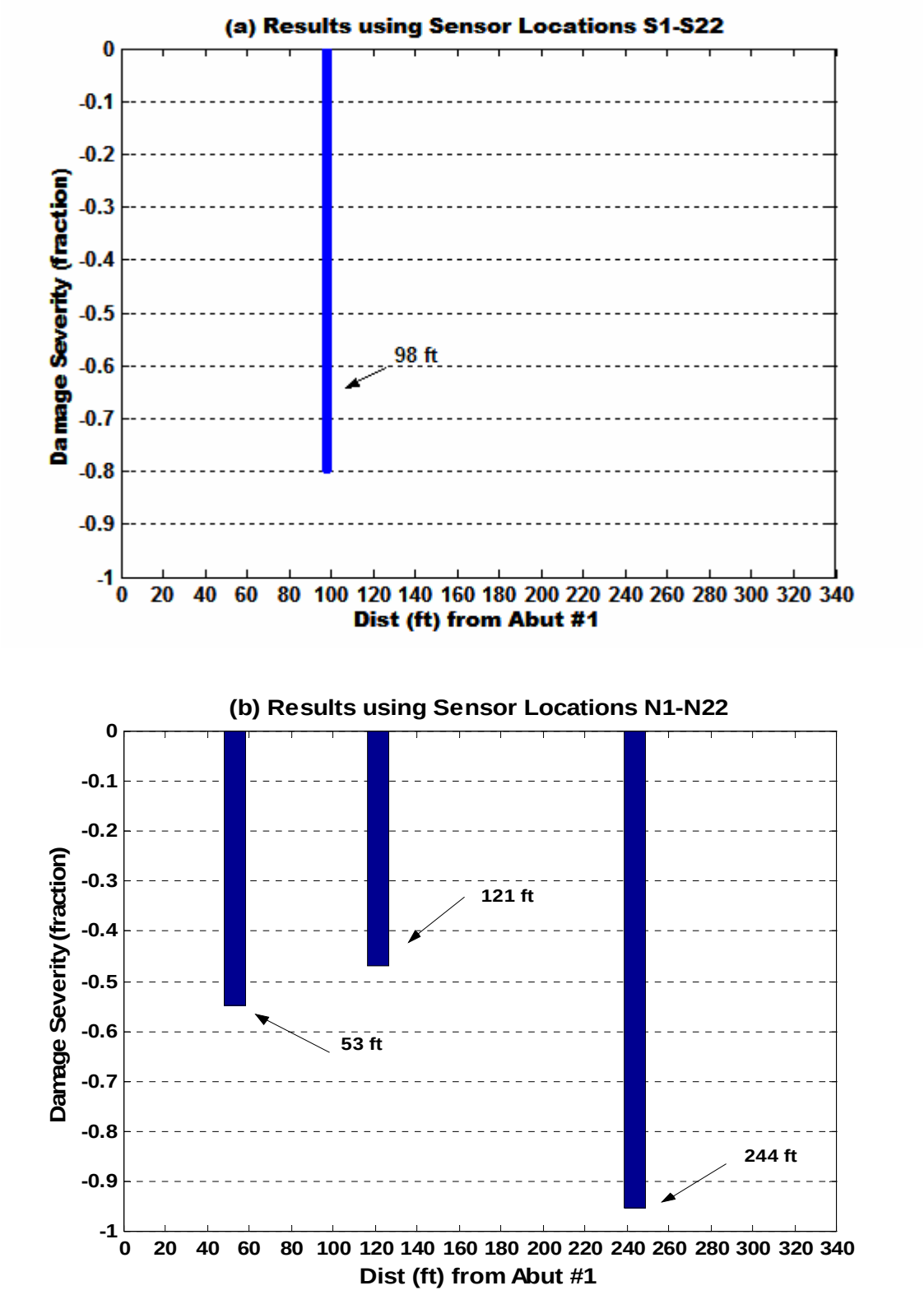

Figure 7.A4.3: T4 damage severity results using all modes

APPENDIX 7-5:
PHOTOGRAPHIC RECORD OF DISTRESS PATTERNS AND CRACK GROWTH

In order to facilitate the placement of the composite reinforcement the deck soffits were sand blasted and cleaned. In cases where extensive microcracking was seen, the cracks were filled with epoxy, and a layer of adhesive was placed in the local region as in Figure A5.1.

Figure 7.A5.1: Local repair

In general, however, the primary strategy was to hold cracks closed through the use of appropriately distributed external reinforcement. Pull-off tests conducted prior to rehabilitation showed that although local areas of the soffits had undergone substantial distress and cracking, the overall pull-off strength was between 1.0 and 2.5 N/mm^2. Pull-off tests conducted at level T3 indicated an average value on concrete of 1.6 N/mm^2 and through the composite of 3.0 N/mm^2. However, further degradation was seen through testing conducted at level T4 with some loss in pull-off strengths in local areas. However, no bond loss between the composite and the concrete was seen, indicating that the system as a whole was still operating at acceptable levels.

Visual inspection in T4 and a month thereafter showed that there were indications of increased crack growth due to local degradation of the concrete in the soffit in a few locations, which corresponded to those identified by the NDE technique. Figures A5.2 and A5.3 show two locations. It was seen that the further propagation of these cracks was being halted by the presence of the composite reinforcement. Cracking was seen in the unreinforced primer region but stopped as soon as the fiber was reached, indicating that the system was operating as intended. However, it is likely that over an extended period of time the growth of these cracks would cause further local distress and could potentially result in local debonding or even longitudinal separation of the reinforcement between fibers.

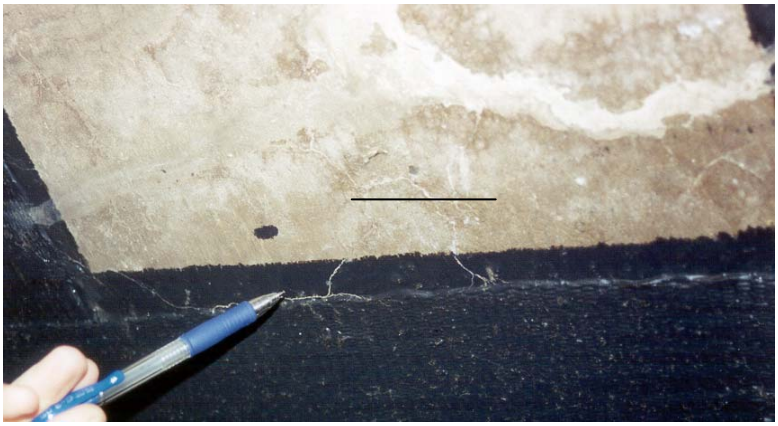

Figure 7.A5.2: Crack propagation through primer and along edge of the composite

Figure 7.A5.3: Crack propagation in region between composite strips and through the primer

Based on the results of the NDE, however, this growth of distress was still not significantly affecting bridge response in the slab. Preventive maintenance through the application of appropriate local patches would be sufficient to forestall long-term damage growth in these areas.

It was, however, noted that there was substantial growth of cracks in girder webs, both in terms of crack extension and in decrease in spacing between cracks. Vertical cracks were seen to extend to the bottom of the girders in some locations and even to extend across the bottom, joining with the vertical crack from the other face (Figure A5.4). The level to which the crack had extended as marked in two previous inspections is also shown for purposes of comparison.

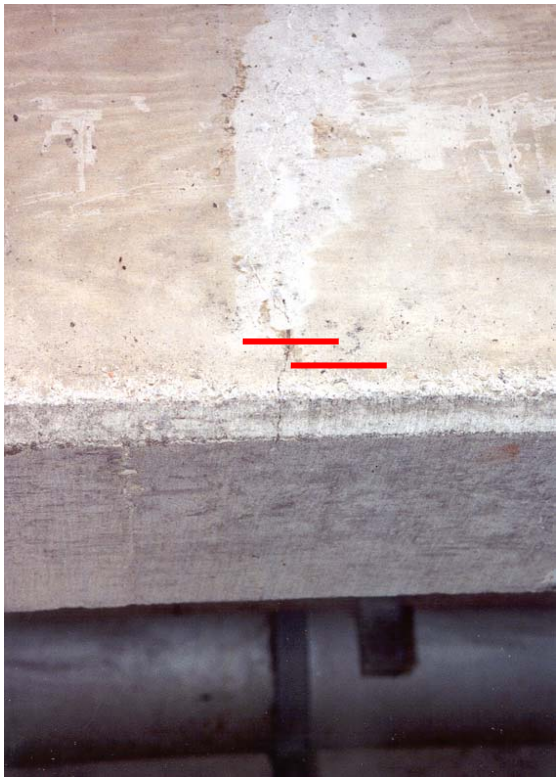

Figure 7.A5.4: Crack extension through the bottom of girder

A second instance is shown in Figure A5.5, clearly showing crack propagation through the bottom face of the girder.

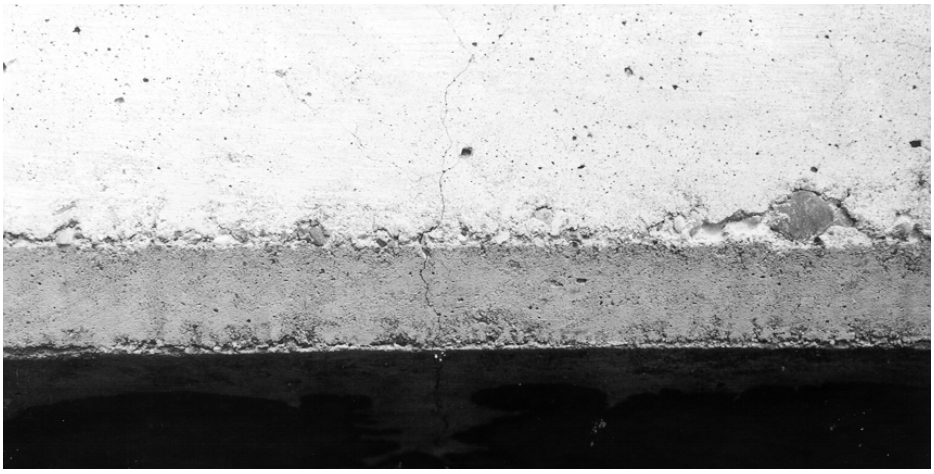

Figure 7.A5.5: Crack propagation through bottom face of girder

In areas indicated by NDE as having undergone further girder distress, crack opening was also noted. Figure A5.6 shows a vertical crack as noted in 2000, and Figure A5.7 shows the same crack at roughly the same time of the year. A marker indicating the distance between gauge points is shown to the same length in both figures for purposes of comparison.

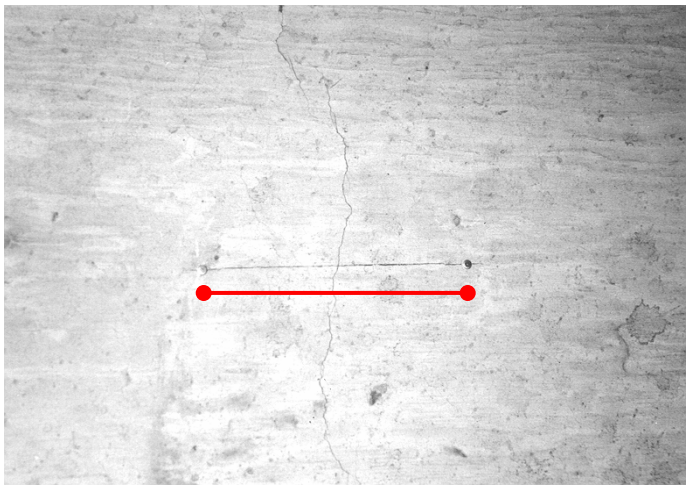

Figure 7.A5.6: Crack at T3 level

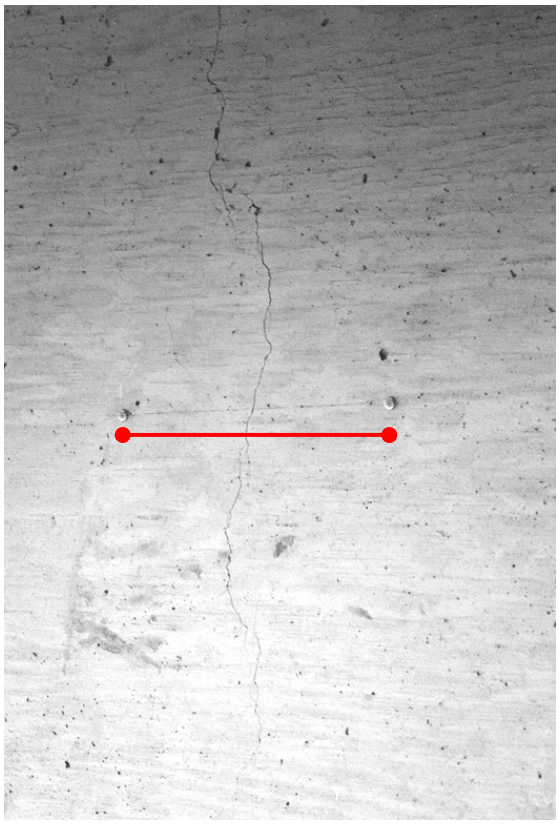

Figure 7.A5.7: Crack after T4

An isolated instance of a vertical crack diverging into two horizontal cracks followed by vertical growth in an area showing poor initial concrete is shown in Figure A5.8. This crack pattern was not noted prior to T4.

Figure 7.A5.8: Crack divergence

Prior to the rehabilitation of the deck through application of composites, the wearing surface had been treated by DWR for purposes of sealing. This application appeared to have been successful until after T4, when indication of moisture transport to the bottom face of the soffit was again noted, as seen through the occurrence of the damp patch in Figure A5.9.

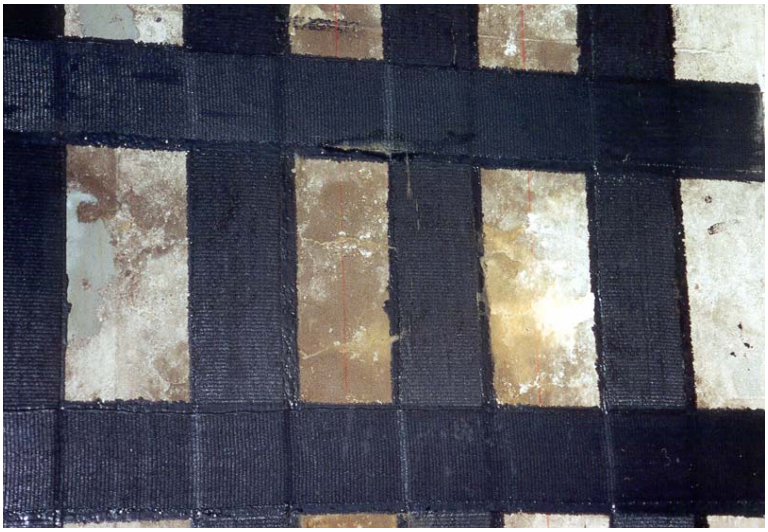

Figure 7.A5.9: Occurrence of damp patches on soffit

In the same bay an isolated instance of splitting within the composite (Figure A5.10) was also seen. It is noted that the spacing of reinforcement in this bay did not follow the initial design but was modified during construction by a field engineer.

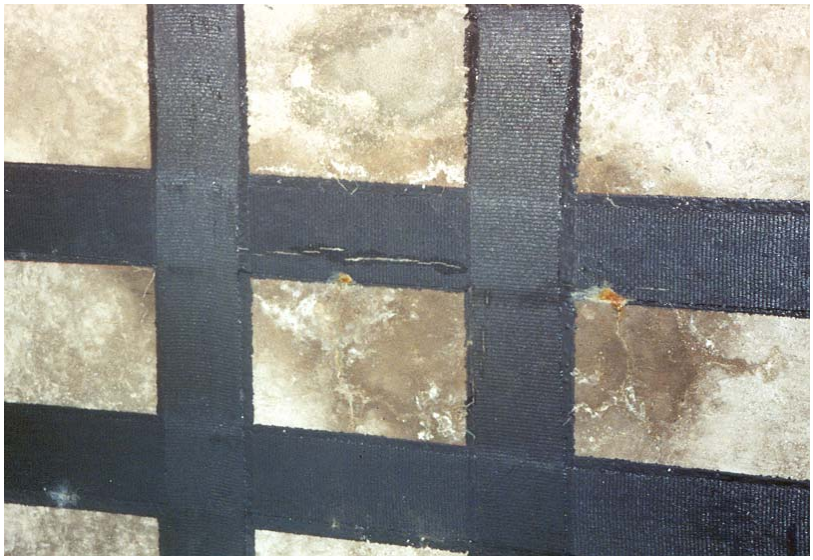

Figure 7.A5.10: Split in composite

8.0 USE OF IR THERMOGRAPHY AS A FORM OF NDE

8.1 INTRODUCTION

Data from the US National Inventory indicate that in the federal aid system, which includes about 276,200 federally maintained bridges, 40% of all bridge deck areas are 15-35 years old. It is also estimated that out of about 575,000 highway bridges in the United States, 230,000 are rated as structurally deficient or functionally obsolete and are thus in need of replacement or serious rehabilitation work [1]. However the scarcity of funds and restrained public spending prevents any investments being made in a majority of these structures. It has been estimated that the worldwide gap between needed and actual infrastructure investment exceeds $900 billion [2]. Thus it is of great importance to carry out periodic condition assessment of these structures to ensure public safety.

The general trend in monitoring the performance of deficient or retrofitted structures is to carry out biennial visual inspections. These inspections, however, can miss many of the signs of subsurface damage and deterioration, not visible from the outside. Thus it is necessary to carry out continuous health monitoring through the application of non-destructive evaluation (NDE) techniques to evaluate the performance of the structure over its useful life. If the structural behavior can be characterized by a field-calibrated finite element model, which integrates experimental, analytical and NDE results, then it would serve as an excellent tool in the prediction of the performance and residual life of the structure.

With the above considerations in mind, considerable efforts are currently being made to understand the definition of structural damage and to come up with cost- and data-effective monitoring systems. It is not sufficient to merely identify the damage. The main challenge lies in the determination of the cause of damage, its location, its severity, and its impact on the performance of the structure as a whole. From this perspective NDE techniques can help to relate the experimental data and results to an analytical model through real-time characterization and assessment of the severity of the defect. With the advances made in image processing, knowledge based systems and new inspection techniques, the conventional NDE techniques can be replaced with faster and more economical techniques with no sacrifice of quality [3]. IR Thermography is one such technique, which is fast emerging as an efficient cost effective NDE method in the detection of flaws and discontinuities in structural systems. It is believed that the use of IR Thermography can result in cost savings of 60 to 75% over ultrasonic testing and radiography, two of the commonly used NDT techniques [3].

Based on a review of NDE techniques, the use of dynamic testing in conjunction with damage detection algorithms, and IR thermography were determined to have high potential for use in defect detection in FRP rehabilitated concrete structures. This chapter provides a review of the use of IR thermography, including steps in its use.

As mentioned in Chapters 1 and 2 of this report, there is a growing need for the development of a fast, cost-effective, non-contact NDE technique specifically modulated and optimized for the detection of sub-surface damage in civil infrastructures. This is necessary not only for regular condition assessment of existing reinforced concrete infrastructure but also to carry out assessment of installation quality and to monitor the performance of structures strengthened with new advanced composite materials. Both the applications are specifically aimed at the detection of subsurface defects in the form of cracks and delaminations in reinforced concrete structures and in the form of debonds, delaminations and defects at the bondline of composite materials used in the external rehabilitation of deficient structures. Infrared thermography has been used as an effective NDE technique in the aerospace industry for the detection of sub-surface defects and anomalies in composite materials and aerospace structural components. Some of the advantages of this technique are as follows:

- It is a non-contact optical technique aimed at detection of subsurface defects with an infrared camera under relevant temperature differentials;

- Real-time inspection and data interpretation allow instant assessment of a structure's integrity and serviceability; and

- It is advantageous in terms of speed and cost compared to traditional NDE methods.

Most of the research and applications of this technique were previously limited to aerospace industry. The recent improvement of infrared thermography with high precision infrared detectors, advanced computing power, and application-specific image processing tools have brought about remarkable progresses in thermographic NDE techniques. This has made it possible to evaluate its effectiveness in applications aimed specifically at the detection of flaws and defects both in reinforced concrete and FRP composite rehabilitated structures.

The objective of this chapter is to evaluate the applicability of IR thermography for the non-destructive evaluation and monitoring of civil infrastructure. A theoretical basis of this technique is first presented to get an understanding of the merits and demerits as well as application constraints. The underlying principles of a number of thermographic methods differing from each other in terms of type of input impulse are discussed with particular emphasis on pulsed thermography, for its promise in civil infrastructure specific applications. A review of the available thermography applications in various fields is presented with emphasis on the defect detection in concrete and composites. The review is presented for applications both at the component level – in order to get an understanding of the defect detectability and the various constraints – and at the system level – in order to evaluate the applicability of this technique to large scale structural applications.

It is to be noted that most of these applications are more aimed at qualitative defect detection. Attempts are currently being made to make the technique more quantitative through utilization of advanced computing power and image processing techniques so that it will not merely identify the location of a defect but also provide information on size, depth, severity and impact of the defect on the overall structure. The underlying principles of such quantitative thermographic inspection are discussed.

A majority of the applications of thermography in defect detection are used under laboratory conditions. But in order to extend this technique for widespread applications in large-scale structures, special attention needs to be given to the environment and surface conditions, and application-specific adjustments might be necessary both in the settings of the camera and the data collection unit. Thus the practical aspects in the applications of thermography in large-scale field projects are discussed.

Finally, applicability of this technique in health monitoring of composite rehabilitated structures through monitoring of damage progression at the composite bondline is studied. Thus, the goal of this chapter is to evaluate the feasibility of IR thermography as an effective NDE technique for sub-surface defect detection in reinforced concrete and composite rehabilitated civil infrastructure through study of previous research and to propose methodologies to extend the technique for quantitative defect identification and effective implementation of the technique under actual field conditions.

8.1.1 NDE flaw detection in concrete

The rapid aging and deterioration of concrete infrastructure, complemented by the scarcity of funds available for the repair or replacement of the structurally deficient or functionally obsolete structures, has underlined the need for the development of advanced NDT techniques. These techniques would help in the rapid, cost effective and reliable condition assessment of the existing infrastructure to ensure public safety [4].

Most of the deteriorating existing concrete structures are subjected to sustained loading in excess of the design load or severe environmental exposures or a combination of both. This results in the formation of major defects such as cracks, delaminations and honeycombs, which can considerably reduce the member's load carrying capacity and corrosion resistance. Since most of these defects are subsurface, they cannot be detected through normal visual surveys and thus require the use of nondestructive evaluation techniques for structural health assessment. Recent advances in signal processing and imaging algorithms, complemented by the high computing speed, have helped in the implementation of imaging techniques as an effective NDT tool for the evaluation of reinforced or prestressed concrete structural components.

8.1.2 NDE of composite concrete bond

The rapid deterioration of infrastructure and the limited funding has promoted the use of advanced composite materials such as Fiber Reinforced Polymers (FRP) as an optimized repair and strengthening technique. In this method, the FRP material (glass or carbon) is externally bonded to the concrete surface using epoxy adhesives. The epoxy, apart from protecting the fabric from the environment, also helps to transfer the load. Thus the performance and durability of the bond between the concrete and the composite is critically important for the integrity and safety of the repaired structure. The use of advanced composite materials for the repair/strengthening of civil infrastructure is a relatively new development, and there is limited information on their long-term performance. Thus further research and experimental data are required on the long-term behavior of the composite-concrete bond and its impact on overall structural performance.

The advantage of NDE testing lies in its capability to detect and characterize subsurface material discontinuities, including debond, delamination or fiber breakage in FRP strengthened structures without damaging or dismantling individual components. Through non-destructive inspection, engineers can obtain valuable information on eventual changes in the state of a material, including the onset of cracking and debonds at microscopic level. IR Thermography is gaining increased acceptance as an effective inspection tool for the maintenance and repair of composite structures. The real-time inspection and data interpretation from this technique can allow instant assessment of a structure's integrity and serviceability. Moreover, for a number of applications it is advantageous in terms of speed and cost compared to traditional methods, and it does not require being in contact with the sample [5].

8.2 INFRARED THERMOGRAPHIC DEFECT RECOGNITION

8.2.1 Background

IR Thermography is a non-contact optical method where an accurate two- dimensional mapping of isothermal contours of steady or transient thermal effects is constructed from the measurement of infrared energy emitted by the target. The first application of IR Thermography as a practical NDE technique was made in 1950 [3]. The early attempts in the implementation of thermographic techniques were qualitative and often were based on the subjective interpretation of the images by the inspector.

In the last two decades, however, recent advances in infrared technology, specifically the development of cost-effective and high-density resolution imaging sensors, have opened a new level of applications unreachable prior to the availability of this technology [7]. Real-time infrared image acquisition and processing allows the implementation of advanced thermographic test methods. The current IR techniques allow automated detection and measurement of subsurface defect depth and area without the intervention of the operator [5].

The principle of IR Thermography is to input heat energy on one surface of the sample to be inspected. The heat energy will tend to diffuse into the material and the rate of heat flow will be a function of the properties of the material. The presence of discontinuities and flaws will cause interruption in the heat flow, resulting in hot spots in these regions. Thus IR Thermography can be used to detect the presence of subsurface defects through observation of discontinuities in the spatial or temporal profile of the surface temperature.

Two methods of thermography, namely active and passive, are generally used. In passive thermography the discontinuities in temperature profiles are generated by ambient environmental conditions (such as the sun) or operating conditions (such as heat generated in machinery by means of internal friction). However, the disadvantage of passive thermography is that the heat emitted from the source cannot usually be quantified. An alternative to passive thermography is active thermography in which an external heat source is used to induce energy in the specimen. In this technique the duration, magnitude and frequency of the source electromagnetic wave are known entities and thus can be used to characterize defects on a more quantitative basis.

8.2.2 Theoretical basis

The use of Infrared Thermography as an effective non-destructive testing technique is based on the theory that the flow of heat through a material is altered through the presence of internal discontinuities, cracks, delaminations or other anomalies. Heat is usually transferred within the material and from one material to another through conduction, which is described by Fourier's law, expressed by:

$$Q = \frac{k}{t \cdot A_h \cdot \Delta T} \qquad \textbf{(8-1)}$$

where k is the material's thermal conductivity.

From the above expression of heat transfer, it is evident that materials with a high k-value, such as metals, can conduct heat quickly compared to an air gap (or vacuum), which is characterized by close to zero conductivity of heat. Composite materials also have much lower thermal conductivity as compared to metals. A comparison of the thermal conductivities of metals, concrete and composites is presented in Table 8.1. Thus the rate of the heat flow will be a function of the media in which the energy transfer is taking place and the presence of any discontinuities in the media.

Table 8.1: Thermal Conductivity of Various Materials [8]

SUBSTANCE	THERMAL CONDUCTIVITY, k [W/m-°C]
Steel (20°C)	36-54†
Concrete (20°C)	1.37
Carbon Fibers (longitudinal)	84
Carbon Fibers (transverse)	0.84
Epoxy Resin	0.18
CFRP (transverse, V_f = 65%)	0.72

† depending on carbon-content

In most cases the thermal response of a thick, semi-infinite solid is described by the 3-dimensional diffusion equation, expressed by:

$$\frac{\delta^2 T}{\delta x^2} + \frac{\delta^2 T}{\delta y^2} + \frac{\delta^2 T}{\delta z^2} = \frac{1}{\alpha}\frac{\delta T}{\delta t} \qquad \textbf{(8-2)}$$

where α = thermal diffusivity of the material.

In the absence of any defects in the material, at a point far away from any edges, the lateral heat flow components in Equation 8-2 will cancel out and the heat flow can be approximated by a 1-dimensional diffusion equation, expressed as:

$$\frac{\delta^2 T}{\delta z^2} = \frac{1}{\alpha}\frac{\delta T}{\delta t} \quad \textbf{(8-3)}$$

However, in the presence of a subsurface defect in the path of propagation of the "heat-wave," the incident thermal energy will be trapped between the defect and the sample surface and will tend to flow laterally outwards towards the cooler areas surrounding the defect. Under such circumstances, the diffusion equation followed can be expressed as:

$$\frac{\delta^2 T}{\delta x^2} + \frac{\delta^2 T}{\delta y^2} = \frac{1}{\alpha}\frac{\delta T}{\delta t} \quad \textbf{(8-4)}$$

Due to the difference in the thermal diffusion equation in the presence of any abnormalities or discontinuities in the material, there will be non-uniformity in the temperature profile, producing a "defect signature" that can be detected through the Infrared Thermography technique. Monitoring of the spatial and temporal profile at the surface using IR Thermography can thus be an effective NDE technique for the detection of any subsurface defects.

8.2.3 Application constraints

When heat energy is applied to a material, a portion of it is reflected and the rest is transmitted through the material. The application of Infrared Thermography in defect detection is based on the thermal diffusion incompatibilities in the material in the presence of discontinuities. This requires that a considerable portion of the source heat energy should diffuse through the material. If the material reflects all the heat energy and acts like a mirror, then no assessment can be made about the internal discontinuities and anomalies. This is applicable for highly reflective metal surfaces and also reflections produced by surface artifacts. Thus the surface reflectance characteristics and ambient conditions have to be taken into account to perform reliable NDE with IR thermography. In order to get the best thermal response, the surface of the material should be prepared properly and in some instances must be painted black.

Emissivity characterizes the ability of the material to radiate heat with the high emissivity surfaces radiating more heat. An ideal material called "black body" has an emissivity of one. All real bodies have emissivities below this value, with shiny surfaced metals having an emissivity approaching zero. Infrared Thermography works best for materials with low reflective properties. Generally, it is not recommended to make IR measurements on materials with emissivity below 50% [9]. For most nonmetals, such as composite materials, emissivity lies in the range between 0.8-1 indicating their suitability for thermographic inspection [8]. The emissivity of a material can be affected by artifacts such as surface markings, blemishes (e.g., dirt, oil, scratches), reflection of stray IR radiation and environmental factors. Thus, surface condition, temperature, and angle of view must be monitored carefully to ensure consistency of results [9].

Another parameter that should be given due importance in the successful application of the IR Thermography technique is that the IR radiation emitted from the material surface must be effectively transmitted to the detecting unit. In most applications, the emitted radiation passes through air before reaching the receiving unit. The heat radiation is found to be most effectively

transmitted in one of two wavebands, 2 to 6-μm and 8 to 14-μm [8]. In between these ranges, only limited transmission of the infrared radiation is allowed in air. Consequently the detection devices have to be calibrated such that they can receive the emitted radiation signals in the specified ranges.

The ambient temperature will change through the day and also through the season and has to be taken into account in conducting passive thermography. Moreover in active thermography using externally applied thermal field technique, there will be an increase in the specimen temperature; thus this temperature needs to be monitored to maintain the specimen temperature range during the test within the infrared camera range.

Each material system also requires slight adjustments in the inspection settings to obtain the best results in the detection of the discontinuities. Depending on the sample thickness, flaw depth and size, it might be necessary to make adjustments in the field of view (FOV), contrast, brightness, illumination, scanning speed and heat direction. The interactions of the various inspection settings are usually found to be complicated, and a statistical design of the thermographic variables is usually necessary to arrive at the best interaction of the settings for flaw detection. The goal of an effective thermographic inspection is to detect all flaws and make no false calls [3].

8.3 IR THERMOGRAPHY TECHNIQUES

IR Thermography has been applied as an effective inspection technique on several material systems. It has been used to inspect fiber-reinforced composites, insulation materials and composites bonded to metals, composite-concrete bonds and flaws in concrete. Each material system requires a slightly different technique because the infrared absorption and discontinuities for each case causes the heat to flow differently. Thus, a variety of thermographic methods have been developed to suit individual material and geometric configurations. Three general methods are usually used to generate the thermal fields for the detection of flaws, cracks or damaged zones.

8.3.1 Externally Applied Thermal Field (EATF)

EATF Thermographic NDT methods involve the application of external heat to the structural surface and study of the resulting transient thermal gradient. In the absence of any defects, the gradient is uniform and the isotherms will be straight lines. Consequently no discontinuities in the temporal profile will be observed. In the presence of a flaw, however, the discontinuous thermal conductivity would cause a perturbation in the heat flux and temperature field, resulting in curved isotherms and non-uniform temperatures near the flaw [10].

As discussed previously, depending on the external heat source used, EATF thermography can be classified into active and passive. Traditionally, for large projects, with a large overall dimension of the structure, it is more feasible to use an ambient source of heating (the sun); and Passive Infrared Thermography inspection is performed following periods of heating or cooling. This technique has been found to be effective in the measurement of the variations of thermal diffusivity in the inspection of heat loss in sections of an entire building [11]. This method tends

to be qualitative, however, and predicts the performance of the system on the structural level. For more quantitative measurement and characterization of defects, Active Thermography is usually a better option. In this technique, the heat is applied using an incandescent light bulb, heat gun, flash lamp or quartz lamp. Since the magnitude and duration of individual source heat pulses are known and are easily adjustable, an exact quantitative study on internal properties and defect characterization can be pursued.

EATF Thermography can be further classified into Parallel and Normal, depending on the orientation of the discontinuities [12]. Interior flaws such as delaminations, which interrupt the heat flux normal to the surface under inspection and result in hot spots on the heated surface will result in Normal EATF. Thus in normal EATF the flaw detectability is greater for higher temperature difference around and away from the defect. Flaws such as surface cracks, which interrupt heat flow parallel to the surface under inspection and produce local convexities in the isotherms or steps in the surface temperature will result in Parallel EATF. In this type, the defect detectability is governed by the step in the temperature across the crack and the length of time over which the thermal pattern remains.

Based on the input temperature signals used in Active Thermography, two of the most commonly used EATF Thermography techniques are Pulsed Thermography and Lock-In Thermography.

8.3.1.1 Pulsed thermography

Pulsed Thermography (PT) is one of the most commonly used NDE techniques, effectively applied for a broad range of applications including defect detection in composites and concrete. In PT applications, a heat pulse of relatively short duration is directed at the test surface and this launches a thermal front, which propagates through the sample under inspection, by diffusion according to the diffusion equations presented earlier. Either a ‘‘warm’’ or a ‘‘cold’’ stimulation can be used in PT, since the main objective of this technique is to generate a temperature differential in the sample. Usually the heat pulse is deployed by means of lamps, flashes, laser beam and air jets. Moreover the Normal EATF method requires uniform heat flux for effective detection of flaws.

The duration of the pulse is variable from μs (microseconds) to several seconds depending to the thickness of material to be probed and its thermal properties. As a constant heat flux is applied to the surface of the sample, the temperature difference – Δt – between the flawed and the unflawed regions will reach an asymptote with time even though the temperatures through the specimen will continue to increase. Thus for most applications, the heat application can be stopped after the elapse of the time necessary to produce about 90% maximum obtainable Δt [12].

The inspection equipment usually consists of a heat source (usually a high intensity flashlight), an infrared camera, an infrared thermometer and a data collection unit. When the heat pulse is applied to the specimen, there is a rise in the surface temperature, and the heat flux will thus move towards the colder regions inside the specimen. The presence of any subsurface defects will alter the rate of diffusion with respect to the surrounding area, due to the low thermal conductivity of defects (usually air pockets) as well as the

comparatively high heat flow rate in the surrounding material. As a result, the areas with discontinuities will be subjected to a buildup of thermal energy and serve as hot spots during the heating cycle. These areas will also restrict loss of thermal energy during the cooling cycle. Consequently, the operator can make a qualitative assessment of the presence of defects in the specimen in terms of the magnitude and configurations of the thermal gradient through subjective interpretation of the thermal image. A schematic of a pulsed thermography test setup is presented in Figure 8.1.

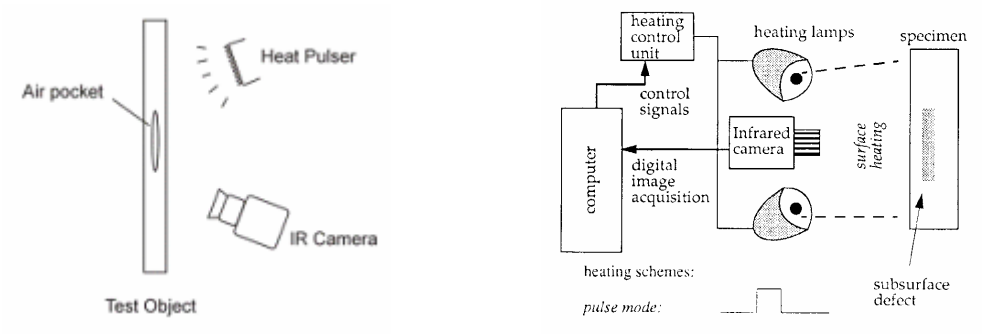

Figure 8.1: Pulsed thermography test setup [13]

For quantitative flaw detection and direct interpretation of the condition, depth, size and progression of the defect, automated PT techniques have been developed. In these methods, upon completion of the thermal stimulation, the temperature decay curve of the specimen surface is continuously monitored and recorded by one or multiple external recording devices either during the rising surface temperature or the decay. In PT, the thermal propagation time t and the depth z of a subsurface defect are often related by the following expression:

$$t \approx \frac{z^2}{\alpha} \qquad \textbf{(8-5)}$$

where α is the material thermal diffusivity ($m^2\ s^{-1}$), such that $\alpha = \frac{K}{\rho C}$; with K being the thermal conductivity, ρ is mass density, and C is specific heat.

The quantitative thickness and depth measurement is generally based on a thermal contrast image recorded through either its whole evolution or at its peak. However this requires identification of a defect-free reference region by the operator so as to compute temperature differences in the region with flaws. The contrast definition often used is expressed as:

$$C(t) = \frac{T_i(t) - T_i(t_0)}{T_s(t) - T_s(t_0)} \qquad \textbf{(8-6)}$$

where *i* and *s* refer, respectively, to a suspected defective location and a non-defect area.

$C(t)$ is computed with respect to the temperature distribution before heating at time t_o and is normalized by the behavior of the non-defect area. Moreover, $C(t)$ is a function of time and for quantitative analysis its maximum value C_{max}, computed at t_{max} is usually of interest. A unit value will be obtained over a non-defect area [13].

However the contrast curve methods (e.g., peak slope time, peak amplitude time) sometimes do not prove to be reliable, as results depend on the placement of the reference region [5]. Moreover in these methods, the defect detection is based on either temporal analysis of each pixel in the image or on contrast in a single image. Thus the presence of surface markings, emissivity variations, reflections off the surface of the sample and variations in the composition of the material might result in false calls.

In order to analyze the PT data without any a priori knowledge of the sample and without any subjective decision of the operator, an automated data processing algorithm has been developed by Shepard, et al. making use of the 3-D diffusion equations in the material [5]. As discussed in Section 8.2.2, the diffusion equations governing the heat flow in the material after illumination by a spatially uniform light pulse, are expressed as:

Without defects:
$$\frac{\delta^2 T}{\delta z^2} = \frac{1}{\alpha}\frac{\delta T}{\delta t} \qquad \textbf{(8-3)}$$

With defects:
$$\frac{\delta^2 T}{\delta x^2} + \frac{\delta^2 T}{\delta y^2} = \frac{1}{\alpha}\frac{\delta T}{\delta t} \qquad \textbf{(8-4)}$$

In general, the depth measurement of the defect through the identification of the peak slope or peak contrast amplitude in the contrast curves is based on Equation 8-3. However, as seen above, the difference in the diffusion equations before and after the heat flux travels from the surface to the subsurface defect, classifies the PT data into two distinct time regimes and can thus be utilized for automated depth detection and measurement. The time at which the transition between the two regimes occurs, represent the "onset time" from the flash pulse to the time at which the defect at a particular depth is detected [5]. Before the onset time, the heat flow is similar in the regions both above and away from the defect. However after the transition time, the surface temperature profile above the defect will not be uniform despite the fact that the input pulse is uniform and the defect may be planar, since the heat closer to the defect is trapped while the heat away from the defect will move towards cooler surrounding areas. An automated algorithm can be used to detect these "signature characteristics" and identify subsurface defects without human intervention.

This hypothesis was tested by Shepard, et al. using three carbon/epoxy samples with a non-symmetrical $|0,90|_{15}$ ply lay-up sequence with a total thickness of 0.208 inches and with simulated voids at varying depths in the three samples [5]. The difference in behavior of a single pixel above the defect from a large kernel is presented in Figure 8.2. The behaviors of the two were found to be identical until the transition time t_o, and the

breakpoints were also found to be appearing at progressively later times for deeper defects.

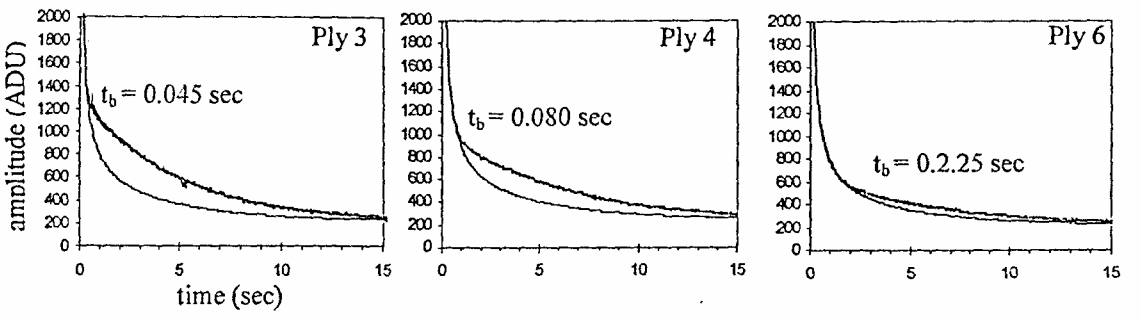

Figure 8.2: Temporal profile from IR thermography [5]

An alternative to monitoring the temperature decay on the heated side of a component is a transmission scheme. In this scheme, transmission of heat is allowed through the specimen, and an infrared detector and stimulation unit is placed on either side of the specimen to capture the heat signature on the far surface. The heat flow through the specimen will thus be restricted in regions of low thermal conductivity, resulting in regions of lower temperature observed in the heat-contour image. Since this arrangement requires access to both sides of a part, the applicability of through transmission is mainly restricted to parts of minimal thickness. On structural components, this method would typically require dismantling or may not be possible at all. The reflection scheme is thus preferred over the transmission scheme due to the ease of deployment.

The main advantage of the PT approach is the ease of deployment for in-situ inspections. It is also inherently fast, as the whole area of the specimen can be analyzed due to surface wide heating. Moreover, as evident from Equation 8-5, typical NDE thickness for most common materials requires an observation time of less than 1 min (~e.g., about 0.5 min for 2 mm of graphite/epoxy) [13].

8.3.1.2 Modulated thermography

Modulated Thermography (MT), also referred to as Lock-in Thermography, is used for a number of applications in the evaluation of CFRP materials. In this technique, instead of being subjected to a heat pulse, the specimen is exposed to sinusoidal temperature stimulation (Figure 8.3), whose magnitude and phase depend on the input frequency. For a point inspection, the specimen is heated by a modulated laser beam while for the inspection of a surface, the area is exposed to sinusoidal illumination, usually by means of a modulated heating beam. The thermal stimulation causes an oscillating temperature field inside the specimen, which can be remotely recorded through IR detectors.

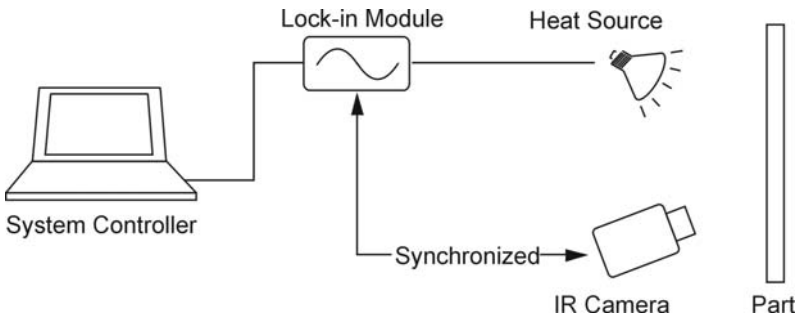

Figure 8.3: Modulated heating in lock-in thermography [8]

A lock-in amplifier is used to synchronize the input and output signals and thus the magnitude and the phase of the input and output thermal waves can be computed with respect to the reference modulation. In recent applications of MT, development in imaging techniques have made it possible to obtain the output signals through the analysis of the digitized data without using the amplifier. The magnitude of the signal is proportional to local optical and infrared surface features while the phase is related to the propagation time delay. Since the magnitude and phase of the signals differ between good and defective regions of the specimen, the presence of subsurface defects can be detected by monitoring the signals [14].

As compared to PT, MT is usually found to have a better depth resolution, which can be tuned depending on the modulation frequency, and MT is usually more insensitive to surface artifacts [13]. For slow thermal response materials, such as CFRP, the use of modest power illumination sources operating in the long pulse mode are often found to produce good results [38]. However the setup is more complicated in order to produce the sinusoidal modulated heating, and the process is much slower as compared to PT. As an example, 2 min will be required to inspect a 2-mm-thick CFRP laminate at a modulation frequency of 0.03 Hz. while, a PT inspection will require about 30 sec [15].

8.3.1.3 Automated transient thermography technique

The test setups for pulsed and modulated thermography techniques as described in the previous sections work quite well in a controlled laboratory environment. However several constraints are imposed on the application of thermography in the field, where it is much more difficult to control the required temperature ranges due to variations in the ambient temperature and the presence of several unwanted or 'parasitic' heat sources. Thus in order to ensure repeatability of the test measurements from a specimen under different working environments, transient thermography techniques are often used in field applications of pulsed or lock-in thermography.

In this technique the heat source and the IR camera are mounted on a trolley-type setup and are moved parallel to the surface of the specimen under inspection. The speed of the trolley is controlled such that each surface element after being heated by the external heat

source will travel under the IR camera and will be in its field of view for a certain time period. The evolution of the thermal pattern, which is a function of the specimen material and the location of the defect, will be recorded in a sequence of thermograms and will translate into a corresponding trajectory in the IR images stack [16]. A schematic of the test setup is presented in Figure 8.4.

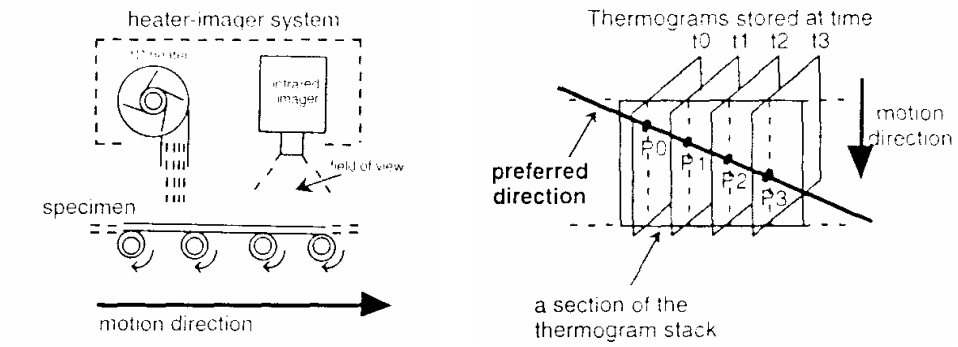

Figure 8.4: Test setup and preferred direction identification inside IR image stack [16]

In Figure 8.4, *Pi* represents a pixel at time *ti* containing a surface element, S, whose response under the thermal stimulus produced by the heat source is to be studied. Thus the pixel *Pi* will follow a predictable trajectory, referred to as "Preferred Direction" and the time evolution of the pixels along their trajectory in the thermogram stack will image the heat patterns produced by a defect under the surface S. A linear motion (constant velocity) will thus result oblique line trajectory with its direction being in the preferred direction while an accelerated motion will result in parallelogram trajectory in the thermogram stack. A directional operator would then be used to enhance the signals in the preferred direction. Moreover, only the defects at a particular depth can be detected by studying only a subset of the thermogram stack.

This technique, referred to as D2D (Defect to Direction) has been used for the detection of structural heterogeneities in solids [16]. A 30x30 cm square, 5 mm thick CFRP plate with a stacking sequence of 25 plies placed at [0,90] and with nine square defects embedded at different depths was investigated using this technique. The distance between the heat source and the imager was selected so as to allow initiation of defect evolution a little after the defect area enters the field of view while the velocity was chosen so that the full defect evolution could be studied. A velocity of 2 cm/sec, a 1000W heat source and a thermogram acquisition rate of 15 per second was selected for the study. From a sequence of 300 thermograms obtained it was observed that a pixel stayed in the imager's field of view for about 121 thermograms. After the application of the directional integrator on the thermogram stacks, the defects at different depths in the CFRP plate were successfully constructed in the thermal maps using different subsets of the thermograms.

Some of the inherent advantages in the application of transient thermography include real time imaging of the defects and the convenience of large surface exploration capability with a decision free operation. As long as a fixed velocity and proper direction of propagation can be ensured, the technique can be fairly automated. A continuous sequence of thermogram stacks can be obtained in the preferred direction for practically unlimited length while the width is limited by the field of view of the imager. Usually the imaging is carried out in parallel directions over the entire surface area of the specimen and the thermograms are then superimposed to get a 3-D thermal map.

8.3.2 Stress generated thermal field

The behavior of most materials in the inelastic portion of the load range is characterized by the hysteresis loops produced upon subsequent loading and unloading. The energy, which is generated in the loading/unloading cycles, is dissipated as heat energy and the thermal gradient is higher in regions of high stress or deformation [10]. Cracks, flaws and other defects and damages in the material act as stress concentrators under externally applied loading. Inside the specimen, the transmitted mechanical energy is converted to heat energy through non-conservative micro mechanical deformation processes such as dislocation motion, impurity diffusion, and other complex atomic activity [17]. Thus thermal patterns will be generated near the defect areas and flaws as 'hot spots', which can be detected and monitored using real time infrared thermography.

The application of infrared thermography in the imaging of stress generated thermal field was studied through conducting cyclic loading tests on flawed tensile specimens [10]. The stress concentrations produced by the presence of holes and simulated delaminations were found to produce thermal patterns as shown in Figure 8.5, which were found to correspond well with the local stress analysis. The thermal patterns were usually found to develop near the flaws in composite specimens at 0.2 to 0.8 of the static ultimate load and at cyclic frequencies of 15 to 50 Hz. However some applications of thermography have also been demonstrated at lower maximum loads and cyclic frequencies as low as 0.5 to 5 Hz in the detection of heat patterns produced by cyclic tensile loading in composite laminates [10].

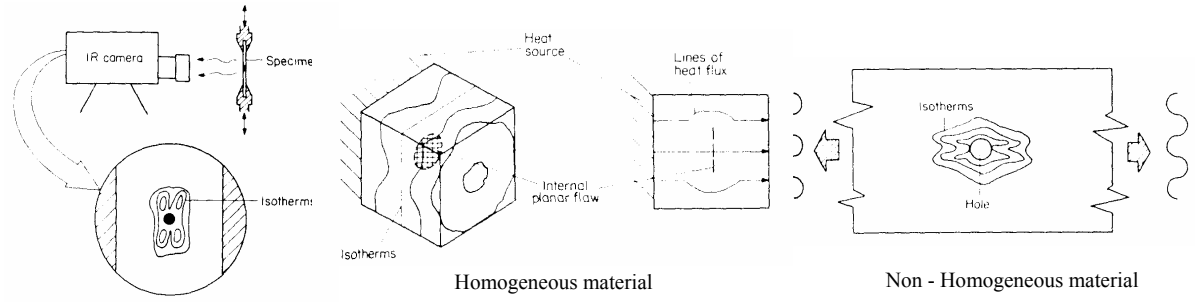

Figure 8.5: Stress generated thermal fields under cyclic loading [10]

8.3.2.1 Externally applied vibration field (vibro-thermography)

In this thermography technique, the specimen under inspection is subjected to forced mechanical vibrations as an external stimulus. The external steady state vibrations are usually applied to the specimen under inspection using a piezoelectric shaker. Figure 8.6 shows a schematic of the test method. Both the amplitude and the frequency of applied time varying loading can be increased. In practice, either a low frequency, high amplitude loading (such as in a fatigue test) or a high frequency, low amplitude loading (usually done through attachment to a high frequency shaker) is usually applied.

The fatigue type of loading is used in applications where it might be necessary to cause initiation or progression of a damage. The high frequency, low amplitude loadings are usually inertial loadings and do not cause additional mechanical damage in the material [18]. Moreover the high frequency of oscillation is used to enhance the efficiency of heating while a low frequency of amplitude modulation is found to improve the depth range [19.].

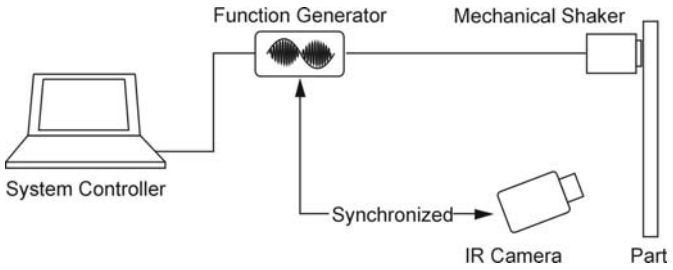

Figure 8.6: Test setup for vibro-thermography [18]

In the thermography techniques involving externally applied thermal fields, the development of the thermal pattern is contingent on the difference in the conductivity of the defect from that of the material. Thus the defect has to be detected on the background of the signal in "good areas." For some applications this can be time consuming, and the thermal patterns might not be evident in the presence of hidden flaws. It will be advantageous to use techniques that will stimulate the defect directly, causing it to produce a heat pattern that is a function of the defect itself, so that only the defect areas will be displayed when imaged by real time infrared thermography.

In vibro-thermography the specimens are subjected to forced mechanical vibrations, which will result in stress concentrations in defect areas. Stress concentrations will cause hysteresis in the stress-strain curves, which corresponds to the energy lost per cycle [19]. This 'lost energy' gets converted to heat energy; thus the areas with defects will develop preferential heating because of the larger hysteresis loops associated with stress concentrations in the defect areas.

Real time infrared thermography can be used to detect and monitor the temperature gradients developed at the locations with discontinuities. However the formation of the

thermal patterns is highly sensitive to the applied frequency for high frequency, low amplitude vibrations. It has been observed that variations in the applied frequency of the order of ±0.5-kHz can cause thermal gradients to appear or vanish [18]. Hence, in most vibro-thermography applications the frequency is gradually increased until a distinct thermal pattern can be observed. For composite laminates the frequency band typically used is 10 to 40 kHz.

Apart from the 'classical' vibro-thermography technique described above, the oscillatory part of the heat generated can also be monitored to obtain the amplitude and phase information [19]. Referred to as "phase sensitive lock-in vibro-thermography", the local variations of phase angle reveal the defect areas where the thermal diffusivity has been modified. The amplitude of the temperature modulation on the surface of the specimen indicates the efficiency of heat generation, while the phase angle as a propagation time effect depends on the depth at which the heat is generated [19].

The vibrothermography technique is most effective in applications where it is necessary to detect and monitor defects and damages that might affect the mechanical properties such as strength and stiffness of the material. In this application the thermal patterns created are functions of the stress concentrations around the defect sites, which are related to the mechanical properties of the body rather than to the thermal conductivity (the principle behind application of pulsed and modulated thermography techniques). Thus, vibro-thermography can be used to detect defects such as closed cracks or delaminated regions, which may not be detectable by pulsed or lock-in thermography.

8.4 THERMOGRAPHIC DEFECT DETECTION IN CONCRETE

IR Thermography imaging of concrete structures has been successfully applied for the detection and characterization of delamination defects in concrete structures, and it is gaining rapid acceptance as an effective NDT technique because it is non-contact, time saving, cost effective and does not damage or impair the serviceability of the structure. However proper care has to be taken in the interpretation of the thermal patterns in concrete, since concrete is a highly non-homogeneous material and is produced with limited quality control. Thus concrete is usually characterized by variable grain size and properties of constituent materials. Moreover most concrete structures are associated with complex geometries and restricted access [4].

Concrete structures deteriorate over time, due to both sustained and fatigue loading and environmental effects. These adversely affect the service life, safety and maintenance costs. The most common defects in concrete structures are cracks, delaminations and honeycombs, and they grow with time under service conditions. Corrosion of the steel reinforcement is also usually associated with most concrete structures. The corroding steel expands in volume and causes further cracking or subsurface fracture planes (delaminations), resulting in further deterioration and reduction in load carrying capacity. Thus the primary objectives of IR thermography in the evaluation of concrete structures are detection and characterization of subsurface delaminations, cracks or voids and assessment of structural health.

It is usual practice to use manual methods such as striking with hammers and steel rods and dragging chains over deck slabs to detect any delaminations in the concrete. However these techniques are only qualitative, since defect detection depends on the operator's interpretation of the sound produced. Thus it is difficult to characterize the depth, size and cause of a defect and is usually inconvenient and time-consuming, causing disruption of structural use. Also in the hammer and steel rod sounding techniques the sound produced depends on their vibration characteristics, and a large number of such readings need to be taken to get a proper two-dimensional surface mapping of delamination throughout the deck. Moreover, though widely used in detection of delamination in concrete bridge decks, these techniques cannot be conveniently applied in the evaluation of other concrete infrastructures, e.g., buildings, water and sewer systems, harbors and airports.

Thus acoustic and thermography techniques have proven to be viable techniques for rapid, cost effective and reliable condition assessment of concrete structures. As mentioned earlier, it is believed that the use of IR Thermography can result in cost savings of 60% to 75% over ultrasonic testing and radiography [3]. Moreover, since most concrete structures have large overall dimensions, IR thermography can be used to quickly scan large areas and pinpoint potential problem areas on which the inspector can focus [29].

The detection of delamination in concrete structures through the use of IR thermography is based on the basic principle of difference in the thermal conductivity of sound versus delaminated concrete, resulting in the formation of heat patterns that can be imaged by thermography techniques as described in Section 8.3. The surface over the delamination is found to heat up faster, as the defect acts as an insulator and heat is not dissipated at the same rate as other areas. The temperature variations in sound and delaminated concrete during a period of moderate heating in a deck slab are illustrated in Figure 8.7 [30]. It is usually found that the delaminated concrete is 2 to 3 ºF warmer than the surrounding solid concrete.

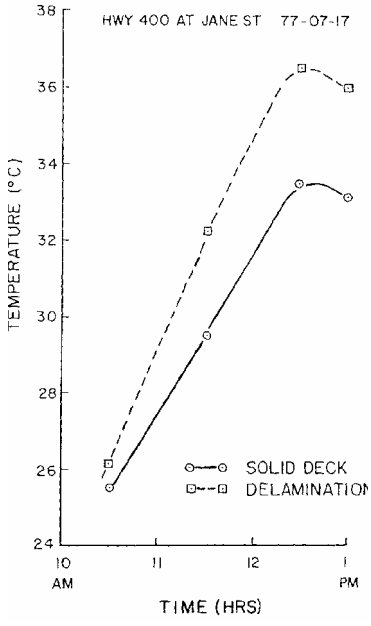

Figure 8.7: Temperature difference between solid and delaminated concrete [30]

The Pulsed Thermography technique (as discussed in section 8.3.1.1) is usually preferred in the thermographic flaw detection of concrete structures. Also for large projects, with large overall dimension of the structure, it is more feasible to use an ambient source of heating (the sun), and passive thermography inspection is performed following periods of heating or cooling. This technique has been found to be effective in the measurement of the variations of thermal diffusivity in the inspection of heat loss in sections of an entire building [11]. The technique has also been applied to investigate waterproofing and surface integrity characteristics of buildings [29]. Water damaged roofs usually have a different heat capacity as compared to non-damaged roofing and can be imaged by IR thermography.

The thermography imaging of masonry walls is slightly different from concrete. For concrete the sun causes the change in the surface temperatures, while for the masonry walls water changes the surface temperatures [29]. Thus masonry walls are usually imaged after a soaking rain or through artificial wetting. In the wall the defect areas will absorb more water than solid masonry, and as this reserve of water gradually evaporates it cools off the area and causes the thermograph of the defect area to appear as a "cold spot." This technique works best after a good soaking rainfall, relative humidity below 85% and usually around sunset.

The defect detection of bridge decks and pavements is usually found to be more challenging, because the thermal patterns generated from the heat reflected from the specimen surface are sensitive to environmental factors. ASTM C4788 specifies the methods for the detection of delaminations in concrete bridge decks. It states that 80 to 90% of the delaminations in a bridge deck can be located by IR thermography and inspection of the same deck by four different operators resulted in a variation of only about ±5% in terms of the predicted delaminated area.

In the pavements and bridge decks, deterioration can be in the form of delaminations, debonding of overlays, loss of cross-section subsurface, deterioration of joints, and subsurface voids [31]. Passive thermography has been used as an effective tool for the detection of delaminations and debonding in pavements and bridge deck components. In the periods of solar heating and cooling after sunrise and before sunset temperature differentials were created in the sound and delaminated concrete. The temperature differential increases with solar heating and stabilizes at about 1.5 to 4.5 ºC during mid-afternoon. It usually disappears for a short period just after sunrise and sunset during the transitions between periods of heating and cooling [30]. The differentials are also found to vary between seasons and with changes in ambient conditions such as wind and cloud cover. Usually a temperature differential of 1.5 ºC is suitable for thermal imaging, and testing should be avoided during winter/rainy seasons and for wind speeds exceeding 25 km/hr [30]. Moreover surface artifices such as debris, moisture and polishing of the concrete in the wheel paths can cause differences in emissivity and mask the surface temperature differentials.

In order to get a thermal surface map of the pavement or bridge deck, the equipment is mounted on a car and the infrared data are collected continuously with the car traveling at a constant speed [31]. Thus a stack of thermograms is obtained and the thermal patterns of the pavement surface are obtained through processing of the images recorded. This procedure has been explained in Section 8.3.1.3. The technique has been applied successfully for the inspection of an 18.5-mile stretch of the Dan Ryan Expressway in Chicago, Illinois [31]. Delaminated areas as small as 4 in. in diameter could be detected using IR thermography and helped in comprehensive assessment

of extent of repairs and estimation of rehabilitation costs. The effectiveness of the technique was also evaluated for 79 miles of reinforced concrete pavements. Some of the advantages of the technique observed from the studies included accuracy and speed of data collection and the ability to inspect a full lane width in a single pass, resulting in very little traffic congestion. It was also observed that the thermograms were easily pieced together for true vertical images.

Imaging of concrete pavements and bridge decks by IR thermography from the air was also tried out for faster inspection and no interruption of traffic [30]. During this inspection the equipment was mounted in a helicopter and several bridge decks and pavements were imaged for detection of delaminations. Though this reduced the time required for processing the thermograms since a wider field of view could be imaged, this also reduced level of precision and detail from the images. Moreover the results were affected by the weather and wind conditions and the flight heights ranged from 15 to 400 m. The thermal images were generally poor and the delaminations were not visible in some thermograms. Thus the airborne imaging technique is currently not feasible but is a promising tool since in this technique the inspection can be carried out through remote sensing without any closure of the traffic lanes.

Application of IR thermography in the inspection of concrete subsurface defects in large and complex structures can be observed in the non-destructive evaluation of the 33,445 m^2 reinforced concrete shell roof of the Kingdome in Seattle [33]. The primary objective of the investigation was to evaluate in-situ concrete conditions and to detect planar-type locations of deep voiding or delaminations associated with the consolidation and reinforcement placement conditions. The passive thermography technique was carried out during periods of relative heating or cooling of the roof to locate the areas containing subsurface defects. The unique and non-repeating thermal signatures with significant thermal gradients were identified as possible defects and delaminations and are illustrated in Figure 8.8. At the sites identified by thermography to be possible defect locations detailed investigation were performed, including visual inspection, impact echo testing, local exploratory openings and core sample collection. The anomalous areas identified by thermography were found to correspond well with locations of honeycomb, paste voiding and delaminations.

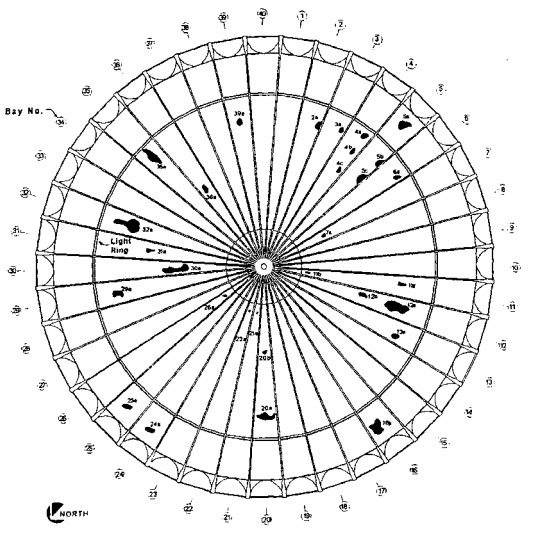

Figure 8.8: Defects observed in Seattle Kingdome roof through thermographic inspection [33]

Clarke, et al. used thermography in an attempt to detect delaminations on the underside of bridge decks in the field. Inspection was carried out from the ground level, and the distance of the camera from the object was 12 m (39 feet) [40]. The technique was found to be time efficient and was fairly successful in identifying delamination areas (Figure 8.9). However, weather and temperature of the surrounding objects were found to have a considerable impact on the inspections. Another common application of IR thermography has been in the assessment of heat loss in houses (Figure 8.10) to determine the thermal insulation quality [40]. However this application is more aimed towards non-structural objectives.

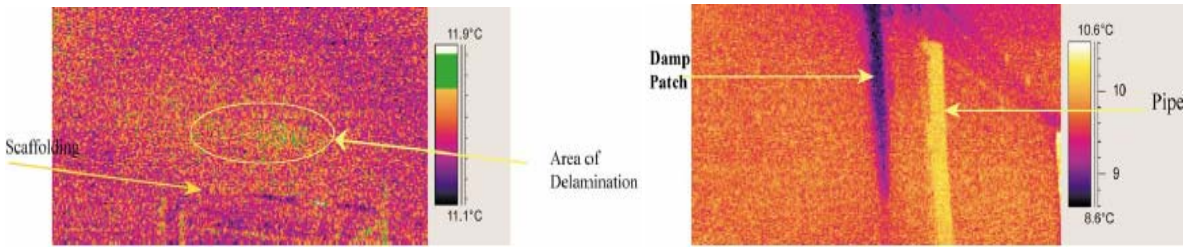

Figure 8.9: Thermograms of underside of a RC bridge deck [40]

Figure 8.10: Thermography survey of a house for assessment of heat loss [40]

Another application of thermography has been in the detection of moisture ingress in reinforced concrete and masonry structures. It is to be noted that the high specific heat of water causes it to act as a sink for incident heat from the sample surface. Thus an area with water ingress will appear as a cold (dark) spot in a thermographic image and can be easily separated from an area with debond/delamination, which will appear as a hot (bright) spot. Clarke, et al. investigated the use of thermography in the identification of defect areas, such as presence of moisture in the fill of a single span, low rise, masonry arch bridge [40]. The presence of dark spots in the brick arch (Figure 8.11) was identified as potential areas of moisture ingress.

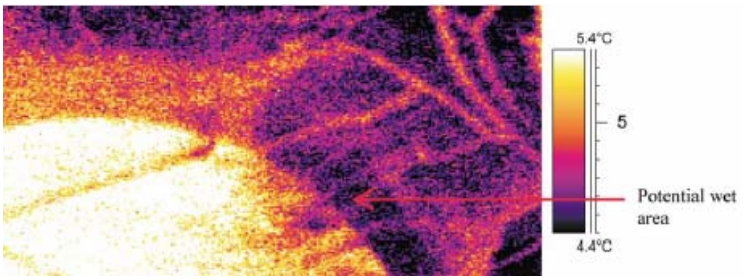

Figure 8.11: Thermographic image showing area of moisture ingress [40]

Lock-in thermography was also applied in the detection and characterization of delamination defects in concrete box culverts under a railroad [32]. The tests were carried out for three different heating periods, and the location and size of the defects could be estimated from the contrast changes in the phase delay images. From the calibration curves of the relationship between the phase difference and heating period for different defect depths, as illustrated in Figure 8.12, the depths of the delamination defects in the specimens could be estimated.

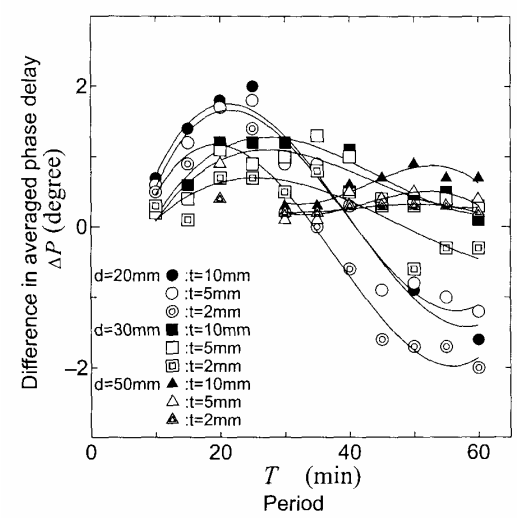

Figure 8.12: Relation between phase difference and heating period at different depths [32]

Attempts have also been made to use IR thermography for the monitoring of progressive damage and mechanisms of concrete failure [34]. As mentioned previously, stress generated thermal fields can be used for defect detection and quality assurance. In reinforced concrete structural components subjected to inelastic loading, heat will be generated due to intrinsic energy dissipation in the hysteresis loops in the areas of stress concentrations in the loaded zones. At the macroscopic level, the energy dissipation is a result of loss of stiffness and accumulation of irrecoverable deformations. At the structural level it is a result of micro cracking and slippage at the aggregate-cement paste interfaces [34].

The micro cracks are usually formed at regions of stress concentration, and with sustained loadings there will be progressive growth of the cracks and increased plastic deformations. This results in non-linearity and softening of the stress strain curves, and the work done to produce the plastic deformation causes heat generation until the concrete reaches ultimate strain resulting in fracture. Thus the primary objective in the monitoring of the heat patterns in the defect critical regions using IR thermography is to image damage progression during plastic deformations. The vibrothermography technique can be applied for the development of heat patterns in the specimens under fatigue loading. Tests carried out on plain concrete specimens under vibratory compressive excitation demonstrated the following [34]:

a. For vibratory excitation ranging between 25% and 50% of the nominal uniaxial compression, the heat dissipation observed over 2,000 load cycles was small.

b. For excitations between 50% and 75%, the stress concentrations around cracks or defects could be observed in the $1{,}000^{th}$ load cycle.

The thermography technique is a very promising NDE tool for the evaluation of damage propagation in earthquake resistant concrete structures. Attempts have been made to monitor the development of plastic hinges at the base of columns in a reinforced building frame subjected to seismic loading [34]. The inelastic deformations at the plastic hinge regions result in progressive evolution of heat generation. Thus IR thermography can be used for detection of damage progression and its effect on the strength and ductility of the structural component.

8.5 THERMOGRAPHIC DEFECT DETECTION IN COMPOSITES

8.5.1 Composite-composite and composite-concrete bond

Externally bonded glass or carbon FRP systems may be used for the enhancement of the flexural or shear strength and/or confinement of a deficient structural component. The loss of bond between the composite layers or between the composite and concrete will thus result in the degradation of strength of the retrofitted specimen. Three types of bond defects are usually observed in FRP retrofitted structures:

1. Unbonded Area, which is usually not caused by structural failure but due to initial lack of bond during application;

2. Debonded Area, which occurs due to separation between the composite and the underlying concrete surface; and

3. Delaminated Area, due to separation of two layers of composite.

The acceptable limits for unbonded, debonded and delaminated areas as specified by the ACI 440 2002, “Guide for the Design and Construction of Externally Bonded FRP Systems for Strengthening Concrete Structures” are as follows:

a. Inspection methods should be capable of detecting delaminations of 2 in2 or greater.

b. Small delaminations less than 2 in2 each are permissible, so long as the delaminated area is less than 5% of the total laminate area and there are no more than 10 such delaminations per 10 ft2.

c. Large delaminations greater than 25 in2 can affect the performance of the installed FRP and should be repaired by selectively cutting away the affected sheet and applying an overlapping sheet patch of equivalent plies.

d. Delaminations less than 25 in2 may be repaired by resin injection or ply replacement, depending on the number and size of delaminations and their locations.

In order to verify the above specifications in a composite retrofitted structure, IR thermography can be used as an effective NDT technique for rapid, cost effective and reliable condition assessment.

8.5.2 Detection of disbonds in composites

IR Thermography can be used as an effective NDE technique to monitor the installation quality and long-term efficacy of repair in FRP rehabilitated bridge decks, girders or columns. One of the inherent advantages in the use of Thermography techniques in composites is that composites are relatively poor conductors of heat. As a result, differences in the heat pattern, which are representative of temporal anomalies, approach thermal equilibrium at a relatively slow rate. Hence, discontinuities can be distinguished over a longer period, leaving more time for inspection and data acquisition. Moreover, most polymer and ceramic matrix composites have reasonably good light and IR absorption properties, as well as good IR emissivity [45]. Thus for composites with a clean surface no additional surface preparation is typically required.

The inspection equipment consists of an infrared thermometer, infrared camera, a video recorder and a heat source (flash light or heat gun, for active external heating). The heat pulser is used to develop a temperature differential on the composite surface (Figure 8.13). For laminates thicker than 1 mm, incandescent light bulbs, infrared lamps and radiant heaters are usually used, while xenon flash light and pulsed lasers are used to provide a short duration / high intensity heat for thin laminates [12]. Commercial heat guns are also used in some applications but usually not preferred as they produce a non-uniform surface temperature.

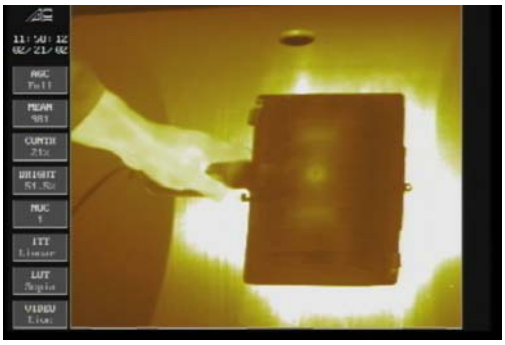

Figure 8.13: Thermal stimulation [8]

Initially the composite laminate and the concrete are at the same temperature. When heat is applied, the temperature rises uniformly in the composite surface due to diffusion of heat towards the cold concrete interface. The rate of heat flow is a function of the intimacy of contact between the composite layers and between composite and the concrete. In the areas with disbonds and delaminations, the transfer of heat is slower resulting in higher temperature ("hot spots"), which can be detected with the IR camera (Figure 8.14).

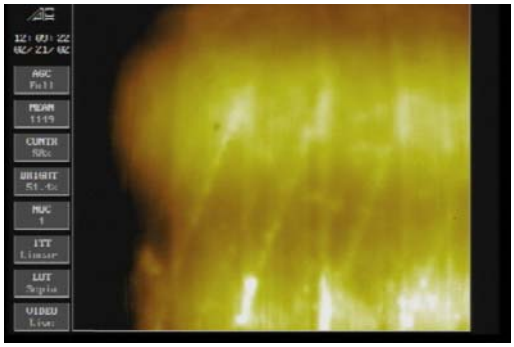

Figure 8.14: IR image of hot spots [8]

In laminated composites the conductivity is also found to vary significantly in different configurations and depend on the fiber type, layup sequence, and fiber, resin, and void contents. Being a non-homogeneous material, the individual properties of the fiber and the matrix will determine the heat conduction. The in-plane anisotropy of the material in terms of different ply orientation in a layup is usually negligible, and a multiple ply laminate behaves as a quasi-isotropic material. Heat propagation usually occurs more rapidly along the fiber than through the matrix, and glass fiber (GFRP) composites generally show a lower conductivity as compared to graphite fibers. Hence, to capture the temperature decay of CFRP to the desired detail, higher frame rates may be required.

This is illustrated in Figure 8.15, in which it is shown that the heat front will advance uniformly in the homogeneous materials such as metals, while in the composites the heat front will tend to advance more rapidly in the direction of the composite fibers. However, even though heat conduction is significantly higher in the direction of the fibers, there is significantly more axial surface area of the fiber wall exposed to the matrix than there is surface area available for heat conduction through the fibers [45]. Consequently, there will be a significant amount of heat conduction into the composite sample.

In most large-scale applications, such as retrofitted bridge decks and girders, passive thermographic testing is given preference, as it is more convenient and uses an ambient source of heat [11]. However, in many cases, passive thermographic testing generates only qualitative results, which are relevant only for evaluation on a structural level. Thus, in order to detect and characterize defects quantitatively, active "pulsed" or "lock-in" thermography with an externally applied thermal field (EATF) is used in many composite applications.

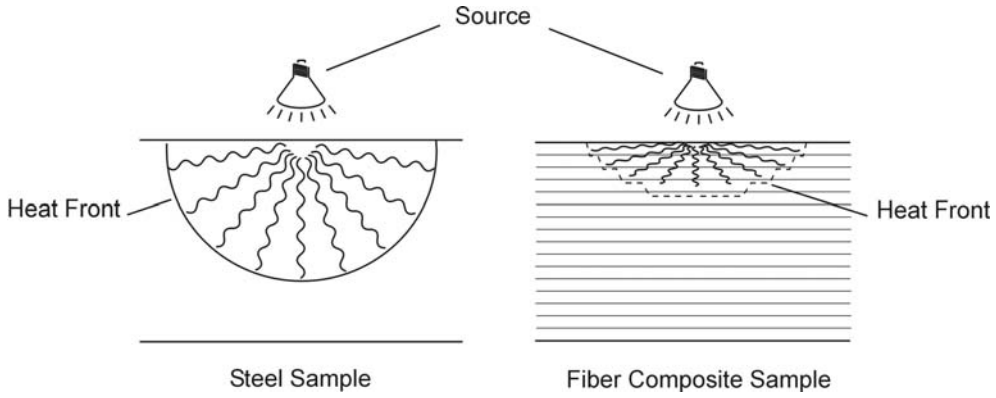

Figure 8.15: Thermal conduction in steel and composite samples [8]

8.5.2.1 EATF thermography in composite defect detection

There have been quite a number of successful applications of EATF IR Thermography in the defect detection between composite layers. This research has been mainly instigated by the aerospace industry for detection and monitoring of delaminations between composite layers in aerospace structural components. However, they are equally applicable towards the understanding of defect detection using IR thermography in composites used for the structural rehabilitation of civil engineering components. With the growing focus towards rehabilitation of the rapidly deteriorating infrastructure and the need to use advanced NDT techniques such as thermography for rapid, cost effective and reliable condition assessment of both deficient and retrofitted infrastructure, more thermography research is currently being done with the main focus on civil infrastructure.

EATF Thermography has proven to be an effective NDE approach for a range of applications including detection of trapped water in honeycomb panels, detection of debonds/delaminations, and evaluation of composite repairs [5]. Dutton investigated the effect of defect size and depth on detectability using the PT technique [20]. Glass-polyester composite specimens with different sized defects located at various depths were studied. The defect consisted of an envelope of polyamide film filled with air simulating an air void. Figure 8.16 illustrates the detectability of varying depths of flaws for three different flaw sizes. It was observed that the size and depth of the flaw controls the maximum signal amplitude of the heat pattern that can be detected at the surface using IR thermography.

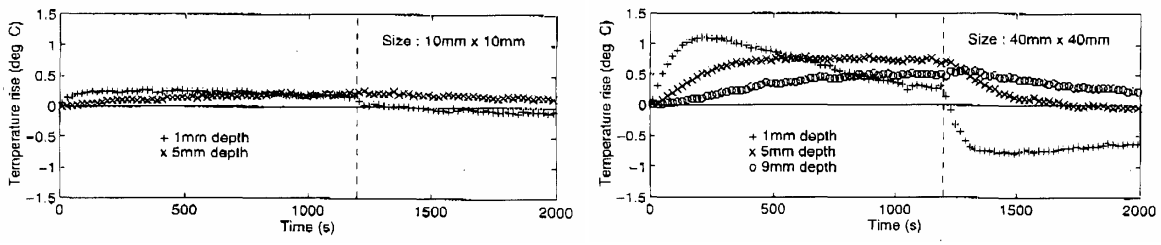

Figure 8.16: Effect of depth and size of defect on thermographic detectability [20]

An analytical heat flow analysis was carried out by Jones, et al. to look at the effects of defect size and depth on their detectability using thermography technique [23]. A solid graphite epoxy laminate, 0.5 cm thick, with typical quasi-isotropic properties of graphite-epoxy was used for the analysis. Discontinuities were simulated at various depths of the model as a percentage of the laminate thickness. Two defect sizes, 3.6 cm x 3.6 cm and 1.2 cm x 1.2 cm area were also used for two separate cases. Analysis was then done to study the effects of a thermal pulse traveling through the graphite-epoxy solid element with the impregnated defects in terms of the thermal intensity at the surface of the laminate. An explicit finite difference solution of the heat conduction partial differential equation was used. The heat intensity at the surface of the laminate generated by a large flaw, 3.6 x 3.6 cm in area, located at various depths is illustrated in Figure 8.17a. It is evident that the peak intensity diminishes rapidly with an increase of defect depth and is only barely detectible when located at halfway through the laminate.

The results obtained for a smaller defect size, 1.2 x 1.2 cm area, is illustrated in Figure 8.17b. It is interesting to note the difference between Figures 17a and 17b. First, the intensities measured at the surface decrease with a decrease in the defect size. Second, the rate of thermal decay as the defects move deeper through the thickness is higher for the smaller defects. Finally, the widths of the intensity peaks are narrower for the smaller discontinuities, indicating that the thermal signatures will be available only for a short time interval for detection. All these effects can be explained by the in-plane conduction of heat in composites. In composites the in-plane conductivity is higher as compared to that in the direction of its thickness. As the size of the defect decreases, this higher in-plane conductivity has an increased blurring effect on the thermal intensity observed at the surface and causes a reduction in the intensity and shifts the peak to an earlier time since the in-plane heat flow quenches the intensity before the anticipated peak can be reached [23].

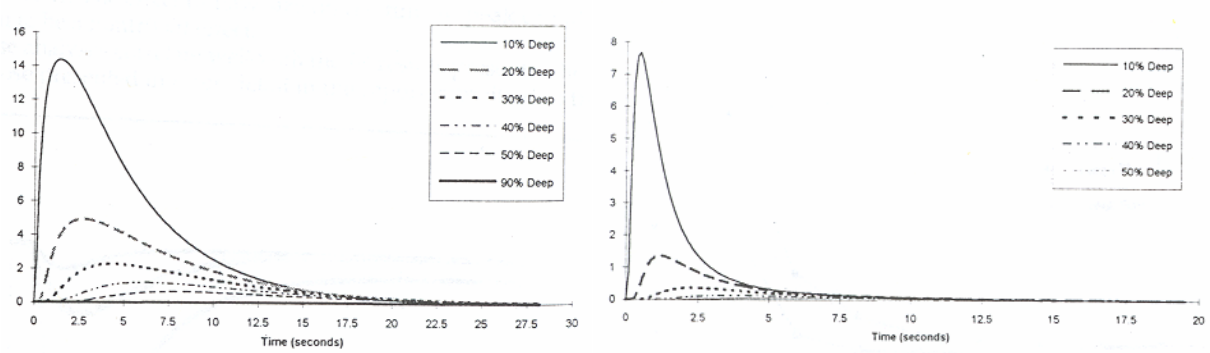

Figure 8.17: a) Thermal intensity for large flaws; b) Thermal intensity for small flaws [23]

Similar conclusions were arrived at by Cielo, et al. through experimental tests on multiple graphite-epoxy laminates with simulated subsurface delaminations of different sizes and at different depths [21]. The smaller defects and the defects located at larger depths required a higher heat energy input for clear discernability. The thermal image became

blurred and had a low defect visibility when the thermal path to the depth of the delaminated area was of the order of the thermal path corresponding to the radius of the delamination. In an isotropic material defects become difficult to detect with radius/depth ratio equal to or smaller than unity. In thermally anisotropic materials such as composites, the thermal diffusivity α_1 in the direction of the fibers is usually larger than the thermal diffusivity, α_2 transverse to the direction of the fibers. This further increases the radius/depth ratio for proper visibility on the thermal image [21].

In another study it was found that the surface temperature increased by up to 50% as the size of the delamination increased from 3x3 mm to 25x25 mm, and the temperature increased by 5% as the delamination depth decreases from 1.9 to 0.6 mm [22]. The numbers are representative of a particular composite type, however, and can vary for different orientations, stacking sequence and material properties.

It is to be noted that deeper defects can be detected for materials with high thermal conductivity such as graphite. However because of the high in-plane conductivity, the thermal intensity changes observed at the surface of the specimen would disappear very quickly and thus the temperature measurements have to be completed within a short time interval [37]. Thus, though the thermography technique works well for the detection of flaws close to the surface, it loses application for defect detection far away from the surface or for small sized defects. For most composite retrofitting of civil infrastructure, the laminates are externally bonded to concrete, and thus thermography techniques can be used for successful defect detection in the near surface composite-composite or composite-concrete interface.

One of the useful applications of thermography is in the NDE of composite sandwich constructions, which have become popular by virtue of the high strength, low weight and high stiffness achieved, and which have a large field of applications ranging from aircraft to naval structures. Vikstrom evaluated the effectiveness of thermography for the detection of defects within sandwich panels with faces of glass FRP composite laminates and a core of rigid cellular PVC foam [41]. The main challenge lay in the detection of any disbonds at the joints that existed between subsequent core blocks and the bondline between the face sheets and the core, since they induce stress concentrations and thus have an adverse effect on the structural strength of the entire sandwich. Thus the simulated disbonds in the tests were placed between the core blocks and between the face and the core as well as inside the core. The camera was placed at a distance of 0.6 m (2 feet) from the test sample. The inspections were able to pick up defect areas at the interface of the core and the facing and between the core blocks, but they were not able to pick up the cavity areas simulating defects within the core.

The viability of the use of thermography for NDE of large-scale sandwich constructions was evaluated by Dattoma, et al. to investigate a wind turbine blade, 17m (56 feet) in length [42]. Two portions of the blade were investigated. The spar, which provided strength to the blade in the length directions and carried the majority of the load, was constructed of glass FRP with the fibers running lengthwise. The shell, which formed the external part of the blade and had a wing profile, was manufactured in a sandwich structure, with the face made up of GFRP laminates with the fibers randomly oriented

and the core was low-density expanded PVC foam. Thermography inspections were conducted to detect any defect areas in the sandwich structure of the shell as well as the adhesive joint between the shell and the spar. The inspection was done in the cooling phase. A thermographic image obtained from the study of the sandwich structure shell is presented in Figure 8.18 and shows debonded areas between the outer skin face and the core. In addition, thermography was able to detect the presence of glue filtering in some of the fissures of the foam core.

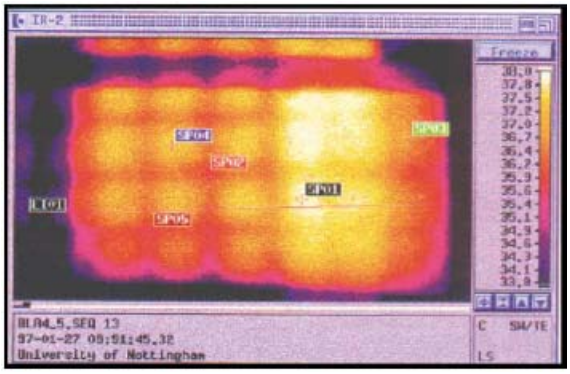

Figure 8.18: Thermogram of an area of the turbine blade [42]

As seen in the previous applications, joints form an important part of structural performance since they generally represent a weak point. Thus the presence of any defects in the joints will lead to degradation of the structural performance and reduction of life. A joint can either be adhesively or mechanically joined and in either case it is susceptible to cracks, delaminations and impact damages [43]. Thus there is a need for NDE of such joined components, and thermography can be used as a viable inspection tool in such applications.

Shroeder, et al. investigated the use of thermography for quality assessment of structural adhesive bonding in automotive applications [44]. A composite pickup truck box structural inner assembly was used for the inspection. The truck box was made up of random chopped GFRP manufactured by injection molding. It was supported by composite cross-sills running horizontally across the underside of the box and connected to the box using epoxy adhesives. The objective of the investigation was to evaluate the quality of the bond at the joints. Pulsed thermography inspection was conducted using a commercial thermographic NDT system (Figure 8.19a).

The inspections revealed “starved” bonds where insufficient adhesive was applied, as illustrated in Figure 8.19b. One of the difficulties faced in this inspection was degradation of the image, to some extent due to the chopped fibers in the composite. However the inspections gave a clear indication that it might be possible to have effective quality control during the manufacture of components with adhesively bonded composite joints through the use of thermographic NDE. Inspections were also carried out after spread

load testing of the composite box, and a new debonded area at the side of the box sidewalls was observed to appear as a result of the load (Figure 8.19c). Inspections were also carried out to detect the quality of the bond after being subjected to impact damage.

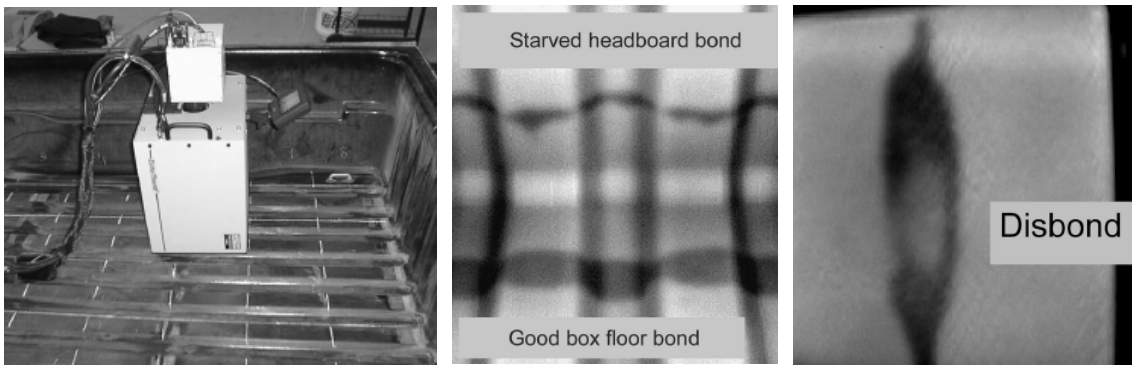

Figure 8.19: a) Thermography inspection; b) Thermogram of bondline quality; c) Disbond after spread loading [44]

Composites are also finding growing applications in the naval industry in the design and fabrication of surface ships and submersibles. Thus there is a need for non-destructive characterization and defect detection in the composite component. Such inspections carried out over the lifetime of the structure will give indications on whether the structure can be left in service or whether it needs to be replaced or repaired. Applications of thermography in naval structures are reported by Lipetzky [36]. A number of NDE techniques including thermography, tap, ultrasonics, shearography and microwave were used for the evaluation of the composite mast aboard a surface combatant, USS Radford (Figure 8.20), for disbonds, delaminations and impact damages.

One of the main challenges in this research was the detection of "kissing disbonds" which represent defect regions in intimate physical contact with each other but without any mechanical bonding. Sample specimens were tested in the lab in which such kissing disbonds were simulated using Teflon sheets or a release agent in between the E-glass composite laminate layers. Pulsed flash lamps were used as the heat source for thermography inspections. The disbonds could be detected well using thermography.

Figure 8.20: Thermography application in large-scale composite naval structures [36]

Apart from defect detection, thermography techniques have also been used for quality control purposes of composite laminates through the detection of epoxy-starved regions in the cured laminates, which might be produced under excessive squeezing of the epoxy out of the laminate [21]. The heat pattern was found to have higher amplitude in the epoxy rich regions as compared to the epoxy starved zones. However the changes were very subtle, and operators and image enhancement software were used for visibility of the difference in heat patterns.

Reports on impact damage have shown that IR imaging is an effective tool for detection of barely visible impact damage in composites [23]. The impact damage in the composites is a combination of fiber fracture and interlaminar defects. Inspection was done on 6.35-mm (0.25-in) thick CFRP samples that had suffered a range of impact delamination after being impacted at energies of 27 and 30.5 J (20 and 22.5 ft-lb). The samples showed mild surface indentations, some front-surface cracking and back-surface blistering [23]. Inspection in both transmission and one-sided modes showed the effectiveness of IR Thermography in the detectability of damage.

The IR inspections of the impact-damaged samples were also effective in revealing that different levels of impact energy produced differences in the delamination damage. Use of some image processing tools, such as frame averaging and contrast manipulations helped to reduce the noise of the signal and were also effective in boosting the details in the smaller discontinuities. Cielo, et al also investigated the use of thermography in detection of impact damages in graphite-epoxy specimens with satisfactory results [21]. Thermographic images of impact damages and cracks in composites are presented in Figure 8.21.

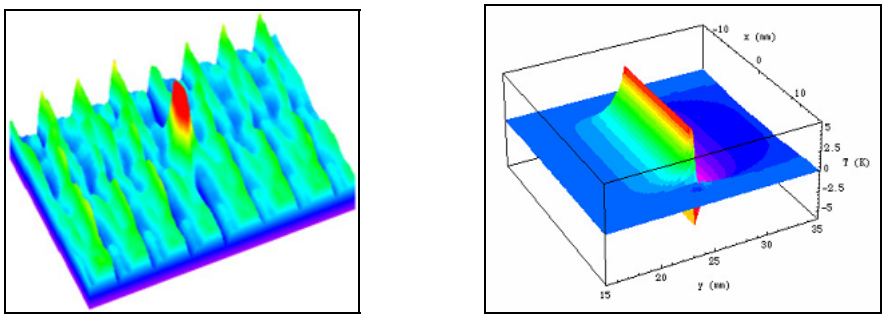

Figure 8.21: a) Crack in a composite; b) Impact damage in a lamina

8.5.2.2 Thermography for NDE of composite applications in civil infrastructure

Advanced composite materials are gaining rapid acceptance in the construction and retrofit industry, both as a new construction material and for the rehabilitation of deficient existing structures. Fiber Reinforced Polymer (FRP) composite materials, exhibit superior performance levels in terms of high strength-weight and stiffness-weight ratios and resistance to environmental factors, such as corrosion. These characteristics make

them potentially viable for use either for the construction of new durable civil infrastructure components with longer service lives, or as an add-on in rehabilitation/retrofit applications for performance enhancements of deficient existing structural components.

However, being a relatively new material in civil infrastructure applications, there is a lack of data on their long-term performance and overall durability under sustained loading and harsh environmental conditions. Thus there is a need for the development and standardization of non-destructive testing techniques for quality control during installation as well as evaluation of the long-term performance of these materials. The weak links in the use of these materials exist: 1) at the bondline; 2) at the micro-level as voids or discontinuities; 3) at the macro-level as debonds or delaminations between composite laminates or between the composite and the surface to which it is bonded; and 4) at the structural level in adhesively bonded composite joints. The NDE techniques need to focus on these weak links and to evaluate the performance of the structure based on the behavior of these components.

Thermography has long being recognized as an effective NDE technique in defect detection in the aerospace industry. Based on this platform, a number of research programs have been undertaken to evaluate its effectiveness in civil infrastructure specific applications, particularly in the field of defect/damage detection and monitoring in FRP composite rehabilitated structural components.

Miceli investigated the use of IR thermography in the health monitoring of FRP bridge decks [24]. The primary objective was to evaluate the behavior and structural integrity of a pultruded glass fiber reinforced polymer bridge deck using thermography. The main research focus was on the detection of debonding of composite components within the deck system under fatigue loading. The bridge deck components were made from alternating layers of random glass mat fibers and unidirectional glass fiber rovings in polyester resin. The overall deck dimension was 15 ft length, 5 ft width and 7 in. depth and was composed of square tubes sandwiched between glass fiber plates (Figure 8.22).

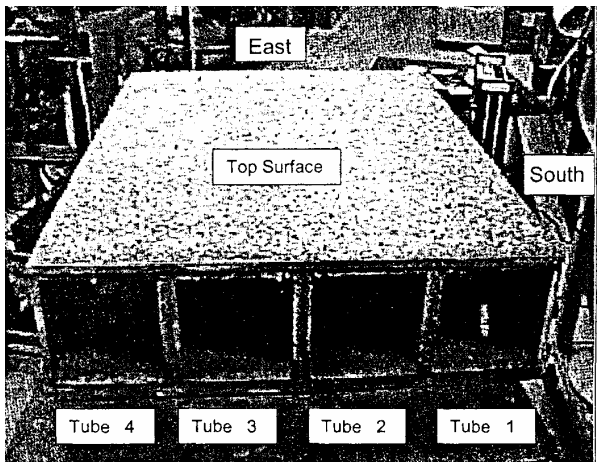

Figure 8.22: FRP bridge deck used for thermographic inspection [24]

Unusual thermal patterns were observed in the areas of inadequate adhesion between the components. After the laboratory testing, two in-situ polymer bridge decks on I-81 in Troutville, Virginia were inspected using thermography. The investigation revealed that thermography had the potential to provide valuable information regarding the debonding between critical FRP bridge deck components and could be used as a valuable tool for the health monitoring of bridge decks.

Most applications of IR thermography in composites have been in the defect detection between composite laminate layers. Some work has also been done in terms of debond detection at steel-composite and aluminum-composite interfaces [25, 21]. For civil infrastructures, however, debond detection at composite-concrete interface is of great importance.

Levar, et al. investigated the use of IR thermography to evaluate bonded CFRP composites used to strengthen reinforced concrete beams [26]. IR inspections were conducted on the beams, strengthened with several configurations of CFRP composites before loading to determine the extent of the bond. The beams were then statically tested to failure, and IR inspections were done periodically to determine the amount and characteristics of bond damage. The main objectives of the research were:

1. To determine the effectiveness of IR thermography in the inspection of FRP strengthening systems for both initial application and long term performance.

2. To monitor the progression of debonded areas under loading till failure.

3. To estimate the installation quality expected from different strengthening systems.

The beams were 16 ft long and had a 4 in. x 12 in. cross-section with concrete strength of 5 ksi (35 MPa). The beams were strengthened with two systems of CFRP laminates using wet layup. Quartz lamps were used as the heat source, and the pulse thermography technique was used. Initial thermographic investigation revealed that unbonded areas at the composite-concrete interface could exceed 20% of the total CFRP area. Coin tap tests conducted simultaneously revealed that the tap tests were unable to detect about 20% to 30% of the defects.

Inspections were also done during loading at 60%, 80% and 100% of the calculated capacity of the beams. The unbonded and delamination areas were distinguished on the basis of their depth of occurrence, identified from sample tests carried out before full scale testing. The inspections revealed the growth of debonded and delamination areas at different stages of loading. A comparative evaluation of the two systems tested could also be made in terms of debonded areas. IR images obtained from the study are presented in Figure 8.23.

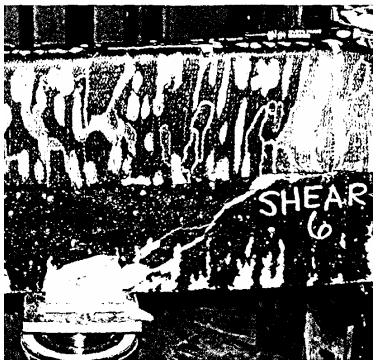

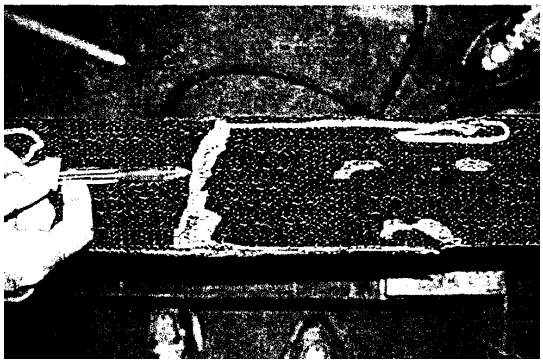

Figure 8.23: Defect detection in wrapped beams using thermography [26]

Hawkins, et al. investigated the utility of thermographic methods for the inspection of debonds on composite overwraps for circular concrete bridge columns in an in-situ environment [27]. The bridge columns were located under the I-10 freeway in Los Angeles, California. Three systems of column retrofitting – hand layup, pre-cured shells and machine wraps – were evaluated. Both active heating (using high intensity heat lamps) and passive heating (making use of solar radiation) were used as heat sources for the inspection of the retrofitted columns.

Prior to the thermographic inspection the columns were tap tested. The IR survey from over 50 feet away showed clear indications of the presence of debonded regions in the form of entrapped air pockets of about 2-in diameter in the columns with hand layup overwraps. In the columns with pre-cured shells, debonds were noticed close to the slits or butt ends where the cinching straps might not have been effective in confining the shell. The amount of defects in the machine wrapped columns were found to be much less.

The application of thermography for the in-service evaluation of an FRP strengthening system in a reinforced concrete T-beam bridge was reported by Elsafi, et al. [35]. The bridge, built in 1932, was a 42 ft. long and 120 ft. wide RC structure with 26 simply supported T-beams. FRP composites were used for flexure and shear strengthening of the beams in view of the loss of capacity due to section loss of the reinforcing steel to corrosion and extensive cracking.

The bridge was instrumented and load tested before and after installation of the FRP system for global assessment of the effectiveness of the FRP retrofit. Thermographic inspection (Figure 8.24) was conducted for detection of any localized bond flaws after the retrofit system was in service for two years. No major deterioration in the bond quality was observed in these inspections, and this observation was supported through load tests. The purpose of this thermography inspection, however, was only to detect any major deterioration in the composite bond and was performed more on a qualitative basis.

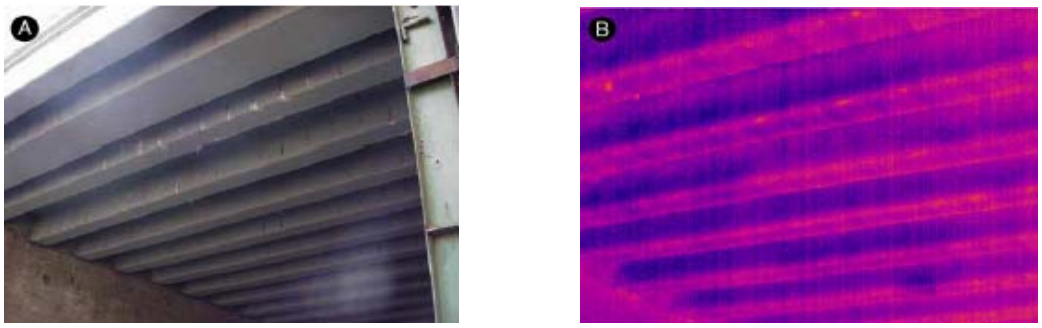

Figure 8.24: Thermography inspection of FRP rehabilitated T girders of a RC bridge [35]

Morton used thermography to perform quality assurance tests on composites used to rehabilitate the beams in two concrete T-girder bridges [39]. Both of the structures had spans of over 34 feet and were 30 feet wide with 6 T beams. Three different rehabilitation schemes were used to upgrade the T-beams: 1) Replark carbon sheet, 2) 5" carbon plate, and 3) carbon unidirectional sheet. From load testing, all the rehabilitation schemes were found to produce around 8% stiffness increase and 15% decrease in strain. Thermography was then used to evaluate the quality of the bond between the concrete and composite. Voids in the bondline could be detected down to ½" diameter. The Replark carbon sheet rehabilitation scheme showed a significant number and size of voids. This was attributed to the irregular contours of concrete formed by ridges in the forms and droplet sized cured primer. The Replark sheets did not conform to these irregularities, and this resulted in the voids in these regions, which totaled about 15% of the total bonded area. The CFRP sheets, because of their flexibility, were able to conform better to the surface irregularities and consequently had much fewer voids: less than 2% of the total bonded area.

8.5.2.3 Lock-in thermography in defect detection in composites

Pulse thermography techniques are the most commonly used thermographic defect detection method in composites. Limited applications of the Lock-in or Modulated Thermography technique (in which a modulated (usually sinusoidal) continuous heat wave is applied instead of a pulse) are also present for composite defect detection. Bai and Wong inspected specimens with 30 layers of CFRP lamina (totaling approximately 4.2-mm in thickness), containing various artificially implanted layers of Teflon film [14]. Defect sizes ranged from 1 to 11 mm (0.04 to 0.43 in) in diameter at depths between 0.28 and 2.8 mm (0.01 to 0.11 in). The heat modulation frequency was varied over a predefined range to evaluate its effect on defect detectability.

It was found that, depending on the defect size and depth, a "blind frequency" existed at which no distinct phase difference was apparent. Optimum frequencies also existed that were most suitable for displaying defects of certain size and depth. While large defects could be detected throughout the entire depth range, phase differences of defects ranging from 1 to 6 mm (0.04 to 0.24 in) in diameter were not sufficient for detection. However, because differences between the thermal properties of Teflon and CFRP are less

pronounced than between air and CFRP, the measured detectivity of this specific application can be considered as conservative.

8.5.2.4 Vibro-thermography in defect detection in composites

Vibro-thermography can be used for the evaluation of defects or delaminations in composite laminates or the composite-concrete interface. High amplitude, low frequency mechanical excitation is usually used to study the progression of damage in composites subjected to fatigue type vibrational loading. Under fatigue or cyclic loading the initiation and progression of damage in composites may be a combination of several damage modes, including matrix cracking, fiber matrix debonding, delamination, void growth, local fiber breakage or interface debonding, depending upon the material system, stacking sequence and specimen geometry. Thus vibro-thermography can be used as an effective tool to monitor the mode of failure in composites. A low amplitude, high frequency excitation is usually used for the detection of pre-existing defects.

One of the earliest applications of vibro-thermography for detection of defects in composites was in studying the fatigue damage in composites [28]. Boron-epoxy laminates with a stacking sequence of [0, ±45, 0] and a 0.25 in. diameter hole were subjected to fatigue loading. The progression of damage was observed through the development of thermal patterns around the hole. The observed heat patterns were found to correspond well with the stress distribution obtained through stress analysis. The detection of delamination in composites using the vibro-thermography technique was studied by Henneke in $[0, \pm 45, 0]_S$ boron-epoxy laminates [18]. The surface heat pattern, monitored through real time vibro infrared thermography, was found to correspond well with the shape of the damaged/delaminated regions inside the composite.

8.5.3 Effectiveness and limitations

The main advantages of IR Thermography testing for evaluation of composite-composite and composite-concrete bonds are the ease of deployment for in-situ inspection and the relatively short inspection time due to surface-wide heating and monitoring. Also, since no physical contact is required, the inspection personnel can work at a safe distance from traffic and not cause any interruption to the traffic flow. This technique can be used as an effective tool both for quality assurance during the installation of the composite system and for the health monitoring of the structure through its life span by providing a quick and comprehensive insight to material properties. Due to its capability of covering large areas at a relatively short duration, it can be applied in both near- and full-field measurements. The high sensitivity of modern recording equipment (±0.1°K temperature difference) provides a very high spatial resolution for successful detection of the defect location.

However, the sensitivity of the technique can be affected in a subtle way. One of the main requirements of this technique is uniform heating over the surface. Thus care should be taken in the field to obtain a uniform heating. This can be accomplished by using a linear array of heating lamps or flashlights mounted on a wheeled base (e.g., the D2D technique discussed previously). The base can be contoured to match the surface under inspection. Even with uniform heating, the ambient temperature variations (due to changes in temperature or wind speed) can affect the

heating / cooling rate of the structure and the quality of the thermographic image [27]. Also the degree of thickness variation in the composite material or the adhesive (particularly for pre-cured composite shells used in columns) can cause variations in the heat diffusivity.

The presence of surface artifacts such as dust, grease and paint can cause changes in the emissivity. Moreover, thermography is more effective for the detection of bond defects at shallow depths, and internal defects must be of sufficient magnitude to affect heat transfer at the surface. As a result, small defects at considerable depth can rarely be identified. This is generally not a problem for the defect evaluation of externally FRP-retrofitted structural components, however, since debonds will usually be at a shallow depth.

8.6 FIELD APPLICATION OF IR THERMOGRAPHY – A PRACTICAL PERSPECTIVE

Infrared Thermography has been effectively used over a broad range of applications in the aerospace industry with considerable research work on the viability of the technique in defect detection in composites. With the recent advances in computing power complemented by the development of efficient imaging algorithms, research conducted on the application of this technique for defect detection in civil engineering infrastructure has been discussed in the previous sections of this chapter. The results are very promising; however, successful implementation of the technique under actual field conditions holds the key to its widespread acceptability in the infrastructure industry.

As discussed in the previous sections, there has been research on the evaluation of viability of this technique in several areas:

- health monitoring of FRP bridge decks [24];
- quality assurance and damage detection of FRP rehabilitated girders of RC bridges [35,39];
- detection and monitoring of debonds/ delaminations in RC beams [26];
- inspection of debonds on composite wraps for concrete bridge columns [27];
- inspection of heat loss, waterproofing and surface integrity characteristics in buildings [11, 29]; and
- detection of delaminations in concrete pavements, box culverts and reinforced concrete roof shell [30, 31, 32, 33].

The main focus of most of this research has been on the mere detection of the defect/damage, rather than on the quantitative evaluation of the damage, its severity and effect on the structure as a whole and subsequent progression of the damage under sustained loading. Thus more research is needed in this regard for widespread application of the technique as an effective NDE tool by the engineer for quantitative evaluation of the performance level of a structure. The current research is aimed at this aspect of making the technique automated and quantitative, but a basic understanding of its application constraints in the field must always be kept in mind for best

results. This section aims to present some of the practical aspects of application of thermography in the field and its promise as a successful health-monitoring tool for civil infrastructure.

8.6.1 Practical aspects of thermography application

As previously discussed, thermography techniques require a thermal field for the detection of defect/damage and this thermal field can either be heat or stress generated. From a practical standpoint, for large field projects dealing with large overall dimensions of the structure, it is more feasible to use an ambient source of heating (the sun) following periods of heating and cooling. This would make the process much faster and convenient to use. However the drawback is that the amount of heat received from the sun would vary throughout the year, making it difficult to monitor the structure at regular time intervals on a common platform. Thus spot temperatures need to be taken and the results should be calibrated accordingly.

This technique is more suitable for evaluating the performance of the system on the structural level. However for better characterization of defects and to evaluate performance on the local level, active thermography needs to be used in which the heat is applied by a heat gun, propane torch, kerosene lamp, xenon flash lamp, quartz lamp, halogen lamp, IR heating lamp or even a photographer's flash [26, 46]. Some of the relative merits and demerits of the different forms of external heating are briefly described below:

a) Xenon Flashlamps: The xenon flash lamp has been found to be one of the most effective sources of external heating for pulsed thermography. The advantage of using a flash lamp is that the magnitude and duration of the individual source heat pulses are known and can be adjusted if necessary. This helps in quantitative analysis, and the high intensity flash supplies enough thermal energy for detecting defects/damages at greater depths from the surface. Moreover, uniform heating is provided over the entire surface to be inspected. The effectiveness of the xenon flashlamps can be improved by mounting them inside a hood and with parabolic reflectors in order to concentrate the heat pulse towards the target. For most thermography applications for the inspections of near surface defects a typical flash duration of around 5 ms is used. However a higher flash duration or multiple flashes might be necessary for defect detection at larger depths.

b) Halogen Lamps: High intensity Halogen lamps (500 Watt) have been used in some applications and have proved to be fairly successful in providing the necessary thermal unit [46]. However the amount of heat input is less than that supplied by Xenon flashlamps, and a longer duration of heating might be necessary to provide sufficient thermal energy for the inspection of deeper defects. To get the best results out of this heat source for the inspection of composites, it is recommended that a thermal shield be placed between the heat source and the specimen and that the lamp be pre-warmed for some time [46]. The thermal shield should then be taken off and the thermal images recorded with the lamp on. After about 30 to 60 sec, depending on the thickness of the composite, the lamp should be turned off and the images recorded as the sample cools down. Thus the main disadvantages of this heat source are the longer inspection time and the lower heat energy input. The halogen lamps, however, are usually a preferred source of heat input in lock-in thermography applications, as a continuous harmonically modulated heating source operating in the long pulse mode [38].

c) IR heating lamps: 125 Watt IR heating lamps have been used in some applications, but the area of heating is limited to a narrow beam and it becomes difficult to heat the surface evenly [46]. It is necessary to move the lamp across the surface of the inspection sample to input the thermal energy; thus the thermal images cannot be collected from the sample during heating. Also the heat input cannot be quantified.

d) Photographer's Flash: 3200 Joule-sec photographer's flash has been tried in some applications for inspections of subsurface defects in composites [46]. But the heat input is too low and might work only for single layered composite.

For field applications, considerable attention also needs to be paid to the surface preparation of the area to be inspected. The emissivity of a material can be considerably affected by surface markings, dirt and grease or overhead lights, leading to false calls while performing the thermography. Thus it is recommended to clean the surface and if necessary to paint it black to get the best results. Usually a thin matt black coating with an emissivity value of 0.9 helps to eliminate spurious reflections [38]. The same applies to very shiny surfaces with high reflective properties. One of the common difficulties faced in the inspection of composite rehabilitated civil structures in the field is that after the rehabilitation work, the composite layers are coated with a thick layer of paint or epoxy for protection from environmental and impact damage as well as from aesthetic considerations. With such thick and dense coating materials on the surface, it becomes practically impossible to detect any subsurface defects in the composite layers, since these coatings allow very little diffusion of heat into the composite subsurface. This is one of the main limitations in the application of thermography in the field on structures with surface coatings.

The effect of the presence of a dirt layer over a composite sandwich structure was studied by Dattoma [42]. It was observed that the areas with the dust layer looked lighter on the thermogram, thus indicating higher thermal intensity as compared to clean areas. The layer of dust acted as a thin layer of a different material with a different emissivity value. Thus, while comparing between images collected from different parts of a structure with different orders of cleanliness or with different surface coatings, the emissivity of the surface material needs to be taken into account, and the surface thermal intensities obtained from the thermographic inspections need to be suitably adjusted. The same applies to inspections carried out for a structure with components made up of different materials. Since the emissivity will be different for the different materials, their thermal signatures in the presence of defects will be different in terms of absolute intensity values and thus will have to be modified to compare the severity of the defects in the different components. It should also be recognized that materials with emissivity values less than one will reflect radiation from surrounding objects as well as radiating its own radiation. Thus in such cases the thermal signature of an object will be influenced by those of the surrounding objects.

The settings of the infrared camera and the data collection unit also need to be given due consideration. They must be calibrated so that they can receive the emitted radiation signals in certain specified wave lengths which allow best transmission of the IR radiations through air. The infrared radiation is found to be most effectively transmitted in one of two wavebands, 2 to 6-μm and 8 to 14-μm [8]. In between these ranges, only limited transmission of the infrared

radiation is allowed in air. Consequently the detection devices must be calibrated such that they can receive the emitted radiation signals in the specified ranges.

The frame rate of data acquisition also needs to be given due consideration. For a multi-layer composite the use of a lower frame rate of data acquisition is usually recommended for best results. For single or thin-layered composites a frame rate of 60 Hz is usually adopted for inspection.

The distance of the camera from the surface and the angle of view can also affect the consistency of the results. For field applications it might not always be practically feasible to maintain the same distance and angle of the camera due to space constraints. Thus the results will need to be calibrated for the particular variables in order to compare them on a common platform. For field inspections of large structures it will be more practical to get a larger field of view by having the camera at a greater distance from the target. The disadvantage is that such inspections will not be able to detect minor defects. Moreover, the attenuation of radiation in the atmosphere caused by the absorption of energy by suspended particles and subsequent re-radiation in random directions can affect the obtained results. The camera-to-target distance will thus be governed by the level of precision desired for a particular application. For example, generally for aerospace structures the degree of accuracy necessary to pinpoint a defect will be much higher than for civil infrastructure applications.

In some applications, it might be necessary to monitor the condition of existing defects over a period of time, in terms of their growth or progression under sustained loading or detrimental environmental conditions. In order to carry out such monitoring with consistency, it is necessary to ensure repeatability of the test measurements, so that by keeping all the other variables fixed, only the progression of damage with time and loading can be easily extracted from the data.

This can be accomplished to a satisfactory level by using the automated transient thermography technique as discussed in Section 8.3.1.3. As discussed before, in this technique the camera and the heat source are mounted on a trolley which can be moved on rails supported by a formwork that helps to ensure constant distance of the camera and the heat source from the surface. Apart from the distance, there are other environmental variables such as temperature, humidity, and surface cleanliness, and camera variables such as input thermal pulse magnitude and duration, focus, and frame rate of data acquisition, all of which have to be kept within reasonable bounds.

The thermography images can be taken with the camera being static at a certain location and then moved to the next location to take the subsequent image so as to obtain the temperature profile along the length of the structure as a set of thermograms.

Another technique investigated is that the camera can be kept moving at a certain speed so that each segment will be in its field of view for a certain period of time. The evolution of the thermal pattern along the length of the specimen can then be studied by looking at the sequence of thermograms taken. Referred to as the D2D technique, this has not yet been tested on real structural components in the field, and further study is needed to evaluate its feasibility in the field [16]. For defect detection of pavements or bridge decks or surfaces which are accessible from the top, the camera and the heat source can also be mounted at the back of a car and a rapid, cost efficient condition assessment of the structure can be done.

Some applications of IR Thermography have also been discussed in this chapter where instead of an external heat source, external mechanical vibrations can be applied which will result in stress concentrations in defect areas. The energy generated in the hysteresis cycles will be dissipated as heat, with the thermal gradient being higher in the regions of stress concentration, thereby leading to the identification of the damage through IR Thermography. Such vibro-thermography technique has been studied to monitor the development of heat patterns in specimens under fatigue loading but needs further investigation for any widespread applications [34].

8.6.2 Quantitative pulsed thermography

The preceding sections have demonstrated the feasibility of using IR thermography for non-destructive evaluation of structural components in a wide range of applications in aerospace, automotive, naval and civil industry for detection of subsurface damage/defects. Most of these applications have been aimed towards qualitative assessment and thus were limited to the detection of defects and the use of thermography more as just a quality assurance tool. With the advancement of image processing tools and availability of high performance IR cameras, efforts are being made to quantify the defect size and depth obtained from thermography inspections so that it will be possible to integrate the thermography data into finite element models, with the goal of predicting the true behavior and performance level of the structural component.

In order to get a quantitative measurement of the temporal profile, the temperature decay curve of the specimen surface needs to be monitored and recorded. The data can then be recast as a set of equations, each a function of time, that describe the time evolution of a particular pixel [44, 45]. This technique, also referred to as the Thermographic Signal Reconstruction (TSR) method [45], helps to reduce noise and extraneous non-thermal signal components from the raw signal and at the same time accentuates those signals from the defect areas, which deviate from typical cooling behavior. This is particularly advantageous for defects of small size or located at great depths where the noise level of the IR camera makes it difficult to distinguish such defects directly from the raw data.

As discussed previously, the presence of subsurface debonds or delaminations will alter the rate of diffusion with respect to the surrounding area. The diffusion equations for areas without and with defects are repeated below for convenience:

Without defects:
$$\frac{\delta^2 T}{\delta z^2} = \frac{1}{\alpha}\frac{\delta T}{\delta t} \qquad \textbf{(8-3)}$$

With defects:
$$\frac{\delta^2 T}{\delta x^2} + \frac{\delta^2 T}{\delta y^2} = \frac{1}{\alpha}\frac{\delta T}{\delta t} \qquad \textbf{(8-4)}$$

The separation of the diffusion equations puts the thermography data, collected from a defect free and a damaged region, into two separate time regimes – before and after the incident thermal energy reaches the defect. This principle can be used in the TSR process, in which for each pixel an equation is generated that is a noise-reduced replica of the original [45]. These equations can then be used to reconstruct an image at any point in time. The advantages of this technique are an increase in the sensitivity of the thermography process towards detection of low-aspect ratio features and a reduction in storage space required for the data [45]. Being represented

mathematically in the closed form, it becomes easy to perform mathematical operations such as differentiation, FFT or logarithmic plotting that might be necessary to enhance the image quality.

If the temporal profiles of two points on the surface are plotted, then the presence of a disbond will be indicated by a break in the temporal profile as compared to the one without any defects. This is illustrated in Figure 8.25 as normal and logarithmic surface temperature vs. time plots. A straight line with slope of –0.5 will represent the logarithmic temperature-time history solution of the heat diffusion differential equation of a point on the surface over a defect-free region. For a point on the surface located over a defect, the logarithmic temporal profile will follow similar linear behavior until the incident heat reaches the defect area, beyond which the temporal profile will deviate from the linearity. Knowing the instant of time, t_o, at which the breaking point occurs, the depth of the defect can be found out from depth calibration curves generated by using a reference defect at a known depth using the following relation:

$$d = (\alpha t_b)^{1/2} \qquad \textbf{(8-7)}$$

where d is the defect depth, α is the thermal diffusivity and t_b is the break time.

Thus it is possible to exploit the separation of diffusion equations for automated defect detection and depth measurement [5, 45].

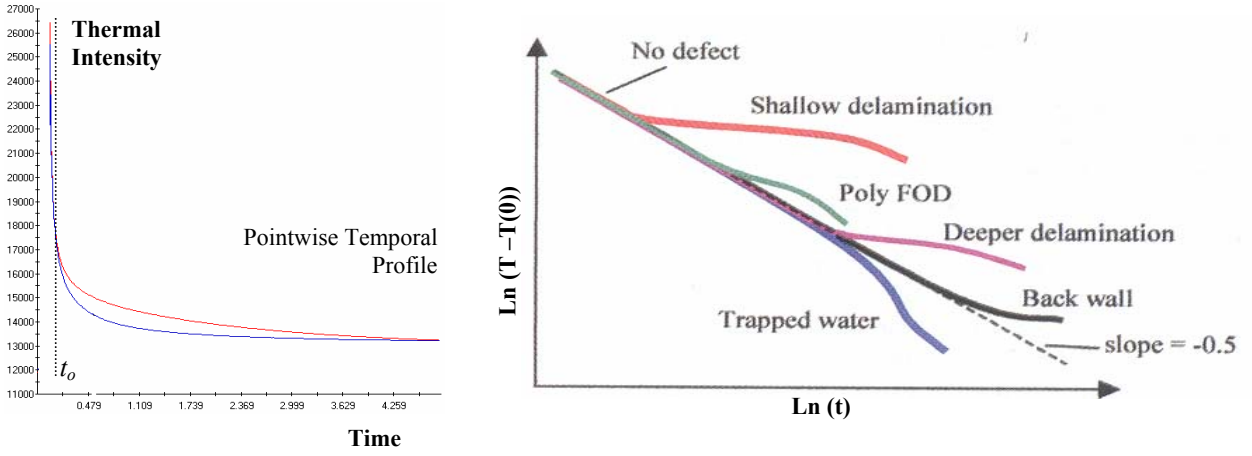

Figure 8.25: a) Surface temperature vs. time; b) Log-log plot of surface temperature vs. time [45]

The thermography data can be visualized in a number of ways depending on convenience. A 2-D surface profile or 3-D volumetric profile (Figure 8.26) can be generated, and this will give information on the size of the defect and location. A linear profile (Figure 8.26) is usually generated to get quantitative information on the thermal intensity along the length of the specimen as well as to compare between the baseline intensity and the test inspection intensity to observe the appearance of new defects or the growth of existing damage/defect areas. The point-wise temporal profiles are used to get information on the depth of the defect (Figure 8.25).

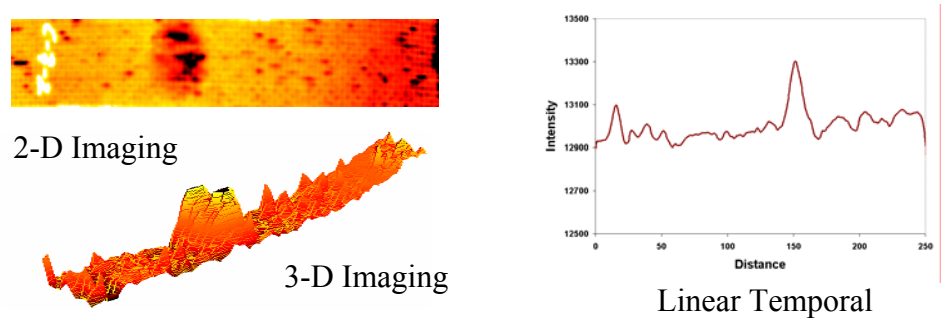

Figure 8.26: IR image of thermal gradient caused by disbonds in composites

Other than quantified defect depth and size determination, another requirement of automated thermography would be to identify the type of defect. In composites some of the typical defects are caused by moisture ingress, impact damage, delamination and disbonds, skin to core disbonds in sandwich panels, breakdown of the repair patch integrity and anomalous resin distribution.

Usually most of these defects exhibit a unique thermal signature and thus it is possible to separate these defects. Trapped water would act as a heat sink and would thus appear as a cold (dark) spot in the thermal image. Disbonds and delaminations would on the other hand be represented as hot (bright) spots because they block the heat flow to the substrate. Skin to core disbonds in sandwich panels would appear as areas of higher temperature as compared to normal voids or facing delaminations, since in the sandwich structure there is no conduction path from the surface through the honeycomb. Impact damage is characterized by compression at the point of impact and thus the delamination would grow in size and rotate with the ply orientation as it propagates deeper into the laminate [45].

The characteristic temporal profiles for some defect types are presented in Figure 8.25 and the typical spatial profiles of the thermal intensity as observed from a thermogram of some common defects in aerospace composites are presented in Figures 8.27 and 8.28.

It should be remembered that a defect closer to the surface would have a higher thermal intensity than a deeper defect of the same severity, since it takes more time for the deeper defect to be detected and thus a greater amount of thermal energy will get diffused. This was evident in the surface temperature vs. time plot (Figure 8.25), in which the temporal profile of a shallow delamination was found to deviate much earlier from that of a deeper delamination. Thus, while determining the relative severity of damage areas in multiple ply laminates, it is not only necessary to compare the thermal intensities but also to look at the depths of those defects, and an adjustment factor must be applied to the intensities to be able to compare them on a common platform.

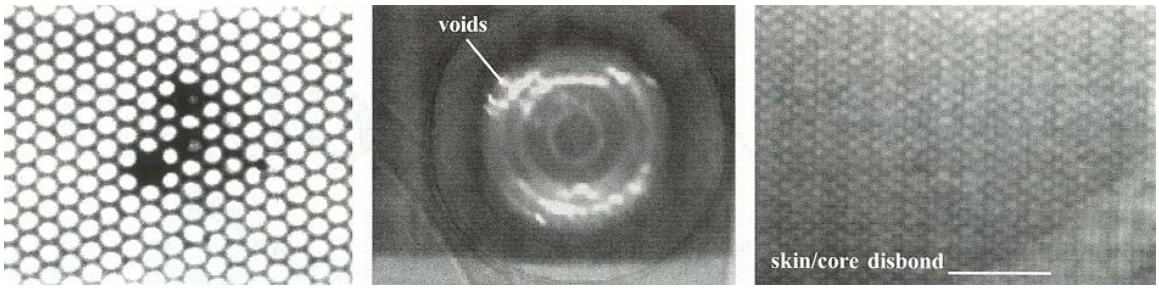

Figure 8.27: Typical defects in composites: a) Trapped water; b) Voids in a graphite patch; c) Skin to core disbond between graphite epoxy skin and nomex core [45]

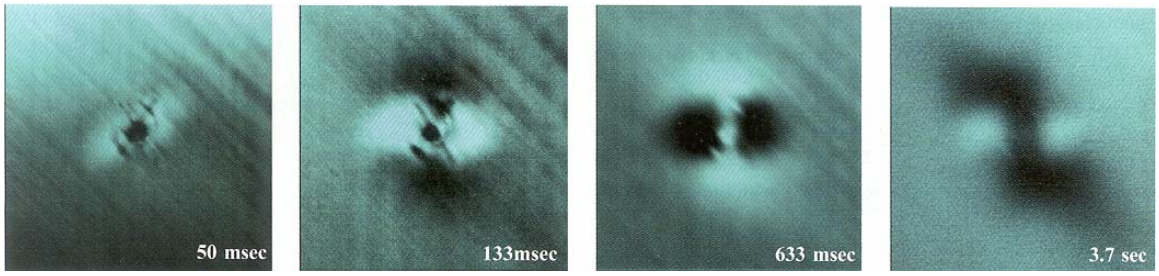

Figure 8.28: Impact damage with delamination following ply orientation at progressively deeper levels of the layup [45]

The complete automated quantified pulsed thermography process (Figure 8.29) would combine production of the thermal excitation pulse, data acquisition, and processing of the data into a single operation that can be performed by any operator without any prior experience of thermographic inspection or without any prior knowledge of the location of the defect.

Figure 8.29: Automated thermographic inspection of a composite jet engine cowling [45]

After the inspection, either in the laboratory or in the field, a thermography expert can then look at the data in the office. The use of the Thermographic Signal Reconstruction (TSR) technique will also allow the study of a number of image sequences simultaneously in the form of a single large array which will help to determine the time frame at which a defect becomes visible in the thermogram and to detect any changes in the properties of the defect from thermograms obtained at two different points of time for the same target. Image processing software can also be used to combine individual shots taken of a large structure into a single shot.

8.6.3 Further applications in damage progression/evolution

With the rapid deterioration of infrastructure there is a growing need for the health monitoring and continuous condition assessment of selected existing structures by rapid, cost efficient and reliable NDE techniques to ensure public safety. Bonded FRP composites are being looked upon as a viable solution for the repair and strengthening of the deficient structures. But with these relatively new construction materials there is a need to evaluate the installation quality and the long-term efficacy of the repair using NDE techniques.

Thus the primary objective of such a technique would be not only to detect and locate the anomaly (which might be in the form of delaminations, thickness variations, deteriorated zones and moisture in reinforced concrete structures and in form of debonds and delaminations in FRP retrofitted structures) but also to be able to monitor the structure on a continuous basis through assessment of the damage/defect in terms of its severity and impact on the structure as a whole. This makes it necessary to carry out further research in the extension of the thermographic inspection technique for the monitoring of damage progression or evolution over a period of time so as to evaluate any degradation in the structural performance under the effects of sustained fatigue loading or detrimental environmental conditions.

The progression of damage in composites is further complicated by the wide array of damage modes involved depending on the composite properties, ply orientations, geometry of the material/structure and loading conditions. Thus at the micro mechanics level, the process of damage accumulation in the composite materials under sustained loading will be due to interaction of the various damage modes, including matrix cracking, delamination, and fiber fracture, which will continuously change the structure of the composite and redistribute the stresses in the laminate. Moreover, the initiation of an individual damage mode is not independent of the state of damage in the material [47,48].

The initiation of matrix cracks is not a single, instantaneous event, but is a series of sequential events dependent on the local distribution of stress and on local variations of strength throughout the laminate [47]. The progressive initiation of matrix cracks forms a regularly spaced pattern of cracks in the off-axis plies, which changes the local stress field, causing the interlaminar stresses along the edge to be redistributed along the ply interfaces. The redistributed stresses initiate interfacial debonds which produce delamination along the length of the free edge. The matrix cracks also change the local stress field in the adjacent plies to produce a stress concentration near the crack tip. Figure 8.30 illustrates the progressive development of the damage modes during the fatigue life of a laminate with several off-axis plies.

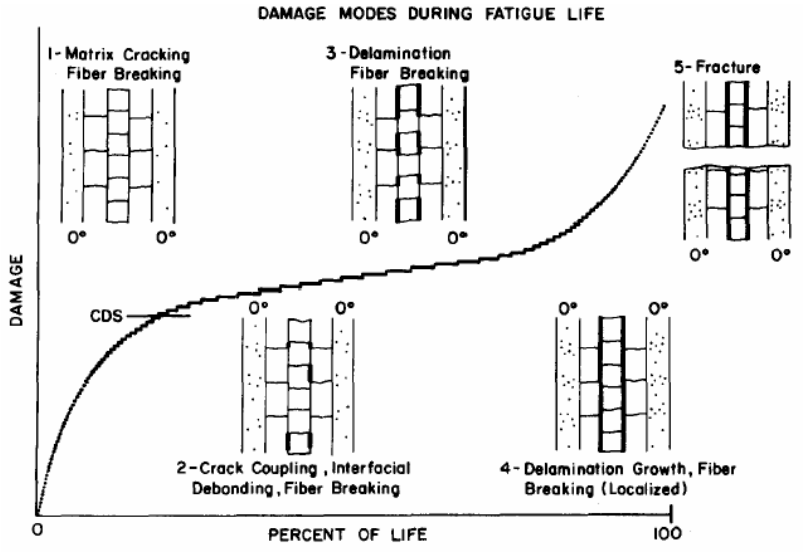

Figure 8.30: Damage accumulation in composite laminates [47]

Such damage accumulation/evolution being at the microscopic level can only be studied using microscopy techniques. However, in monitoring the appearance or progression of defect / damage areas in civil structures greater emphasis is laid on the global extent and influence of such defects on the performance of the structure rather than looking at the progression of different damage modes at the microscopic level. This makes it feasible to use NDE techniques such as IR thermography for evaluation of damage in terms of changes in the state of the material (appearance or growth of debond/delamination with can be looked upon as the appearance of a new material) and their consequences on the engineering response of the structure. Thus rather than trying to identify the appearance or growth of a matrix crack or fiber rupture, the aim of such NDE techniques will be to identify damage modes which will have significant influence on the degradation of strength and life of a structural component.

8.7 SUMMARY

The primary objective of this chapter was to evaluate the effectiveness of IR thermography as an advanced NDE technique for rapid, cost efficient and reliable condition assessment of structural components with particular emphasis on the civil infrastructure. The chapter looked into the theoretical basis of the different thermography techniques, with particular emphasis on pulsed thermography and its viability in defect detection in both reinforced concrete and composite retrofitted structures. Relevant research work in these areas were studied and discussed.

It is evident from previous research that IR Thermography has the potential of being used for both condition assessment and health monitoring of infrastructure. However, a considerable portion of the research on thermography was specifically aimed at aerospace structures, since thermography inspections have long being accepted in the aerospace industry as a viable and effective NDE technique for defect detection and quantification. Thus there is a need for further research in the study of composite-concrete bond, the feasibility of using the technique in initial

production quality assurance, and the monitoring of deficient and retrofitted structures, subjected to sustained loading and detrimental environmental conditions. Such research would focus on detection of the extent and characteristics of flexural and shear cracking in reinforced concrete and debond/delamination/discontinuities in composites.

The database created from such inspections can be used to develop a field-calibrated finite element model. Such a model would be able to integrate experimental, analytical and NDE results and would serve as an excellent tool in the prediction of the performance and residual life of a structure by taking into account the presence of defect/damage areas in the structural components and by considering their severity and their impact on the structure.

8.8 CHAPTER 8 REFERENCES

1. Bonacci, J.F. and Maalej, M., "Externally Bonded FRP for Service Life Extension of RC Infrastructure." Journal of Infrastructure Systems, ASCE, March 2000, pp 41-51.

2. Innovator, Newsletter of the Canadian Network of Centers of Excellence on Intelligent Sensing for Innovative Structures, ISIS Canada, April 1997.

3. Bouvier, Carl G., "Investigating Variables in Thermographic Composite Inspections." [Journal Article] Materials Evaluation, v 53, n 5, May 1995, pp 544-551.

4. Buyukozturk, O., "Imaging of Concrete Structures." NDT&E International, v 31, n 4, 1998, pp 233-243.

5. Shepard, S.M., Rubadeux, B.A. and Ahmed, T., "Automated Thermographic Defect Recognition and Measurement." CP 497, Nondestructive Characterization of Materials IX, American Institute of Physics, 1999, pp 373-378.

6. Shepard, S M., "Advances in Pulsed Thermography." [Conference Paper] Proceedings of SPIE - The International Society for Optical Engineering, v 4360, 2001, pp 511-515.

7. Connolly, M. and Copley, D., "Thermographic Inspection of Composite Materials." Materials Evaluation, v 48, no. 12, 1990, pp 1461-1463.

8. Kaiser, H., "Assessment of Defect Criticality and Non-destructive Monitoring in CFRP Rehabilitated Civil Structures." M.S. Thesis, Dept. of Structural Engineering, UCSD, 2002.

9. Hellier, C.J., Handbook of Nondestructive Evaluation, 2001, New York: McGraw-Hill.

10. McLaughlin, P.V., McAssey, E.V. and Deitrich, R.C., "Non-Destructive Examination of Fibre Composite Structures By Thermal Field Techniques." NDT&E International, v 13, n 2, April 1980, pp 56-62.

11. Titman, D.J., "Application of Thermography in Non-Destructive Testing of Structures." NDT&E International, 2001, v 34, pp 149-154.

12. McLaughlin, Philip V Jr., "Defect Detection and Quantification in Laminated Composites by EATF (Passive) Thermography." [Journal Article] Review of Progress in Quantitative Nondestructive Evaluation, v 7B, 1988, pp 1125-1132.

13. Maldague, X. and Marinetti, S., "Pulse Phase Infrared Thermography." Journal of Applied Physics, v 79, n 5, 1996, pp 2694-2698.

14. Bai, W. and Wong, B.S., "Evaluation of Defects in Composite Plates under Convective Environments Using Lock-in Thermography." Measurement Science and Technology, 2001, v 12, pp 142-150.

15. Busse, G., “Nondestructive Evaluation of Polymer Materials.” V 27, n 5, Oct. 1994, pp 234-296.

16. Braggiotti, A., Marinetti, S. and Mazzoldi, A., “D2D: A Robust Technique for Detection of Structural Heterogeneities in Solids based on Transient Thermography.” [Journal Article] Review of Progress in Quantitative Nondestructive Evaluation, v 17B, 1988, pp 1761-1768.

17. Henneke, E.G., “Vibrothermography Applied to Polymer Matrix Composites.” Manual on Experimental Methods for Mechanical Testing of Composites, C.H. Jenkins (Editor), 1998, The Fairmont Press, Lilburn, USA, pp 213-221.

18. Henneke, E. G., “Vibrothermography Applied to Composite Laminates.” [Conference Paper] SESA (Society for Experimental Stress Analysis), Published by SESA, Brookfield Center, Conn, USA, pp 50-51.

19. Rantala, J., Wu, D. and Busse, G., “Lock-In Vibrothermography Applied for Nondestructive Evaluation of Polymer Materials.” Materials Science Forum, v 210-213, 1996, pp 433-438, © Transtec Publications, Switzerland.

20. Dutton, A G., “Flaw Detection In Composite Materials Using Infra-Red Thermography by the Method of External Heating.” [Journal Article] Proceedings of the Institution of Mechanical Engineers, Part C - Journal of Mechanical Engineering Science, v 210, n 5, 1996, pp 399-407.

21. Cielo, P., Maldague, X., Deom, A. and Lewak, R., “Thermographic Nondestructive Evaluation of Industrial Materials and Structures.” [Journal Article] Materials Evaluation, v 45, n 4, April 1987, pp 452-460.

22. Roth, D.J., Bodis, J.R. and Bishop, C., “Thermographic Imaging for High Temperature Composite Materials – A Defect Detection Study.” Res Nondestructive Evaluation, v 9, 1997, pp 147-169.

23. Jones, T. and Berger, H., “Thermographic Detection of Impact Damage in Graphite-Epoxy Composites.” Materials Evaluation, v 50, n 12, 1992, pp 1446-1453.

24. Miceli, M., Duke, J.C. and Horne, M., “Health Monitoring of Fiber Reinforced Polymer Bridge Decks with Infrared Thermography.” Materials Evaluation, 2002, pp 1245-1252.

25. Quinn, M.T., Hribar, J.R., Ruiz, R.L. and Hawkins, G.F., “Thermographic Detection of Buried Debonds.” [Journal Article] Review of Progress in Quantitative Nondestructive Evaluation, v 7B, 1988, pp 1116-1124.

26. Levar, J.L. and Hamilton, H.R., “NDE of CFRP-Concrete Bond using Infrared Thermography.” ACI Materials Journal – Manuscript, pp 1-28.

27. Johnson, E.C., Nokes, J.P. and Hawkins, G.F., “NDE of Composite Seismic Retrofits to Bridges.” CP 497, Nondestructive Characterization of Materials IX, American Institute of Physics, 1999, pp 367-372.

28. Marcus, L.A. and Stinchcomb, W.W., “Measurement of Fatigue Damage in Composite Materials.” Experimental Mechanics, v 15, 1975, pp 55-60.

29. Everett, B. and Morriss, R., “Thermographic Analysis of Concrete and Masonry Structures - Recent Developments.” [Conference Paper] Book I, Published by AGEMA Infrared Systems, Secaucus, NJ, USA, pp 73-77.

30. Manning, D.G. and Holt, F. B., “Detecting Delamination in Concrete Bridge Decks.” Concrete International, Design & Construction, v 2, n 11, Nov 1980, pp 34-41.

31. Holt, F. B. and Eales, J. W., “Nondestructive Evaluation of Pavements.” [Journal Article] Concrete International, Design & Construction, v 9, n 6, June 1987, pp 41-45.

32. Sagakami, T. and Kubo, S., “Development of a New Non-destructive Testing Technique for Quantitative Evaluations of Delamination Defects in Concrete Structures Based on Phase Delay Measurement using Lock-In Thermography.” Infrared Physics and Technology, v 43, 2002, pp 311-316.

33. Weil, G.J. and Rowe, T.J., “Nondestructive Testing and Repair of the Concrete Roof Shell at the Seattle Kingdome.” NDT&E International, v 31, n 6, 1998, pp 389-400.

34. Luong, M. P., “Fatigue Damage Detection on Concrete under Compression using Infrared Thermography.” [Conference Paper] Mechanics of Deformation and Flow of Particulate Materials, ASME-ASCE-SES Joint Summer Meeting 1997, ASCE, New York, NY, USA, pp 199-213.

35. Hag-Elsa, O., Alampalli, S. and Kunin, J., “In-service Evaluation of a Reinforced Concrete T-beam Bridge FRP Strengthening System.” Composite Structures, v 64, 2004, pp 179–188

36. Lipetzky, K. and Bandos, B., “Composite Structures and Adhesive Joints: NDE Techniques for Naval Applications.” SAMPE Journal, v 39, n 5, Sept/Oct. 2003, pp 66-74.

37. Sakagami, T. and Kubo, S., “Applications of Pulse Heating Thermography and Lock-In Thermography to Quantitative Nondestructive Evaluations.” Infrared Physics and Technology, v 43, 2002, pp 211-218.

38. Bates, D., Smith, G., Lu, D. and Hewitt, J., “Rapid Thermal Non-destructive Testing of Aircraft Components.” Composites: Part B, v 31, 2000, pp 175-185.

39. Morton, S., “Externally Bonded Composites for Strengthening Concrete Bridges.” 33rd International SAMPE Technical Conference, November 5-8, 2001, pp 808-821.

40. Clark, M., McCann, D. and Forde, M., “Application of Infrared Thermography to the Non-destructive Testing of Concrete and Masonry Bridges.” NDT&E International, v 36, 2003, pp 265-275.

41. Vikstrom, M., Backlund, J. and Olsson, K., “Non-destructive Testing of Sandwich Constructions Using Thermography.” Composite Structures, v 13, 1989, pp 49-65.

42. Dattoma, V., Marcuccio, R., Pappalettere, C. and Smith, G., “Thermographic Investigation of Sandwich Structure made of Composite Material.” NDT&E International, v 34, 2001, pp 515-520.

43. Meola, C, Carlomagno, G., Squillace, A. and Giorleo, G., “The Use of Infrared Thermography for Nondestructive Evaluation of Joints.” Infrared Physics and Technology, 2004.

44. Schroeder, J., Ahmed, T., Chaudhry, B. and Shepard, S., “Non-destructive Testing of Structural Composites and Adhesively Bonded Composite Joints : Pulsed Thermography.” Composites: Part A, v 33, 2002, pp 1511-1517.

45. Shepard, S., Lhota, J., Ahmed, T. and Hou, Y., “Thermographic Inspection of Composite Structures.” SAMPE Journal, v 39, n 5, Sept-Oct 2003, pp 53-59.

46. Brown, J. and Hamilton, H., “NDE of Reinforced Concrete Strengthened with Fiber-Reinforced Polymer Composites using Infrared Thermography.” InfraMation 2003.

47. Stinchcomb, W., “Nondestructive Evaluation of Damage Accumulation Processes in Composite Laminates.” Composites Science and Technology, v 25, 1986, 103-118.

48. Chow, C., Xian, X. and Lam, J., “Experimental Investigation and Modeling of Damage Evolution/Propagation in Carbon/Epoxy Laminated Composites.” Composites Science and Technology, v 39, 1990, 159-184.

9.0 IR THERMOGRAPHY DEMONSTRATION CASE STUDY

9.1 INTRODUCTION

A test program was undertaken to evaluate the behavior of bridge decks prior to and after being strengthened with externally bonded FRP composites, taking into account the progression of damage. The four specimens tested in this program constitute sections cut out from an actual bridge deck during demolition of the bridge as part of a replacement program of aging infrastructure. Composite strips were used to extend the life of this bridge a few years prior to the demolition.

The specimens tested are representative of bridge deck components being subjected to realistic deterioration and damage over time. NDE tests using Infrared Thermography and forced excitation based dynamic testing were conducted to study the behavior of the slabs with the progression of damage under monotonically increasing loads simulating wheel loads.

The primary objective of this test program was to correlate the test data on the failure modes, capacity loads and specimen behavior under progressive damage propagation, to the behavior of a full bridge deck in the field being subjected to similar deterioration and environmental exposures.

9.2 FIELD REHABILITATION

Field rehabilitation using FRP composites was undertaken for a 225.86 m (741 ft.) long, reinforced concrete T-girder bridge consisting of 18 spans and 5 bays. The bridge deck had a longitudinal girder c/c spacing of 2.134 m (7 feet) and had a longitudinal span length of 12.8 m (42 feet). The bridge was constructed in 1970 and some of the main problems associated with the bridge were transverse and longitudinal cracking at the bottom of the bridge deck, susceptibility of the bridge deck to punching shear type failure and efflorescence in the cracks resulting from water penetration.

The transverse cracks were found to develop at an approximate spacing of 5.5 inches, which correspond to the average spacing of the transverse reinforcement in the bridge deck. Moreover the interaction of the longitudinal and the transverse cracks made the deck susceptible to punching shear. Finally, being designed as per Caltrans BDS of 1969, the existing reinforcement in the structure was found to be inadequate to satisfy current load demands.

In order to extend the service life of the bridge, segments of the bridge deck were strengthened with externally bonded FRP composite materials in the form of prefabricated pultruded carbon strips and site impregnated carbon fabric laminates. The rehabilitation scheme was designed to help in the redistribution of the wheel loads, to satisfy the current code demands in terms of added reinforcement requirement, to enhance the capacity of the decks and control crack widths

thereby preventing punching shear type failures. Figures 9.1(a) and 9.1(b) illustrate the rehabilitation of the Watson Wash Bridge decks with pultruded carbon strips and carbon fabric laminates, respectively. The bridge was demolished however in the middle of 2003, in view of the extensive damage and susceptibility to punching shear failures of the spans not strengthened with the composite materials.

Figure 9.1: Onsite rehabilitation of bridge deck

9.3 LABORATORY TESTING OF DECK SLAB COMPONENTS

9.3.1 Development of the test specimens

Four specimens were cut out from the deck slabs of the bridge during its demolition for testing in the laboratory. Two of these were control specimens: one (S1) was cut off from the positive moment area of the bridge deck and showed significant deterioration; the other (S4) was cut off from the negative moment area near the supports and showed lesser cracking and damage. These two specimens were used as the baseline against which the capacity and performance enhancement of the other two specimens were evaluated: S3 strengthened with the pultruded strips; and S2 strengthened with the fabric laminates. All the specimens were 3.048 m (10 feet) x 1.372 m (4.5 feet) in size and the slab thickness was 155.6 mm (6.125 inches).

The slab boundary and loading conditions were designed to simulate the behavior and performance of the complete bridge deck from the component test specimens. Since the actual bridge deck was susceptible to punching shear type failure, it was the objective of the test program to develop the boundary and the loading conditions such that the control specimens would fail in punching shear. In order to arrive at the proper boundary conditions for the test specimens, a detailed finite element model of the actual bridge was constructed and analyzed. The analysis was conducted under the application of a concentrated wheel load having a footprint area of 508 mm (20”) x 203.2 mm (8”), which is representative of the actual HS20 wheel load configuration.

The finite element model used for the analysis of the actual bridge deck is shown in Figure 9.2a. Shell elements were used to model the deck slabs, longitudinal and transverse girders and the

abutments. 3-D solid elements were used to model the footing, while the footing restraints were modeled using spring elements.

Finite element models of the specimens cut out from the bridge decks were then analyzed under the same concentrated wheel load with a footprint area of 508 mm (20") x 203.2 mm (8"), applied at the center of the specimens. The specimen boundary conditions were designed to be simply supported along the two longer edges, with a center-to-center distance between the supports of 1.067 m (3.5 feet). This was based on the analysis results that most of the load transfer in the actual bridge deck is one-way with the load from the deck slabs being transferred to the girders predominantly because of the much longer longitudinal span length of the slabs as compared to the center-to-center distance between the girders.

The finite element model used to analyze the test specimens is shown in Figure 9.2b. Contours of the transverse membrane forces from the finite element models of the actual bridge deck and the test specimens were found to match closely. The capacities of the test specimens were then determined using design oriented analytical models to ensure that the control specimens would fail in punching shear and the strengthened specimens in flexure.

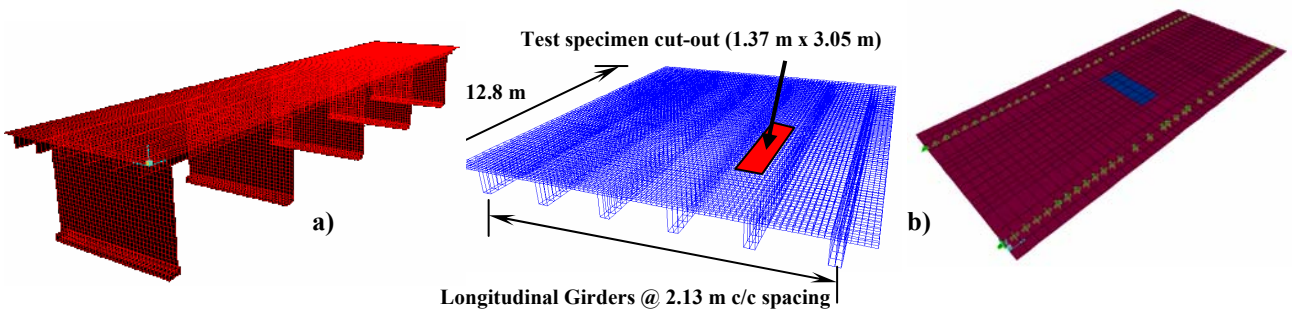

Figure 9.2: Finite element models used to analyze a) Bridge deck; b) Test specimen

9.3.2 Specimen details

The test specimens consisted of #5 rebar spaced at approximately 139.7 mm (5.5 inches) c/c in the transverse direction and #5 rebar spaced at 243.8 mm (9.6 inches) c/c in the longitudinal direction. The laminate strips in S2 had two layers of fabric in the transverse direction and consisted of a single layer in the longitudinal direction. All the strips were 152.4 mm (6 inches) wide. All the pultruded strips in S3 were 50.8 mm (2 inches) wide and consisted of only a single layer in both the longitudinal and the transverse directions. The external composite reinforcement ratio was higher in S2 since it was strengthened to carry a permit truck load, while S3 was rehabilitated to prevent local punching shear failures through control of the crack width opening. Composite strengthening details in specimens S2 and S3 are presented in Figure 9.3.

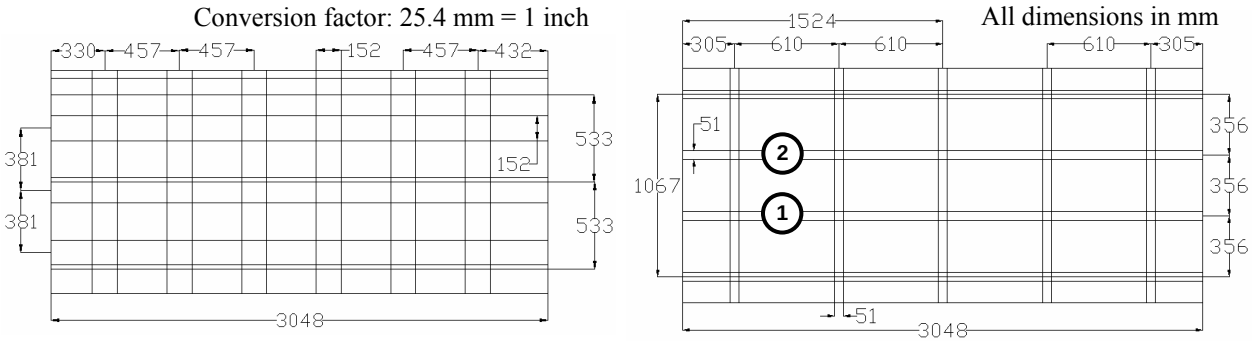

Figure 9.3: Strengthening scheme in test specimens S2 and S3

Specimen S4 was cut off from the negative moment region of the bridge deck close to the bridge support. Being subjected to lower moment demands, this specimen had fewer existing cracks and was subjected to lesser damage over its life span. All the test specimens had considerable existing cracks in both the transverse and longitudinal directions resulting from over 30 years of traffic loading as well as from the effects of severe environmental exposure. The transverse cracks were usually spaced at 139.7 mm (5.5 inches), which corresponds to the spacing of the internal transverse steel reinforcement. Secondary cracks were also observed in both the transverse and the longitudinal directions in between the main cracks. The test specimens as obtained from the Watson Wash Decks are shown in Figure 9.4.

The concrete and reinforcement properties used in the computation of the flexural and shear capacities of the test specimens were assumed based on Caltrans BDS-1969 design practices. The composite properties, however, were determined based on tension tests from samples cut out from the composites used for the strengthening of the actual bridge deck. The concrete compressive strength, f_C', was assumed to be 27.3 MPa (4000 psi) for all the test specimens and the steel reinforcement was assumed to have a yield strength, f_Y, of 410 MPa (60,000 psi).

9.3.3 Predicted capacities

The punching shear capacities of the test specimens were computed as per the design equations of Caltrans BDS as well as AASHTO. The computations were made for a concentrated wheel load with a footprint area of 508 mm (20”) x 203.2 mm (8”). Most of the punching shear models assume a 45^o failure cone from the perimeter of the loading area. However experimental results from punching shear tests of reinforced concrete slabs often predict values less than the typical value of 45^o used in the design codes. Thus shear capacity of the current control test specimens was computed for a shear angle value of 38^o as suggested from experimental results by Klingner, et al. [1]. The punching shear capacity thus computed was predicted to be at 503 kN (113 kips).

Nominal flexural capacities in the longitudinal and transverse directions of the test specimens were calculated based on the available information on the concrete properties and reinforcement details. Sectional analysis was used to compute the flexural capacity for a maximum concrete

compressive strain of 0.003. The nominal flexural capacity of the control specimens was computed to be reached for a wheel load of 512 kN (115 kips), and this ensured that punching shear failure would occur in the control specimens before the occurrence of flexural failure.

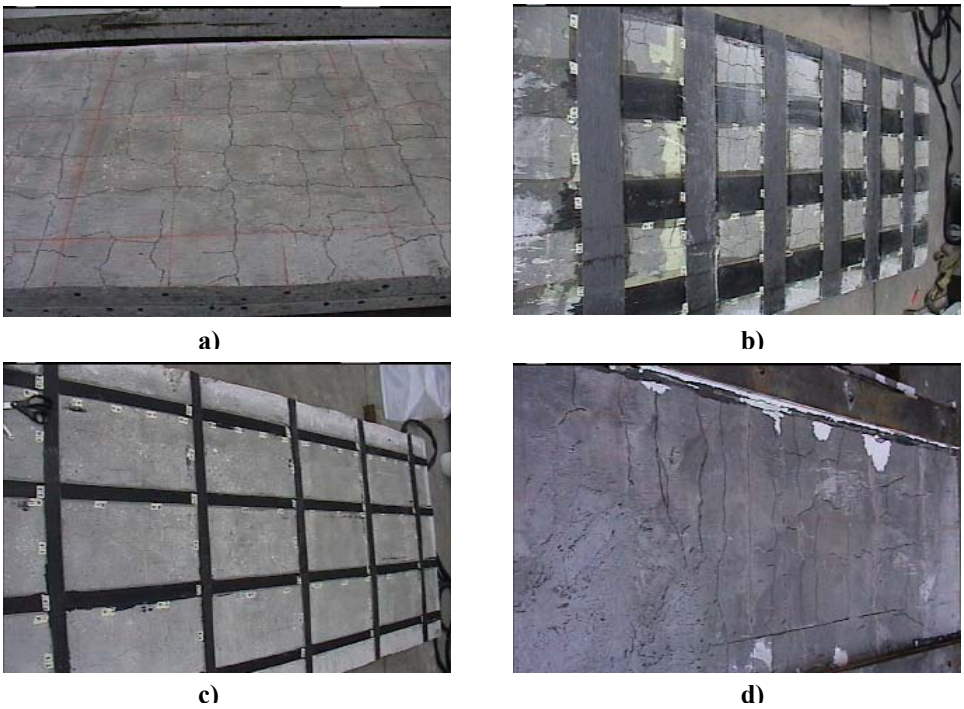

Figure 9.4: Test specimens: a) S1; b) S2; c) S3; d) S4

For the two test specimens strengthened with FRP composite strips and laminates, it was expected that the strengthening scheme would change the mode of failure from punching shear to flexural failure, culminating in the debonding of the laminates or strips at failure of the specimens. Thus the flexural capacities of the strengthened specimens were computed as the loads required to cause debonding of the composite strips/laminates. Table 9.1 summarizes the predicted shear and flexural capacities of the test specimens.

Table 9.1: Predicted failure loads of the test specimens from analysis results

Specimen Description	Predicted failure load	Predicted mode of failure
Control Specimens (S1 and S4)	503 kN (113 kips)	Punching shear failure
Specimen strengthened with carbon fiber composite laminate for permit truck load (S2)	801 kN (180 kips)	Flexural failure with debonding of the composite laminate
Slab strengthened with prefabricated carbon composite strips to resist punching shear failure (S3)	690 kN (155 kips)	Flexural failure with debonding of the composite strips

9.3.4 Loading and test setup

The test specimens were placed on roller supports, simulating simply supported conditions, running continuously along the two 3.048 m (10 feet) long edges and at a distance of 152 .4 mm (6 inches) from the outer edge of the specimens, thereby giving a center-to-center distance between the supports of 1.0668 m (3.5 feet). The two shorter outer edges of the slab were free edges. Two steel bearing plates were also mounted between the roller supports and the underside of the slab and two 6.35 mm (¼ inch) thick durometer neoprene bearing strips were placed in between the concrete and the steel bearing plates to ensure uniform bearing of the test specimens on the supports. The test setup is presented in Figure 9.5.

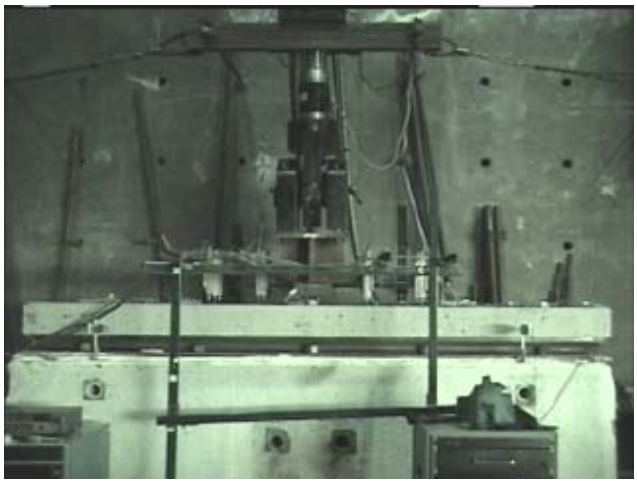

Figure 9.5: Test setup

All the specimens were tested under monotonically increasing load applied by a 979 kN (220 kips) capacity hydraulic actuator. The load from the actuator was transferred to the test specimens through load bearing plates having a loading footprint area of 508 mm (20 inches) x 203.2 mm (8 inches). The load was applied at the center of the test specimens. A 76.2 mm (3-inch) thick elastomeric bearing pad was also placed between the load bearing plates and the concrete surface to obtain a uniformly distributed constant pressure on the slab. A displacement control mode of loading was used. The loading was cycled every 44.5 kN (10 kips). The loading was continued until there was a significant decrease in the capacity of the specimens.

9.3.5 Instrumentation and data acquisition

Vertical deflections in the area around the load application were measured using 15, ± 76.2 mm (3 inch) linear potentiometers. Three of these potentiometers along the centerline of the specimens were used to measure deflections from the underside of the specimens so as not to interfere with the load actuator. The remaining 12 potentiometers were used to measure deflections from the top of the specimens. In addition to the vertical linear potentiometers, four horizontal potentiometers were used along the long edge of the specimens, two on each side of

the long edges. These potentiometers were used to measure any horizontal movement of the specimens during the test. Four rotation sensors were also used, two on each outer unsupported shorter edge. These were placed right over the supports to measure the rotations of the test specimens over the supports.

Forced excitation based dynamic testing was conducted to study the behavior of the specimens with the progression of damage. A total of 15 PCB piezoelectric accelerometers were used to capture the major natural frequencies. Electrical resistance strain gages with a gage length of 20 mm were also used on the composite laminates and strips in specimens S2 and S3 respectively, to monitor the strains in the composite material with the progression of damage.

A data acquisition system was used to record the data from the actuator, linear pots, rotation sensors and the strain gages. A second data acquisition system was used to record the piezoelectric accelerometer data during each forced excitation based dynamic testing. A third system was used to record the data from Infrared Thermography inspection of S2 and S3.

9.4 TYPICAL TEST RESULTS

S1 and S4 were control specimens and their boundary conditions were designed to ensure punching shear failure representing the behavior of the actual bridge deck. S1 failed in punching shear at 501.1 kN (112.6 kips), and the shear failure was followed by the yielding of the internal steel reinforcement resulting in the plateau in the load-displacement plot as shown in Figure 9.6. Failure was caused by opening of preexisting cracks and punching of the load pad through the concrete. Thus damage was mostly localized around the loading footprint area with the main transverse cracks at the bottom of the specimen forming at 180 mm and 230 mm on either side of the centerline of the slab.

S2 failed at 862 kN (193.7 kips) with a corresponding mid-span deflection of 13.46 mm (0.53 inches). Failure was initiated in flexure by debonding of the transverse composite strips and was followed by punching of the load pad through the concrete. The rehabilitation scheme resulted in the enhancement in the capacity of the specimen as compared to the control specimen while at the same time changing the failure mode from punching shear to flexure. The rehab also helped to distribute the load and thus the failure zone was spread over a larger area with the main transverse cracks forming at around 530 mm on either side from the centerline of the slab with considerable deflections in the longitudinal direction.

S3 failed at 791 kN (177.76 kips) with a corresponding mid-span deflection of 11.7 mm (0.46 inches). The purpose of this rehab was to prevent punching shear failure through control of the crack widths as opposed to the strength enhancement objective in specimen S2. Consequently, S3 had a lower strength and failed at a lower mid-span deflection level. Slab failure was initiated in flexure by debonding of the prefabricated strips and was followed by punching of the load pad through the concrete. The main transverse cracks were formed at around 550 mm on the right and at 360 mm on the left from the centerline of the slab. There were also considerable deflections in the longitudinal direction.

S4 was also a control specimen but with fewer preexisting cracks and damage regions as compared to S1. The specimen failed in punching shear at 702.2 kN (157.8 kips) at a mid-span deflection of 9.1 mm (0.36 inches). Thus this specimen could withstand a much higher load as compared to S1 though the midspan deflection was less. After the failure it was observed by lifting off the spalled concrete that there were three steel rebar in the region just below the load footprint area at the top of the specimen running in the transverse direction. It is believed that the locations of the rebar just below the load area also resulted in increasing the failure load by preventing the load pad from punching through into the concrete.

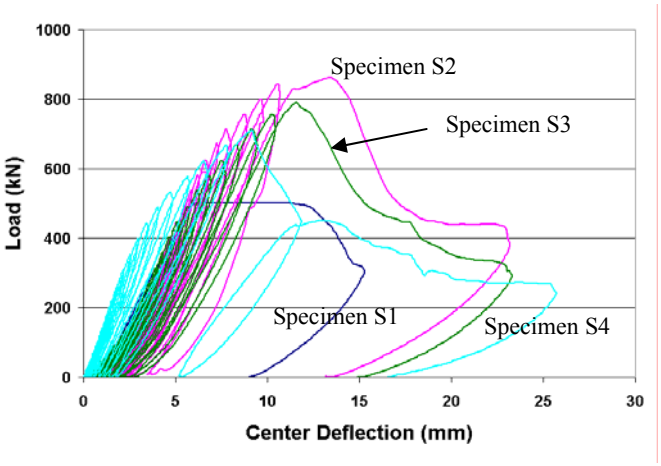

Figure 9.6: Characteristic load – mid-span displacement response

9.5 PROGRESSIVE DAMAGE EVALUATION USING IR THERMOGRAPHY

One of the primary objectives of testing the slab components in the laboratory was to characterize the progression of damage in the composite strips with the increase in loading and to link it to the degradation of strength and crack formation. The general trend of monitoring the performance of retrofitted structures is to carry out biennial visual inspections. These inspections, however, can miss many of the signs of subsurface damage and deterioration at the composite-concrete or composite-composite interface not visible from the outside. Thus it is necessary to carry out continuous health monitoring through the application of non-destructive evaluation (NDE) techniques for detection of debond and delamination defects in composite materials so as to correctly predict the true condition and residual strength of a rehabilitated structural component and thereby evaluate the performance level of the entire structure. If the structural behavior can be characterized by a field-calibrated finite element model which integrates experimental, analytical and NDE results, then it would serve as an excellent tool in the prediction of the performance and residual life of the structure.

With the above considerations in mind, considerable efforts are currently being made to understand the definition of structural damage and to come up with cost and data effective

monitoring systems. It is not sufficient to merely identify the damage. The main challenge lies in the determination of the cause of damage, its location, its severity, and its impact on the performance of the structure as a whole. From this perspective NDE techniques can help to relate the experimental data and results to an analytical model through real-time characterization and assessment of the severity of the defect structures without damaging or dismantling individual components.

With the advances made in image processing, knowledge based systems and new inspection techniques, the conventional NDE techniques can be replaced with faster and more economical techniques with no sacrifice of quality [2]. IR Thermography is one such technique, which is fast emerging as an efficient cost effective NDE method in the detection of defects and debonds in rehabilitated structural systems. The real-time inspection and data interpretation from this technique can allow instant assessment of a structure's integrity and serviceability. Moreover, for a number of applications it is advantageous in terms of speed and cost compared to traditional methods and does not require being in contact with the sample [3]. It is believed that the use of IR Thermography can result in cost savings of 60% to 75% over ultrasonic testing and radiography, two of the commonly used NDT techniques [2].

9.5.1 Background and theoretical basis of IR thermographic inspections

IR Thermography is a non-contact optical method where an accurate two-dimensional mapping of isothermal contours of steady or transient thermal effects is constructed from the measurement of infrared energy emitted by the target. The principle of IR Thermography is to input heat energy on one surface of the sample to be inspected. The heat energy will tend to diffuse into the material and the rate of heat flow will be a function of the properties of the material. The presence of discontinuities and flaws, such as debonds and delaminations, will cause an interruption in the heat flow resulting in 'hot' or 'cold' spots in these regions. Thus IR Thermography can be used to detect the presence of subsurface defects through observation of discontinuities in the spatial or temporal profile of the surface temperature.

In most cases the thermal response of a thick, semi-infinite solid is described by the 3-dimensional diffusion equation, expressed by:

$$\frac{\delta^2 T}{\delta x^2} + \frac{\delta^2 T}{\delta y^2} + \frac{\delta^2 T}{\delta z^2} = \frac{1}{\alpha}\frac{\delta T}{\delta t} \qquad \textbf{(9-1)}$$

where α = thermal diffusivity of the material.

In the absence of any defects in the material, at a point far away from any edges, the lateral heat flow components in the above equation will cancel out and the heat flow can be approximated by a 1-dimensional diffusion equation, expressed as:

$$\frac{\delta^2 T}{\delta z^2} = \frac{1}{\alpha}\frac{\delta T}{\delta t} \qquad \textbf{(9-2)}$$

However, in the presence of a subsurface defect in the path of propagation of the "heat-wave", the incident thermal energy will be trapped between the defect and the sample surface and will

tend to flow laterally outwards towards the cooler areas surrounding the defect. Under such circumstances, the diffusion equation followed can be expressed as:

$$\frac{\delta^2 T}{\delta x^2} + \frac{\delta^2 T}{\delta y^2} = \frac{1}{\alpha}\frac{\delta T}{\delta t} \qquad \textbf{(9-3)}$$

Due to the difference in the thermal diffusion equation in the presence of any abnormalities or discontinuities in the material, there will be non-uniformity in the temperature profile producing a "defect signature" that can be detected through the Infrared Thermography technique. Monitoring of the spatial and temporal profile at the surface using IR Thermography can thus be used as an effective NDE technique for the detection of any subsurface defects.

Two methods of thermography, namely active and passive, are generally used. In passive thermography the discontinuities in the temperature profiles are generated by ambient environmental conditions (such as the sun) or operating conditions (such as heat generated in machinery by means of internal friction). However, the disadvantage of passive thermography is that the heat emitted from the source cannot usually be quantified. An alternative to passive thermography is active thermography in which an external heat source, such as incandescent light bulb, heat gun, flash lamp or quartz lamp, is used to induce energy to the specimen. In this technique the duration, magnitude and frequency of the source electromagnetic wave are known entities and are easily adjustable and thus can be used to characterize defects on a more quantitative basis. The relative time and amplitude of the measured signal provides information about the depth and size of the subsurface defects. Pulsed Thermography (PT) is one of the most commonly used active thermography techniques, in which a heat pulse of relatively short duration, such as provided by a flash lamp, is directed at the test surface, and this launches a thermal front, which propagates through the sample under inspection by diffusion according to the diffusion equations presented earlier.

9.5.2 Pulsed thermography NDT evaluation of FRP composite rehabilitated slab specimens

The objective of using IR Thermography in the current test program was two-fold, one being the detection of any pre-existing defect/damage areas in the composite strips and the other being the characterization of damage progression in the strips with loading. Inspection was done before the test for both of the rehabilitated specimens, S2 and S3, to form the baseline for subsequent inspections. The data was acquired using a commercial thermographic NDT system (Figure 9.7a). Flash heating was provided by 2 xenon flashtubes with 5 ms flash duration, each powered by a 6.4 kJ capacitor bank. This heat source was used to simulate temperature differential between the composite and any potential debond/delamination areas. The infrared camera was equipped with a 256 x 256 pixel InSb focal plane array, operating in the 2 – 5 μm spectral range. Continuous 12 bit data was acquired at a 60 Hz frame rate for 20 sec after flash heating for each shot. The field of view of the Thermography system used was 305 mm (12 inches) x 230 mm (9 inches). Thus the surface of the test specimens was divided into a number of grids and each grid was imaged independently. An overlap of about 51 mm (2 inches) was maintained between the adjacent shots so that during the processing of the thermography data the adjacent thermal

profiles could be brought together and superimposed. The initial thermography inspection of the rehabilitated specimens is shown in Figure 9.7b.

Figure 9.7: a) Thermography data acquisition; b) Initial thermography inspection of specimens

Thermographic inspection was also carried out during the testing of the rehabilitated test specimens, S2 and S3, under cyclic fatigue loading. The data was acquired every 178 kN (40 kips), both under loading at the maximum load level of each cycle and after unloading the specimen. To facilitate the thermographic inspection at the bottom of the specimens, all the vertical displacement measuring linear potentiometers were instrumented at the top of the specimens so as to leave clear space at the bottom of the slabs. The data could be acquired only up to 801 kN (180 kips) for Slab S2 and up to 712 kN (160 kips) for Slab S3, since beyond that load level, inspection under the test specimen was deemed to be unsafe.

Both 2-D and 3-D mapping of the thermal intensities over the composite surface was performed to determine the time frame within each shot at which any pre-existing or new damage/defects became visible. Linear thermal profiles along the length of each shot were then combined to construct the thermal profile along the entire length of the composite strips for each load level. The profiles from subsequent load levels were then compared to each other to determine the appearance or progression of defect areas.

9.5.3 Damage detection/progression from IR thermography data

In Slab S3, rehabilitated with prefabricated carbon composite pultruded strips, the appearance of damage areas (indicated by changes in the thermal intensity when compared to previous load stages) at some locations of the longitudinal composite strips were observed during the inspection at 623 kN (140 kips). At the inspection carried out at 712 kN (160 kips) these damage areas were found to grow along with the appearance of new ones. Figure 9.8 shows the progression of damage in longitudinal strip 2 (refer to Figure 9.3) as indicated by the linear profiles as well as 2-D and 3-D mapping of the thermal intensities acquired at unloading after reaching the desired load level so as to compare with the baseline intensity at zero load. The

appearance of damage areas at other locations of the strip at 712 kN (160 kips) is illustrated in Figure 9.9. The appearance of damage/debond areas in longitudinal strip 1 (refer to Figure 9.3) is illustrated in Figure 9.10 and Figure 9.11.

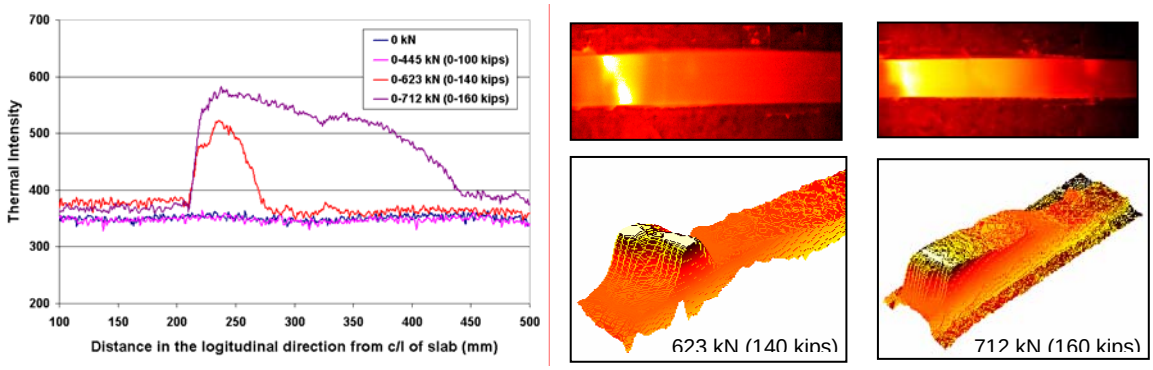

Figure 9.8: Progression of damage in longitudinal composite strip 2 of Slab S3

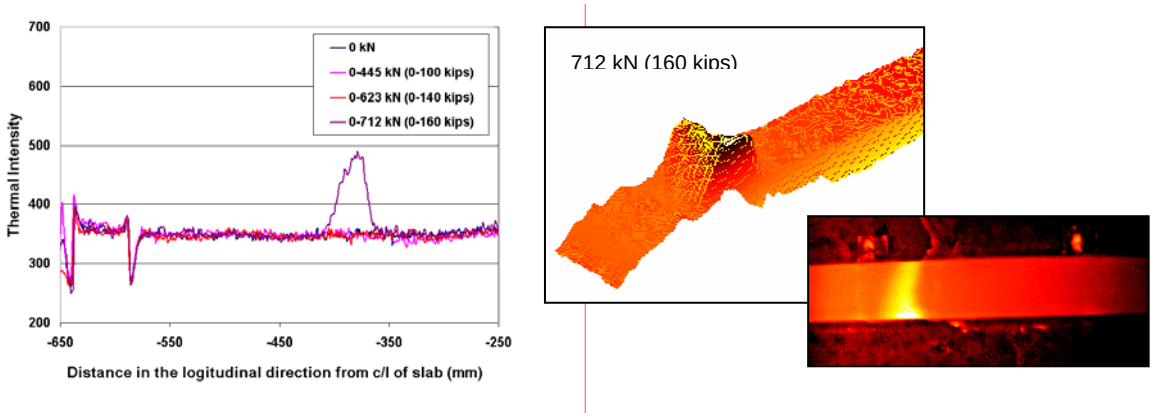

Figure 9.9: Appearance of debond areas in longitudinal composite strip 2 of Slab S3

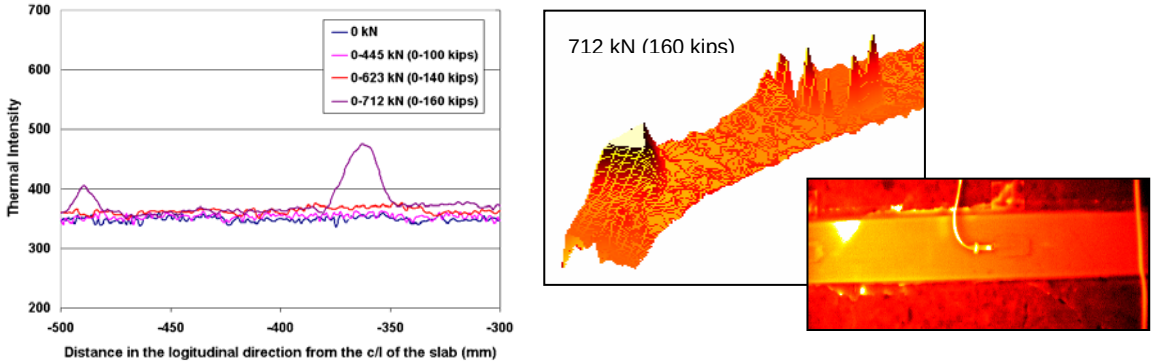

Figure 9.10: Appearance of debond areas in longitudinal composite strip 1 of Slab S3

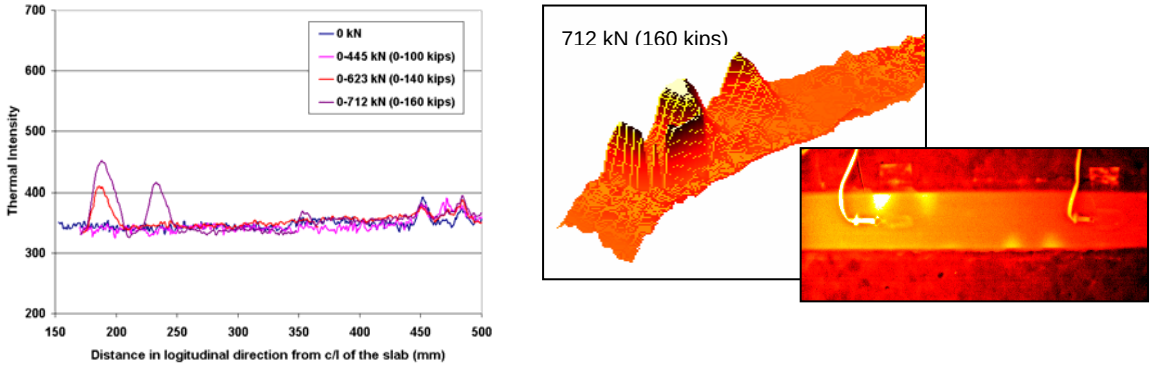

Figure 9.11: Appearance of debond areas in longitudinal composite strip 1 of Slab S3

It is evident from Figures 9.8 to 9.11 that damage in the composite strips started out as a localized phenomenon resulting in sharp changes in the thermal intensity with peaks at the location of the defects. In order to verify the validity of these defects, the thermography profiles were compared to the crack patterns observed in the slabs and illustrated in Figure 9.12. As mentioned earlier, failures in all the test specimens were caused by the opening up of pre-existing cracks. In Slab S3, the cracks widths were kept under control by the rehabilitation scheme up to 623 kN (140 kips), beyond which the opening up of the cracks was observed visually through the falling of fine sand and small pieces of concrete. This corresponds well with the thermography data where significant changes in the thermal intensity were observed only beyond 623 kN (140 kips). The falling of debris accelerated beyond 757 kN (170 kips) and failure occurred at 791 kN (177.76 kips) with the opening up of gaping cracks at the bottom surface of the slab.

On close inspection, the primary cracks were found to intersect longitudinal strip 1 at approximately 550 mm, 190 mm and –355 mm (distances being measured w.r.t. the center-line of the slab) and intersected longitudinal strip 2 at 555 mm, 130 mm and –360 mm. The locations of the cracks were found to coincide well with the locations of the thermal intensity peaks, thereby indicating that debonding of the strips was initiated by the high stress concentration at the cracks. However since the inspections were conducted up to 712 kN (160 kips), most of these intensity peaks were localized over a region of only 30 to 50 mm around the crack since away from the crack, the strain in the composite was lower than the debonding strain.

The only exception was in composite strip 2, where thermographic inspection at 623 kN (140 kips) showed intensity changes indicating debonding over a region of about 70 mm and at 712 kN (160 kips) a significant change in thermal intensity w.r.t. the baseline was observed over a region of 232 mm. On close inspection of the test specimen a horizontal crack was observed to propagate along the longitudinal strip between the main transverse cracks at 130 mm and 555 mm resulting in the debonding of the strip. It is to be noted that the thermal intensity change gradually decreases towards the right because the restraint offered by the transverse composite strips checked the growth of damage (debonding) in the longitudinal strip. A thermal intensity

peak with magnitude lower than the other peaks was also observed at –488 mm in longitudinal strip 1 which coincides with the location of a secondary crack at approximately –490 mm.

Figure 9.12: Crack pattern in Slab 3

In Slab S2, rehabilitated with site-impregnated carbon composite fabric strips, thermographic inspection was carried out both before the test, to characterize pre-existing damage/defect areas and to form a baseline for further inspections after loading the specimen. In contrast to Slab S3, where no major pre-existing defects were observed in the composite pultruded strips, the composite fabric laminates were found to have a number of pre-existing defect locations indicated by thermal intensity peaks observed in the 2-D and 3-D intensity maps. These defects were primarily located at the intersection regions of the longitudinal and transverse strips, indicating the potential presence of defects in the form of voids, crimps in the fabric, or resin rich areas in such locations. This is illustrated in Figure 9.13.

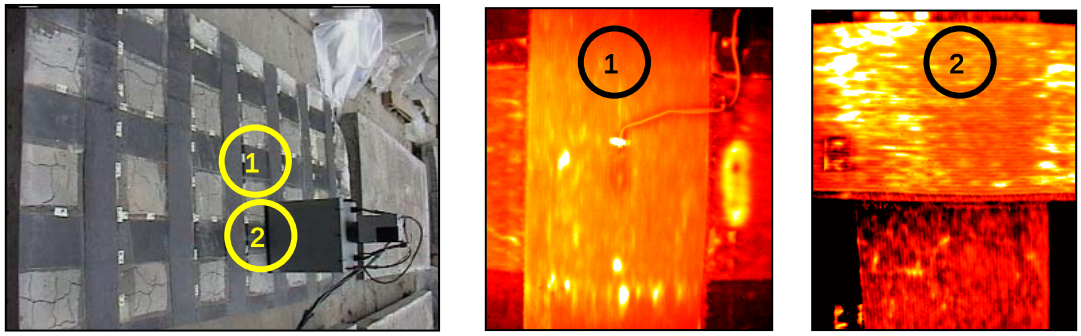

Figure 9.13: Detection of pre-existing damage/defects in composite strips of Slab 2

Thermographic inspections were also conducted in S2 at intervals of 178 kN (40 kips) during the test, up to 801 kN (180 kips), beyond which inspection was deemed to be unsafe. No significant changes in thermal intensity as compared to the baseline intensity were observed in the composite laminates. This can be explained by the fact that no major growth or appearance of damage areas took place in the composite laminates at the load levels up to which thermographic

inspection was carried out. This was confirmed later from the strain gage profiles where the strains in the composite strips were observed to remain below the debonding strains at the load stages of thermographic inspection. However, the ability of thermography to detect the presence of the existing defect areas justify its use as an effective NDT technique for quality assurance, detection, and monitoring of defect areas in site-impregnated composite fabrics.

9.5.4 Co-relation of damage progression to strain gage data

Test specimens S2 and S3 were instrumented with 20 mm gage electrical resistance strain gages in order to monitor the strains in the composite laminates and strips respectively, with the progression of loading. The axial strain profiles along the length of the longitudinal composite strips in specimens S2 and S3 (longitudinal strip 1) are presented in Figure 9.14. In Slab S3, a significant increase in the axial strain in composite strip 1 can be observed to occur at 712 kN (160 kips) in the strain gage located at –405 mm and matches with the crack pattern and the appearance of the damage area in thermographic inspection at that load stage. Moreover the strain recorded by the gage at 205 mm was relatively high and was validated through the appearance of a major transverse crack at 190 mm and the detection of damage areas through thermographic inspection at 623 kN (140 kips), which was found to propagate along with the appearance of a new damage at an adjacent location at 712 kN (160 kips).

The debonding strain of the pultruded strips was estimated to be around 2500 microstrains from fracture energy based analysis. It is observed from the thermal profiles that the axial strain reaches the debonding strain only at 623 kN (140 kips) thus explaining the appearance of damage areas in the thermographic inspections at this load level.

Since the composite strip 2 was not instrumented with strain gages no direct co-relation between the strain gage data and the thermography data could be obtained. However the thermal intensity profiles in this strip also followed the general trend in terms of appearance of intensity peaks, as that of strip 1. Also the progression of damage in terms of growth of debonded areas was evident in strip 2 (as illustrated in Figure 9.8).

It is to be noted that IR Thermography inspection data indicated the initiation of damage areas, which were found to correspond well with the locations of the main cracks. However, apart from the one location in strip 2, progression of these damage areas were not too evident since even at the final load levels of inspection, the strains in the composite strips were below the debonding strains, as are indicated by the strain profiles in Figure 9.14. The debonding strain was exceeded only at the localized areas near the cracks, resulting in the initiation of damage/debonds that was detected by the thermographic inspections as areas with higher thermal intensities than the surrounding area.

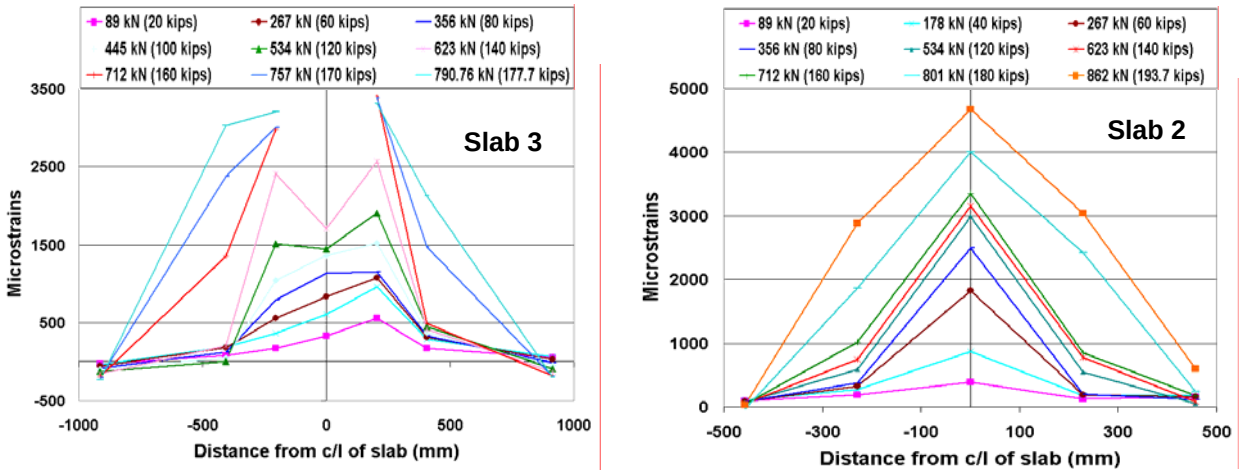

Figure 9.14: Axial strain profiles along longitudinal composite strips of rehabilitated slabs

The strain profiles in S3 were much more irregular as compared to that of S2. This was because S3 was rehabilitated only to control the cracks widths to prevent punching shear while S2 was rehabilitated with the purpose of strength enhancement for the permit truck load and had a higher composite reinforcement ratio. Moreover, the alignment of the transverse composite strips (Figure 9.3) was such that the longitudinal strip in S2 was overlapped by a transverse strip at 230 mm from the c/l of the slab, while the longitudinal strip in S3 was overlapped by the transverse strip at 610 mm. The transverse strips acted as restraints for the longitudinal strips and thus helped to control the crack widths and subsequent debonding of the strips much more effectively in S2. This was substantiated by the regular strain profiles and gradual strength degradation along with no visual observation of significant crack growth at 801 kN (180 kips) and no appearance or progression of damage areas in the thermographic inspections.

The debonding strain of the carbon fabric laminate strips was predicted to be around 3200 microstrains through fracture energy analysis. From the strain gage data of S2, the strains in the composite were found to be below this level at 712 kN (180 kips). This, along with the effective control of crack widths in specimen S2 explains why no major damage areas were observed in the composite through thermographic inspection at these load levels.

Research is currently underway to determine the degradation of strength and stiffness with the progression of damage, from the forced excitation based dynamic tests and to correlate the modal analysis results with the thermography inspection results.

9.6 SUMMARY

The control specimens were found to fail in punching shear with the damage being localized around the load area and the load pad punching through the concrete with the shear cracks following close to the typical 45^{o} dispersion failure pattern. The second control specimen, which was cut out from the negative moment area of the bridge deck and had lesser damage, had a higher capacity than the other control specimen cut out from the positive moment area of the

deck subjected to higher moment demands and damage. Thus sections of the bridge deck in regions of higher moment demand would be more susceptible to punching shear type failures.

The two rehabilitation schemes, namely strengthening with the composite fabric laminates and prefabricated pultruded strips resulted in enhancement of capacity of the specimens along with a better load distribution. Specimen S2, strengthened with the laminate strips had a strength enhancement around 73% and specimen S3, strengthened with the pultruded strips had a strength enhancement around 59% as compared to the control specimen S1.

In the strengthened specimens the damage was spread out over a larger area because of better load distribution, and the failure was transformed to flexural mode rather than punching. This was evident from the main transverse cracks resulting in failure, which were formed at a greater distance from the centerline in the strengthened specimens than in the control slabs. There were considerable deflections in the strengthened specimens away from the load area and the pre-existing cracks in the specimens were held together by the composite strips, thereby preventing punching failure until debonding of the composite strips.

Failures in all the specimens resulted from opening of the pre-existing cracks rather than formation of any new cracks. This goes to show that the loading and the boundary conditions in the test specimens closely simulated those of the actual bridge deck, thereby resulting in similar behavior of the specimens. Thus it is possible to correlate the test data on the failure modes, capacity loads and specimen behavior under progressive damage propagation to the behavior of a full bridge deck in the field being subjected to fatigue deterioration and environmental exposures.

The progression of damage in the rehabilitated specimens was monitored using IR Thermography inspections. The thermography results indicated the appearance of localized damage areas around the cracks along with their progression with the increase of loading in the specimen strengthened with the pultruded strips. This damage progression could also be linked to the crack pattern and the strain profiles along the length of the composite strips. Appearance of new damage areas was not observed in the specimen strengthened with the carbon fabric laminates, since the strains in the composite were below the debonding strains at the load level of thermographic inspection. However, baseline thermographic inspection could detect the presence of pre-existing defects/damage in the laminates in the form of fiber crimps, voids or resin rich areas.

9.7 CHAPTER 9 REFERENCES

1. J.C. Graddy, J. Kim, J.H. Whitt, N.H. Burns and R.E. Klingner, “Punching Shear Behavior of Bridge Decks under Fatigue Loading.” ACI Structural J., 99 (3), 2002, pp 257-266.

2. C.G Bouvier, “Investigating Variables in Thermographic Composite Inspections.” [Journal Article] Materials Evaluation, v 53, n 5, May 1995, pp 544-551.

3. Shepard, S.M., Rubadeux, B.A. and Ahmed, T., “Automated Thermographic Defect Recognition and Measurement.” CP 497, Nondestructive Characterization of Materials IX, American Institute of Physics, 1999, pp 373-378.